

# Separation and characterisation of elementary kenaf fibres as reinforcement in high-density polyethylene-matrix composites and tensile behaviour of flax fibres as reinforcement in vinyl ester-matrix composites

**Author:**

Soatthiyanon, Niphaphun

**Publication Date:**

2014

**DOI:**

<https://doi.org/10.26190/unsworks/2574>

**License:**

<https://creativecommons.org/licenses/by-nc-nd/3.0/au/>

Link to license to see what you are allowed to do with this resource.

Downloaded from <http://hdl.handle.net/1959.4/53585> in <https://unsworks.unsw.edu.au> on 2024-04-27

**Separation and Characterisation of Elementary  
Kenaf Fibres as Reinforcement in High-Density  
Polyethylene-Matrix Composites and Tensile  
Behaviour of Flax Fibres as Reinforcement in  
Vinyl Ester-Matrix Composites**

**Niphaphun Soatthiyanon**

A thesis in fulfilment of the requirements for the degree of

Doctor of Philosophy



School of Materials Science and Engineering

Faculty of Science

July 2014



PLEASE TYPE

THE UNIVERSITY OF NEW SOUTH WALES  
Thesis/Dissertation Sheet

Surname or Family name: **Soatthiyanon**

First name: **Niphaphun**

Other name/s: -

Abbreviation for degree as given in the University calendar: **PhD**

School: **School of Materials Science and Engineering**

Faculty: **Faculty of Science**

Title: Separation and characterisation of elementary kenaf fibres as reinforcement in high-density polyethylene-matrix composites and tensile behaviour of flax fibres as reinforcement in vinyl ester-matrix composites

Abstract 350 words maximum: (PLEASE TYPE)

The work consisted of two parts. The first examined the use of high aspect ratio short fibres in thermoplastic matrix composites. This required that the technical fibres were first broken down into elementary fibres. Kenaf fibres were used in this part of the study with HDPE as the matrix.

Several different treatments were examined for isolating the elementary fibres, the most successful being 60% HNO<sub>3</sub> treatment and 20% H<sub>2</sub>O<sub>2</sub>/CH<sub>3</sub>COOH treatment. The H<sub>2</sub>O<sub>2</sub>/CH<sub>3</sub>COOH treatment produced full length elementaries with an average length of 2.3 mm and aspect ratio of 180. However, the HNO<sub>3</sub> treatment caused fragmentation of the elementary fibres resulting in an average length of 0.2 mm and aspect ratio of 15.

The elementary fibres were used to produce HDPE composites with a 40 wt% fibre fraction. The behaviour of these composites was then compared with that of composites of the same fibre fraction, prepared using chopped technical fibres with an average length of 0.7 mm and aspect ratio of 8. Breakup of the elementaries occurred during extrusion reducing the fibre length by as much as a factor of 10. No improvement in modulus or strength over that of the chopped fibre composites was obtained for the HNO<sub>3</sub> treated fibre composites. However, improvements of 20% were obtained for the H<sub>2</sub>O<sub>2</sub>/CH<sub>3</sub>COOH treated fibre composites.

The second part of the work examined the suitability of using the results obtained from single fibre and flat fibre bundle testing to predict the tensile properties of unidirectional composites. Flax fibres were used in this part of the study. Unidirectional composites were prepared with a fibre volume fraction of 25% using vinyl ester as the matrix.

The modulus and strength obtained by backing out the fibre properties from tensile data obtained from the composites were both within 7% of those obtained from single fibre testing, once proper account was taken of the true fibre cross sectional shape and the effect of fibre length on fibre strength. The flat fibre bundle tests gave values which were only 43% of the single fibre data. However, the scatter in results was much lower.

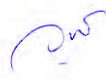
Declaration relating to disposition of project thesis/dissertation

I hereby grant to the University of New South Wales or its agents the right to archive and to make available my thesis or dissertation in whole or in part in the University libraries in all forms of media, now or here after known, subject to the provisions of the Copyright Act 1968. I retain all property rights, such as patent rights. I also retain the right to use in future works (such as articles or books) all or part of this thesis or dissertation.

I also authorise University Microfilms to use the 350 word abstract of my thesis in Dissertation Abstracts International (this is applicable to doctoral theses only).

นิภาพรรณ ไส้ตถิยานนท์

Signature



Witness

5<sup>th</sup> July, 2014

Date

The University recognises that there may be exceptional circumstances requiring restrictions on copying or conditions on use. Requests for restriction for a period of up to 2 years must be made in writing. Requests for a longer period of restriction may be considered in exceptional circumstances and require the approval of the Dean of Graduate Research.

FOR OFFICE USE ONLY

Date of completion of requirements for Award:

THIS SHEET IS TO BE GLUED TO THE INSIDE FRONT COVER OF THE THESIS

## ORIGINALITY STATEMENT

'I hereby declare that this submission is my own work and to the best of my knowledge it contains no materials previously published or written by another person, or substantial proportions of material which have been accepted for the award of any other degree or diploma at UNSW or any other educational institution, except where due acknowledgement is made in the thesis. Any contribution made to the research by others, with whom I have worked at UNSW or elsewhere, is explicitly acknowledged in the thesis. I also declare that the intellectual content of this thesis is the product of my own work, except to the extent that assistance from others in the project's design and conception or in style, presentation and linguistic expression is acknowledged.'

Signed ..... นันทพรพรณ ไส้ตมิชานนท์ .....

Date ..... 5<sup>th</sup> July, 2014 .....



## COPYRIGHT STATEMENT

'I hereby grant the University of New South Wales or its agents the right to archive and to make available my thesis or dissertation in whole or part in the University libraries in all forms of media, now or here after known, subject to the provisions of the Copyright Act 1968. I retain all proprietary rights, such as patent rights. I also retain the right to use in future works (such as articles or books) all or part of this thesis or dissertation.

I also authorise University Microfilms to use the 350 word abstract of my thesis in Dissertation Abstract International (this is applicable to doctoral theses only).

I have either used no substantial portions of copyright material in my thesis or I have obtained permission to use copyright material; where permission has not been granted I have applied/will apply for a partial restriction of the digital copy of my thesis or dissertation.'

Signed ..... นันทพรพรณ ไส้ตถิชาเนก

Date ..... 5<sup>th</sup> July, 2014

## AUTHENTICITY STATEMENT

'I certify that the Library deposit digital copy is a direct equivalent of the final officially approved version of my thesis. No emendation of content has occurred and if there are any minor variations in formatting, they are the result of the conversion to digital format.'

Signed ..... นันทพรพรณ ไส้ตถิชาเนก

Date ..... 5<sup>th</sup> July, 2014



## ACKNOWLEDGEMENTS

I would like to express my greatest appreciation to my supervisor Professor Alan Crosky for his invaluable support, assistance, guidance and suggestions throughout my study. Without his precious contribution, this thesis would not have been possible. I would particularly like to thank not only my supervisor, but also Dr Andrew Beehag for bringing this very challenging project from the Cooperative Research Centre for Advanced Composite Structures Ltd. (CRC-ACS). I have learnt a lot from this project and I would like to express my deepest gratitude to the CRC-ACS.

Special thanks to the University of New South Wales for awarding an International Postgraduate Research Scholarship (IPRS) and the CRC-ACS for granting a supplementary postgraduate scholarship during my study. My thanks are also extended to the Malaysian Agricultural Research and Development Institute (MARDI) for providing kenaf fibres, Composite Evolution Ltd. for providing Biotex unidirectional untreated flax fabric, Clariant (Australia) Pty Ltd. and Clariant Produkte (Deutschland) GmbH for providing a maleated polyethylene coupling agent, the Composite Innovation Centre (CIC) for fabricating the unidirectional composites, the Industrial Technology Centre (ITC) for testing the unidirectional composites, and Scion for examining defects of the kenaf fibres.

In addition, I would like to offer my special thanks to Dr Michael Heitzmann, Dr Amandeep Singh Virk, Angelica Legres, Dr Timothy Nicholson, Dr Luigi Vandi, Nicolas Drout and Rob for their helpful assistance and guidance throughout my experimental work at Griffith University, the University of Queensland and Australian Aerospace Composites in Queensland. I would also like to acknowledge my debt to Dr Amandeep Singh Virk again and Paresh Parmar for their important guidance and suggestions in fibre testing. Furthermore, I received valuable suggestions regarding tensile testing of extruded strands from Dr Peter Lescher. I would also like to extend my thanks to Dr Renee Whan and Dr Alexander Macmillan for their generous suggestions regarding image analysis.

I would like to express my sincere gratitude to Professor Robert Shanks, Associate Professor Allan Easteal, Associate Professor Ittipol Jangchud, Dr Dongyan Liu, Dr Mohd Nazarudin Zakaria and Duangdao Channei who gave me worthwhile

guidance in elementary fibre separation. I am grateful for the assistance provided by Associate Professor Rowan Truss, who gave me professional guidance in X-ray photoelectron spectroscopy (XPS) and assistance in interpreting experimental results of the kenaf fibres examined using the XPS at the University of Queensland. Additionally, insightful advice regarding the use of a solvent to dissolve high-density polyethylene (HDPE) given by Associate Professor Grainne Moran, and helpful assistance in statistical analysis provided by Pattarasuda Sudsaen were greatly appreciated. I also appreciate the help provided by Dr Victor Wong, Rodman Chan, Sunil Patel, Silvia Duo and Stefan Audick throughout my experimental work in the School of Chemical Engineering, the School of Biotechnology and Biomolecular Science, and the Graduate School of Biomedical Engineering.

Furthermore, I would like to thank Dr George Srzednicki and Professor Andrew Ruys for their permission to use freeze dryers at the School of Chemical Engineering (UNSW) and the University of Sydney, respectively. I would also like to thank Professor Robert Burford for his permission to use a thermogravimetric analyser (TGA) in the School of Chemical Engineering. In addition, my thanks go to Associate Professor John Foster for his permission to use a tensile testing machine in the School of Biotechnology and Biomolecular Science.

I would like to offer my heartfelt thanks to Jenny Norman, Eugene White, Dr Karen Privat, Leah Koloadin and Dr Deming Zhu for their assistance and training in using a scanning electron microscope. I would also like to thank Dr James Hook, Dr Donald Thomas and Dr Aditya Rawal for their help with solid-state  $^{13}\text{C}$  nuclear magnetic resonance (NMR) studies. Additionally, I would like to express my thanks to Dr Yu Wang for his help and training in X-ray Diffraction (XRD) measurements. My thanks also go to Dr Anne Rich and Dr Chris Marjo for their suggestions and training in using Fourier transform infrared (FTIR) and Raman spectrometers. Furthermore, I received valuable assistance from Terry Flynn.

I would like to express my great appreciation to the academic, technical and administrative staff and research academics at the School of Materials Science and Engineering, especially my committee members Associate Professor Sri Bandyopadhyay and Dr Owen Standard for their useful advice and comments. In addition, I would like to thank Professor Paul Munroe, Professor Chris Sorrell, Associate Professor Sammy Lap Ip Chan, Dr John Daniels, Dr George Yang, Anthony

Zhang, Bill Joe, Jane Gao, Dr Rahmat Kartono, Dr Thiam Teck, NM Saha-Chaudhury, Danny Kim, Thwin Htoo, Lana Strizhevsky, Judy Lim, Qing Xia, Lucy Zhang, Courtenay Atwell, Dr Pramod Koshy, Dr Wanquiang Xu and Dr Xing Xing for their enormous help and support.

I am particularly grateful for the useful guidance given by Linda Burnett and Monica O'Brien in my thesis writing. Moreover, I am in debt to Akhila Mukkavilli for her meticulous comments on several parts of my thesis writing, especially the chapter on fibre treatment and fibre characterisation.

I would like to offer my sincere thanks to various individuals who assisted, supported and encouraged me in several ways during my study. They includes Jieqing Gan, Chanes Egobal, Ismail Sinan Atli, Dr Farhana Hayazi, Gavin Feldman, Patavee Ewsawas, Norazimah Duraman, Supphatuch Ukritnukun, Dr Liana Madaleno, Carole Autoric, Dr David Ruys, Dr Shiqiang Deng, Dr Auppatham Nakaruk, Dr Somyote Kongkarat, Dr Magdalena Zaharia, Dr Navavan Thongmee, Dr Warangkana Srichamnong, Dr Pimpinan Somsong, Dr Sharifah Syed Bakar, Dr Alexander Blagus, Dr Pat Photongkam, Dr Wathukan Laopongsit, Leonie Farr, Pritipal Baweja, Paul Hallahan, Denise Bennett, John Starling, Beibei Zhu, Yin Yao, Liam Bull, Alireza Hedayati, Nabihah Sallih, Dr Sutthida Panyain, Yusuf Valentino Kaneti, Ming-Ze Lin, Orapin Namsa, Dr Man Tuiprae, Habib Fahandej Sadi, Rey Luis Teh, Irshadahmed Mansuri, Pornwan Pornprasitpol, Bronwyn Sexton, Kwanwuk Park, Kwan Hyun Ko, Zhuozhu Ye, Hsin Chen, Yongli Cui, Fran Kurnia, Dr Chanick Wangphanich and Benjamaporn Chaitachwong.

Last but not least, I would like to express my deepest gratitude to my father, Woodthikrai Soatthiyanon, my mother, Tipvimon Soatthiyanon, and my sister, Chanoksuda Soatthiyanon, for their unconditional love, tireless assistance, extraordinary support and warm encouragement.





## ABSTRACT

The work involved studies of two separate aspects of natural fibre composites. The first part of the work examined the use of high aspect ratio short fibres in thermoplastic matrix composites. This required that the technical fibres were first broken down into elementary fibres. Kenaf fibres were used in this part of the study with high-density polyethylene (HDPE) as the matrix.

Several different treatments were examined for isolating the elementary fibres from the technical fibres, the most successful being 60% nitric acid treatment and 20% hydrogen peroxide/glacial acetic acid treatment. The hydrogen peroxide/acetic acid treatment produced full length elementaries with an average length of 2.3 mm and an average aspect ratio of 180. However, the nitric acid treatment caused fragmentation of the elementary fibres resulting in an average length of only 0.2 mm and an average aspect ratio of 15. It also caused an increase in the defect density of the fibres. Both treatments increased the cellulose crystallinity but caused some oxidation of the fibres.

The elementary fibres were used to produce HDPE composites with a 40 wt% fibre fraction. The behaviour of these composites was then compared with that of composites of the same fibre fraction, prepared using chopped technical fibres with an average length of 0.7 mm and an average aspect ratio of 8. Breakup of the elementaries occurred during extrusion reducing the fibre length by as much as a factor of 10. However, the chopped technical fibres were unaffected. No improvement in modulus or strength over that of the chopped fibre composites was obtained for the nitric acid treated fibre composites, due to the very low fibre aspect ratio. However, an improvement of 20% in both modulus and strength was obtained for the hydrogen peroxide/acetic acid treated fibre composites.

The second part of the work examined the suitability of using the results obtained from single fibre testing and from flat fibre bundle testing to predict the tensile properties of unidirectional composites made from the fibres. Flax fibres were used in this part of the study. Unidirectional composites were prepared with a fibre volume fraction of 25% using vinyl ester as the matrix resin.

The modulus and strength obtained by backing out the fibre properties from tensile data obtained from the composites were both within 7% of those obtained from

single fibre testing, once proper account was taken of the true fibre cross sectional shape and the effect of fibre length on fibre strength. The flat fibre bundle tests gave values which were only 43% of the single fibre data. However, the scatter in results was much lower indicating that this test may be useful for assessing batch to batch variation.

# Table of Contents

	<b>Page</b>
<b>Originality Statement</b>	<b>i</b>
<b>Copyright Statement</b>	<b>iii</b>
<b>Authenticity Statement</b>	<b>iii</b>
<b>Acknowledgements</b>	<b>v</b>
<b>Abstract</b>	<b>ix</b>
<b>List of Figures</b>	<b>xix</b>
<b>List of Tables</b>	<b>xxxv</b>
<b>Publication</b>	<b>xli</b>
 <b>Chapter 1 Introduction</b>	 <b>1</b>
1.1 Scope of Study	4
1.2 Thesis Outline	5
 <b>Chapter 2 Literature Review</b>	 <b>7</b>
2.1 Introduction	9
2.2 Natural Fibres	9
2.2.1 Kenaf Fibres	16
2.2.1.1 Properties of Kenaf Fibres	22
2.2.2 Flax Fibres	25
2.2.2.1 Properties of Flax Fibres	28
2.3 Interface Modification of Natural Fibres	29
2.3.1 Treatments of Natural Fibre Surfaces	30
2.3.1.1 Chemical Treatments	30
(2.3.1.1.1) Alkaline Treatment	30
(2.3.1.1.2) Silane Treatment	32
(2.3.1.1.3) Acetylation Treatment	34
2.3.1.2 Physical Treatments	34
2.3.1.3 Thermal Treatment	36

	<b>Page</b>
2.3.2 Modification of Fibre/Matrix Interface by Adding Coupling Agents to the Matrix Resin	36
2.4 Natural Fibre-Reinforced Polymer-Matrix Composites	37
2.4.1 Natural Fibre-Reinforced Thermoplastic-Matrix Composites	38
2.4.1.1 Thermoplastics	38
2.4.1.2 Processing Methods	39
2.4.1.3 Properties of Kenaf Fibre-Reinforced Polyolefin-Matrix Composites	42
(2.4.1.3.1) Mechanical Properties	43
(2.4.1.3.2) Thermal Properties	45
(2.4.1.3.3) Dynamic Mechanical Properties	46
(2.4.1.3.4) Moisture Absorption	47
2.4.2 Natural Fibre-Reinforced Thermoset-Matrix Composites	48
2.4.2.1 Thermosets	48
2.4.2.2 Fabrication Techniques	50
2.4.2.3 Mechanical Properties of Unidirectional Natural Fibre- Reinforced Thermoset-Matrix Composites	53
2.4.3 Advantages and Disadvantages of Natural Fibre Composites	60
2.4.3.1 Advantages of Natural Fibre Composites	60
2.4.3.2 Disadvantages of Natural Fibre Composites	61
2.5 Summary	61
 <b>Chapter 3 Kenaf Fibre Separation and Characterisation</b>	 <b>63</b>
3.1 Introduction	65
3.2 Materials	66
3.3 Experimental	67
3.3.1 Isolation of Elementary Fibres	67
3.3.1.1 Chemical Treatment	67
(3.3.1.1.1) Ethylenediaminetetraacetic Acid (EDTA) Treatments	67
(3.3.1.1.2) Sulphuric Acid Treatment	68

	<b>Page</b>
(3.3.1.1.3) Nitric Acid Treatment	69
(3.3.1.1.4) Hydrogen Peroxide/Glacial Acetic Acid Treatment	69
(3.3.1.1.5) Glacial Acetic Acid Treatment	70
3.3.1.2 Nitric Acid and Hydrogen Peroxide/Acetic Acid Treatment of Alpha-Cellulose	70
3.3.1.3 Drying of Elementary Fibres	70
3.3.1.4 Untreated Fibres	71
3.3.2 Scanning Electron Microscopy (SEM)	71
3.3.3 Fibre Length, Diameter and Aspect Ratio	71
3.3.4 Defects in Elementary Fibres	71
3.3.5 Fourier Transforms Infrared (FTIR) Spectroscopy	72
3.3.6 Raman Spectroscopy	72
3.3.7 X-Ray Photoelectron Spectroscopy (XPS)	73
3.3.8 Cellulose Crystallinity	74
3.3.9 Degree of Oxidation	75
3.3.10 Thermogravimetric Analysis (TGA)	77
3.4 Results	77
3.4.1 Isolation of Elementary Fibres	77
3.4.1.1 Ethylenediaminetetraacetic Acid (EDTA) Treatments	77
3.4.1.2 Sulphuric Acid Treatment	77
3.4.1.3 Nitric Acid Treatment	78
3.4.1.4 Hydrogen Peroxide/Glacial Acetic Acid Treatment	80
3.4.1.5 Glacial Acetic Acid Treatment	82
3.4.1.6 Nitric Acid and Hydrogen Peroxide/Acetic Acid Treatment of Alpha-Cellulose	82
3.4.1.7 Untreated Fibres	83
3.4.2 Aspect Ratios of Elementary Fibres	83
3.4.3 Defect Density of Elementary Fibres	89
3.4.4 FTIR Spectra	101
3.4.5 Raman Spectra	105

	<b>Page</b>
3.4.6 XPS Spectra	108
3.4.7 Crystallinity of Cellulose	116
3.4.7.1 X-Ray Diffraction (XRD)	116
3.4.7.2 Solid State <sup>13</sup> C Nuclear Magnetic Resonance (NMR)	118
3.4.7.3 FTIR	121
3.4.8 Degree of Oxidation	122
3.4.9 TGA	123
3.5 Discussion	125
3.5.1 Elementary Kenaf Fibres	125
3.5.2 Aspect Ratio of Elementary Fibres	129
3.5.3 Defect Density of Elementary Fibres	131
3.5.4 FTIR Spectra	133
3.5.5 Raman Spectra	135
3.5.6 XPS Spectra	135
3.5.7 Crystallinity of Cellulose	139
3.5.8 TGA	143
3.6 Summary	144
<b>Chapter 4 Extruded Kenaf Fibre-Reinforced HDPE-Matrix Composites</b>	<b>147</b>
4.1 Introduction	149
4.2 Materials	149
4.3 Experimental Methods	151
4.3.1 Extrusion of Composites	151
4.3.2 Fibre Weight Fractions of Extruded Composites	156
4.3.3 Transverse and Longitudinal Microstructures of Composites	157
4.3.4 Tensile Testing	158
4.3.4.1 Rod Composites	158
4.3.4.2 Strip Composites	159
4.3.5 Fractographic Examination	160
4.4 Results	161
4.4.1 Extruded Neat HDPE and Composites	161

	<b>Page</b>
4.4.1.1 Rod Composites	161
4.4.1.2 Strip Composites	163
4.4.2 Fibre Weight Fractions of Extruded Composites	166
4.4.3 Transverse and Longitudinal Microstructures of Composites	174
4.4.4 Tensile Properties	178
4.4.4.1 Rod Composites	178
4.4.4.2 Strip Composites	182
4.4.5 Fracture Surfaces of Tensile Specimens	194
4.5 Discussion	201
4.5.1 Extrusion	201
4.5.1.1 Rod Composites	201
4.5.1.2 Strip Composites	202
4.5.2 Tensile Properties	203
4.5.2.1 Rod Composites	203
4.5.2.2 Strip Composites	204
4.5.3 General Discussion	205
4.6 Summary	206
 <b>Chapter 5 Tensile Properties of Flax Fibres and Unidirectional Flax Fibre/ Vinyl Ester Composites</b>	 <b>209</b>
5.1 Introduction	211
5.2 Materials	211
5.3 Experimental Procedures	212
5.3.1 Characterisation of Fibres	212
5.3.1.1 Optical and Scanning Electron Microscopy	212
5.3.1.2 Measurement of Fibre Length	212
5.3.1.3 Fibre Defects	212
5.3.2 Tensile Testing of Single Technical Fibres	212
5.3.2.1 Specimen Preparation	212
5.3.2.2 Determination of Fibre Cross-Sectional Area	213
5.3.2.3 Fibre Testing	214



	<b>Page</b>
5.3.2.4 Weibull Analysis	215
5.3.2.5 Determination of Fibre Area Correction Factor	217
5.3.2.6 Determination of True Modulus and True Strength	218
5.3.3 Testing of Fibre Bundles	219
5.3.3.1 Introduction	219
5.3.3.2 Fibre Bundle Preparation	220
5.3.3.3 Fibre Bundle Testing	223
5.3.3.4 Scanning Electron Microscopy of Fractured Fibre Bundles	225
5.3.4 Unidirectional Flax Fibre-Reinforced Vinyl Ester Matrix Composites	225
5.3.4.1 Fabrication of Composites	225
5.3.4.2 Tensile Testing of Composites	226
5.3.4.3 Optical and Scanning Electron Microscopy of Composites	227
5.3.4.4 Fibre Volume Fraction Measurement	227
5.3.4.5 Scanning Electron Microscopy of Fracture Surfaces of Composites	228
5.4 Results	228
5.4.1 Characterisation of Flax Fabric	228
5.4.2 Defect Density of Flax Fibres	231
5.4.3 Flax Technical Fibres	233
5.4.3.1 Fibre Length	233
5.4.3.2 Diameter and Cross-Sectional Area of Flax Technical Fibres	234
5.4.3.3 Fibre Area Correction Factor	236
5.4.3.4 Tensile Properties of Flax Technical Fibres	238
5.4.3.5 Weibull Analysis	242
5.4.4 Testing of Fibre Bundles	244
5.4.4.1 Tensile Properties of Fibre Bundles	244
5.4.4.2 Fracture of Fibre Bundles	248

	<b>Page</b>
5.4.5 Unidirectional Composites	248
5.4.5.1 Characterisation of Unidirectional Composites	248
5.4.5.2 Fibre Volume Fraction	251
5.4.5.3 Tensile Properties of Unidirectional Composites	255
5.4.5.4 Fracture Surface of Unidirectional Composites	258
5.5 Discussion	259
5.5.1 Defects in Flax Fibres	259
5.5.2 Technical Fibres	260
5.5.2.1 Fibre Area Correction Factor	260
5.5.2.2 Tensile Properties of Technical Fibres	260
5.5.3 Fibre Bundle Tests	263
5.5.3.1 Tensile Properties of Fibre Bundles	263
5.5.3.2 Fracture of Flax Fibres	270
5.5.4 Unidirectional Flax Fibre/Vinyl Ester Composites	273
5.5.4.1 Tensile Properties of Unidirectional Composites	273
(5.5.4.1.1) Stress-Strain Behaviour	273
(5.5.4.1.2) Calculation of Fibre Modulus and Strength from Composite Tensile Test Data	273
5.6 General Discussion	277
5.7 Summary	278
 <b>Chapter 6 Summary and Conclusions</b>	 <b>281</b>
 <b>References</b>	 <b>287</b>
 <b>Appendix I:</b> Chemical Treatment of Fibres and Alpha-Cellulose	
<b>Appendix II:</b> Defect Density of Elementary Kenaf Fibres	
<b>Appendix III:</b> T Test Output for Defect Density of Elementary Kenaf Fibres	
<b>Appendix IV:</b> Material Data Sheets for HDPE and MAPE	
<b>Appendix V:</b> Tensile Specimens of Extruded HDPE and Composite Strips after Testing	

**Appendix VI:** Process for Determining Fibre Weight Fraction of Extruded Composites

**Appendix VII:** Measured Fibre Weight Fractions of Extruded Composites

**Appendix VIII:** Process for Soaking Untreated and Treated Kenaf Fibres in Hot Trichlorobenzene

**Appendix IX:** Peak Assignations for FTIR Spectra of Residue from Filtered Solution of Untreated and Treated Kenaf Fibres Soaked in Hot Trichlorobenzene

**Appendix X:** SEM Micrographs of Transverse Sections of Extruded Composites

**Appendix XI:** SEM Micrographs of Longitudinal Section of Extruded Composites

**Appendix XII:** T Test and One-Way Analysis of Variance (ANOVA) Output for Tensile Property Test Data for Extruded HDPE and Short Kenaf Fibre/HDPE Rod Composites

**Appendix XIII:** Tensile Stress-Strain Curves of Extruded HDPE and Short Kenaf Fibre/HDPE Strip Composites

**Appendix XIV:** Material Data Sheets for Flax Fabric and Vinyl Ester Resin

**Appendix XV:** Identification of Wrapping Threads Using Fourier Transforms Infrared (FTIR) and Raman Spectroscopy

**Appendix XVI:** SEM Images of Cross-Sections of Flax Technical Fibres

**Appendix XVII:** Calculations for the Log-Normal Distributions of Measured and True Cross-Sectional Areas of Flax Technical Fibres

**Appendix XVIII:** Calculations for the Weibull Property Plot for True Tensile Strength and Strain to Failure of Flax Technical Fibres

**Appendix XIX:** Tensile Test Data for Flax Fibre Bundles

## List of Figures

	<b>Page</b>
<b>Figure 1.1:</b> Schematic diagram showing a flax stem separated down to an elementary flax fibre (Van den Oever, Bos & Van Kemenade, 2000).	4
<b>Figure 2.1:</b> Natural fibre classification (Mohanty et al., 2005).	10
<b>Figure 2.2:</b> Structure of natural fibres (Kabir et al., 2012).	11
<b>Figure 2.3:</b> Structural organisation of the cellulose, hemicellulose and lignin in the natural fibre cell wall (Kabir et al., 2012).	12
<b>Figure 2.4:</b> Structures of (a) cellulose (Biagiotti et al., 2004), (b) hemicellulose, (c) lignin (Gwon, Lee, Chun, Doh & Kim, 2010) and (d) pectin (Williams, Hosur, Theodore, Netravali, Rangari & Jeelani, 2011).	13
<b>Figure 2.5:</b> Non-textile applications of bast fibres (Suddell & Evans, 2005).	14
<b>Figure 2.6:</b> Physical appearance of kenaf (Aji, Sapuan, Zainudin & Abdan, 2009).	17
<b>Figure 2.7:</b> (a) Optical micrograph and (b) scanning electron micrograph of the cross-section of the kenaf stem consisting of the bark and core (Nishino, 2004).	17
<b>Figure 2.8:</b> Kenaf stem cross-sections (P: pith; X: xylem; VC and arrow: vascular cambium; PF: phloem (bast) fibre bundles; CE: cortex and epidermis) (Ayre et al., 2009).	18
<b>Figure 2.9:</b> (a) Scanning electron micrograph of kenaf bark fibre and schematic representations of (b) macrofibril and (c) microfibril of natural fibres (Nishino, 2004).	18
<b>Figure 2.10:</b> Transmission electron micrograph of cross-section of kenaf fibres (CW: cell wall; P: primary wall; S <sub>1</sub> , S <sub>2</sub> and S <sub>3</sub> : secondary wall sub-layers; L: lumen; ML: middle lamella; CML: compound middle lamella) (Abdul Khalil et al., 2010).	19
<b>Figure 2.11:</b> FTIR spectrum of kenaf stem in the frequency range of 400-4000 cm <sup>-1</sup> (Abdul Khalil et al., 2010).	21

<b>Figure 2.12:</b> SEM micrographs of microcrystalline cellulose (MCC): MCC-B (MCC from kenaf bast) and MCC-C (MCC from kenaf core) (Wang et al., 2010).	24
<b>Figure 2.13:</b> SEM micrograph of cross-section of flax fibre bundle (Oksman, Mathew, Långström, Nyström & Joseph, 2009).	26
<b>Figure 2.14:</b> Structure of flax from the stem to the cellulose fibrils (d = diameter) (Charlet, Eve, Jernot, Gomina & Breard, 2009).	26
<b>Figure 2.15:</b> Structure of flax stem (Bismarck, Mishra & Lampke, 2005) .	27
<b>Figure 2.16:</b> FTIR spectra of alkali treated and untreated kenaf fibres (Han et al., 2007).	31
<b>Figure 2.17:</b> FTIR spectra of alkali and silane treated and untreated kenaf fibres (Sgriecia et al., 2008).	33
<b>Figure 2.18:</b> FTIR spectra of EBI treated and untreated kenaf fibres (Han et al., 2007).	35
<b>Figure 2.19:</b> Reaction mechanism between maleated polypropylene (MAPP) and lignocellulosic fibres (Karnani et al., 1997).	37
<b>Figure 2.20:</b> Structures of molecules in amorphous (left) and semi- crystalline (right) polymers (Campbell, 2004).	38
<b>Figure 2.21:</b> (a) Extrusion and (b) injection moulding (Ashby & Jones, 2006).	40
<b>Figure 2.22:</b> Schematic diagram of natural fibre dispersion and distribution during mixing (Vázquez & Alvarez, 2009).	42
<b>Figure 2.23:</b> Typical stress-strain curves for pure polypropylene (PP), 50 wt% kenaf fibre/PP composites without MAPP coupling agent (u) as well as 20-60 wt% kenaf fibre/PP composites with MAPP coupling agent (c) (Rowell et al., 1999).	43
<b>Figure 2.24:</b> Chemical structure of a typical polyester resin (Ray & Rout, 2005).	48
<b>Figure 2.25:</b> Chemical structure of a typical epoxy resin (Ray & Rout, 2005).	48
<b>Figure 2.26:</b> Chemical structure of a typical vinyl ester resin (Ray & Rout, 2005).	49

<b>Figure 2.27:</b>	Stages of cure for thermoset resin. (a) Polymer and curing agent prior to reaction. (b) Curing initiated with size of molecules increasing. (c) Gelation with full network formed. (d) Fully cured and crosslinked (Campbell, 2010a).	49
<b>Figure 2.28:</b>	Flow diagram of resin transfer moulding (Karak, 2012).	51
<b>Figure 2.29:</b>	Filament winding technique (Campbell, 2010b).	52
<b>Figure 2.30:</b>	Pultrusion technique (Campbell, 2010b).	52
<b>Figure 2.31:</b>	Locations of the flax stems in the oriented tows (Charlet et al., 2007).	55
<b>Figure 2.32:</b>	SEM micrograph of fracture surface of unidirectional flax fibre/epoxy composites (Charlet et al., 2007).	55
<b>Figure 3.1:</b>	Kenaf fibres as received.	66
<b>Figure 3.2:</b>	Kenaf fibre bundles cut to 100 mm length.	67
<b>Figure 3.3:</b>	X-ray diffraction pattern showing measurement of peak intensity for determination of the crystallinity index (Park, Baker, Himmel, Parilla & Johnson, 2010).	74
<b>Figure 3.4:</b>	Solid state $^{13}\text{C}$ NMR spectrum of the commercial cellulose (Avicel PH-101). (a) Whole spectrum showing the assignment of peaks to the carbons in a glucopyranose repeat unit and (b) sub-spectrum showing peaks assigned to the C4 in cellulose. The crystallinity index is calculated by $X/(X+Y)$ (Park et al., 2010).	75
<b>Figure 3.5:</b>	Structure of oxidised cellulose (Kumar & Yang, 2002).	76
<b>Figure 3.6:</b>	Generation of nitrogen oxides in situ (Kumar & Yang, 2002).	76
<b>Figure 3.7:</b>	Oxidation mechanism of cellulose (Kumar & Yang, 2002).	76
<b>Figure 3.8:</b>	Photograph of freeze-dried KFTS elementary fibres	77
<b>Figure 3.9:</b>	KFTN fibres (a) air-dried, (b) freeze-dried (low fibre to water ratio) and (c) freeze-dried (high fibre to water ratio).	78
<b>Figure 3.10:</b>	Photographs of freeze-dried KFTN elementary fibres.	78
<b>Figure 3.11:</b>	Optical microscope image of KFTN elementary fibre.	79

<b>Figure 3.12:</b> SEM micrographs of air-dried KFTN elementary fibres at $\times 150$ (left) and $\times 400$ (right) magnifications.	79
<b>Figure 3.13:</b> SEM micrographs of freeze-dried KFTN elementary fibres (low fibre to water ratio) at $\times 150$ (left) and $\times 400$ (right) magnifications.	80
<b>Figure 3.14:</b> SEM micrographs of freeze-dried KFTN elementary fibres (high fibre to water ratio) at $\times 150$ (left) and $\times 400$ (right) magnifications.	80
<b>Figure 3.15:</b> Photographs of freeze-dried KFTHA1 elementary fibres.	81
<b>Figure 3.16:</b> SEM micrographs of freeze-dried KFTHA1 elementary fibres at $\times 150$ (left) and $\times 400$ (right) magnifications.	81
<b>Figure 3.17:</b> Photographs of freeze-dried KFTHA2 elementary fibres.	82
<b>Figure 3.18:</b> SEM micrographs of freeze-dried KFTHA2 elementary fibres at $\times 150$ (left) and $\times 400$ (right) magnifications.	82
<b>Figure 3.19:</b> SEM micrographs of chopped kenaf fibre bundles (UKF) at $\times 50$ (left) and $\times 150$ (right) magnifications.	83
<b>Figure 3.20:</b> Typical optical microscope images of (a) chopped technical fibres (UKF) and (b) freeze-dried elementary fibres obtained from the $\text{HNO}_3$ treatment (KFTN).	83
<b>Figure 3.21:</b> Histogram of measured lengths of UKF.	84
<b>Figure 3.22:</b> Histogram of measured diameters of UKF.	84
<b>Figure 3.23:</b> Histogram of measured lengths of freeze-dried KFTN.	85
<b>Figure 3.24:</b> Histogram of measured diameters of freeze-dried KFTN.	86
<b>Figure 3.25:</b> Typical optical microscope images of KFTHA1.	86
<b>Figure 3.26:</b> Histogram of measured lengths of KFTHA1.	87
<b>Figure 3.27:</b> Histogram of measured diameters of KFTHA1.	87
<b>Figure 3.28:</b> Typical optical microscope images of KFTHA2.	88
<b>Figure 3.29:</b> Histogram of measured lengths of KFTHA2.	88
<b>Figure 3.30:</b> Histogram of measured diameters of KFTHA2.	89
<b>Figure 3.31:</b> Transmitted light micrographs of the KFTN fibres showing kinks (a-c), initial breaks (d) and micro-compressions (e-f).	90

<b>Figure 3.32:</b>	SEM micrographs (BSE) of uncoated KFTN fibres showing micro-compressions (a-b) and initial breaks (c-f) at 2,500× (a-c), 2,000× (d), 4000× (e), and 800× (f) magnification.	91
<b>Figure 3.33:</b>	SEM micrographs (BSE) of coated KFTN fibres showing initial breaks (a-c), micro-compressions (d-e) and node (f) at 5000× magnification.	92
<b>Figure 3.34:</b>	Transmitted light micrographs of the wet KFTN fibres showing micro-compressions.	93
<b>Figure 3.35:</b>	Cross-polarised light micrograph of KFTN fibres showing dislocations.	94
<b>Figure 3.36:</b>	Cross-polarised light micrograph of KFTHA2 fibres showing nodes and dislocations.	94
<b>Figure 3.37:</b>	SEM micrographs (SE) of coated KFTN fibres (at 2000× magnification) showing initial breaks (a-d), kinks (e-g) and micro-compression (h).	95
<b>Figure 3.38:</b>	SEM micrographs (SE) of coated KFTN fibres (at 4700× magnification) showing initial breaks (a-b), dislocations (c-d), micro-compressions (e-g) and pits (h).	96
<b>Figure 3.39:</b>	SEM micrographs (SE) of coated KFTHA1 fibres (at 2000× magnification) showing nodes (a-c), dislocations (d), pits (e-f) and kinks (f-h).	97
<b>Figure 3.40:</b>	SEM micrographs (SE) of coated KFTHA1 fibres (at 4700× magnification) showing micro-compression (a) and kinks (b-h).	98
<b>Figure 3.41:</b>	SEM micrographs (SE) of coated KFTHA2 fibres (at 2000× magnification) showing nodes (a-b), pits (c-d), micro-compressions (e), initial break (f) and kinks (g-h).	99
<b>Figure 3.42:</b>	SEM micrographs (SE) of coated KFTHA2 (at 4700× magnification) showing nodes (a), micro-compressions (b-e) and kinks (f-h).	100
<b>Figure 3.43:</b>	Average defect density of KFTN, KFTHA1 and KFTHA2 fibres. Error bars represent one standard deviation.	101



	<b>Page</b>
<b>Figure 3.44:</b> FTIR spectra of (a) UKF, (b) KFTN, (c) KFTHA1 and (d) KFTHA2.	102
<b>Figure 3.45:</b> FTIR spectra of (a) AC, (b) ACTN, (c) ACTHA1 and (d) ACTHA2.	102
<b>Figure 3.46:</b> Raman spectra of (a) UKF, (b) KFTN, (c) KFTHA1 and (d) KFTHA2.	106
<b>Figure 3.47:</b> Raman spectra of (a) AC, (b) ACTN, (c) ACTHA1 and (d) ACTHA2.	106
<b>Figure 3.48:</b> XPS survey spectrum of UKF.	108
<b>Figure 3.49:</b> XPS survey spectrum of KFTN.	109
<b>Figure 3.50:</b> XPS survey spectrum of KFTHA1.	109
<b>Figure 3.51:</b> High resolution XPS spectrum of C 1s peaks of UKF.	110
<b>Figure 3.52:</b> High resolution XPS spectrum of N 1s peaks of UKF.	111
<b>Figure 3.53:</b> High resolution XPS spectrum of O 1s peaks of UKF.	111
<b>Figure 3.54:</b> High resolution XPS spectrum of C 1s peaks of KFTN.	112
<b>Figure 3.55:</b> High resolution XPS spectrum of O 1s peaks of KFTN.	112
<b>Figure 3.56:</b> High resolution XPS spectrum of C 1s peaks of KFTHA1.	113
<b>Figure 3.57:</b> High resolution XPS spectrum of O 1s peaks of KFTHA1.	113
<b>Figure 3.58:</b> X-ray diffraction patterns of (a) UKF, (b) KFTN, (c) KFTHA1 and (d) KFTHA2.	116
<b>Figure 3.59:</b> X-ray diffraction patterns of (a) AC, (b) ACTN, (c) ACTHA1 and (d) ACTHA2.	117
<b>Figure 3.60:</b> Solid state <sup>13</sup> C NMR spectra of (a) UKF, (b) KFTN, (c) KFTHA1 and (d) KFTHA2.	119
<b>Figure 3.61:</b> Solid state <sup>13</sup> C NMR spectra of (a) AC, (b) ACTN, (c) ACTHA1 and (d) ACTHA2.	120
<b>Figure 3.62:</b> TGA curves of UKF, KFTN and KFTHA2.	124
<b>Figure 3.63:</b> DTG curves of UKF, KFTN and KFTHA2.	124
<b>Figure 3.64:</b> Flax fibres treated with (a) EDTA and (b) EDTA and enzyme (Stuart et al., 2006).	126

<b>Figure 3.65:</b> SEM micrograph of treated kenaf fibres using chemical treatments and 300-kGy electron beam irradiation treatment (Shin et al., 2012).	127
<b>Figure 3.66:</b> SEM micrographs of hemp fibres (a) in original condition, (b) after STEX and water extraction, (c) after STEX, water extraction and NaOH extraction and (d) after STEX, water extraction, NaOH extraction and bleaching (Garcia-Jaldon, Dupeyre & Vignon, 1998).	128
<b>Figure 3.67:</b> SEM micrograph of untreated kenaf fibre (Aziz & Ansell, 2004).	129
<b>Figure 3.68:</b> Micrograph of HCl treated hemp fibres (Thygesen, 2008).	130
<b>Figure 3.69:</b> Average defect density of the elementary kenaf fibres obtained in the present study and hemp and flax sliver (elementaries) obtained by Ruys (2007).	131
<b>Figure 3.70:</b> Defect types of elementary hemp fibres: (A) kink band (500× magnification), (B) node (500× magnification), (C) dislocation (200× magnification), (D) slip plane (200× magnification) and (E) initial break (500× magnification) (Fan, 2010).	132
<b>Figure 3.71:</b> FTIR spectrum of kenaf stem (Öztürk et al., 2010).	133
<b>Figure 3.72:</b> FTIR spectrum of pure cellulose (Garside & Wyeth, 2003).	134
<b>Figure 3.73:</b> Raman spectrum (785 nm excitation) of untreated kenaf fibres (Ooi, Rambo & Hurtado, 2011).	135
<b>Figure 3.74:</b> Crystallinity indexes of cellulose in the UKF, KFTN, KFTHA1, KFTHA2, AC, ACTN, ACTHA1 and ACTHA2 examined using the XRD, NMR and FTIR.	140
<b>Figure 3.75:</b> X-ray diffraction patterns of amorphous cellulose examples: (a) amorphous portion extracted by the peak deconvolution method, (b) amorphous cellulose produced by the DMSO/PF method, (c) ball-milled cellulose and (d) commercial xylane (Park et al., 2010).	141
<b>Figure 3.76:</b> $^{13}\text{C}$ NMR spectrum of cellulose from kenaf (Focher et al., 2001).	142

<b>Figure 3.77:</b>	TGA curve (—), derivative weight loss DTG (---) and second derivative weight loss 2DTG (.....) of cellulose nitrate (Huang & Li, 1998).	144
<b>Figure 4.1:</b>	Eurolab co-rotating twin-screw extruder (top) and screws inside Eurolab extruder (bottom).	151
<b>Figure 4.2:</b>	Photographs of (a) materials mixed in PRISM feeder and (b) mixed materials fed into hopper of Eurolab extruder.	152
<b>Figure 4.3:</b>	(a) Thermo Scientific Eurolab 16 twin-screw extruder with two feeders and (b) control panel.	153
<b>Figure 4.4:</b>	Inside of Feeder 2 used for feeding the kenaf fibres.	154
<b>Figure 4.5:</b>	Large barrel of feeder 2 for feeding the treated kenaf fibres.	154
<b>Figure 4.6:</b>	(a) Water jet cutting into dog-bone specimens and (b) schematic diagram of Type V tensile specimen in accordance with ASTM standard D638-10.	155
<b>Figure 4.7:</b>	Setup using silicone rubber strip fixtures for tensile testing of an extruded composite rod using an Instron universal testing machine.	159
<b>Figure 4.8:</b>	(a) Lloyd EZ50 universal testing machine, (b) mechanical extensometer and (c) testing a tensile specimen of HDPE.	160
<b>Figure 4.9:</b>	Extruded neat HDPE rods.	161
<b>Figure 4.10:</b>	Extruded UKF/HDPE rod composites.	162
<b>Figure 4.11:</b>	Extruded KFTN/HDPE rod composites.	162
<b>Figure 4.12:</b>	SEM micrographs of surface of UKF/HDPE (left) and KFTN/HDPE (right) rod composites.	163
<b>Figure 4.13:</b>	Extruded (a) neat HDPE and (b) HDPE/MAPE strips.	163
<b>Figure 4.14:</b>	Extruded strip composites: (a) UKF/HDPE, (b) KFTN/HDPE and (c) KFTHA/HDPE.	164
<b>Figure 4.15:</b>	Hot pressed extruded HDPE (HDPE_H) strip.	164
<b>Figure 4.16:</b>	Hot pressed extruded HDPE/MAPE (HDPE/MAPE_H) strip.	165
<b>Figure 4.17:</b>	Hot pressed extruded UKF/HDPE (UKF/HDPE_H) strip.	165
<b>Figure 4.18:</b>	Hot pressed extruded KFTN/HDPE (KFTN/HDPE_H) strip.	166

	<b>Page</b>
<b>Figure 4.19:</b> Hot pressed extruded KFTHA/HDPE (KFTHA/HDPE_H) strip.	166
<b>Figure 4.20:</b> Fibres after extraction from rod composites: (a) untreated fibres (b) nitric acid treated fibres.	167
<b>Figure 4.21:</b> Fibres after extraction from rod composites shown at higher magnification: (a) untreated fibres and (b) nitric acid treated fibres.	167
<b>Figure 4.22:</b> Fibres after extraction from strip composites (a) as-extruded and (b) hot pressed untreated fibres; (c) as-extruded and (d) hot pressed nitric acid treated fibres; (e) as-extruded and (f) hot pressed hydrogen peroxide/acetic acid treated fibres.	169
<b>Figure 4.23:</b> Fibres after extraction from as-extruded strip composites shown at higher magnification: (a) untreated fibres, (b) nitric acid treated fibres and (c) hydrogen peroxide/acetic acid treated fibres.	170
<b>Figure 4.24:</b> Average measured fibre weight fractions of untreated and treated fibre composite strips in both as-extruded and hot pressed conditions. Error bars represent one standard deviation.	171
<b>Figure 4.25:</b> Fibres after treatment in trichlorobenzene: (a) untreated fibres, (b) nitric acid treated fibres and (c) hydrogen peroxide/acetic acid treated fibres.	172
<b>Figure 4.26:</b> SEM micrographs of transverse sections of UKF/HDPE rod composites.	174
<b>Figure 4.27:</b> SEM micrographs of transverse sections of KFTN/HDPE rod composites.	175
<b>Figure 4.28:</b> SEM micrographs of transverse sections of UKF/HDPE strip composites.	175
<b>Figure 4.29:</b> SEM micrographs of transverse sections of KFTN/HDPE strip composites.	175
<b>Figure 4.30:</b> SEM micrographs of transverse sections of KFTHA/HDPE strip composites.	176

	<b>Page</b>
<b>Figure 4.31:</b> SEM micrographs of longitudinal section of UKF/HDPE rod composite (a) at centre and (b) at edge of specimen.	176
<b>Figure 4.32:</b> SEM micrographs of longitudinal section of KFTN/HDPE rod composite (a) at centre and (b) at edge of specimen.	176
<b>Figure 4.33:</b> SEM micrographs of longitudinal section of UKF/HDPE strip composite (a) at centre and (b) at edge of specimen.	177
<b>Figure 4.34:</b> SEM micrographs of longitudinal section of KTFN/HDPE strip composite (a) at centre and (b) at edge of specimen.	177
<b>Figure 4.35:</b> SEM micrographs of longitudinal section of KTFHA/HDPE strip composite (a) at centre and (b) at edge of specimen.	177
<b>Figure 4.36:</b> Tensile stress-strain curves of extruded neat HDPE rods.	178
<b>Figure 4.37:</b> Tensile stress-strain curves of extruded UKF/HDPE rod composites.	179
<b>Figure 4.38:</b> Tensile stress-strain curves of extruded KFTN/HDPE rod composites.	179
<b>Figure 4.39:</b> Tensile modulus of extruded HDPE, UKF/HDPE and KFTN/HDPE rod composites. Error bars indicate one standard deviation.	180
<b>Figure 4.40:</b> Ultimate tensile strength of extruded HDPE, UKF/HDPE and KFTN/HDPE rod composites. Error bars indicate one standard deviation.	181
<b>Figure 4.41:</b> Strain at maximum stress of extruded HDPE, UKF/HDPE and KFTN/HDPE rod composites. Error bars indicate one standard deviation.	181
<b>Figure 4.42:</b> Stress-crosshead displacement curve of extruded HDPE strip.	183
<b>Figure 4.43:</b> Stress-crosshead displacement curves of extruded UKF/HDPE strip composites.	184
<b>Figure 4.44:</b> Stress-crosshead displacement curves of extruded KFTN/HDPE strip composites.	184
<b>Figure 4.45:</b> Stress-crosshead displacement curves of extruded KFTHA/HDPE strip composites.	185

	<b>Page</b>
<b>Figure 4.46:</b> Stress-crosshead displacement curves of hot pressed extruded HDPE (HDPE_H) strips.	185
<b>Figure 4.47:</b> Stress-crosshead displacement curves of hot pressed extruded HDPE/MAPE (HDPE/MAPE_H) strip composites.	186
<b>Figure 4.48:</b> Stress-crosshead displacement curves of hot pressed extruded UKF/HDPE (UKF/HDPE_H) strip composites.	186
<b>Figure 4.49:</b> Stress-crosshead displacement curves of hot pressed extruded KFTN/HDPE (KFTN/HDPE_H) strip composites.	187
<b>Figure 4.50:</b> Stress-crosshead displacement curves of hot pressed extruded KFTHA/HDPE (KFTHA/HDPE_H) strip composites.	187
<b>Figure 4.51:</b> Relative modulus for HDPE, HDPE/MAPE, UKF/HDPE, KFTN/HDPE and KFTHA/HDPE strip composites with and without hot pressing. Error bars indicate one standard deviation.	189
<b>Figure 4.52:</b> Ultimate tensile strength for HDPE, HDPE/MAPE, UKF/HDPE, KFTN/HDPE and KFTHA/HDPE strip composites with and without hot pressing. Error bars indicate one standard deviation.	189
<b>Figure 4.53:</b> Relative strain at maximum stress for HDPE, HDPE/MAPE, UKF/HDPE, KFTN/HDPE and KFTHA/HDPE strip composites with and without hot pressing. Error bars indicate one standard deviation.	190
<b>Figure 4.54:</b> Relative modulus as a function of true weight fraction for as-extruded strip composites.	192
<b>Figure 4.55:</b> Ultimate tensile strength as a function of true weight fraction for as-extruded strip composites.	192
<b>Figure 4.56:</b> Relative modulus as a function of true weight fraction for as hot pressed strip composites.	193
<b>Figure 4.57:</b> Ultimate tensile strength as a function of true weight fraction for as hot pressed strip composites.	193
<b>Figure 4.58:</b> SEM micrographs of fracture surfaces of tested specimens of UKF/HDPE (left) and KFTN/HDPE (right) rod composites at (a) 200×, (b) 400×, (c) 600× and (d) 800× magnification.	195

<b>Figure 4.59:</b>	SEM micrographs of fracture surfaces of (a) UKF/HDPE, (b) UKF/HDPE_H, (c) KFTN/HDPE, (d) KFTN/HDPE_H, (e) KFTHA/HDPE and (f) KFTHA/HDPE_H strip composites at 200× magnification.	196
<b>Figure 4.60:</b>	SEM micrographs of fracture surfaces of (a) UKF/HDPE, (b) UKF/HDPE_H, (c) KFTN/HDPE, (d) KFTN/HDPE_H, (e) KFTHA/HDPE and (f) KFTHA/HDPE_H strip composites at 400× magnification.	197
<b>Figure 4.61:</b>	SEM micrographs of fracture surfaces of (a) UKF/HDPE, (b) UKF/HDPE_H, (c) KFTN/HDPE, (d) KFTN/HDPE_H, (e) KFTHA/HDPE and (f) KFTHA/HDPE_H strip composites at 800× magnification.	198
<b>Figure 4.62:</b>	SEM micrographs of fracture surfaces of (a) UKF/HDPE, (b) UKF/HDPE_H, (c) KFTN/HDPE, (d) KFTN/HDPE_H, (e) KFTHA/HDPE and (f) KFTHA/HDPE_H strip composites at 1,200× magnification.	199
<b>Figure 4.63:</b>	SEM micrographs of fracture surfaces of (a) UKF/HDPE, (b) UKF/HDPE_H, (c) KFTN/HDPE, (d) KFTN/HDPE_H, (e) KFTHA/HDPE and (f) KFTHA/HDPE_H strip composites at 2,000× magnification.	200
<b>Figure 4.64:</b>	KFTHA fibres fed into a hopper of a twin-screw extruder.	202
<b>Figure 5.1:</b>	Biotex unidirectional flax fabric.	211
<b>Figure 5.2:</b>	Schematic diagram of mounting tab for single fibre testing (After Virk, 2010).	213
<b>Figure 5.3:</b>	Photograph of a flax technical fibre specimen for single fibre testing.	213
<b>Figure 5.4:</b>	Single fibre test specimen in a universal testing machine.	214
<b>Figure 5.5:</b>	Schematic diagram of cross-section of a flax technical fibre (Baley, 2002).	217
<b>Figure 5.6:</b>	Set of the aluminium fixtures connecting the Stelometer clamps to the grips of the universal testing machine.	219

<b>Figure 5.7:</b>	Tools used for fibre preparation: fibre clamp apparatus (A), Stelometer clamps (B), fine comb (C), small clamp (D), cutting knife (E), pair of tweezers (F), Petri dishes (G) and female Allen key (H).	220
<b>Figure 5.8:</b>	Clamping the fibre bundles.	221
<b>Figure 5.9:</b>	Combing the fibre bundles.	221
<b>Figure 5.10:</b>	Steps for aligning and fixing the fibre bundles inside the fibre clamp using the fibre clamp apparatus: 1 <sup>st</sup> Step - fixing the fibre clamp in the fibre clamp apparatus using the knob of the clamp apparatus; 2 <sup>nd</sup> Step -sliding up the spring and pressing the top part; 3 <sup>rd</sup> Step - inserting the fibre bundle held using a small clamp, and fixing the small clamp on the clamp apparatus by releasing the finger from the top part; 4 <sup>th</sup> Step - letting the spring pull the fibres across the clamp apparatus by releasing the thumb; 5 <sup>th</sup> Step - closing the fibre clamp; 6 <sup>th</sup> Step - tightening the fibre clamp using a female Allen key.	222
<b>Figure 5.11:</b>	Assembled Stelometer clamps with fibre bundles held firmly.	223
<b>Figure 5.12:</b>	Stelometer clamps inserted into the aluminium fixtures fixed in the universal testing machine.	225
<b>Figure 5.13:</b>	Schematic diagram of tensile specimen in accordance with ASTM standard D638.	227
<b>Figure 5.14:</b>	Optical microscope images of a yarn from the unidirectional flax fabric.	229
<b>Figure 5.15:</b>	SEM micrographs of the flax yarns.	229
<b>Figure 5.16:</b>	FTIR spectrum of wrapping threads from flax fabric.	230
<b>Figure 5.17:</b>	Raman spectra of wrapping threads from flax fabric using (a) 785-nm and (b) 514-nm excitation.	230
<b>Figure 5.18:</b>	SEM micrographs of the flax technical fibres showing kinks (arrowed).	231
<b>Figure 5.19:</b>	SEM micrographs of the flax technical fibres showing nodes (arrowed).	232



	<b>Page</b>
<b>Figure 5.20:</b> SEM micrographs of the flax technical fibres showing micro-compressions (arrowed).	232
<b>Figure 5.21:</b> SEM micrographs of the flax technical fibres showing initial break (arrowed).	233
<b>Figure 5.22:</b> Histogram showing lengths of flax technical fibres.	234
<b>Figure 5.23:</b> Typical optical microscope image of flax technical fibre.	235
<b>Figure 5.24:</b> Histogram of measured diameters of flax technical fibres.	235
<b>Figure 5.25:</b> Histogram of measured cross-sectional areas of flax technical Fibres.	236
<b>Figure 5.26:</b> Examples of cross-sectional shape of technical fibres.	236
<b>Figure 5.27:</b> Histogram of true cross-sectional areas of flax technical fibres.	237
<b>Figure 5.28:</b> Log-normal distributions of measured and true cross-sectional areas of flax technical fibres.	237
<b>Figure 5.29:</b> Tested flax fibre specimen in the universal testing machine.	238
<b>Figure 5.30:</b> Representative tensile stress-strain curves of flax technical fibres.	239
<b>Figure 5.31:</b> Histogram of measured tensile modulus of flax technical fibres.	240
<b>Figure 5.32:</b> Histogram of measured tensile strength of flax technical fibres.	240
<b>Figure 5.33:</b> Histogram of measured strain to failure of flax technical fibres.	241
<b>Figure 5.34:</b> Weibull probability plot for true tensile strength of flax technical fibres.	243
<b>Figure 5.35:</b> Weibull probability plot for strain to failure of flax technical fibres.	243
<b>Figure 5.36:</b> Representative tensile stress-strain curves of flax fibre bundles.	244
<b>Figure 5.37:</b> Histogram of linear mass density of flax fibre bundles.	245
<b>Figure 5.38:</b> Histogram of tenacity of flax fibre bundles.	245
<b>Figure 5.39:</b> Histogram of tensile modulus of flax fibre bundles.	246
<b>Figure 5.40:</b> Histogram of tensile strength of flax fibre bundles.	246
<b>Figure 5.41:</b> SEM micrographs of fracture surfaces of tested flax fibre bundles at 400× (top) and 800× (bottom) magnification.	247

<b>Figure 5.42:</b> Optical microscope images of polished unidirectional composites in transverse direction at 5× (top) and 10× (bottom) magnification.	248
<b>Figure 5.43:</b> SEM micrographs of polished unidirectional composites in transverse direction at 200× magnification.	249
<b>Figure 5.44:</b> Optical microscope images of polished unidirectional composites in longitudinal direction at 5× (top) and 10× (bottom) magnification.	249
<b>Figure 5.45:</b> SEM micrographs of polished unidirectional composites in longitudinal direction at 200× magnification .	250
<b>Figure 5.46:</b> Optical microscope images of polished unidirectional composites in parallel surface direction at 5× (top) and 10× (bottom) magnification.	250
<b>Figure 5.47:</b> SEM micrograph (top) of unidirectional composites (Image No. 1) and their binary images including wrapping threads (middle) and excluding wrapping threads (bottom).	252
<b>Figure 5.48:</b> SEM micrograph (top) of unidirectional composites (Image No. 2) and their binary images including wrapping threads (middle) and excluding wrapping threads (bottom).	253
<b>Figure 5.49:</b> SEM micrograph (top) of unidirectional composites (Image No. 3) and their binary images including wrapping threads (middle) and excluding wrapping threads (bottom).	254
<b>Figure 5.50:</b> Tensile stress-strain curves of unidirectional composites.	256
<b>Figure 5.51:</b> Tensile stress-strain curves of neat vinyl ester resin.	256
<b>Figure 5.52:</b> Failed tensile specimens.	257
<b>Figure 5.53:</b> Cracking in parallel sided region of tensile specimens.	257
<b>Figure 5.54:</b> SEM micrographs of fracture surfaces of unidirectional composites at (a) 50×, (b) 75×, (c and d) 150×, (e) 200× and (f) 500× magnification.	258
<b>Figure 5.55:</b> Defects of flax fibres (Baley, 2002).	259
<b>Figure 5.56:</b> Shear deformation in the leather pads.	265

	<b>Page</b>
<b>Figure 5.57:</b> Simulated load-strain curve for Bundle 9.	267
<b>Figure 5.58:</b> Corrected simulated load-strain curve for Bundle 9.	269
<b>Figure 5.59:</b> Simulated experimental load-strain curve for Bundle 9.	269
<b>Figure 5.60:</b> Failure sequence in a flax technical fibre: (a) debonding and fibrillation in the longitudinal direction along the elementary fibres; (b) cracking in the elementary fibres in the transverse direction due to stress concentration; (c) “tearing-type” fracture within and through the elementary fibres; (d) and (e) long-range fracture completed by fracture of the elementary fibres and their constituting microfibrils (Romhány, Karger-Kocsis & Czigány, 2003).	271
<b>Figure 5.61:</b> SEM micrographs of fracture surfaces of tested flax fibres at low (left) and high (right) magnification (Baley, 2002).	272
<b>Figure 5.62:</b> Diagram showing the failure sequence of flax fibres: axial splitting (debonding), transverse cracking, and multiple elementary fibre fracture (Romhány, Karger-Kocsis & Czigány, 2003).	272

## List of Tables

	<b>Page</b>
<b>Table 1.1:</b> Inventory of major potential world fibre sources (Rowell, 2008).	3
<b>Table 2.1:</b> Fibre content by weight in straw (Urbanczyk, 1985, cited in Zimniewska, Wladyka-Przybylak & Mankowski, 2011).	10
<b>Table 2.2:</b> Factors affecting fibre quality (Dittenber & GangaRao, 2012).	11
<b>Table 2.3:</b> Use of natural fibres for serial parts in the automotive industry in 1997-2001 (Karus & Kaup, 2002).	15
<b>Table 2.4:</b> Climate requirements for kenaf fibres (Rowell, 2008).	16
<b>Table 2.5:</b> Characteristics and properties of kenaf stems (values in brackets represent one standard deviation) (Abdul Khalil et al., 2010).	20
<b>Table 2.6:</b> Lengths of kenaf bast and core elementary fibres (values in brackets represent one standard deviation) (Abdul Khalil et al., 2010).	21
<b>Table 2.7:</b> Chemical compositions of different fractions of kenaf fibres (Abdul Khalil et al., 2010).	21
<b>Table 2.8:</b> Thermal properties of kenaf fibres (Ashby, 2013).	22
<b>Table 2.9:</b> Tensile properties of kenaf bast fibre bundles at temperatures of 110-190°C for 3, 6 and 9 hours (Du et al., 2008).	23
<b>Table 2.10:</b> Properties of microcrystalline cellulose (MCC) from kenaf fibres (Wang et al., 2010).	24
<b>Table 2.11:</b> Climate requirements for flax fibres (Rowell, 2008).	26
<b>Table 2.12:</b> Major chemical components of flax fibres (Dittenber & GangaRao, 2012; Wanjale & Jog, 2011; Zimniewska, Wladyka-Przybylak & Mankowski, 2011).	27
<b>Table 2.13:</b> Tensile properties of flax fibres (Ashby, 2013; Cheung, Ho, Lau, Cardona & Hui, 2009; Saheb & Jog, 1999; Wanjale & Jog, 2011).	28
<b>Table 2.14:</b> Thermal properties of flax fibres (Ashby, 2013).	29
<b>Table 2.15:</b> Comparison between different plasma sources (Lee et al., 2011).	35

	<b>Page</b>
<b>Table 2.16:</b> Properties of synthesis thermoplastics (Schwartz & Goodman, 1982 and Van de Velde & Kiekens, 2001, cited in Sain & Panthapulakkal, 2004).	39
<b>Table 2.17:</b> Details of the pure HDPE and the 50% kenaf fibre/HDPE composites (Lundin et al., 2004).	44
<b>Table 2.18:</b> Flexural properties of the pure HDPE and the 50% kenaf fibre/HDPE composites (Lundin et al., 2004).	45
<b>Table 2.19:</b> Storage modulus ( $E'$ ), loss modulus ( $E''$ ) and $\tan \delta$ values of the kenaf fibre/ polypropylene composites (Tajvidi, Falk et al., 2006).	47
<b>Table 2.20:</b> Properties of polyester, epoxy and vinyl ester resins (Iijima et al., 1991, Mukherjee et al., 1984, Sarkar et al., 1997, cited in Ray & Rout, 2005).	49
<b>Table 2.21:</b> Advantages and disadvantages of polyester, epoxy and vinyl ester resins (Kroschwitz, 1985, Pritchard, 1980, Sarkar et al., 1997, cited in Ray & Rout, 2005).	50
<b>Table 2.22:</b> Tensile properties of epoxy resin and unidirectional flax fibre/epoxy composites (values in brackets represent one standard deviation) (Oksman, 2001).	53
<b>Table 2.23:</b> Mechanical properties of jowar, sisal and bamboo fibre/polyester composites (Ratna Prasad & Mohana Rao, 2011).	54
<b>Table 2.24:</b> Tensile properties of the unidirectional flax fibre/epoxy composites (values in brackets represent one standard deviation) (Charlet et al., 2007).	55
<b>Table 2.25:</b> Tensile properties of 45% unidirectional Alfa/unsaturated polyester composites with different fibre-tensile load angles in the longitudinal direction (Brahim & Cheikh, 2007).	56
<b>Table 2.26:</b> Tensile properties of unidirectional Alfa/unsaturated polyester composites with different fibre volume fraction in the longitudinal direction (Brahim & Cheikh, 2007).	56

<b>Table 2.27:</b>	Tensile properties of epoxy resin and unidirectional kenaf fibre/epoxy composites (Abdullah, Khalina & Ali, 2011).	57
<b>Table 2.28:</b>	Tensile properties of epoxy resin and untreated and 18% NaOH treated unidirectional sisal fibre/epoxy composites (Padmavathi, Naidu & Rao, 2012).	57
<b>Table 2.29:</b>	Compressive strength of epoxy resin and untreated and 18% NaOH treated unidirectional sisal fibre/epoxy composites (Padmavathi, Naidu & Rao, 2012).	58
<b>Table 2.30:</b>	Impact property of untreated and 18% NaOH treated unidirectional sisal fibre/epoxy composites (Padmavathi, Naidu & Rao, 2012).	58
<b>Table 2.31:</b>	Flexural properties of the untreated and treated flax fibre/epoxy composites (Van de Weyenberg et al., 2006).	59
<b>Table 2.32:</b>	Compression properties of the unidirectional kenaf fibre/unsaturated polyester composites (Nosbi et al., 2010).	60
<b>Table 3.1:</b>	Chemical analysis (wt%) of MARDI kenaf fibres (Zakaria, 2014).	66
<b>Table 3.2:</b>	Raman spectrum measurement conditions.	73
<b>Table 3.3:</b>	Measured lengths, diameters and aspect ratios of UKF, KFTN, KFTHA1 and KFTHA2 fibres (values in brackets represent one standard deviation).	85
<b>Table 3.4:</b>	Assignments of peak positions of FTIR bands of kenaf fibres and $\alpha$ -cellulose in untreated and treated conditions.	103
<b>Table 3.5:</b>	Sources for assignments of peak positions of FTIR spectra.	104
<b>Table 3.6:</b>	Assignments of Raman bands of kenaf fibres and $\alpha$ -cellulose in untreated and treated conditions.	107
<b>Table 3.7:</b>	Atomic composition (%) and O/C ratio at surface of UKF, KFTN and KFTHA1 fibres.	110
<b>Table 3.8:</b>	XPS carbon (C) 1s, nitrogen (N) 1s and oxygen (O) 1s binding energies and atomic composition of UKF, KFTN and KFTHA1.	114

	<b>Page</b>
<b>Table 3.9:</b> Percentage crystallinity indexes of cellulose in kenaf fibres and $\alpha$ -cellulose examined from the XRD patterns subtracted background using Segal's equation.	117
<b>Table 3.10:</b> Percentage crystallinity indexes of cellulose in kenaf fibres and $\alpha$ -cellulose examined from the NMR spectra.	121
<b>Table 3.11:</b> Percentage crystallinity indexes of cellulose in kenaf fibres and $\alpha$ -cellulose examined from the FTIR spectra using the ratio of the peaks at $1420\text{ cm}^{-1}$ to $893\text{ cm}^{-1}$ .	122
<b>Table 3.12:</b> Degree of oxidation of cellulose in treated kenaf fibres and treated $\alpha$ -cellulose. Values in brackets represent one standard deviation.	123
<b>Table 3.13:</b> Summary of decomposition temperatures of UKF, KFTN and KFTHA2.	125
<b>Table 3.14:</b> Atomic composition (%) in surfaces of the untreated kenaf fibres obtained in the present work and that of Sgriccia et al. (2008).	136
<b>Table 3.15:</b> O/C ratios and atomic percentages of C 1s of cellulose, hemicellulose, lignin and extractives.	137
<b>Table 3.16:</b> Atomic percentages of C 1s of kenaf fibres, hemp fibres, flax fibres (linen), wood fibres, wood flour and kraft fibres.	138
<b>Table 3.17:</b> Atomic percentages of O 1s of kenaf fibres and hemp fibres.	139
<b>Table 3.18:</b> Summary of significant findings.	145
<b>Table 4.1:</b> Physical characteristics of HDPE powder.	150
<b>Table 4.2:</b> Physical and chemical properties of MAPE powder.	150
<b>Table 4.3:</b> Weight loss of fibres after soaking in hot trichlorobenzene (values in brackets represent one standard deviation) and correction factors of fibre weight fractions of the composite samples.	173
<b>Table 4.4:</b> Measured and true fibre weight fractions of composite samples.	173
<b>Table 4.5:</b> Tensile test data for extruded HDPE and short kenaf fibre/HDPE rod composites.	180

	<b>Page</b>
<b>Table 4.6:</b> Tensile test data for extruded HDPE and short kenaf fibre/ HDPE strip composites.	188
<b>Table 4.7:</b> True fibre weight fraction of extruded strip composites.	191
<b>Table 5.1:</b> Strain ranges used for determination of tensile modulus.	215
<b>Table 5.2:</b> Defects in flax technical fibres.	233
<b>Table 5.3:</b> Location parameters, scale parameters, geometric mean and geometric standard deviation of the measured and true cross-sectional areas of the flax technical fibres.	238
<b>Table 5.4:</b> Measured tensile properties of flax technical fibres.	241
<b>Table 5.5:</b> True tensile properties of flax technical fibres.	242
<b>Table 5.6:</b> True tensile properties of flax technical fibres and their Weibull modulus and scale parameters (values in brackets represent one standard deviation).	244
<b>Table 5.7:</b> Test results for flax fibre bundles.	247
<b>Table 5.8:</b> Fibre volume fraction of unidirectional composites and flax fibre contents in unidirectional flax fabrics.	255
<b>Table 5.9:</b> Measured tensile properties of neat resin and unidirectional composites.	257
<b>Table 5.10:</b> Comparison of single fibre and bundle strengths.	266
<b>Table 5.11:</b> Results from simulated fibre bundle tests.	268
<b>Table 5.12:</b> Data used for predicting the tensile modulus and strength of the flax fibres.	276





## **PUBLICATION**

### **Book Chapter**

Crosky, A., Soatthiyanon, N., Ruys, D., Meatherall, S., & Potter, S. (2014). Thermoset matrix natural fibre-reinforced composites. In A. Hodzic & R. Shanks (Eds.), *Natural fibre composites: Materials, processes and applications* (pp. 233-270): Woodhead Publishing Limited.



CHAPTER 1

**INTRODUCTION**

---



## 1. INTRODUCTION

Natural plant fibres are attractive for use as the reinforcement in plastic matrix composites because of their low density, low cost, non-abrasiveness, biodegradability, high electrical resistance, high specific properties, low energy consumption and utilization, and decrease of greenhouse gas (CO<sub>2</sub>) emissions. Their use can also lead to the development of non-food agricultural/farm-based economies thereby creating job opportunities in rural areas (Rowell, Sanadi, Jacobson & Caulfield, 1999; Sain & Panthapulakkal, 2004; Sanadi, Caulfield, Jacobson & Rowell, 1995; Sreekumar & Thomas, 2008). Moreover, the fibres are harmless to workers and do not cause health issues such as lung cancer (Lee, Kim & Yu, 2009, cited in Wanjale & Jog, 2011). Major sources of plant fibres are listed in Table 1.1.

**Table 1.1:** Inventory of major potential world fibre sources (Rowell, 2008)

<b>Fibre Source</b>	<b>World (dry tonnes)</b>
Wood	1,750,000,000
Straw (wheat, rice, oat, barley, rye, flax and grass)	1,145,000,000
Stalks (corn, sorghum and cotton)	970,000,000
Sugar cane bagasse	75,000,000
Reeds	30,000,000
Bamboo	30,000,000
Cotton staple	15,000,000
Corn (jute, kenaf and hemp)	8,000,000
Papyrus	5,000,000
Bast (jute, kenaf and hemp)	2,900,000
Cotton linters	1,000,000
Esparto grass	500,000
Leaf (sisal, abaca and henequen)	480,000
Sabai grass	200,000
<b>Total</b>	<b>4,033,080,000</b>

Plant fibres are extracted as technical fibres which are 50-100  $\mu\text{m}$  in diameter and run the length of the plant, as shown in Figure 1.1. The technical fibres are themselves made up of smaller shorter fibres having diameters of 10-20  $\mu\text{m}$ . These are referred to as elementary fibres and are also shown in Figure 1.1.

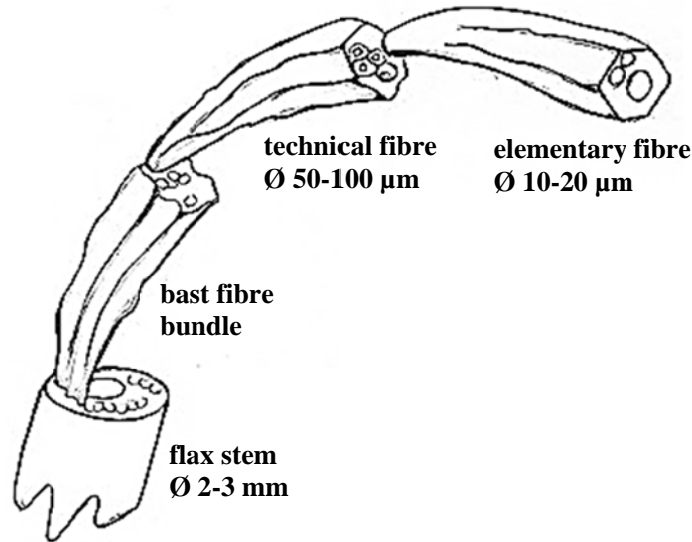


**Figure 1.1:** Schematic diagram showing a flax stem separated down to an elementary flax fibre (Van den Oever, Bos & Van Kemenade, 2000).

## 1.1 Scope of Study

This thesis examines the use of high aspect ratio fibres in extruded thermoplastic and resin transfer moulded thermoset natural plant fibre composites. Since the technical fibres run the length of the plant they have an inherently high aspect ratio which can be retained in thermoset composites made from yarn. It can also be retained in thermoplastic composites manufactured by comingling or film stacking. However the fibres require chopping when used for more automated processes such as extrusion and injection moulding, which are more desirable for thermoplastic composite fabrication. Unfortunately chopping of the fibres results in a low aspect ratio which reduces the mechanical performance of the composite.

The aspect ratio of short fibres can be improved if the technical fibres are first reduced to elementary fibres. This was investigated for kenaf fibre/polyethylene composites. Kenaf was used as the reinforcing fibre because of its importance as a commercial crop in the South East Asia region.

The work involved development of a suitable process for reducing the technical fibres to elementaries which were then analysed to establish any effect of the process on the fibre chemistry. The elementaries were subsequently used to produce extruded composites and the mechanical properties of the composites then determined.

A major issue affecting commercial uptake of natural fibre composites is variability in the fibre properties from batch to batch, since this flows on into the resulting composite. One possible method of managing this variability would be to grade each batch of fibres mechanically and use the mechanical grading as an indicator for the performance of the composites. This was investigated for flax/vinyl ester composites. Flax fibres were used rather than kenaf since untwisted flax unidirectional fabrics are now available which overcome the inherent difficulty of making unidirectional natural fibre composites with good fibre alignment.

One way of mechanically grading fibres is to measure the tensile strength of individual (technical) fibres. However, even within a batch, there is considerable variability and this necessitates testing of a large number of fibres (typically 100), which is very time consuming. A simpler method, which is widely used for grading in the textiles industry, is flat fibre bundle testing. The work in this part of the study involved measuring the mechanical properties of the flax fibres using both methods and then evaluating how well these properties compared with fibre properties determined from unidirectional composites.

## **1.2 Thesis Outline**

Chapter 2 presents a review of existing literature on natural fibres and natural fibre composites. The review focuses on kenaf and flax, kenaf fibre-reinforced polyolefin composites and unidirectional natural fibre-reinforced thermoset-matrix composites.

The methods used to break down kenaf fibre bundles into elementary fibres by chemical treatment are described in Chapter 3. The elementary fibres obtained are then characterised physically and chemically to determine the effect of the chemical treatments.

Successful treatments are then used to produce larger quantities of elementaries which are compounded with HDPE to produce extruded composites. Mechanical testing is then conducted to evaluate the performance of the composites. This part of the work is described in Chapter 4.



The tensile properties of flax fibres determined using single fibre tests and also flat bundle testing are given in Chapter 5. These are compared with fibre tensile properties obtained from tests conducted on unidirectional flax/vinyl ester composites.

Chapter 6 presents the conclusions and recommendations.

CHAPTER 2

**LITERATURE REVIEW**

---



## **2. LITERATURE REVIEW**

### **2.1 Introduction**

In this chapter, natural fibres and natural fibre composites are reviewed. This chapter is divided into three parts: natural fibres, interface modification of natural fibres and natural fibre composites. Firstly, the structure of natural fibres, chemical composition and properties of natural fibres, with particular focus on kenaf and flax fibres, are reviewed. Secondly, chemical, physical and thermal treatments of natural fibre surfaces, particularly for kenaf fibres, are described in detail. The modification of fibre-matrix interfaces by the addition of coupling agents is also described in this section. Finally, processing methods and properties of kenaf fibre-reinforced polyolefin-matrix composites and unidirectional natural fibre-reinforced thermoset-matrix composites are reviewed. The advantages and disadvantages of natural fibre composites are also discussed.

### **2.2 Natural Fibres**

Natural fibres used as reinforcements in polymer composites are classified into non-wood and wood fibres as shown in Figure 2.1. Non-wood fibres include bast fibres, leaf fibres, seed/fruit fibres, grass fibres and straw fibres, whereas wood fibres consist of soft and hard woods and recycled wood fibres (Mohanty, Misra, Drzal, Selke, Harte & Hinrichsen, 2005). This research focuses on bast fibres, especially kenaf and flax.

Bast fibres are extracted from the inner bark or phloem of plant stems (Rowell, 2008; Zimniewska, Wladyka-Przybylak & Mankowski, 2011). The quantity of phloem and fibres for kenaf, flax, hemp, jute and ramie is given in Table 2.1. Yields and qualities of the bast fibres are dependent on the type of plants, the climatic conditions and the soil (Munder, Fürll & Hempel, 2005). Factors affecting the fibre quality are shown in Table 2.2. The structure of natural fibres from the outside to the inside includes the primary wall and three layers of secondary wall referred to as  $S_1$ ,  $S_2$  and  $S_3$  (Kabir, Wang, Lau & Cardona, 2012), as shown in Figure 2.2.

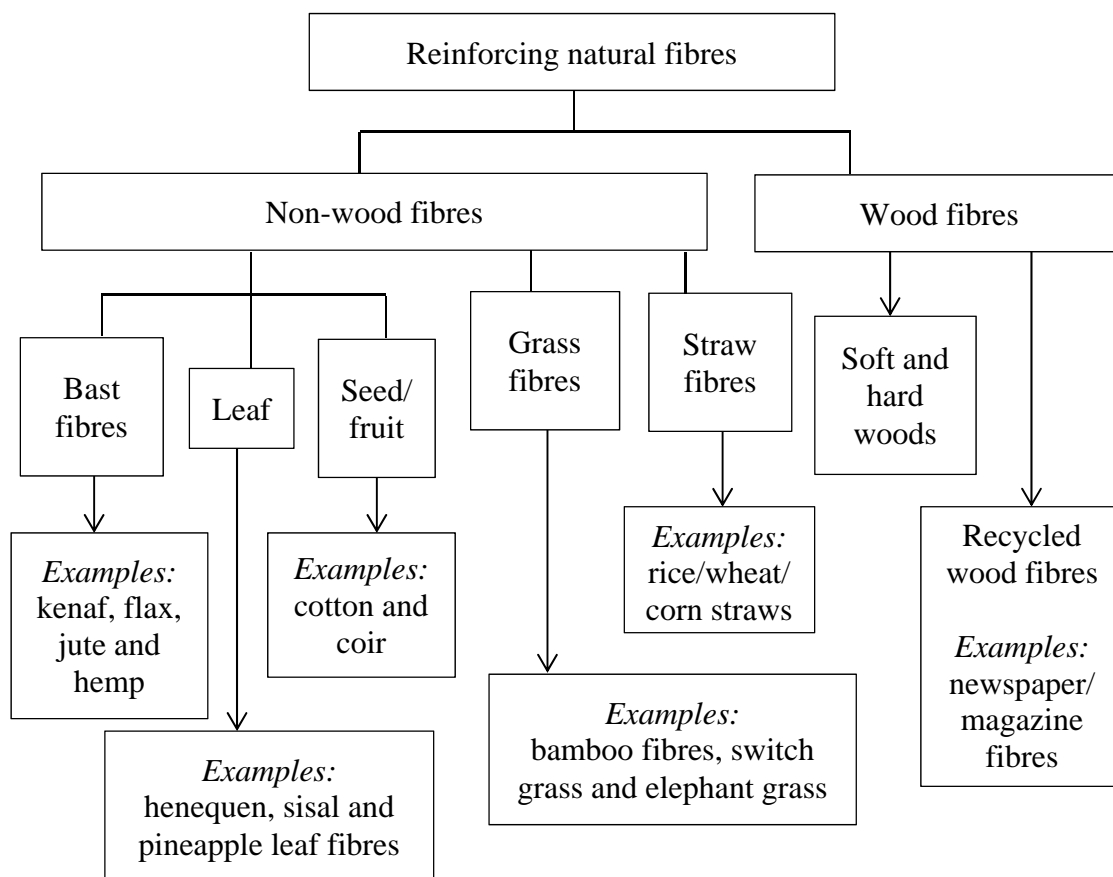


**Figure 2.1:** Natural fibre classification (Mohanty et al., 2005).

**Table 2.1:** Fibre content by weight in straw (Urbanczyk, 1985, cited in Zimmiewska, Wladyka-Przybylak & Mankowski, 2011)

<b>Fibrous plant</b>	<b>Phloem content in dry straw (%)</b>	<b>Fibre content in phloem (%)</b>	<b>Fibre content in dry straw (%)</b>
Kenaf	23-28	48	16-17
Flax	36-42	47-54	17-22
Hemp	22-32	46-49	10-15
Jute	30-48	-	19-20
Ramie	20-35	24-48	4-21

**Table 2.2:** Factors affecting fibre quality (Dittenber & GangaRao, 2012)

Stage of Natural Fibre Production	Factors Affecting Fibre Quality
Plant growth stage	<ul style="list-style-type: none"> <li>- Species of plant</li> <li>- Crop cultivation</li> <li>- Crop location</li> <li>- Fibre location in plant</li> <li>- Local climate</li> </ul>
Harvesting stage	<ul style="list-style-type: none"> <li>- Fibre ripeness, which affects: <ul style="list-style-type: none"> <li>- Cell wall thickness</li> <li>- Coarseness of fibres</li> <li>- Adherence between fibres and surrounding structure</li> </ul> </li> </ul>
Fibre extraction stage	<ul style="list-style-type: none"> <li>- Decortication process</li> <li>- Type of retting methods</li> </ul>
Supply stage	<ul style="list-style-type: none"> <li>- Transportation conditions</li> <li>- Storage conditions</li> <li>- Age of fibres</li> </ul>

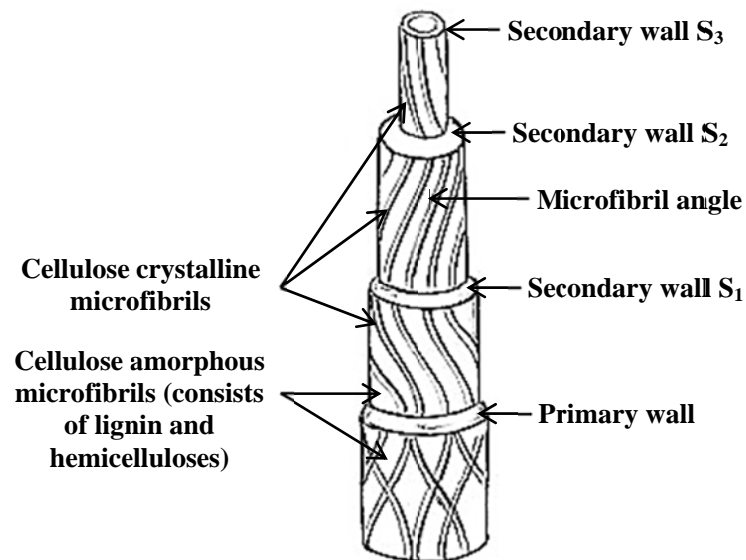


**Figure 2.2:** Structure of natural fibres (Kabir et al., 2012).

The main chemical constituents of bast fibres are cellulose, hemicellulose and lignin. Figure 2.3 shows the structural organisation of the main chemical components in the natural fibre cell wall (Kabir et al., 2012).



**Figure 2.3:** Structural organisation of the cellulose, hemicellulose and lignin in the natural fibre cell wall (Kabir et al., 2012).

Cellulose (Figure 2.4a) is a natural homopolymer of D-glucopyranose rings linked with  $\beta$ -(1 $\rightarrow$ 4)-glycosidic bonds (polysaccharides), (Akil, Omar, Mazuki, Safiee, Ishak & Abu Bakar, 2011). It is a hydrophilic linear polymer (Sain & Panthapulakkal, 2004) consisting of long linear chains of linking glucose units (4,000 to 8,000 glucose molecules). The repeating unit in cellulose contains two glucose units and a glucose monomer, the latter containing three hydroxyl groups which result in strong hydrogen bonds between the cellulose chains (Biagiotti, Puglia & Kenny, 2004). Cellulose is semi-crystalline. Its microcrystalline structure consists of a combination of highly crystalline regions and amorphous regions (Sain & Panthapulakkal, 2004). Cellulose is stable in normal environments and has the ability to resist hydrolysis (Garcia-Jaldon, Dupeyre & Vignon, 1998). Most properties of cellulose are dependent on the degree of polymerisation (Kaith, Mittal, Jindal, Maiti & Kalia, 2011). Generally, cellulosic fibres have more than 500,000 cellulose molecules. The strong hydrogen bonding between the molecules results in high tensile strength (Biagiotti et al., 2004). A number of different types of cellulose exist. Each has its own cell geometry which affects the mechanical properties of natural fibres (Thomas, Paul, Pothan & Deepa, 2011).

Hemicellulose (Figure 2.4b) is a highly branched polysaccharide consisting of glucose, mannose, galactose, xylose, rhamnose, arabinose and other sugars (Mohamed, Bhardwaj, Hamma & Webber, 1995, cited in Akil et al., 2011; Kaith et al., 2011). It is also very hydrophilic (Olesen & Plackett, 1999, cited in Lee, Delille & Bismarck, 2011). It is amorphous and has a random structure with low strength. Hemicellulose is easily hydrolysed by dilute acids or bases. In the case of acid hydrolysis, hemicellulose

is degraded into sugar molecules. Hemicellulose can absorb water which results in swelling. This affects the dimensional stability of the fibres (Biagiotti et al., 2004).

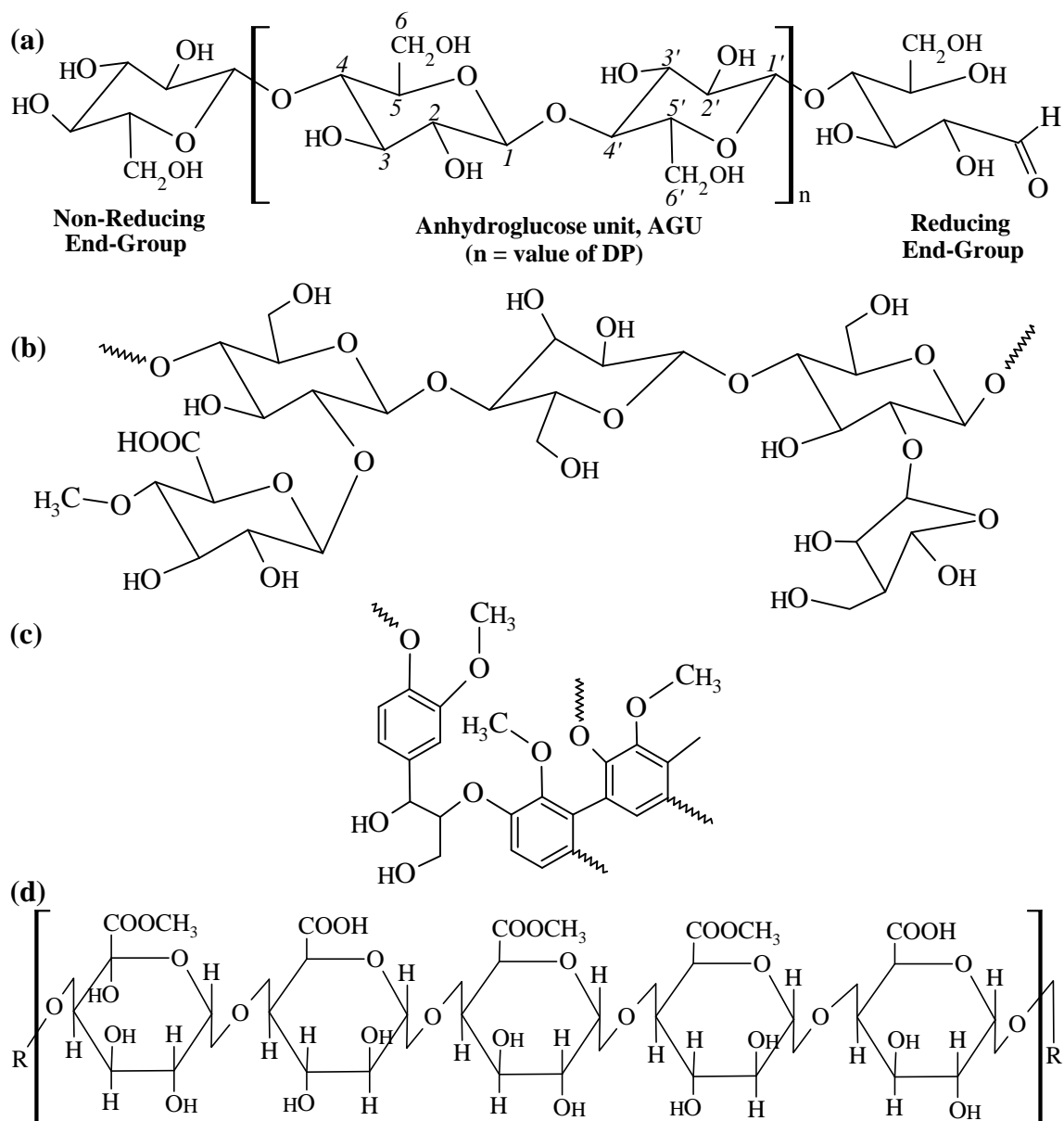


**Figure 2.4:** Structures of (a) cellulose (Biagiotti et al., 2004), (b) hemicellulose, (c) lignin (Gwon, Lee, Chun, Doh & Kim, 2010) and (d) pectin (Williams, Hosur, Theodore, Netravali, Rangari & Jeelani, 2011).

Lignin (Figure 2.4c) has a crosslinked aromatic structure. It is strongly resistant to most microorganism attack (Biagiotti et al., 2004). Lignin is hydrophobic and amorphous. Lignin dissolves in hot alkali, however, it is not acid hydrolysed (Thomas et



al., 2011). A function of lignin in plants is to support and hold polysaccharide fibres together. Another function is to protect the cellulose in plants (Sain & Panthapulakkal, 2004). The glass transition temperature and melting temperature of lignin are approximately 90°C and 170°C, respectively (Thomas et al., 2011).

The decomposition temperature of cellulose, hemicellulose and lignin ranges from 360-370°C, 280-320°C and 230-500°C, respectively (Li, Li & Zhang, 2002, cited in Han, Han, Cho, & Kim, 2007).

Other chemical components of natural fibres are pectins and waxes. Pectin (Figure 2.4d) is heteropolysaccharide including polygalacturon acid. A function of pectin in plants is to give flexibility (Thomas et al., 2011). Pectin can dissolve in hot alkali (Wong & Shanks, 2009). Waxes include different alcohols (Thomas et al., 2011).

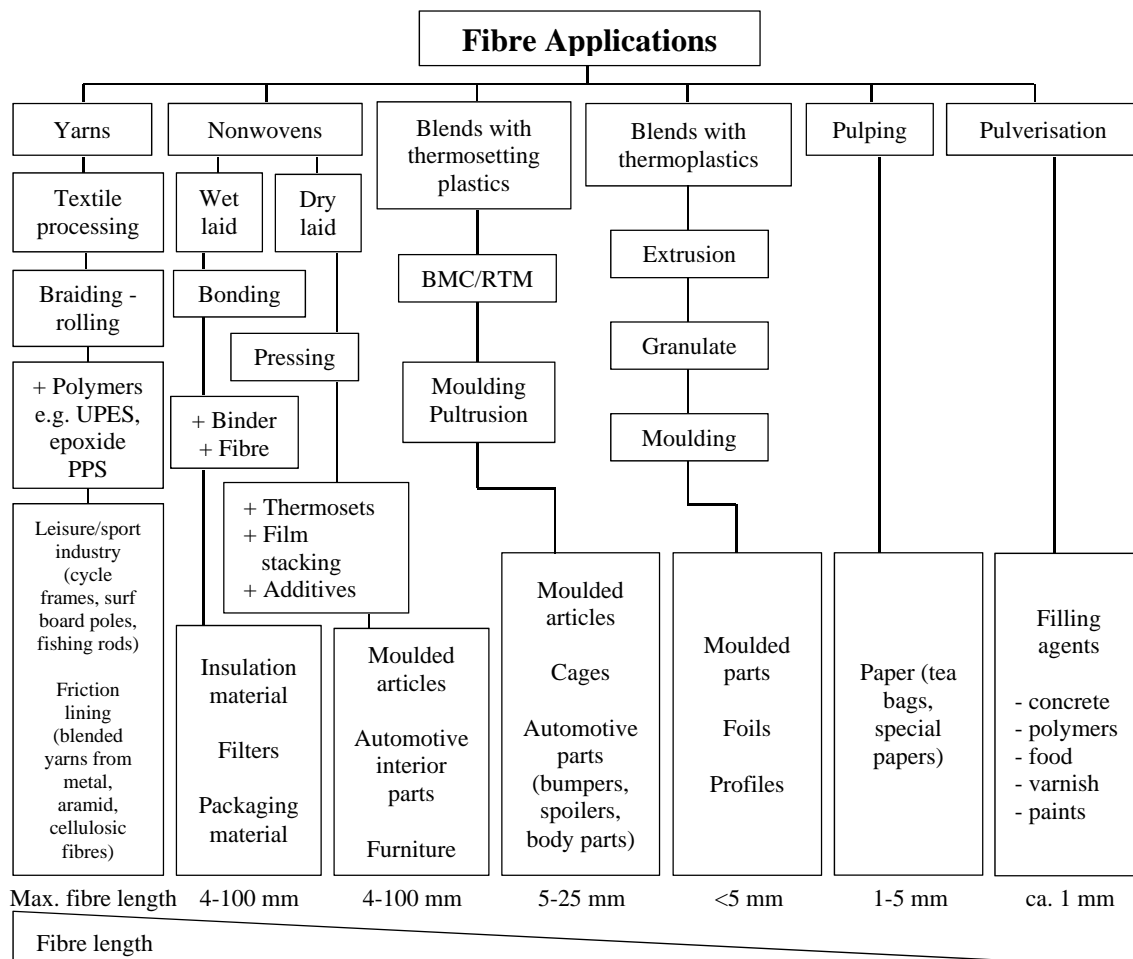


**Figure 2.5:** Non-textile applications of bast fibres (Suddell & Evans, 2005).

**Table 2.3:** Use of natural fibres for serial parts in the automotive industry in 1997-2001 (Karus & Kaup, 2002)

<b>Manufacturers /Customers</b>	<b>Model/Application (dependent on model)</b>
Audi	TT, A2, A3, A4, A4 Avant (1997), A4 Variant (1997), A6, A8 (1997), Roadster and Coupe Seat back, side and back door panels, parcel tray, boot lining, rear flap lining, rear storage panel and spare tire lining
BMW	3, 5 and 7 Series and others Door inserts/door panels, headliner panel, boot lining and seat back
Citroen	C4 (2001) Door inserts
DaimlerChrysler	A-Klasse, C-Klasse, E-Klasse and S-Klasse Door inserts, windshield/dashboard, business table and column cover
Fiat	Punto, Brava, Marea, Alfa Romeo 146, 156 and Sportwagon
Ford	Mondeo CD 162 (1997), Cougar (1998), Mondeo (2000) and Focus Door inserts, B-column cover, parcel tray and in the future also motor protection (cover undershield)
MAN	Bus (1997) Headliner panel
Mitsubishi	Miscellaneous models (since 1997)
Nissan	Miscellaneous models
Opel	Astra, Vectra and Zafira Headliner panel, door inserts, column cover, instrument panel and rear shelf panel
Peugeot	New model 406
Renault	Clio and Twingo
Rover	Rover 2000 and others Insulation and rear storage panel
Saab	Coupe (1998) Door inserts
SEAT	Door inserts and seat backs
Toyota	Miscellaneous models
Volkswagen	Golf A4, Golf 4 Variant (1998), Passat Variant and Bora Door inserts Seat backs , rear flap lining and parcel tray
Volvo	C70, V70 and Coupe (1998) Door inserts and parcel tray

Bast fibres are used in several non-textile applications as shown in Figure 2.5. The particular applications are dependent on the fibre length (Suddell & Evans, 2005).

Table 2.3 shows the use of natural fibres for various parts in the automotive industry during the period 1997-2001 (Karus & Kaup, 2002).

### 2.2.1 Kenaf Fibres

Kenaf (*Hibiscus cannabinus* L.) is an annual crop which grows in temperate climates (Rowell & Han, 1999). It goes through 5 stages in its life cycle, these being germination, growth, flowering, seed formation and death. Kenaf is cultivated in India, China, Bangladesh, United States of America, Indonesia, Malaysia, South Africa, Vietnam, Thailand, parts of Africa, and some areas in southeast Europe (Zimniewska et al., 2011). The ideal climatic conditions for growing of kenaf are given in Table 2.4 (Rowell, 2008). Kenaf can grow up to more than 3 m in height and 3-5 cm in base diameter under a variety of weather conditions (Nishino, 2004). The growth of kenaf can be up to 10 cm/day in height under optimum ambient conditions (Rowell & Han, 1999, cited in Nishino, 2004). Kenaf absorbs nitrogen and phosphorous during growth and also absorbs high amounts of carbon dioxide (Michell, 1986, cited in Zampaloni et al., 2007). The average nitrogen and phosphorous absorption rates of kenaf are 0.81 g/m<sup>2</sup>/day and 0.11 g/m<sup>2</sup>/day, respectively (Abe & Ozaki, 1998, cited in Nishino, 2004).

**Table 2.4:** Climate requirements for kenaf fibres (Rowell, 2008)

Requirement	
Optimum temperature (°C)	22-30
Minimum water (mm) required during the growing season	120
Optimum soil pH	6.0-6.8
Growing cycle (days)	150-180
Fibre yield (kg/hectare)	1,700

The physical appearance of kenaf is shown in Figure 2.6 while optical and scanning electron micrographs of the cross section of a kenaf stem are shown in Figure 2.7. The kenaf stem contains both inner core fibres (~0.5-0.8 mm; 75-60%) and outer bast fibres (~2-2.5 mm; 25-40%) (Abdul Khalil, Yusra, Bhat & Jawaid, 2010; Wang, Shang, Song & Lee, 2010). As is discussed later in this section, the properties of the bast fibres are superior to those of the core fibres.

The structure of a mature kenaf stem is also shown in Figure 2.8. The stem is shown viewed under white light in Figure 2.8a and viewed using UV epifluorescence, to

emphasise the presence of lignified cells, in Figure 2.8b. A schematic diagram of primary phloem (bast) fibre bundles is shown in Figure 2.8c. Lignin in the primary cell walls and middle lamella is shown as light blue whilst lignin in the secondary walls is shown as dark blue. The hollow lumen is shown in black (Ayre et al., 2009). The phloem (bast) fibres play a major role in protection and mechanical support (Raven, Evert & Eichhorn, 2005, cited in Ayre et al., 2009).

*Figure 2.6 has been removed due to Copyright restrictions.*

**Figure 2.6:** Physical appearance of kenaf (Aji, Sapuan, Zainudin & Abdan, 2009).

*Figure 2.7 has been removed due to Copyright restrictions.*

**Figure 2.7:** (a) Optical micrograph and (b) scanning electron micrograph of the cross-section of the kenaf stem consisting of the bark and core (Nishino, 2004).

*Figure 2.8 has been removed due to Copyright restrictions.*

**Figure 2.8:** Kenaf stem cross-sections (P: pith; X: xylem; VC and arrow: vascular cambium; PF: phloem (bast) fibre bundles; CE: cortex and epidermis) (Ayre et al., 2009).

There are several factors that are important for the separation of kenaf fibres from the plant. These include stem size, moisture content in the fibres, humidity of the ambient air, the type of machine used and the processing rate (Abdul Khalil et al., 2010).

*Figure 2.9 has been removed due to Copyright restrictions.*

**Figure 2.9:** (a) Scanning electron micrograph of kenaf bark fibre and schematic representations of (b) macrofibril and (c) microfibril of natural fibres (Nishino, 2004).

A scanning electron micrograph of a bundle of kenaf bast fibres, together with schematic diagrams showing their structure, is given in Figure 2.9 (Nishino, 2004). The fibre bundles are made up of macrofibrils, also referred to as microfibrils or primary/elementary fibres. As noted earlier, the fibres consist of a primary cell wall and the  $S_1$ ,  $S_2$  and  $S_3$  secondary cell walls. These, in turn, are made up of cellulose microfibrils which, as noted earlier, consist of both crystalline and amorphous regions.

*Figure 2.10 has been removed due to Copyright restrictions.*

**Figure 2.10:** Transmission electron micrograph of cross-section of kenaf fibres (CW: cell wall; P: primary wall;  $S_1$ ,  $S_2$  and  $S_3$ : secondary wall sub-layers; L: lumen; ML: middle lamella; CML: compound middle lamella) (Abdul Khalil et al., 2010).

A kenaf fibre bundles is shown in more detail in Figure 2.10. The individual elementary fibres (microfibrils), are bound into the fibre bundles by the middle lamella at their triple point and by the compound middle lamella along their sides. Most of the lignin (~90%) is in the middle lamella although some is also present in the  $S_1$  and  $S_2$  layers and the compound middle lamella. The highest cellulose concentration (~50%) is in the  $S_2$  layers. These are the thickest layer in the kenaf cell walls and have a strong influence on the properties of the fibres (Abdul Khalil et al., 2010).

The kenaf bast fibre bundles are located under the kenaf bark, as shown in Figure 2.6, and are aligned parallel to the length of the stem (Rowell, 2008). The bast fibres have a thicker cell wall and smaller lumen diameter than the core fibres. The thickness of the  $S_2$  layers is 1.5 to 2.5  $\mu\text{m}$  and 0.3 to 1.6  $\mu\text{m}$  in the bast fibres and core fibres, respectively. The average lumen diameter is approximately 2.8  $\mu\text{m}$  and 6.7  $\mu\text{m}$  for the bast fibres and core fibres, respectively (Abdul Khalil et al., 2010). Calamari et al. (1999) found that the average length and diameter of single (elementary) kenaf fibres

were 2.45 mm (1.17-4.94 mm) and 12  $\mu\text{m}$  (5.63-21.25  $\mu\text{m}$ ), respectively. Zimniewska et al. (2011) have reported a somewhat greater elementary fibre length of 1.5 mm to 11 mm. This probably reflects differences within the plant species and/or in the growing conditions.

The characteristics of kenaf bast and core stems are shown in Table 2.5 while the lengths of the elementary bast and core fibres are shown in Table 2.6. The bast elementary fibres have lengths approximately three-times those of the core fibres. The bast elementary fibres are longest in the middle of the plant and shortest at the top while the core fibres are longest at the top of the plant and shortest at the bottom, Table 2.6, (Abdul Khalil et al., 2010).

**Table 2.5:** Characteristics and properties of kenaf stems (values in brackets represent one standard deviation) (Abdul Khalil et al., 2010)

Characteristics/Properties	Bast	Core	Stem
Dimension (cm)			
Height (range)		145-250	145-250
Diameter		1.52 (0.095)	1.74 (0.212)
Perimeter		5.73 (0.131)	6.60 (0.101)
Proportion (%)			
Cross-section area	21.96 (2.03)	78.04 (2.51)	
Weight proportion	32.2	68.5	
Density ( $\text{g}/\text{cm}^3$ )	1.2 <sup>1</sup>	0.21 (0.038)	0.29 (0.044)
Acidity (pH)	7.13	5.21	5.87

<sup>1</sup>Zimniewska et al. (2011)

The chemical components of kenaf fibres include  $\alpha$ -cellulose, holocellulose (cellulose and hemicellulose (Owen & Thomas, 1989)), lignin, extractive and ash, as given in Table 2.7. As can be seen from Table 2.7 the bast fibres have a higher  $\alpha$ -cellulose and lower lignin content than the core fibres and this results in higher strength (Abdul Khalil et al., 2010).

**Table 2.6:** Lengths of kenaf bast and core elementary fibres (values in brackets represent one standard deviation) (Abdul Khalil et al., 2010)

Position from the top of plants <sup>1</sup>	Fibre lengths, $\mu\text{m}$			Average
	A	B	C	
Kenaf bast				
Fibre length	3370 (211)	3980 (319)	3560 (286)	3637 (419)
Kenaf core				
Fibre length	1360 (191)	1050 (112)	890 (93)	1100 (153)

<sup>1</sup> A, B and C: correspond to the top, middle and base of the both kenaf bast and core stems

**Table 2.7:** Chemical compositions of different fractions of kenaf fibres (Abdul Khalil et al., 2010)

	Kenaf whole (bast + core)	Kenaf bast	Kenaf core
$\alpha$ -Cellulose (%)	53.8	55.0	49.0
Holocellulose (%)	87.7	86.8	87.2
Lignin (%)	21.2	14.7	19.2
Extractive (%)	6.4	5.5	4.7
Ash (%)	4.0	5.4	1.9

*Figure 2.11 has been removed due to Copyright restrictions.*

**Figure 2.11:** FTIR spectrum of kenaf stem in the frequency range of 400-4000  $\text{cm}^{-1}$  (Abdul Khalil et al., 2010).

A Fourier transform infrared (FTIR) spectrum from a kenaf stem is shown in Figure 2.11 (Abdul Khalil et al., 2010). An OH stretching absorption peak presents at 3,390  $\text{cm}^{-1}$ , and an OH bending absorption peak appears at 1,190  $\text{cm}^{-1}$ . A CH<sub>2</sub> stretching absorption peak appears at 2,910  $\text{cm}^{-1}$ . The carbonyl stretching (C=O) peaks for acetyl



groups in hemicellulose and for the aldehyde groups in lignin appear at  $1,739\text{ cm}^{-1}$  and  $1,650\text{ cm}^{-1}$  (Abdul Khalil et al., 2010).

The traditional applications of kenaf are in ropes, canvas and sacking (Nishino, Hirao, Kotera, Nakamae & Inagaki, 2003). Recent applications of kenaf include paper products, building materials (decking, railing, flooring and wall frames), absorbents, animal feeds (Edeerozey, Akil, Azhar & Ariffin, 2007; Sain & Panthapulakkal, 2004), automotive structural parts (Du, Zhang & Xue, 2008), furniture, toys, gardening equipment and packaging (Rowell et al., 1999; Sain & Panthapulakkal, 2004).

Harvesting of kenaf before full maturity can be of benefit to its use in both paper and composites. This is because lignin is lower in immature plants than in mature plants. This is particularly significant for paper manufacturing, since chemical removal of lignin is required in the pulping process (Rowell & Han, 1999). Likewise, if lignin needs to be removed from the fibres before composite manufacture, the use of immature plants is attractive.

### **2.2.1.1 Properties of Kenaf Fibres**

As for other plant fibres, the properties of the kenaf fibres are anisotropic (Xue, Du, Elder, Wang & Zhang, 2009). Kenaf fibre properties also depend on the source, cultivation, age, separation techniques and kenaf fibre history (Feng et al., 2001; Sanadi et al., 1995). The density of the kenaf fibres is approximately  $1.38\text{--}1.40\text{ g/cm}^3$  (Liu, Drzal, Mohanty & Misra, 2007; Rowell et al., 1999; Sanadi et al., 1995; Zampaloni et al., 2007). The modulus of kenaf fibres is approximately 60 GPa (Liu et al., 2007) while the tensile strength is 217-740 MPa, the yield strength is 195-666 MPa and the strain to failure is 1.3-5.5% (Ashby, 2013). Thermal properties of kenaf fibres are given in Table 2.8.

**Table 2.8:** Thermal properties of kenaf fibres (Ashby, 2013)

<b>Thermal property</b>	
Glass temperature ( $^{\circ}\text{C}$ )	107-117
Thermal conductor or insulator?	Poor insulator
Thermal conductivity ( $\text{W/m}\cdot^{\circ}\text{C}$ )	0.25-0.35
Specific heat capacity ( $\text{J/kg}\cdot^{\circ}\text{C}$ )	1,200-1,220
Thermal expansion coefficient ( $\mu\text{strain}/^{\circ}\text{C}$ )	15-30

The effect of strain rate on the tensile properties of kenaf bast fibre bundles (also known as technical fibres) has been examined by Xue et al. (2009) using strain rates of 2.5, 25 and 250  $\mu\text{m/s}$ . Both Young's modulus and tensile strength increased progressively with strain rate, with the increase in Young's modulus being from 12.7 to 17.2 GPa and the increase in tensile strength being from 146 to 223 MPa. However, the maximum failure strain of 1.5% occurred at a strain rate of 25  $\mu\text{m/s}$  with values of 1.1-1.2% and 1.2-1.3% being obtained at the lower and higher strain rates respectively. Two failure mechanisms were observed, fibre pullout from the bundles and complete bundle breakage.

**Table 2.9:** Tensile properties of kenaf bast fibre bundles at temperatures of 110-190°C for 3, 6 and 9 hours (Du et al., 2008)

Condition		Tensile Property		
Time (hours)	Temperature (°C)	Tensile Modulus (GPa)	Tensile Strength (MPa)	Failure Strain (%)
3	110	12.0	136.5	1.17
	130	13.8	162.6	1.13
	150	14.4	140.1	1.05
	170	15.0	147.8	0.92
	190	9.2	49.7	0.72
6	110	15.3	214.0	1.39
	130	14.2	173.2	1.20
	150	13.4	152.7	1.13
	170	15.3	133.1	0.83
	190	8.0	72.8	0.81
9	110	13.0	176.6	1.33
	130	14.3	166.7	1.24
	150	13.7	146.3	1.02
	170	14.3	91.3	0.57
	190	6.8	41.4	0.47

The effect of exposure at elevated temperature on the room temperature tensile properties of kenaf bast fibre bundles has also been examined. Du et al. (2008) treated

fibres at temperatures from 110-190°C in 20° increments for times of 3, 6 and 9 hours. It was found that the tensile modulus was not affected by elevated temperature exposure except at the highest temperature of 190°C, where it decreased markedly, Table 2.9. The tensile strength and strain to failure also decreased markedly at this temperature, although some decrease in both these properties was also evident at 170°C for the longer exposure times, Table 2.9. The changes in the tensile properties at the higher temperatures were attributed to degradation of cellulose, hemicellulose and lignin. In contrast, Xue et al., (2009) reported that the strength and strain to failure of kenaf bast fibre bundles treated at 180°C for 1 hour were higher than for fibre bundles treated at 170°C for the same length of time. However, Young's modulus was slightly lower at the higher temperature, consistent with the findings of Du et al. (2008).

*Figure 2.12 has been removed due to Copyright restrictions.*

**Figure 2.12:** SEM micrographs of microcrystalline cellulose (MCC): MCC-B (MCC from kenaf bast) and MCC-C (MCC from kenaf core) (Wang et al., 2010).

**Table 2.10:** Properties of microcrystalline cellulose (MCC) from kenaf fibres (Wang et al., 2010)

Sample	Degree of polymerization	Yield (%)	Crystallinity index (%)	Moisture content (%)	Bulk density (g/cm <sup>3</sup> )
MCC-B <sup>1</sup>	324	80	77.7	3.62	0.24
MCC-C <sup>2</sup>	310	77	68.6	5.10	0.11

<sup>1</sup>MCC-B: microcrystalline cellulose from kenaf bast

<sup>2</sup>MCC-C: microcrystalline cellulose from kenaf core

Both bast and core kenaf fibres have been used to prepare microcrystalline cellulose (MCC) (Wang et al., 2010). MCC is composed of subunits of poly-β-

cellobiose which is produced by acid hydrolysis of cellulose (Battista, 1971, cited in Wang et al., 2010). SEM micrographs of the MCC from both bast and core fibres are shown in Figure 2.12. The properties of the MCC are given in Table 2.10.

The degree of polymerization ( $DP$ ) was calculated as follows:

$$DP = 95 \cdot [\eta] \cdot \frac{c}{w} \quad (2.1)$$

where  $w$  is the dried weight (g) of MCC taken;  $c$  is the MCC concentration (g/mol) in 0.5 M cupriethylenediamine solution.  $[\eta]$  is the intrinsic viscosity (ml/g) of the solution. As shown in Table 2.10, the degree of polymerization was slightly higher for the bast MCC (MCC-B) than for the core MCC (MCC-C) (Wang et al., 2010).

The crystallinity index ( $CrI$ ) was obtained from x-ray diffraction data using the intensity measurements at  $2\theta$  values of 22.0-22.5° (crystalline region) and 18.0-18.5° (amorphous background)  $2\theta$  using Segal's equation:

$$CrI = \frac{I_{002} - I_{am}}{I_{002}} \quad (2.2)$$

where  $I_{002}$  denotes the maximum intensity of the 002 peak at about  $2\theta = 22.0-22.5^\circ$  and  $I_{am}$  is the lowest intensity corresponding to  $2\theta$  value near 18.0-18.5° (Segal, Creely, Martin & Conrad, 1959; Wang et al., 2010). As shown in Table 2.10, the crystallinity index was substantially higher for the bast MCC than for the core MCC, indicating a higher level of crystallinity. The bast MCC also absorbed less moisture than the core MCC which was attributed to its higher level of crystallinity (Wang et al., 2010).

### 2.2.2 Flax Fibres

Flax (*Linum usitatissimum* L.) is an annual herbaceous plant, grown in mild climates (Ehrensing, 2008). The climatic conditions most suitable for growing flax are given in Table 2.11 (Rowell, 2008). Flax grows up to 80-150 centimetres in height in 80-110 days. The bast fibres are produced from the central section of the flax plant only. The lengths and diameters of flax fibre bundles (Figure 2.13) range from 60-140 centimetres and from 40-80  $\mu\text{m}$ , respectively (Bismarck, Mishra & Lampke, 2005). The technical fibre lengths and elementary fibre lengths of flax fibres range from 0.2-1.4 meters and from 13-40 millimetres, respectively. The diameter of elementary flax fibres ranges from 17-20  $\mu\text{m}$ . The density and linear density of flax fibres are 1.50  $\text{g/cm}^3$  and 0.289 tex, respectively (Zimniewska, Wladyka-Przybylak & Mankowski, 2011). The

structure of flax from the stem to the cellulose fibrils is shown schematically in Figure 2.14 while a section through a flax stem is shown in Figure 2.15. The structure of the flax stem from the inside to the outside consists of a hollow core (also referred to as a lumen), a pith layer, a cambium layer, the phloem or parenchyma (which contains the bast fibres), the cortex, the epidermis and a waxy cuticula, Figure 2.15.

**Table 2.11:** Climate requirements for flax fibres (Rowell, 2008)

<b>Requirement</b>	
Optimum temperature (°C)	10-20
Minimum water (mm) required during the growing season	150
Optimum soil pH	5.5-7.0
Growing cycle (days)	85-120
Fibre yield (kg/hectare)	1,100

*Figure 2.13 has been removed due to Copyright restrictions.*

**Figure 2.13:** SEM micrograph of cross-section of flax fibre bundle (Oksman, Mathew, Långström, Nyström & Joseph, 2009).

*Figure 2.14 has been removed due to Copyright restrictions.*

**Figure 2.14:** Structure of flax from the stem to the cellulose fibrils (d = diameter) (Charlet, Eve, Jernot, Gomina & Breard, 2009).

*Figure 2.15 has been removed due to Copyright restrictions.*

**Figure 2.15:** Structure of flax stem (Bismarck, Mishra & Lampke, 2005).

**Table 2.12:** Major chemical components of flax fibres (Dittenber & GangaRao, 2012; Wanjale & Jog, 2011; Zimniewska, Wladyka-Przybylak & Mankowski, 2011)

Major Chemical Component	Reference		
	Dittenber & GangaRao (2012)	Wanjale & Jog (2011)	Zimniewska, Wladyka-Przybylak & Mankowski (2011)
Cellulose	62-72 wt%	71%	64-84 wt%
Hemicellulose	18.6-20.6 wt%	18.6-20.6%	16-18 wt%
Lignin	2-5 wt%	2%	0.6-5.0 wt%
Pectin	2.3 wt%	-	1.8-2.0 wt%
Waxes or fat	1.5-1.7%	-	1.5 wt%

Chemical analyses of flax fibres from three recent studies: Dittenber & GangaRao, 2012, Wanjale & Jog, 2011, Zimniewska, Wladyka-Przybylak &

Mankowski, 2011, are given in Table 2.12. While there is some variation amongst the different results, the analysis all lie within the range 64-84 wt% cellulose, 16-21 wt% hemicellulose, 0.6-5.0 wt% lignin, 1.8-2.3 wt% pectin and 1.5-1.7 wt% wax. Comparison with the data given for kenaf in Table 2.7 shows that flax has a substantially higher cellulose content than kenaf while the hemicellulose and lignin contents are substantially lower.

Flax fibres have been used extensively in the textile industry to make linen fabrics. More recently, they have been used as the reinforcement in polymer composites used as components in the automotive and transportation industry (Foulk, Akin, Dodd & Ulven, 2011).

### ***2.2.2.1 Properties of Flax Fibres***

As for other plant fibres, including kenaf, the reported tensile properties for flax fibres vary widely, Table 2.13. As noted in Section 2.2.1.1, this is due to differences within the species, differences in the growth conditions, differences in age, differences in separation technique, etc. The gauge length used for testing can also have a substantial effect on the measured tensile strength and strain to failure (Romhány, Karger-Kocsis & Czigány, 2003).

**Table 2.13:** Tensile properties of flax fibres (Ashby, 2013; Cheung, Ho, Lau, Cardona & Hui, 2009; Saheb & Jog, 1999; Wanjale & Jog, 2011)

<b>Tensile Property</b>	<b>Reference</b>			
	Ashby (2013)	Cheung et al. (2009)	Saheb & Jog (1999)	Wanjale & Jog (2011)
Young's modulus (GPa)	75-90	24-80	27	27.6
Tensile strength (MPa)	750-940	300-1,500	344	45-1,100
Yield strength (MPa)	150-338	-	-	-
Elongation (%)	1.2-1.8	1.3-10%	-	-

Ashby (2013) reported a Young's modulus of 75-90 GPa, a tensile strength of 750-940 MPa, a yield strength of 150-338 MPa and strain to failure of 1.2-1.8% for flax

fibres. Wanjale & Jog (2011) reported that the Young's modulus and tensile strength were 27.6 GPa and 45-1,100 MPa, respectively, while Saheb & Jog (1999) reported that the tensile modulus and strength were 27 GPa and 344 MPa, respectively. Cheung, Ho, Lau, Cardona & Hui (2009) reported a Young's modulus of 24-80 GPa, a tensile strength of 300-1,500 MPa and an elongation at break of 1.3-10%.

Thermal properties of flax fibres are given in Table 2.14. In terms of electrical properties, flax fibres are good insulators (Ashby, 2013). Rowell (2008) has reported that the equilibrium moisture content (EMC) of flax fibres is 7% at 21°C and 65% relative humidity (RH). Dittenber & GangaRao (2012) reported moisture contents of 8-12 wt%.

**Table 2.14:** Thermal properties of flax fibres (Ashby, 2013)

<b>Thermal property</b>	
Glass temperature (°C)	110-130
Thermal conductor or insulator?	Poor insulator
Thermal conductivity (W/m·°C)	0.25-0.3
Specific heat capacity (J/kg·°C)	1,220-1,420
Thermal expansion coefficient (μstrain/°C)	15-30

Baley, Le Duigou, Bourmaud & Davies (2012) examined the effect of drying on the tensile properties of flax fibres, with average fibre diameters of 21.6 μm and 23.9 μm. The undried flax fibres had Young's moduli of 64.1 and 51.3 GPa, tensile strengths of 1,499 and 1,317 MPa and failure strains of 2.9 and 3.3%, for the 21.6 μm and 23.9 μm diameter fibres, respectively. After drying at 105°C for 14 h the average fibre diameters decreased only marginally to 20.9 μm and 23.8 μm. However, the strength and failure strain decreased substantially with values of 870 and 711 MPa being obtained for the strength and 2.1 and 1.7% for the failure strain, for the two fibre diameters, respectively. The modulus appeared unaffected by drying with values of 59.2 and 58.7 GPa being recorded.

## 2.3 Interface Modification of Natural Fibres

Several different methods are used for surface modification of natural fibres for use in composites. The major methods are chemical treatment, physical treatment,



thermal treatment, and the use of coupling agents. These methods are discussed below with particular reference to kenaf fibres since surface treatment was used in the present study for these fibres only.

## **2.3.1 Treatments of Natural Fibre Surfaces**

### **2.3.1.1 Chemical Treatments**

Chemical treatment of kenaf fibres can modify the fibre surface, retarding moisture absorption and increasing surface roughness. The chemical treatments also improve fibre-matrix adhesion and fibre strength (Li, Tabil & Panigrahi, 2007). Several different chemical treatments are used.

#### *(2.3.1.1.1) Alkaline Treatment*

An effective and inexpensive chemical treatment (Edeerozey et al., 2007) is alkaline treatment (also known as mercerization) using alkalis such as sodium hydroxide (NaOH), potassium hydroxide (KOH) or lithium hydroxide (LiOH) (Wanjale & Jog, 2011). Alkaline treatment enhances fibre surface roughness, removes wax and oils, but also increases the amount of amorphous cellulose (Li et al., 2007; Zimniewska et al., 2011). The chemical reaction between natural fibres and aqueous sodium hydroxide (Agrawal, Saxena, Sharma, Thomas & Sreekala, 2000, cited in Li et al., 2007) is given as follows:



Edeerozey et al. (2007) examined the alkaline treatment of kenaf fibres using concentrations of 3, 6 and 9% NaOH at room temperature and at a temperature of 95°C. They found that a concentration of at least 6% NaOH was required to effectively remove impurities from the fibre surfaces at both of the temperatures, although the 3% NaOH treatment improved the tensile strength of the fibres. The highest strength was obtained at 6%, with the strength being reduced substantially below the untreated fibre value when the 9% NaOH treatment was used. Other workers have also reported that high concentrations of alkali, such as 10% NaOH, have negative effects on the fibres (Mishra et al., 2000, cited in Li et al., 2007). Based on their study, Edeerozey et al. (2007) concluded that 6% NaOH was the optimum concentration for treating kenaf

fibres, since it cleaned the fibre surface and also improved strength. Aziz & Ansell, (2004) also reported that 6% NaOH does not produce cell wall damage in kenaf fibres.

In their study, Aziz & Ansell (2004) determined the bulk density of untreated and 6% alkali treated kenaf fibres. It was found that the bulk density of the untreated and treated fibres was 1,192.6 kg/m<sup>3</sup> and 1,221.7 kg/m<sup>3</sup>, respectively. They attributed the higher bulk density of the treated fibres to a lower level of porosity in the fibres.

*Figure 2.16 has been removed due to Copyright restrictions.*

**Figure 2.16:** FTIR spectra of alkali treated and untreated kenaf fibres (Han et al., 2007).

Han et al. (2007) carried out FTIR spectroscopy of untreated and alkali treated kenaf fibres. The alkali treatments were carried out at ambient temperature using 2, 5 and 10 wt% NaOH. The spectra for the different treatments are shown in Figure 2.16. The absorption peaks at 3,200-3,400 cm<sup>-1</sup> and 2,900-2,950 cm<sup>-1</sup> represent the typical –OH stretching and the typical aliphatic (CH<sub>2</sub> and CH) stretching, respectively. The absorption peaks at 1,735 cm<sup>-1</sup>, 1,595 cm<sup>-1</sup>, 1,373 cm<sup>-1</sup> and 1,245 cm<sup>-1</sup> also represent carbonyl group stretching, free carbonyl bond, O-H groups in plane bending and C-H, respectively. Additionally, the absorption peaks at 1,000-1,500 cm<sup>-1</sup> represent the aromatic region. It was found that there were reductions in the intensity of the O-H stretching absorption peaks at 3,200-3,400 cm<sup>-1</sup> and the O-H in-plane bending at 1,373 cm<sup>-1</sup> with increasing NaOH concentration due to the formation of glycosidic bonds. The intensity of the carbonyl group stretching absorption peak at 1,736 cm<sup>-1</sup> was also decreased due to the removal of hemicellulose. Han et al. (2007) found that the 5 wt%

NaOH treatment gave the best mechanical performance when the kenaf fibres were incorporated into thermoplastic matrix composites

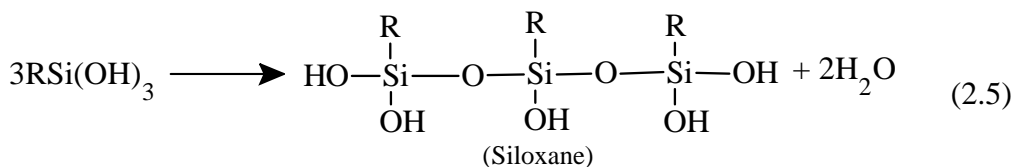
#### (2.3.1.1.2) Silane Treatment

Silane coupling agents are chemical compounds containing  $\text{SiH}_4$ . They modify the interface between natural fibres and the polymer matrix, increasing the interfacial strength. Silanes can also decrease the level of hydroxyl groups in cellulose in natural fibres. The silanes are converted to silanols by moisture and hydrolysable alkoxy groups. The silanols can then react with the hydroxyl groups of the fibres (Li et al., 2007). Factors including silane type, concentration of silane, temperature, time of silanization, quantity of moisture and fibre volume fraction all affect the extent to which the treatment improves fibre-matrix adhesion in composites (Abdalla & Pickering, 2002; Abdalla et al., 2002; Bledzki & Gassan, 1997, cited in Zimniewska et al., 2011). The chemical reaction steps (Karnani, Krishnan, & Narayan, 1997) are given as follows:

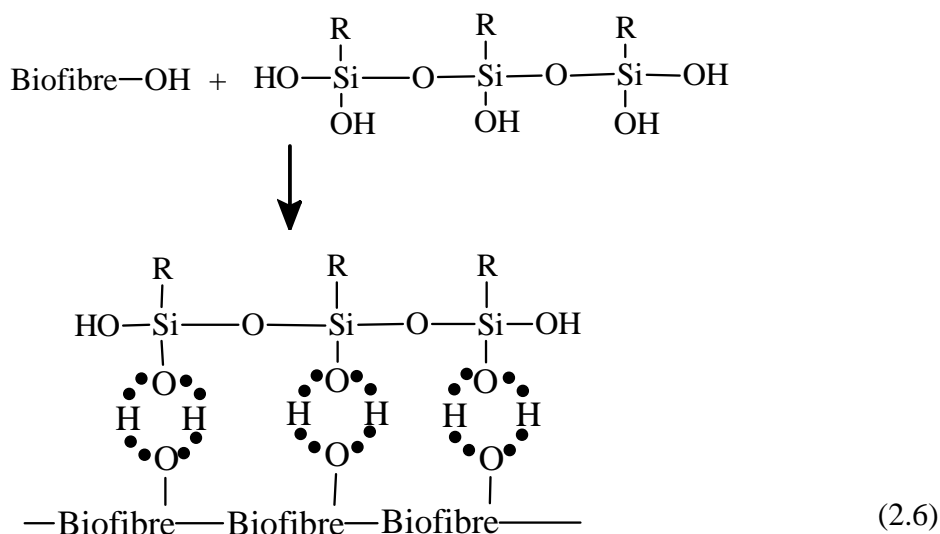
##### *Hydrolysis*



##### *Condensation*



##### *Hydrogen bonding*



### Surface grafting

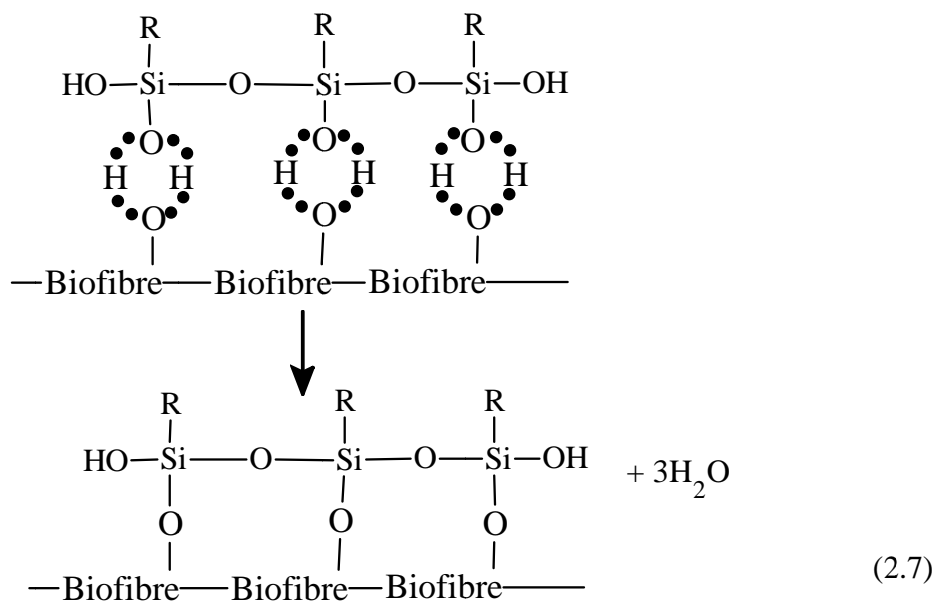


*Figure 2.17 has been removed due to Copyright restrictions.*

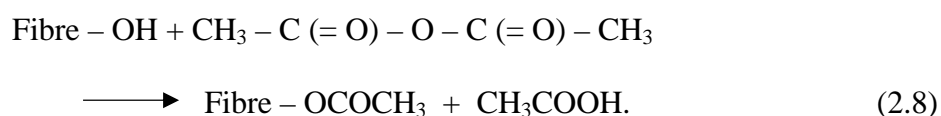
**Figure 2.17:** FTIR spectra of alkali and silane treated and untreated kenaf fibres (Sgriccia et al., 2008).

Alkaline pre-treatment is commonly used to increase the efficiency of the silane treatment (Wanjale & Jog, 2011). Sgriccia, Hawley, & Misra (2008) examined the effect of alkaline treatment (5% sodium hydroxide), silane treatment (1% 3-glycidoxypyltrimethoxysilane) and alkali treatment followed by silane treatment on kenaf fibres using FTIR, Figure 2.17. It was found that the carbonyl peak of the acetyl groups of hemicellulose at  $1,730 \text{ cm}^{-1}$  was not affected by silane treatment alone but was absent after alkaline treatment, both with and without subsequent silane treatment. This indicates that the alkali pretreatment removes hemicellulose from the fibres. The

intensity of the C – O stretching peak of the acetyl group of lignin at 1,239 cm<sup>-1</sup> was also reduced more by the alkaline treatment than by the silane treatment alone indicating that alkali pretreatment also partly removes lignin from the fibres.

#### *(2.3.1.1.3) Acetylation Treatment*

Acetylation treatment is an esterification method. It involves reacting the hydroxyl groups (OH-) of the fibres with acetyl groups (CH<sub>3</sub>CO-) (Zafeiropoulos, 2008). The acetylation generates acetic acid (CH<sub>3</sub>COOH) as a byproduct. The treatment improves the fibre-matrix adhesion and dimensional stability of natural fibre composites (Li et al., 2007). The chemical reaction between natural fibres and acetic anhydride (CH<sub>3</sub>-C(=O)-O-C(=O)-CH<sub>3</sub>) (Hill, Abdul Khalil & Hale 1998, cited in Li et al., 2007) is given as follows:



#### **2.3.1.2 Physical Treatments**

The physical treatments used to modify the fibres include stretching, calendaring, thermotreatment and electrical discharge (corona and cold plasma) treatments. These treatments can change the fibre structure and/or the fibre surface, thereby improving the fibre-matrix bonding (Bledzki & Gassan, 1999; Wanjale & Jog, 2011). For example, the surface of the fibres can be changed and free radicals, ions and electrons can be formed by using plasma treatment (Morales et al., 2006, cited in Lee et al., 2011). This leads to changes in the surface properties of the fibres, such as chemistry, wettability, and roughness of the surface, depending on the nature of the plasma feed gas. There are five types of plasma source, these being arc and torches, corona, dielectric barriers, low-pressure discharge and atmospheric pressure discharge (Lee et. al., 2011). The characteristics of the different plasma sources are shown in Table 2.15.

The fibre surface can also be modified by electron beam irradiation (EBI). This technique is dry, clean and environmentally friendly (Han et al., 2007). The process is reported to change the structure and properties of cellulose in the fibres (Takacs, Wojnarovits, Foldvary, Hargittai, Borsa & Sajo, 2000, cited in Han et al., 2007). However this is contrary to the findings of Han et al. (2007) who conducted an FTIR

study of untreated and EBI treated kenaf fibres. As shown in Figure 2.18, their results indicated that there was no significant difference in the spectra obtained from untreated fibres and from fibres given 100 kGy, 200 kGy and 500 kGy EBI treatments. However, they did find that EBI treatment improved the performance of thermoplastic composites, made with the kenaf fibres, with the 200 kGy dosage being the most effective. This may indicate that surface modification occurs only to a shallow depth which is beyond the resolution of FTIR.

**Table 2.15:** Comparison between different plasma sources (Lee et al., 2011)

Plasma Source	Glass Temperature (°C)	Electron Temperature (eV)	Applied Voltage (kV)	Charge Density (cm <sup>-3</sup> )
Arc and torches	7,000-65,000	2.5-6.8	10-50	10 <sup>16</sup> -10 <sup>19</sup>
Corona	50-400	4-6	10-50	10 <sup>9</sup> -10 <sup>13</sup>
Dielectric barriers	50-400	2-10	5-25	10 <sup>12</sup> -10 <sup>15</sup>
Low-pressure discharge	10-500	1-10	0.2-0.8	10 <sup>8</sup> -10 <sup>13</sup>
Atmospheric pressure discharge	25-200	1-2	0.05-0.2	10 <sup>11</sup> -10 <sup>12</sup>

*Figure 2.18 has been removed due to Copyright restrictions.*

**Figure 2.18:** FTIR spectra of EBI treated and untreated kenaf fibres (Han et al., 2007).

### **2.3.1.3 Thermal Treatment**

Thermal treatment is carried out at the glass transition temperature of lignin (Rinne, Boettger, Loader, Robertson, Switsur & Waterhouse, 2005), to remove lignin and some hemicellulose from the fibres (Sain & Panthapulakkal, 2004). The glass transition temperature of lignin in kenaf ranges from 66°C to 70°C (Lora & Glasser, 2002). The physical and chemical properties of cellulose also change when cellulose is heated. The physical properties affected include enthalpy, weight, strength, colour and crystallinity. The chemical properties affected include a decrease in degree of polymerization due to bond scission, free radical creation, formation of carbonyl, carboxyl and peroxide groups, and evolution of water and carbon dioxide (Shafizadeh, 1985, cited in Zafeiropoulos, 2008).

As a result of these changes thermal treatment can improve the compatibility between the fibres and the polymer matrix. The effectiveness is dependent on the atmosphere used with heating in an inert atmosphere being considered to give better results than heating under normal conditions (Sain & Panthapulakkal, 2004). As noted in Section 2.2.1.1, heating to temperatures above ~170°C can, however, reduce the mechanical properties of kenaf fibres due to chemical degradation.

### **2.3.2 Modification of the Fibre/Matrix Interface by Adding Coupling Agents to the Matrix Resin**

Fibre treatments using chemical and physical techniques are effective methods for improving fibre-matrix adhesion in composites. However, these techniques increase the cost of manufacturing the composites. An alternative inexpensive method for improving adhesion between the fibres and the matrix is the addition of a coupling agent to the matrix resin. As for coupling agents applied directly to the fibres, this technique enhances stress transfer from the polymer matrix to the fibres, improving the properties of the composite (Bledzki et al., 2008; Rowell, Sanadi, Caulfield, & Jacobson, 1997).

Grafted maleic anhydride is commonly used as the coupling agent in thermoplastic matrix composites. The addition of maleic anhydride grafted polypropylene (MAPP) has been shown by several workers to improve the mechanical properties of polypropylene composites (Clemons & Sanadi, 2007; Feng et al., 2001; Ganster, Fink, & Pinnow, 2006). Yang, Wolcott, Kim, Kim & Kim (2007) have also

demonstrated that the form in which the maleic anhydride is used is important, with maleated polyethylene (MAPE) addition being less effective than MAPP addition in polypropylene composites.

The reaction mechanism between the coupling agent and natural fibres is shown in Figure 2.19 (Karnani et al., 1997). The improvement in properties brought about by addition of the coupling agent is attributed to the formation of ester linkages between the maleic anhydride of the MAPP and hydroxyl groups of the cellulose fibres (Ganster et al., 2006).

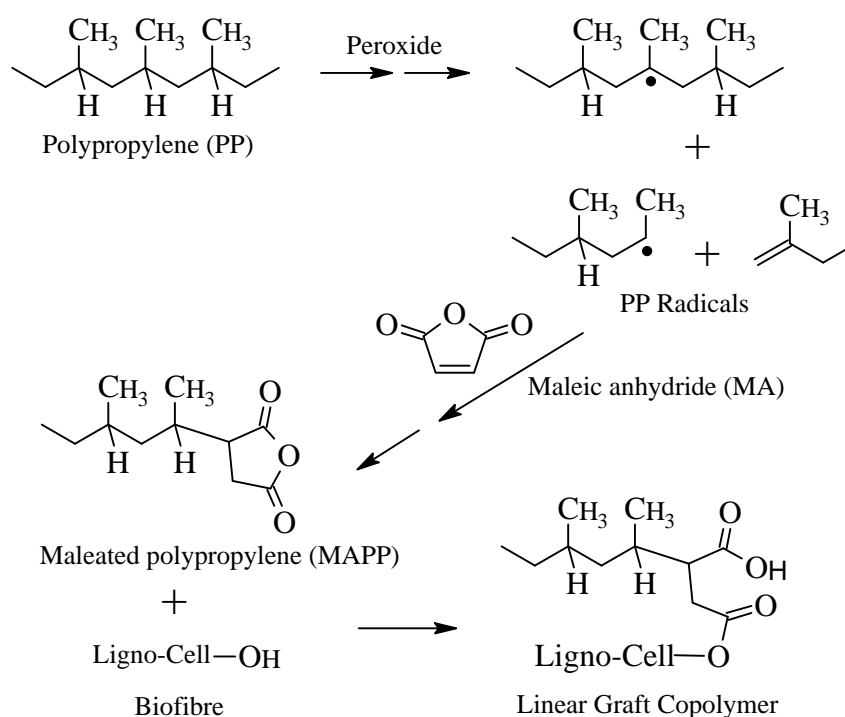


**Figure 2.19:** Reaction mechanism between maleated polypropylene (MAPP) and lignocellulosic fibres (Karnani et al., 1997).

## 2.4 Natural Fibre-Reinforced Polymer-Matrix Composites

Natural fibres have become attractive materials for reinforcing polymers because of their low cost and good environmental credentials. The present study examines both short kenaf fibre reinforced thermoplastic composites and long flax fibre reinforced thermoset matrix composites. Accordingly, this section is divided into two parts, natural fibre-reinforced thermoplastic-matrix composites and natural fibre-reinforced thermoset-matrix composites. The first part is focused on kenaf fibre-reinforced



polyolefin-matrix composites, whereas the second part is focused on unidirectional natural fibre-reinforced thermoset-matrix composites.

## 2.4.1 Natural Fibre-Reinforced Thermoplastic-Matrix Composites

### 2.4.1.1 Thermoplastics

Thermoplastics are commonly used as the matrix in polymer composites. They do not contain crosslinks between the polymer chains and this allows them to be melted and infuse the fibres when used in fibre reinforced composites. Some thermoplastics are completely amorphous but others are semi-crystalline containing both amorphous and crystalline regions. The arrangement of the molecules in amorphous and semi-crystalline polymers is shown in Figure 2.20. The molecular arrangement in the amorphous regions is random whilst that in the crystalline regions is ordered (Mazumdar, 2002).

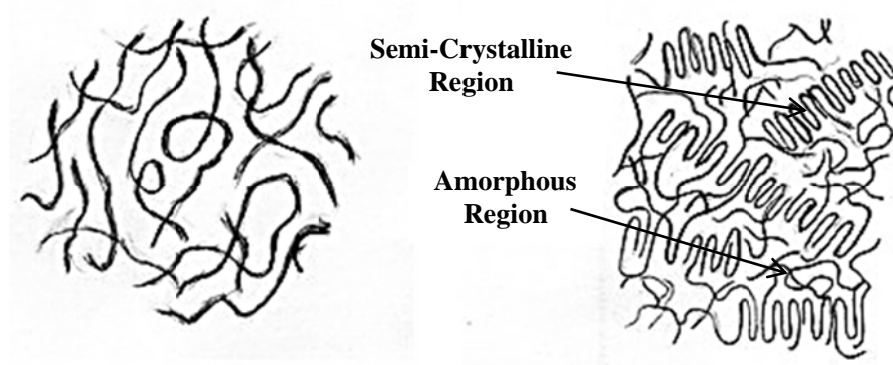


**Figure 2.20:** Structures of molecules in amorphous (left) and semi-crystalline (right) polymers (Campbell, 2004).

Polyethylene (PE), polypropylene (PP), polystyrene (PS) and polyamides (nylon 6 and 6,6), which are all synthetic thermoplastics, are most commonly used for natural fibre thermoplastic composites (Sain & Panthapulakkal, 2004). The physical, mechanical and thermal properties of these thermoplastics are shown in Table 2.16. PE is the cheapest thermoplastic and requires the lowest processing temperatures. It also has excellent impact strength and toughness (Saxena, Pappu, Haque & Sharma, 2011). However, PP is the most commonly used polymer for thermoplastic matrix composites because of its good combination of properties, which include low density, excellent processability, good mechanical properties, high temperature resistance, excellent

electrical properties, good dimensional stability and good impact strength (Sain & Panthapulakkal, 2004).

**Table 2.16:** Properties of synthesis thermoplastics (Schwartz & Goodman, 1982 and Van de Velde & Kiekens, 2001, cited in Sain & Panthapulakkal, 2004)

Property	PP	HDPE	LDPE	PS	Nylon 6	Nylon 6,6
Density (g/cm <sup>3</sup> )	0.899-0.920	0.941-1	0.910-0.925	1.04-1.09	1.09-1.14	1.090-1.19
Water absorption after 24 hours (%)	0.01-0.02	0.01-0.2	<0.015	0.03-0.10	1.3-1.8	1.0-1.6
T <sub>g</sub> (°C)	-10 to -23	-133 to -100	-125	-	48	80
T <sub>m</sub> (°C)	160-176	120-140	105-116	110-135	215-216	250-269
Heat deflection temp. (T <sub>d</sub> ) at 1.8 MPa (°C)	50-63	43-60	32-50	Max. 220	56-80	75-90
Coefficient of linear thermal expansion ( $\alpha_T$ ) (mm/mm/°C × 10 <sup>5</sup> )	6.8-13.5	12-13.0	10	6-8	8-8.6	7.2-9.0
Tensile strength (MPa)	26-41.4	14.5-38	4-78.6	-	43-79	12.4-94
Young's modulus (GPa)	0.95-1.776	0.413-1.490	0.055-0.38	4-5	2.9	2.5-3.9
Elongation (%)	15-700	12-1000	90-800	1-2.5	20-150	35 to >300
Izod impact strength (J/m)	21.4-267	26.7-1068	>845	0.05-0.55 <sup>1</sup>	42.7-160	16.0-654

<sup>1</sup>Units ft lb/inch.

#### 2.4.1.2 Processing Methods

Common processing methods used in fabricating natural fibre-reinforced thermoplastic composites include extrusion, injection moulding and compression

moulding. Extrusion (Figure 2.21a) is a process which produces a continuous extruded product called an extrudate. The shape of the product depends on the die shape. Materials are fed into a hopper and then mixed by a screw and melted in the barrel of the extruder. The screw then forces the melted materials through a die (Ashby & Jones, 2006). Extrusion can be carried out using a single-screw extruder or a twin-screw extruder. Single-screw extruders are suitable for mixtures that do not require very high mixing effects whilst twin-screw extruders, running either co- or counter-rotating, are better for compounding. Twin-screw extruders are most appropriate for compounding natural fibres with thermoplastics as this ensures even distribution of the fibres in the extrudates. Extruders which have higher L/D (barrel length/barrel diameter) ratios are more effective at removing moisture from the fibres due to the longer degassing sectors (Bledzki et al., 2008). Advantages of extrusion are high speed and low cost (Ashby & Jones, 2006).

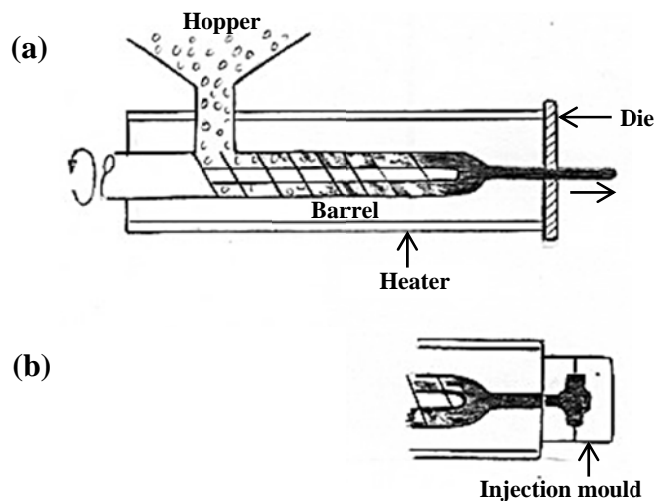


**Figure 2.21:** (a) Extrusion and (b) injection moulding (Ashby & Jones, 2006).

Injection moulding (Figure 2.21b) involves injecting a melted material into a mould under pressure. Injection moulding machines can produce complex geometric products in short periods of time (Bledzki et al., 2008) with typical cycle times of 1 to 5 minutes. The properties of injection moulded materials are anisotropic (Ashby & Jones, 2006).

In compression moulding, materials are pressed into a mould under heat and pressure. The cycle time is short (approximately 10 seconds) for small thin moulds, but long (approximately 10 minutes) for large thick moulds. The capital cost of the

equipment for compression moulding is less than that for injection moulding, due to lower pressure requirements (Ashby & Jones, 2006). Compression moulding is appropriate when producing simple and flat products. However, compression moulding machines cannot produce complex geometric products (Bledzki et al., 2008).

There are three major concerns when compounding natural fibres and thermoplastics for fabricating natural fibre/thermoplastic composites. Firstly, it is difficult to feed the compounder because the bulk density of the fibres and the thermoplastic is different. Secondly, dispersion of the fibres in the thermoplastic matrix is difficult because of intramolecular and intermolecular bonding in the fibres. This can bring about fibre agglomeration leading to inefficient reinforcement of the composites. Thirdly, the degree of shear produced during compounding is important since this can lead to fibre attrition (reduction in the fibre length) (English, Chow & Bajwa, 1996, cited in Sain & Panthapulakkal, 2004).

The level of fibre attrition depends on the type of compounding and moulding. In addition to the shearing forces generated in the equipment, other important factors affecting the level of attrition are loading contents, residence time, temperature and blend viscosity (Czarnecki & White, 1980, cited in Rowell et al., 1997). The level of the fibre attrition is also dependent on the screw configuration in the extruder. Modified screw configurations can be used to decrease fibre attrition (Yam, Gogoi, Lai & Selke, 1990, cited in Rowell et al., 1997).

In addition to affecting fibre length, processing can also affect fibre dispersion and/or fibre orientation, all of which have significant effects on the mechanical properties of polymer composites. Injection moulding can enhance fibre dispersion in the polymer composites, bringing about improvements in the mechanical properties of the composites (Mohanty, Wibowo, Misra & Drzal, 2004, cited in Liu et al., 2007). However, injection moulding causes fibre damage which leads to a decrease in fibre length and diameter (Carneiro & Maia, cited in Liu et al., 2007). Although injection moulding has an adverse effect on the fibres, it can produce better consolidation of the polymer composites than is achievable with compression moulding. This is attributed to the closed mould, which allows higher transmission of pressure into the composites during processing (Mohanty et al., 2004, cited in Liu et al., 2007). Although polymer composites fabricated using compression moulding in a frame mould do not receive as high transmitted pressure as composites fabricated using injection moulding in a closed

mould, compression moulding does not cause fibre damage and changes in fibre orientation (Liu et al., 2007). Liu et al. (2007) reported that, as a result of the lower level of fibre damage, compression moulded composites had higher impact strength than injection moulded composites.

#### ***2.4.1.3 Properties of Kenaf Fibre-Reinforced Polyolefin-Matrix Composites***

The major factors affecting the properties of short fibre composites, particularly the mechanical properties, are fibre content (usually expressed as fibre volume fraction), fibre aspect ratio (the ratio of fibre length to fibre diameter) (Vázquez & Alvarez, 2009), dispersion and orientation of the fibres, fibre length distribution, fibre-matrix adhesion, stress transfer from the matrix to the fibres (Milewski, 1992, cited in Rowell et al., 1997), and processing conditions (Vázquez & Alvarez, 2009). Figure 2.22 gives a schematic diagram showing the effects of shear stress during mixing and fibre-matrix compatibility on the dispersion and distribution of natural fibres in the resulting composite. When a high shear stress is produced during mixing and fibre agglomerations are avoided, good fibre dispersion and distribution will be obtained (Vázquez & Alvarez, 2009).

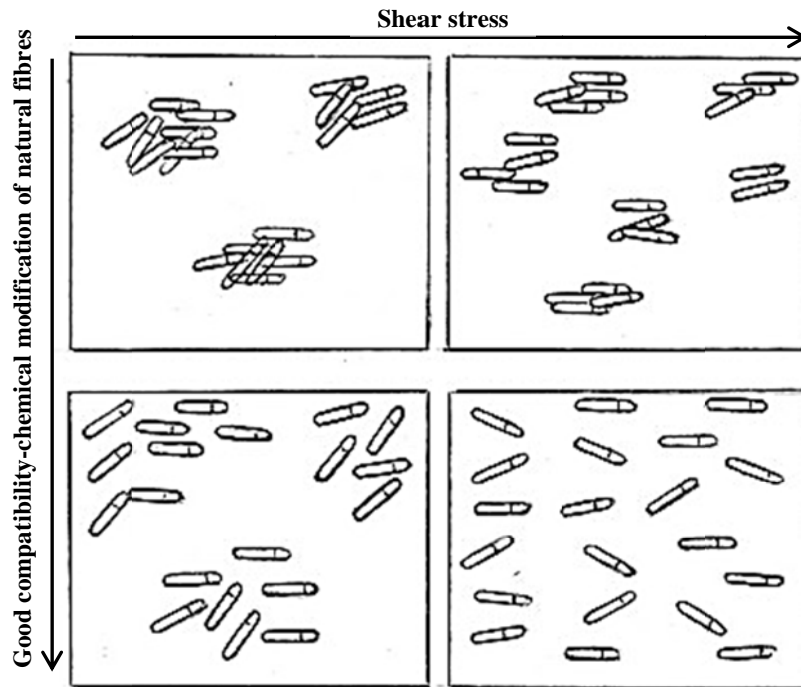


**Figure 2.22:** Schematic diagram of natural fibre dispersion and distribution during mixing (Vázquez & Alvarez, 2009).

The properties of polymer composites depend not only on the fibre properties, but also on the properties of the polymer matrix. The following discussion focuses on short kenaf fibre thermoplastic composites.

#### *(2.4.1.3.1) Mechanical Properties*

The mechanical properties of natural fibre composites depend on fibre type, fibre content, fibre length and fibre geometry. Most of the mechanical properties of composites can be improved by increasing the aspect ratio of the fibres (Liu, Drzal, Mohanty & Misra, 2007, cited in Bledzki et al., 2008).

*Figure 2.23 has been removed due to Copyright restrictions.*

**Figure 2.23:** Typical stress-strain curves for pure polypropylene (PP), 50 wt% kenaf fibre/PP composites without MAPP coupling agent (u) as well as 20-60 wt% kenaf fibre/PP composites with MAPP coupling agent (c) (Rowell et al., 1999).

Rowell et al. (1999) examined the mechanical properties of kenaf fiber/polypropylene composites with and without the addition of 2 wt% MAPP coupling agent. The stress-strain curves obtained for composites containing 20-60 wt% kenaf, together with the curve for pure polypropylene, are shown in Figure 2.23. It was found

that the failure strain of the composites was significantly less than that of the neat polypropylene and this was attributed to obstruction of the mobility of the polymer molecules by the presence of the fibres. For the composites with the MAPP addition, the strength increased progressively with fibre content while the failure strain decreased. Only one fibre content (50 wt%) was examined without MAPP addition and this composite achieved only half the strength of its MAPP treated counterpart. The superior performance of the MAPP treated composite was attributed to the formation of covalent bonds between the anhydride groups in the MAPP and the hydroxyl groups in the fibre surface. Feng et al. (2001) also reported that the tensile strength of 50 wt% short fibre kenaf/polypropylene composites was improved by the addition of 3 wt% maleated polypropylene (MAPP).

The MAPP treated 50 wt% kenaf fibre/polypropylene composites examined by Rowell et al. (1999) had a tensile modulus of 8.3 GPa, a tensile strength of 65 MPa, a flexural modulus of 7.3 GPa, a flexural strength of 98 MPa, an elongation at break of 2.2% and a notched Izod impact strength of 32 J/m (Rowell et al., 1999). It is noted that the impact strength of composites is dependent on the type of impact test used. For notched impact testing, energy absorption occurs from the crack propagation mechanism, but for un-notched impact testing, energy absorption occurs from both crack initiation and crack propagation. High stress concentration regions, such as at fibre defects and fibre ends, can readily act as crack initiation sites (Sanadi et al., 1995).

**Table 2.17:** Details of the pure HDPE and the 50% kenaf fibre/HDPE composites (Lundin et al., 2004)

Material	Sample	
	HDPE	50% Kenaf/HDPE
HDPE	100.0%	48.6%
UV stabilizer	-	0.4%
Antioxidant	-	0.2%
Kenaf fibres	-	48.6%
MAPE	-	2.1%

Lundin, Cramer, Falk & Felton (2004) examined the flexural properties of pure high-density polyethylene (HDPE) and 50% kenaf fibre/HDPE composites. The

materials, used are given in Table 2.17 while their flexural properties are given in Table 2.18. The flexural modulus of the 50% kenaf fibre/HDPE composites was approximately ten times higher than for the pure HDPE while the strength was approximately three and a half times higher.

**Table 2.18:** Flexural properties of the pure HDPE and the 50% kenaf fibre/HDPE composites (Lundin et al., 2004)

Sample	Flexural Property	
	Flexural Modulus (MPa)	Flexural Strength (MPa)
HDPE	668	14.0
50% Kenaf/HDPE	5,950	48.2

#### (2.4.1.3.2) Thermal Properties

Feng et al. (2001) examined the thermal properties of untreated and 3 wt% MAPP treated 50 wt% kenaf fibre/polypropylene composites using differential scanning calorimetry (DSC). The specimens were initially heated from 25°C to 230°C at a rate of 20°C/minute in order to remove previous thermal history. After that, the specimens were cooled to -100°C at a rate of 10°C/minute in order to determine the crystallisation temperature ( $T_c$ ). The specimens were then reheated from -100°C to 230°C at a rate of 20°C/minute to determine the melting temperature ( $T_m$ ) and heat of fusion. The  $T_c$  and  $T_m$  were found to be slightly decreased (from 120.7°C to 120.0°C and 167.3°C to 166.5°C) respectively in the MAPP treated composites. The crystallisation and melting behaviour of the MAPP treated composites depend on two important factors, these being the interactions between the anhydride groups of the MAPP and the hydroxyl groups of the fibres, and the interactions of the anhydride groups with themselves (Jarvela, Li & Jarvela, 1996, cited in Feng et al., 2001). When good interaction between the fibre surfaces and the MAPP exist, the mobility of molecules is limited and this depresses  $T_m$ . Likewise interactions of anhydride groups between themselves obstructs crystallisation and this depresses  $T_c$  (Feng et al., 2001).

The thermal stability of a 30 wt% kenaf fibre/polypropylene composite has also been examined using thermogravimetric analysis (TGA) (Han et al., 2007). The study was conducted over the temperature range of 30-500°C under a nitrogen atmosphere



with a heating rate of 5°C/min. The decomposition temperature of the composite was found to be approximately 455°C.

#### *(2.4.1.3.3) Dynamic Mechanical Properties*

Dynamic mechanical analysis (DMA) is a common technique for analysing dynamic mechanical properties of natural fibre/polyolefin composites. The dynamic mechanical properties are dependent on the type, length, content, orientation and dispersion of the fibres, the fibre loading, and the adhesion between the fibres and the matrix since these properties all affect the mechanical properties of the end products (Tajvidi, Falk & Hermanson, 2006; Tajvidi, Falk, Hermanson & Felton, 2003).

DMA studies of kenaf fibre/polypropylene composites have been conducted by Feng et al. (2001) and Tajvidi, Falk et al. (2006), in both cases at a heating rate of 2°C/minute and a test frequency of 1 Hz. Feng et al. (2001) conducted their study over the temperature range -100°C to 180°C. They found that addition of 3 wt% MAPP increased the softening temperature of the composites which they attributed to improved fibre-matrix adhesion (Feng et al., 2001)

Tajvidi, Falk et al. (2006) examined 25 wt% and 50 wt% kenaf fibre/polypropylene composites with additions of 1 wt% and 2 wt% MAPP. Their study was carried out over the temperature range -60°C to 120°C. The storage modulus ( $E'$ ), loss modulus ( $E''$ ) and  $\tan \delta$  values obtained from this work are given in Table 2.19. The results showed that increasing the fibre content increased the stiffness (storage modulus and loss modulus). There was no effect of fibre content on the mechanical loss factor,  $\tan \delta$ , (damping) at temperatures below 20°C but the 50 wt% composite had a lower  $\tan \delta$  at temperatures above 20°C.

Tajvidi et al. (2003) also examined the dynamic mechanical properties of kenaf/HDPE composites. They again used 25 and 50 wt% fibre, but used maleated polyethylene, again at 1 wt % and 2 wt%, as the coupling agent. The study was carried out over the temperature range -110°C to 100°C at a heating rate of 2°C/minute, a frequency of oscillation of 1 Hz, and a strain amplitude of 0.1%. It was found that the storage modulus and loss modulus were higher for the kenaf fibre/HDPE composites than for the pure HDPE. As for the kenaf/PP composites, the 50 wt% kenaf/PE composite had a higher storage modulus and loss modulus than its 25 wt% counterpart. Also, the  $\tan \delta$  values the two PE composites were similar at temperatures below 20°C while the 50 wt% composite had a lower  $\tan \delta$  at temperatures above 20°C. The  $\tan \delta$  of

pure HDPE was the same as that of the kenaf fibre/HDPE composites at temperatures below 20°C, but higher than that of the kenaf fibre/HDPE composites at temperatures above 20°C.

**Table 2.19:** Storage modulus ( $E'$ ), loss modulus ( $E''$ ) and  $\tan \delta$  values of the kenaf fibre/ polypropylene composites (Tajvidi, Falk et al., 2006)

Temperature (°C)	Composite formulation	$E'$ (GPa)	$E''$ (GPa)	$\tan \delta$
-60	25 KF-PP	5.530	0.164	0.030
	50 KF-PP	7.349	0.219	0.030
-20	25 KF-PP	5.118	0.156	0.030
	50 KF-PP	6.701	0.198	0.030
+20	25 KF-PP	3.126	0.189	0.060
	50 KF-PP	4.733	0.225	0.048
+60	25 KF-PP	1.835	0.117	0.064
	50 KF-PP	3.132	0.182	0.058
+100	25 KF-PP	1.047	0.096	0.092
	50 KF-PP	2.001	0.166	0.083

#### (2.4.1.3.4) Moisture Absorption

It is important to evaluate the moisture absorption of natural fibre composites since it has a substantial effect on their service performance. Moisture absorption leads to fibre swelling and this affects the dimensional stability of the composites (Tajvidi, Najafi & Moteei, 2006). Moisture absorption also brings about an increase in heat conductivity and fungal sensitivity (Bledzki et al., 2008). Moisture absorption is dependent principally on the chemical structure of both the fibres and the polymer matrix, the presence or absence of coupling agents, and the service temperature and relative humidity (George, Bhagawan & Thomas, 1997). Moisture absorption can be reduced by improving bonding between the fibres and the matrix (Rowell et al., 1997).

The water absorption of 25 wt% and 50 wt% natural fibre/polypropylene composites with 1 wt% and 2 wt% maleic anhydride polypropylene (MAPP) was studied by Tajvidi, Najafi et al. (2006). The natural fibres used included kenaf fibres, wood flour, rice hulls and newsprint fibres. It was found that water absorption by the

kenaf fibres was higher than that for the other natural fibres due to higher cellulose and hemicellulose contents and a lower lignin content. The maximum water absorption over 5 weeks for the 25 wt% and 50 wt% composites was 2.1% and 13.2%, respectively, indicating that the rate of moisture absorption was strongly dependent on fibre content. It is noted that the moisture absorption had not reached the equilibrium level in either of the composites during the 5-week water immersion period.

Rowell et al. (1999) reported a moisture absorption level of 1.1% after 24 hours immersion for a 50 wt% kenaf/PP composite with MAPP coupling agent.

## 2.4.2 Natural Fibre-Reinforced Thermoset-Matrix Composites

### 2.4.2.1 Thermosets

Synthetic thermosets commonly used as matrices in natural fibre composites are polyester, epoxy and vinyl ester resins (Ray & Rout, 2005). The chemical structure of polyester, epoxy and vinyl ester resins is shown in Figures 2.24 to 2.26, respectively. Unlike thermoplastics, thermoset resins crosslink during curing (Campbell, 2010a). The stages of cure of a thermoset resin are shown in Figure 2.27. As a result of crosslinking, thermoset plastics are unable to be reshaped by heating (Aranguren & Reboredo, 2007). Physical and mechanical properties of polyester, epoxy and vinyl ester resins are given in Table 2.20. Advantages and disadvantages of these thermosets are shown in Table 2.21.

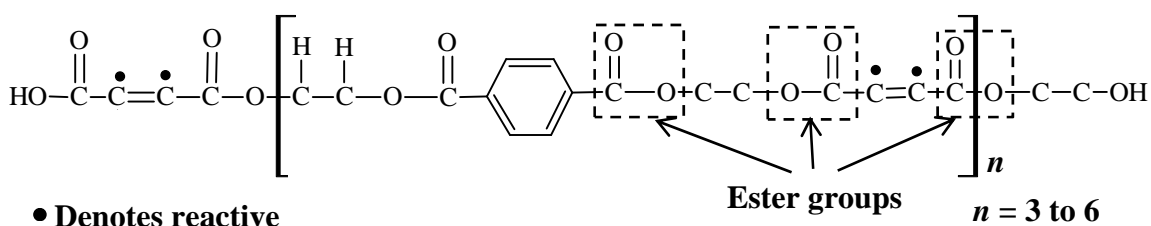


**Figure 2.24:** Chemical structure of a typical polyester resin (Ray & Rout, 2005).

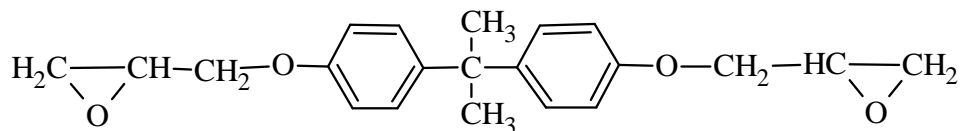
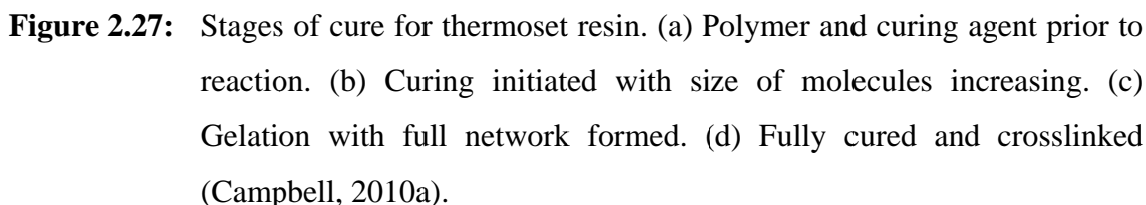
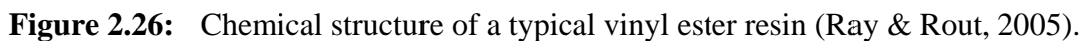


**Figure 2.25:** Chemical structure of a typical epoxy resin (Ray & Rout, 2005).



Property	Polyester	Epoxy	Vinyl Ester
Density (g/cm <sup>3</sup> )	1.2-1.5	1.1-1.4	1.2-1.4
Young's modulus (GPa)	2-4.5	3-6	3.1-3.8
Tensile strength (MPa)	40-90	35-100	69-83
Compressive strength (MPa)	90-250	100-200	-
Elongation at break (%)	2	1-6	4-7
Cure shrinkage (%)	4-8	1-2	-
Water absorption at 20°C for 24 h	0.1-0.3	0.1-0.4	-
Fracture energy (kJ/m <sup>2</sup> )	-	-	2.5

**Table 2.21:** Advantages and disadvantages of polyester, epoxy and vinyl ester resins (Kroschwitz, 1985, Pritchard, 1980, Sarkar et al., 1997, cited in Ray & Rout, 2005)

<b>Thermoset</b>	<b>Advantage</b>	<b>Disadvantage</b>
Polyester	<ul style="list-style-type: none"> <li>- easy to use</li> <li>- lowest cost of resins available (£1-2/kg)</li> </ul>	<ul style="list-style-type: none"> <li>- only moderate mechanical properties</li> <li>- high styrene emissions in open moulds</li> <li>- high cure shrinkage</li> <li>- limited range of working times</li> </ul>
Epoxy	<ul style="list-style-type: none"> <li>- high mechanical and thermal properties</li> <li>- high water resistance</li> <li>- long working time available</li> <li>- temperature resistance can be up to 140°C wet/220°C dry</li> <li>- low cure shrinkage</li> </ul>	<ul style="list-style-type: none"> <li>- more expensive than vinyl esters (£3-5/kg)</li> <li>- critical mixing</li> <li>- corrosive handling</li> </ul>
Vinyl ester	<ul style="list-style-type: none"> <li>- very high chemical/environmental resistance</li> <li>- higher mechanical properties than polyesters</li> </ul>	<ul style="list-style-type: none"> <li>- postcure generally required for high properties</li> <li>- high styrene content</li> <li>- higher cost than polyesters (£2-4/kg)</li> <li>- high cure shrinkage</li> </ul>

#### **2.4.2.2 Fabrication Techniques**

Fabrication techniques commonly used for manufacturing natural fibre-reinforced thermoset-matrix composites are hand lay-up, compression moulding, resin infusion, filament winding and pultrusion (Ray & Rout, 2005).

The hand lay-up technique involves laying fibres over a mould surface coated with a release agent. The thermoset resin is then applied to the mould (Higgins, 1994). Rollers or brushes are used to compact the material to remove air bubbles and extra resin. Composites of only low fibre volume fraction can be manufactured using this technique (Ray & Rout, 2005).

The compression moulding technique consists of sheet moulding, bulk moulding, cold pressing and hot pressing. The technique is similar to the hand lay-up technique, except that it uses a set of matched dies to which pressure is applied. As a result of the applied pressure, composites with substantially higher fibre loadings can be produced (Ray & Rout, 2005).

A widely used process for manufacturing natural fibre composites is resin infusion. In this process resin is infused into a mat or fabric preform under the application of pressure and/or vacuum. Two different types of process are used. The first, known as resin transfer moulding (RTM), utilises a two-piece closed mould into which the fibre preform is placed and the resin then infused. Figure 2.28 shows a flow diagram of the RTM technique.

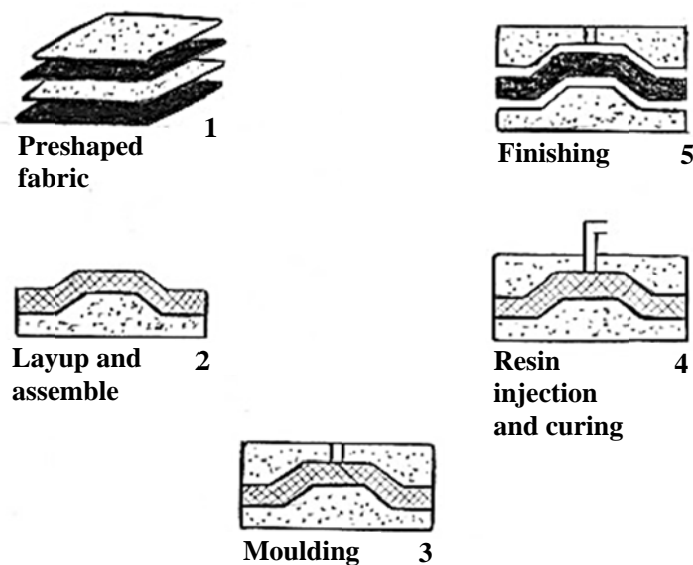


**Figure 2.28:** Flow diagram of resin transfer moulding (Karak, 2012).

A simpler resin infusion process is vacuum bag resin infusion. This uses a single mould into which the fibre preform is placed. A plastic film is then placed over the preform, sealed around the edges to form a vacuum bag, and vacuum then applied to the mould cavity, i.e., the space between the vacuum bag and the mould. The vacuum acts to draw resin into the mould cavity, thereby infusing the preform. These closed mould processes have the advantage over open mould processes, such as the hand lay-up technique, of producing more consistent parts and avoiding emission of volatiles from the resin into the atmosphere.

The filament winding technique involves impregnating continuous fibres in a resin bath, and winding the fibres onto a rotating mandrel (Ray & Rout, 2005) as shown in Figure 2.29.

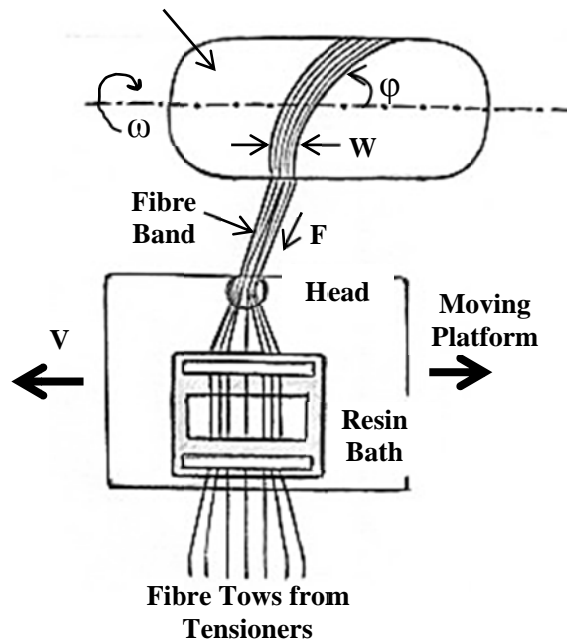


**Figure 2.29:** Filament winding technique (Campbell, 2010b).

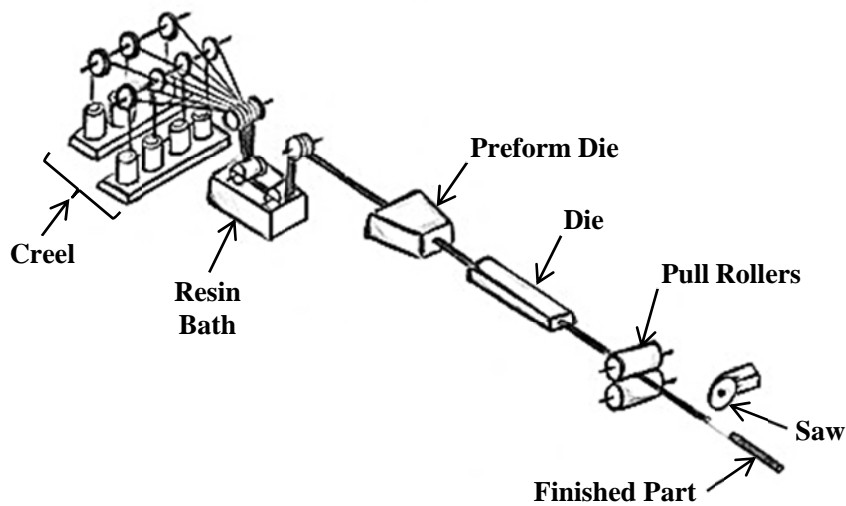


**Figure 2.30:** Pultrusion technique (Campbell, 2010b).

Pultrusion (Figure 2.30) is used to make continuous products (Ray & Rout, 2005). The continuous fibres are impregnated in a liquid thermoset resin bath and then

pulled through a preform die, followed by a finishing die. Heated dies are commonly used to accelerate curing.

#### ***2.4.2.3 Mechanical Properties of Unidirectional Natural Fibre-Reinforced Thermoset-Matrix Composites***

Natural fibre thermoset matrix composites have been fabricated using a wide range of fibre forms, including mats, rovings and fabrics. The present study examined unidirectional fibre reinforced thermoset matrix composites and only these composites are considered here. A detailed review of thermoset matrix composites made using a wider range of fibre forms is given in Crosky et al. (2014).

**Table 2.22:** Tensile properties of epoxy resin and unidirectional flax fibre/epoxy composites (values in brackets represent one standard deviation) (Oksman, 2001)

<b>Sample</b>	<b>Fibre Volume Fraction (%)</b>	<b>Tensile Modulus (GPa)</b>	<b>Tensile Strength (MPa)</b>	<b>Elongation at Break (%)</b>
Epoxy resin	-	3.1-3.2 <sup>1</sup>	76 <sup>1</sup>	73 <sup>1</sup>
UD-Flax <sup>2</sup> /Epoxy	32	15 (0.6)	132 (4.5)	1.2
ArcticFlax <sup>3</sup> /Epoxy 1	21	22 (4)	193 (30)	0.9
ArcticFlax <sup>3</sup> /Epoxy 2	42	35 (3)	280 (15)	0.9
ArcticFlax <sup>3</sup> /Epoxy 3	47	39 (6)	279 (14)	0.8

<sup>1</sup>Data supplied by the manufacturer

<sup>2</sup>UD-Flax is unidirectional flax fibre mat from Mühlmeier GmbH

<sup>3</sup>ArcticFlax is a trade name of unidirectional flax fibre mat from FinFlax Oy, Kiiminki, Finland

Oksman (2001) examined the tensile properties of unidirectional flax fibre/epoxy composites, fabricated using resin transfer moulding. Composites with 21, 42 and 47 volume% fibres were fabricated using flax fibres from a Finnish supplier while a 32 volume% composite was fabricated using flax fibres from a German supplier. The tensile modulus and strength of the composites made with the Finnish-sourced fibres increased with increasing fibre volume fraction, while the strain to failure remained constant, Table 2.22. This behaviour is consistent with that observed for synthetic fibre composites (Harris, 1999). Interestingly, the modulus and strength of the 32% composite made with the German-sourced fibres were only half the values



obtained by interpolation of the data for the composites made with the Finnish-sourced fibres to the same fibre fraction, Table 2.22. This indicates the substantial variation in the properties of fibres from different sources.

Ratna Prasad & Mohana Rao (2011) fabricated 40 volume% unidirectional jowar, sisal and bamboo fibre/polyester composites using the hand lay-up compression moulding technique. The mechanical properties of the composites were determined and are given in Table 2.23. The jowar and bamboo composites both had similar mechanical properties, except for the flexural modulus which was substantially higher in the jowar composites. The sisal composites had lower mechanical properties than the other two composites.

**Table 2.23:** Mechanical properties of jowar, sisal and bamboo fibre/polyester composites (Ratna Prasad & Mohana Rao, 2011)

Composite	Tensile Property		Flexural Property	
	Strength (MPa)	Modulus (GPa)	Strength (MPa)	Modulus (GPa)
Cured polyester resin	31.5	0.63	55.1	1.54
Jowar/polyester	124	2.75	134	7.87
Sisal/polyester	65.5	1.90	99.5	2.49
Bamboo/polyester	126	2.48	128	3.70

Charlet, Baley, Morvan, Jernot, Gomina & Bréard (2007) examined the tensile properties of fabricated 20 volume% unidirectional Hermès flax fibre/epoxy composites fabricated using wet impregnation. The flax fibres used were selected from 3 different locations of the stems, these being the top, middle and bottom as shown in Figure 2.31. The tensile properties of the composites are given in Table 2.24. It was found that the composites made with fibre from the middle of the stems had higher tensile properties than those made with fibre from the other two locations. The composites made from the bottom of the stems had the lowest tensile properties. A fracture surface from the flax fibre/epoxy composites is shown in Figure 2.32.

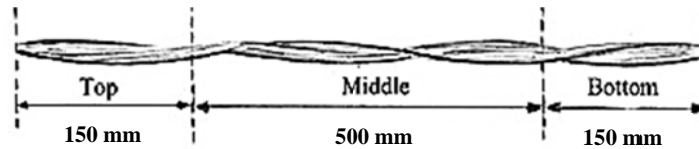


**Figure 2.31:** Locations of the flax stems in the oriented tows (Charlet et al., 2007).

**Table 2.24:** Tensile properties of the unidirectional flax fibre/epoxy composites (values in brackets represent one standard deviation) (Charlet et al., 2007)

Location of Fibre Stems	Tensile Property		
	Young's Modulus (GPa)	Strength (MPa)	Ultimate Strain (%)
Top	12.4 (1.3)	126 (14)	1.3 (0.2)
Middle	16.7 (3.7)	127 (14)	0.9 (0.2)
Bottom	11.1 (1.4)	113 (11)	1.5 (0.1)

*Figure 2.32 has been removed due to Copyright restrictions.*

**Figure 2.32:** SEM micrograph of fracture surface of unidirectional flax fibre/epoxy composites (Charlet et al., 2007).

Brahim & Cheikh (2007) examined the effect of loading direction on the tensile properties of 45 volume% unidirectional Alfa fibre/unsaturated polyester composites fabricated using the wet lay-up technique. They examined a range of loading directions from 0° (parallel to the fibres) to 90° (perpendicular to the fibres), as shown in Table 2.25. As for synthetic fibre composites (Harris, 1999), the Young's modulus and strength decreased progressively as the loading direction was changed from 0° to 90°. Young's modulus parallel to the fibres was 12.3 GPa while perpendicular to the fibres it

was 5.0 GPa. The strength parallel and perpendicular to the fibres was 150 MPa and 18 MPa, respectively. The shear modulus was also determined and a value of 2.5 GPa was obtained.

**Table 2.25:** Tensile properties of 45% unidirectional Alfa/unsaturated polyester composites with different fibre-tensile load angles in the longitudinal direction (Brahim & Cheikh, 2007)

Angle between the fibres and tensile load (degree)	Modulus (GPa)	Strength (MPa)
0	12.3	150
10	11.5	104
30	8.1	43
45	6.4	33
90	5.0	18

Brahim & Cheikh (2007) also examined the influence of fibre volume fraction on the tensile properties of composites loaded in the longitudinal direction, using volume fractions from 0% to 44%, Table 2.26. As for the flax fibre composites examined by Oksman (2001), the modulus and strength increased progressively with increasing fibre content while the strain to failure remained constant.

**Table 2.26:** Tensile properties of unidirectional Alfa/unsaturated polyester composites with different fibre volume fraction in the longitudinal direction (Brahim & Cheikh, 2007)

Fibre Volume Fraction (%)	Modulus (GPa)	Stress (MPa)	Strain (%)
0	4.1	64	2.7
12	6.6	75	2.3
21	8.2	96	2.3
32	10.2	118	2.6
44	12.3	149	3.1

Abdullah, Khalina & Ali (2011) fabricated 15 volume% and 45 volume% unidirectional kenaf fibre/epoxy composites using hand lay-up compression moulding at

room temperature. The tensile properties obtained are given in Table 2.27. Consistent with the results obtained for flax fibre composites, the modulus and strength were higher at the higher volume fraction while the strain to failure remained unchanged.

**Table 2.27:** Tensile properties of epoxy resin and unidirectional kenaf fibre/epoxy composites (Abdullah, Khalina & Ali, 2011)

<b>Sample</b>	<b>Modulus of Elasticity (GPa)</b>	<b>Tensile Strength at Break (MPa)</b>	<b>Tensile Strain at Break (%)</b>
Epoxy resin	1.78	32.19	3.40
15% Kenaf/epoxy	3.96	57.95	2.11
45% Kenaf/epoxy	7.76	100.53	1.90

**Table 2.28:** Tensile properties of epoxy resin and untreated and 18% NaOH treated unidirectional sisal fibre/epoxy composites (Padmavathi, Naidu & Rao, 2012)

<b>Sample</b>	<b>Fibre Weight Fraction (%)</b>	<b>Tensile Modulus (GPa)</b>	<b>Tensile Strength (MPa)</b>
Epoxy resin	-	3.50	70.0
Untreated sisal/epoxy	38.8	7.10	185.1
Treated sisal/epoxy 1	15.7	5.62	161.3
Treated sisal/epoxy 2	22.8	6.02	172.4
Treated sisal/epoxy 3	26.4	6.36	189.3
Treated sisal/epoxy 4	29.3	6.39	198.8
Treated sisal/epoxy 5	33.5	6.40	203.5
Treated sisal/epoxy 6	39.2	6.42	235.0

Another study of the effect of fibre fraction was made by Padmavathi, Naidu & Rao (2012) for alkali treated unidirectional sisal fibre/epoxy composites fabricated using the wet lay-up technique. The fibre weight fraction was varied between 16% and 39% They also examined a 40% fibre volume fraction untreated sisal fibre/epoxy composites. Their results are given in Table 2.28. Again the modulus and strength increased progressively with fibre weight fraction. For the 39-40% treated and untreated

composites it was found that the modulus was about 10% higher for the untreated composite, but the reverse was true for strength with the treated fibre composite being about 21% stronger than its untreated counterpart.

**Table 2.29:** Compressive strength of epoxy resin and untreated and 18% NaOH treated unidirectional sisal fibre/epoxy composites (Padmavathi, Naidu & Rao, 2012)

<b>Sample</b>	<b>Fibre Weight Fraction (%)</b>	<b>Compressive Strength (MPa)</b>
Epoxy resin	-	90.0
Untreated sisal/epoxy	38.8	115.5
Treated sisal/epoxy 1	15.7	76.2
Treated sisal/epoxy 2	22.8	84.9
Treated sisal/epoxy 3	26.4	96.0
Treated sisal/epoxy 4	29.3	117.2
Treated sisal/epoxy 5	33.5	123.8
Treated sisal/epoxy 6	39.2	136.6

**Table 2.30:** Impact property of untreated and 18% NaOH treated unidirectional sisal fibre/epoxy composites (Padmavathi, Naidu & Rao, 2012)

<b>Sample</b>	<b>Fibre Weight Fraction (%)</b>	<b>Impact Energy (J)</b>
Untreated sisal/epoxy	38.8	4.3
Treated sisal/epoxy 1	15.7	2.3
Treated sisal/epoxy 2	22.8	3.7
Treated sisal/epoxy 3	26.4	7.0
Treated sisal/epoxy 4	29.3	7.5
Treated sisal/epoxy 5	33.5	9.2
Treated sisal/epoxy 6	39.2	11.1

Padmavathi, Naidu & Rao (2012) also determined the compressive strength and impact strength of their composites, Tables 2.29 and 2.30, respectively. As for tensile strength, the compressive strength increased progressively with fibre weight fraction.

The compressive strength of the 39% treated fibre composite was also about 15% higher than that of the untreated 40% fibre composite, Table 2.29.

The impact strength also increased progressively with fibre weight fraction, Table 2.30. Moreover, the impact strength of the 39% treated fibre composites was almost 3 times that of its untreated fibre counterpart.

Van de Weyenberg, Chi Truong, Vangrimde & Verpoest (2006) studied the effect of alkali treatment on the flexural properties of 40 volume% unidirectional flax fibre/epoxy prepreg composites fabricated using autoclave curing. Three concentrations of NaOH were examined, 1, 2 and 3%, while composites were also prepared from untreated fibres, Table 2.31. The longitudinal flexural strength increased progressively with increasing NaOH concentration with the 3% treatment producing a 30% improvement over the untreated fibres. In the transverse direction, the improvement was even greater with 1% NaOH treatment producing a doubling in the flexural strength. However, there was no further improvement with increased NaOH concentration. The longitudinal flexural modulus increased by 28% with 1% NaOH treatment but showed no further improvement with the higher NaOH concentrations. The transverse modulus increased 6 fold with 1% NaOH treatment but the improvement was only about 3 fold for the higher concentrations.

**Table 2.31:** Flexural properties of the untreated and treated flax fibre/epoxy composites (Van de Weyenberg et al., 2006)

Flexural Property	Fibre Treatment			
	Untreated	1% NaOH	2% NaOH	3% NaOH
<b>Longitudinal Direction</b>				
Strength (MPa)	218	237	261	283
Modulus (GPa)	18	23	20	22
<b>Transverse Direction</b>				
Strength (MPa)	8	20	15	19
Modulus (GPa)	0.4	2.3	1.1	1.2

Nosbi, Akil, Mohd Ishak & Abu Bakar (2010) examined the effect of water absorption on the compression properties of 70 wt% unidirectional kenaf

fibre/unsaturated polyester composites fabricated by pultrusion. The composites were soaked in distilled water, seawater and an acidic solution at room temperature, Table 2.32. The compression strength and modulus were both reduced by the soaking treatments and this was attributed to hydrogen bonding of the water molecules to the kenaf fibres. There was no effect on failure strain. The degradation in compression strength and modulus was much greater in sea water and acid solution than in distilled water.

**Table 2.32:** Compression properties of the unidirectional kenaf fibre/unsaturated polyester composites (Nosbi et al., 2010)

<b>Condition</b>	<b>Strength (MPa)</b>	<b>Young's Modulus (GPa)</b>	<b>Failure Strain (%)</b>
No soaking	45.3	2.32	31.4
Distilled water	40.7	1.57	28.3
Seawater	32.4	1.02	36.0
Acidic solution	32.7	1.02	35.3

## 2.4.3 Advantages and Disadvantages of Natural Fibre Composites

### 2.4.3.1 Advantages of Natural Fibre Composites

Natural fibre composites have substantially lower density than glass fibres. As a result, they have specific strengths and stiffnesses which are comparable to those of glass fibres. Natural fibre composites can be easily formed into complex shapes in a single manufacturing process, with little tool abrasion (Anandjiwala & Blouw, 2007). They are also environmentally friendly and are generally considered to have a much low embodied energy than synthetic fibre composites, although this is not necessarily true when high levels of post-harvest processing are used (Dissanayake, Summerscales, Grove & Singh, 2009). Manufacturing processes for natural fibre composites are generally considered harmless to workers in terms of the fibres used. However, consideration should be given to the effect of any chemicals used as well as the effect of the composite fabrication process itself. The use of natural fibres is a low capital investment due to the low cost of the fibres. Natural fibres also have good thermal and acoustic insulation properties (Anandjiwala & Blouw, 2007).

#### ***2.4.3.2 Disadvantages of Natural Fibre Composites***

Natural fibre composites have low impact strength and poor fire resistance. The fibres also absorb high amounts of moisture and this causes dimensional changes of the composites. Natural fibres have low resistance to ultra-violet radiation and this leads to structural degradation of the composites. Adhesion between the natural fibres and the polymer matrix is often poor and this requires fibre surface treatments. Natural fibre preparation is time-consuming and labour intensive. The quality of natural fibres is inconsistent due to the intrinsic variability in the fibre properties, which is dependent on fibre source and cultivation. Natural fibres are also susceptible to fungal attack and mildew. The price of natural fibres depends on the global demand and production and this brings about price fluctuation (Anandjiwala & Blouw, 2007).

### **2.5 Summary**

The use of natural fibres in polymer-matrix composites is attractive since they have similar specific stiffness and strength to glass fibres, while also having much better environmental credentials. Moisture absorption and adhesion of the fibres to the matrix are problematic but can be largely overcome by the use of appropriate surface treatments.

Extrusion and injection moulding are potential processes for high volume production of natural fibre composite thermoplastic products. Chopped fibres must be used in these processes. However chopped plant fibres have much lower aspect ratios than synthetic fibres because of their much larger diameter. Low aspect ratios result in reduced mechanical performance.

One way of addressing this problem would be to reduce the plant fibres to elementary fibres. These have diameters similar to synthetic fibres and could thus provide short fibres with high aspect ratios, which could then be used in extruded and injection moulded thermoplastic composites. This was examined in the present study for kenaf/high density polyethylene (HDPE) composites.

Natural fibre composites also show pronounced variability in their properties, even within a single species, due to climatic conditions, soil conditions, extraction conditions, etc. This causes difficulty in reliably predicting the behaviour of natural fibre composites in service and this has limited their commercial uptake. One way of addressing this problem would be to grade the fibres on a mechanical basis and use this



data to predict their performance in the composite. This was undertaken in the present study for composites fabricated from vinyl ester resin reinforced with untwisted yarns made from flax technical fibres.

CHAPTER 3

**KENAF FIBRE SEPARATION AND  
CHARACTERISATION**

---



## **3. KENAF FIBRE SEPARATION AND CHARACTERISATION**

### **3.1 Introduction**

The first part of the study involved an examination of the effectiveness of using elementary fibres to produce high aspect ratio extruded thermoplastic matrix composites. This was done using kenaf fibres and a polyethylene matrix. The work involved developing a suitable process for reducing the technical fibres to elementaries and then analysing the fibres to establish any effect of the process on the fibre chemistry. This work is reported in this chapter.

The elementary fibres were subsequently used to produce extruded composites and the mechanical properties of the composites then determined. This work is reported in Chapter 4.

Several different chemical treatments identified in the literature were evaluated, these being ethylenediaminetetraacetic acid (EDTA) (Stuart, Liu, Hughes, McCall, Sharma & Norton, 2006), ethylene-diaminetetraacetic acid (EDTA)/pectinase (Stuart et al., 2006), sulphuric acid ( $\text{H}_2\text{SO}_4$ ) (Orts, Shey, Imam, Glenn, Guttman & Revol, 2005), nitric acid ( $\text{HNO}_3$ ) (Ogbonnaya, 1990, cited in Ogbonnaya, Roy-Macauley, Nwalozie & Annerose, 1997), a 50:50 mixture of hydrogen peroxide ( $\text{H}_2\text{O}_2$ ) and glacial acetic acid ( $\text{CH}_3\text{COOH}$ ) (Hughes, Sebe, Hague, Hill, Spear & Mott, 2000), and glacial acetic acid on its own.

The elementary fibres were physically characterised to determine their width and length. The defects present in the fibres were also examined. The elementaries were also characterised chemically using Fourier transform infrared spectroscopy (FTIR) and Raman spectroscopy, while the level of cellulose crystallinity and the degree of oxidation were determined by X-ray diffraction (XRD) and solid state nuclear magnetic resonance (NMR) spectroscopy. Thermal gravimetric analysis (TGA) was also carried out. Untreated fibres were chemically characterised by these techniques also and the results compared with those obtained from the elementary fibres. X-ray photon spectroscopy (XPS) was used to examine the surface chemistry of the elementaries and untreated fibres.

Selected treatments were also carried out on alpha-cellulose to provide standards against which the results obtained from the fibres could be compared.

### 3.2 Materials

Untreated kenaf fibres (UKF) were obtained from the Malaysian Agriculture Research and Development Institute (MARDI), Malaysia. The fibres are shown as received in Figure 3.1. These fibres had been previously characterised by Zakaria (2014) and their analysis is given in Table 3.1.



**Figure 3.1:** Kenaf fibres as received.

**Table 3.1:** Chemical analysis (wt%) of MARDI kenaf fibres (Zakaria, 2014)

Description	Test Method	Analysis (wt%)
Holocellulose	TAPPI T 249-75	91.2
Cellulose	TAPPI T 203 os-74	60.9
Hemicelluloses	TAPPI T 203 cm-99	30.3
Pentosan	TAPPI T 223 cm-01	17.3
Alkali solubility	TAPPI T 212 om-02	16.8
Lignin content	TAPPI T 222 om-02	11.1
Moisture content	TAPPI T 264 om-88	10.0
Hot water soluble	TAPPI T 207 cm-99	1.19
Ethanol-toluene	TAPPI T 204 cm-97	0.73
Ash content	TAPPI T 211 om-02	0.65

70% nitric acid, 30% hydrogen peroxide, glacial acetic acid, sulphuric acid and sodium hydroxide (NaOH) pellets were supplied by Ajax Finechem. Alpha-cellulose, ethylenediaminetetraacetic acid (EDTA), Triton<sup>TM</sup> X-100, and Pectinex<sup>®</sup> Ultra SPL (pectinase from *Aspergillus aculeatus*) were supplied by Sigma-Aldrich.

### 3.3 Experimental

#### 3.3.1 Isolation of Elementary Fibres

##### 3.3.1.1 Chemical Treatment

Prior to undertaking the chemical treatments, the as-received fibre bundles were cut to 100 mm lengths, as are shown in Figure 3.2.



**Figure 3.2:** Kenaf fibre bundles cut to 100 mm length.

##### (3.3.1.1.1) Ethylenediaminetetraacetic Acid (EDTA) Treatments

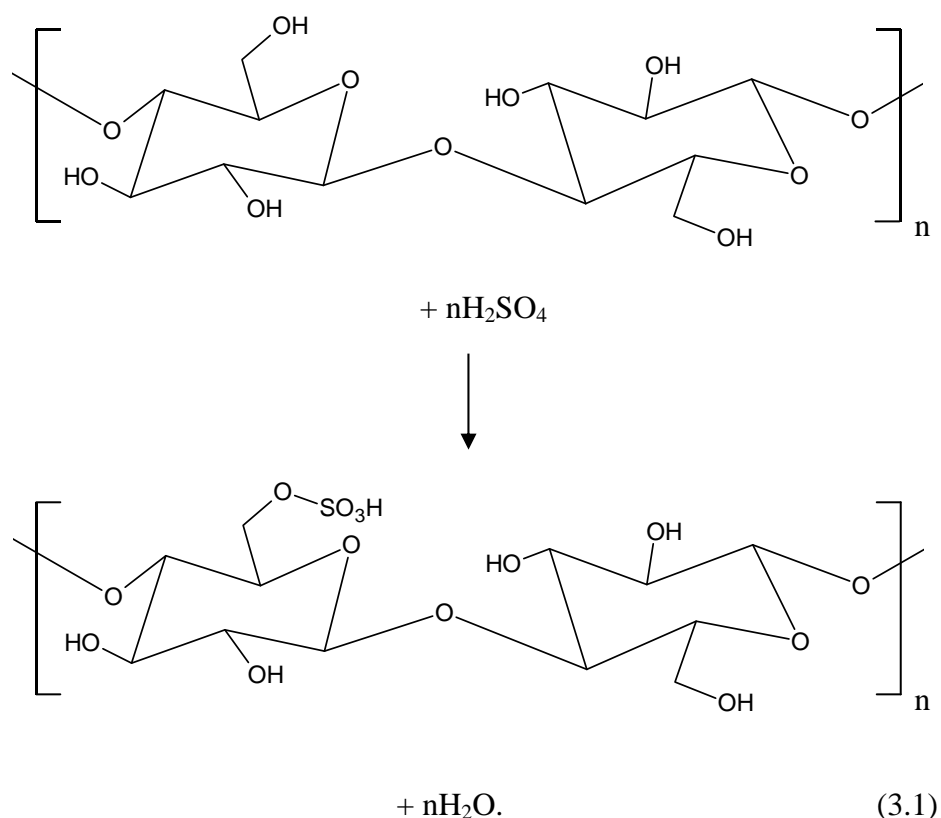
EDTA treatment was carried out using the method given by Stuart et al., (2006). The cut fibre bundles were soaked in EDTA (5 g/L) at a pH of 11 with 20%w/v sodium hydroxide and 20 drops of 0.1% Triton<sup>TM</sup> X-100 at 60°C for 3.5 and 24 hours. Liquor to fibre ratios were 40:1 and 133:1 for the 3.5-hour and 24-hour treatments, respectively. The treated fibres were then washed in cold running tap water for 2 hours. Subsequently, the fibres were dried in air. The EDTA-treated fibres are referred to hereafter as KFTE treated fibres.

A second EDTA treatment which involved a subsequent pectinase treatment was also carried out, again using a method given by Stuart et al., (2006). The fibres bundles were soaked in EDTA using the same conditions as for the 3.5 hour treatment described

above except that the treatment time was reduced to 3 hours and the amount of 0.1% Triton<sup>TM</sup> X-100 was increased to 40 drops. Washing and drying were again carried out as described above. A second solution was then prepared from distilled water. Acetic acid containing 5 ml/L Pectinex<sup>®</sup> Ultra SPL was added to the distilled water to adjust the pH to a value of 4.5 and 40 drops of 0.1% Triton<sup>TM</sup> X-100 then added. The EDTA treated kenaf fibres were then soaked in this solution for 2 hours at 40°C with a liquor to fibre ratio of 40:1. The treated fibres were washed in cold running tap water for 2 hours, then dried in air. The resulting fibres are referred to hereafter as KFTEDP treated fibres.

#### (3.3.1.1.2) Sulphuric Acid Treatment

Sulphuric acid treatment was carried out using a method based on those used by Orts et al. (2005) and Liu, Yuan, Bhattacharyya & Easteal (2010). The esterification between hydroxyl groups of cellulose in the fibres and sulfate ions from H<sub>2</sub>SO<sub>4</sub> is given as follows (Bondeson, Kvien & Oksman, 2006):

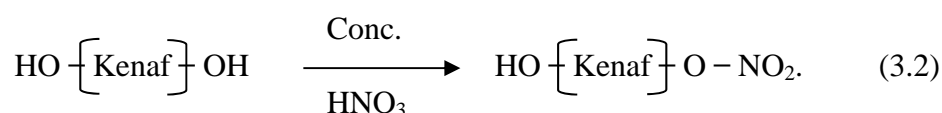


Cut fibre bundles were soaked in 60% H<sub>2</sub>SO<sub>4</sub> (Orts et al., 2005), in a 150:1 liquor to fibre ratio, at 55°C (Liu et al., 2010) for 75 minutes (Orts, et al., 2005). The fibres were then filtered and washed, first with tap water, then with distilled water and,

finally, with deionized water. Subsequently, the fibres were freeze dried using the procedure given in Section 3.3.1.3. The resulting fibres are referred to hereafter as KFTS treated fibres.

#### (3.3.1.1.3) Nitric Acid Treatment

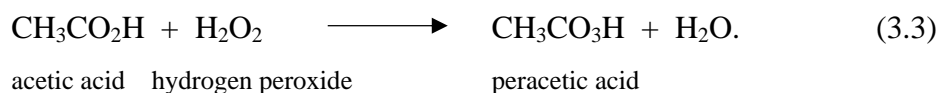
Nitric acid treatment is referred to as nitration. The chemical reaction between kenaf fibres and  $\text{HNO}_3$  is given as follows (Samal & Ray, 1997):



The treatment was carried out using 60%  $\text{HNO}_3$  in a 20:1 liquor to fibre ratio, at  $80 \pm 2^\circ\text{C}$  for 30 minutes (Ogbonnaya, 1990, cited in Ogbonnaya et al., 1997). The yield from this process was low so the treatment was continued in the same solution at room temperature in a fume cupboard for a minimum of 5 weeks. The treated fibres were then filtered and washed to remove  $\text{HNO}_3$ , first using tap water, then distilled water and, finally, deionized water. The fibres were then washed until the pH value of the solution was approximately 6-7. They were then dried in air at room temperature or freeze dried, as described in Section 3.3.1.3. The fibres obtained from this treatment are referred to hereafter as KFTN treated fibres. This process was one of two processes subsequently used for large scale extraction of elementary fibres.

#### (3.3.1.1.4) Hydrogen Peroxide/Glacial Acetic Acid Treatment

Fibre bundles were also treated using a 50:50 mixture of hydrogen peroxide and glacial acetic acid (50:50) as used by Hughes et al., (2000). The chemical reaction between the  $\text{H}_2\text{O}_2$  and  $\text{CH}_3\text{COOH}$  is given as follows (Kitis, 2004):



Two different methods were evaluated for this treatment. In the first method, the fibre bundles were immersed in a 50:50 mixture of 30% hydrogen peroxide and glacial acetic acid, in a 100:1 liquor to fibre ratio, at  $60 \pm 2^\circ\text{C}$  for 24 hours (Franklin, 1945; Rautiainen & Alen, 2009). Soaking in the solution was continued at room temperature



for 4 months. The treated fibres were subsequently filtered, washed with water until the pH reached approximately 7, then freeze dried as described in Section 3.3.1.3. The fibres treated in this manner are referred to hereafter as KFTHA1 treated fibres.

The second treatment involved soaking the bundles in a 50:50 mixture of 20% hydrogen peroxide and glacial acetic acid (Gominho, Fernandez, & Pereira, 2001), in a 75:1 liquor to fibre ratio, at  $98 \pm 2^\circ\text{C}$  for 7 hours (Mazumder, Ohtani, Cheng, & Sameshima, 2000). The treated fibres were then filtered, washed with water, again until the pH of the solution was approximately 7, then freeze dried using the method described in Section 3.3.1.3. The fibres treated in this manner are hereafter referred to as KFTHA2 treated fibres. This method was the second method used to extract elementary fibres on a large scale.

#### *(3.3.1.1.5) Glacial Acetic Acid Treatment*

The treatment given above was successful in producing elementary fibres and it was therefore decided to examine the efficacy of glacial acetic acid on its own. Accordingly, fibres were treated with glacial  $\text{CH}_3\text{COOH}$ , in a 70:1 liquor to fibre ratio, at  $98 \pm 2^\circ\text{C}$  for 7 hours. The treated kenaf fibres were then washed with water and dried in air. The  $\text{CH}_3\text{COOH}$  treated fibres are hereafter referred to as KFTA treated fibres.

### ***3.3.1.2 Nitric Acid and Hydrogen Peroxide/Acetic Acid Treatment of Alpha-Cellulose***

As for other plant fibres, cellulose is the major component in kenaf fibres, Table 3.1. To examine the effect of the treatments in the absence of the other components in the kenaf fibres,  $\alpha$ -cellulose (AC), was treated with the nitric acid treatment given above (KFTN) and both of the hydrogen peroxide/acetic acid treatments (KFTHA1 and KFTHA2). As for these treatments the treated cellulose was freeze dried using the method given in Section 3.3.1.3. The nitric acid treated  $\alpha$ -cellulose is referred to hereafter as ACTN while the hydrogen peroxide/acetic acid treated  $\alpha$ -cellulose is referred to as ACTHA1 (treatment KFTHA1) and ACTHA2 (treatment KFTHA2).

#### ***3.3.1.3 Drying of Elementary Fibres***

Two different drying techniques were used. The first involved drying the washed treated fibres in air at room temperature for several days. The second, which was used in most cases, involved first freezing the washed treated kenaf fibres and then

placing them in a Lyovac GT 2 freeze drier (Rennekar, Zink-Sharp, Esker, Johnson & Glasser, 2006; Sain & Panthapulakkal, 2004) for 1-2 days. For both techniques, the dried fibres were subsequently stored in desiccators to avoid moisture absorption.

#### ***3.3.1.4 Untreated Fibres***

Analysis was also carried out on untreated kenaf fibres in the as-received condition for the purpose of comparison. For this, the fibre bundles were hand-cut to a length of approximately 2 mm and then manually separated to give chopped technical fibres. These fibres are referred to hereafter as UKF fibres. UKF fibres were also used for comparison in the extruded composites examined in Chapter 4.

### **3.3.2 Scanning Electron Microscopy (SEM)**

The fibres obtained from the UKF, KFTN, KFTHA1 and KFTAH2 processes were imaged using a Hitachi S3400-X scanning electron microscope (SEM). The fibre specimens were first sputter coated with gold using an Emitech K550x gold sputter coater. The SEM was operated in high vacuum mode at an accelerating voltage of 10 kV.

### **3.3.3 Fibre Length, Diameter and Aspect Ratio**

The length and diameter were measured for 500 UKF, 500 KFTN, 50 KFTHA1, and 50 KFTHA2 fibres and the aspect ratio then determined for each process using the average values of these two parameters. The fibres were sprinkled onto glass slides and then examined using a Nikon Eclipse ME600 optical microscope. The measurements were made using UTHSCSA ImageTool program.

### **3.3.4 Defects in Elementary Fibres**

The defects present in the elementary fibres were examined for the KFTN, KFTHA1 and KFTHA2 processes. Several different techniques were trialled. These included examination of fibres that had been placed wet onto glass slides then air dried on the slides (Hughes et al., 2000). The samples were then examined using a Nikon Eclipse ME600 optical microscope using transmitted light and also using a Hitachi TM3000 tabletop scanning electron microscope imaging with backscattered electrons (BSE). Both uncoated samples, and samples sputter coated with gold using the method described in Section 3.3.2, were examined using the TM3000 scanning electron microscope.

Fibres were also examined after placing them wet onto a glass slide using a dropper. The fibres were then dried, mounted in Eukitt mounting medium and examined under cross-polarised light using a Leica DMRB microscope. Digital images were recorded using a Leica EC3 digital camera. This work was carried out by Scion, New Zealand, and the images provided to UNSW.

The final method used was to examine gold coated dry fibres using a Hitachi S3400-X scanning electron microscope, using the method described in Section 3.3.2, but with an accelerating voltage of 15 kV. In this technique, imaging was done using secondary electrons (SE). This technique was considered the most successful for imaging defects and was used to determine the defect density for the different fibre treatments. Ten elementary fibres were examined in each case.

### **3.3.5 Fourier Transforms Infrared (FTIR) Spectroscopy**

Fourier transform infrared (FTIR) spectroscopy is a technique used to identify the molecular structure of components or groups of atoms absorbing in the infrared (IR) radiation region. Absorption occurs when an incident beam of radiation causes vibration of molecular dipoles. The radiation is absorbed at the same frequency as that of the molecular vibration (Kim & Mai, 1998).

The untreated fibres (UKF), the fibres treated with  $\text{HNO}_3$  (KFTN), and the fibres treated with the two  $\text{H}_2\text{O}_2/\text{CH}_3\text{COOH}$  solutions (KFTHA1 and KFTHA2) were analysed using FTIR spectroscopy.  $\alpha$ -cellulose (AC),  $\alpha$ -cellulose treated with  $\text{HNO}_3$  (ACTN), and  $\alpha$ -cellulose treated with the two  $\text{H}_2\text{O}_2/\text{CH}_3\text{COOH}$  solutions (ACTHA1 and ACTHA2) were also analysed. The analyses were carried out using a Perkin Elmer Spotlight 400 FTIR microscope in universal attenuated total reflectance (UATR) mode in the range of  $4,000\text{--}650\text{ cm}^{-1}$ , with a resolution of  $4\text{ cm}^{-1}$ . Sufficient material ( $\sim 1\text{ g}$ ) was placed on the crystal window to completely cover its area. A single sample was analysed for each different material and condition.

### **3.3.6 Raman Spectroscopy**

Raman spectroscopy is a complementary technique to IR spectroscopy for chemical characterisation. Raman spectroscopy depends on the change in polarisability of the molecule associated with the vibrational motion, whereas FTIR spectroscopy depends on the permanent dipole moment of the molecule associated with the vibrational motion (Michielsen, 2001).

Samples of both the fibres and  $\alpha$ -cellulose in both the untreated and treated conditions were analysed using a Perkin Elmer Ramanstation 785-nm (near-IR) laser-based Raman spectrometer. A single sample approximately 1 g in weight was analysed for each different material and condition. The measurement conditions used are given in Table 3.2.

**Table 3.2:** Raman spectrum measurement conditions

<b>Instrument Conditions</b>	
Excitation source	785-nm (near IR) laser
Laser energy	100%
Microscope objective	50 times
Exposure time	30 per second
Spectrum range or Raman shift	200-2,000 $\text{cm}^{-1}$

### 3.3.7 X-Ray Photoelectron Spectroscopy (XPS)

X-ray photoelectron spectroscopy (XPS) is used to identify elements at a depth of 2-10 nm in the surface of samples. This technique is also known as electron spectroscopy for chemical analysis (ESCA). An X-ray beam is used to eject electrons from the inner orbital of atoms with kinetic energies characteristic of the parent atoms. The intensities of the kinetic energy are analysed and the characteristic binding energies then used to determine the chemical composition (Kim & Mai, 1998). The total absorbed X-ray photon energy ( $h\nu$ ) is given by

$$h\nu = E_K + E_B \quad (3.4)$$

where  $E_K$  is the kinetic energy and  $E_B$  is the electron binding energy (Kim & Mai, 1998).

The chemical and elemental species present at the surface of the untreated fibres and the fibres in the two treated conditions were studied using a Kratos Axis Ultra X-ray photoelectron spectrometer (XPS). Low resolution XPS survey spectra of all of the samples and also high resolution XPS spectra of the C 1s, N 1s and O 1s peaks of all of the samples were obtained.

### 3.3.8 Cellulose Crystallinity

The level of crystallinity (crystallinity index) in the cellulose was determined for both the fibres and  $\alpha$ -cellulose in both the untreated and treated conditions using a Philips X'pert Multipurpose X-ray Diffraction (XRD) System. Both untreated fibres and  $\alpha$ -cellulose, as well as the fibres and  $\alpha$ -cellulose in the three treated conditions, were examined. The specimens were scanned from  $8^\circ$  to  $55^\circ$  at  $2\Theta$ . A step size of  $0.026^\circ$ , a voltage of 45 kV and a current of 40 mA were used. Time per step was 51 seconds and revolution time was 4 seconds. Percentage crystallinity indexes were calculated using Segal's equation (equation 2.2 in Chapter 2) and multiplying by 100 (Sayeba, Marzouga, Hassena, Saklia & Rodeslib, 2010). Peak intensity was measured as shown in Figure 3.3.

*Figure 3.3 has been removed due to Copyright restrictions.*

**Figure 3.3:** X-ray diffraction pattern showing measurement of peak intensity for determination of the crystallinity index (Park, Baker, Himmel, Parilla & Johnson, 2010).

The crystallinity index of cellulose was also determined for the same materials using solid-state  $^{13}\text{C}$  nuclear magnetic resonance (NMR), using a Bruker Avance III 300 Solid State NMR. Figure 3.4 shows an example of the cellulose NMR spectrum. Peak deconvolution was carried out using TopSpin<sup>TM</sup> peak deconvolution software. The Lorentzian distribution function was also used for deconvolution and curve fitting. The crystalline and amorphous peaks at 89 ppm and 84 ppm, respectively, in the C4 region (from 80 ppm to 93 ppm) were used for determining the crystallinity index of the cellulose (Park et al., 2010).

The crystallinity index was also determined using FTIR from the ratio of the intensity of the peaks at  $1,420\text{ cm}^{-1}$  to  $893\text{ cm}^{-1}$  which correspond to crystalline and amorphous cellulose, respectively (Dai & Fan, 2010).

For each of the three methods, the results were obtained from a single analysis of each of the different materials.

*Figure 3.4 has been removed due to Copyright restrictions.*

**Figure 3.4:** Solid state  $^{13}\text{C}$  NMR spectrum of the commercial cellulose (Avicel PH-101). (a) Whole spectrum showing the assignment of peaks to the carbons in a glucopyranose repeat unit and (b) sub-spectrum showing peaks assigned to the C4 in cellulose. The crystallinity index is calculated by  $X/(X+Y)$  (Park et al., 2010).

### 3.3.9 Degree of Oxidation

Treatment of both the fibres and  $\alpha$ -cellulose in nitric acid and hydrogen peroxide/acetic acid would be expected to cause some oxidation of the cellulose. Figure 3.5 shows the structure of oxidised cellulose (Kumar & Yang, 2002). Commercial  $\text{HNO}_3$  as used in the present work generally contains nitrogen oxides such as  $\text{NO}_2$ ,  $\text{HNO}_2$ ,  $\text{NO}$ ,  $\text{N}_2\text{O}_3$  and  $\text{N}_2\text{O}_5$  (Ogata, 1978, cited in Kumar & Yang, 2002). The

generation of nitrogen oxides in  $\text{HNO}_3$  is shown in Figure 3.6. while the oxidation mechanism of cellulose due to  $\text{HNO}_3$  is shown in Figure 3.7 (Kumar & Yang, 2002).

The degree of oxidation of cellulose in the treated kenaf fibres and treated  $\alpha$ -cellulose was determined from solid state  $^{13}\text{C}$  NMR spectra by integrating the peak at 174 ppm ( $\text{C6}'$ ) corresponding to the carboxyl groups (Lasseuguette, 2008). The integration was performed using the C1, the C4 and the C2,3,5 peaks separately as calibration to allow three separate estimates to be made. The degree of oxidation indicates the weight percent of the carboxyl in the cellulose (Ashton & Moser, 1968).

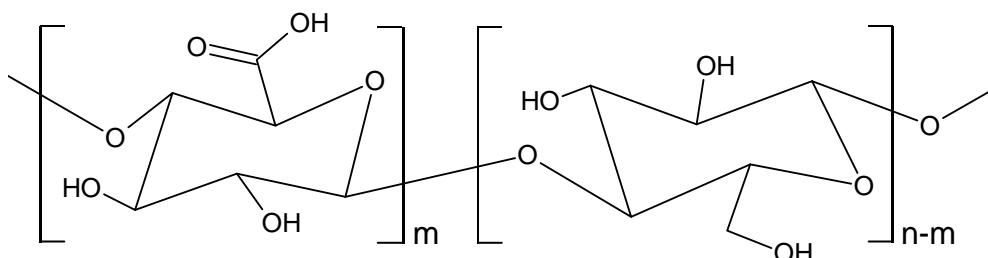


**Figure 3.5:** Structure of oxidised cellulose (Kumar & Yang, 2002).

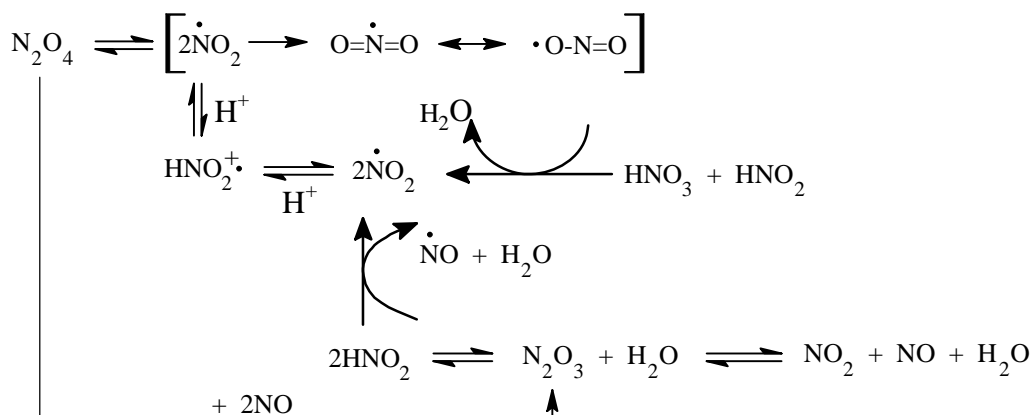


**Figure 3.6:** Generation of nitrogen oxides in situ (Kumar & Yang, 2002).

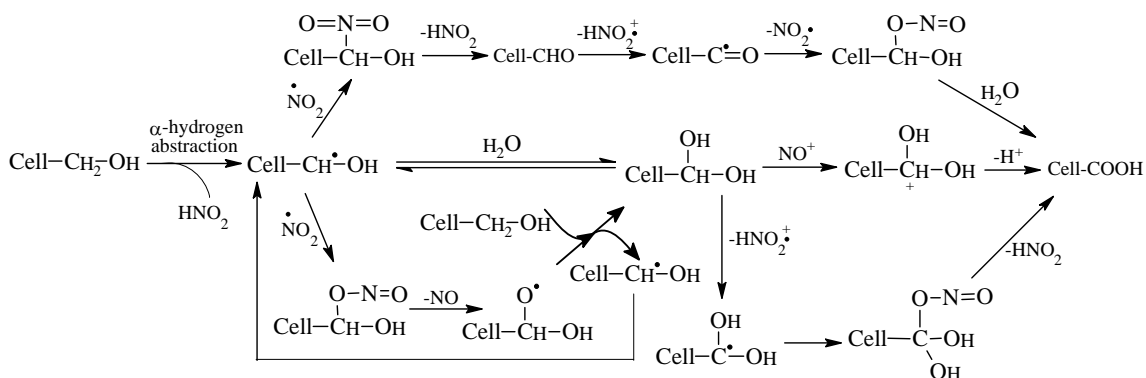


**Figure 3.7:** Oxidation mechanism of cellulose (Kumar & Yang, 2002).

### 3.3.10 Thermogravimetric Analysis (TGA)

Thermogravimetric analysis (TGA) measurements were conducted on the untreated (UKF), nitric acid treated (KFTN), and 20% hydrogen peroxide/acetic acid treated (KFTHA2) fibres using a TGA Q5000 thermogravimetric analyser under an air atmosphere with a flow rate of 15 ml/min. The fibres were heated from room temperature to 700°C at a heating rate of 10°C/min. A platinum pan was used for the measurements.

## 3.4. Results

### 3.4.1 Isolation of Elementary Fibres

The results obtained using the different chemical treatments are given below. Stages during each of the processes are shown in Appendix I.

#### 3.4.1.1 Ethylenediaminetetraacetic Acid (EDTA) Treatments

Neither of the two EDTA treatments examined proved to be successful in breaking the fibre bundles down into elementary fibres, Appendix I. In view of the poor performance of these treatments, they were not pursued further.

#### 3.4.1.2 Sulphuric Acid Treatment



**Figure 3.8:** Photograph of freeze-dried KFTS elementary fibres.

The sulphuric acid treatment (KFTS) produced some success in breaking down the fibre bundles into elementaries. However, the yield was very low (2%). Moreover,



the fibres became blackened by the treatment, Figure 3.8, indicating that substantial reaction had occurred. As a result, this treatment was not examined further.

### 3.4.1.3 Nitric Acid Treatment

The nitric acid treatment proved more successful and elementary fibres were obtained.

The KFTN elementaries are shown after air-drying and freeze-drying (both low fibre to water ratio (~5 volume % fibres) and high fibre to water ratio (~70 volume % fibres)) in Figure 3.9, while KFTN elementaries obtained from several batches are shown Figure 3.10. Unlike the kenaf technical fibres which were yellow in colour, Figure 3.2, the elementary fibres can be seen to be white. An optical microscope image of a KFTN elementary fibre after drying is shown in Figure 3.11. The high aspect ratio is evident.

The process gave a yield of only 36% due to loss of elementaries principally during the washing and filtering processes.



**Figure 3.9:** KFTN fibres (a) air-dried, (b) freeze-dried (low fibre to water ratio) and (c) freeze-dried (high fibre to water ratio).



**Figure 3.10:** Photographs of freeze-dried KFTN elementary fibres.

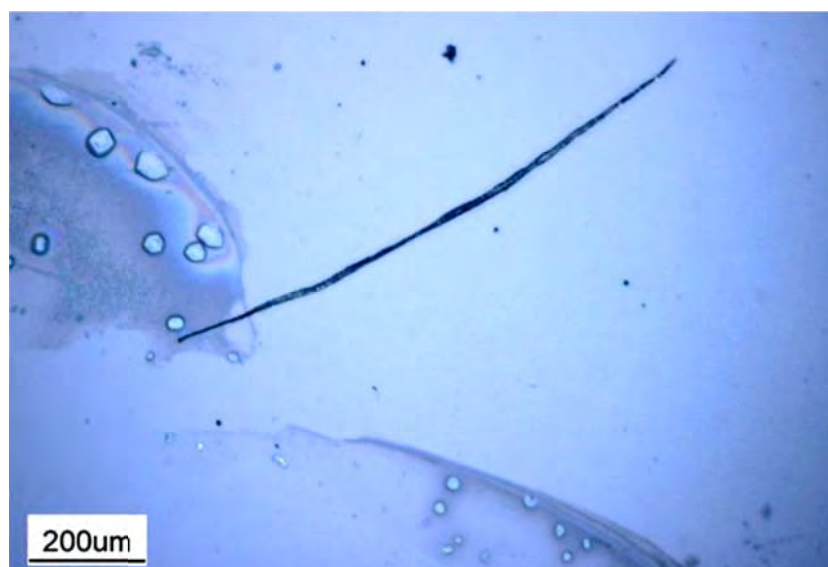


**Figure 3.11:** Optical microscope image of KFTN elementary fibre.

Figures 3.12 to 3.14 show SEM micrographs of the air-dried KFTN, freeze-dried KFTN (low fibre to water ratio) and KFTN (high fibre to water ratio), respectively. The surface of the air-dried KFTN can be seen to be quite clean, Figure 3.12 whereas agglomerated microfibrils are evident on the surface of the freeze-dried elementaries, Figures 3.13 and 3.14. Some interconnection of the fibres can also be seen in Figure 3.14.

The fibres obtained from both the air-drying and freeze-drying processes generally had wide square ends, rather than the narrow tapered ends that are usual for elementary fibres.

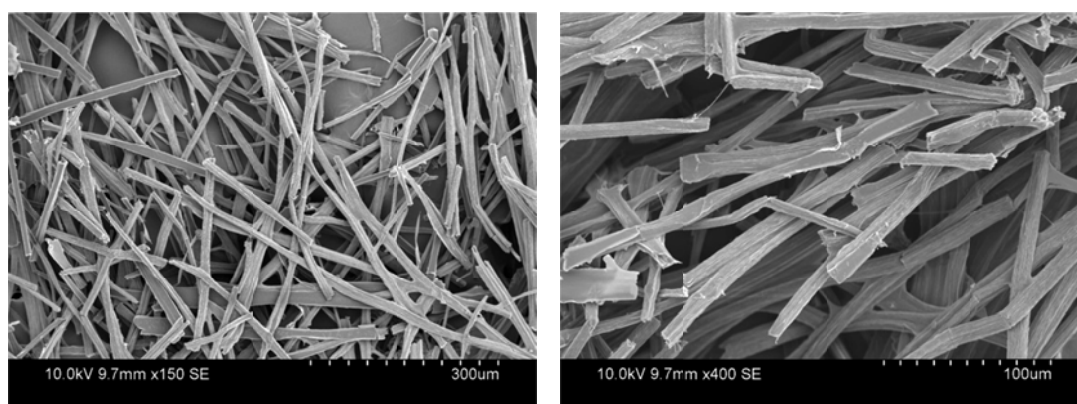


**Figure 3.12:** SEM micrographs of air-dried KFTN elementary fibres at  $\times 150$  (left) and  $\times 400$  (right) magnifications.

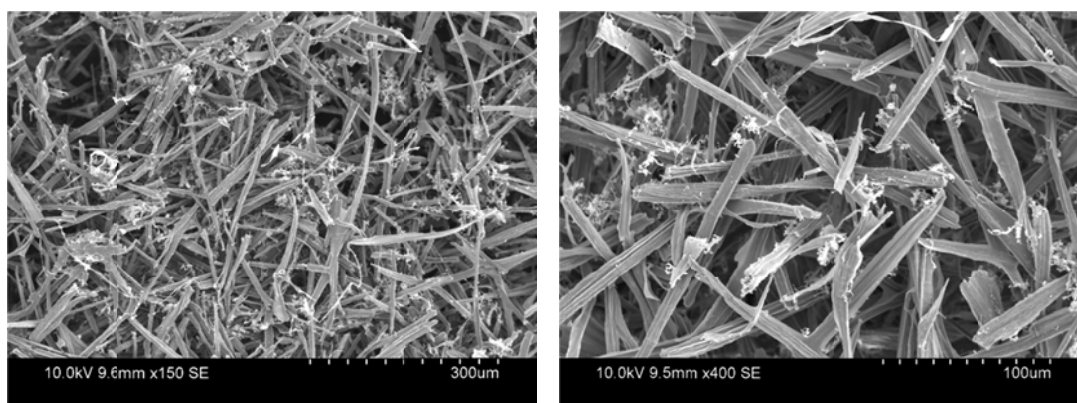


**Figure 3.13:** SEM micrographs of freeze-dried KFTN elementary fibres (low fibre to water ratio) at  $\times 150$  (left) and  $\times 400$  (right) magnifications.

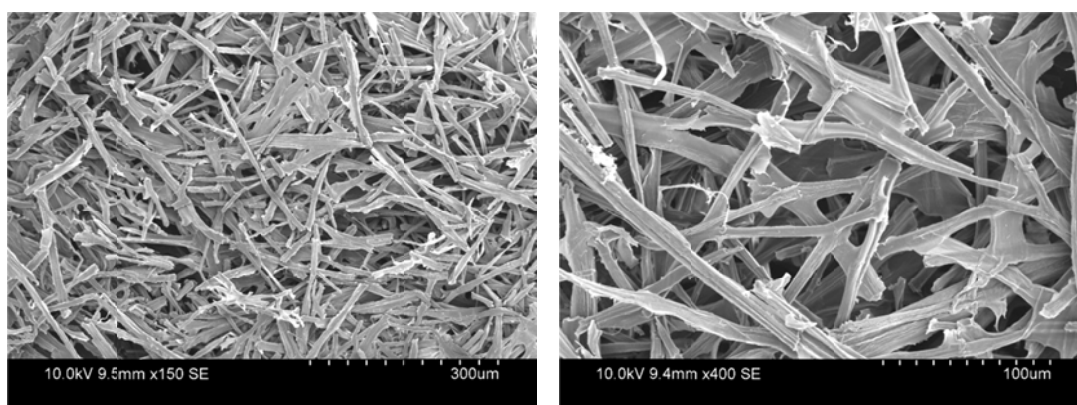


**Figure 3.14:** SEM micrographs of freeze-dried KFTN elementary fibres (high fibre to water ratio) at  $\times 150$  (left) and  $\times 400$  (right) magnifications.

#### ***3.4.1.4 Hydrogen Peroxide/Glacial Acetic Acid Treatment***

Both of the two hydrogen peroxide/glacial acetic acid treatments were also successful in isolating the elementary fibres.

Photographs and SEM micrographs of the freeze-dried 30% hydrogen peroxide/acetic acid treated fibres (KFTHA1) are shown in Figures 3.15 and 3.16, respectively. Macroscopically, the elementaries have a similar appearance to those obtained from the nitric acid process, Figures 3.15. Microscopically, the fibres can be seen to be much longer than those obtained from the nitric acid process and have narrow tapered ends rather than square ends, Figures 3.16. Some microfibrils can be seen attached to the fibres.

The yield from this process was 57%, again due to the loss of elementaries principally during the washing and filtering process.



**Figure 3.15:** Photographs of freeze-dried KFTHA1 elementary fibres.

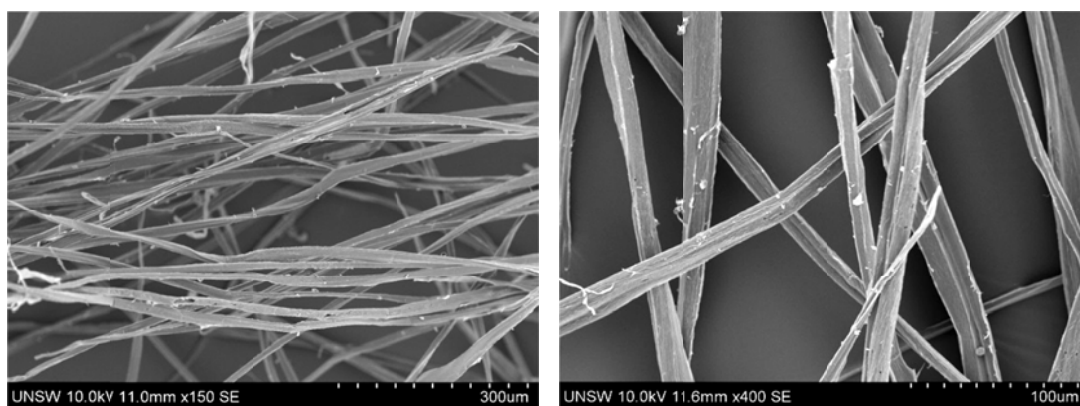


**Figure 3.16:** SEM micrographs of freeze-dried KFTHA1 elementary fibres at  $\times 150$  (left) and  $\times 400$  (right) magnifications.

The elementaries obtained from the 20% hydrogen peroxide/acetic acid treatment (KFTHA2) had a similar appearance, both macroscopically, Figure 3.17, and microscopically, Figure 3.18, to those obtained from the KFTHA1 treatment, except that the fibre surfaces had a much cleaner appearance with minimal attachment of microfibrils. As for the KFTHA1 treatment the fibres were long with highly tapered ends, Figure 3.18.

The yield for the KFTHA2 process was 58%.





**Figure 3.17:** Photographs of freeze-dried KFTHA2 elementary fibres.

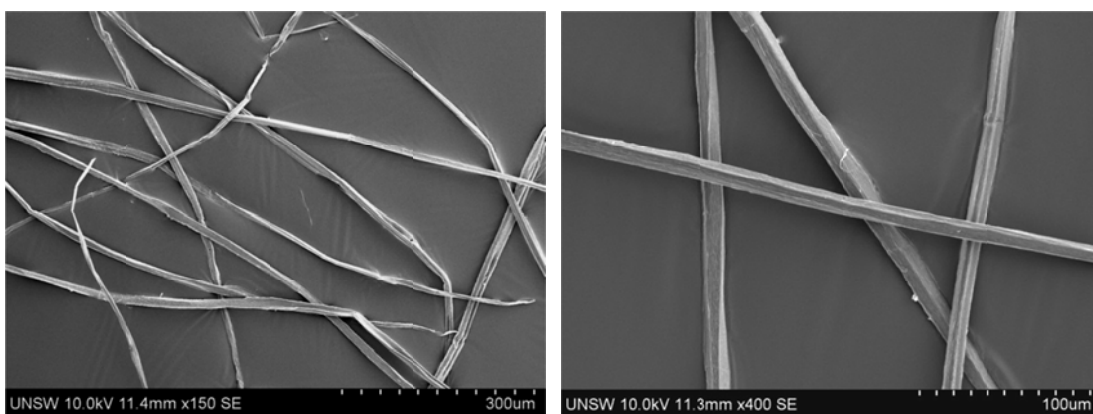


**Figure 3.18:** SEM micrographs of freeze-dried KFTHA2 elementary fibres at  $\times 150$  (left) and  $\times 400$  (right) magnifications.

#### ***3.4.1.5 Glacial Acetic Acid Treatment***

Treatment of the fibres in glacial acetic acid alone at 98°C, was also undertaken. However, there was no evidence of breakdown of the fibre bundles during the 7 hour treatment used, Appendix I.

#### ***3.4.1.6 Nitric Acid and Hydrogen Peroxide/Acetic Acid Treatment of Alpha-Cellulose***

Nitric acid treatment and the two hydrogen peroxide/acetic acid treatments were also carried out on  $\alpha$ -cellulose. Various stages during the processes are shown in Appendix I.

### 3.3.1.7 Untreated Fibres

SEM micrographs of chopped fibres (UKF), which were used for comparison with the elementary fibres obtained from the fibre treatments, are shown in Figure 3.19. While the intended fibre length was 2 mm, considerable variation can be seen. Some impurities are also evident on the fibre surfaces.

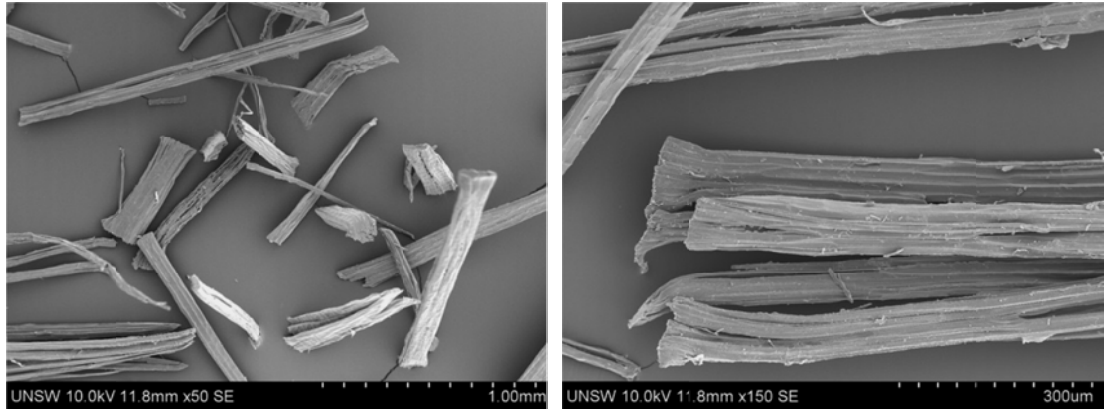


**Figure 3.19:** SEM micrographs of chopped kenaf fibre bundles (UKF) at  $\times 50$  (left) and  $\times 150$  (right) magnifications.

### 3.4.2 Aspect Ratios of Elementary Fibres

A typical optical microscope image of the chopped fibres (UKF) is shown in Figure 3.20a, while histograms of the measured length and diameter of the UKF fibres are shown in Figures 3.21 and 3.22, respectively. Both distributions are positively skewed.

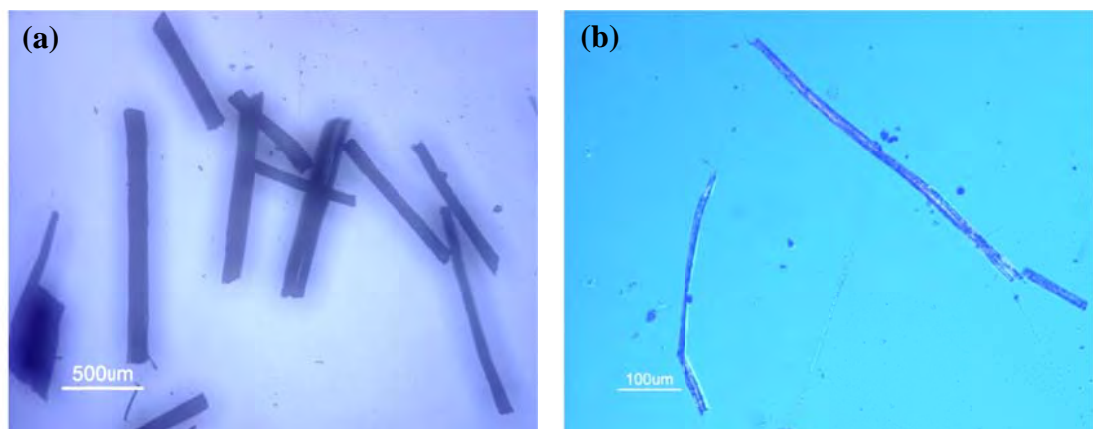


**Figure 3.20:** Typical optical microscope images of (a) chopped technical fibres (UKF) and (b) freeze-dried elementary fibres obtained from the  $\text{HNO}_3$  treatment (KFTN).

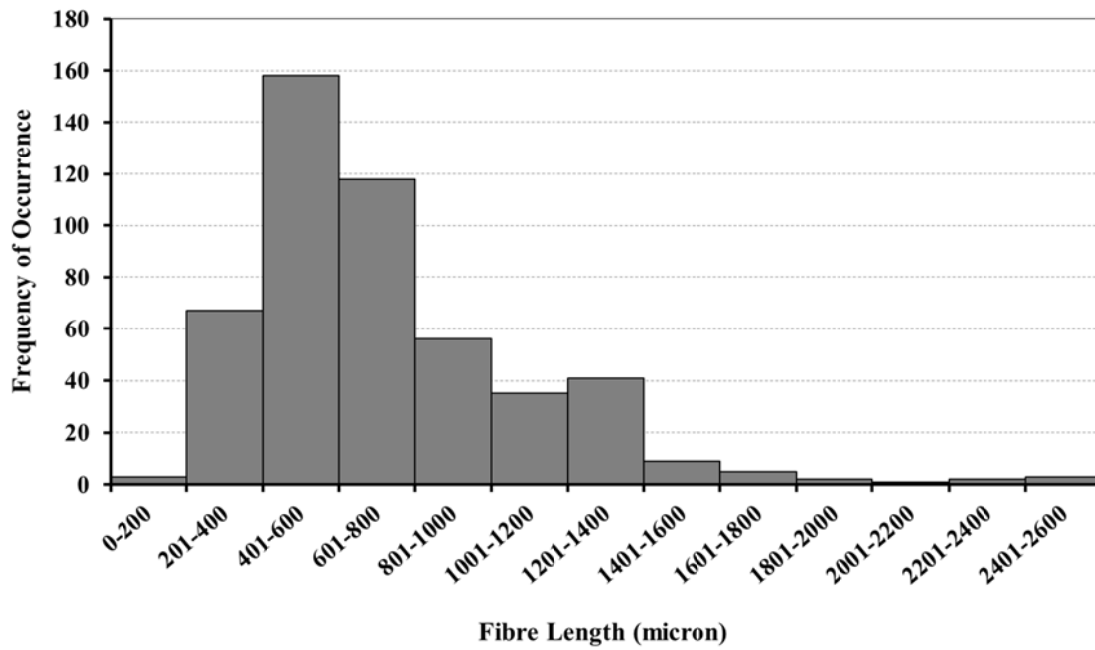


**Figure 3.21:** Histogram of measured lengths of UKF.

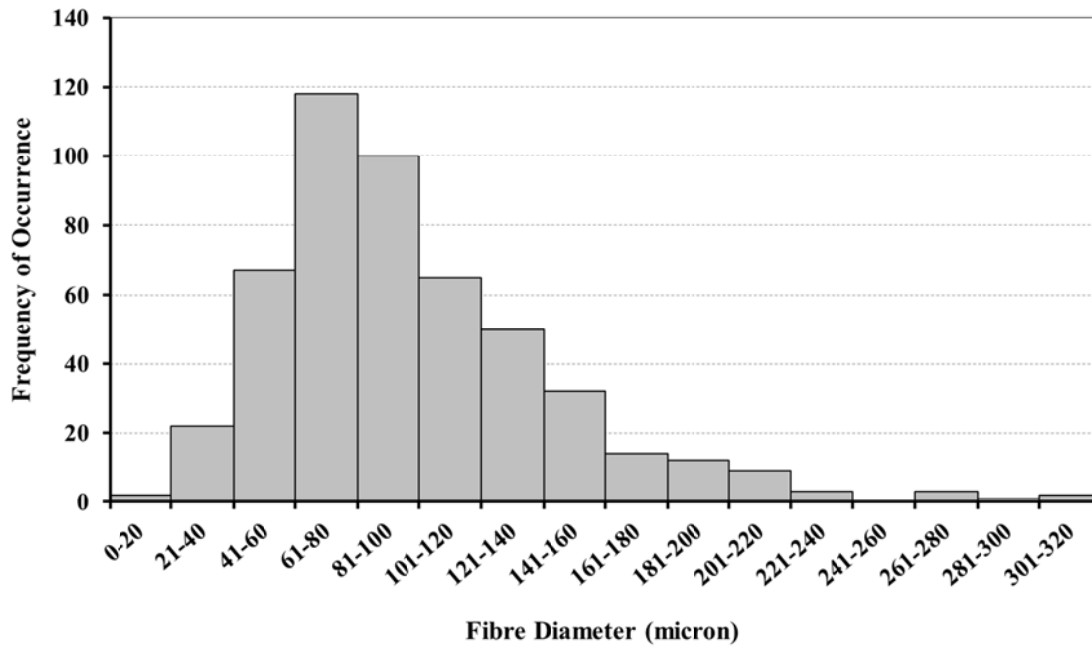


**Figure 3.22:** Histogram of measured diameters of UKF.

The average values are given in Table 3.3. The chopped fibres had an average length of 730  $\mu\text{m}$ , with a standard deviation of 51%, and an average diameter of 97  $\mu\text{m}$ , with standard deviation of 47%. This gave an aspect ratio of 7.5, Table 3.3.

**Table 3.3:** Measured lengths, diameters and aspect ratios of UKF, KFTN, KFTHA1 and KFTHA2 fibres (values in brackets represent one standard deviation)

Sample	Measured Fibre Length ( $\mu\text{m}$ )			Measured Fibre Diameter ( $\mu\text{m}$ )			Aspect Ratio
	Minimum Length	Maximum Length	Average Length	Minimum Diameter	Maximum Diameter	Average Diameter	
UKF	167.2	2,486.8	729.9 (371.1)	13.4	316.4	97.4 (45.9)	7.5
KFTN	53.5	685.0	179.5 (95.6)	3.7	24.0	11.7 (3.1)	15.3
KFTHA1	809.1	3,882.4	2,274.4 (564.1)	8.6	30.0	16.6 (3.6)	137.4
KFTHA2	872.1	3,462.4	2,312.3 (627.3)	6.9	21.9	13.0 (3.0)	178.5

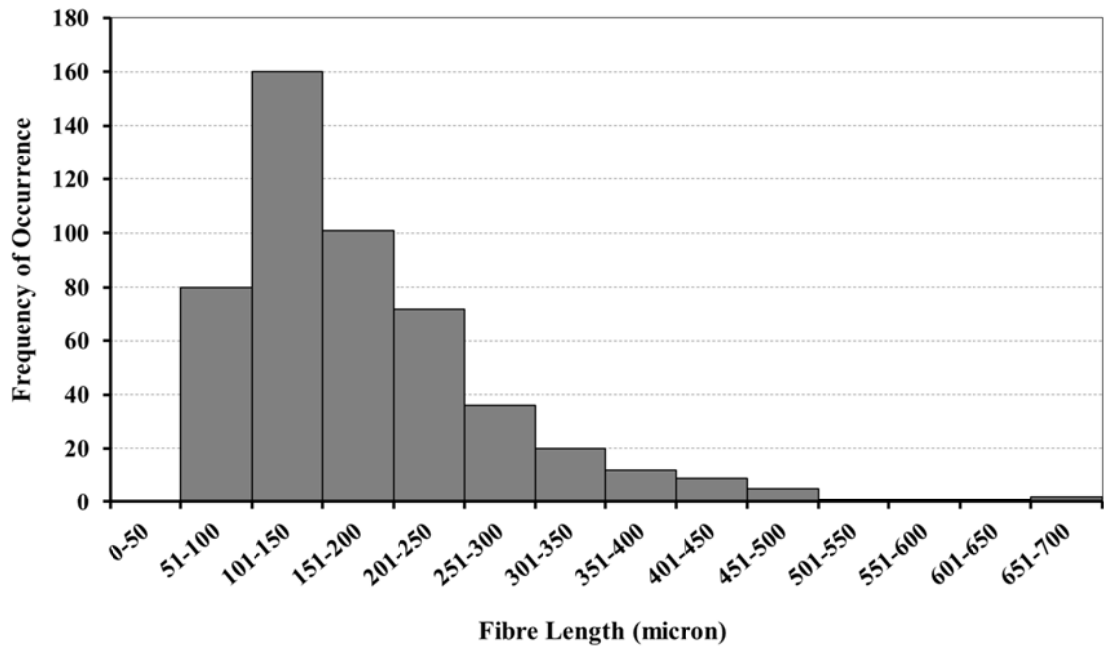


**Figure 3.23:** Histogram of measured lengths of freeze-dried KFTN.

A typical optical microscope image of the elementaries obtained using the  $\text{HNO}_3$  (KFTN) treatment (freeze-dried) is given in Figure 3.20b. Histograms of the measured lengths and diameters of the KFTN fibres are given in Figures 3.23 and 3.24,



respectively. The length is positively skewed but the width shows an essentially normal distribution. The mean length was 180  $\mu\text{m}$  (standard deviation 53%), the mean width was 11.7  $\mu\text{m}$  (standard deviation 26%), while the aspect ratio was 15.3, Table 3.3.

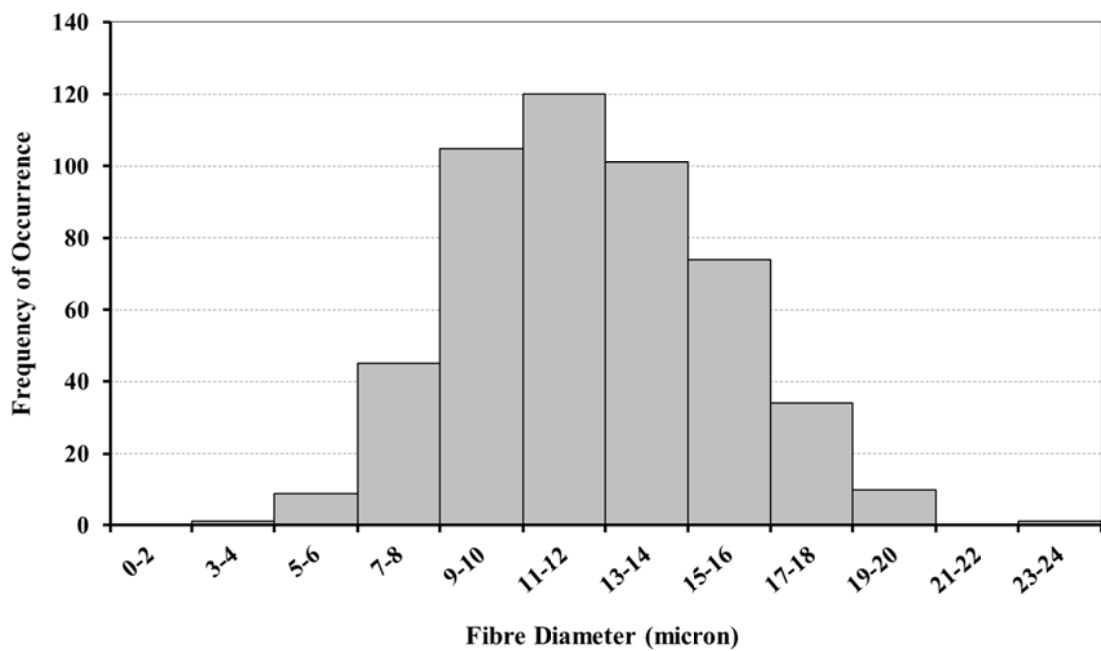


**Figure 3.24:** Histogram of measured diameters of freeze-dried KFTN.

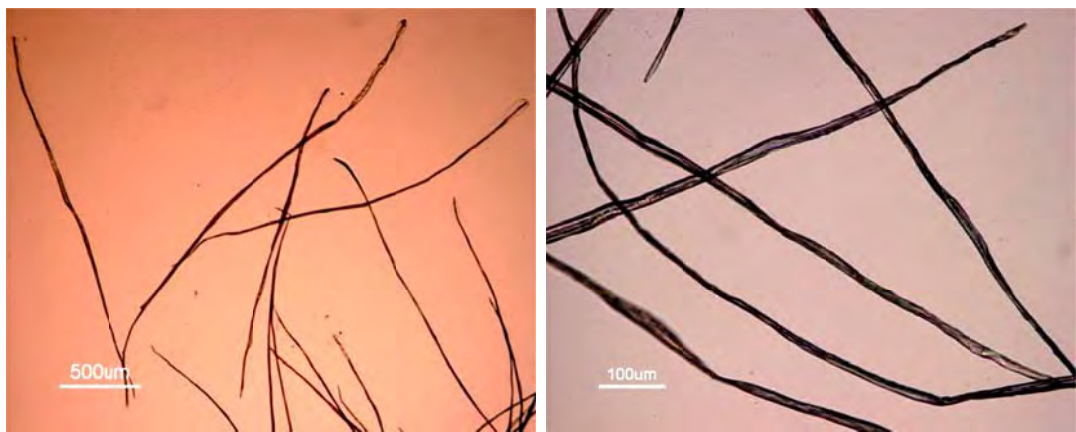


**Figure 3.25:** Typical optical microscope images of KFTHA1.

Typical optical microscope images and length and diameter histograms for the elementaries obtained from the 30% and 20% hydrogen peroxide/acetic acid treatments (KFTHA1 and KFTHA2, respectively) are shown in Figures 3.25-3.30, while the average values and the aspect ratios are included in Table 3.3. The histograms show essentially normal distributions. The mean length and diameter of the KFTHA1 fibres

were 2274  $\mu\text{m}$  (standard deviation 25%), and 16.6  $\mu\text{m}$  (standard deviation 22%), respectively, while the aspect ratio was 137. For the KFTHA2 fibres, the mean length and diameter were 2312  $\mu\text{m}$  (standard deviation 27%), and 13.0  $\mu\text{m}$  (standard deviation 23%), respectively, with the aspect ratio being 179.

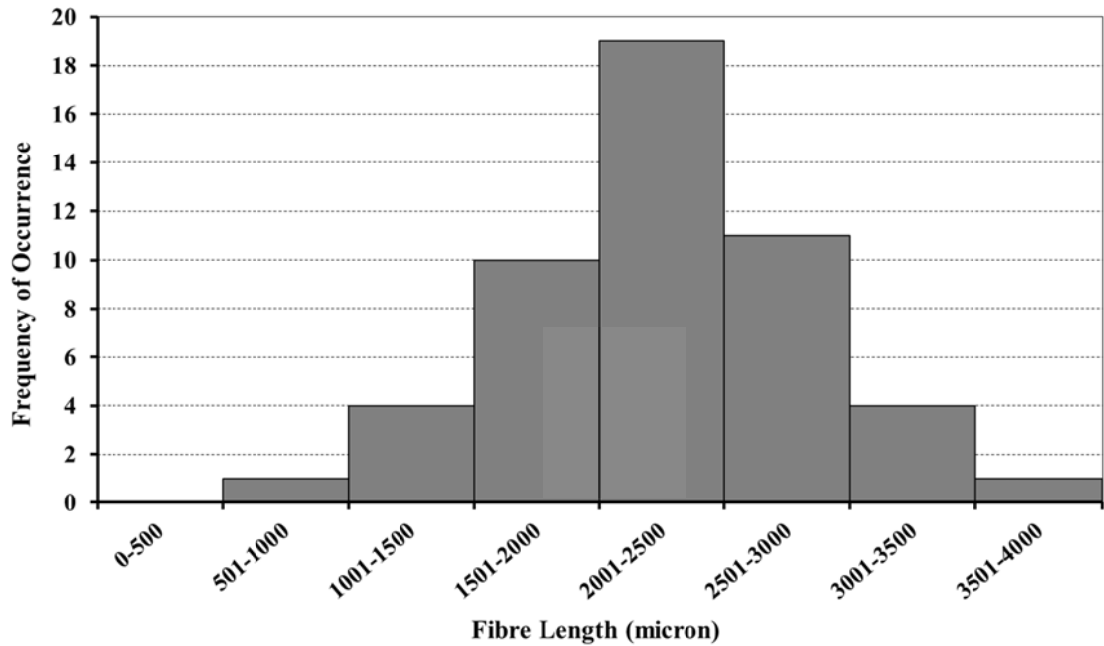


**Figure 3.26:** Histogram of measured lengths of KFTHA1.

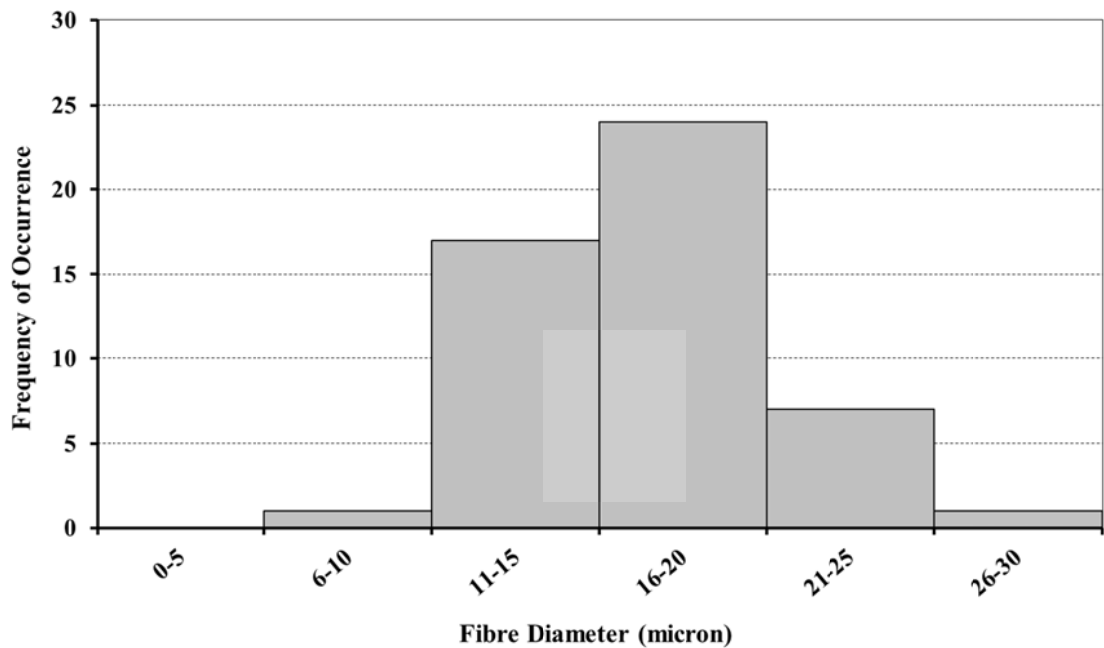


**Figure 3.27:** Histogram of measured diameters of KFTHA1.

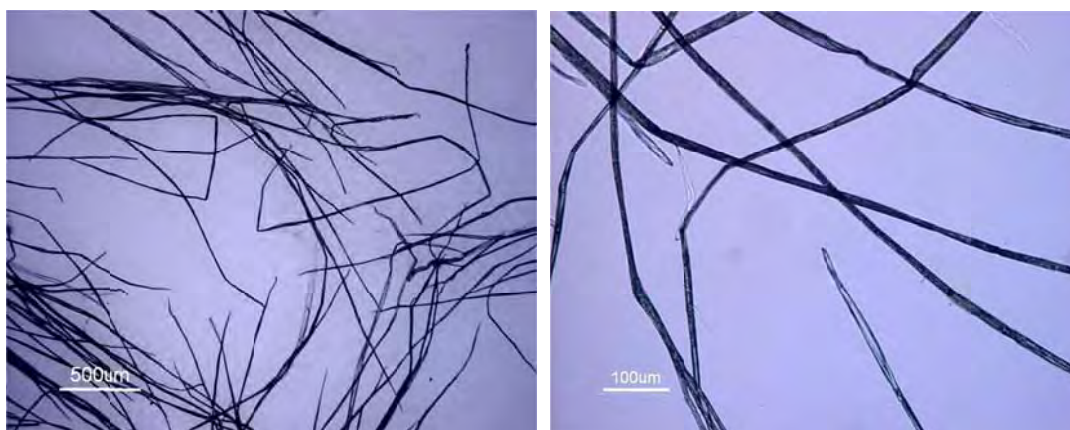


**Figure 3.28:** Typical optical microscope images of KFTHA2.

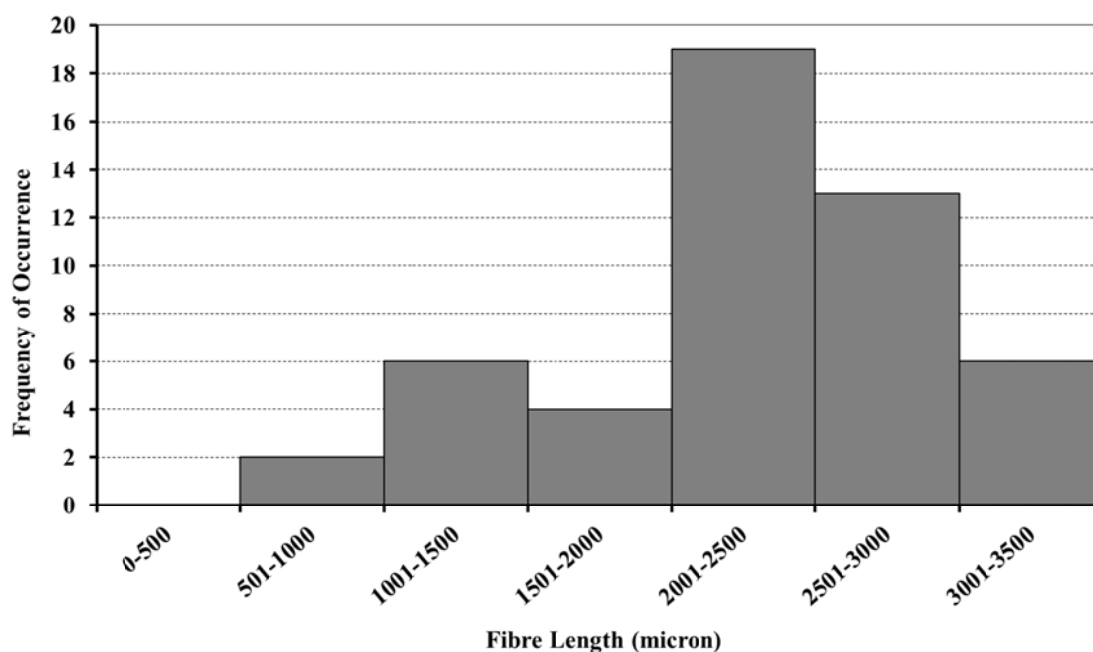


**Figure 3.29:** Histogram of measured lengths of KFTHA2.

The average fibre diameter was reasonably similar for all three treatments, ranging from 11.7 to 16.6  $\mu\text{m}$ . These values are within the range of 10-20  $\mu\text{m}$  considered to be indicative of elementary fibres (Van den Oever et al., 2000), and this provides quantitative evidence that the three processes had been successful in converting the fibre bundles to elementaries. However, there was a very substantial difference in the fibre lengths, with the elementaries obtained from the hydrogen peroxide/acetic acid treatments being an order of magnitude longer (average length of 2.3 mm) than those obtained from the nitric acid treatment (average length of 0.2 mm).

Accordingly, the aspect ratios also differed by an order of magnitude (~140-180 compared with 15 for the two different types of treatment, respectively).

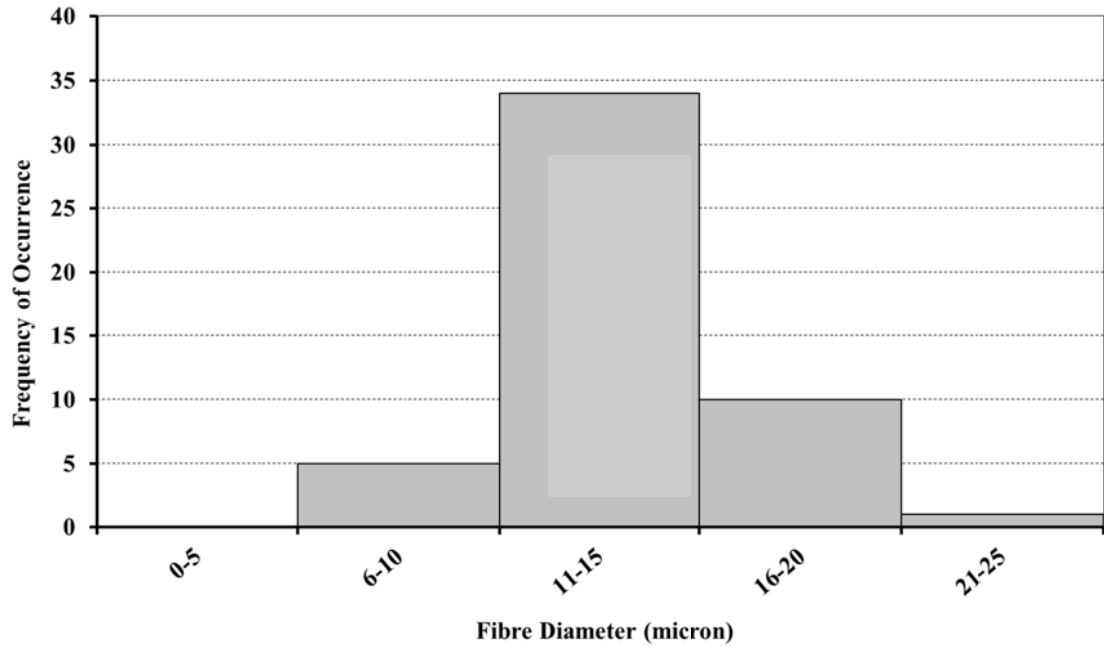


**Figure 3.30:** Histogram of measured diameters of KFTHA2.

### 3.4.3 Defect Density of Elementary Fibres

Examples of the defects seen in the elementary fibres using the initial techniques described in Section 3.3.4 are shown in Figures 3.31-3.36, while the defects observed using a scanning electron microscope operated in secondary electron mode are shown for the KFTN, KFTHA1 and KFTHA2 fibres in Figures 3.37-3.42. The defects present were similar for all three treatments and were nodes, pits, dislocations, micro-compressions, initial breaks, and kinks.

The defect density for the three treatments is shown in Figure 3.43 while the data for each of the ten fibres examined for each treatment is given in Appendix II. The defect density was significantly higher (t-test output, Appendix III) for the KFTN fibres than for the KFTHA1 and KFTHA2 fibres with the values being 21 (standard deviation of 9), 14 (standard deviation of 8) and 14 (standard deviation of 4) defects per millimeter, respectively.

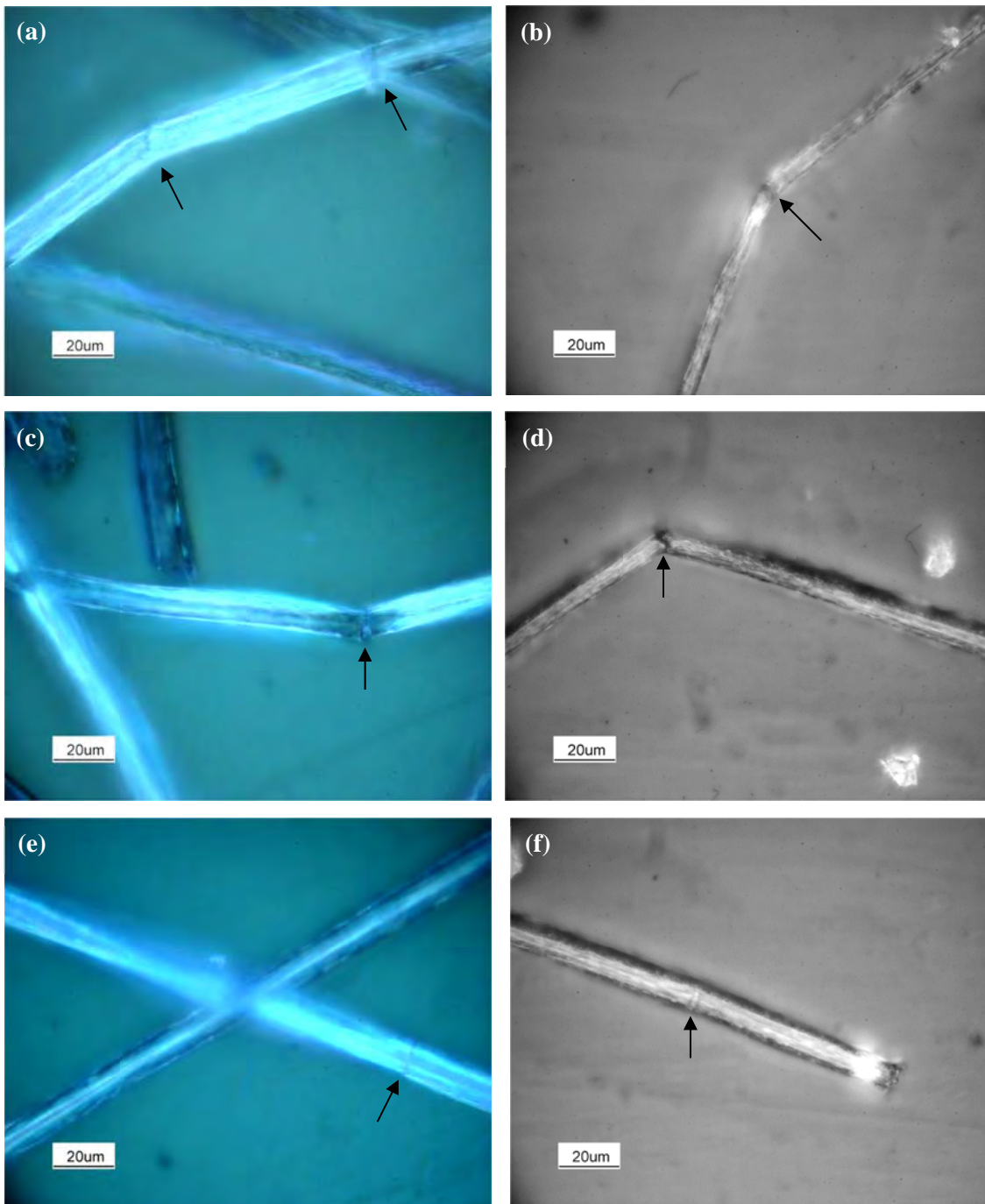


**Figure 3.31:** Transmitted light micrographs of the KFTN fibres showing kinks (a-c), initial breaks (d) and micro-compressions (e-f).

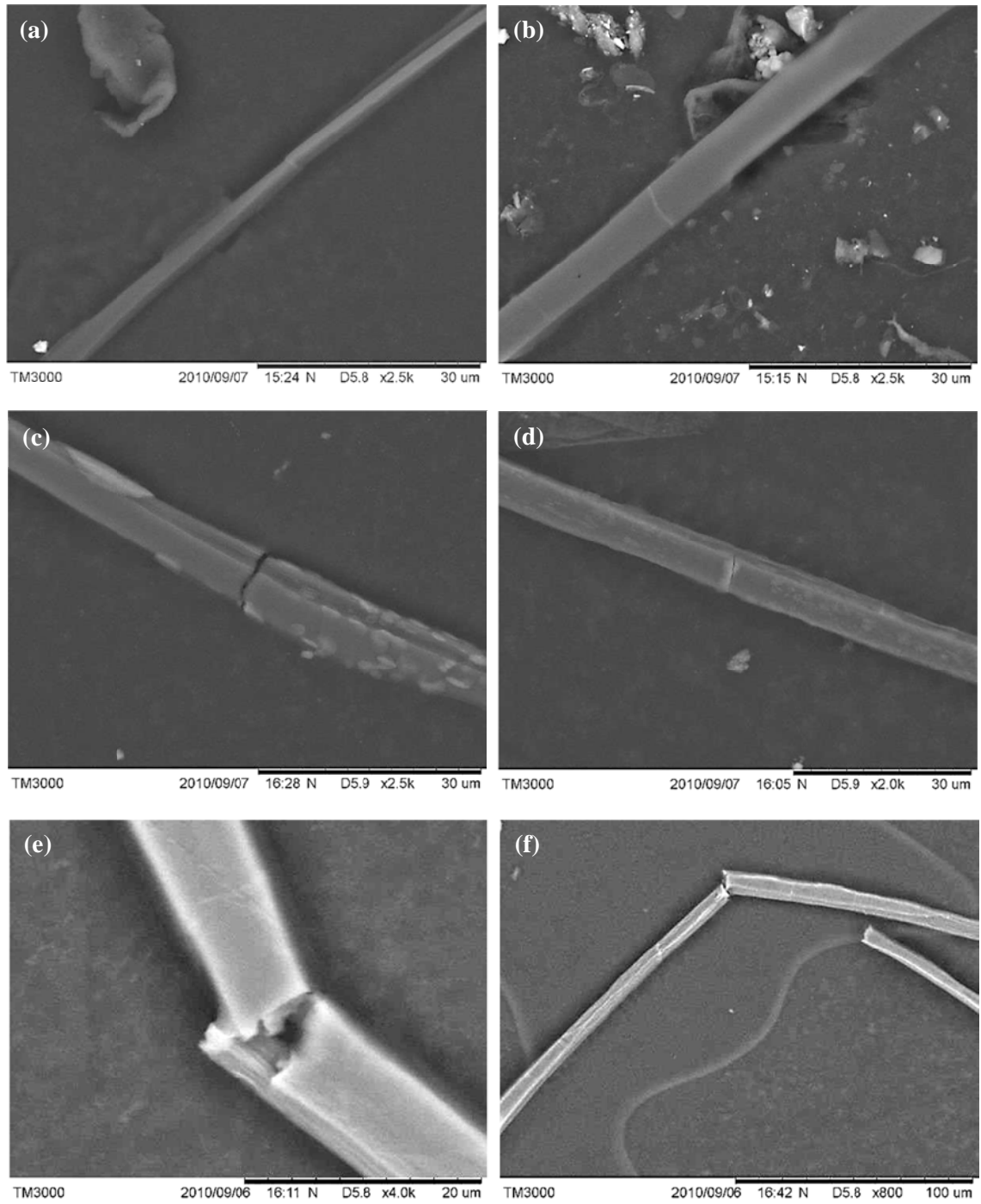


**Figure 3.32:** SEM micrographs (BSE) of uncoated KFTN fibres showing micro-compressions (a-b) and initial breaks (c-f) at 2,500 $\times$  (a-c), 2,000 $\times$  (d), 4000 $\times$  (e), and 800 $\times$  (f) magnification.

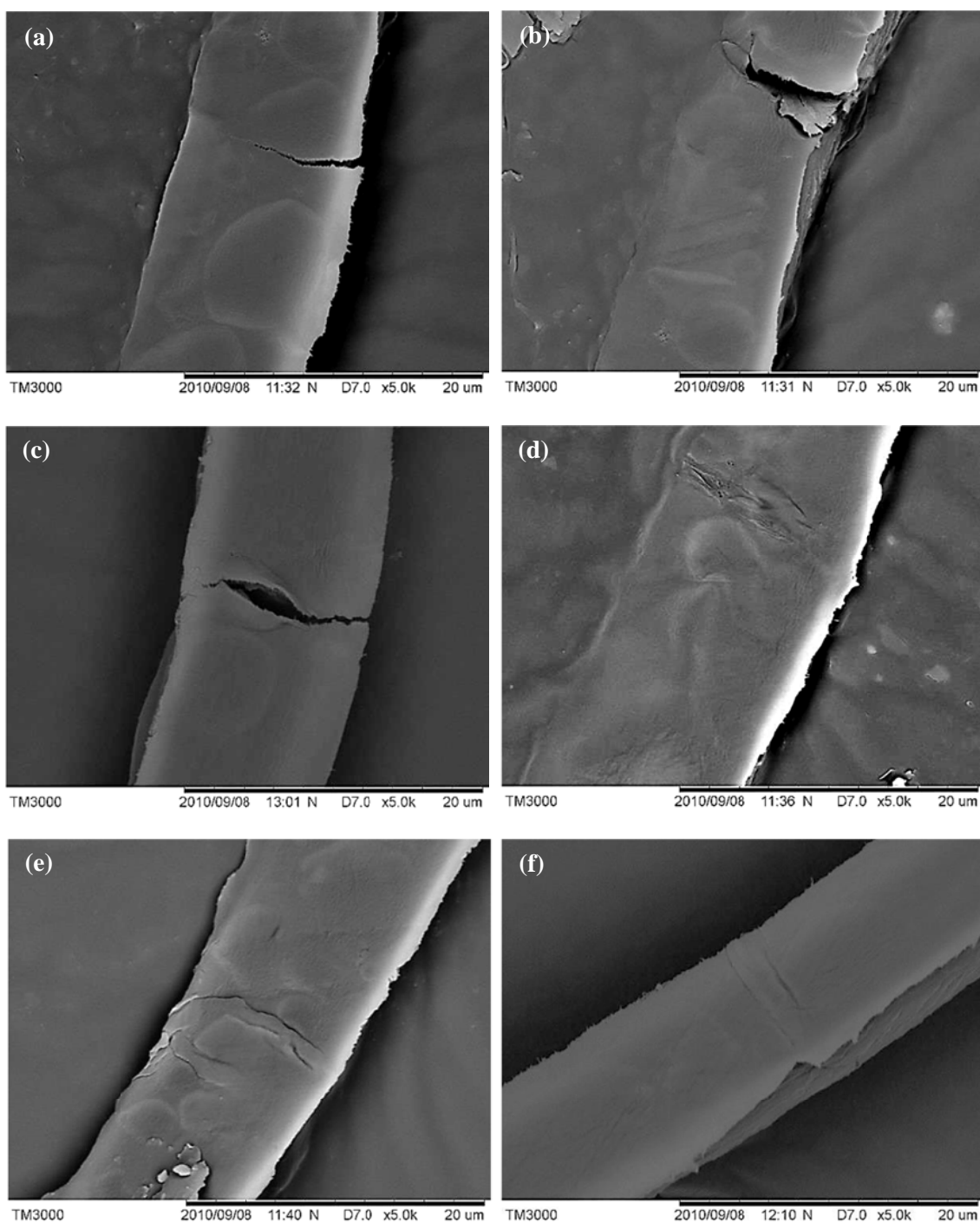


**Figure 3.33:** SEM micrographs (BSE) of coated KFTN fibres showing initial breaks (a-c), micro-compressions (d-e) and node (f) at 5000× magnification.



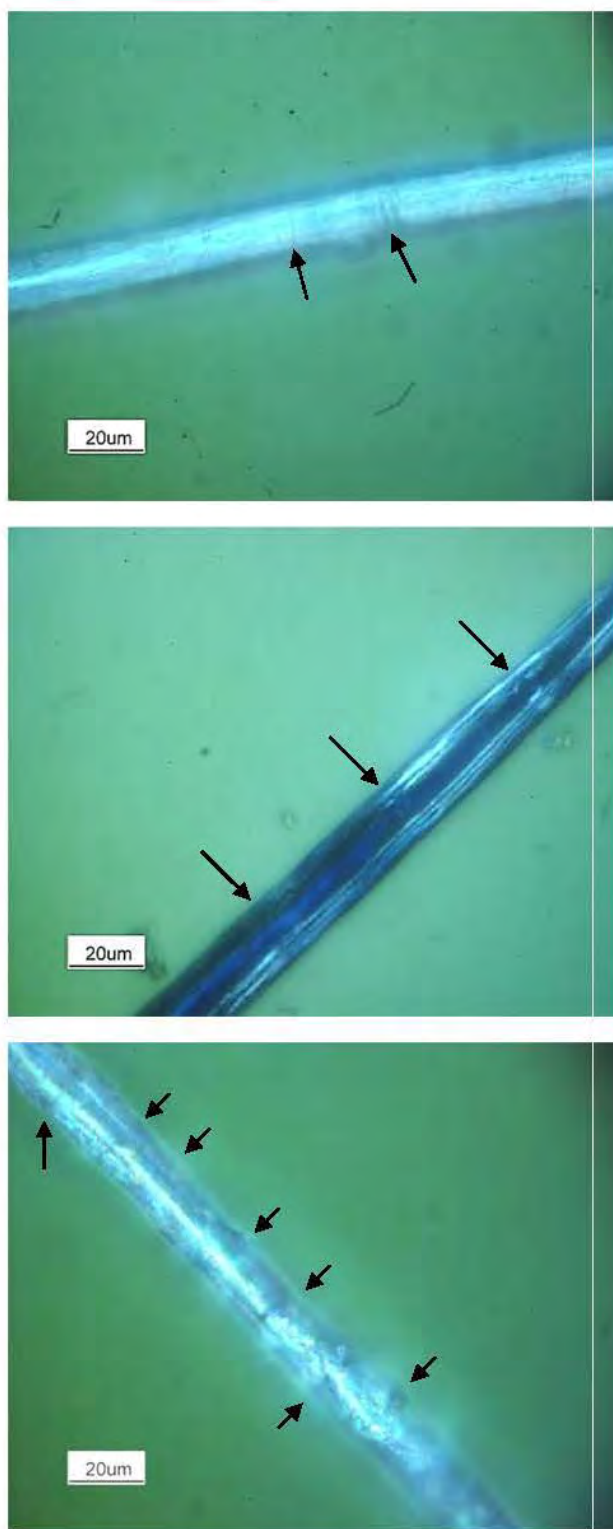


**Figure 3.34:** Transmitted light micrographs of the wet KFTN fibres showing micro-compressions.



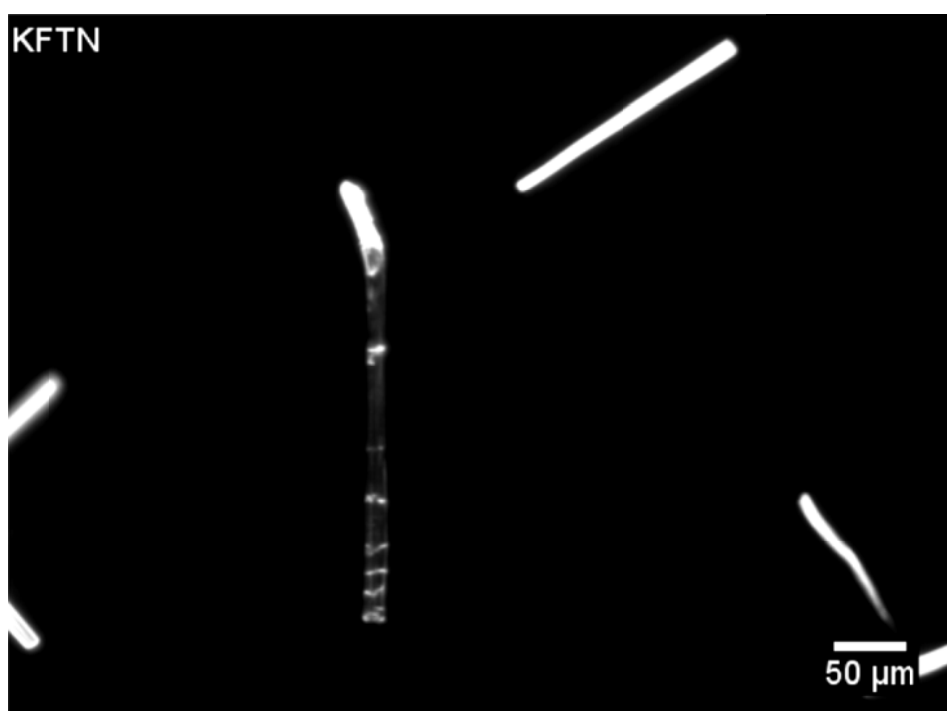


**Figure 3.35:** Cross-polarised light micrograph of KFTN fibres showing dislocations.



**Figure 3.36:** Cross-polarised light micrograph of KFTHA2 fibres showing nodes and dislocations.

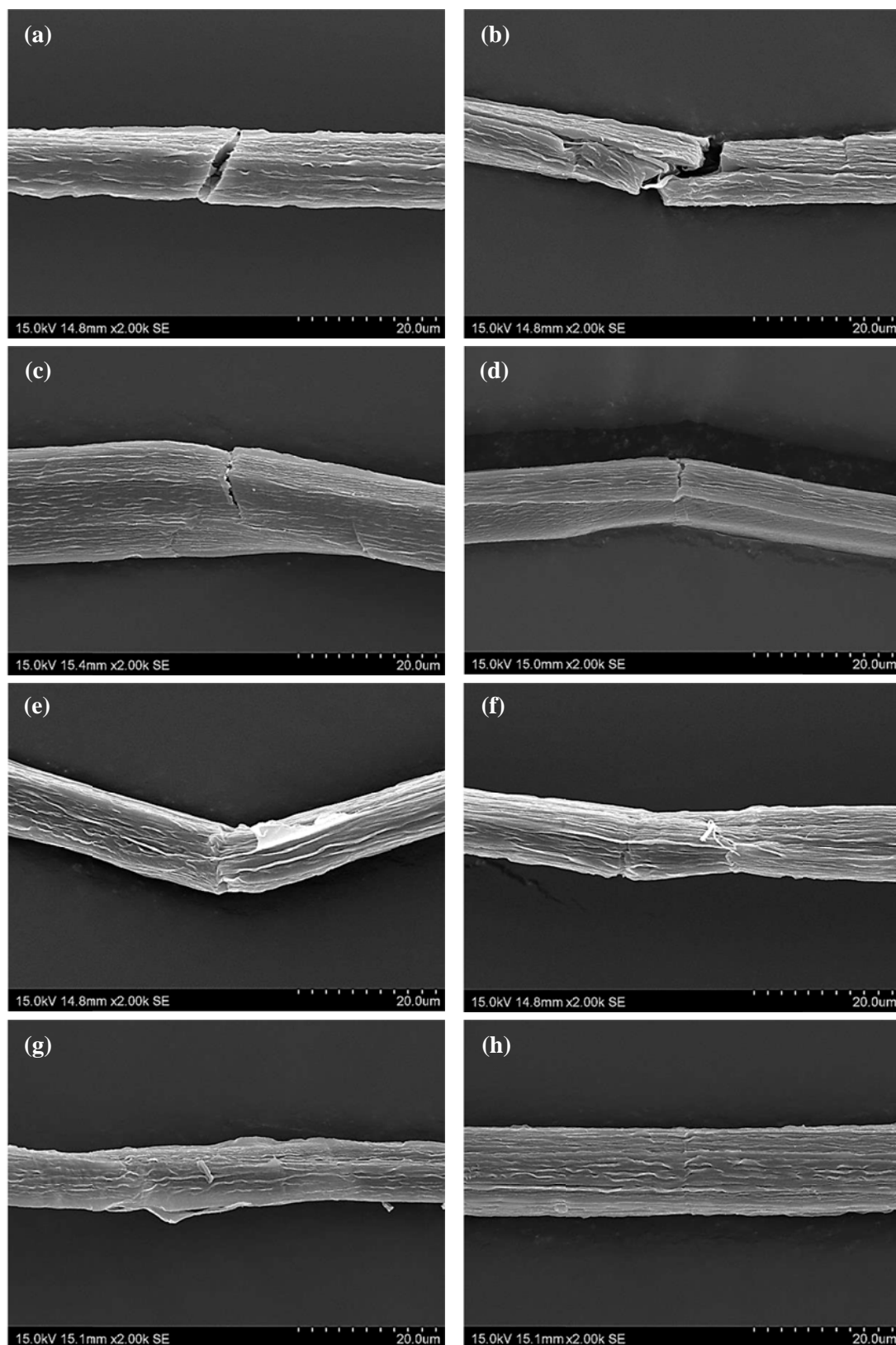


**Figure 3.37:** SEM micrographs (SE) of coated KFTN fibres (at 2000 $\times$  magnification) showing initial breaks (a-d), kinks (e-g) and micro-compression (h).

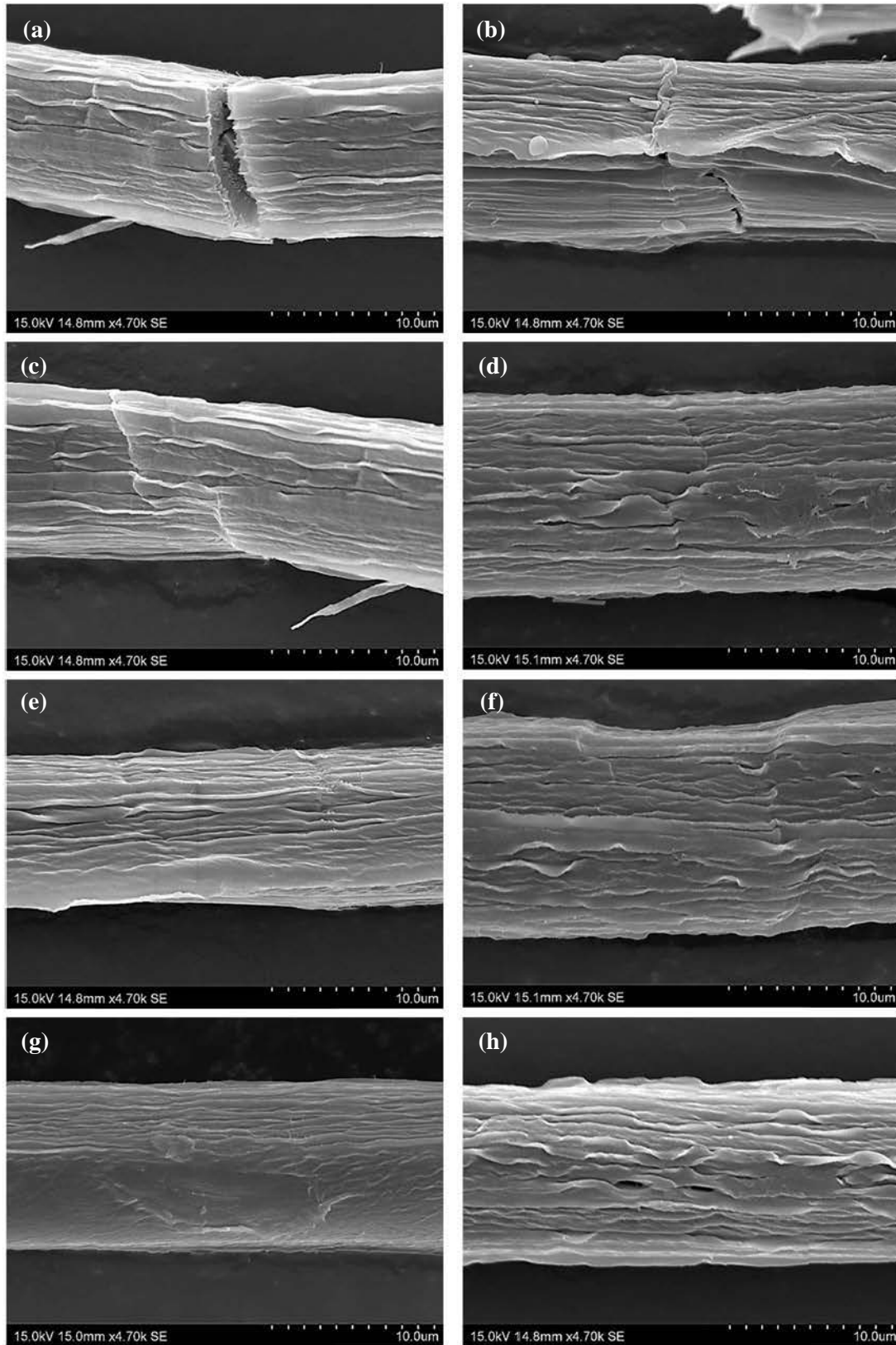


**Figure 3.38:** SEM micrographs (SE) of coated KFTN fibres (at 4700 $\times$  magnification) showing initial breaks (a-b), dislocations (c-d), micro-compressions (e-g) and pits (h).

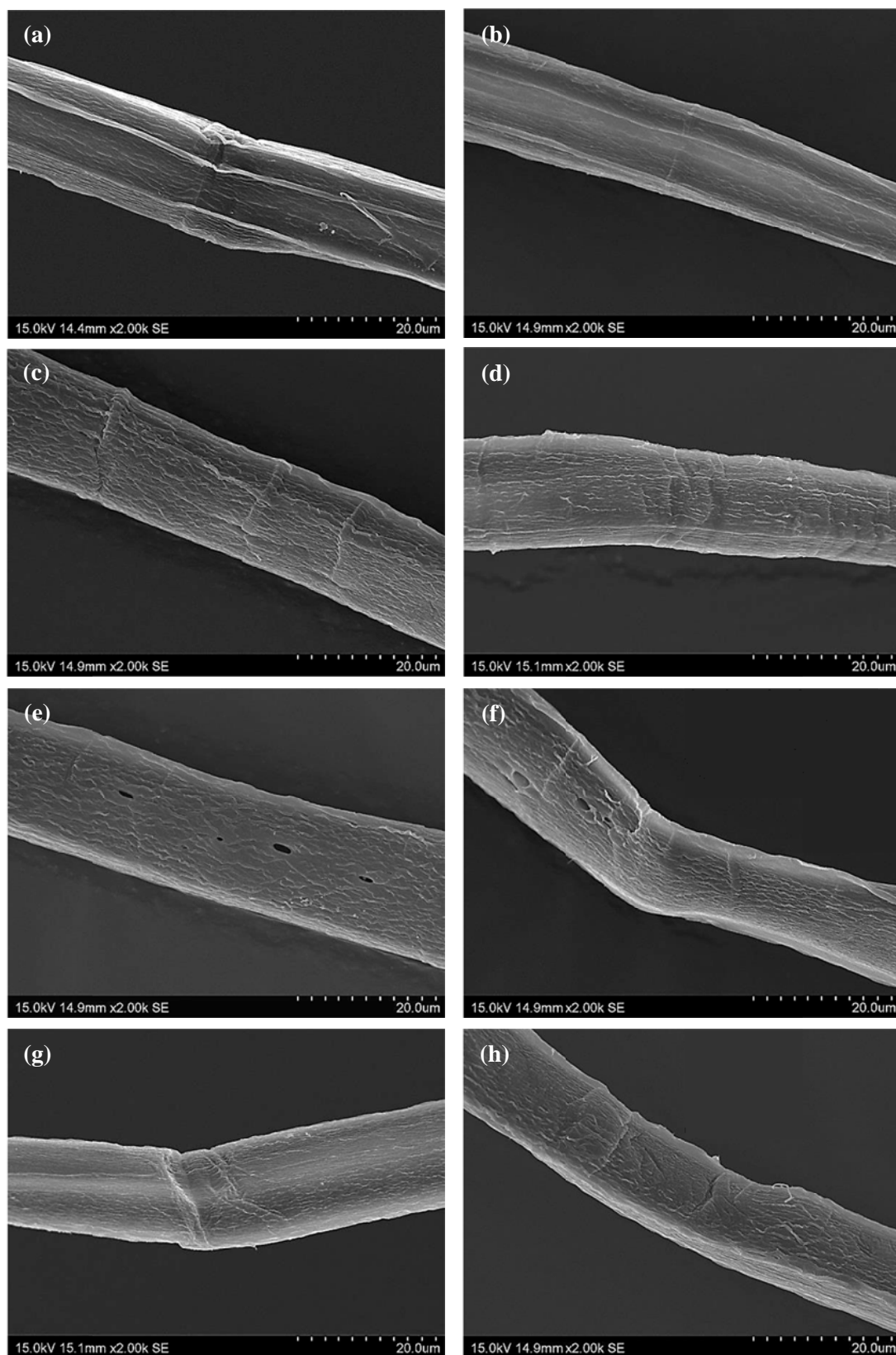


**Figure 3.39:** SEM micrographs (SE) of coated KFTHA1 fibres (at 2000 $\times$  magnification) showing nodes (a-c), dislocations (d), pits (e-f) and kinks (f-h).

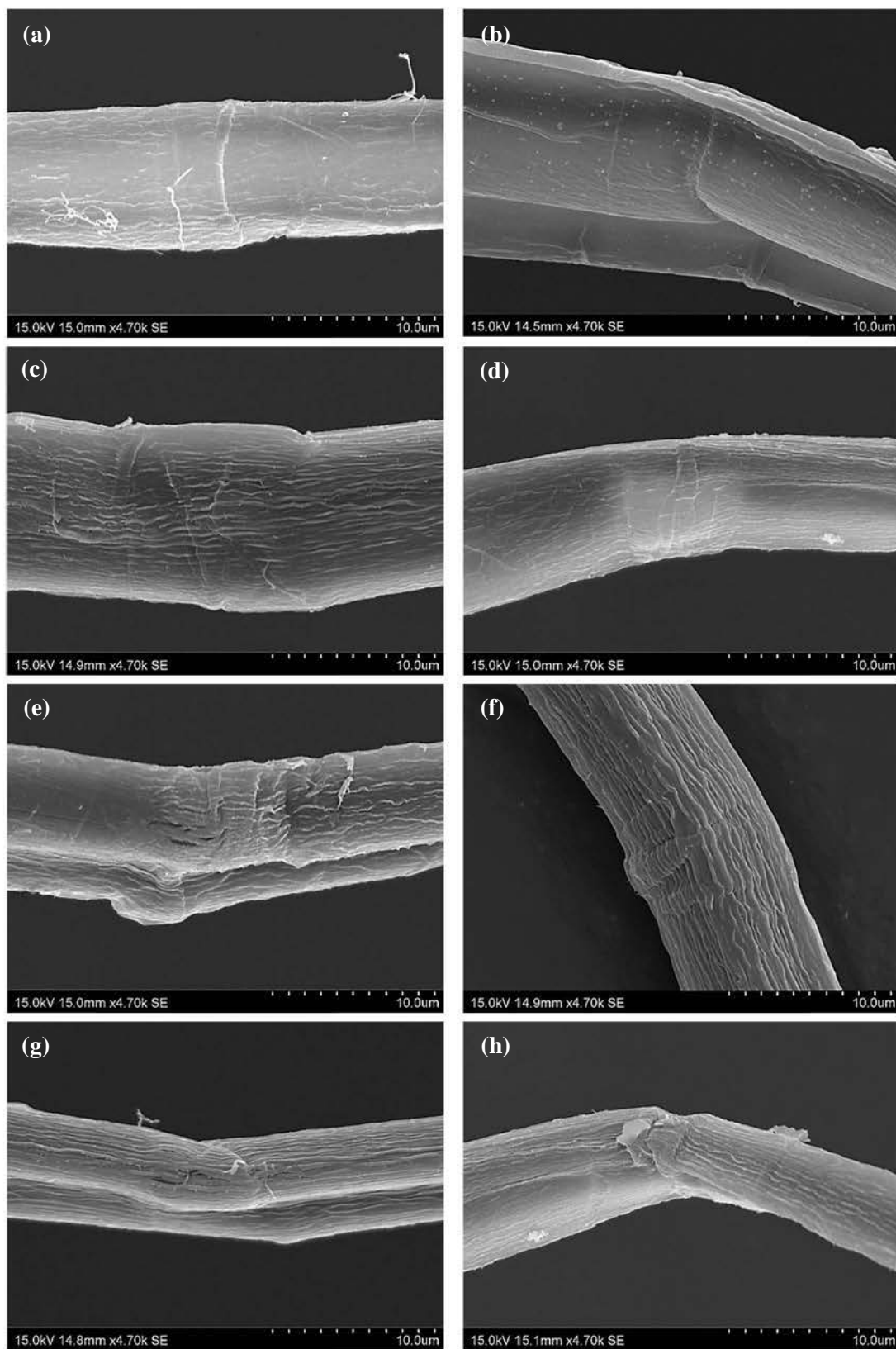


**Figure 3.40:** SEM micrographs (SE) of coated KFTHA1 fibres (at 4700 $\times$  magnification) showing micro-compression (a) and kinks (b-h).

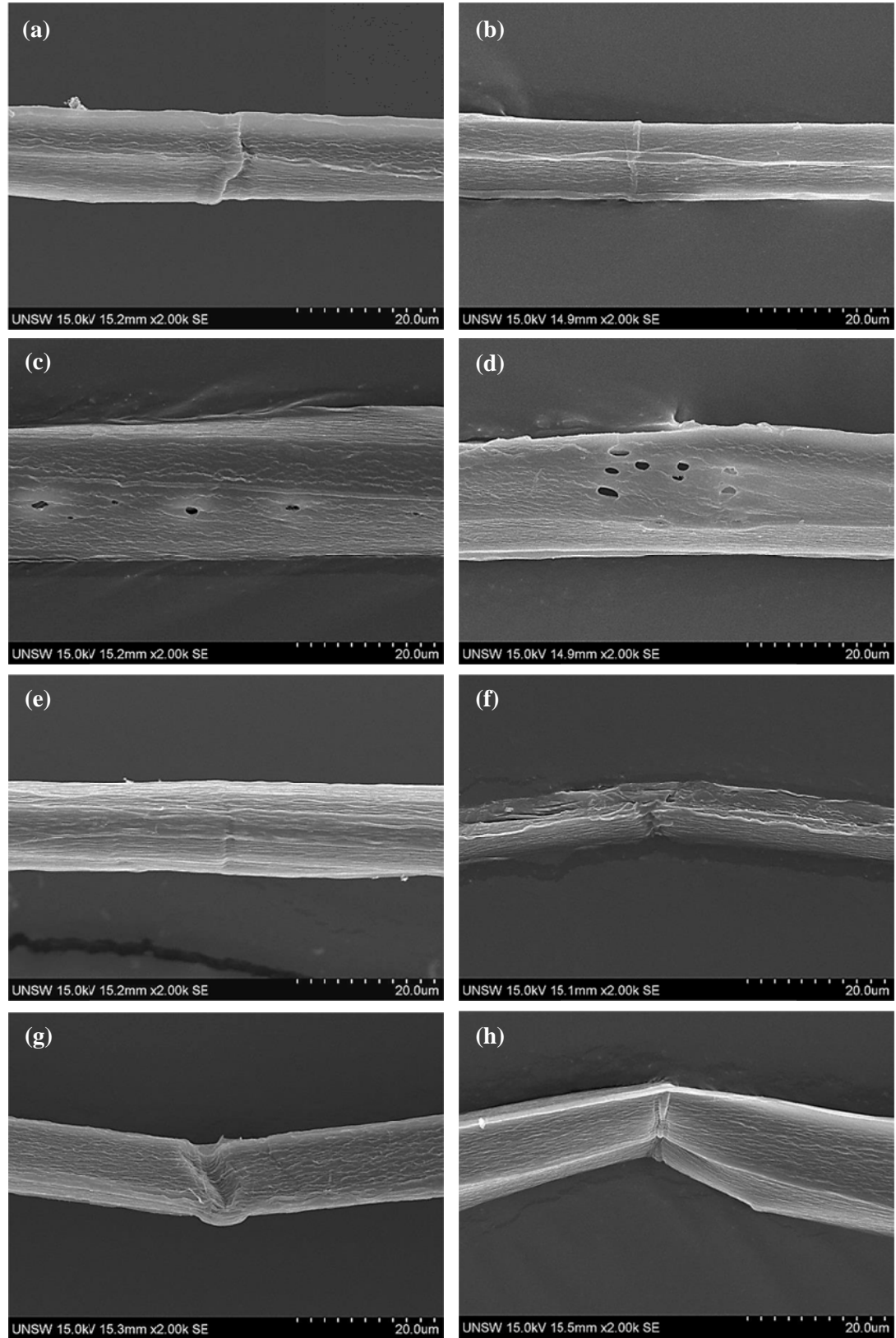


**Figure 3.41:** SEM micrographs (SE) of coated KFTHA2 fibres (at 2000 $\times$  magnification) showing nodes (a-b), pits (c-d), micro-compressions (e), initial break (f) and kinks (g-h).

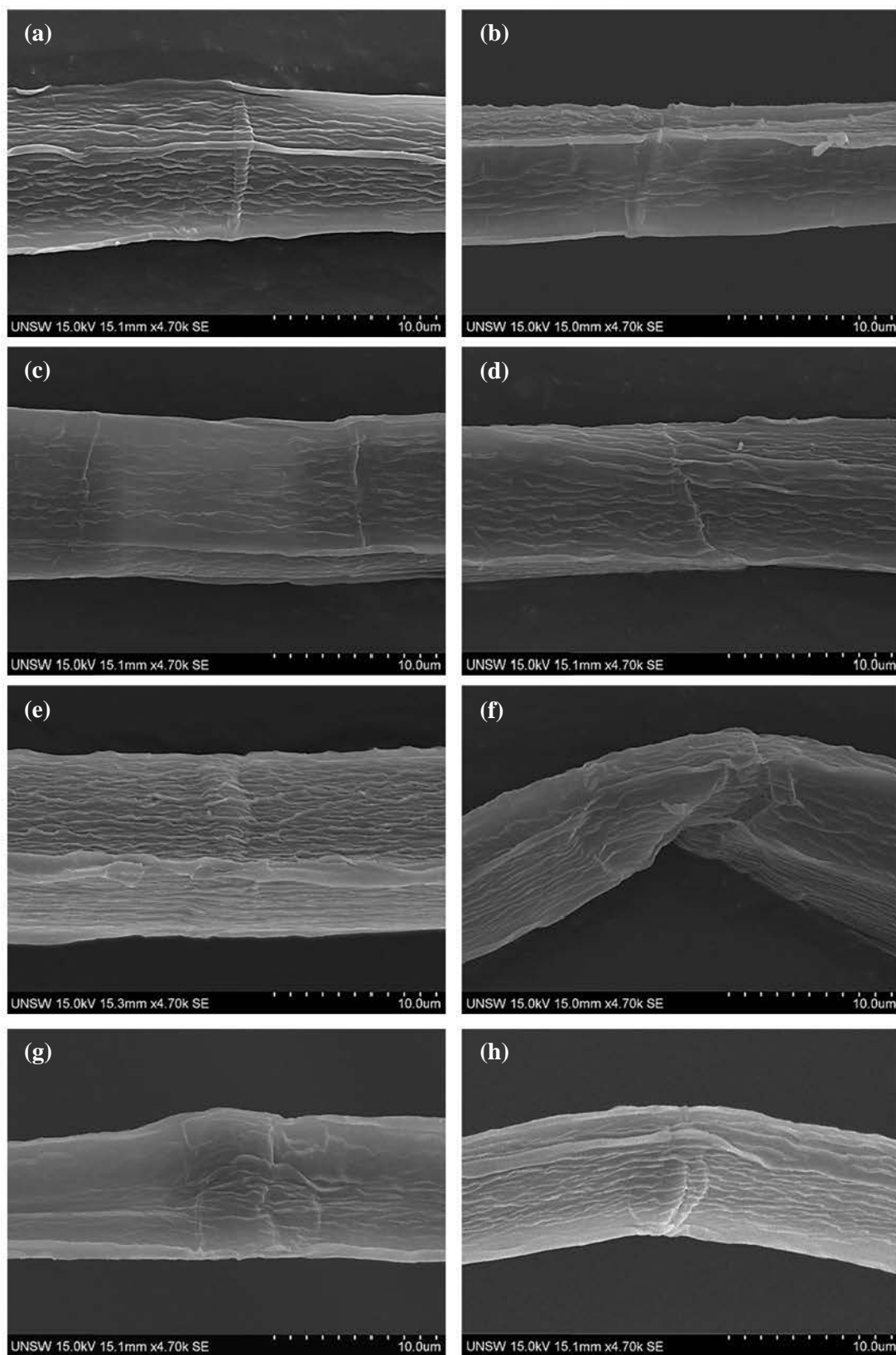


**Figure 3.42:** SEM micrographs (SE) of coated KFTHA2 (at 4700× magnification) showing nodes (a), micro-compressions (b-e) and kinks (f-h).

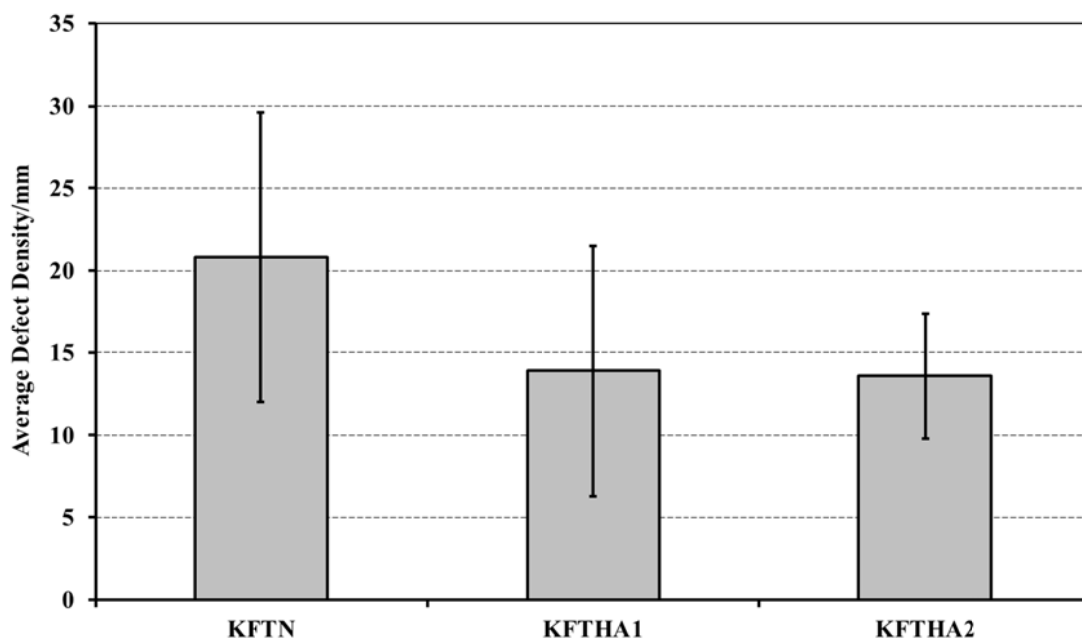


**Figure 3.43:** Average defect density of KFTN, KFTHA1 and KFTHA2 fibres. Error bars represent one standard deviation.

### 3.4.4 FTIR Spectra

FTIR spectra of the untreated fibre bundles (UKF), fibres treated with  $\text{HNO}_3$  (KFTN), fibres treated with 30%  $\text{H}_2\text{O}_2/\text{CH}_3\text{COOH}$  (KFTHA1) and fibres treated with 20%  $\text{H}_2\text{O}_2/\text{CH}_3\text{COOH}$  (KFTHA2) are shown in Figure 3.44, while spectra obtained for  $\alpha$ -cellulose in the untreated condition (AC), after treatment with  $\text{HNO}_3$  (ACTN), and after the two  $\text{H}_2\text{O}_2/\text{CH}_3\text{COOH}$  treatments (ACTHA1 and ACTHA2) are shown in Figure 3.45. The peak assignments obtained from the literature are summarized in Table 3.4 while the sources for the assignments are given in Table 3.5.

The spectra from the fibres all show peaks at  $3,329\text{ cm}^{-1}$  (O-H stretching (Moran, Alvarez, Cyras & Vazquez, 2008)),  $2,900\text{ cm}^{-1}$  (C-H stretching (Moran et al., 2008)),  $1,635\text{ cm}^{-1}$  (O-H bending (Han, et al., 2007; Moran, et al., 2008))  $1,420\text{ cm}^{-1}$  (- $\text{CH}_2$  and OCH in-plane bending (Dai & Fan, 2010)),  $1,360\text{ cm}^{-1}$  (C-H bending (Dai & Fan, 2010)),  $1,313\text{ cm}^{-1}$  (- $\text{CH}_2$  wagging (Dai & Fan, 2010)),  $1,170\text{-}1,082\text{ cm}^{-1}$  (pyranose ring skeletal C-O-C (Dai & Fan, 2010)),  $1,102\text{ cm}^{-1}$  (C-OH group (Dai & Fan, 2010)) and  $893\text{ cm}^{-1}$  (COC, CCO and CCH deformation and stretching (Dai & Fan, 2010)). These peaks are all characteristic of cellulose, although the peaks at  $3,329\text{ cm}^{-1}$ ,  $2,900$



$\text{cm}^{-1}$  and  $1,102 \text{ cm}^{-1}$  are also seen in hemicellulose and lignin. The spectra also show a peak at  $1,635 \text{ cm}^{-1}$  which is attributed to the presence of moisture.

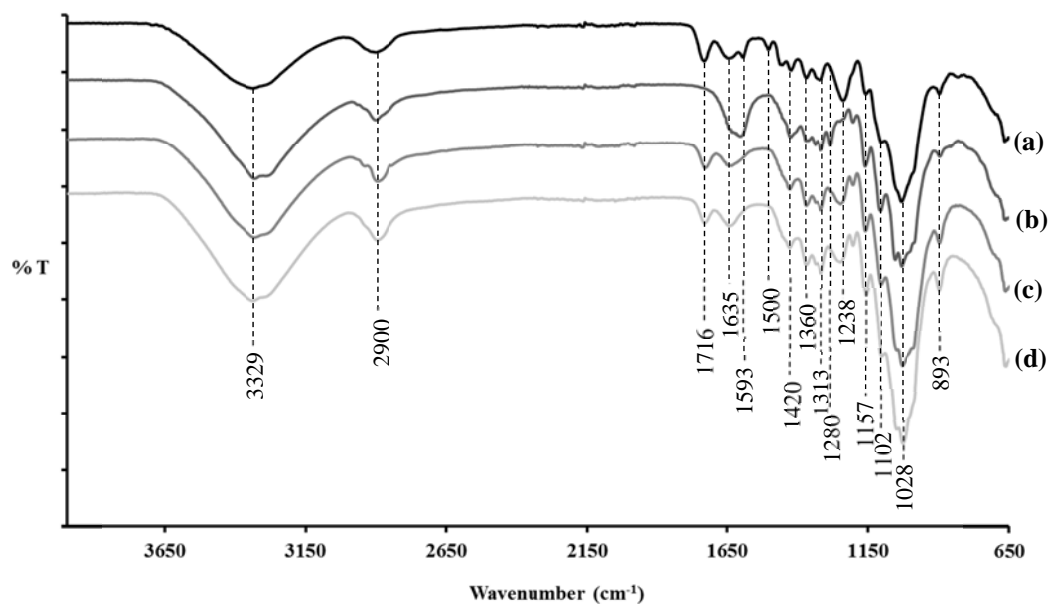


**Figure 3.44:** FTIR spectra of (a) UKF, (b) KFTN, (c) KFTHA1 and (d) KFTHA2.

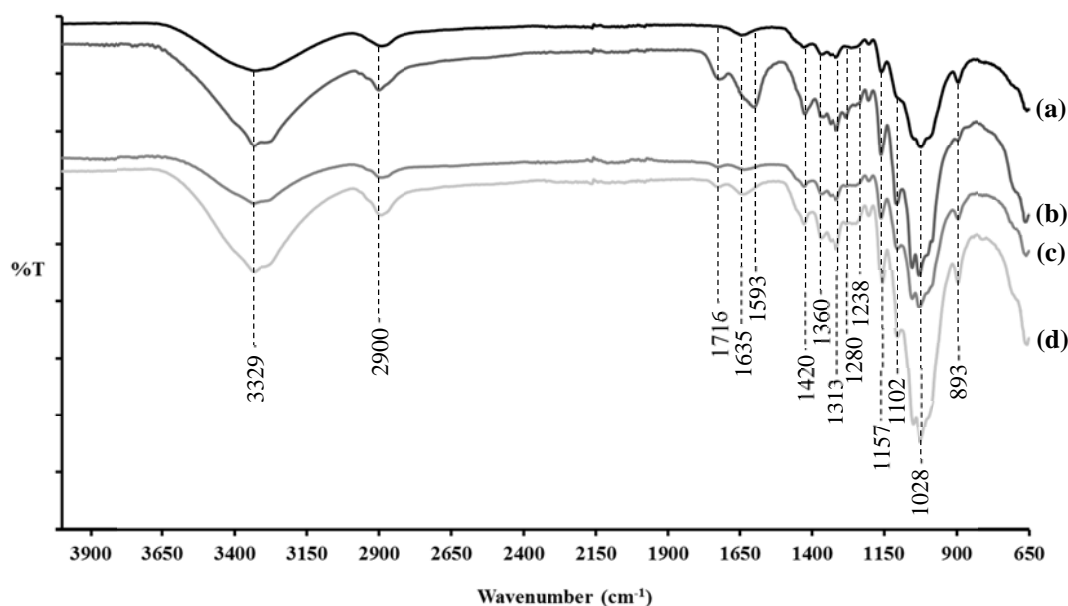


**Figure 3.45:** FTIR spectra of (a) AC, (b) ACTN, (c) ACTHA1 and (d) ACTHA2.

**Table 3.4:** Assignments of peak positions of FTIR bands of kenaf fibres and  $\alpha$ -cellulose in untreated and treated conditions

Peak Position (cm <sup>-1</sup> )	Assignment	Sample								Source
		UKF	KFTN	KFTHA1	KFTHA2	AC	ACTN	ACTHA1	ACTHA2	
3,329	O-H stretching vibrations in cellulose, hemicellulose and lignin	×	×	×	×	×	×	×	×	1
2,900	C-H stretching vibrations in cellulose, hemicellulose and lignin	×	×	×	×	×	×	×	×	2
1,716	C=O stretching vibrations of ketone and carbonyl groups in hemicellulose, pectin and waxes	×		×	×		×	×	×	3
	C=O stretching vibrations of carboxylic groups in oxidised cellulose and/or those of acetyl groups due to mixtures of H <sub>2</sub> O <sub>2</sub> and CH <sub>3</sub> COOH									4
1,635	O-H bending vibrations due to moisture absorption	×	×	×	×	×	×	×	×	5
1,593	C=C aromatic in-plane vibrations combined with C=O stretching vibrations in lignin	×	×				×			6
	-NO <sub>2</sub> asymmetrical stretching vibrations									7
1,500	C=C aromatic in-plane vibrations in lignin	×								8
1,420	-CH <sub>2</sub> and OCH in-plane bending vibrations in cellulose	×	×	×	×	×	×	×	×	9
1,360	C-H bending vibrations in cellulose	×	×	×	×	×	×	×	×	10
1,313	-CH <sub>2</sub> wagging vibrations in cellulose	×	×	×	×	×	×	×	×	11
1,280	-NO <sub>2</sub> symmetrical stretching vibrations		×				×			12
1,238	C-O stretching vibrations of acetyl groups in lignin	×		×	×			×	×	13
	C-O stretching vibrations of acetyl groups due to mixtures of H <sub>2</sub> O <sub>2</sub> and CH <sub>3</sub> COOH									14
1,170-1,082	Pyranose ring skeletal in cellulose	×	×	×	×	×	×	×	×	15
1,102	C-OH group frequency in cellulose, hemicellulose and lignin	×	×	×	×	×	×	×	×	16
893	COC, CCO and CCH deformation and stretching vibrations in cellulose	×	×	×	×	×	×	×	×	17

**Table 3.5:** Sources for assignments of peak positions of FTIR spectra

Source	
1	Moran et al. (2008)
2	Moran et al. (2008)
3	Dai & Fan (2010), Li & Pickering (2008), and Moran et al. (2008)
4	Luz et al. (2008) and Silverstein, Webster & Kiemle (2005)
5	Han, et al. (2007) and Moran, et al. (2008)
6	Garside & Wyeth (2003) and Kubo & Kadla (2005)
7	Samal & Ray (1997)
8	Kubo & Kadla (2005)
9	Dai & Fan (2010)
10	Dai & Fan (2010)
11	Dai & Fan (2010)
12	Edge et al. (1990) and Silverstein, Webster & Kiemle (2005)
13	Sgriccia et al. (2008)
14	Tserki et al. (2005)
15	Dai & Fan (2010)
16	Dai & Fan (2010)
17	Dai & Fan (2010)

There are however significant differences between the spectra obtained for the different fibre treatments, Figure 3.44. The untreated fibres (UKF) show a peak at  $1,500\text{ cm}^{-1}$  which is attributed to the C=C aromatic in plane vibrations in lignin (Kubo & Kadla, 2005). This peak is absent in the treated fibres indicating that all three treatments have removed the lignin.

The untreated fibres also show a peak at  $1,716\text{ cm}^{-1}$  which is attributed to C=O stretching of ketone and carbonyl groups in hemicellulose (Moran et al., 2008), pectin and waxes (Dai & Fan, 2010; Li & Pickering, 2008). This peak is again absent for KFTN but a peak at the same wavenumber is present for the two KFTHA treatments. However, for these treatments the peak is attributed to C=O stretching corresponding to carboxylic groups (Silverstein, Webster & Kiemle, 2005) from oxidised cellulose and/or acetyl groups (Luz, Del Tio, Rocha, Goncalves & Del'Arco Jr, 2008) due to the  $\text{H}_2\text{O}_2/\text{CH}_3\text{COOH}$  treatment. The results are therefore considered to indicate that pectin and waxes have been removed by the fibre treatments.

In addition, the untreated fibres show a peak at  $1,593\text{ cm}^{-1}$ . This is attributed to C=C aromatic in-plane vibrations combined with C=O stretching, which is again indicative of lignin (Garside & Wyeth, 2003; Kubo & Kadla, 2005). This peak is absent for the two KFTHA treatments although a peak at the same wavenumber is present for KFTN. This peak is however considered to be due to  $-\text{NO}_2$  asymmetrical stretching

vibrations (Samal & Ray, 1997) resulting from the reaction between cellulose and  $\text{HNO}_3$  (Gert, Morales, Zubets & Kaputskii, 2000).

A further peak is evident for the untreated fibres at  $1,238\text{ cm}^{-1}$  and this is attributed to C-O stretching of acetyl groups from lignin (Sgriccia et al., 2008). A peak is also present at the same wavenumber for the two KFTHA treatments but this is attributed to C-O stretching of acetates (Tserki, Zafeiropoulos, Simon & Panayiotou, 2005) resulting from reaction of cellulose with  $\text{H}_2\text{O}_2/\text{CH}_3\text{COOH}$ . The assignment of this peak to species other than lignin is consistent with the absence of the  $1,500\text{ cm}^{-1}$  lignin peak in the treated fibres.

The KFTN fibres exhibit a peak at  $1,280\text{ cm}^{-1}$  which is not present for the other treatments. This peak is attributed to  $-\text{NO}_2$  symmetrical stretching (Edge, Allen, Hayes, Riely, Horie & Luc-Gardette, 1990; Silverstein, Webster & Kiemle, 2005) due to reaction between cellulose and  $\text{HNO}_3$  (Gert et al., 2000) and is not considered to be due to the presence of lignin.

The FTIR spectrum of the untreated  $\alpha$ -cellulose (AC) was similar to that for the untreated fibres (UKF), Figure 3.44a except for the absence of the  $1,716\text{ cm}^{-1}$ ,  $1,593\text{ cm}^{-1}$ ,  $1,500\text{ cm}^{-1}$ , and  $1,238\text{ cm}^{-1}$  peaks. This confirms that the presence of these peaks in the untreated fibre spectrum was due to the presence of hemicellulose, lignin, pectin or waxes, all of which are absent in  $\alpha$ -cellulose.

The spectrum from  $\alpha$ -cellulose treated with  $\text{HNO}_3$  (ACTN) contained the same peaks as the nitric acid treated fibres (KFTN), except for the addition a peak at  $1,716\text{ cm}^{-1}$ , which is attributed to the presence of some oxidized cellulose.

The spectra from  $\alpha$ -cellulose treated with the two  $\text{H}_2\text{O}_2/\text{CH}_3\text{COOH}$  solutions (ACTHA1 and ACTHA2) contained the same peaks as the fibres treated with the same solutions (KFTHA1 and KFTHA2).

### 3.4.5 Raman Spectra

Raman spectra of the untreated (UKF), and treated (KFTN, KFTHA1 and KFTHA2) fibres are shown in Figure 3.46 while spectra from the  $\alpha$ -cellulose in the untreated (AC) and treated (ACTN, ACTHA1 and ACTHA2) conditions are shown in Figure 3.47. The assignment of Raman bands is given in Table 3.6 (Agarwal, 1999; Eichhorn, Sirichaisit & Young, 2001; Ooi, Rambo & Hurtado, 2011; Wiley & Atalla, 1987).

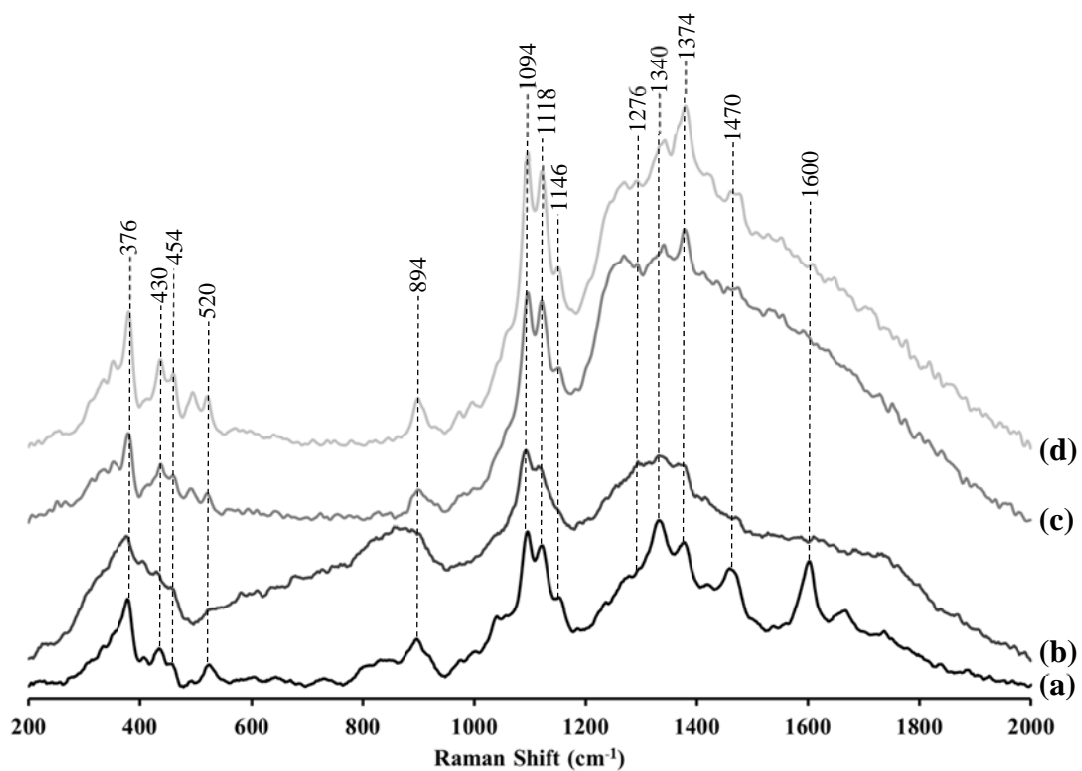


**Figure 3.46:** Raman spectra of (a) UKF, (b) KFTN, (c) KFTHA1 and (d) KFTHA2.

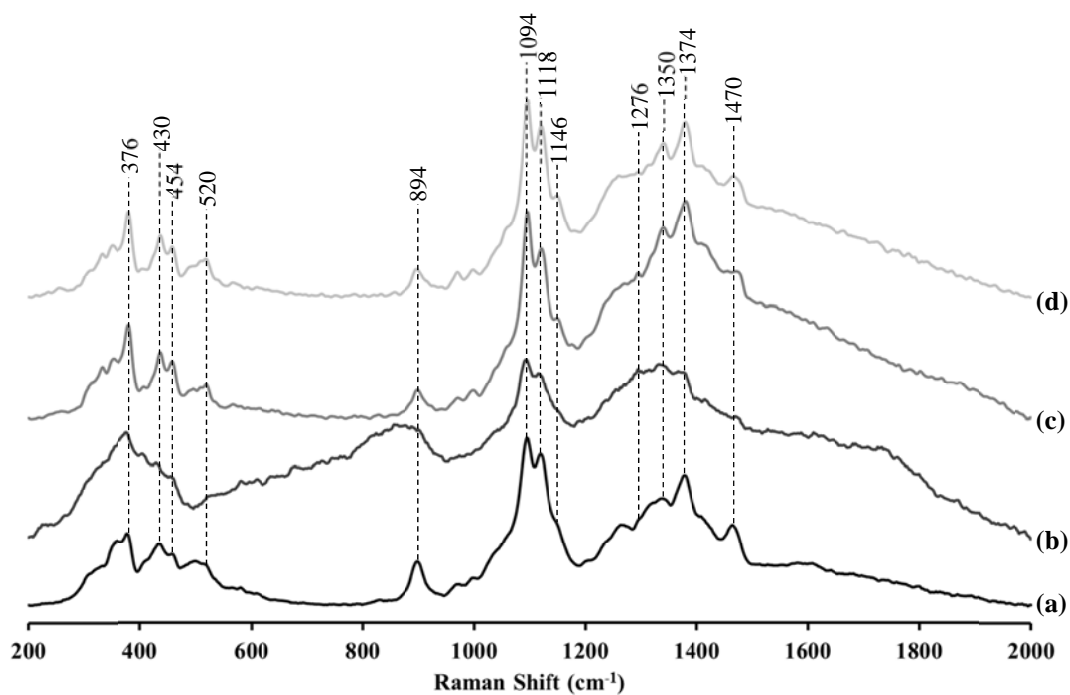


**Figure 3.47:** Raman spectra of (a) AC, (b) ACTN, (c) ACTHA1 and (d) ACTHA2.

**Table 3.6:** Assignments of Raman bands of kenaf fibres and  $\alpha$ -cellulose in untreated and treated conditions

Peak Position (cm <sup>-1</sup> )	Assignment	Sample							
		UKF	KFTN	KFTHA1	KFTHA2	AC	ACTN	ACTHA1	ACTHA2
376	Some heavy atom stretching vibrations <sup>1,2</sup>	×	×	×	×	×	×	×	×
430	Some heavy atom stretching vibrations <sup>1,2</sup>	×	×	×	×	×	×	×	×
454	Some heavy atom stretching vibrations <sup>1,2</sup>	×	×	×	×	×	×	×	×
520	Some heavy atom stretching vibrations <sup>1,2</sup>	×	×	×	×	×	×	×	×
894	Mixed modes (H-C-C, C-H-O at C6) including angle bending vibrations <sup>1,3</sup>	×	×	×	×	×	×	×	×
1,094	Cellulose C-O ring stretching vibrations <sup>3</sup>	×	×	×	×	×	×	×	×
1,118	Heavy atom (CC and CO) stretching vibrations <sup>1</sup>	×	×	×	×	×	×	×	×
1,146	Heavy atom (CC and CO) stretching plus HCC and HCO bending vibrations <sup>1</sup>	×	×	×	×	×	×	×	×
1,276	HCC and HCO bending vibrations <sup>1,2</sup>	×	×	×	×	×	×	×	×
1,340 or 1,350	HCC and HCO bending vibrations <sup>1</sup>	×	×	×	×	×	×	×	×
1,374	HCC, HCO and HOC bending vibrations <sup>1,2</sup>	×	×	×	×	×	×	×	×
1,470	HCH and HCO bending vibrations <sup>2</sup>	×	×	×	×	×	×	×	×
1,600	Aromatic polymer in lignin <sup>4</sup>	×							

<sup>1</sup>Agarwal (1999)<sup>2</sup>Wiley & Atalla (1987)<sup>3</sup>Eichhorn, Sirichaisit & Young (2001)<sup>4</sup>Ooi, Rambo & Hurtado (2011)

The spectrum from the untreated fibres contains Raman bands at  $376\text{ cm}^{-1}$ ,  $430\text{ cm}^{-1}$ ,  $454\text{ cm}^{-1}$ ,  $520\text{ cm}^{-1}$ ,  $894\text{ cm}^{-1}$ ,  $1,094\text{ cm}^{-1}$ ,  $1,118\text{ cm}^{-1}$ ,  $1,146\text{ cm}^{-1}$ ,  $1,276\text{ cm}^{-1}$ ,  $1,340\text{ cm}^{-1}$ ,  $1,374\text{ cm}^{-1}$  and  $1,470\text{ cm}^{-1}$ , Figure 3.46. These bands are also present in the spectra from both the untreated and treated  $\alpha$ -cellulose and are therefore attributed to cellulose Figure 3.47.

The untreated fibres additionally contain a band at  $1,600\text{ cm}^{-1}$  which is attributed to the aromatic components in lignin (Agarwal, 2006; Atalla & Agarwal, 1986; Ooi, Rambo & Hurtado, 2011). This band is however absent in the treated kenaf fibres, providing further confirmation that lignin has been removed.

### 3.4.6 XPS Spectra

The XPS survey spectra of the untreated fibres (UKF), the nitric acid treated fibres (KFTN) and the fibres treated with 30%  $\text{H}_2\text{O}_2/\text{CH}_3\text{COOH}$  (KFTHA1) are shown in Figures 3.48 to 3.50, respectively. Atomic composition and O/C ratios at the fibre surfaces are also given in Table 3.7.

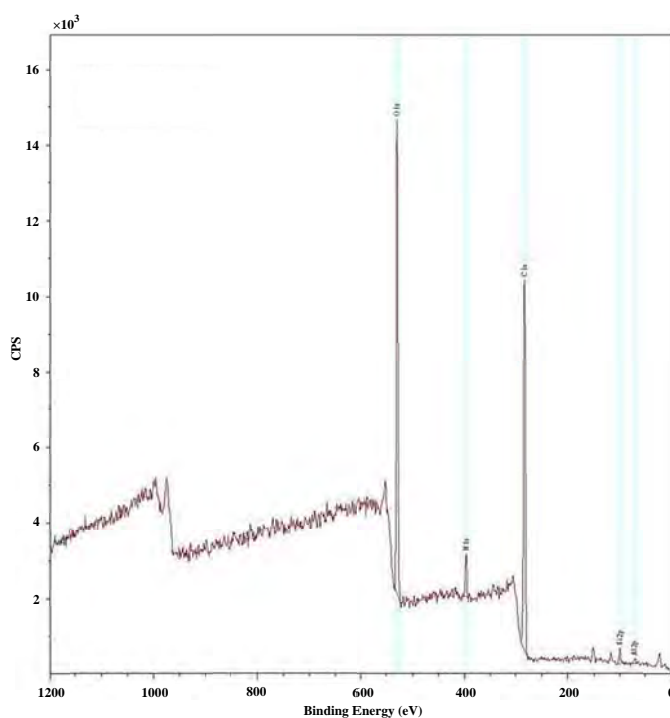


**Figure 3.48:** XPS survey spectrum of UKF.

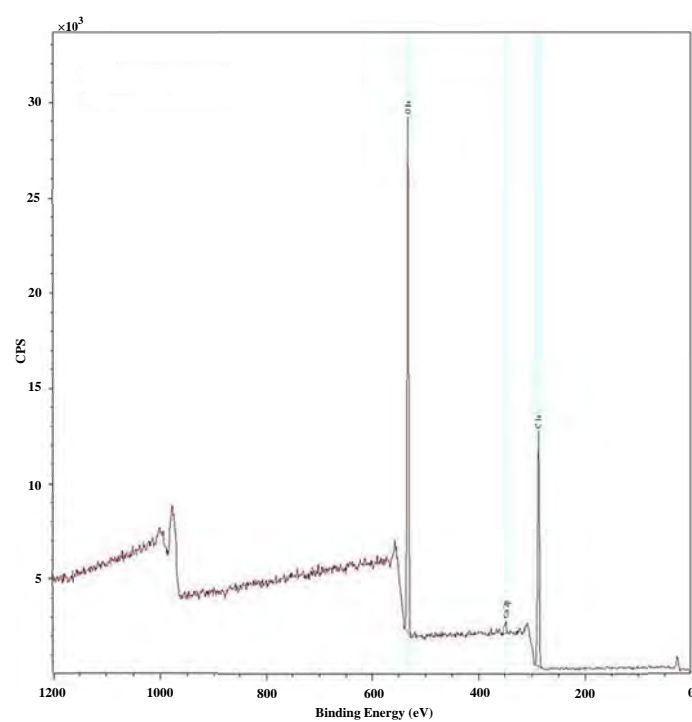


**Figure 3.49:** XPS survey spectrum of KFTN.

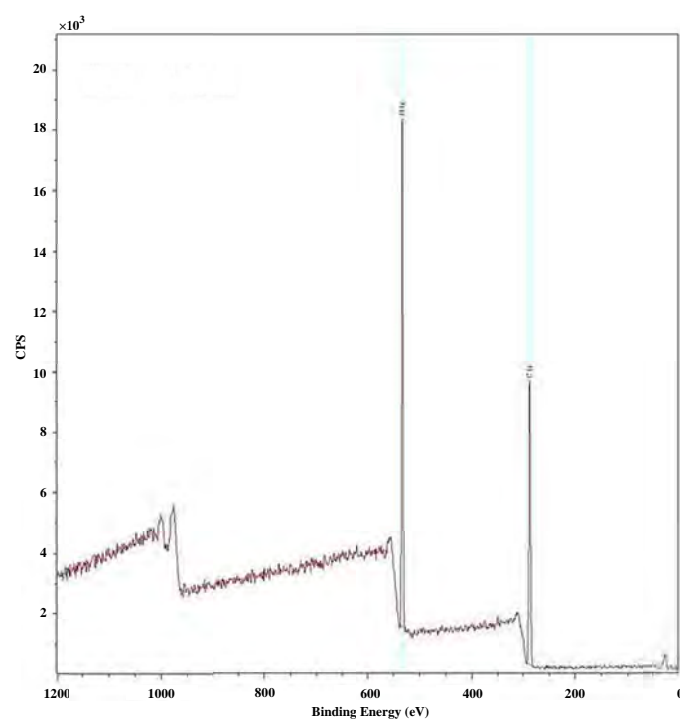


**Figure 3.50:** XPS survey spectrum of KFTHA1.



**Table 3.7:** Atomic composition (%) and O/C ratio at surface of UKF, KFTN and KFTHA1 fibres

Sample	O (1s)	C (1s)	N (1s)	Ca (2p)	Si (2p)	Al (2p)	O/C
UKF	26.24	66.51	2.83	-	3.05	1.37	0.39
KFTN	40.07	59.25	-	0.67	-	-	0.68
KFTHA1	35.09	64.91	-	-	-	-	0.54

The O/C ratios for the UKF, KFTN and KFTHA1 fibres were 0.39, 0.68 and 0.54, respectively. This indicates that the two acid treatments have made the fibre surfaces more hydrophilic since higher O/C ratios are indicative of higher hydrophilicity (Sgriccia et al., 2008). It is noted that the O/C ratios were, however, all lower than those for cellulose, hemicellulose and pectin, all of which have an O/C ratio of 0.83 (Sgriccia et al., 2008; Tserki et al., 2005).

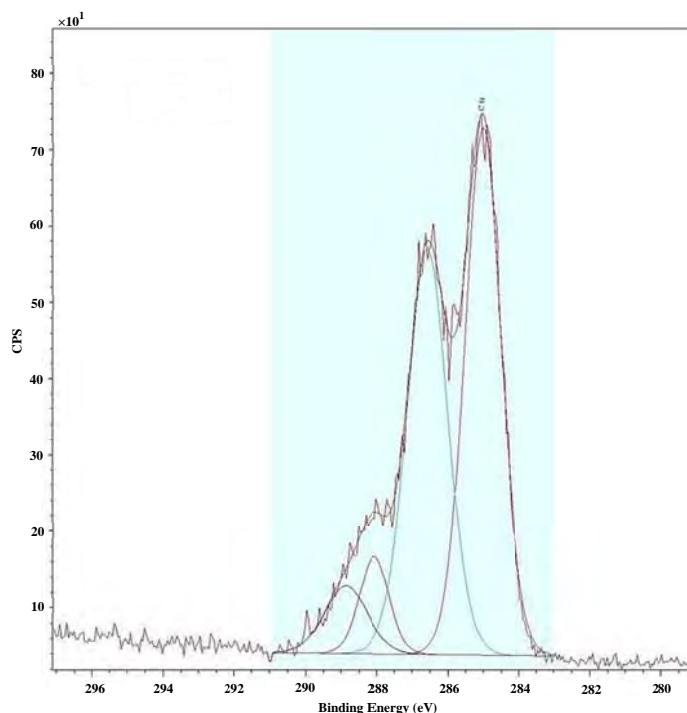


**Figure 3.51:** High resolution XPS spectrum of C 1s peaks of UKF.

High resolution XPS spectra of the C 1s, N 1s and O 1s peaks for the UKF fibres are shown for the UKF fibres in Figures 3.51 to 3.53, respectively. High resolution XPS spectra of the C 1s and O 1s peaks are shown for the KFTN fibres in Figures 3.54 and 3.55, respectively, and for the KFTHA1 fibres in Figures 3.56 and 3.57, respectively.

XPS C 1s, N 1s and O 1s binding energies and atomic composition of the UKF, KFTN and KFTHA1 are given in Table 3.8.

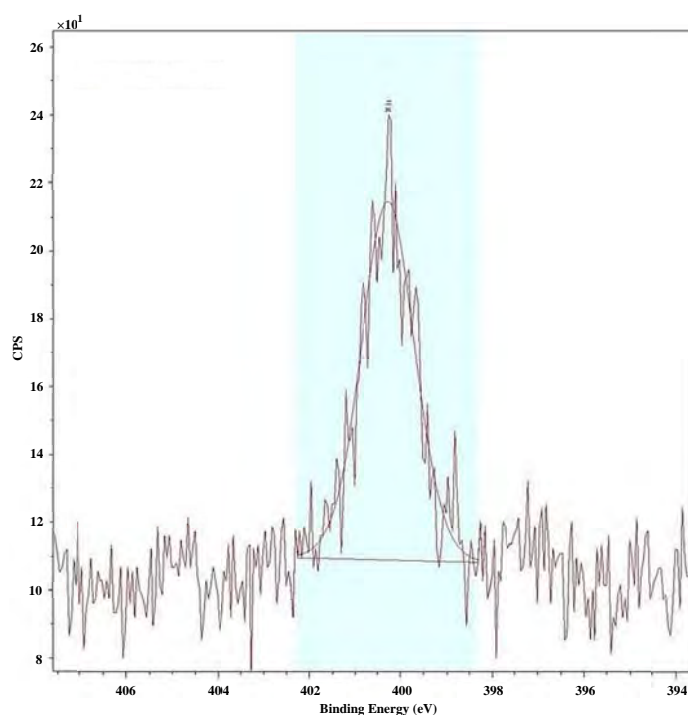


**Figure 3.52:** High resolution XPS spectrum of N 1s peaks of UKF.

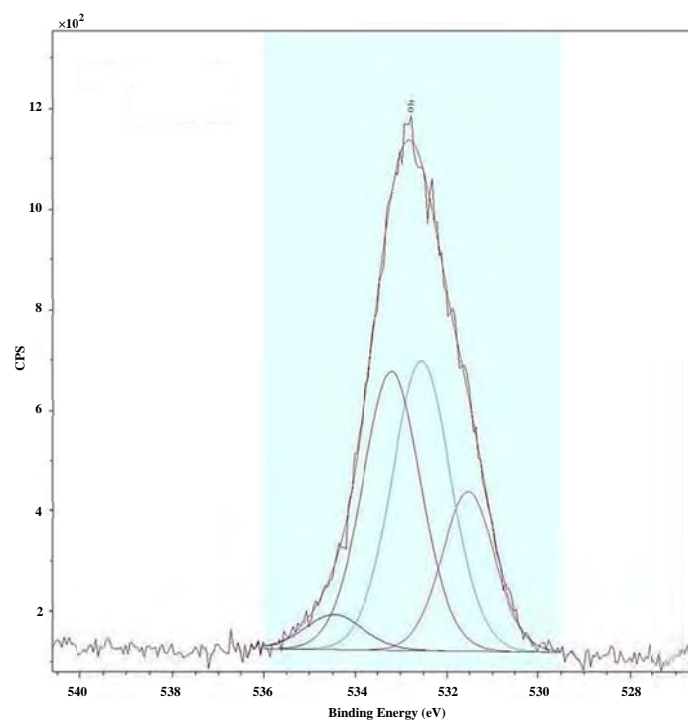


**Figure 3.53:** High resolution XPS spectrum of O 1s peaks of UKF.

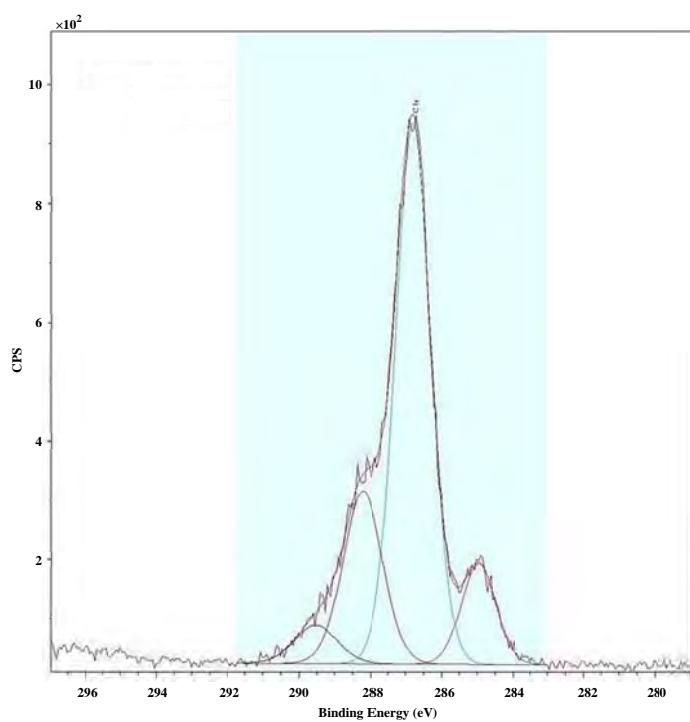


**Figure 3.54:** High resolution XPS spectrum of C 1s peaks of KFTN.

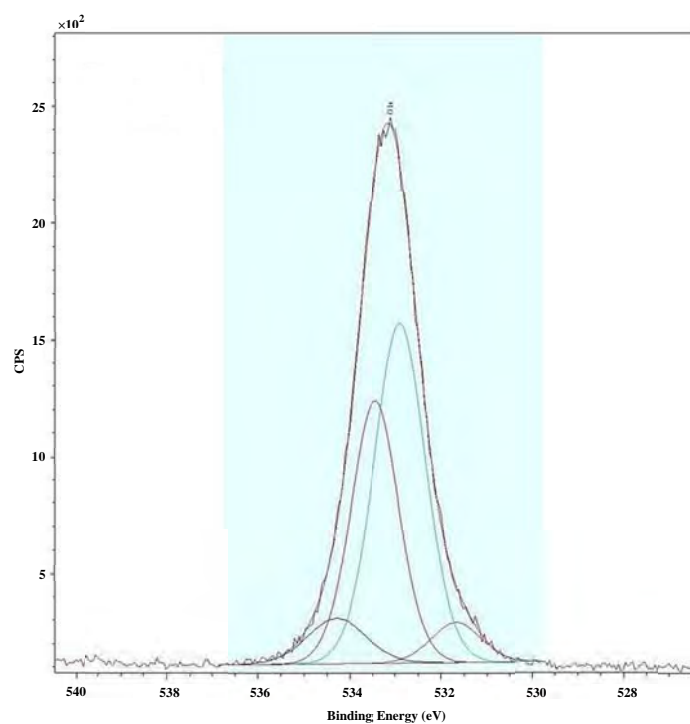


**Figure 3.55:** High resolution XPS spectrum of O 1s peaks of KFTN.

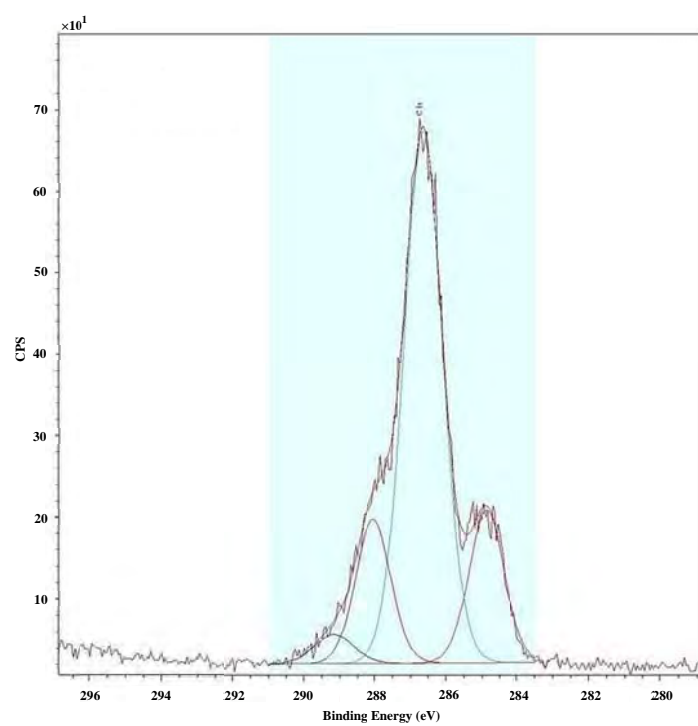


**Figure 3.56:** High resolution XPS spectrum of C 1s peaks of KFTHA1.

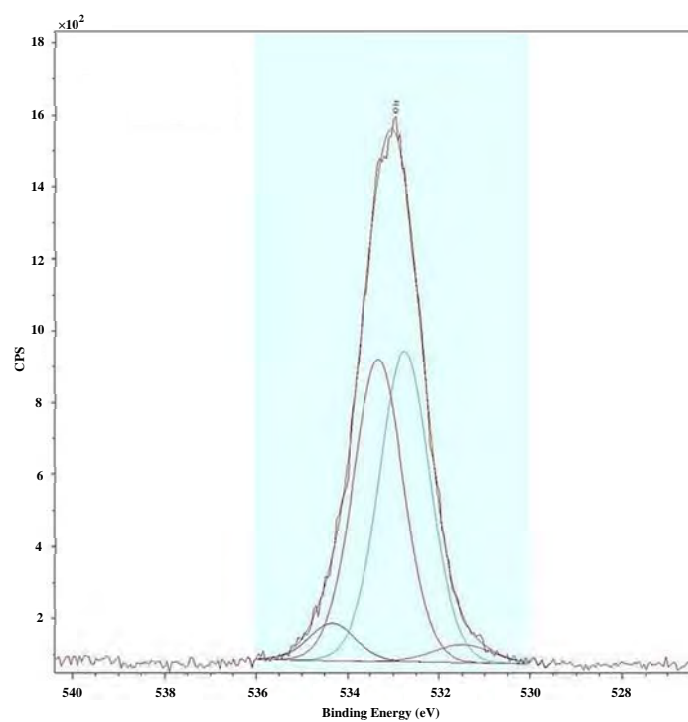


**Figure 3.57:** High resolution XPS spectrum of O 1s peaks of KFTHA1.

**Table 3.8:** XPS carbon (C) 1s, nitrogen (N) 1s and oxygen (O) 1s binding energies and atomic composition of UKF, KFTN and KFTHA1

Sample	Atomic Composition								
	C 1s				N 1s	O 1s			
	C1	C2	C3	C4	N	O1	O2	O3	O4
<b>UKF</b>									
Binding Energy (eV)	285.0	286.6	288.1	288.9	400.3	531.5	532.5	533.2	534.5
Total atomic % for each atom	46.38	39.79	6.94	6.89	100	19.07	38.85	37.38	4.70
Total atomic % for all the atoms	32.4	27.8	4.9	4.9	3.0	5.1	10.5	10.1	1.3
<b>KFTN</b>									
Binding Energy (eV)	285.0	286.8	288.2	289.5	-	531.7	532.9	533.5	534.3
Total atomic % for each atom	11.22	61.42	22.08	5.28	-	5.79	50.23	36.32	7.65
Total atomic % for all the atoms	6.7	36.5	13.1	3.1	-	2.4	20.4	14.8	3.1
<b>KFTHA1</b>									
Binding Energy (eV)	284.9	286.6	288.1	289.2	-	531.5	532.7	533.3	534.3
Total atomic % for each atom	16.72	63.77	15.91	3.59	-	3.19	46.48	45.18	5.14
Total atomic % for all the atoms	10.6	40.5	10.1	2.3	-	1.2	16.9	16.5	1.9

The C 1s peaks of the UKF, KFTN and KFTHA1 include C1, C2, C3 and C4 peaks. The C1 peak at 284.9-285.0 eV corresponds to C-C and/or C-H bonds (Buchert, Pere, Johansson & Campbell, 2001; Shchukarev, Sundberg, Mellerowicz & Persson, 2002) due to lignin, hemicellulose and extractives, such as fatty acids (Merdy, Guillon, Dumonceau & Aplincourt, 2002; Shen, Mikkola & Rosenholm, 1998). The C2 peak at 286.6-286.8 eV corresponds to C-OH bonds due to cellulose, hemicellulose, lignin and extractives, OCH bonds due to lignin, and C-O-C bonds due to cellulose, hemicellulose and extractives. The C3 peak at 288.1-288.2 eV corresponds to C=O bonds from lignin and extractives, and O-C-O bonds from cellulose and hemicellulose. The C4 peak at 288.9-289.5 eV corresponds to CH<sub>3</sub>CO groups due to hemicellulose, O-C=O and COOH groups due to hemicellulose and extractives (Buchert et al., 2001; Shen, Mikkola & Rosenholm, 1998) and carboxyl groups from oxidized lignin or cellulose (de Lange, de Kreek, van Linden & Coenjaarts, 1992).

The atomic percentage of the C1 in the fibres was reduced very substantially by the acid treatments with the values being 46.4%, 11.2% and 16.7% for the UKF, KFTN and KFTHA1 fibres, respectively, Table 3.8. Smaller reductions were also seen in the C4 for which the values were 6.9%, 5.3% and 3.6%, respectively. However, the atomic percentages of the C2 and C3 were increased substantially by the treatments, with the values for the C2 being 39.8%, 61.4% and 63.8%, respectively, while the values for the C3 were 6.9%, 22.1% and 15.9%, respectively.

The N 1s peak at 400.3 eV corresponds to C-N of amine groups (Watling, Parr, Rintoul, Brown & Sullivan, 2011) and O=CN from pectin or proteins (Truss & Wood, 2011). This peak appears in the high resolution XPS spectrum of the UKF; however, it disappears in the high resolution XPS spectra of the treated kenaf fibres (KFTN and KFTHA1).

The O 1s peaks of the UKF, KFTN and KFTHA1 consist of O1, O2, O3 and O4 peaks. The O1 peak at 531.5-531.7 eV corresponds to Ph-C=O\*O groups. The O2 peak at 532.6-532.9 eV corresponds to C-O-C and C-OH bonds. The O3 peak at 533.2-533.5 eV corresponds to C-O-C bonds and Ph-OH groups. The O4 peak at 534.3-534.5 eV corresponds to ester groups and/or oxygen of phenyl rings due to lignin and/or water absorption (Truss & Wood, 2011).

The atomic percentage of the O1 in the kenaf fibres was considerably decreased by the treatments with values of 19.1%, 5.8% and 3.2% being observed for the UKF,

KFTN and KFTHA1 fibres, respectively, Table 3.8. However, the treatments generally increased the atomic percentage of the O2, (values of 38.9%, 50.2% and 46.5%, respectively), the O3 (values of 37.4%, 36.3% and 45.2%, respectively) and the O4 (values of 4.7%, 7.7% and 5.1%, respectively).

### 3.4.7 Crystallinity of Cellulose

Three different methods were used for determining the crystallinity index of cellulose of the fibres and  $\alpha$ -cellulose in the untreated and treated conditions. The methods used were X-ray diffraction (XRD), solid state nuclear magnetic resonance (NMR) and FTIR spectroscopy.

#### 3.4.7.1 X-Ray Diffraction (XRD)

X-ray diffraction patterns of the untreated (UKF) and treated (KFTN, KFTHA1 and KFTHA2) fibres are shown in Figure 3.58, while diffraction patterns from the  $\alpha$ -cellulose in the corresponding conditions (AC, ACTN, ACTHA1 and ACTHA2), are shown in Figure 3.59. The percentage crystallinity index calculated using Segal's equation is given for each material in Table 3.9.

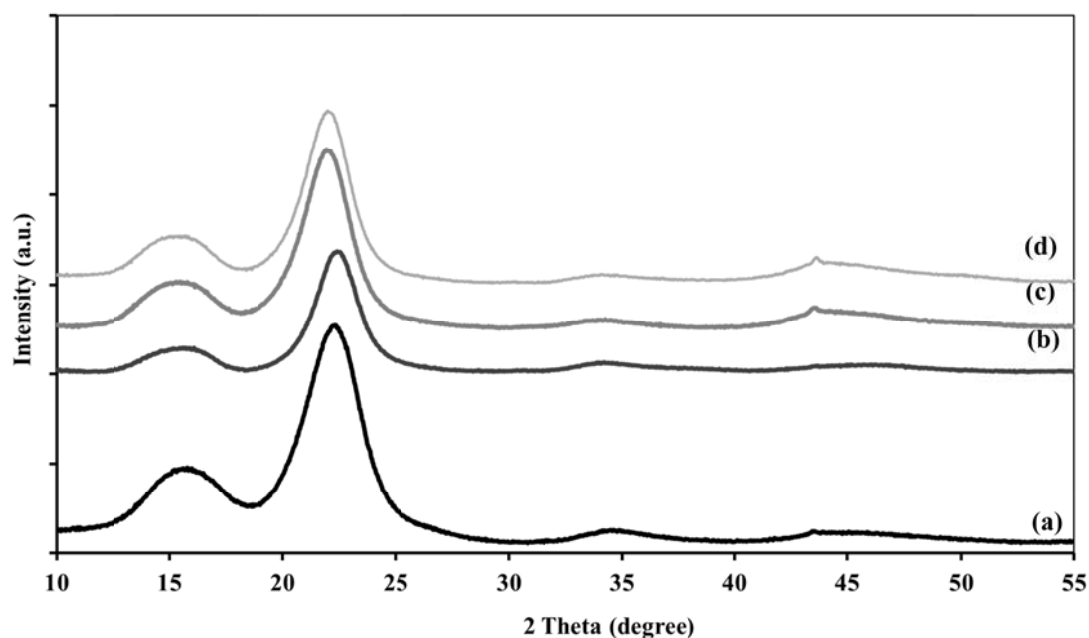


**Figure 3.58:** X-ray diffraction patterns of (a) UKF, (b) KFTN, (c) KFTHA1 and (d) KFTHA2.

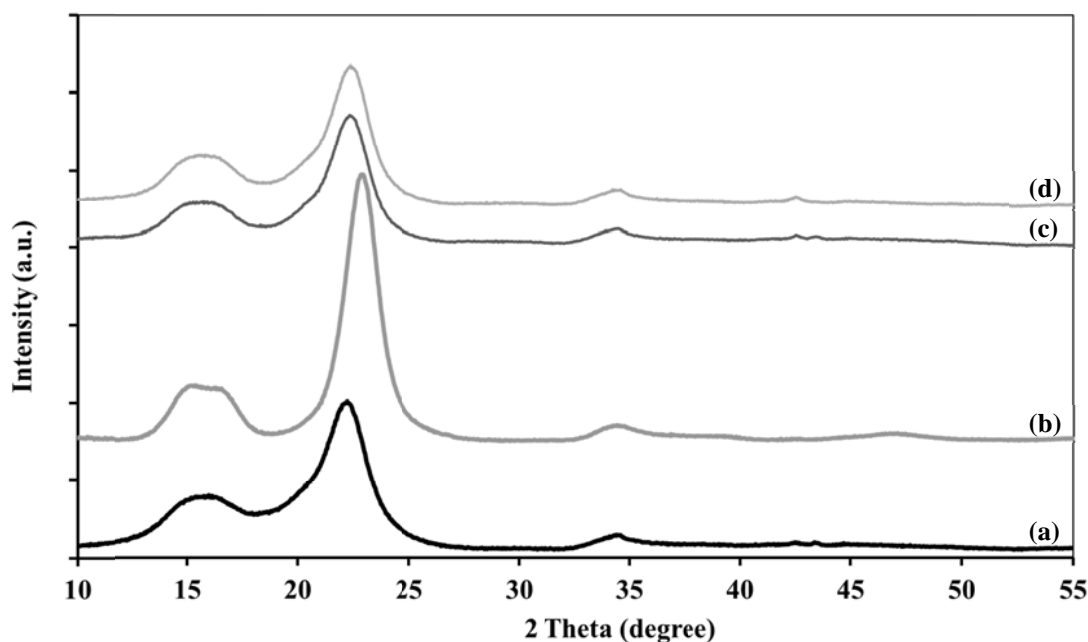


**Figure 3.59:** X-ray diffraction patterns of (a) AC, (b) ACTN, (c) ACTHA1 and (d) ACTHA2.

**Table 3.9:** Percentage crystallinity indexes of cellulose in kenaf fibres and  $\alpha$ -cellulose examined from the XRD patterns subtracted background using Segal's equation

Sample	Intensity (counts)		Crystallinity Index (%)
	$I_{am}$	$I_{002}$	
UKF	8,359	48,345	83
KFTN	1,057	27,288	96
KFTHA1	3,994	39,626	90
KFTHA2	3,517	38,496	91
AC	9,488	37,789	75
ACTN	2,171	68,797	97
ACTHA1	5,494	33,960	84
ACTHA2	6,803	36,821	82

The crystallinity indexes range from 75% to 97%. The values are generally lower for  $\alpha$ -cellulose than for the fibres. They are also lower for the untreated than the treated materials. The crystallinity index for untreated  $\alpha$ -cellulose was 75% compared



with 83% for untreated fibres. The nitric acid treatment substantially increased the crystallinity index with values of 96% and 97% being obtained for the KFTN and ACTN materials, respectively. The hydrogen peroxide/acetic acid treatments also increased the level of crystallinity, but to a lesser extent, especially in the  $\alpha$ -cellulose. There was only minimal difference between the crystallinity indexes for the two different hydrogen peroxide/acetic acid treatments, with the values being 90% and 91% for KFTHA1 and KFTHA2, respectively, and 84% and 82% for ACTHA1 and ACTHA2, respectively, Table 3.9.

#### **3.4.7.2 Solid State $^{13}\text{C}$ Nuclear Magnetic Resonance (NMR)**

Solid state  $^{13}\text{C}$  NMR spectra are shown for the untreated and treated fibres in Figure 3.60 and for the corresponding  $\alpha$ -cellulose samples in Figure 3.61. The NMR spectrum of UKF, Figure 3.60, absorbs at 21 ppm and 56 ppm due to acetyl groups and methoxyl groups (Newman, 2004), respectively, in lignin (Evans, Newman, Roick, Suckling & Wallis, 1995). It exhibits a chemical shift at 153 ppm also corresponding to lignin (Newman, 2004) while there is a signal at 174 ppm which corresponds to carboxylic groups and/or ester groups (Silverstein et al., 2005). This signal appears in the spectrum of UKF due to the carboxylic ester in pectin and wax (Li & Pickering, 2008).

The signals at 21 ppm, 56 ppm and 153 ppm are no longer present in the spectrum for KFTN, consistent with the removal of lignin. A signal is still present at 174 ppm, but in this case it is attributed to the presence of carboxylic groups and/or ester groups (Silverstein et al., 2005) produced as result of oxidation (Lasseguette, 2008).

The 56 ppm and 153 ppm signals are also absent in the spectra for KFTHA1 and KFTHA2, although signals are still present at 21 ppm and 174 ppm. However in these spectra the 21 ppm signal is attributed to acetyl groups (Newman, 2004) resulting from the  $\text{H}_2\text{O}_2/\text{CH}_3\text{COOH}$  treatment, while the 174 ppm signal is attributed to carboxylic groups and/or ester groups (Silverstein et al., 2005) resulting from oxidation. Collectively, the results indicate that the treatments have removed lignin, pectin and waxes, consistent with the findings from the FTIR and Raman studies.

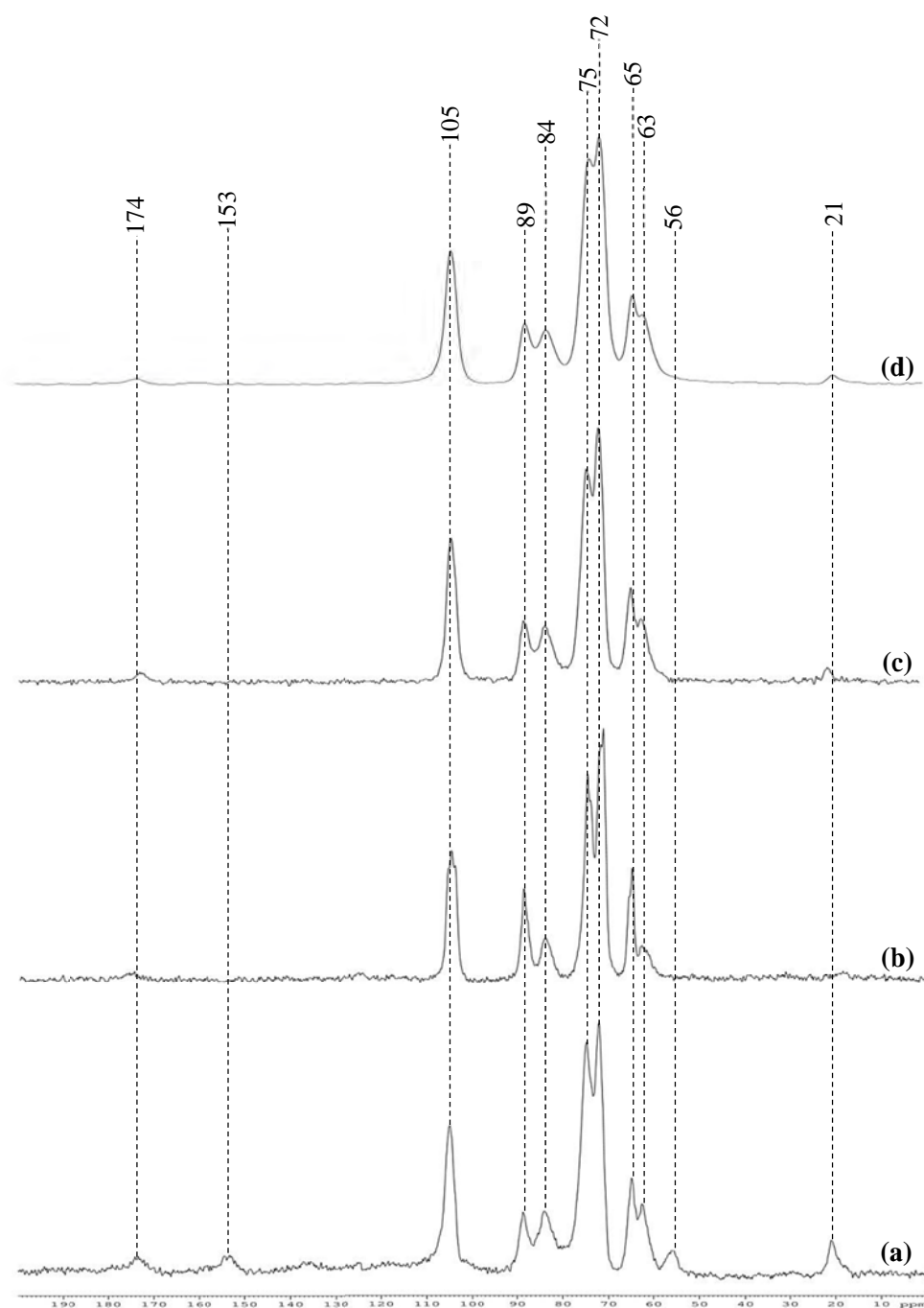


**Figure 3.60:** Solid state  $^{13}\text{C}$  NMR spectra of (a) UKF, (b) KFTN, (c) KFTHA1 and (d) KFTHA2.

The spectra for untreated  $\alpha$ -cellulose (AC) contain the same signals as that for UKF, except for the absence of the lignin and the pectin/waxes signals at 21, 56, and 153 ppm and at 174 ppm, respectively, Figure 3.61. The spectra for the treated  $\alpha$ -cellulose samples (ACTN, ACTHA1 and ACTHA2) contain the same signals as for the

untreated  $\alpha$ -cellulose, but also exhibit a signal at 174 ppm, as was seen in the treated fibres. Again this chemical shift is attributed to the presence of carboxylic groups and/or ester groups resulting from oxidation. The signal at 21 ppm seen in the hydrogen peroxide/acetic acid treated fibres is at the best very weak in the similarly treated  $\alpha$ -cellulose samples.

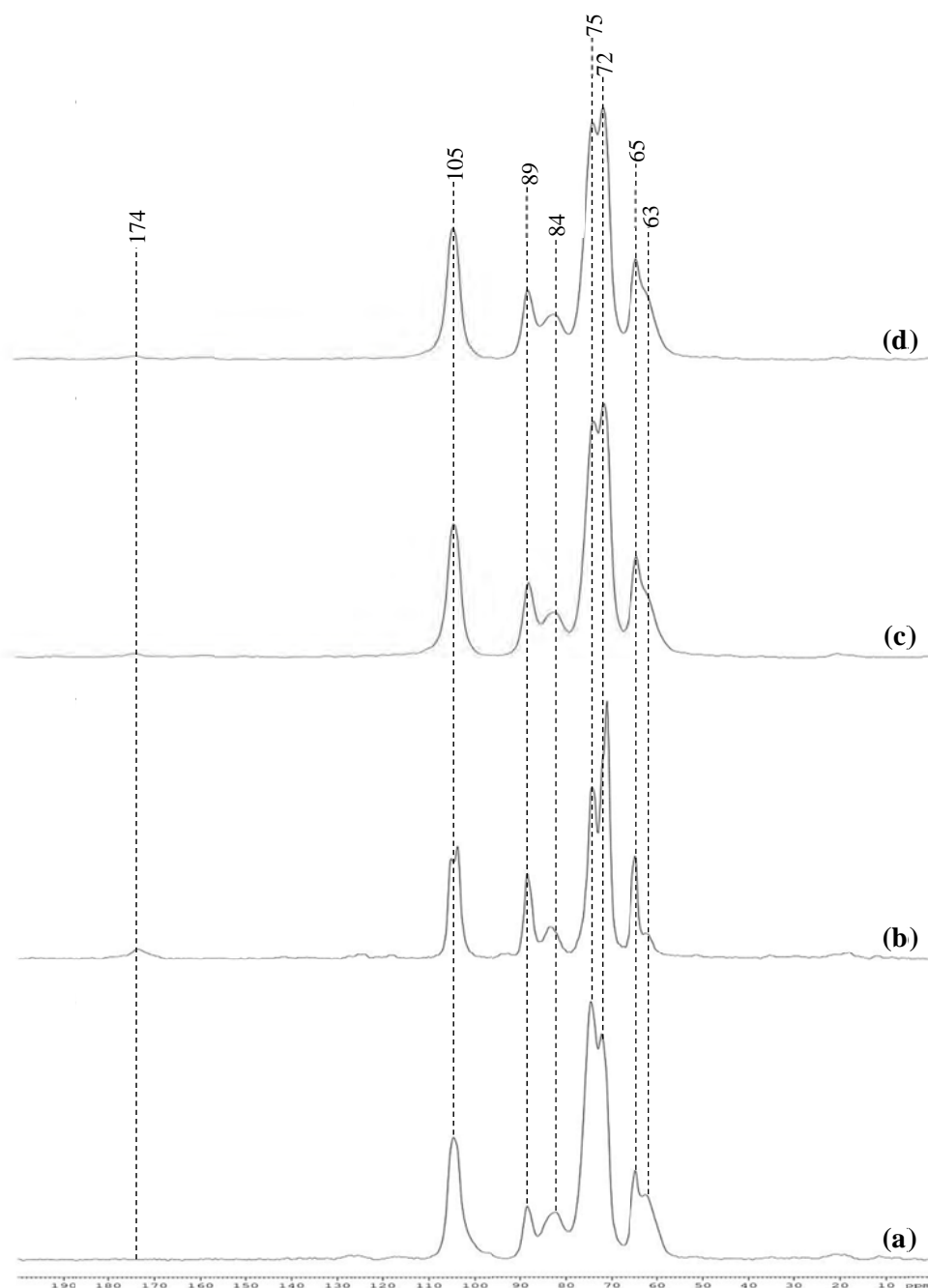


**Figure 3.61:** Solid state  $^{13}\text{C}$  NMR spectra of (a) AC, (b) ACTN, (c) ACTHA1 and (d) ACTHA2.

The crystallinity indexes for the untreated and treated fibres and for the corresponding  $\alpha$ -cellulose samples are given in Table 3.10. The values obtained are much lower than those obtained by XRD, ranging from 30-56% compared with 75-97%. The trends were however generally similar. The untreated fibres and cellulose had the lowest crystallinity indexes (36% and 30%, respectively) while the nitric acid treated samples had the highest crystallinity indexes (56% and 55%, respectively). The crystallinity indexes were intermediate for the two hydrogen peroxide/acetic acid treatments (40% and 38-39%, respectively) but there was now no difference in the crystallinity levels in the fibre and  $\alpha$ -cellulose samples, Table 3.10.

**Table 3.10:** Percentage crystallinity indexes of cellulose in kenaf fibres and  $\alpha$ -cellulose examined from the NMR spectra

<b>Sample</b>	<b>Area of Crystalline Peak in the C4 Region (X)</b>	<b>Area of Amorphous Peak in the C4 Region (Y)</b>	<b>Crystallinity Index (X/(X+Y))</b>	<b>Crystallinity Index (%)</b>
UKF	221.07	400.17	0.36	36
KFTN	191.19	150.60	0.56	56
KFTHA1	161.64	246.00	0.40	40
KFTHA2	387.02	598.89	0.39	39
AC	59.12	140.43	0.30	30
ACTN	77.30	62.31	0.55	55
ACTHA1	437.56	657.15	0.40	40
ACTHA2	427.74	709.29	0.38	38

### 3.4.7.3 FTIR

The crystallinity indexes determined as the ratio of the absorption peak at  $1,420\text{ cm}^{-1}$  to the absorption peak at  $893\text{ cm}^{-1}$  from the FTIR spectra (Figures 3.44 and 3.45) are given for the fibres and  $\alpha$ -cellulose for the different treatments in Table 3.11. The values were intermediate between those obtained using XRD and NMR ranging from 42-74%. As before the crystallinity index was lowest for the untreated  $\alpha$ -cellulose (42%) and highest for nitric acid fibres and  $\alpha$ -cellulose (73% and 74%, respectively). However, the value for the untreated fibres (69%) was disproportionately high when

compared with the values obtained using the other two techniques, while the values for the hydrogen peroxide/acetic acid treated fibres (50% and 59%, respectively) were now lower than the value for the untreated fibres. The values for hydrogen peroxide/acetic acid treated  $\alpha$ -cellulose samples (58% and 52%, respectively) were, however, intermediate between those for the untreated and nitric acid treated  $\alpha$ -cellulose, as was found for both the fibres and the  $\alpha$ -cellulose samples using the other two techniques.

**Table 3.11:** Percentage crystallinity indexes of cellulose in kenaf fibres and  $\alpha$ -cellulose examined from the FTIR spectra using the ratio of the peaks at  $1420\text{ cm}^{-1}$  to  $893\text{ cm}^{-1}$

Sample	Absorbance		Crystallinity Index (%)
	At $1420\text{ cm}^{-1}$	At $893\text{ cm}^{-1}$	
UKF	0.09	0.13	69
KFTN	0.11	0.15	73
KFTHA1	0.10	0.20	50
KFTHA2	0.10	0.17	59
AC	0.05	0.12	42
ACTN	0.14	0.19	74
ACTHA1	0.07	0.12	58
ACTHA2	0.11	0.21	52

### 3.4.8 Degree of Oxidation

The degree of oxidation of cellulose was calculated from integration of the signal at 174 ppm in the NMR spectra (Figures 3.60 and 3.61) of the treated fibres and  $\alpha$ -cellulose samples. The values are given in Table 3.12 and range from 4-15%. As noted in Section 3.3.9, the degree of oxidation indicates the weight percent of carboxyl in the cellulose (Ashton & Moser, 1968).

The results for the nitric acid treatment (KFTN and ACTN) were 7.4% and 14.5% for the fibres and  $\alpha$ -cellulose, respectively. Substantially lower values of 6.9% and 4.4%, respectively, were obtained from the 20% hydrogen peroxide/acetic acid treatment (KFTHA2 and ACTHA2). However, the results for the 30% hydrogen peroxide/acetic acid treatment were less consistent with a value of 11.8% being

obtained for the treated fibres (KFTHA1) while a value of 4.0% was obtained for the treated  $\alpha$ -cellulose (ACTHA1).

**Table 3.12:** Degree of oxidation of cellulose in treated kenaf fibres and treated  $\alpha$ -cellulose. Values in brackets represent one standard deviation.

Sample	<sup>13</sup> C NMR Peak Integration				Average Degree of Oxidation (%)
	At C6'	At C1	At C4	At C2,3,5	
KFTN	7.32	100.00	93.46	315.51	<b>7.4 (0.4)</b>
	7.84	106.99	100.00	337.58	
	6.96	95.08	88.87	300.00	
KFTHA1	11.57	100.00	93.82	299.96	<b>11.8 (0.4)</b>
	12.34	106.59	100.00	319.73	
	11.58	100.01	93.83	300.00	
KFTHA2	6.62	100.00	91.81	293.16	<b>6.9 (0.3)</b>
	7.21	108.93	100.00	319.33	
	6.77	102.33	93.95	300.00	
ACTN	14.25	100.00	93.06	309.61	<b>14.5 (0.8)</b>
	15.31	107.46	100.00	332.70	
	13.81	96.89	90.17	300.00	
ACTHA1	3.83	100.00	89.53	290.07	<b>4.0 (0.2)</b>
	4.27	111.70	100.00	324.01	
	3.96	103.42	92.59	300.00	
ACTHA2	4.11	100.00	87.62	287.82	<b>4.4 (0.3)</b>
	4.69	114.13	100.00	328.49	
	4.29	104.23	91.33	300.00	

### 3.4.9 TGA

The thermogravimetric analysis (TGA) and first derivative thermogravimetric analysis (DTG) curves of the untreated fibres (UKF), the nitric acid treated fibres (KFTN) and the fibres treated with 20% H<sub>2</sub>O<sub>2</sub>/CH<sub>3</sub>COOH (KFTHA2) obtained from analyses under an air atmosphere are shown in Figures 3.62 and 3.63, respectively. Table 3.13 gives the extrapolated onset and endset decomposition temperatures of the

fibres, and the maximum weight loss temperatures as defined by the maxima in the derivative curves, Figure 3.63. The TGA curves show three steps as indicated in Table 3.13.

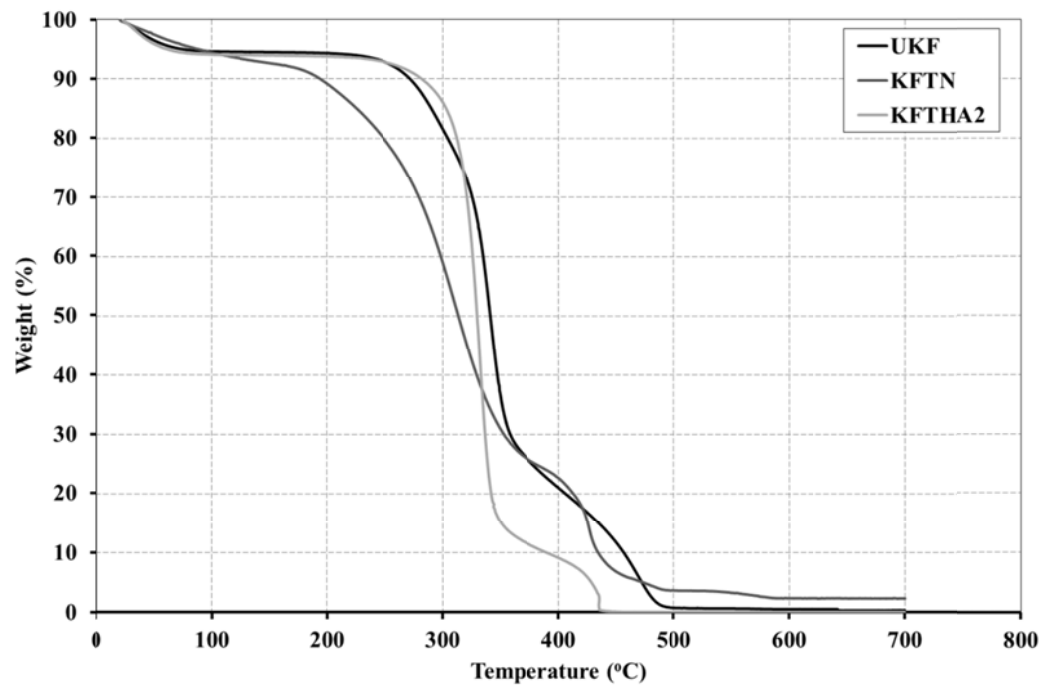


**Figure 3.62:** TGA curves of UKF, KFTN and KFTHA2.

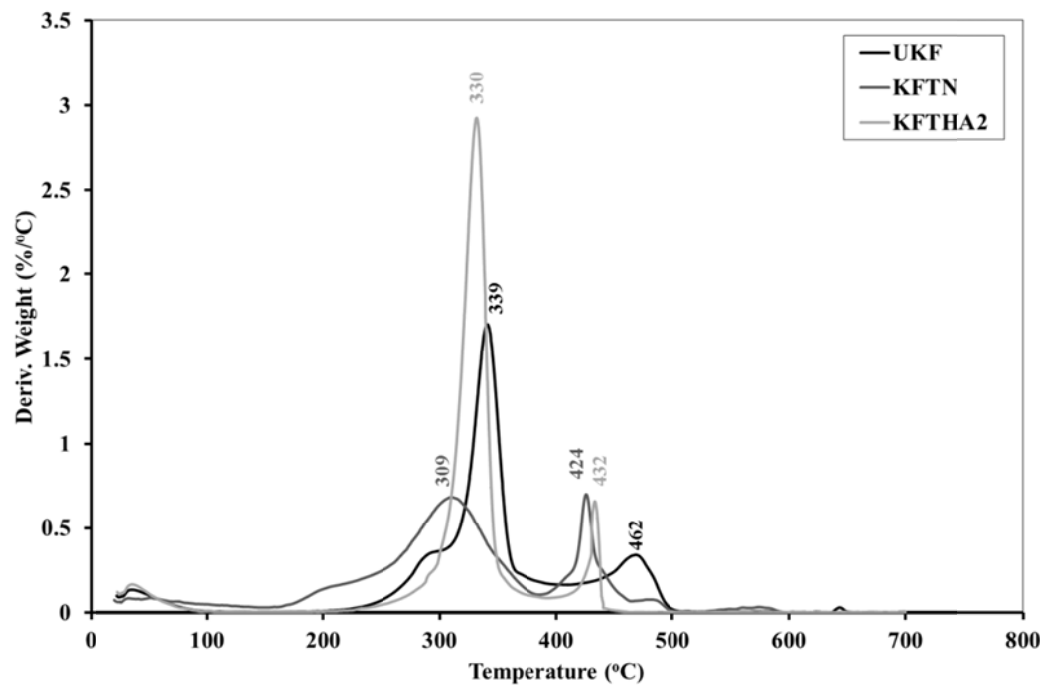


**Figure 3.63:** DTG curves of UKF, KFTN and KFTHA2.

**Table 3.13:** Summary of decomposition temperatures of UKF, KFTN and KFTHA2

Temperature		Sample		
		UKF	KFTN	KFTHA2
1 <sup>st</sup> Step	T <sub>onset</sub> (°C)	23	21	24
	T <sub>max</sub> (°C)	-	-	-
	T <sub>endset</sub> (°C)	60	87	58
2 <sup>nd</sup> Step	T <sub>onset</sub> (°C)	258	187	310
	T <sub>max</sub> (°C)	339	309	330
	T <sub>endset</sub> (°C)	353	347	343
3 <sup>rd</sup> Step	T <sub>onset</sub> (°C)	439	413	422
	T <sub>max</sub> (°C)	462	424	432
	T <sub>endset</sub> (°C)	481	441	440

The onset temperature for each of the three steps was lower for the nitric acid treated fibres than for the untreated fibres, indicating that the treatment reduced the thermal stability of the fibres, particularly at the second step for which the onset temperatures were 187°C for the treated fibres (KFTN) compared with 258°C for the untreated ones (UKF). In contrast, the onset temperature for the second step was higher for the hydrogen peroxide/acetic acid treated fibres than for the untreated fibres (310°C compared with 258°C) indicating that this treatment substantially increased the thermal stability. The endset temperature at the second step was slightly lower for the hydrogen peroxide/acetic acid treated fibres than for the untreated and nitric acid treated fibres (343°C compared with 353°C and 347°C) indicating that degradation occurred faster in the KFTHA2 fibres during this step.

## 3.5 Discussion

### 3.5.1 Elementary Kenaf Fibres

The fibre treatments evaluated for isolation of the elementary kenaf fibres were EDTA, EDTA/pectinase, sulphuric acid, nitric acid, acetic acid, and hydrogen peroxide/acetic acid. Of these treatments, only the sulphuric acid, nitric acid, and hydrogen peroxide/acetic acid treatments were successful in liberating the elementary fibres. The sulphuric acid treatment produced blackening of the fibres indicating that



adverse reactions had occurred. Additionally, the yield was very low (~2%) and this treatment was therefore not examined further.

Even for the nitric acid and hydrogen peroxide/acetic acid treatments the yield of elementary fibres was still quite low with a yield of 36% being obtained for the nitric acid treated fibres (KFTN) and 57-58% for the two hydrogen peroxide/acetic acid treatments (KFTHA1 and KFTHA2). These are however slightly higher than the yields of 34% and 48% obtained by Mazumder et al. (2000) using similar treatments also on kenaf fibres. The low yield of elementaries is attributed to the washing step and fibre degradation during the treatments (Bondenson et al., 2006).

From the present study, it is concluded that the hydrogen peroxide/acetic acid treatment is the better of the two treatments in terms of both yield and treatment time. Moreover, this treatment is milder than the nitric acid treatment and is less likely to degrade the cellulose in the fibres (Zhao, van der Heide, Zhang & Liu, 2010).

One of the main problems encountered in isolating the elementaries was fibre agglomeration, which occurs due to hydrogen bonding between the amorphous parts of the fibres (Spence et al., 2011). This was an important issue in this research but was overcome by using freeze drying which minimized the level of agglomeration.

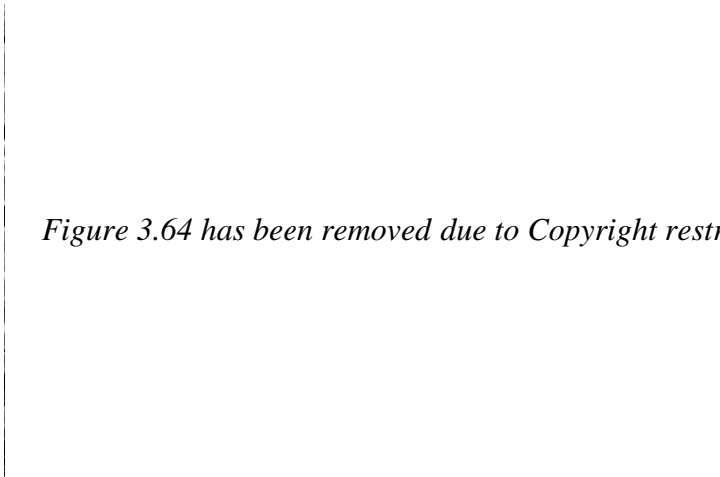


*Figure 3.64 has been removed due to Copyright restrictions.*


**Figure 3.64:** Flax fibres treated with (a) EDTA and (b) EDTA and enzyme (Stuart et al., 2006).

The techniques which were not successful in isolating the elementary fibres in the present study have been used with some success previously. Stuart et al. (2006) used

EDTA and EDTA/enzyme treatments to break down flax technical fibres and the result is shown in Figure 3.64. Some breakdown of the technical fibres has occurred but the resulting fibres are bundles of elementaries rather than individual elementary fibres. Even this level of breakdown was not observed in the present study suggesting that kenaf technical fibres may be more difficult to break down than flax technical fibres.

Treatment with 60%  $\text{H}_2\text{SO}_4$ , has been used previously by Orts et al., (2005) for obtaining nano-fibres. The same method was used in the present study but, as noted above, proved to be unsuccessful.

Several other studies have attempted to isolate kenaf elementary fibres. Shin, Jeun, Kim & Kang (2012) treated kenaf fibres in an autoclave using 12% sodium hydroxide ( $\text{NaOH}$ ) and 0.15% anthraquinone (AQ). The fibres were then bleached using 2% sodium chlorite ( $\text{NaClO}_2$ ) and 3% acetic acid ( $\text{CH}_3\text{COOH}$ ) at  $70^\circ\text{C}$  for 90 minutes. Subsequently, the fibres were bleached using 1.2% sodium hypochlorite ( $\text{NaOCl}$ ) at room temperature for 60 minutes. It was found that lignin removal was imperfect. As a result, separated individual fibres were only partially obtained.



*Figure 3.65 has been removed due to Copyright restrictions.*

**Figure 3.65:** SEM micrograph of treated kenaf fibres using chemical treatments and 300-kGy electron beam irradiation treatment (Shin et al., 2012).

Shin et al. (2012) also treated kenaf fibres using water at  $120^\circ\text{C}$  for 120 minutes and then bleached them, as in the treatment given above. The treated kenaf fibres were subsequently treated using electron beam irradiation treatments with 6 doses of irradiation consisting of 10, 20, 50, 100, 200 and 300 kGy. It was found that with the higher irradiation doses, more isolated individual kenaf fibres were obtained. Removal

of lignin from the kenaf fibres took place completely when the fibres were treated at 300 kGy. Consequently, individual kenaf fibres were obtained as shown in Figure 3.65.

Garcia-Jaldon, Dupeyre & Vignon (1998) isolated semi-retted decorticated hemp fibres using a steam explosion treatment (STEX). This treatment was conducted in a flash hydrolysis laboratory pilot unit purpose-built for lignocellulosic material processing. The exploded hemp fibres were then washed with distilled water and treated with 2% w/w NaOH. Subsequently, the hemp fibres were bleached using NaClO<sub>2</sub>. SEM micrographs of the untreated and treated hemp fibres are shown in Figure 3.66. It can be seen from Figure 3.66d that the elementary hemp fibres were completely separated by the end of the process.

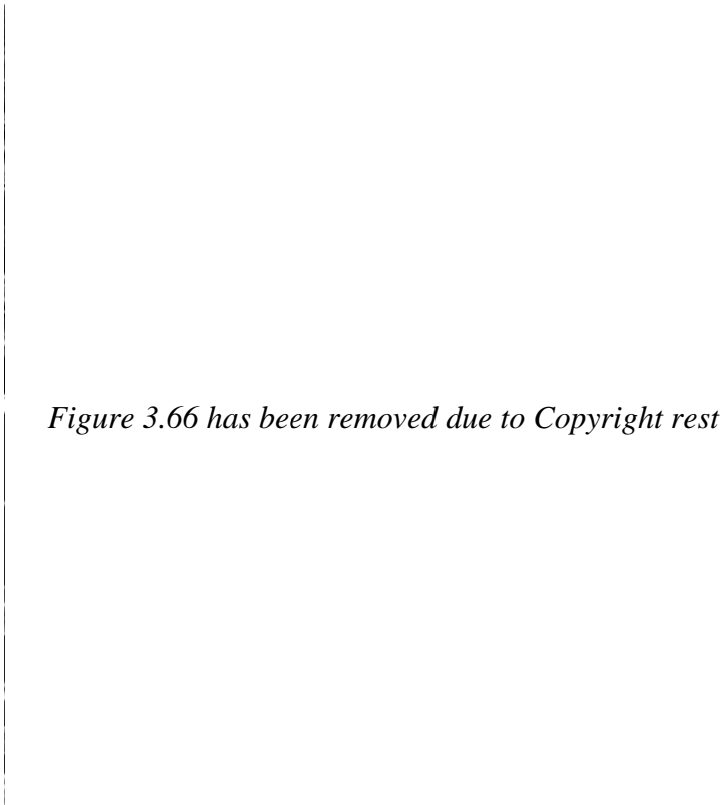


*Figure 3.66 has been removed due to Copyright restrictions.*

**Figure 3.66:** SEM micrographs of hemp fibres (a) in original condition, (b) after STEX and water extraction, (c) after STEX, water extraction and NaOH extraction and (d) after STEX, water extraction, NaOH extraction and bleaching (Garcia-Jaldon, Dupeyre & Vignon, 1998).

*Figure 3.67 has been removed due to Copyright restrictions.*

**Figure 3.67:** SEM micrograph of untreated kenaf fibre (Aziz & Ansell, 2004).

The untreated kenaf fibres used for comparison in the present study showed surface impurities. These were similar to those seen by Aziz & Ansell (2004) in untreated kenaf fibres, Figure 3.67.

### **3.5.2 Aspect Ratio of Elementary Fibres**

Both the modulus and strength of short fibre composites can be improved by increasing the aspect ratio of the fibres (Rowell et al. 1999; Tajvidi, 2005). This can be done by separating the fibres into elementaries which increases the interface area between the fibres and the matrix (Feng et al., 2001). Accordingly breakdown of the kenaf technical fibres into elementary fibres was undertaken with a view to producing high aspect ratio short fibres which could be used to improve the properties of extruded composites.

The length of the elementaries obtained from the nitric acid treatment was quite short with an average value of only 180  $\mu\text{m}$  giving an aspect ratio of 7.5. In contrast, the elementaries obtained from the hydrogen peroxide/acetic acid treatments were much longer with average lengths of  $\sim 2,300 \mu\text{m}$  and aspect ratios of approximately 160. Kenaf elementaries 640  $\mu\text{m}$  in length were obtained by Mazumder et al. (2000) using a 10%  $\text{HNO}_3$  treatment for 1 hour under refluxing conditions. This treatment is both milder and shorter than the lengthy 60% nitric acid treatment used here and this is probably the reason for the difference. None the less, the treatment used by Mazumder

et al. (2000) still gave elementaries only one quarter the length of the elementaries obtained in the present study using the hydrogen peroxide/acetic acid treatments, indicating that nitric acid treatment has an adverse effect on the length of the elementaries obtained. As discussed later, this is considered to be due to acid attack of the defects present in the elementary fibres (Hughes, 2012).

The two hydrogen peroxide/acetic acid treatments used in the present study gave slightly different length and aspect ratios these being 2,274  $\mu\text{m}$  and 137, respectively, for the KFTHA1 treatment (30% hydrogen peroxide/acetic acid at 60°C for 24 hours) and 2,312 and 179, respectively for the KFTHA2 treatment (20% hydrogen peroxide/acetic acid at 98°C for 7 hours). In view of the large scatter in the elementary fibre lengths and widths (standard deviations of approximately 25%), these differences are not considered significant.

Mazumder et al. (2000) also treated kenaf fibres in a 20% hydrogen peroxide/acetic acid solution at 60°C for 24 hour and obtained a fibre length of 2,180  $\mu\text{m}$ , which is similar to the value obtained in the present work. Calamari et al. (1999) also treated kenaf fibres with 20% hydrogen peroxide/acetic acid, but in this case they used an alkali pretreatment. They obtained a fibre length of 2,450  $\mu\text{m}$  and an aspect ratio of 204, again in good agreement with the results of the present study.

*Figure 3.68 has been removed due to Copyright restrictions.*

**Figure 3.68:** Micrograph of HCl treated hemp fibres (Thygesen, 2008).

As noted above, the much shorter length of the nitric acid treated fibres is considered to be due to fibre breakage resulting from acid attack at fibre defects. This occurs because the defects are chemically more active (Hughes, 2012). This was also

observed by Thygessen (2008) for hemp yarns treated with 1 N HCl where breakage of the fibres occurred at dislocations. A micrograph of the treated fibres is shown in Figure 3.68. It can be seen that the ends of the HCl treated fibres are square due to fibre breakage. This is similar to the HNO<sub>3</sub> treated fibres obtained in the present study, as shown in Figure 3.20b.

Hänninen, Michud & Hughes (2011) treated flax fibres using 1% w/v of 0.1M HCl. Acid hydrolysis was considered to cause chain scission, particularly at kink bands.

### 3.5.3 Defect Density of Elementary Fibres

The defects within the kenaf elementaries were studied to establish the influence of the chemical processing on the defects. The chemical action includes acid hydrolysis (Hughes, 2012), which can attack the fibres through loosening of the tightly packed structure of the cell wall in defect areas (Ander, Daniel, Garcia-Lindgren, & Marklund, 2005; Hänninen, Michud & Hughes, 2011).

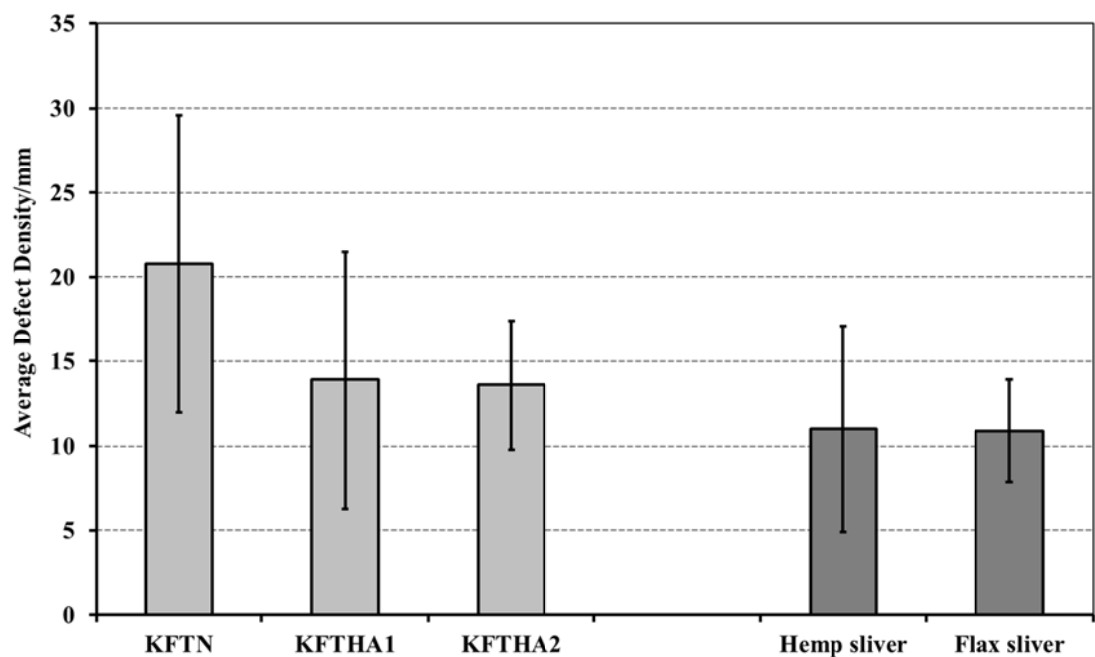


**Figure 3.69:** Average defect density of the elementary kenaf fibres obtained in the present study and hemp and flax sliver (elementaries) obtained by Ruys (2007).

The defect density was significantly higher for the nitric acid treatment which gave 21 defects per millimeter than for either of the hydrogen peroxide/acetic acid treatments both of which gave a defect density of 14. This is attributed to the higher

level of hydrolysis produced by the stronger acid (Bailar, Moeller, Kleinberg, Guss, Castellion & Metz, 1989).

The defect densities from the present study are compared with those obtained by Ruys (2007) for elementary fibres, which were hand separated from mechanically processed hemp and flax sliver, in Figure 3.69. The defect densities for the hydrogen peroxide/acetic acid treated fibres are reasonably similar to the values obtained by Ruys (2007) for flax and hemp, suggesting that level of defects produced by the hydrogen peroxide/acetic acid treatment is minimal. However, the defect density for the nitric acid treated fibres is substantially larger, consistent with the damage produced by this treatment.

*Figure 3.70 has been removed due to Copyright restrictions.*

**Figure 3.70:** Defect types of elementary hemp fibres: (A) kink band (500× magnification), (B) node (500× magnification), (C) dislocation (200× magnification), (D) slip plane (200× magnification) and (E) initial break (500× magnification) (Fan, 2010).

The defects observed in the elementary fibres were initial breaks, micro-compressions, kinks, dislocations, nodes and pits. These are similar to the defects observed by Fan (2010) in elementary hemp fibres, as shown in Figure 3.70.

### 3.5.4 FTIR Spectra

The FTIR spectrum obtained from the untreated kenaf fibres contained the same absorption peaks as the spectrum for a kenaf stem published previously by Öztürk, Irmak, Hesenov & Erbatur (2010), which is shown in Figure 3.71. Likewise, the spectrum obtained from the untreated  $\alpha$ -cellulose sample was similar to that obtained previously by Garside & Wyeth (2003), which is shown in Figure 3.72.

*Figure 3.71 has been removed due to Copyright restrictions.*

**Figure 3.71:** FTIR spectrum of kenaf stem (Öztürk et al., 2010).

In addition to the cellulose peaks, peaks were present at  $1,238\text{ cm}^{-1}$ ,  $1,500\text{ cm}^{-1}$  and  $1,593\text{ cm}^{-1}$  in the spectrum from the untreated kenaf fibres. These are attributed to the presence of lignin (Garside & Wyeth, 2003; Kubo & Kadla, 2005; Sgriccia et al., 2008), consistent with their absence from the spectrum for  $\alpha$ -cellulose. A peak was also present at  $1,716\text{ cm}^{-1}$  which is attributed to hemicellulose (Moran et al., 2008), waxes and pectin (Dai & Fan, 2010; Li & Pickering, 2008). Again this peak was absent from the spectrum for  $\alpha$ -cellulose.

The  $1,500\text{ cm}^{-1}$  was absent from the spectra of the treated fibres indicating that the nitric acid treatment and the two hydrogen peroxide/acetic acid treatments had



removed the lignin from the fibres. This is to be expected since the elementary fibres are bound together in the technical fibres by lignin (Sain & Panthapulakkal, 2004).

*Figure 3.72 has been removed due to Copyright restrictions.*

**Figure 3.72:** FTIR spectrum of pure cellulose (Garside & Wyeth, 2003).

The  $1,238\text{ cm}^{-1}$  peak was absent from the spectrum of the nitric acid treated fibres but a peak at the same wavenumber was present in the hydrogen peroxide/acetic acid treated fibres. However, in this case, the peak is attributed to the presence of acetates (Tserki et al., 2005) produced as a result of the treatment. This peak was also present in the spectra obtained from the hydrogen peroxide/acetic acid treated  $\alpha$ -cellulose, confirming that it had resulted from the acid treatment and was not indicative of the presence of lignin.

The  $1,593\text{ cm}^{-1}$  peak was absent from the spectra from the hydrogen peroxide/acetic acid treated fibres but a peak at the same wavenumber was present in the spectrum from the nitric acid treated fibres. The peak was also present in the nitric acid treated  $\alpha$ -cellulose and again is considered not to be due to lignin, but instead to reaction between  $\text{HNO}_3$  and cellulose (Gert et al., 2000). A second peak attributed to reaction between  $\text{HNO}_3$  and cellulose (Gert et al., 2000) was observed at  $1,280\text{ cm}^{-1}$  in the nitric acid treated fibres and  $\alpha$ -cellulose, but again not in any of the other spectra.

The  $1,716\text{ cm}^{-1}$  peak which is attributed to waxes and pectin was not present in the nitric acid treated fibres but a peak at the same wavenumber was again present in both the hydrogen peroxide/acetic acid treated fibres and the hydrogen peroxide/acetic

acid treated  $\alpha$ -cellulose, indicating that it was again due to the treatment and that the waxes and pectin had been removed. In this case the peak is attributed to oxidised cellulose (Luz et al., 2008).

### 3.5.5 Raman Spectra

The Raman spectrum obtained from the untreated kenaf fibres was similar to that obtained by Ooi, Rambo & Hurtado (2011), which is shown in Figure 3.73. The information obtained from Raman spectroscopy was less extensive than that obtained by FTIR, however the  $1,600\text{ cm}^{-1}$  peak observed in the untreated kenaf, which corresponds with lignin (Ooi, Rambo & Hurtado, 2011), was no longer present after the treatments, providing further confirmation that lignin had been removed.

*Figure 3.73 has been removed due to Copyright restrictions.*

**Figure 3.73:** Raman spectrum (785 nm excitation) of untreated kenaf fibres (Ooi, Rambo & Hurtado, 2011).

### 3.5.6 XPS Spectra

Unlike FTIR and Raman spectroscopy, which obtain information over a depth of  $\sim 1\text{ }\mu\text{m}$  (Holmes-Farley & Whitesides, 1987; Costa, Borowiak-Palen, Kruszyńska, Bachmatiuk & Kaleńczuk, 2008), XPS is a surface technique in which the information is obtained over a depth of only  $\sim 5\text{ nm}$  (Holmes-Farley & Whitesides, 1987).

XPS data from untreated kenaf fibres has been published previously by Sgriccia et al. (2008) and their results are compared with those from the untreated fibres examined in the present study in Table 3.14. The results are reasonably similar although the O/C ratio of 0.45 obtained by them is somewhat higher than the value of 0.39 obtained here. As noted earlier, the O/C ratio is a measure of hydrophilicity (Sgriccia et

al., 2008) but it seems unlikely that this would differ significantly for fibres of the same species. Johansson, Campbell, Koljonen & Stenius (1999) note that the XPS results can be affected by surface contamination and it is considered that the higher O/C ratio is due to contamination with aluminosilicates and possibly silicates. This is consistent with the higher Al and Si values in the results obtained by Sgriccia et al. (2008), Table 3.14. Panthapulakkal & Sain (2007) obtained a value of 0.33 for wood flour, which is lower than the value obtained here.

The O/C ratio was increased by both of the treatments. This is considered to be due to removal of the carbon-rich wax layer from the surface of the fibres (Zhao & Boluk, 2010). This also indicates that the treated fibres were more hydrophilic than the untreated fibres. The nitric acid treated fibres had the highest O/C ratio (0.68) and, accordingly, were the most hydrophilic.

**Table 3.14:** Atomic composition (%) in surfaces of the untreated kenaf fibres obtained in the present work and that of Sgriccia et al. (2008)

Atomic composition	Present Work	Work of Sgriccia et al. (2008)
O (1s)	26.24	27.96
C (1s)	66.51	62.34
N (1s)	2.83	2.68
Ca (2p)	-	-
Si (2p)	3.05	4.26
Al (2p)	1.37	2.76
O/C	0.39	0.45

Table 3.15 lists theoretical data for cellulose, hemicellulose, lignin and extractives obtained by Freudenberg & Neish (1968) cited in Laine, Stenius, Carlsson & Ström (1994), Gustafsson, Ciofica & Peltonen (2003), and Laine et al. (1994). The theoretical values for the O/C ratio are 0.83 for cellulose, 0.78-0.81 for hemicellulose 0.33 for lignin and 0.11-0.12 for extractives. The C2 and C3 values are substantially higher for cellulose and hemicellulose than for lignin and extractives while the reverse is true for the C1. Differences in C4 are only marginal, Table 3.15.

Data obtained for C 1s from previous studies of hemp fibres (Truss & Wood, 2011), linen flax fibres (Buchart et al., 2001), green flax fibres (Zafeiropoulos, Vickers,

Baillie & Watts, 2003), wood fibres (Matuana, Balatinecz, Sodhi & Park, 2001), wood flour (Panthapulakkal & Sain, 2007) and kraft fibres (González, Santos & Parajó, 2011) are compared with the results obtained from the untreated kenaf fibres examined in the present study in Table 3.16.

**Table 3.15:** O/C ratios and atomic percentages of C 1s of cellulose, hemicellulose, lignin and extractives

Compound	O/C	Atomic Percentage			
	Ratio	C1	C2	C3	C4
Cellulose (theoretical) <sup>1</sup>	0.83	-	83	17	-
Hemicellulose (theoretical) <sup>2</sup>	0.80	-	83	17	-
Galaktoglucomannan (theoretical hemicellulose) <sup>2</sup>	0.78	3	78	16	3
Arabinoglucuronoxylan (theoretical hemicellulose) <sup>1</sup>	0.81	-	78	19	3
Lignin (theoretical) <sup>3</sup>	0.33	49	49	2	-
Resin acids (theoretical extractives) <sup>2</sup>	0.11	94	-	-	6
Stearic acid (theoretical extractives) <sup>2</sup>	0.12	94	-	-	6
Oleic acid (theoretical extractives) <sup>1</sup>	0.11	94	-	-	6

<sup>1</sup> Laine, Stenius, Carlsson & Ström (1994)

<sup>2</sup> Gustafsson, Ciofica & Peltonen (2003)

<sup>3</sup> Freudenberg & Neish (1968), cited in Laine et al. (1994)

The C1, C2, C3 and C4 values have similar relative magnitudes amongst the different fibres, although the values for any one parameter vary considerably reflecting chemical differences amongst the fibres. The C1 value for the untreated kenaf fibres obtained in the present study was lower than that of the other natural fibres, except hemp and kraft fibres. The C2 value was however higher than for the other fibres, except kraft fibres, while the C3 value was again lower than for the other fibres, except flax (linen). The C4 value was higher than for the other fibres, except hemp.

Both of the treatments used in the present work produced a marked reduction in the C1 value (Table 3.8) and this is attributed to the removal of lignin and extractives, which as noted above both have high C1 values, Table 3.15. The C2 and C3 were increased after both treatments, consistent with increased cellulose and hemicellulose

contents due to loss of lignin and extractives. A decrease was observed in the C4 value, which is attributed to removal of extractives, Table 3.15. Some C4 was, however, still observed in the treated fibres even though it was not observed for either cellulose or hemicellulose, Table 3.15. Its presence is attributed to oxidised cellulose as was observed using NMR.

**Table 3.16:** Atomic percentages of C 1s of kenaf fibres, hemp fibres, flax fibres (linen), wood fibres, wood flour and kraft fibres

Natural Fibre	Atomic Percentage			
	C1	C2	C3	C4
Untreated kenaf fibres (present work)	46.4	39.8	6.9	6.9
Hemp fibres <sup>1</sup>	43.8	28.5	16.5	11.1
Flax fibres (linen) <sup>2</sup>	66.2	25.9	6.7	2.0
Green flax fibres <sup>3</sup>	52.6	34.7	12.6	-
Wood fibres <sup>4</sup>	57.5	30.3	12.2	-
Wood flour <sup>5</sup>	56.5	31.6	8.6	3.2
Kraft fibres <sup>6</sup>	32.4	48.7	16.8	2.2

<sup>1</sup> Truss & Wood (2011)

<sup>2</sup> Buchert et al. (2001)

<sup>3</sup> Zafeiropoulos, Vickers, Baillie & Watts (2003)

<sup>4</sup> Matuana, Balatinecz, Sodhi & Park (2001)

<sup>5</sup> Panthapulakkal & Sain (2007)

<sup>6</sup> González, Santos & Parajó (2011)

The N 1s peak was present in the untreated kenaf fibres but disappeared after treatment. This is attributed to the removal of pectin.

The atomic percentage of the N 1s obtained for the untreated kenaf fibres was 3.0% which is similar to the value obtained for wood by Shchukarev et al. (2002), while somewhat lower values were obtained by Gauthier, Derenne, Dupont, Guillon, Largeau, Dumonceau & Aplincourt (2002) for wheat straw and wheat bran (1.0% and <1%, respectively)

The O 1s peaks obtained in the high resolution XPS scans in the present study were difficult to utilise to identify the surface chemical composition of the fibres. This is because multiple oxygen bonding peaks overlapped and this led to difficulties in

curve fitting. In this respect, it is noted that O 1s peaks of high resolution XPS scans of natural fibres are rarely found in the literature.

Truss & Wood (2011) examined the O 1s peaks from high resolution XPS scans of hemp fibres. Their results are compared with those from the present study in Table 3.17. The O1, O2, O3 and O4 values are of similar relative magnitudes for the two studies, but there are differences in the individual values. The O1 and O3 atomic percentages obtained by Truss & Wood (2011) were lower than those of the untreated kenaf fibres obtained in the present study. However, the O2 and O4 atomic percentages were higher. In view of the difficulties arising from peak overlap, and the possibility of the results being affected by surface contamination, it is difficult to assess the significance of these differences.

**Table 3.17:** Atomic percentages of O 1s of kenaf fibres and hemp fibres

Natural Fibre	Atomic Percentage			
	O1	O2	O3	O4
Untreated kenaf fibres (present work)	19.1	38.9	37.4	4.7
Hemp fibres (Truss & Wood (2011)'s work)	16.4	40.7	34.4	8.5

### 3.5.7 Crystallinity of Cellulose

The crystallinity of the cellulose before and after treatment was examined for both the fibres and the  $\alpha$ -cellulose using XRD, solid state  $^{13}\text{C}$  NMR and FTIR spectroscopy. The XRD method has been used most widely for measuring the crystallinity index of cellulose, with NMR being used to a much lesser extent. FTIR spectroscopy is the simplest method, but it is not an absolute measurement technique (Park et al., 2010). The other two methods also have limitations and problems (Park et al., 2010) making it difficult to assess which of the three methods is the most appropriate.

The results obtained from the three treatments are compared in Figure 3.74. XRD gave the highest values, NMR the lowest values while intermediate values were obtained from FTIR. It is noted that values obtained by XRD are generally found to be higher than those obtained by NMR (Park et al., 2010).

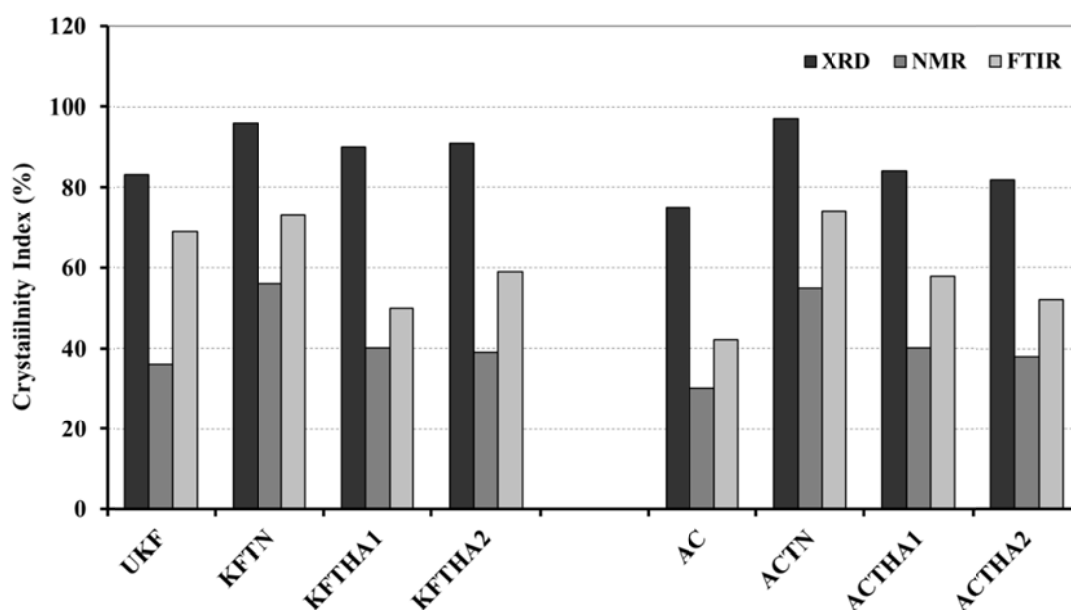


**Figure 3.74:** Crystallinity indexes of cellulose in the UKF, KFTN, KFTHA1, KFTHA2, AC, ACTN, ACTHA1 and ACTHA2 examined using the XRD, NMR and FTIR.

The results obtained by all three techniques for  $\alpha$ -cellulose show that the crystallinity index increases for both the nitric acid and the two hydrogen peroxide/acetic acid treatments with the nitric acid treatment producing the highest level of crystallinity. The same result was obtained for the fibres using XRD and NMR, but FTIR indicated that the hydrogen peroxide/acetic acid treatments caused a reduction in crystallinity. It can be seen that the result for the untreated kenaf fibres obtained from FTIR is anomalously high when compared with the FTIR results for  $\alpha$ -cellulose and also when compared with the XRD and NMR results for the fibres. It is therefore considered that this data is inaccurate and that only the XRD and NMR results should be used. On this basis, it is concluded that all three treatments produced an increase in crystallinity in the fibres. The increase in crystallinity as determined by XRD and NMR was 16% and 56%, respectively, for the nitric acid treated fibres, 8% and 11%, respectively, for the 30% hydrogen peroxide/acetic acid treatment and 10% and 8%, respectively, for the 20% hydrogen peroxide/acetic acid treatment. The increase in crystallinity is attributed to oxidation of the cellulose (Marsh & Wood, 1945, cited in Abdel Moteleb & El Akabawy, 1999) changing the functional groups from primary hydroxyl groups ( $-\text{CH}_2\text{OH}$ ) to carboxylic groups ( $-\text{COOH}$ ) (Kumar & Yang, 2002),

with subsequent formation of ester groups from reaction of the carboxylic groups with unreacted hydroxyl groups in the cellulose. In addition, oxidation would reduce the degree of polymerisation (DP) by constraining movement of cellulose molecules, which would lead to an increase in cellulose crystallinity (Graminski, 1970, cited in Sandy, Manning, & Bollet, 2010).

As noted above, XRD is the most commonly used of the three techniques but it is considered that some inaccuracy could have arisen in three ways. Firstly, the  $I_{am}$  value measured as the highest peak intensity of amorphous cellulose in the XRD spectrum at  $2\theta$  value near  $18.5^\circ$  was underestimated because the maximum height of the amorphous cellulose peak was found at a  $2\theta$  value higher than  $19.5^\circ$  as shown in Figure 3.75. Hence, the crystallinity index calculated by Segal's equation would be overestimated. Secondly, Segal's equation only required the maximum peak intensity for the calculation whilst there were at least four crystallinity peaks in the XRD spectrum. Thirdly, Segal's equation neglects any effect of peak width, which can vary considerably in cellulose due to variation in crystallite size (Park et al. , 2010).

*Figure 3.75 has been removed due to Copyright restrictions.*

**Figure 3.75:** X-ray diffraction patterns of amorphous cellulose examples: (a) amorphous portion extracted by the peak deconvolution method, (b) amorphous cellulose produced by the DMSO/PF method, (c) ball-milled cellulose and (d) commercial xylane (Park et al., 2010).

Park et al. (2010) determined the crystallinity index of  $\alpha$ -cellulose and obtained a value of 78% which is in good agreement with the value of 75% obtained in the present study. Several workers have also used XRD to measure the crystallinity index of



untreated kenaf fibres. Öztürk et al. (2010) obtained a value of 55% for kenaf stems, while Jonoobi, Harun, Shakeri, Misra & Oksman (2009) have reported a similar value of 48% for raw kenaf fibres. Bonatti, Ferrari, Focher, Grippo, Torri & Cosentino (2004) have reported a crystallinity index of 42% for kenaf. These values are substantially lower than the value 83% obtained in the present study. The lower values may however be due to inclusion of core fibres with the bast fibres. This is supported by the value of 78% obtained for kenaf in subsequent work by Jonoobi, Harun, Mathew, Hussein and Oksman (2010) where it was stated explicitly that fibres analysed were bast fibres.

Öztürk et al. (2010) found the crystallinity of their kenaf stems increased from 55% to 74% after hydrolysis in subcritical water at 200°C, consistent with the increases in crystallinity produced by the treatments used in the present study.

*Figure 3.76 has been removed due to Copyright restrictions.*

**Figure 3.76:**  $^{13}\text{C}$  NMR spectrum of cellulose from kenaf (Focher et al., 2001).

NMR studies of crystallinity index are less common. Park et al. (2010) used NMR to determine the crystallinity index of  $\alpha$ -cellulose and obtained a value of 42%, which is in reasonable agreement with the value of 30% obtained in the present study. Focher et al. (2001) determined the crystallinity index of cellulose extracted from kenaf, using the NMR spectrum shown in Figure 3.76, and obtained a value of 42%. This is again in reasonable agreement with the value of 36% obtained here.

It was also possible to examine the chemical effect of the fibre treatments using the NMR data. The NMR spectra of the treated kenaf fibres show a chemical shift at

174 ppm and this indicates that the treated kenaf fibres were oxidized after both the nitric acid and the hydrogen peroxide/acetic acid treatments as discussed earlier.

### 3.5.8 TGA

Three distinct weight loss steps were observed in the TGA (Figure 3.62) and DTG curves (Figure 3.63) of the kenaf fibres. The weight loss at the first step was caused by loss of moisture from the fibres (Pereira, Nascimento, Cordeiro, Morais, Sousa & Rosa, 2010). The second stage of weight loss resulted from thermal decomposition of hemicellulose over the temperature range 280°C to 320°C (Han et al., 2007) and of cellulose over the temperature range 320°C to 380°C (Keshk & Haija, 2011). The weight loss at the third step was due to oxidation of the degradation products from the second step (Ciannamea, Stefani & Ruseckaite, 2010), as well as decomposition of thermally stable residues, such as lignin (Sharma & Kernaghan, 1988; Stuart et al., 2006).

For the nitric acid treated fibres, the second step occurred at a substantially lower temperature than for the untreated fibres, with an onset temperature of 187°C, compared with 258°C, and with the maximum weight loss occurring at 309°C, compared with 339°C, Table 3.13. This is attributed to decomposition of cellulose nitrate produced as result of the nitric acid treatment. The presence of the  $-\text{NO}_2$  group in cellulose nitrate was confirmed by the FTIR results, Figure 3.44b.

TGA curves obtained for cellulose nitrate by Huang & Li, (1998) are shown in Figure 3.77. They found that 90% of the cellulose nitrate decomposed in 1 minute at 212°C. This indicates that, while present, cellulose nitrate was only a minor component of the nitric acid treated fibres.

The hydrogen peroxide/acetic acid treated fibres (KFTHA2) had a higher onset temperatures than the untreated fibres, with a value of 310°C compared with 258°C, Table 3.13. A similar result was obtained by Zhao et al. (2010) for sugarcane bagasse treated using a mixture of 30% hydrogen peroxide and anhydrous acetic acid. They obtained onset temperatures approximately of 265°C and 315°C for the untreated and treated fibres, respectively, and attributed the increase in onset temperature to removal of lignin.

The increased onset temperature of the hydrogen peroxide/acetic acid treated fibres observed in the present study is of particular significance for the use of natural fibres in thermoplastic matrix composites since it would permit higher processing

temperatures. In turn, this would expand the range of thermoplastic polymers that could be used as the matrix for natural fibre thermoplastic composites.

*Figure 3.77 has been removed due to Copyright restrictions.*

**Figure 3.77:** TGA curve ( — ), derivative weight loss DTG ( ---- ) and second derivative weight loss 2DTG ( ..... ) of cellulose nitrate (Huang & Li, 1998).

### 3.6 Summary

The findings from this part of the study are given in Table 3.18 and summarised below.

- Of the different chemical treatments examined only the nitric acid treatment and the hydrogen peroxide/acetic acid treatment were considered suitable for obtaining elementary fibres from kenaf.
- The hydrogen peroxide/acetic acid treatment required a shorter treatment time and gave a 60% higher yield than the nitric acid treatment.
- The elementary fibres obtained for the hydrogen peroxide/acetic acid treatment had an average length and aspect ratio of 2.3 mm and 160, respectively. The

elementary fibres obtained for the nitric acid treatment were only one tenth this length with a similar reduction in their aspect ratio. The reduced elementary length is considered to be due to fibre breakage resulting from chemical attack at defects in the fibres.

- The defect density in the nitric acid treated elementaries was double that found in the hydrogen peroxide/acetic acid treated elementaries. This is again considered to be due to chemical attack of the fibres during the harsher nitric acid treatment.

**Table 3.18:** Summary of significant findings

Property	KFTN	KFTHA1	KFTHA2	Technique
Fibre length (mm)	0.18	2.27	2.31	Microscopy
Fibre aspect ratio	15.3	137	179	Microscopy
Removal of lignin	Yes	Yes	Yes	FTIR, Raman, NMR, XPS
Removal waxes and/or pectin	Yes	Yes	Yes	FTIR
Removal of waxes (only)	Yes	Yes	N/A	XPS (O/C ratios)
Removal of pectin (only)	Yes	Yes	Yes	XPS
Removal of extractives	Yes	Yes	Yes	XPS (C4)
Level of crystallinity	Increased (16-56%)	Increased (8-11%)	Increased (8-10%)	XRD, NMR
Production of -NO <sub>2</sub> groups	Yes	No	No	FTIR
Production of -COOH groups	Yes	Yes	Yes	FTIR, XPS
Production of -C(=O)CH <sub>3</sub> groups	No	Yes	Yes	FTIR
Decomposition temperature	Decreased	Not measured	Increased	TGA (step 2)

- Both chemical treatments removed lignin, pectin, waxes and extractives, as would be expected in isolation of the elementaries. They also increased the

hydrophilicity of the surface of the fibres but caused some oxidation of cellulose to occur.

- Both treatments increased the level of crystallinity in the fibres which is beneficial to their mechanical performance. The crystallinity was increased more by the nitric acid treatment than by the hydrogen peroxide/acetic acid treatment.
- The thermal stability of the fibres was decreased by  $\sim 70^{\circ}\text{C}$  by the nitric treatment but was increased by  $\sim 50^{\circ}\text{C}$  by the hydrogen peroxide/acetic acid treatment. The increase in thermal stability obtained from the latter treatment would permit higher processing temperatures which would allow a wider range of thermoplastics to be used as the matrix material in natural fibre composites.

CHAPTER 4

**EXTRUDED KENAF FIBRE-REINFORCED HDPE-  
MATRIX COMPOSITES**

---



## **4. EXTRUDED KENAF FIBRE-REINFORCED HDPE-MATRIX COMPOSITES**

### **4.1 Introduction**

This chapter describes the work undertaken on extruded thermoplastic matrix composites reinforced with kenaf elementary fibres. The elementaries produced by both the nitric acid treatment (KFTN) and the 20% hydrogen peroxide/acetic acid treatment (KFTHA2) were used for fabricating the composites. These had average lengths of 0.2 and 2.3 mm, respectively, and average aspect ratios of 15 and 179, respectively. In addition, composites were also produced from chopped untreated kenaf technical fibres (UKF) for purposes of comparison. These fibres had an average length of 0.7 mm and an average aspect ratio of 7.5. Details of the treatments and the physical and chemical characteristics for the three types of fibre used have been given in the previous chapter. High-density polyethylene (HDPE) was used as the matrix material with maleated polyethylene (MAPE) being used as the coupling agent.

The components were compounded using twin-screw extruders. Initially, a single feed extruder was used but in subsequent work a twin feed extruder was employed. The extruded composites were metallographically characterised and the fibre weight fraction determined by dissolution of the matrix resin. The tensile properties of the composites, as well as those of the matrix resin without fibre reinforcement, were determined. The fracture surfaces of the composites were also examined after testing.

### **4.2 Materials**

Untreated kenaf technical fibres (UKF), nitric acid treated fibres (KFTN) and 20% hydrogen peroxide treated fibres (KFTHA2) were used to fabricate the composites. Details of the fibres are given in Chapter 3.

ICORENE<sup>®</sup> 3925 or COTENE<sup>™</sup> 3925 (rotational moulding high-density polyethylene (HDPE) powder) obtained from ICO polymers was used as the matrix. Powdered HDPE was used to allow premixing with the fibres. The physical characteristics of the HDPE powder, as given in the product data sheet (Appendix IV), are shown in Table 4.1. Licocene PE MA 4351 fine grain maleated polyethylene



(MAPE) obtained from Clariant (Australia) Pty Ltd was used as the coupling agent. The properties of the MAPE powder as given in the product safety data sheet (Appendix IV), are given in Table 4.2. 1,2,4-trichlorobenzene was obtained from Sigma-Aldrich.

**Table 4.1:** Physical characteristics of HDPE powder

Physical Characteristics	Value	Test Method
Melt Flow Index (MFI)	3.5 g/10min	ASTM D 1238
Annealed Density	0.941 g/cm <sup>3</sup>	ASTM D 1505
Vicat Softening Point	123°C	ASTM D 1525
Environmental Stress-Cracking Resistance (ESCR)		
F <sub>50</sub> (100% Igepal)	>500 h	ASTM D 1693
Environmental Stress-Cracking Resistance (ESCR)		
F <sub>50</sub> (10% Igepal)	- h	ASTM D 1693
Flexural Modulus (1.3 mm/min)*	815 MPa	ASTM D 790
Tensile Modulus (0.5 mm/min)*	695 MPa	ASTM D 638
Tensile Strength at Yield (50 mm/min)	21 MPa	ASTM D 638
Elongation at Break (50 mm/min)	1,500%	ASTM D 638
ARM Impact Strength (3.2 mm sample at -40°C)	95 J	ARM Method
Shore Hardness	61 Shore D	ASTM D 2240
UV Rating (50% Retained Tensile Elongation)	8,000 h	ASTM 2565

\* Mechanical testing was conducted on 3.2 mm compression moulded samples prepared to ASTM D 1928. Type M-II sample dimensions used for tensile testing whilst 25.4 mm sample width used for flexural testing.

**Table 4.2:** Physical and chemical properties of MAPE powder

Property	
Form	Fine Grain
Colour	Yellowish
Drop Forming Point (ASTM D 3954-94)	Approx. 123°C
Density (ISO 1183)	Approx. 0.99 g/cm <sup>3</sup> (23°C)
Solubility in Water	Insoluble (20°C)
Acid number	Approx. 46 mg KOH/g
Viscosity (Dynamic) (DIN 53018)	Approx. 300 mPa.s (140°C)

## 4.3 Experimental Methods

### 4.3.1 Extrusion of Composites

In initial work, extruded HDPE composites were prepared from the chopped untreated kenaf fibres (UKF) and the nitric acid treated fibres (KFTN) by simultaneously compounding and extruding in a EuroLab co-rotating twin-screw extruder, Figure 4.1. The ratio of kenaf fibres to HDPE to MAPE was 40:57:3 by weight.

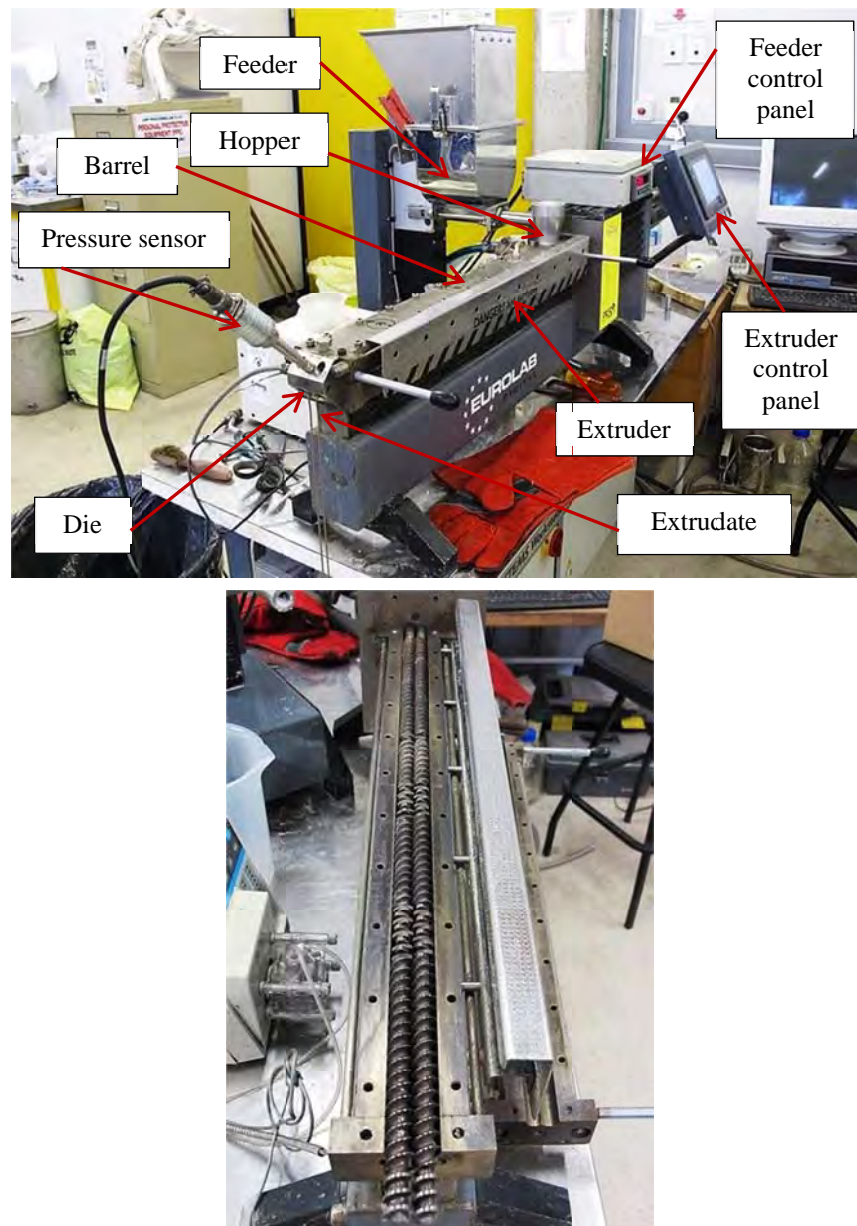


**Figure 4.1:** Eurolab co-rotating twin-screw extruder (top) and screws inside Eurolab extruder (bottom).

Prior to compounding, the UKF, KFTN and MAPE were pre-dried in an oven at 75°C for 24 hours and oven dried at 75°C for at least 3 hours. The kenaf fibres, HDPE and MAPE were mixed in a plastic bag and fed into a PRISM feeder which then fed into the hopper of the extruder, as shown in Figures 4.1 and 4.2, using 30% feeding. Extrusion was carried out with a screw length to screw diameter ratio of 40:1 and a screw speed of 100 rpm, at a pressure of 2 MPa. The temperature of the barrels was approximately 160°C in each zone. The composites were extruded through twin 1 mm diameter circular dies. Pure HDPE was also extruded using the same conditions. Each of the composite extrudates broke into approximately 25 pieces approximately 3 m long after emerging from the die. The extruded HDPE, UKF/HDPE/MAPE and KFTN/HDPE/MAPE samples are referred to hereafter as-extruded HDPE, UKF/HDPE and KFTN/HDPE rod composites, respectively.

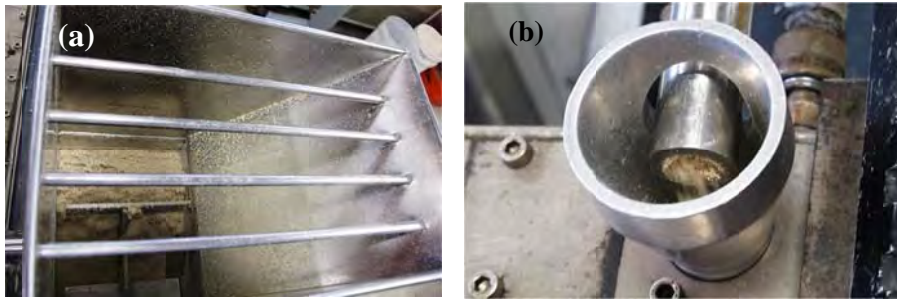


**Figure 4.2:** Photographs of (a) materials mixed in PRISM feeder and (b) mixed materials fed into hopper of Eurolab extruder.

Some variation in fibre fraction was observed along the composites, together with surface roughening, and it was considered that better composites might be obtained using a twin feed extruder in which the fibres and the matrix material could be fed separately. Accordingly, a second set of HDPE/MAPE matrix composites was prepared from the untreated fibres (UKF) and the nitric acid treated fibres (KNTF), and additionally from the 20% hydrogen peroxide/acetic acid treated fibres (KFTHA2). The composites were prepared by simultaneous compounding and extruding using a Thermo Scientific Eurolab 16 twin-screw extruder with a screw length to screw diameter ratio of 25:1. The extruder had two hoppers for separate feeding of the fibres and the matrix material, Figure 4.3. It was decided to extrude the composite as strip since this would allow dog-bone specimens to be used for tensile testing. The die used was a slit die

having dimensions 25.4 mm by 2 mm. The ratio of kenaf fibres to HDPE to MAPE was again 40:57:3 by weight.

Prior to compounding, all of the materials were dried in an oven at 75°C for a minimum of 14 hours. Slightly different processes were then used in the extruder for the untreated and treated fibres.

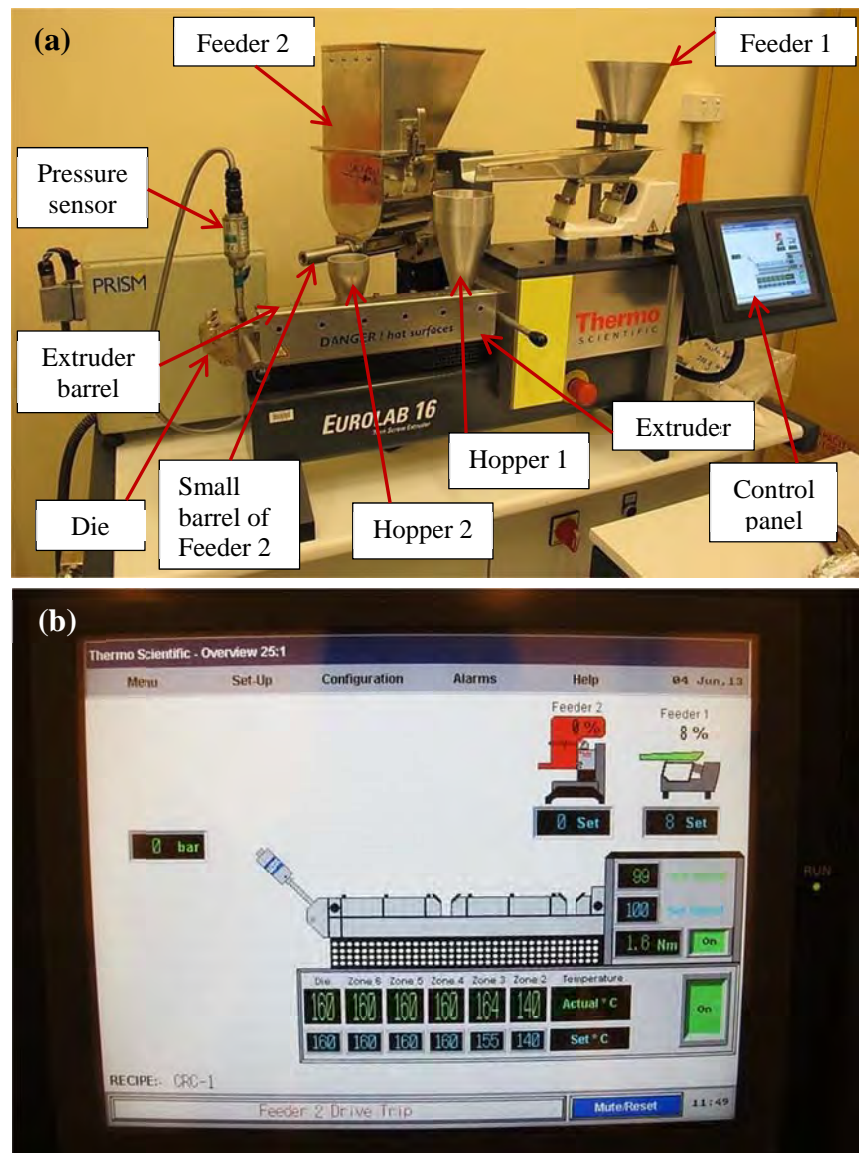


**Figure 4.3:** (a) Thermo Scientific Eurolab 16 twin-screw extruder with two feeders and (b) control panel.

For the untreated fibres, the HDPE and MAPE (57:3) were mixed in a plastic bag and added into Feeder 1, which then fed in Hopper 1, Figure 4.3. The fibres were simultaneously added into Feeder 2, Figure 4.4, which in turn fed into Hopper 2. The



feed rate from the feeder to the hopper for the HDPE/MAPE was 8% (approximately 4.1 g/min), while that for the fibres was 50% (approximately 2.7 g/min), respectively. The screw speed was 100 rpm. The temperature of the barrels was approximately 140°C for zone 2, 155°C for zone 3 and 160°C for zones 4-6 and also at the die, Figure 4.3b. The UKF/HDPE/MAPE extrudates were cut into lengths of 150-200 mm as they emerged from the die and immediately pressed by hand between two panels of carbon fibre composite to minimise warping.

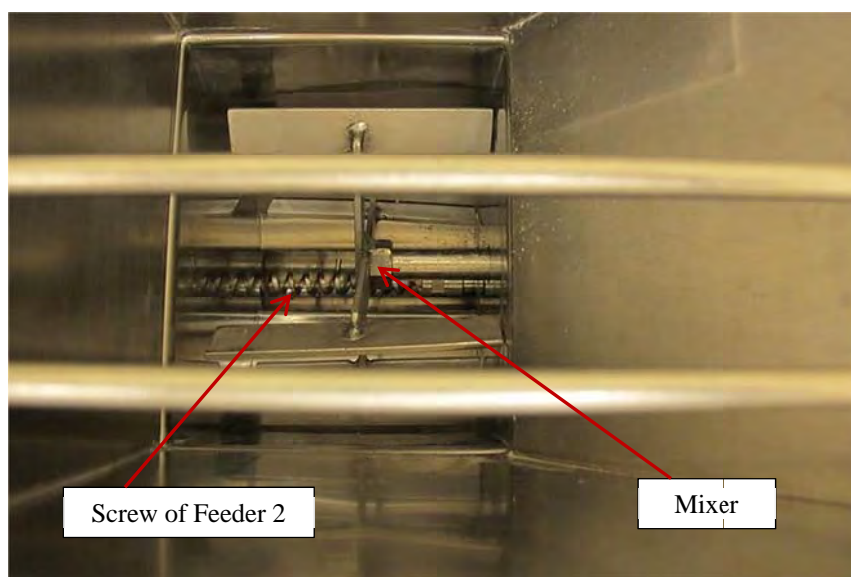


**Figure 4.4:** Inside of Feeder 2 used for feeding the kenaf fibres.

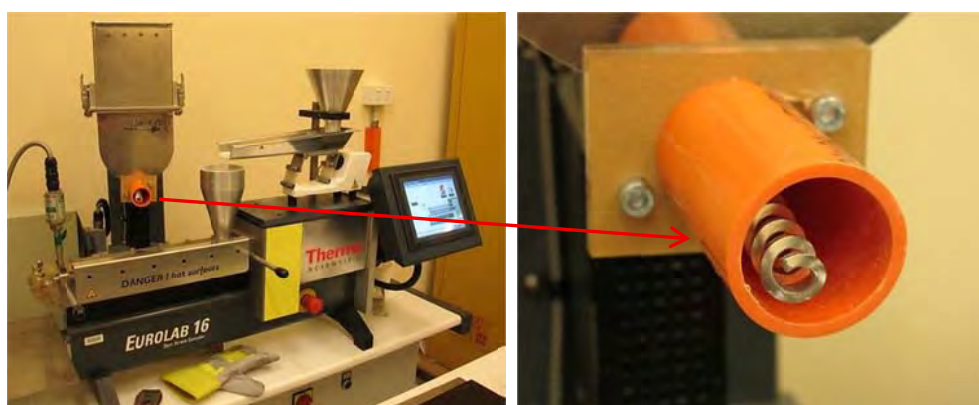


**Figure 4.5:** Large barrel of feeder 2 for feeding the treated kenaf fibres.

HDPE and HDPE/MAPE extrudates were also prepared using the same conditions. The HDPE/MAPE had the same ratio (57:3) as in the composites and was

again premixed in a plastic bag prior to feeding into Feeder 1. Feeder 1 was also used for the HDPE samples.

For the treated kenaf fibres (KFTN and KFTHA2), the barrel of Feeder 2 was changed to a larger barrel, Figure 4.5, while the feed rate was changed to 27% and 100%, respectively, to maintain a feed of approximately 2.7 g/min, as used for the untreated fibres. Otherwise the process remained the same.

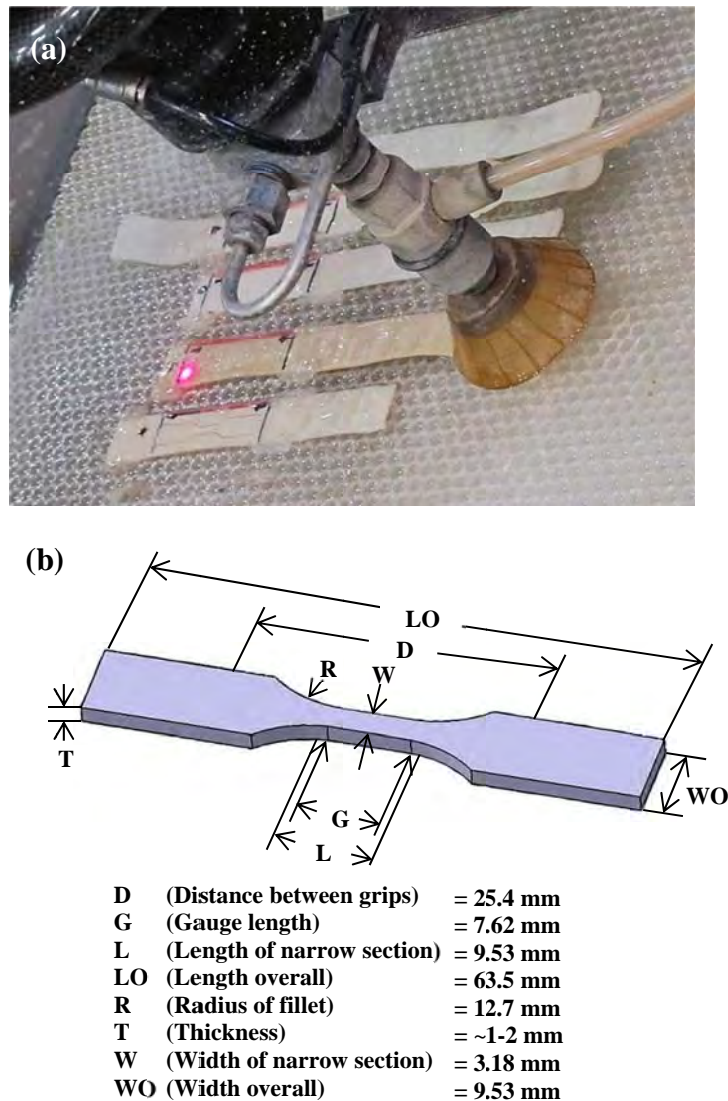


**Figure 4.6:** (a) Water jet cutting into dog-bone specimens and (b) schematic diagram of Type V tensile specimen in accordance with ASTM standard D638-10.

While care was taken to minimise warping by cutting the extrudate into short strips as it emerged from the die and hand pressing these strips before they had cooled to room temperature, it was noticed that the end of the strips which had emerged from the die first usually contained transverse wrinkling. In view of this, it was only possible to obtain samples for tensile testing from the flat end of the strips (i.e., the end which had emerged from the die last) as can be seen in Figure 4.6a. Test samples were however able to be obtained from the more heavily wrinkled strips after first flattening out the wrinkles for 10 minutes at 160°C using a Carver hot press. A pressure of 4 tonnes was used for the HDPE and HDPE/MAPE samples while a pressure of 8 tonnes was used for the kenaf fibre/HDPE/MAPE samples. Different designations were used to allow the hot pressed samples to be distinguished from the as-extruded samples. Accordingly, the as-extruded samples are referred to hereafter as HDPE, HDPE/MAPE, UKF/HDPE, KFTN/HDPE and KFTHA/HDPE strip composites while, the hot pressed samples are referred to as HDPE\_H, HDPE/MAPE\_H, UKF/HDPE\_H, KFTN/HDPE\_H and KFTHA/HDPE\_H strip composites.

The extruded samples with and without hot pressing were water jet cut into Type V dog-bone tensile specimens in accordance with ASTM standard D638-10, as shown in Figure 4.6. The tensile specimens were dried in an oven at 70°C for 1 hour prior to testing to remove moisture.

#### **4.3.2 Fibre Weight Fractions of Extruded Composites**

The weight fraction of the fibres in the composites was determined by dissolving the HDPE/MAPE matrix using 1,2,4-trichlorobenzene as a solvent, as in previous work by Chu, Onclin & Ford (1984) and Macko, Pasch, Kazakevich & Fadeev (2003). For the rod composites, twenty-two specimens of each extrudate were examined. This was done by taking one specimen 6 cm long from each of 22 pieces of extrudate. For the strip composites, four representative specimens were examined for each of the unpressed and pressed materials. The tab section of the tested dog-bone specimens was used for this purpose.

The samples were weighed, then placed into 50 ml of trichlorobenzene in a fume cupboard at approximately  $165 \pm 5^\circ\text{C}$  for 1 hour. The solution was continuously stirred at 400 rpm using a stirrer. After the HDPE had dissolved, the fibres were filtered using a filter paper of known weight, using a Buchner funnel and a side-arm flask connected to a vacuum pump. It was necessary to filter the fibres while the solution and glassware

were hot because the HDPE only remained dissolved while the solution was hot. The fibres and the filter paper were then dried in an oven at 100°C for 1.5 hours. They were then placed in a desiccator, allowed to cool to room temperature, and then weighed. The measured weight fraction was then determined.

Since this method relies on the weight difference before and after immersion in the solvent, it was necessary to also take into account any weight loss resulting from dissolution of material in the fibres. Accordingly, samples of the UKF, KFTN and KFTHA fibres were soaked in hot trichlorobenzene using an identical procedure to that used for the composite samples. Four replicate samples were examined for each fibre type. The fibre weight loss was then determined and was used as a correction factor when determining the true fibre weight fraction of the composites as follows:

$$\text{True fibre weight fraction (\%)} = \frac{\text{Measured fibre weight fraction (\%)}}{100 - \text{Fibre weight loss (\%)}} \times 100 \quad (4.1)$$

$$\text{Correction factor of fibre weight fraction} = \frac{100}{100 - \text{Fibre weight loss (\%)}} \quad (4.2)$$

$$\begin{aligned} \text{True fibre weight fraction (\%)} \\ &= \text{Measured fibre weight fraction (\%)} \\ &\times \text{Correction factor of fibre weight fraction.} \end{aligned} \quad (4.3)$$

The residue from the filtered solution was also analysed using a Perkin Elmer Spotlight 400 FTIR microscope within universal attenuated total reflectance (UATR) mode in the range of 4,000-650 cm<sup>-1</sup>, with a resolution of 4 cm<sup>-1</sup>. Prior to undertaking the analysis the filtered solution was heated at approximately 150°C on a hot plate to evaporate the trichlorobenzene.

### 4.3.3 Transverse and Longitudinal Microstructures of Composites

The transverse and longitudinal microstructure was examined for both the rod and strip composites. The transverse microstructure was examined in three randomly selected pieces approximately 6 metres in length from each of the UKF/HDPE and KFTN/HDPE rod composites. The two ends were cut from each piece and both were examined. Due to die swell, one end of the pieces had a larger diameter than the other end, and the specimen from this end was identified as End A while that from the other



end was identified as End B. Transverse sections were also taken from the gauge length of three representative tensile test specimens for each of the UKF/HDPE, KFTN/HDPE, KFTHA/HDPE, UKF/HDPE\_H, KFTN/HDPE\_H and KFTHA/HDPE\_H composite strips. All specimens were mounted on the transverse plane using cold-setting epoxy resin.

The longitudinal microstructure was determined in four randomly selected samples from the extruded rod composites (again ~ 6 mm long) and three representative tensile specimens from both the as-extruded and hot pressed strip composites. As for the transverse microstructure, the longitudinal microstructure was examined at both ends of the rod composites. All specimens were sectioned longitudinally and mounted in cold-setting epoxy resin. In the case of the strip composites the longitudinal section was made perpendicular to the surface of the strip.

After mounting the specimens were metallographically ground using successively finer emery papers then polished on diamond pads to 1 micron finish. The polished surfaces were then sputter coated with gold using an Emitech K550x gold sputter coater and examined using a Hitachi S3400-X scanning electron microscope (SEM) operated in high vacuum mode at an accelerating voltage of 15 kV. Backscattered electrons were used for imaging since this provided better contrast than was obtained using secondary electrons.

#### **4.3.4 Tensile Testing**

##### ***4.3.4.1 Rod Composites***

Tensile testing of the extruded HDPE and kenaf fibre/HDPE (UKF/HDPE and KFTN/HDPE) rod composites was carried out using an Instron 5565 universal testing machine. The tensile testing was conducted at a crosshead speed of 5 mm/min, using a 5 kN load cell, under ambient conditions of temperature and humidity.

Silicone rubber strips were bonded with double sided tape to each face of the flat grips of the testing machine to allow gripping of the specimens, as shown in Figure 4.7. Specimens 160 mm long were placed in the grips with a gauge length (distance between the two grips) of 20 mm. The diameter of the extruded rods was measured at 3 equally spaced positions along the gauge length.

Six randomly selected specimens were tested for the HDPE rods while 22 specimens were tested for both the untreated fibre/HDPE (UKF/HDPE) and nitric acid

treated fibre/HDPE (KFTN/HDPE) composites. The composite extrudates broke frequently during extrusion and the samples tested were taken from the centre of the longest pieces of extrudate. The tensile modulus was determined as the chord modulus at a strain range of 1% - 3% whilst the ultimate tensile strength was determined as the maximum stress from the stress-strain curve. The strain at maximum stress was also determined from the stress-strain curve.



**Figure 4.7:** Setup using silicone rubber strip fixtures for tensile testing of an extruded composite rod using an Instron universal testing machine.

#### ***4.3.4.2 Strip Composites***

Tensile testing of the HDPE, HDPE\_H, HDPE/MAPE\_H, UKF/HDPE, UKF/HDPE\_H, KFTN/HDPE, KFTN/HDPE\_H, KFTHA/HDPE and KFTHA/HDPE\_H strip composites was carried out using Type V dog-bone specimens in accordance with ASTM standard D638-10. The dimensions of these specimens are shown in Figure 4.6. Testing was conducted using a Lloyd EZ50 universal testing machine, with a mechanical extensometer, having a 9.8 mm gauge length, Figure 4.8.

Testing was carried out under ambient laboratory conditions (at  $23 \pm 2^\circ\text{C}$  and  $50 \pm 5\%$  relative humidity) at a crosshead speed of 5 mm/min using a 5 kN load cell. The distance between the grips at the start of each test was maintained at 25.4 mm using the reset function on the machine controls. A minimum of six replicate specimens were tested for each of the different materials. A HDPE specimen is shown during testing in Figure 4.8c.

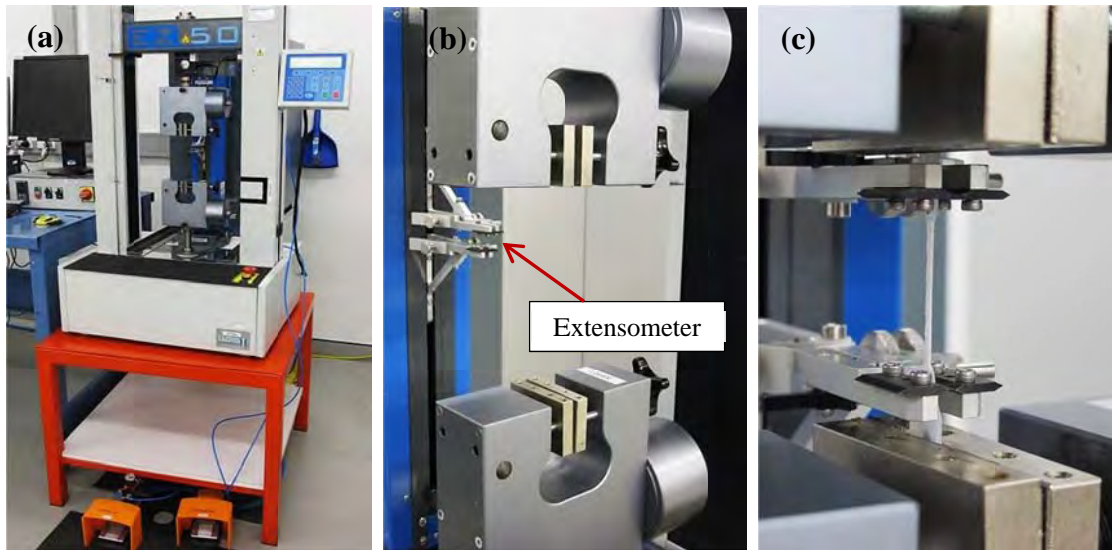


**Figure 4.8:** (a) Lloyd EZ50 universal testing machine, (b) mechanical extensometer and (c) testing a tensile specimen of HDPE.

Prior to testing, the width and thickness was measured at three equally spaced positions along the gauge length of each specimen. The tensile modulus was determined as the chord modulus at a strain range of 0.1% - 0.3% while the ultimate tensile strength was determined as the maximum stress from the stress-strain curve. The strain at maximum stress was also determined from the stress-strain curve.

#### 4.3.5 Fractographic Examination

The fracture surfaces of the tensile specimens (both rod and dog-bone specimens) were examined using a Hitachi S3400-X scanning electron microscope to evaluate the level of bonding between the fibres and the HDPE matrix. The specimens were first sputter coated with gold using an Emitech K550x gold sputter coater and then examined in high vacuum at an accelerating voltage of 15 kV using secondary electrons.

## 4.4 Results

### 4.4.1 Extruded HDPE and Composites

#### 4.4.1.1 Rod Composites

The neat HDPE, UKF/HDPE and KFTN/HDPE rod composites are shown, emerging from the twin dies, and after subsequent coiling, in Figures 4.9 to 4.11, respectively. The presence of fibres produced a brown colouration in the composites with the colour being darkest for the nitric acid treated fibre composites. The surface of the extrudate was smooth for the neat HDPE but was rough for the composites, Figures 4.9 to 4.11, this being most pronounced in the untreated fibre composites, Figure 4.12. Some variation in roughness was also evident along the extrudates.



**Figure 4.9:** Extruded neat HDPE rods.





**Figure 4.10:** Extruded UKF/HDPE rod composites.



**Figure 4.11:** Extruded KFTN/HDPE rod composites.

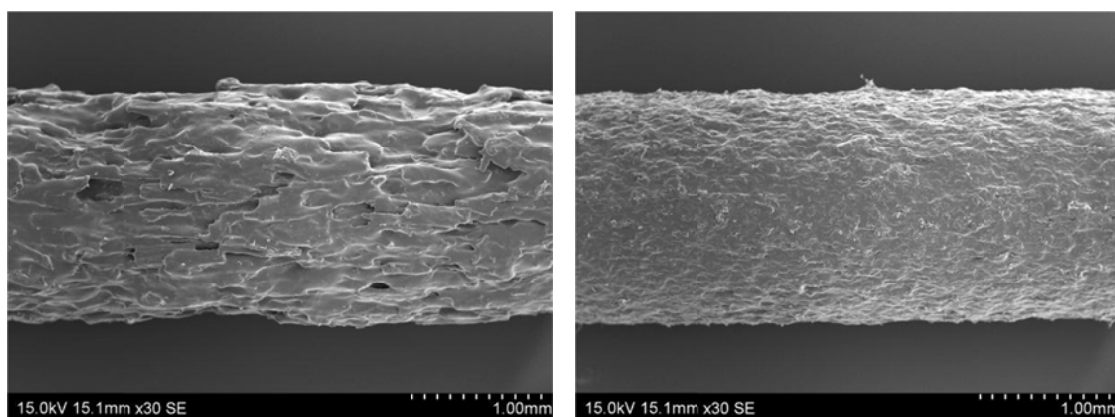


**Figure 4.12:** SEM micrographs of surface of UKF/HDPE (left) and KFTN/HDPE (right) rod composites.

#### ***4.4.1.2 Strip Composites***

The neat HDPE and HDPE/MAPE extruded strips are shown after cutting into lengths in Figure 4.13, respectively. Twisting of the extrudates is readily apparent.

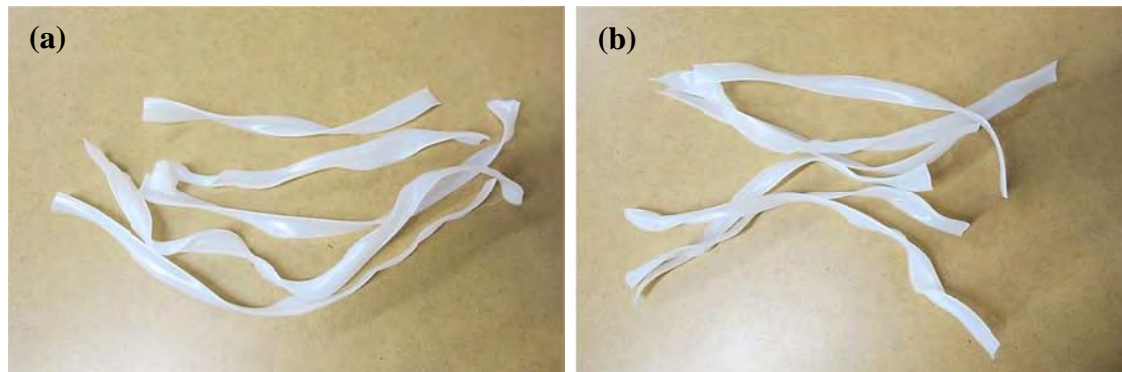


**Figure 4.13:** Extruded (a) neat HDPE and (b) HDPE/MAPE strips.

The extruded strip composites made using untreated fibres, nitric acid treated fibres and hydrogen peroxide/acetic acid treated fibres are shown in Figures 4.14. As noted in Section 4.3.1, the extruded strip was cut into short samples as it emerged from the die to minimise warping.

There was a striking difference between the colour of the composites. The untreated fibre composites and the nitric acid treated fibre composites were light brown and dark brown, respectively, as for the corresponding rod composites, however the hydrogen peroxide/acetic acid treated fibre composites were light cream in colour.

Some variation in colour, suggesting variation in fibre fraction, was observed amongst the different pieces of each type of the composites. This is more evident in Appendix V which shows all the samples after tensile testing.

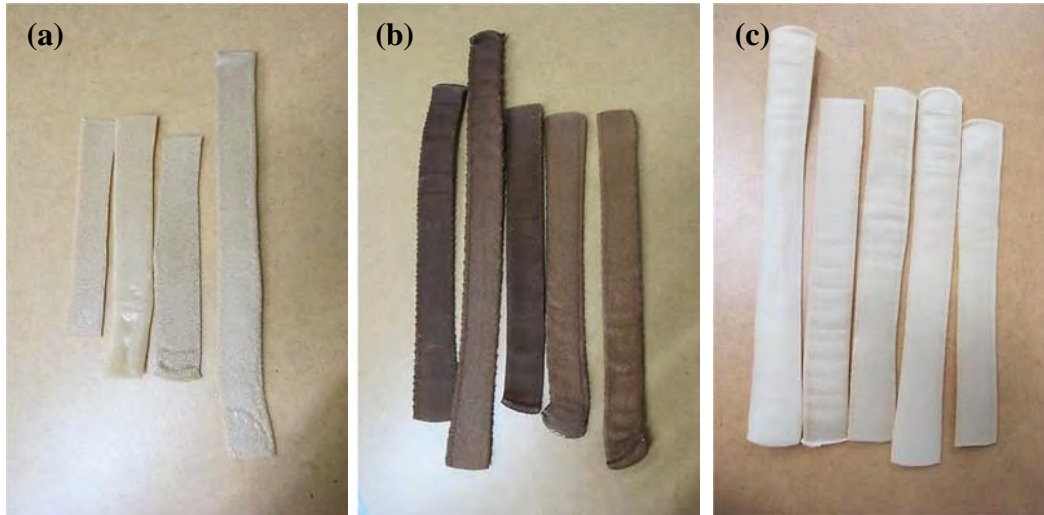


**Figure 4.14:** Extruded strip composites: (a) UKF/HDPE, (b) KFTN/HDPE and (c) KFTHA/HDPE.



**Figure 4.15:** Hot pressed extruded HDPE (HDPE\_H) strip.

The composites did not show the twisting observed for the unreinforced HDPE extrudates. However, transverse wrinkling was present at the front end of the extruded samples, as noted in Section 4.3.1, and only the back end was used for testing.





**Figure 4.16:** Hot pressed extruded HDPE/MAPE (HDPE/MAPE\_H) strip.

The hot pressed samples are shown in Figures 4.15-4.19. The water jet cuts used to produce the tensile samples can be seen in the strips. The strips all had smooth surfaces after hot pressing, but some lateral spreading had occurred. This was most pronounced for the nitric acid treated fibres and least pronounced for the hydrogen peroxide/acetic acid treated fibre composites. It was noticed that the hot pressing also caused darkening of the composites.

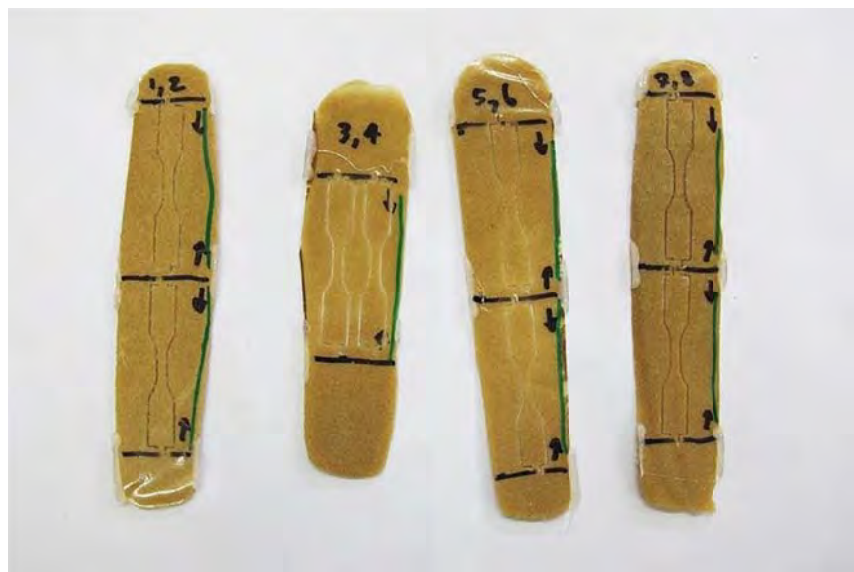


**Figure 4.17:** Hot pressed extruded UKF/HDPE (UKF/HDPE\_H) strip.





**Figure 4.18:** Hot pressed extruded KFTN/HDPE (KFTN/HDPE\_H) strip.

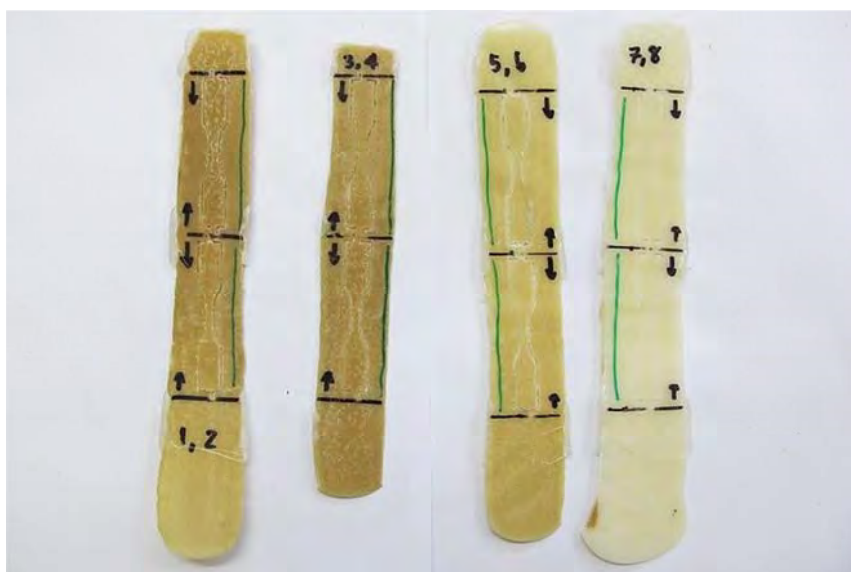


**Figure 4.19:** Hot pressed extruded KFTHA/HDPE (KFTHA/HDPE\_H) strip.

#### 4.4.2 Fibre Weight Fractions of Extruded Composites

The fibres are shown after extraction from the rod composites in Figures 4.20 while the process is shown in Appendix VI. The untreated fibres were found to be lighter in colour than the nitric acid treated fibres, consistent with the difference in colour of the composites.

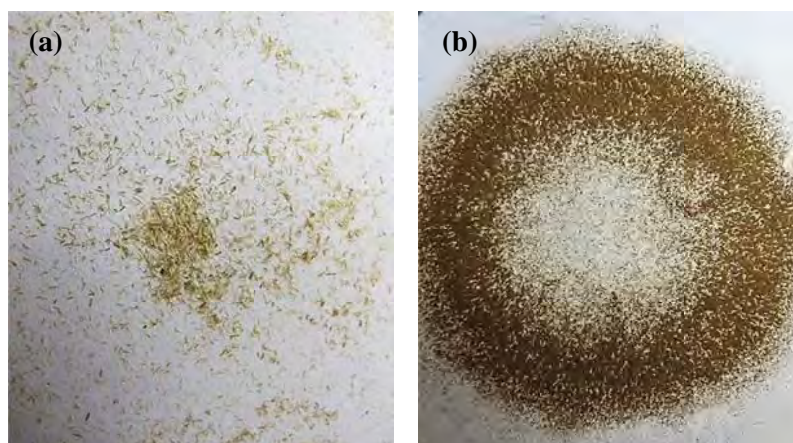


**Figure 4.20:** Fibres after extraction from rod composites: (a) untreated fibres (b) nitric acid treated fibres.

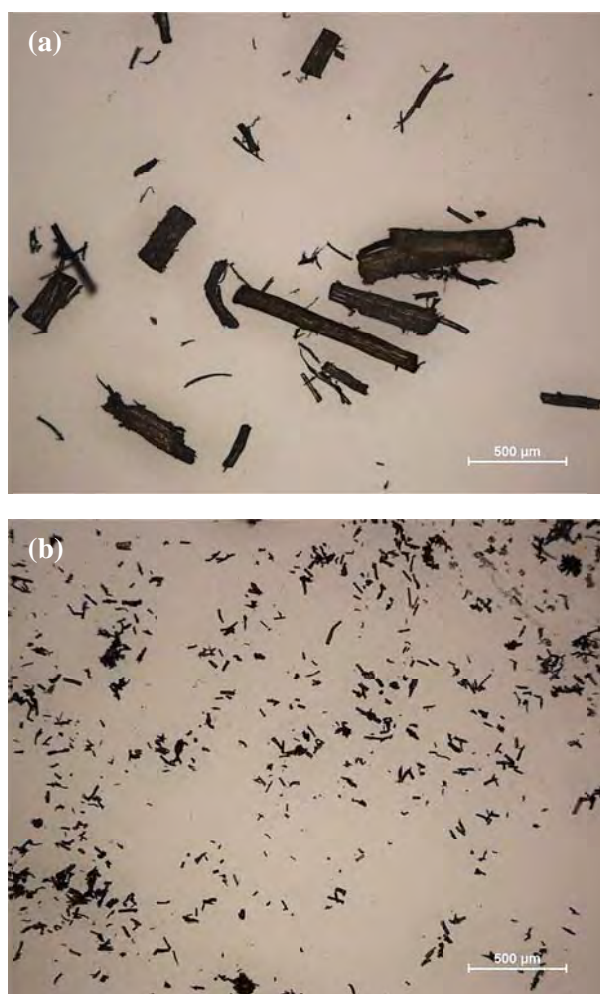


**Figure 4.21:** Fibres after extraction from rod composites shown at higher magnification: (a) untreated fibres and (b) nitric acid treated fibres.

The extracted fibres are shown at higher magnification in Figure 4.21. The untreated fibres appear essentially unchanged after the extrusion process, except for some fibrillation. However, the nitric acid treated fibres have been reduced to less than half their original length.

The measured weight fractions are given for the individual samples in Appendix VII. The average values were 36.7% with a standard deviation of 2.4% (7% of average value), for the untreated fibre composites, and 33.3% with a standard deviation of 3.7% (11% of average value), for the treated fibre composites.

The fibres are shown after extraction for the strip composites in Figure 4.22 while the process is shown in Appendix VI. Again the fibres differ substantially in colour, consistent with the differences seen in the composites.

The extracted fibres are shown at higher magnification in Figure 4.23. Again the untreated fibres show little change after the extrusion process, apart from some fibrillation. However, the hydrogen peroxide/acetic acid treated fibres have been reduced to about one tenth their original length, while the nitric acid treated fibres are very short, often having been reduced essentially to particulate.

The average measured fibre weight fractions for the strip composites in both the as-extruded and hot pressed conditions are shown in Figure 4.24 while the individual results are given in Appendix VII. The results for the untreated fibre composites were similar for both conditions (UKF/HDPE and UKF/HDPE\_H), with values of 16.8% (standard deviation 4.9%) and 14.4% (standard deviation 8.1%) being obtained for the as-extruded and hot pressed composites, respectively.

The results for the hydrogen peroxide/acetic acid treated fibre composites (KFTHA/HDPE and KFTHA/HDPE\_H) were also similar for both the as-extruded and hot pressed conditions, with the values being 30.1% (standard deviation 15.7%) and 29.9% (standard deviation 15.7%), respectively.

The results for the nitric acid treated fibre composites (KFTN/HDPE and KFTN/HDPE\_H) were however quite different for the two conditions with values of 34.4% (standard deviation 25.0%) and 8.1% (standard deviation 1.9%) being obtained for the as-extruded and hot pressed composites, respectively. The weight fraction should be the same for both the as-extruded and hot pressed composites, except for any place-to-place variation in the locations from which the samples were taken from the

extrudate. This is considered to be the source of the discrepancy and is discussed in more detail in Section 4.5.2.

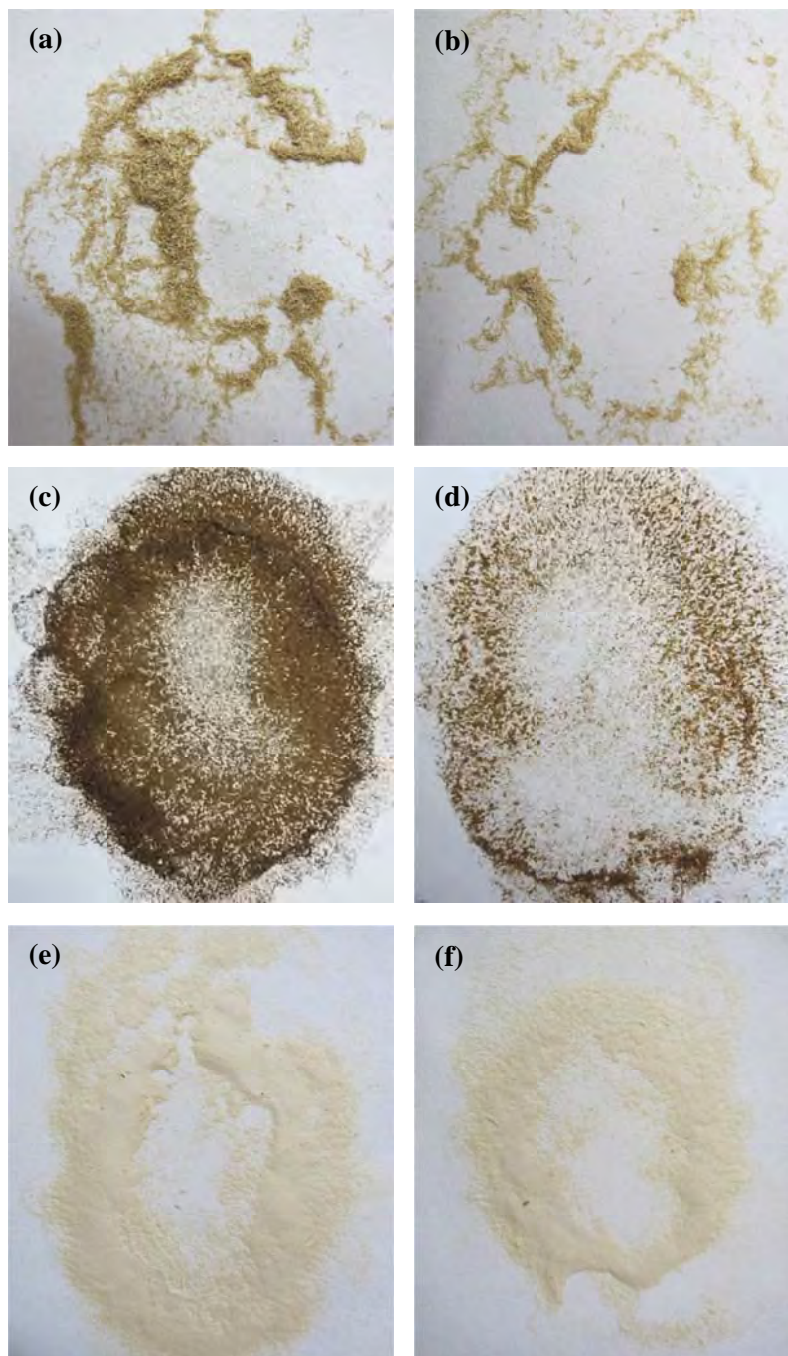


**Figure 4.22:** Fibres after extraction from strip composites (a) as-extruded and (b) hot pressed untreated fibres; (c) as-extruded and (d) hot pressed nitric acid treated fibres; (e) as-extruded and (f) hot pressed hydrogen peroxide/acetic acid treated fibres.



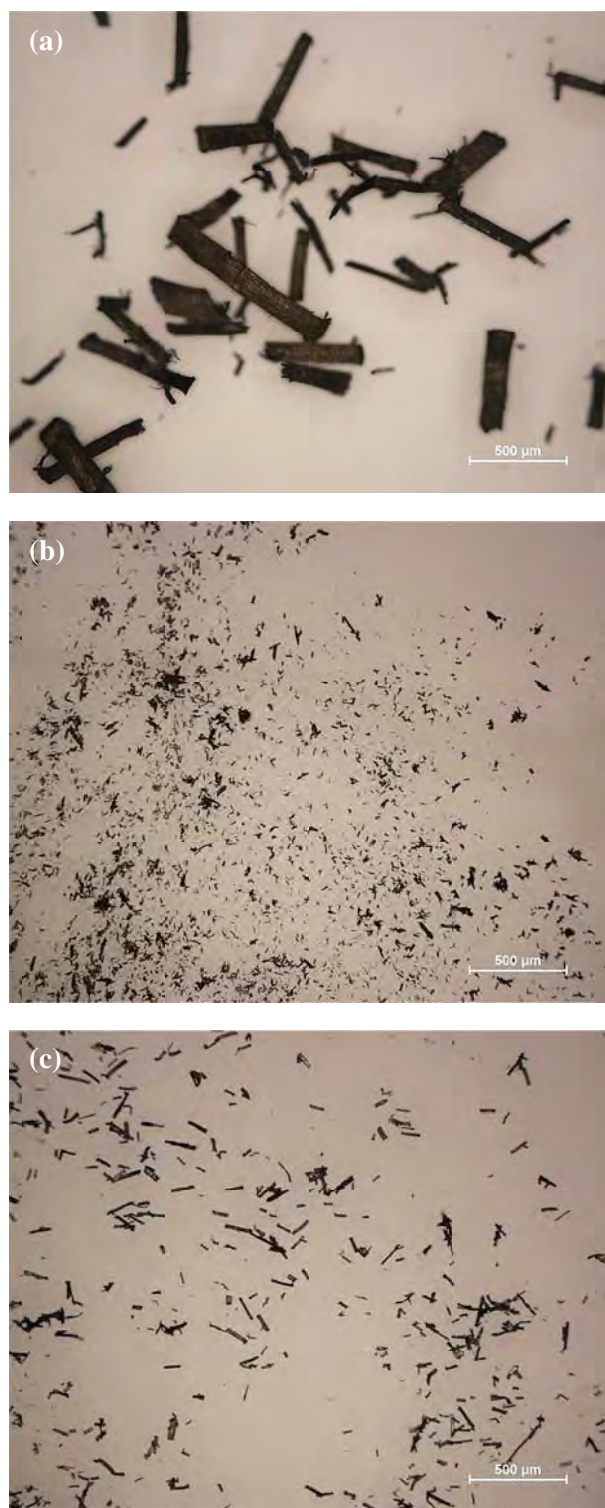


**Figure 4.23:** Fibres after extraction from as-extruded strip composites shown at higher magnification: (a) untreated fibres, (b) nitric acid treated fibres and (c) hydrogen peroxide/acetic acid treated fibres.

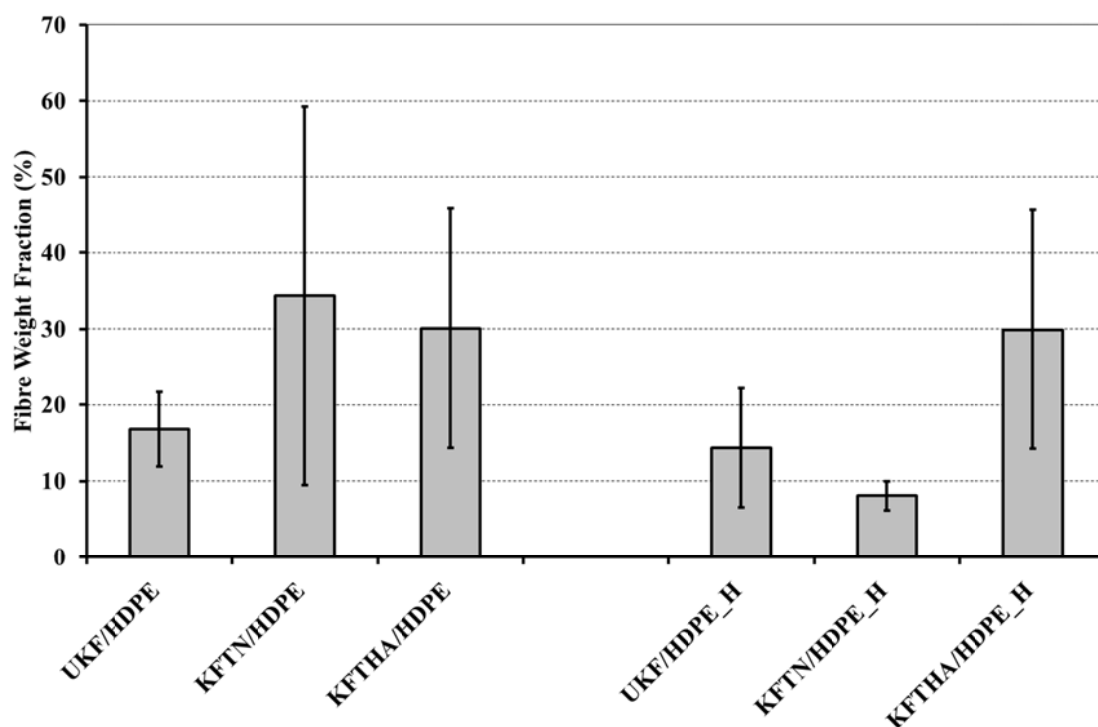


**Figure 4.24:** Average measured fibre weight fractions of untreated and treated fibre composite strips in both as-extruded and hot pressed conditions. Error bars represent one standard deviation.

As noted in Section 4.3.2 the matrix dissolution process may have also caused some dissolution of material in the fibres and this was examined by soaking the untreated and treated fibres in the same solvent under identical conditions to those used for matrix dissolution. The process is shown in Appendix VIII.

The fibres are shown after treatment in Figure 4.25. The fibres appear essentially unchanged after the treatment apart from some possible fibre breakage for the higher aspect ratio hydrogen peroxide/acetic acid treated fibres. This indicates that the substantial reductions in length seen for the elementary fibres after they had been extracted from the composites is due primarily to the extrusion process rather than the extraction process.

Some weight loss occurred for all the fibres, with the values ranging from 3.7% to 12.6%, Table 4.3. The weight loss was lowest for the untreated fibres (3.7%, standard deviation 0.5%), highest for the nitric acid treated fibres (12.6%, standard deviation 0.7%) and intermediate for the hydrogen peroxide/acetic acid treated fibres (5.3%, standard deviation 0.3%).

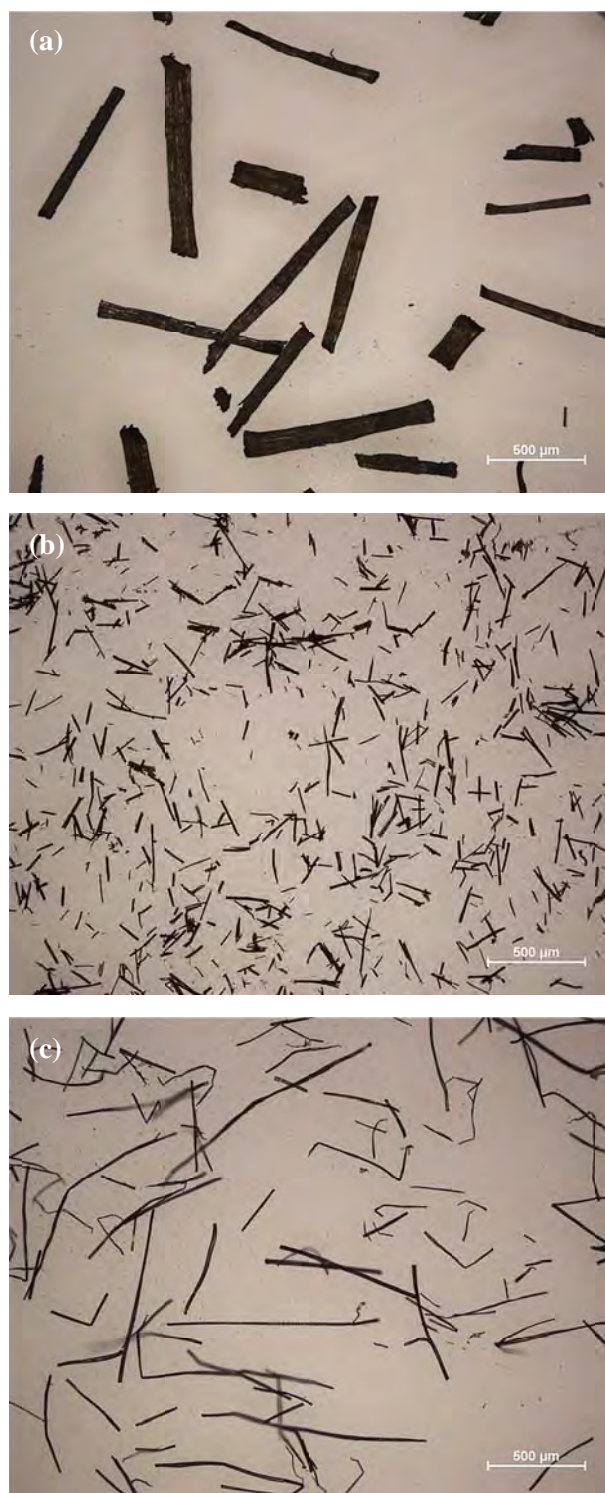


**Figure 4.25:** Fibres after treatment in trichlorobenzene: (a) untreated fibres, (b) nitric acid treated fibres and (c) hydrogen peroxide/acetic acid treated fibres.

**Table 4.3:** Weight loss of fibres after soaking in hot trichlorobenzene (values in brackets represent one standard deviation) and correction factors of fibre weight fractions of the composite samples

<b>Kenaf Fibres</b>	<b>Average Weight Loss of Fibres after Soaking in Hot Trichlorobenzene (%)</b>	<b>Correction Factor of Fibre Weight Fraction</b>
UKF	3.7 (0.5)	1.04
KFTN	12.6 (0.7)	1.14
KFTHA	5.3 (0.3)	1.06

The fibre weight correction factors, determined from these measurements using equation 4.2, are also given in Table 4.3 and range from 1.04 to 1.14. The true weight fractions determined from the measured values multiplied by the correction factors using equation 4.3 are given in Table 4.4. The true weight fractions were 38.1 and 38.0 wt% for the untreated and nitric acid treated fibre rod composites, which are close to the value of 40 wt% used in the formulating the composites, Section 4.3.1.

**Table 4.4:** Measured and true fibre weight fractions of composite samples

<b>Extruded Composites Samples</b>	<b>Measured Fibre Weight Fraction (%)</b>	<b>True Fibre Weight Fraction (%)</b>
UKF/HDPE rods	36.7	38.1
KFTN/HDPE rods	33.3	38.0
UKF/HDPE strip	16.8	17.4
KFTN/HDPE strip	34.4	39.2
KFTHA/HDPE strip	30.1	31.9
UKF/HDPE_H strip	14.4	15.0
KFTN/HDPE_H strip	8.1	9.2
KFTHA/HDPE_H strip	29.9	31.7



For the strip composites, the true weight fractions were 17.4% and 15.0% for the as-extruded and hot pressed untreated fibre composites and 31.9% and 31.7% for the hydrogen peroxide/acetic acid treated fibre composites in the two conditions, respectively. The values for the nitric acid treated fibre composites were 39.2% and 9.2% for the two conditions, respectively. As noted above, this appears to be due to place to place variation in the extrudate.

The fibre weight fractions for the strip composites are generally considerably lower than the intended formulation value of 40%. However, unlike the rod composites, for which the components were premixed then fed using a single hopper, separate feeds were used for the fibres and the matrix when making the strip composites. It appears that the feed rates for the fibres were lower than expected.

The material removed from the fibres as result of treatment in hot trichlorobenzene were analysed by FTIR. The results are given in detail in Appendix IX. The analyses indicated that the weight loss produced in the untreated fibres was due to loss of lignin and waxes. The material removed from both the nitric acid treated and hydrogen peroxide/acetic acid treated fibres appeared to be a product resulting from reaction between oxidized cellulose and hot trichlorobenzene.

#### 4.4.3 Transverse and Longitudinal Microstructures of Composites

Examples of the transverse and longitudinal microstructures of the rod and strip composites are shown in Figures 4.26 to 4.35 while the microstructures of all samples examined are given in Appendices X and XI.

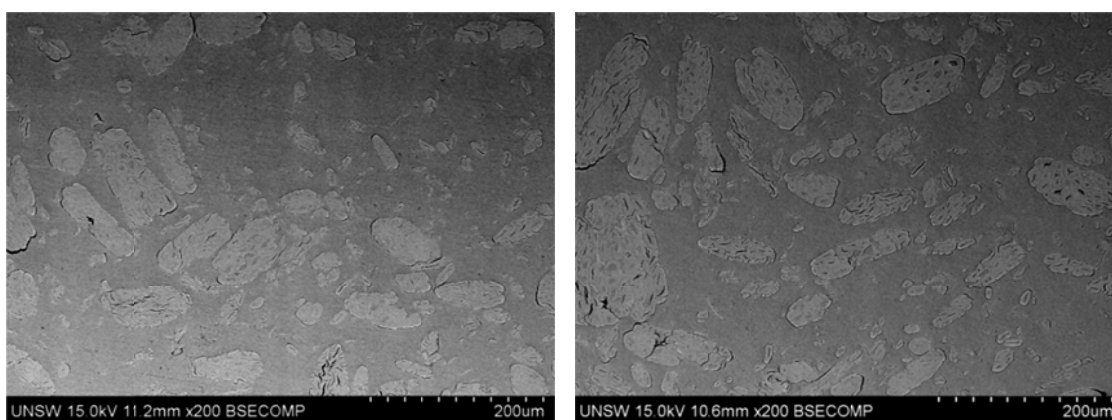


**Figure 4.26:** SEM micrographs of transverse sections of UKF/HDPE rod composites.

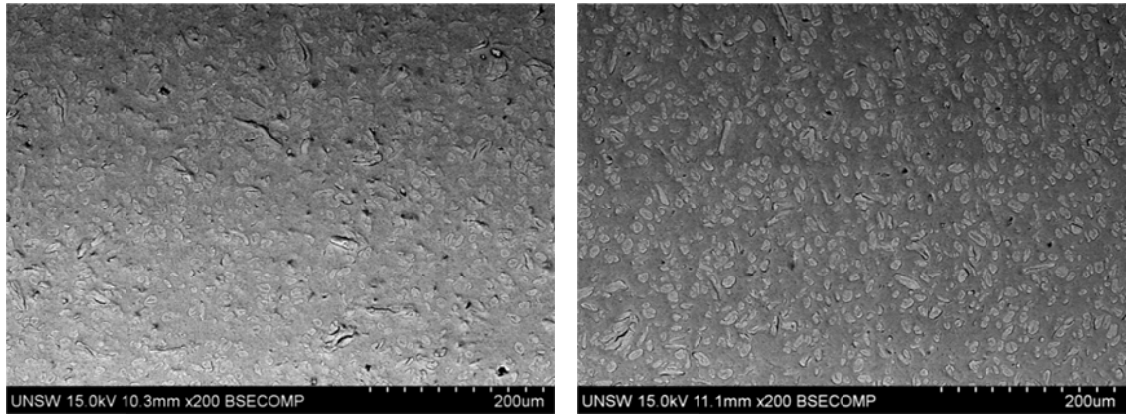


**Figure 4.27:** SEM micrographs of transverse sections of KFTN/HDPE rod composites.

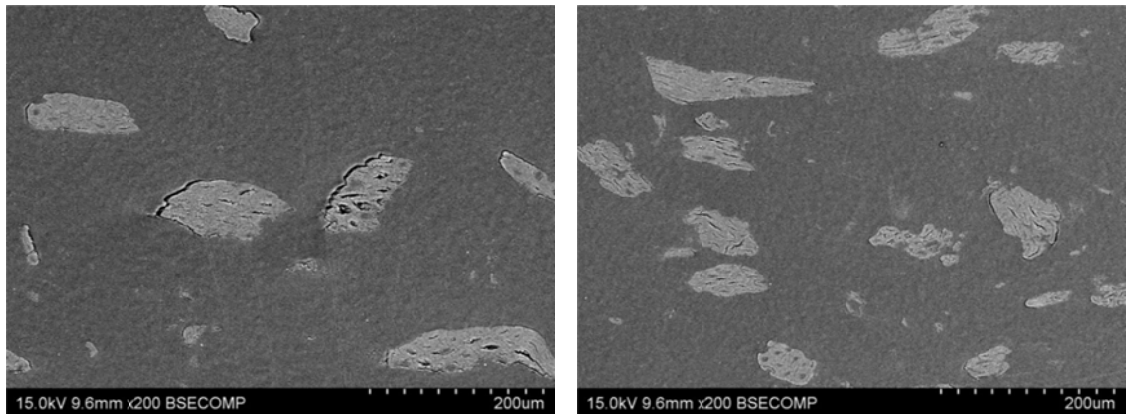


**Figure 4.28:** SEM micrographs of transverse sections of UKF/HDPE strip composites.

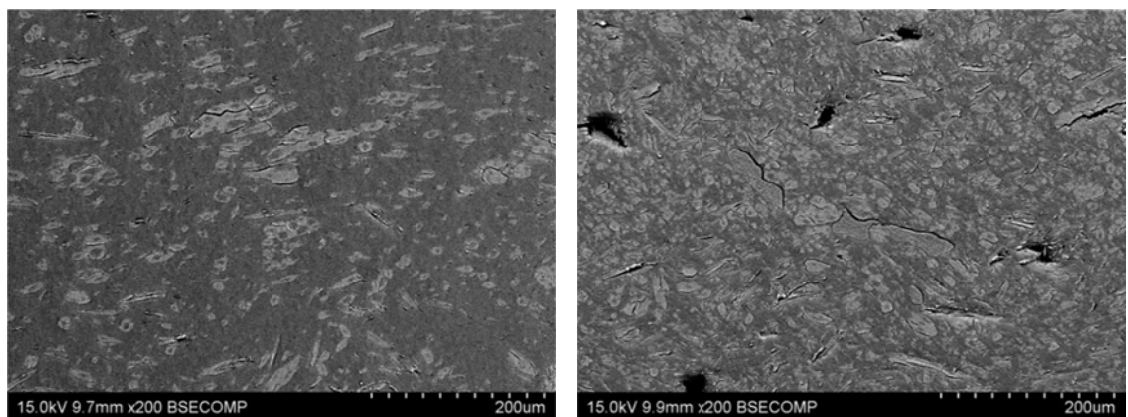


**Figure 4.29:** SEM micrographs of transverse sections of KFTN/HDPE strip composites.

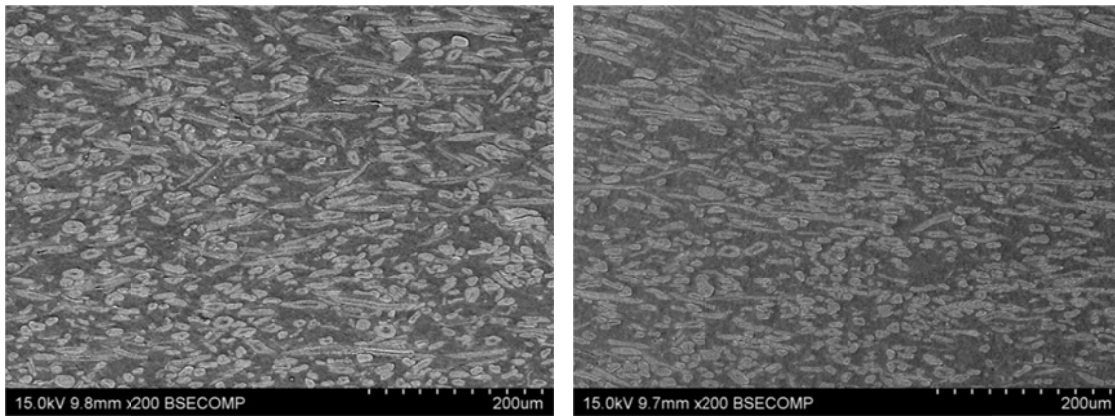


**Figure 4.30:** SEM micrographs of transverse sections of KFTHA/HDPE strip composites.

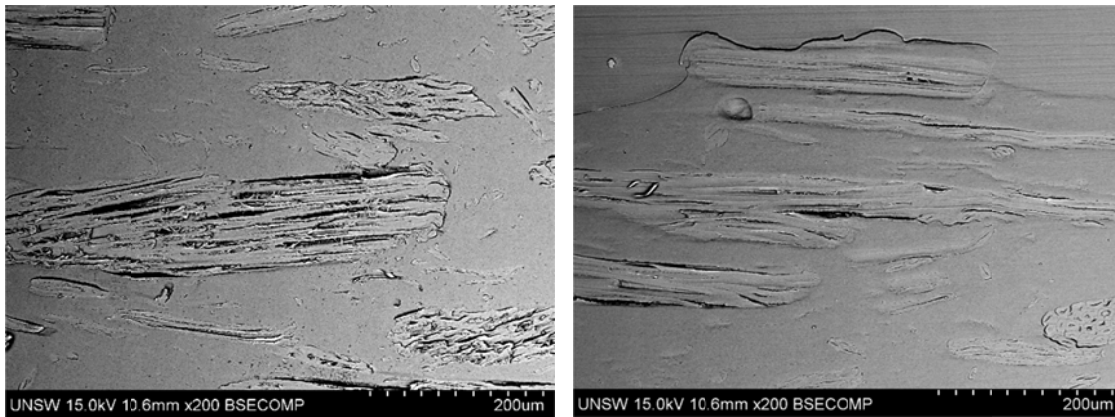


**Figure 4.31:** SEM micrographs of longitudinal section of UKF/HDPE rod composite (a) at centre and (b) at edge of specimen.

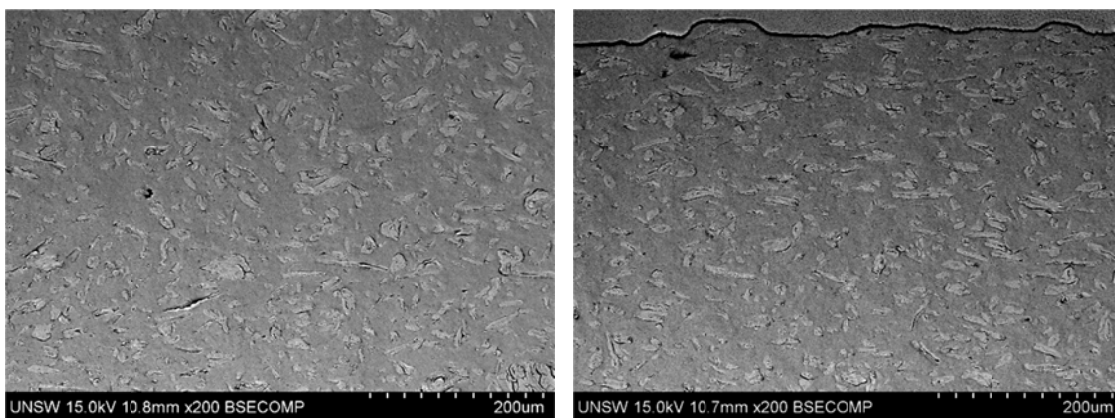


**Figure 4.32:** SEM micrographs of longitudinal section of KFTN/HDPE rod composite (a) at centre and (b) at edge of specimen.

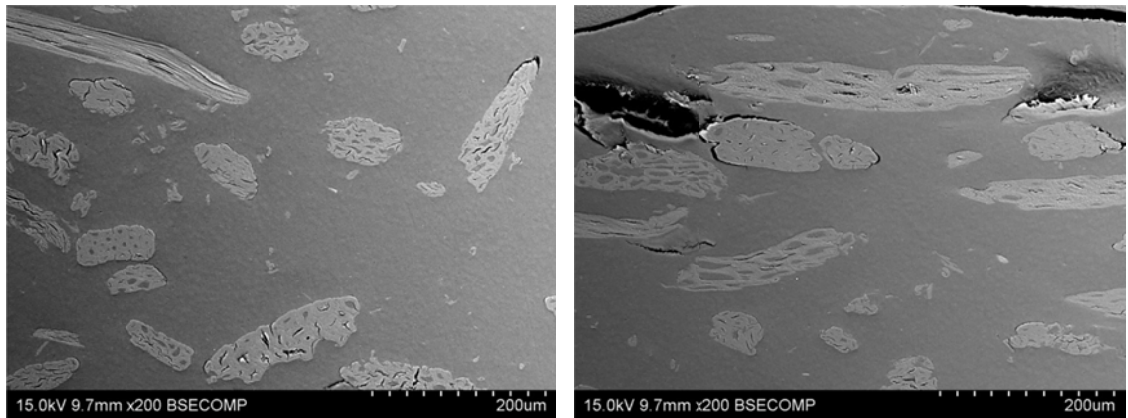


**Figure 4.33:** SEM micrographs of longitudinal section of UKF/HDPE strip composite (a) at centre and (b) at edge of specimen.

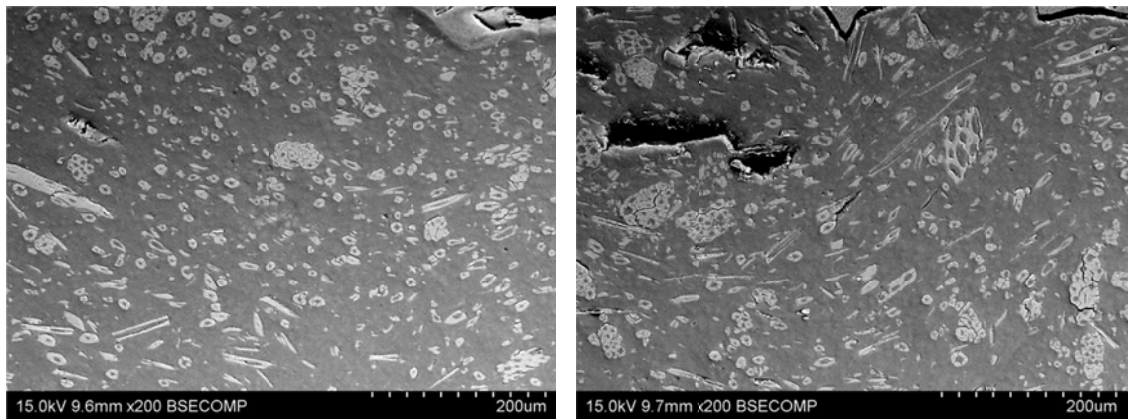


**Figure 4.34:** SEM micrographs of longitudinal section of KTFN/HDPE strip composite (a) at centre and (b) at edge of specimen.

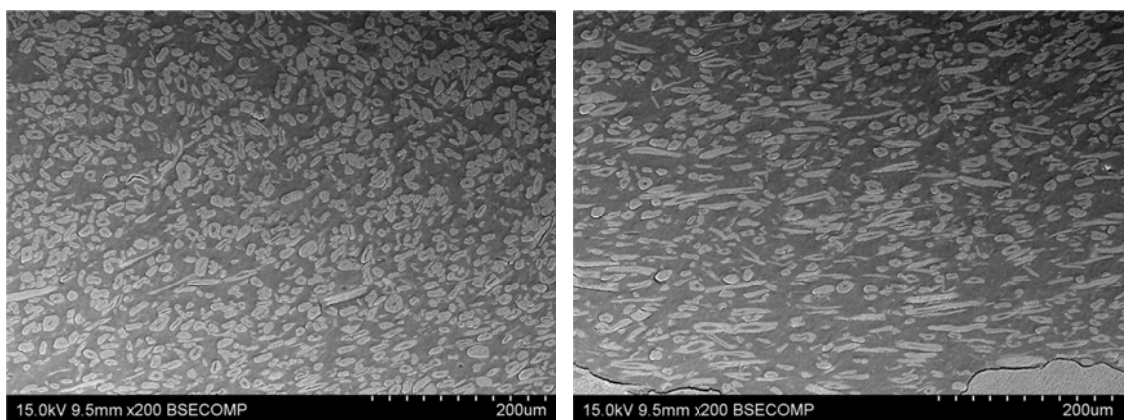


**Figure 4.35:** SEM micrographs of longitudinal section of KTFHA/HDPE strip composite (a) at centre and (b) at edge of specimen.

The fibres were generally well dispersed in the composites. No marked directionality was evident in either the transverse or longitudinal sections indicating that the fibres were reasonably random in orientation. The lumens were generally filled with matrix.

#### 4.4.4 Tensile Properties

##### 4.4.4.1 Rod Composites

Tensile tests were conducted on 6 randomly selected samples from the neat HDPE extruded rods and on 22 samples of both the untreated fibre and the nitric acid treated fibre extruded composite rods.

The tensile stress strain curves are shown in Figures 4.36-4.38. All curves showed a progressive decrease in slope with increasing stress, as is usual for polymeric materials. The curves for the neat HDPE additionally showed the characteristic load drop which occurs at the onset of cold drawing.

All the specimens are shown after failure in Appendix V.

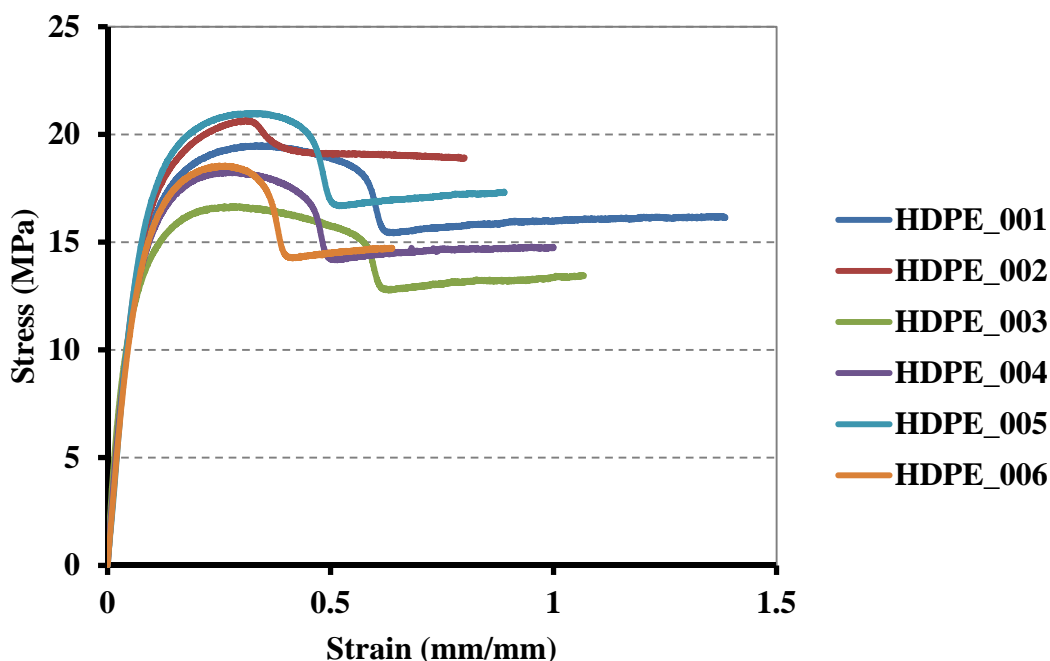
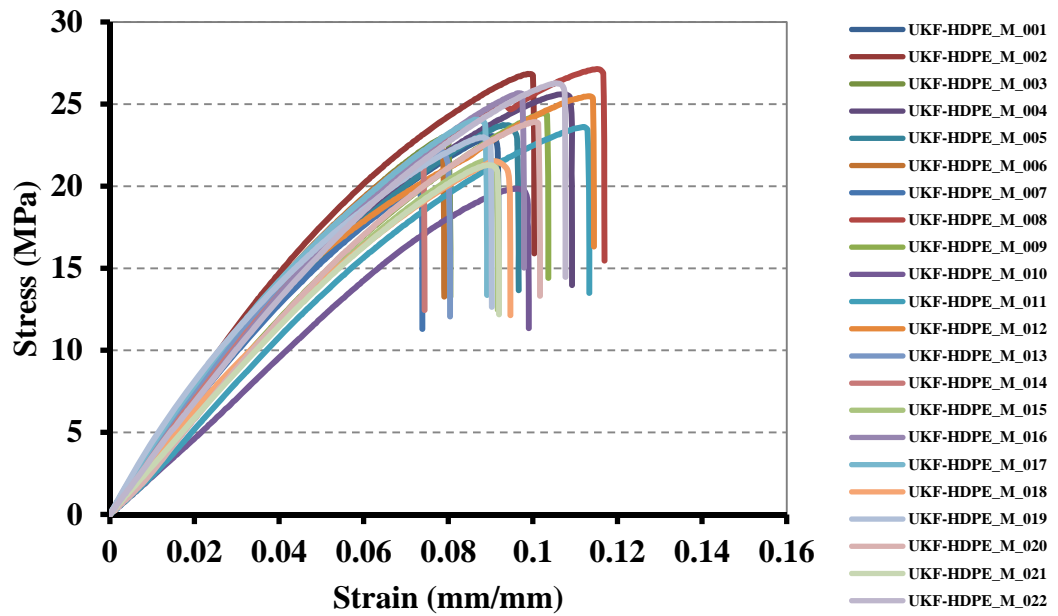
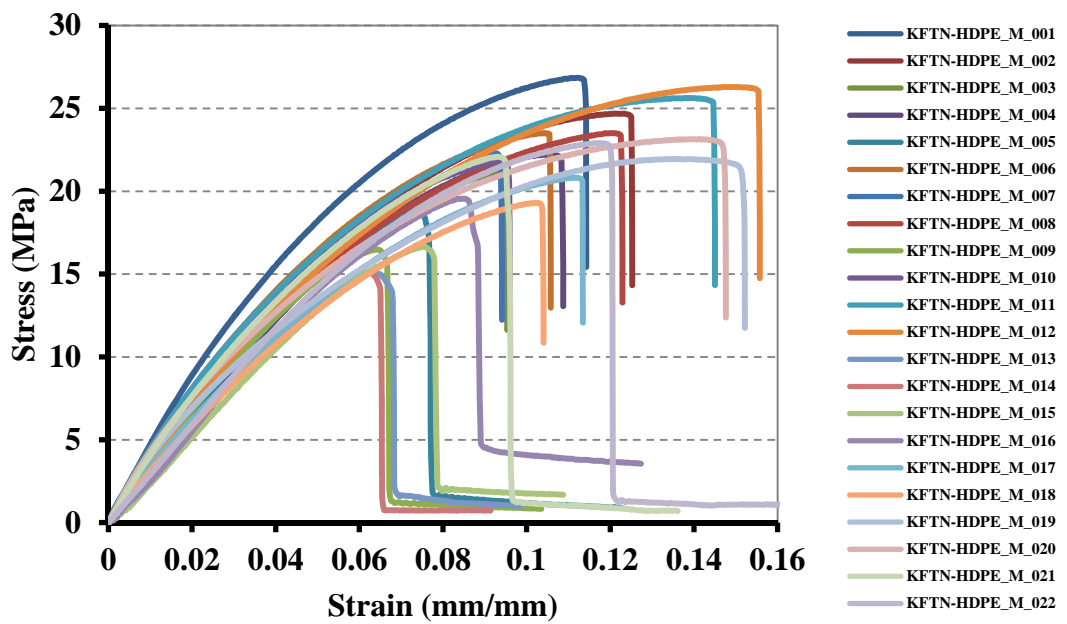


Figure 4.36: Tensile stress-strain curves of extruded neat HDPE rods.



**Figure 4.37:** Tensile stress-strain curves of extruded UKF/HDPE rod composites.



**Figure 4.38:** Tensile stress-strain curves of extruded KFTN/HDPE rod composites.

The tensile modulus, tensile strength and strain at maximum stress are given for the neat HDPE and the rod composites in Table 4.5 and shown in Figures 4.39-4.41. A statistical treatment of the data is given in Appendix XII.

The modulus for the neat HDPE was 238 MPa with a standard deviation of 9 MPa (4%), and was, on average, 33% higher for the two composites. The value for the untreated fibre composite was 325 MPa with a standard deviation of 31 MPa (10%) while that for the nitric acid treated fibre composite was slightly lower being 310 MPa with a standard deviation of 28 MPa (9%). The difference was not however significant, Appendix O.

**Table 4.5:** Tensile test data for extruded HDPE and short kenaf fibre/HDPE rod composites

Tensile Property	Sample		
	HDPE	UKF/HDPE	KFTN/HDPE
Modulus (GPa)	0.238	0.325	0.310
SD (GPa)	0.009	0.031	0.028
Ultimate strength (MPa)	19.1	23.4	21.4
SD (MPa)	1.6	2.1	3.4
Strain at maximum stress (%)	30.3	9.4	10.2
SD (%)	4.2	1.3	2.6

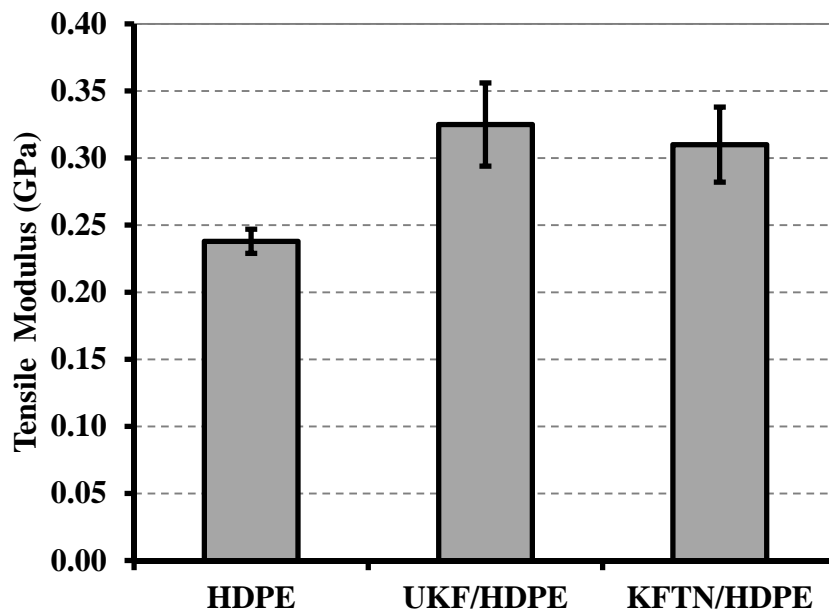


**Figure 4.39:** Tensile modulus of extruded HDPE, UKF/HDPE and KFTN/HDPE rod composites. Error bars indicate one standard deviation.

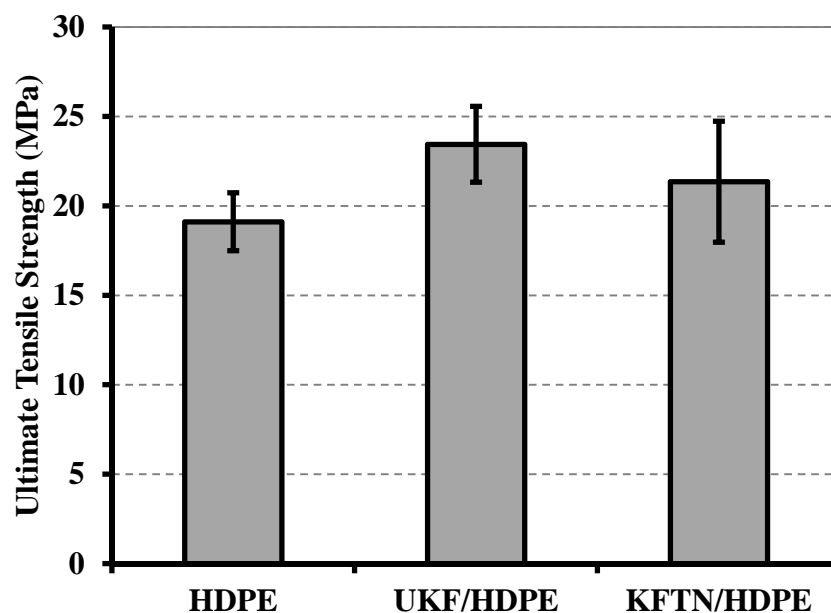


**Figure 4.40:** Ultimate tensile strength of extruded HDPE, UKF/HDPE and KFTN/HDPE rod composites. Error bars indicate one standard deviation.

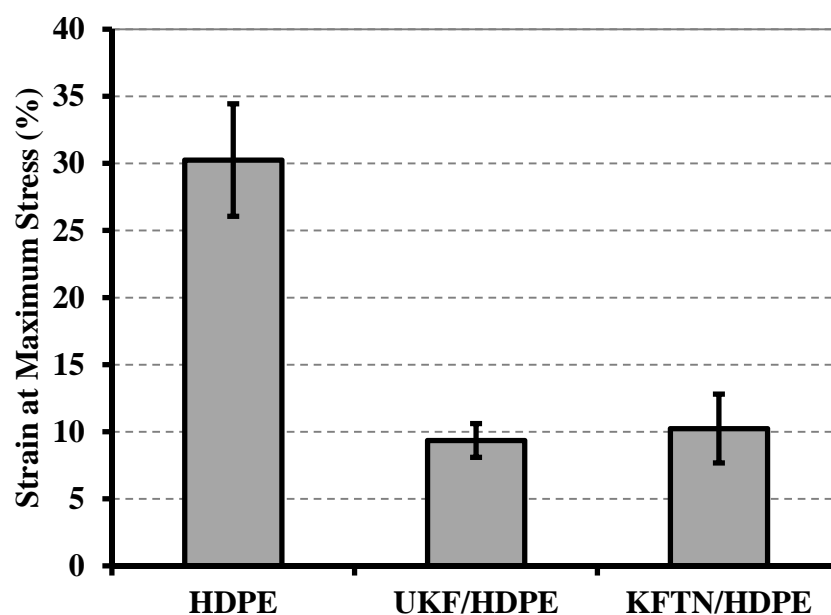


**Figure 4.41:** Strain at maximum stress of extruded HDPE, UKF/HDPE and KFTN/HDPE rod composites. Error bars indicate one standard deviation.

The modulus value of 238 MPa obtained from the neat HDPE was only 34% of the value given in the supplier's data sheet in Table 4.1. The difference is considered to



be due to additional strain occurring in the system, especially in the compliant silicone rubber pads used to grip the specimen. This is discussed in more detail in Section 5.5.3.1. It is expected that the moduli of the composites would be underestimated by a similar amount.

The tensile strength of the HDPE (stress at maximum load) was 19.1 MPa with a standard deviation of 1.6 MPa (8%). This is close to the value of 21 MPa given in the supplier's data sheet, Table 4.1. The strength of the composites was, on average, 17% higher than for the neat HDPE, with the value for the untreated fibre composite being 23.4 MPa with a standard deviation of 2.1 MPa (9%) and that for the nitric acid treated fibre composite being 21.4 MPa with a standard deviation of 3.4 MPa (16%). In this case, the lower value obtained for the nitric acid treated fibre composite was significant, Appendix XII.

The strain at maximum stress was 30.3% (standard deviation 4.2%) for the neat HDPE with much lower values of 9.4% (standard deviation 1.3%) and 10.2% (standard deviation 2.6%) being obtained for the untreated and nitric acid treated fibre composites, respectively. The small difference between the two composites was not significant, Appendix XII.

#### ***4.4.4.2 Strip Composites***

An extensometer was used when testing the strip composites to permit a more accurate determination of strain. However it was noticed after the tests that the extensometer data had corrupted, as is apparent from the stress strain curves given in Appendix XIII, and it was necessary to use the crosshead displacement data instead. This was possible since the distance between the grips was reset to the same value (25.4 mm) after each test so that the same length of specimen was tested in each case. Neglecting any strain occurring in the testing machine, the strain in the gauge length of the specimen is proportional to the crosshead displacement. The crosshead displacement was determined using the time record for each data point (collected at 0.0625 second intervals) and the crosshead speed (5 mm/min.). From the geometry of the specimen it was possible to calculate the approximate crosshead displacement range corresponding to the strain range of 0.001-0.003. This range was 0.0156-0.0521 mm and was used to determine the chord modulus.

The stress-crosshead displacement curves are shown for the different specimens in Figures 4.42 to 4.50. Because of the problems with wrinkling in the as-extruded neat HDPE and HDPE/MAPE specimens, only one specimen could be successfully water cut from the neat HDPE extrudate while it was not possible to obtain any specimens from the HDPE/MAPE extrudate.

The curves for the different specimens were reasonably similar for both the hot pressed HDPE and the hot pressed HDPE/MAPE, but substantial differences were evident in the curves for the different specimens for each of the composites, both as-extruded and hot pressed.

The values of tensile modulus, tensile strength and strain at maximum stress for the different materials are given in Table 4.6 and shown in Figures 4.51 to 4.53, respectively. The modulus values are calculated from the crosshead displacement, which as noted above is considered to be proportional to strain. The values given are therefore not absolute, but instead relative. Likewise the strain at maximum stress is relative and not absolute. These values are referred to hereafter as the relative modulus and relative strain. The tensile strength is independent of strain and the values given are therefore absolute.

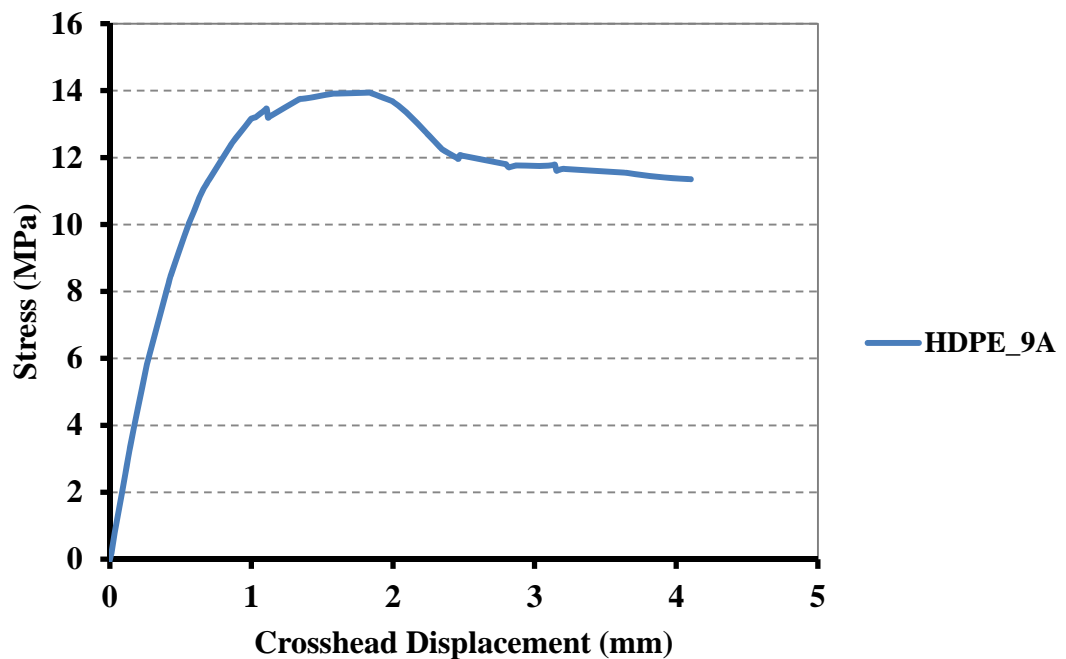


**Figure 4.42:** Stress-crosshead displacement curve of extruded HDPE strip.

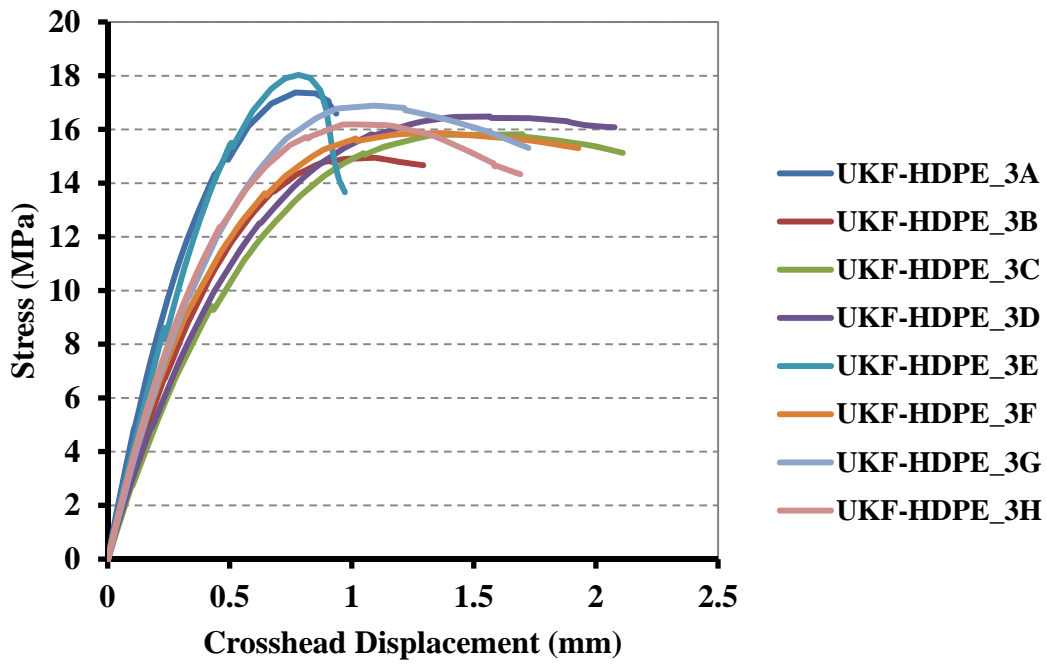


**Figure 4.43:** Stress-crosshead displacement curves of extruded UKF/HDPE strip composites.

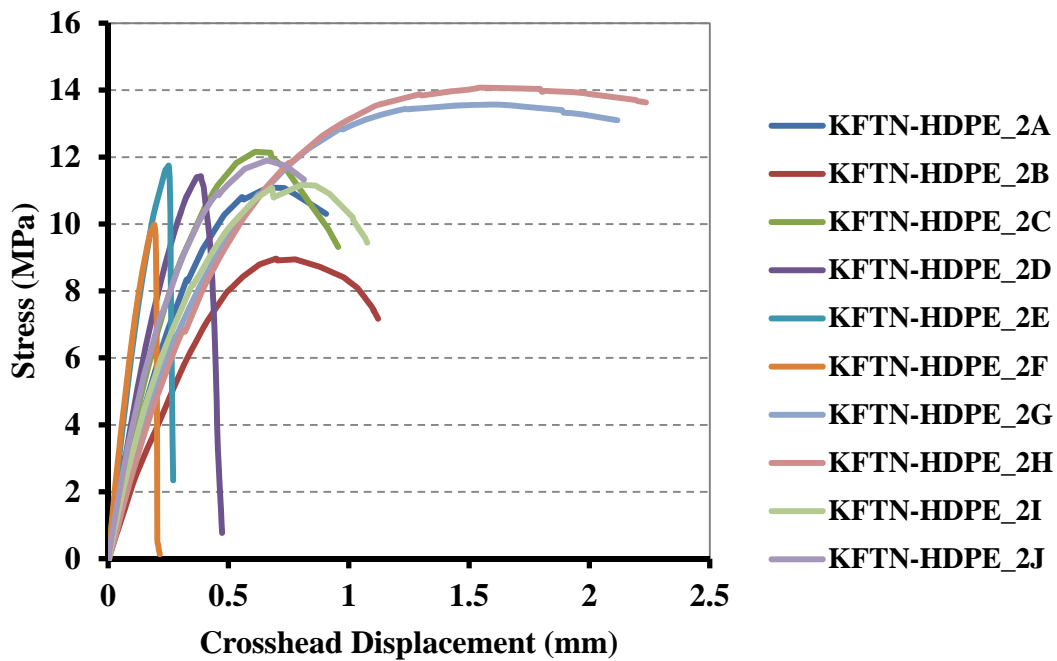


**Figure 4.44:** Stress-crosshead displacement curves of extruded KFTN/HDPE strip composites.

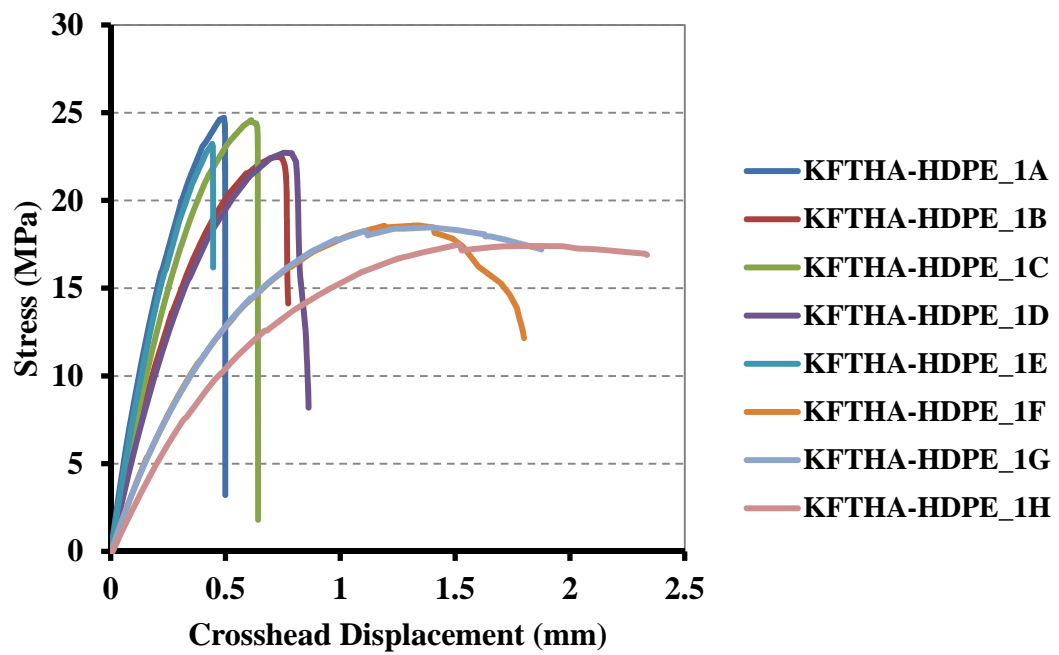


**Figure 4.45:** Stress-crosshead displacement curves of extruded KFTHA/HDPE strip composites.

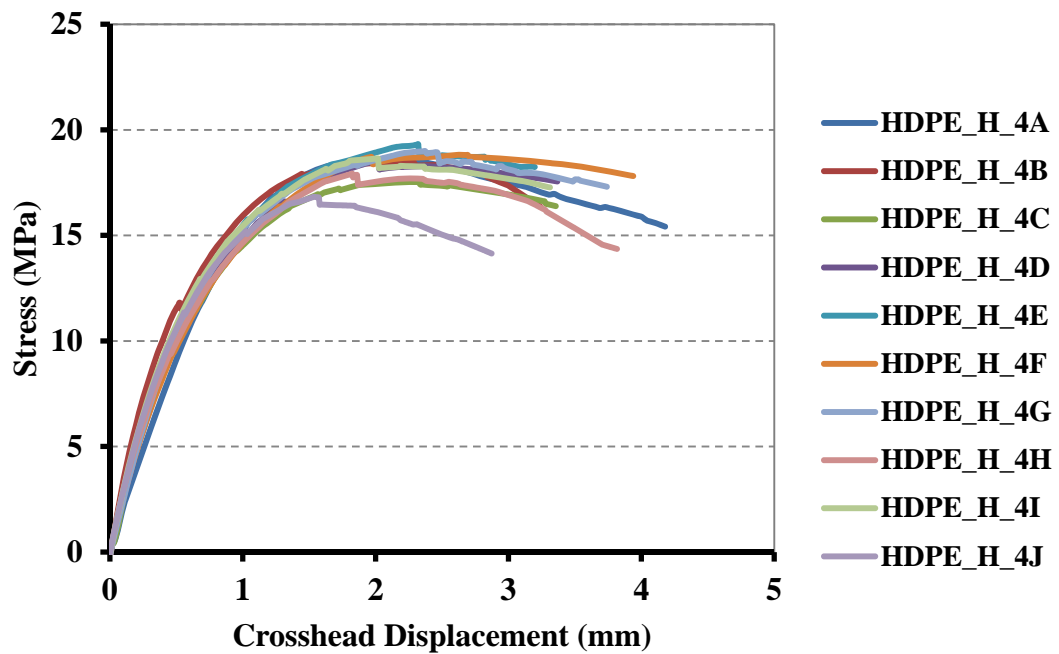


**Figure 4.46:** Stress-crosshead displacement curves of hot pressed extruded HDPE (HDPE\_H) strips.

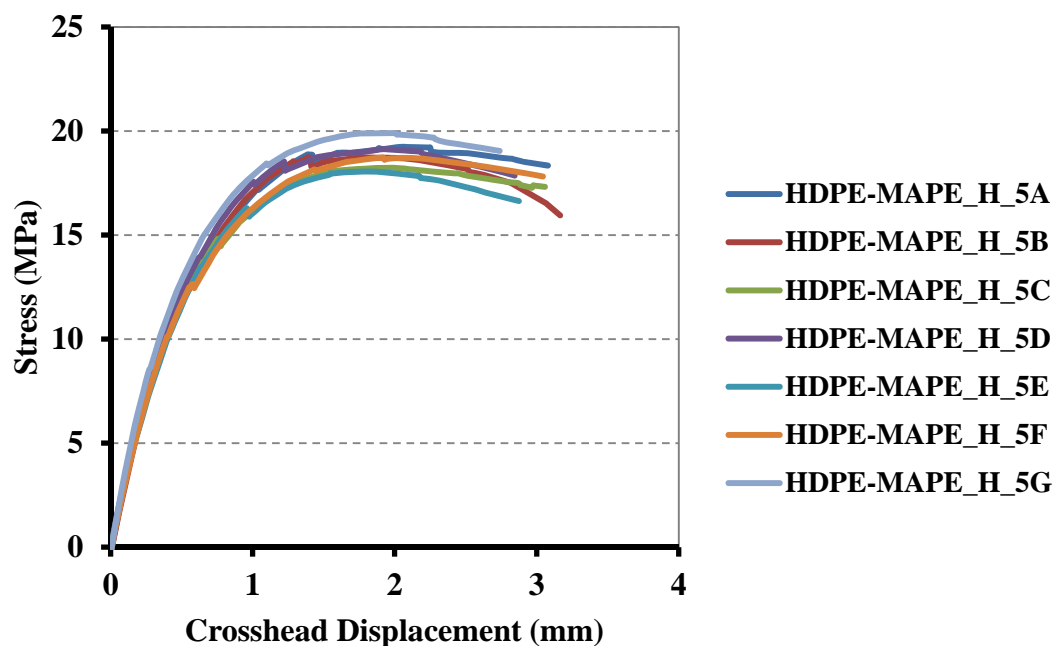


**Figure 4.47:** Stress-crosshead displacement curves of hot pressed extruded HDPE/MAPE (HDPE/MAPE\_H) strip composites.

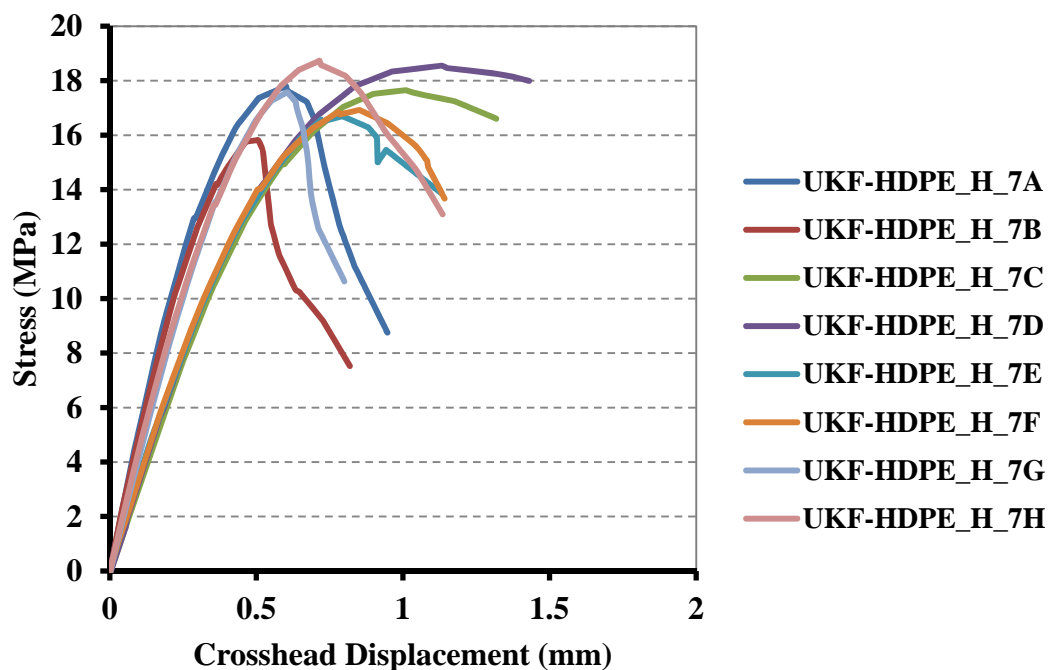


**Figure 4.48:** Stress-crosshead displacement curves of hot pressed extruded UKF/HDPE (UKF/HDPE\_H) strip composites.

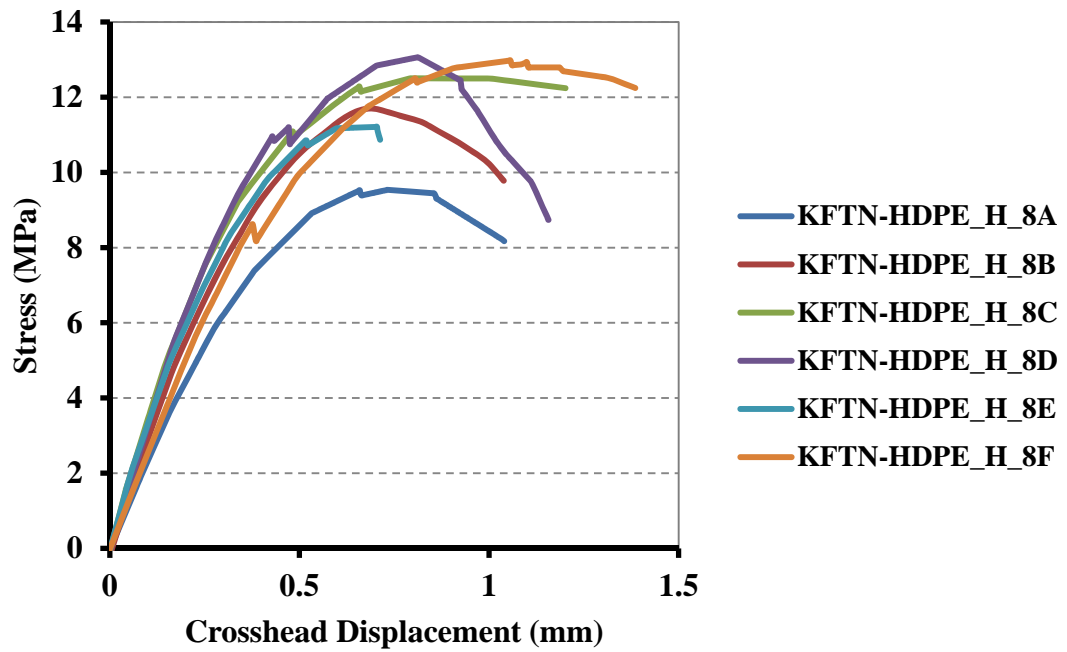


**Figure 4.49:** Stress-crosshead displacement curves of hot pressed extruded KFTN/HDPE (KFTN/HDPE\_H) strip composites.

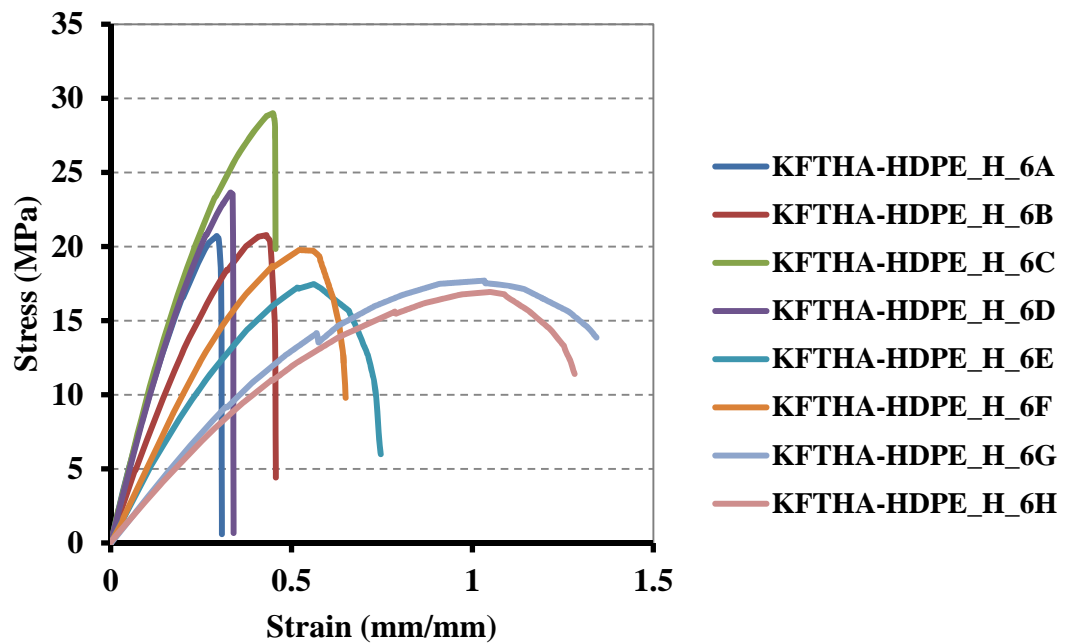


**Figure 4.50:** Stress-strain curves of hot pressed extruded KFTHA/HDPE (KFTHA/HDPE\_H) strip composites.

**Table 4.6:** Tensile test data for extruded HDPE and short kenaf fibre/HDPE strip composites

<b>Sample</b>	<b>Chord Modulus (MPa/mm)</b>	<b>SD (MPa/mm)</b>	<b>SD (%)</b>	<b>Ultimate Tensile Strength (MPa)</b>	<b>SD (MPa)</b>	<b>SD (%)</b>	<b>Crosshead Displacement at Max. Stress (mm)</b>	<b>SD (mm)</b>	<b>SD (%)</b>
HDPE	23.7			13.9	-		1.83	-	
HDPE/MAPE	-----Not measured-----								
UKF/HDPE	35.8	5.8	16.3	16.5	1.0	5.9	1.17	0.34	29.1
KFTN/HDPE	39.9	15.5	38.8	11.6	1.5	13.0	0.74	0.49	65.4
KFTHA/HDPE	56.8	21.3	37.4	21.5	2.9	13.5	0.91	0.44	48.0
HDPE_H	27.8	4.2	15.2	18.4	0.7	4.0	2.11	0.31	14.7
HDPE/MAPE_H	33.4	2.7	8.2	18.9	0.6	3.3	1.93	0.09	4.6
UKF/HDPE_H	40.5	8.7	21.5	17.5	1.0	5.5	0.78	0.22	27.7
KFTN/HDPE_H	31.2	5.4	17.2	11.8	1.3	11.3	0.80	0.14	17.2
KFTHA/HDPE_H	64.8	29.1	44.9	19.3	2.3	12.1	0.58	0.30	50.8

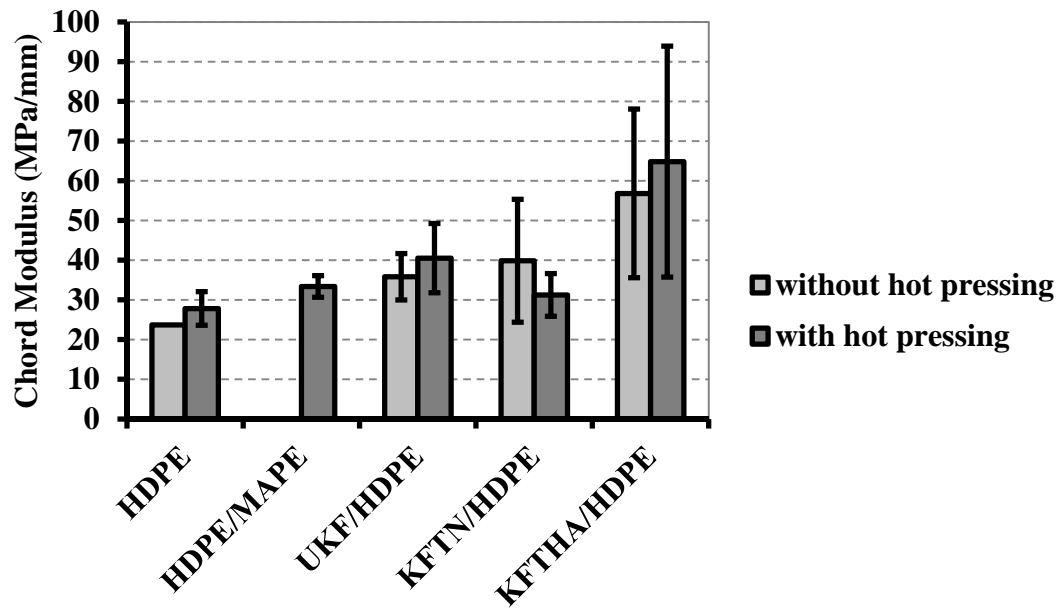


**Figure 4.51:** Relative modulus for HDPE, HDPE/MAPE, UKF/HDPE, KFTN/HDPE and KFTHA/HDPE strip composites with and without hot pressing. Error bars indicate one standard deviation.

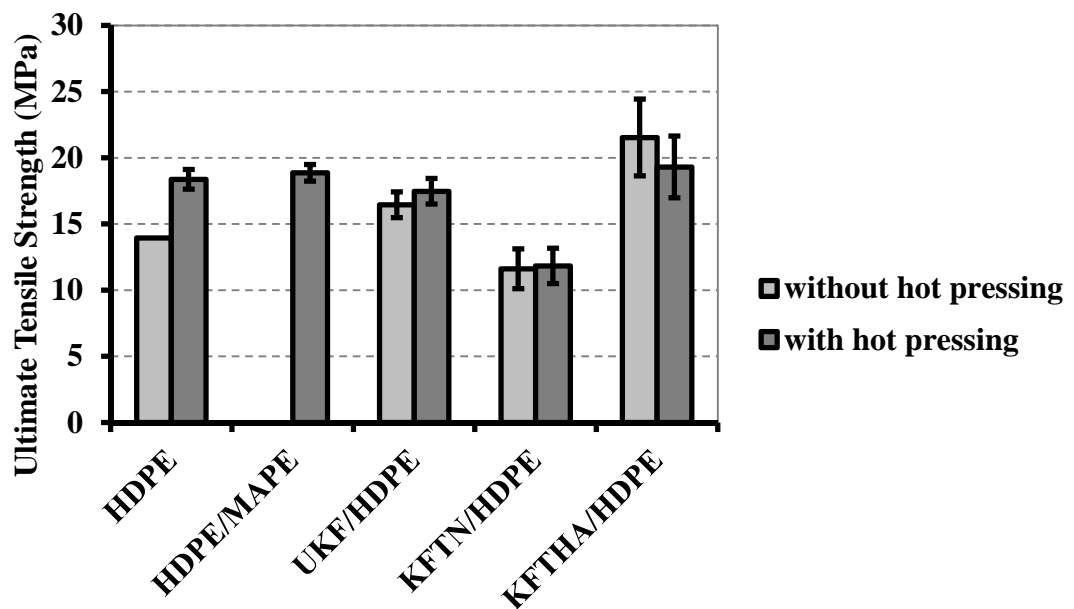


**Figure 4.52:** Ultimate tensile strength for HDPE, HDPE/MAPE, UKF/HDPE, KFTN/HDPE and KFTHA/HDPE strip composites with and without hot pressing. Error bars indicate one standard deviation.



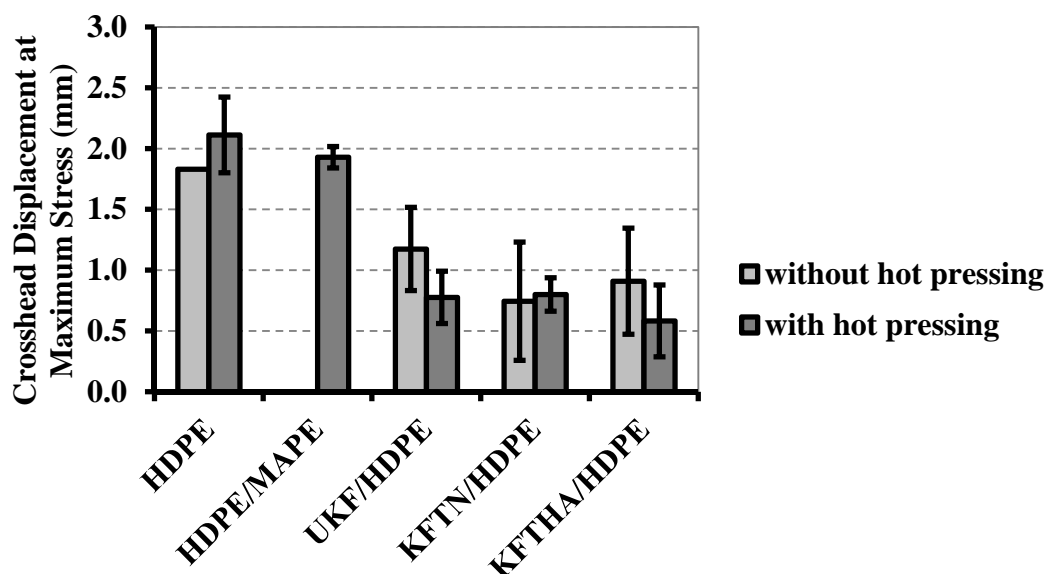


**Figure 4.53:** Relative strain at maximum stress for HDPE, HDPE/MAPE, UKF/HDPE, KFTN/HDPE and KFTHA/HDPE strip composites with and without hot pressing. Error bars indicate one standard deviation.

Both the relative modulus and the tensile strength of the neat HDPE were increased substantially (17% and 32%, respectively) by hot pressing. This is attributed to an increase in the level of crystallinity. The modulus of the hot pressed HDPE was increased further (20%) by the addition of MAPE, but no change in strength was observed.

The relative modulus is generally higher for the composites than for the unreinforced HDPE and HDPE/MAPE, with the difference being greatest for the hydrogen peroxide/acetic acid treated fibre composites, Figure 4.51. The strength is also higher for the hydrogen peroxide/acetic acid treated fibre composites than for the HDPE specimens, but it is similar to that of the HDPE for the untreated fibre composites and lower than that of the HDPE for the nitric acid treated fibres, Figure 4.52. The relative strain at maximum stress is lower for all the composites than for the HDPE specimens, Figure 4.53.

There is, however, considerable scatter in the results for the individual samples from each of the composites, as is evident from the stress-crosshead displacement curves shown in Figures 4.42 to 4.50 and also from the high values of the standard deviations given in Table 4.6. The reason for this becomes apparent when the fibre

fractions are considered. The true fibre weight fraction (measured weight fraction  $\times$  correction factor) for four of the composites of each type are given in Table 4.7 and can be seen to generally vary considerably from specimen to specimen (UKF/HDPE: 11-23%, KFTN/HDPE: 7-61%, KFTHA/HDPE: 9-46%, UKF/HDPE\_H: 9-27%, KFTN/HDPE\_H: 8-12%, KFTHA/HDPE\_H: 9-48%). Measurements of the weight fraction were made for only four specimens of each type in the expectation that the fibre fraction would, in fact, be constant along the extrudate.

**Table 4.7:** True fibre weight fraction of extruded strip composites

<b>Material</b>	<b>Sample No.</b>	<b>Fibre Weight Fraction (%)</b>	<b>Material</b>	<b>Sample No.</b>	<b>Fibre Weight Fraction (%)</b>
UKF/HDPE	3A	23.3	UKF/HDPE_H	7A	26.7
	3D	11.0		7C	10.2
	3G	18.3		7D	14.1
	3H	17.2		7E	8.9
KFTN/HDPE	2A	23.7	KFTN/HDPE_H	8A	12.4
	2D	49.7		8B	7.9
	2E	60.8		8D	8.3
	2G	7.0		8E	8.1
KFTHA/HDPE	1C	42.6	KFTHA/HDPE_H	6B	39.7
	1D	29.4		6D	47.5
	1E	46.1		6F	30.5
	1H	9.4		6H	9.1

The relative modulus and the strength are shown as a function of the true weight fraction for the as-extruded composites in Figures 4.54 and 4.55, respectively, and for the hot pressed composites in Figures 4.56 and 4.57, respectively. The data for neat HDPE has been used as the 0 wt% point for the as-extruded composites (no data was obtained for HDPE/MAPE), while the data for HDPE/MAPE\_H has been used as the 0 wt% point for the hot pressed composites.

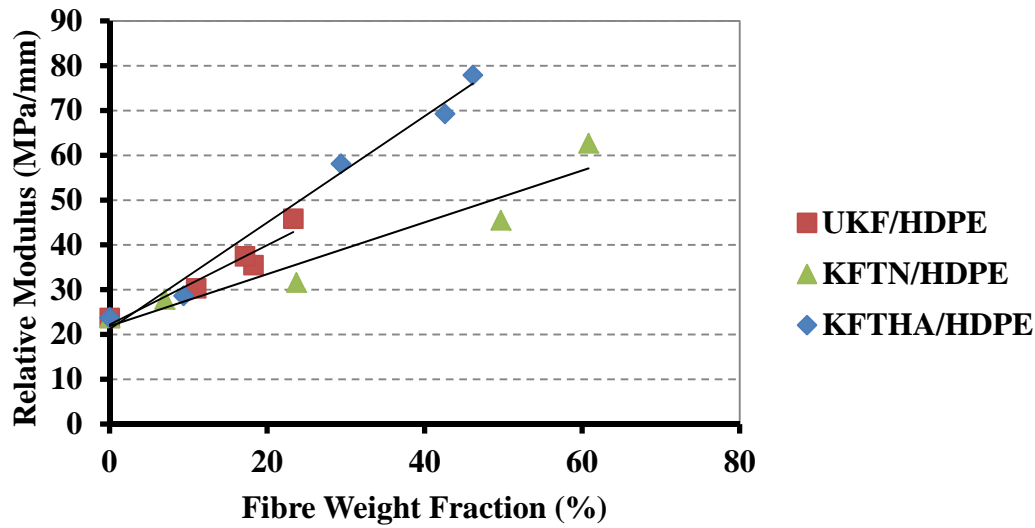


**Figure 4.54:** Relative modulus as a function of true weight fraction for as-extruded strip composites.

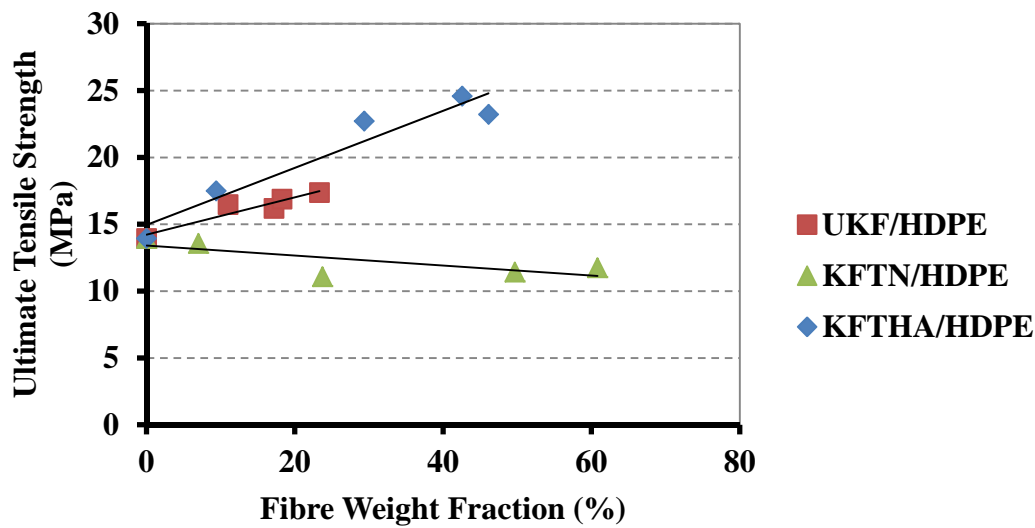


**Figure 4.55:** Ultimate tensile strength as a function of true weight fraction for as-extruded strip composites.

The relative modulus increased progressively with fibre weight fraction for all three composites in the as-extruded condition, Figure 4.54, However, the reinforcing efficiency, as indicated by the slope of the trend lines, was different in the three cases being highest for the hydrogen peroxide/acetic acid treated fibre composite,

intermediate for the untreated fibre composite and lowest for the nitric acid treated fibre composite.

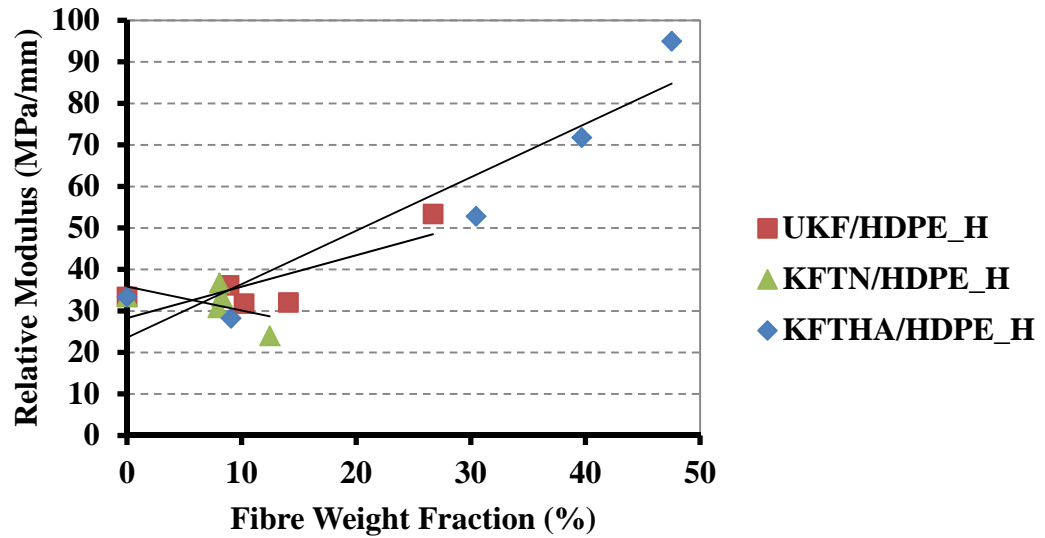


**Figure 4.56:** Relative modulus as a function of true weight fraction for as hot pressed strip composites.

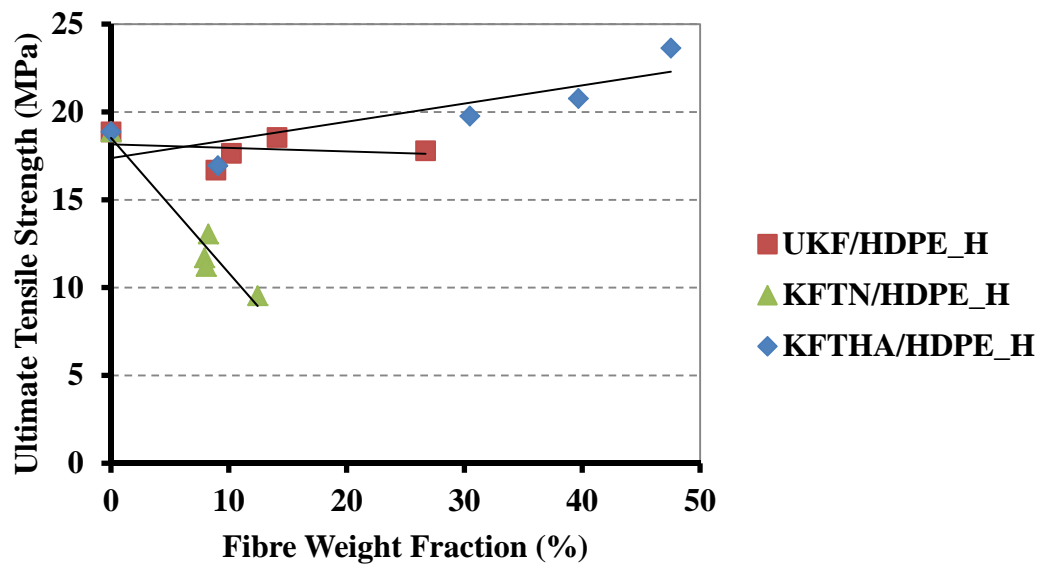


**Figure 4.57:** Ultimate tensile strength as a function of true weight fraction for as hot pressed strip composites.

The tensile strength also increased progressively with fibre weight fraction for both the hydrogen peroxide/acetic acid treated fibre composite, and the untreated fibre composite, with the reinforcing efficiency again being highest for the hydrogen peroxide/acetic acid treated fibre material, Figure 4.55. However the tensile strength decreased slightly with fibre addition for the nitric acid treated fibre composite.

The relative modulus also increased with fibre addition for the hot pressed hydrogen peroxide/acetic acid treated fibre and the untreated fibre composites, with the reinforcing efficiency again being highest for the hydrogen peroxide/acetic acid treated fibre composite, Figure 4.56. However, it showed a slight decrease with fibre addition for the nitric acid treated composite. The strength of the hot pressed composites also increased progressively with fibre fraction for the hydrogen peroxide/acetic acid treated fibre composite, but it was essentially unchanged by fibre addition for the untreated fibre composite, while it decreased strongly with fibre fraction for the nitric acid treated fibre composite, Figure 4.57. It is noted that the level of lateral spread produced by hot pressing was least for the hydrogen peroxide/acetic acid treated fibre composite (Figure 4.19), slightly greater for the untreated fibre composite (Figure 4.17), and much greater for the nitric acid treated composite (Figure 4.18), and this difference may have affected the results.

#### **4.4.5 Fracture Surfaces of Tensile Specimens**

SEM micrographs of the fracture surfaces of the tested rod specimens at varying magnifications are shown in Figure 4.58, while SEM micrographs of the as-extruded and hot pressed composites are shown in Figures 4.59 to 4.63. The micrographs show pulled out fibres with adhering matrix for all the composites, indicating that the fibre matrix adhesion was good. Microfibrils are evident on the fracture surface of the matrix indicating that it had failed in a ductile manner. No obvious differences were apparent between the as-extruded and hot pressed strip composites nor between the strip composites and the rod composites.

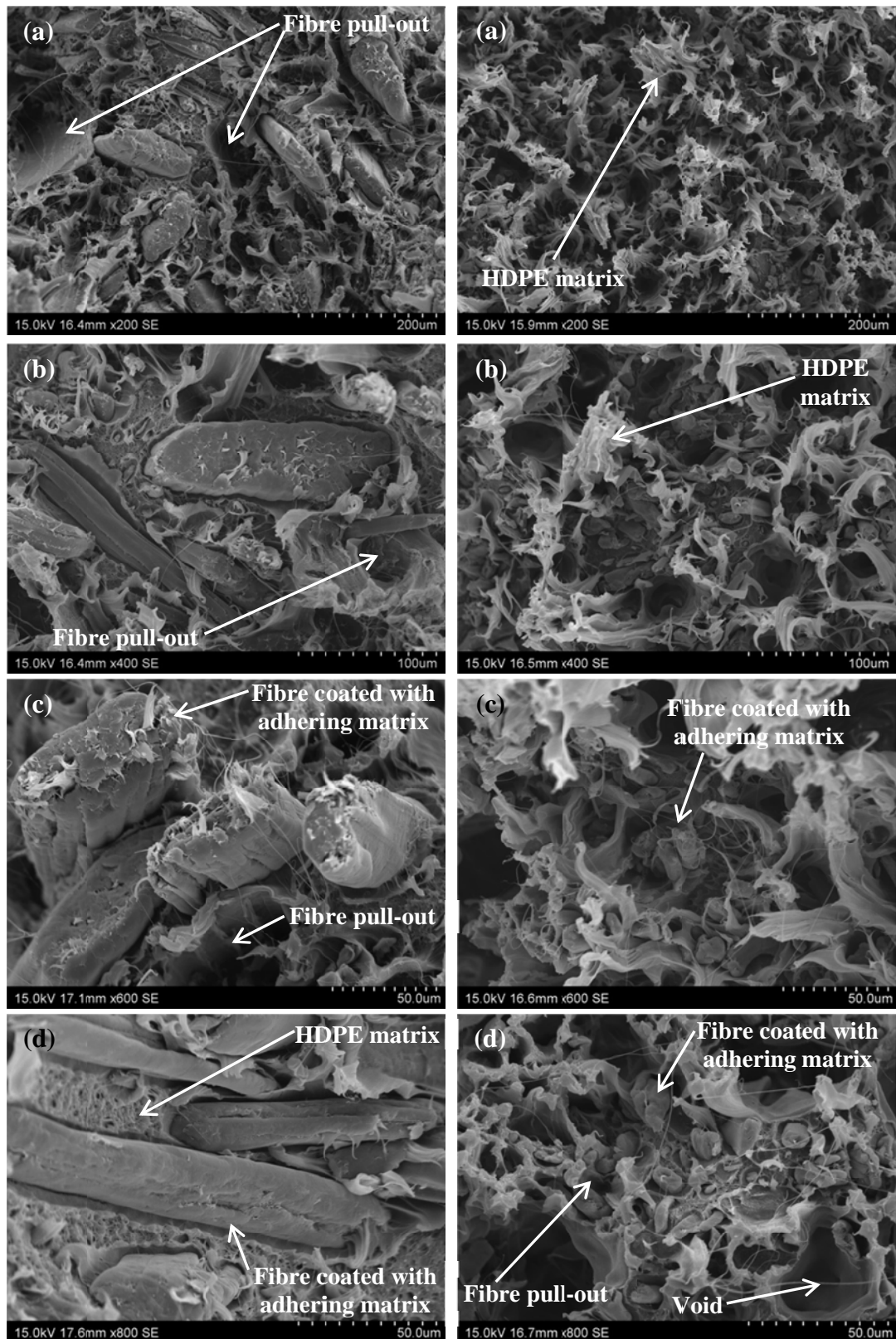


**Figure 4.58:** SEM micrographs of fracture surfaces of tested specimens of UKF/HDPE (left) and KFTN/HDPE (right) rod composites at (a) 200×, (b) 400×, (c) 600× and (d) 800× magnification.

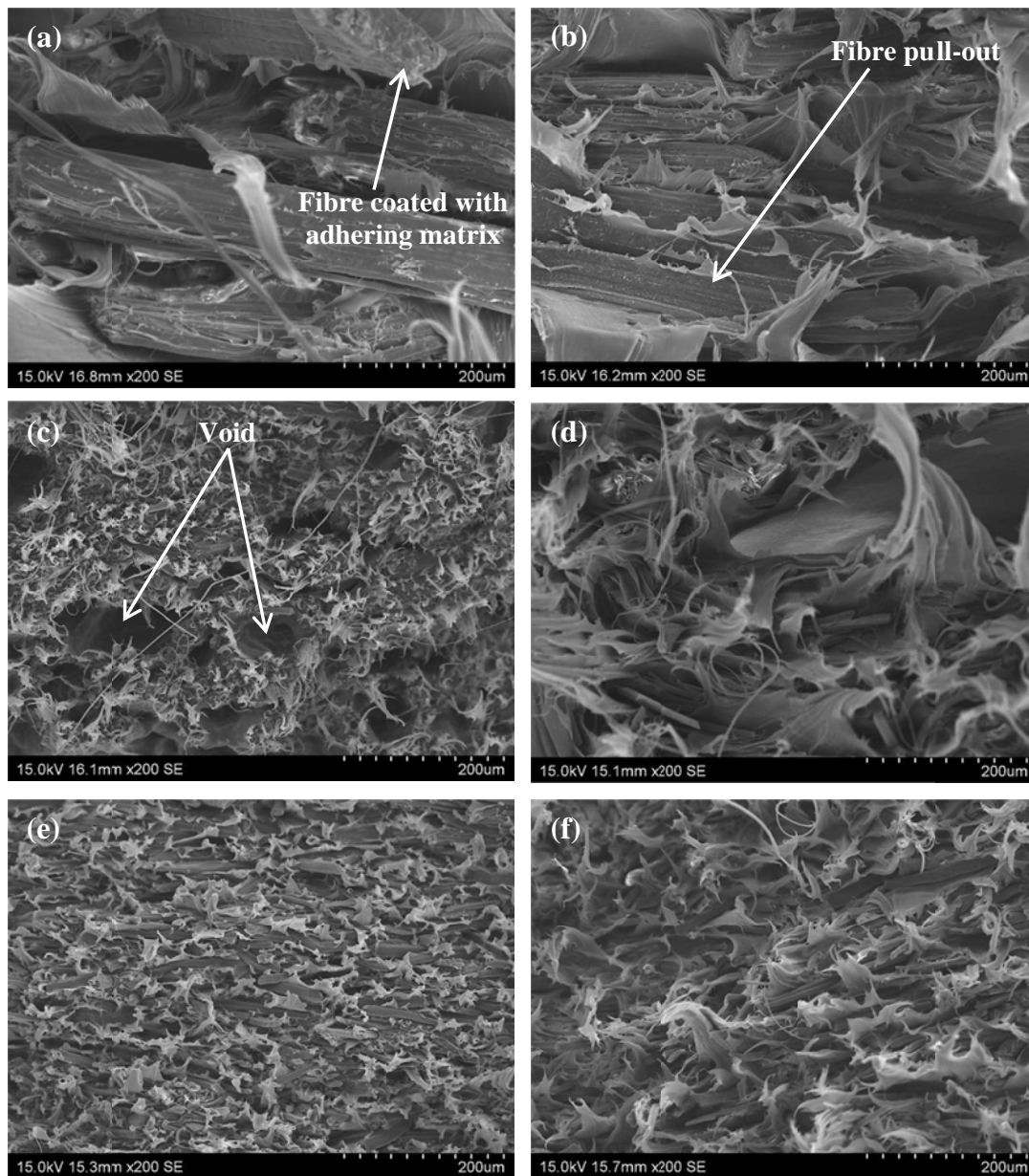


**Figure 4.59:** SEM micrographs of fracture surfaces of (a) UKF/HDPE, (b) UKF/HDPE\_H, (c) KFTN/HDPE, (d) KFTN/HDPE\_H, (e) KFTHA/HDPE and (f) KFTHA/HDPE\_H strip composites at 200× magnification.

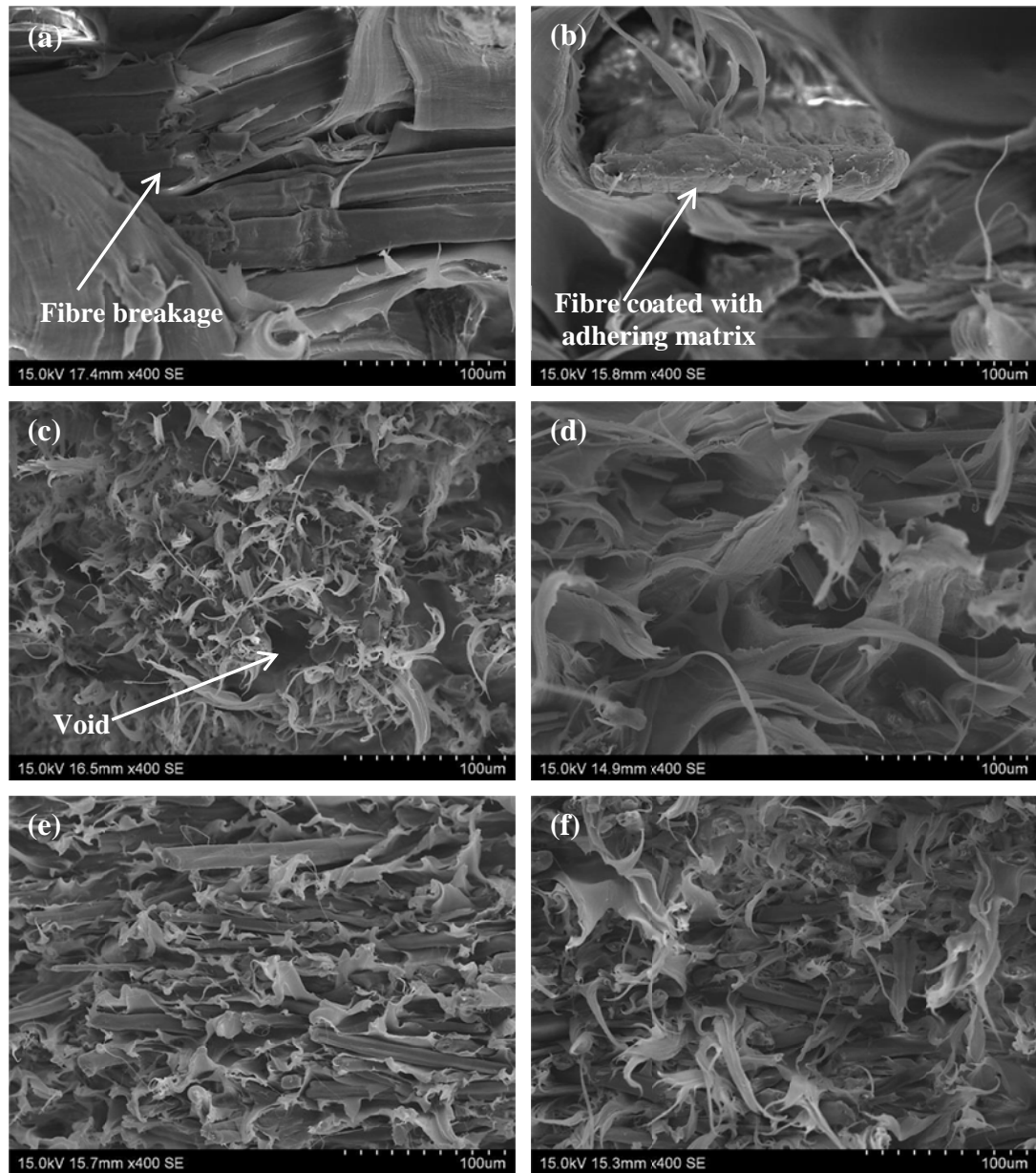


**Figure 4.60:** SEM micrographs of fracture surfaces of (a) UKF/HDPE, (b) UKF/HDPE\_H, (c) KFTN/HDPE, (d) KFTN/HDPE\_H, (e) KFTHA/HDPE and (f) KFTHA/HDPE\_H strip composites at 400× magnification.



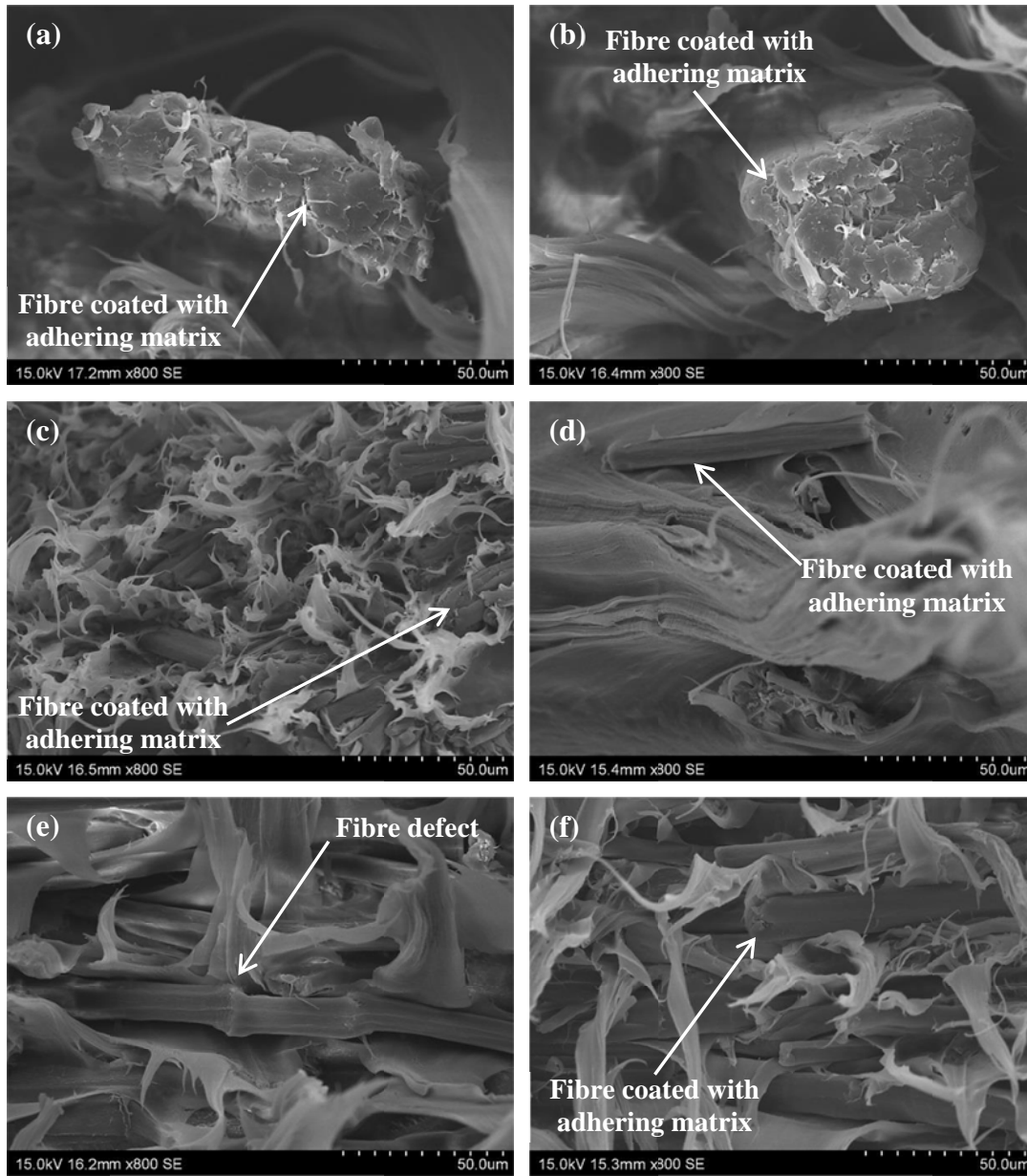


**Figure 4.61:** SEM micrographs of fracture surfaces of (a) UKF/HDPE, (b) UKF/HDPE\_H, (c) KFTN/HDPE, (d) KFTN/HDPE\_H, (e) KFTHA/HDPE and (f) KFTHA/HDPE\_H strip composites at 800 $\times$  magnification.

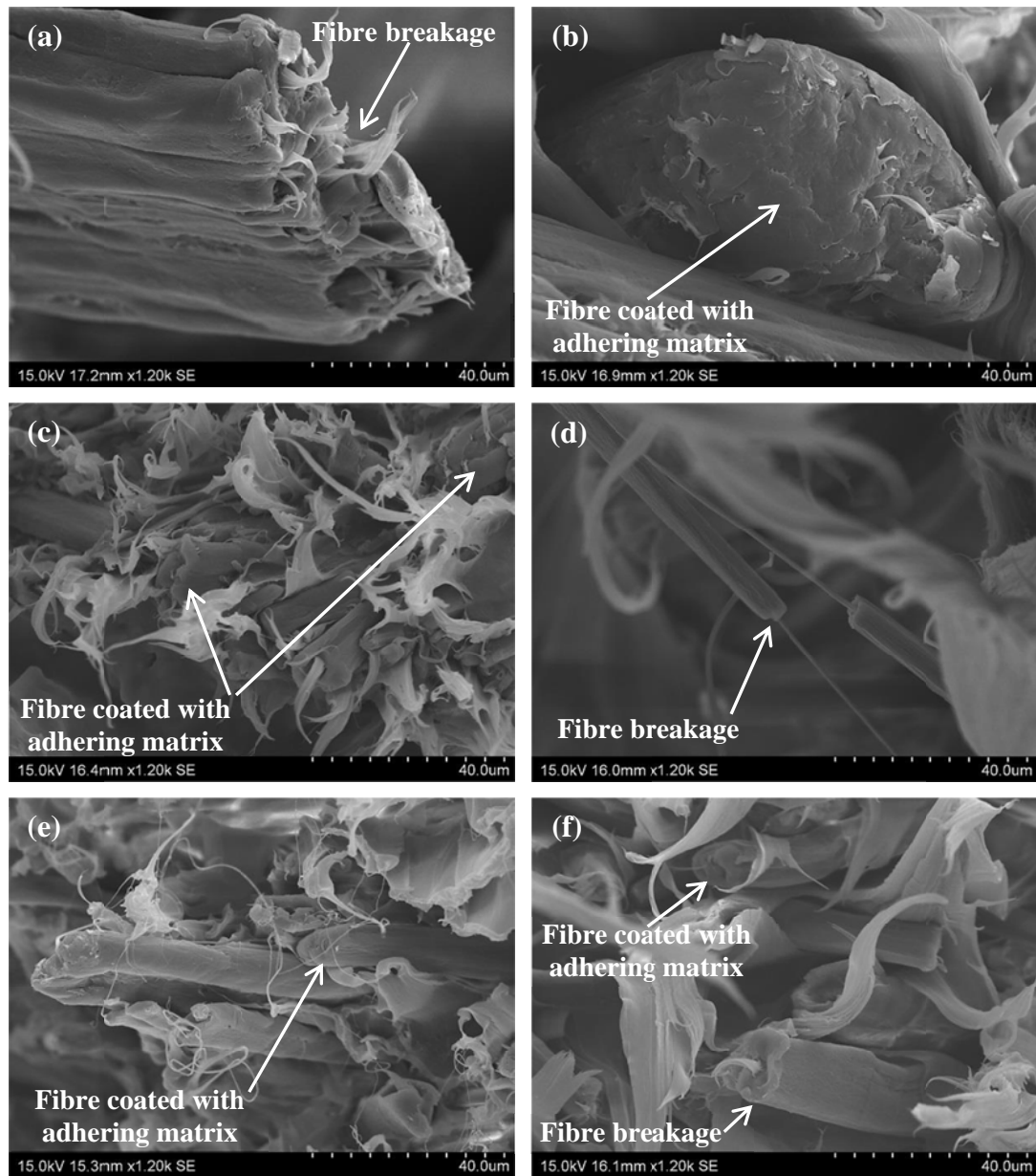


**Figure 4.62:** SEM micrographs of fracture surfaces of (a) UKF/HDPE, (b) UKF/HDPE\_H, (c) KFTN/HDPE, (d) KFTN/HDPE\_H, (e) KFTHA/HDPE and (f) KFTHA/HDPE\_H strip composites at 1,200× magnification.

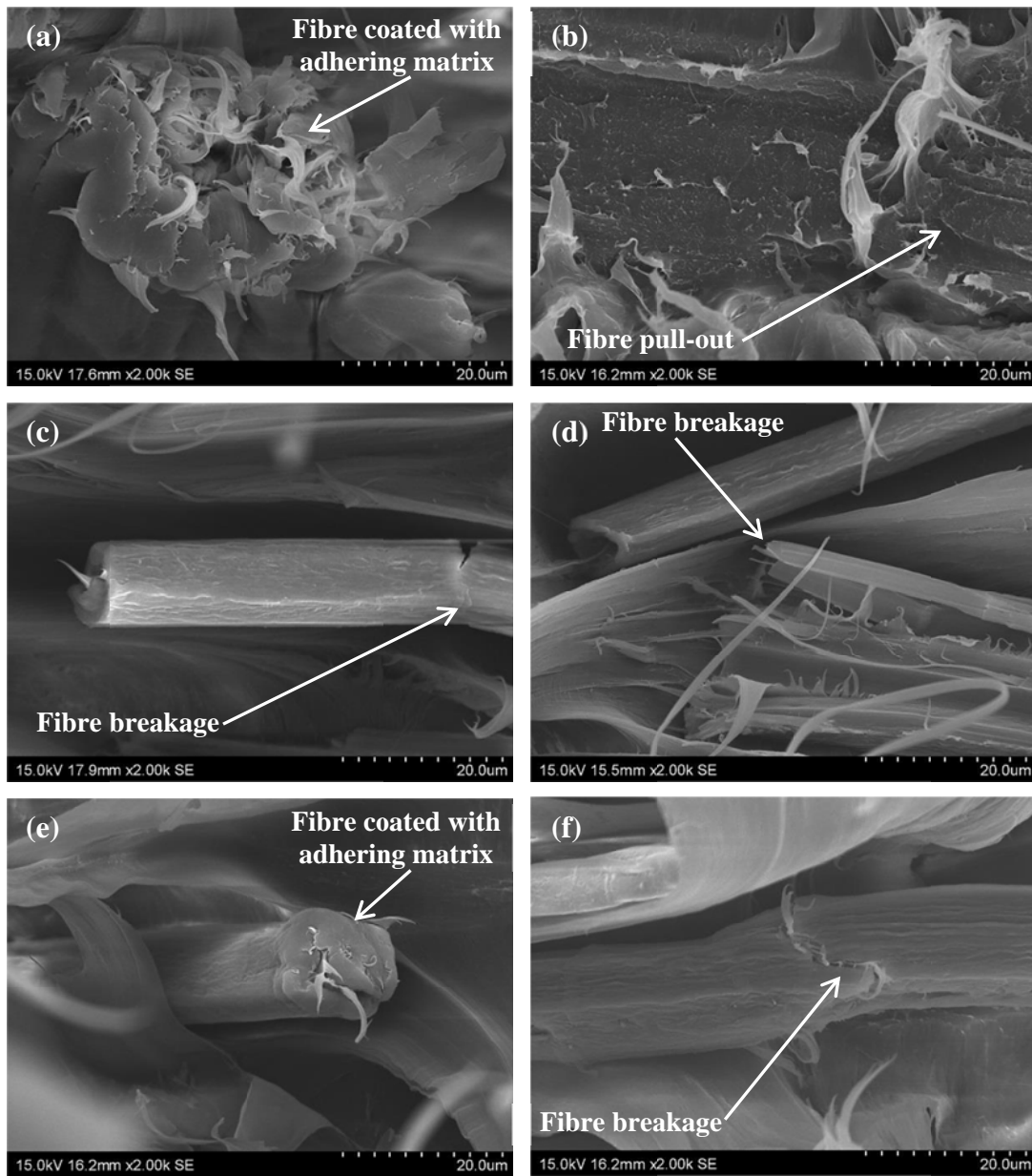


**Figure 4.63:** SEM micrographs of fracture surfaces of (a) UKF/HDPE, (b) UKF/HDPE\_H, (c) KFTN/HDPE, (d) KFTN/HDPE\_H, (e) KFTHA/HDPE and (f) KFTHA/HDPE\_H strip composites at 2,000× magnification.

## 4.5 Discussion

### 4.5.1 Extrusion

#### 4.5.1.1 Rod Composites

As noted in Section 3.3.1 several different techniques were trialled for production of the elementary fibres to be used in the composites. Moreover, a large number of batches of fibres had to be treated to produce sufficient elementaries for an extrusion run. As result of these factors, the nitric acid treated elementaries were available well before the hydrogen peroxide/acetic acid treated fibres and it was decided to undertake an initial extrusion trial using the nitric acid treated elementaries while preparation of the hydrogen peroxide/acetic acid treated fibres was still in progress. Chopped untreated fibres were also used for comparison. The components of the composites were first mixed together at room temperature and the mixture then fed into the extruder using a single hopper.

It was found that while the neat HDPE extruded easily, the composites were substantially more difficult to extrude due to their low melt flow characteristics. In addition, the nitric acid treated fibre composites were more difficult to extrude than the untreated fibre ones. This was because the nitric acid treated fibres were lighter and the mixture fed too quickly into the hopper, making it necessary to stop feeding periodically when the hopper became full. Die swell also occurred, indicating that the process was not run for long enough for full uniformity to occur. Unfortunately longer runs were not possible because of the limited amount of elementary fibres available.

The (true) weight fractions of the untreated and nitric acid treated fibre composites, determined from analysis of 22 samples of each composite, were 38.1 and 38.0%, respectively, with standard deviations of 2.5 and 4.2%, which is consistent with value of 40 wt% used in the formulation. However, some variation was evident along the extrudate with the range of values being from 34-43% for the untreated fibre composite and from 31-46% for the nitric acid treated fibre composites. In addition considerable roughening of the surface occurred for the composites. It was also found that the nitric acid treated elementary fibres were reduced to less than half their original length by the extrusion process, although the untreated chopped technical fibres were essentially unaffected.

#### **4.5.1.2 Strip Composites**

In view of the variation of fibre fraction, surface roughening, and difficulties with feeding, it was decided to use a twin hopper extruder when making the hydrogen peroxide/acetic acid treated fibre composites, since this allowed separate feeding of the fibres and matrix material. Composites were also extruded using a second batch of nitric acid treated fibres while composites were again extruded using untreated chopped fibres for purposes of comparison. A slit die was used rather than a circular die so as to produce strip product that could be used to produce flat dog-bone tensile specimens.

Unfortunately, problems were again experienced with feeding of the fibres which were too light to feed properly and needed to be pushed into the barrel of the extruder. In addition the hydrogen peroxide/acetic acid treated fibres tended to agglomerate, as shown in Figure 4.64. As a result, these composites were the most difficult to extrude, followed by the nitric acid treated fibre composites and then the untreated fibre composites. Difficulties were also experienced with wrinkling of the extruded strip.



**Figure 4.64:** KFTHA fibres fed into a hopper of a twin-screw extruder.

Due to the difficulties experienced in the extrusion process, the intended fibre weight fraction of 40% was not achieved with the average values being 16% for the untreated fibre composites, 24% for the nitric acid treated fibre composites and 32% for the hydrogen peroxide/acetic acid treated fibre composites. Moreover, the composites showed very substantial variation in fibre fraction along their length with the values varying from ~10-25 wt% for the untreated fibre composites and ~10-50 wt% for the treated fibre composites.

It is noted that the nitric acid treated and hydrogen peroxide/acetic acid treated fibre composites were darker and lighter, respectively, than the untreated fibre composites. This may be associated with the different thermal stabilities of the fibres, as reported in Section 3.4.9.

The elementary fibres obtained from both the nitric acid treatment and the hydrogen peroxide/acetic acid treatment were substantially reduced in length by the extrusion process, with the hydrogen peroxide/acetic acid treated fibres being reduced to about one tenth their original length and the nitric acid treated fibres being very short, often having been reduced essentially to particulate.

## **4.5.2 Tensile Properties**

### ***4.5.2.1 Rod Composites***

No significant difference was detected between the modulus of the untreated and nitric acid treated fibre rod composites but the value was 33% higher than that of the extruded HDPE rod. The strength of the composites was also on average 17% higher than that of the neat HDPE. However, there was a significant difference (9%) between the strength of the nitric acid treated fibre composite and that of the untreated fibre composite with the treated fibre composite having the lower value. This is considered to be due to the introduction of defects into the fibres during the nitric acid treatment, as shown in Section 3.4.3, reducing their reinforcing efficiency to below that of the untreated chopped fibres.

The strain at maximum stress was reduced to about one third of the value for neat HDPE by introduction of both the untreated and treated fibres.

#### **4.5.2.2 Strip Composites**

Because of the substantial variation in fibre fraction in the strip composites it was necessary to normalise the data by plotting the modulus and strength as a function of fibre fraction, which then allowed the trend lines to be compared. This showed that the strength and modulus were higher for the hydrogen peroxide/acetic acid treated fibre composites than for those made with untreated fibres but the reverse was seen for the nitric acid treated fibre composites, with the values being lower than those for the untreated fibre composites. These trends were consistent across both the as-extruded and hot pressed composites.

A comparison of the magnitude of these differences was made by assuming a linear relationship between the fibre fraction and both the modulus and strength of the composites, and then using the difference between the linear trend lines given in Figures 4.51-4.54 at a weight fraction of 38% (to be consistent with the weight fraction of the rod composites). As noted in Section 4.4.4.2, differences in the level of lateral spread during hot pressing were seen for the hot pressed composites and this may have affected those results so only the data for the as-extruded composites was considered. This gave an increase of 19% in modulus and 18% in strength for the hydrogen peroxide/acetic acid treated fibre composites, compared with the untreated fibre composites. However, reductions of 21% in modulus and 39% in strength were obtained for the nitric acid treated fibre composites when compared with the untreated fibre composites.

The values given by the trend lines at a weight fraction of 38% were also compared with the values obtained for the neat HDPE. The modulus was increased by 180%, 136% and 85% for the hydrogen peroxide/acetic acid treated, the untreated and the nitric acid treated fibre composites, respectively, over the value obtained for the neat HDPE extrudate. The strength was also increased by 65% and 40% over that of neat HDPE for the hydrogen peroxide/acetic acid treated and untreated fibre composites. However a decrease of 14% in strength was observed for the nitric acid treated composite.

The behaviour of the nitric acid treated fibre composites was unusual since addition of the fibres increased the modulus above that of the matrix, as is expected for fibre reinforcement (Daniel & Ishai, 1994), but decreased the strength. This is attributed to the fibres being reduced essentially to particulate. The addition of higher modulus particulate to a polymer produces an increase in the modulus of the composite, but the

particulates cause stress concentration which results in a decrease in its strength (Ahmed & Jones, 1990).

The nitric acid treated fibre strip composites also performed more poorly than their rod composite counterparts when compared with the corresponding composites made from untreated fibres. This is attributed again to the reduced fibre length in the nitric acid treated fibre strip composites, whereas no difference in fibre length was observed in untreated fibre composites.

It is noted that the improvement in modulus and strength for the untreated fibre composites over that of the neat matrix polymer was greater in the strip composites than in the rod composites, with the increases being 136% and 33%, respectively, for the modulus and 40% and 23% respectively for the strength at 38% fibre weight fraction. The data for the matrix polymer used for the strip composites was for HDPE without MAPE addition (since no results were obtained for as-extruded HDPE/MAPE). However the data for the hot pressed composites indicates that the presence of MAPE raises the modulus of HDPE by 20% and the strength by 3%. Applying these factors to the modulus and strength of the as-extruded HDPE, and replotting the data with these values as the 0 wt% fibre values, reduced the increases produced by the untreated fibres to 81% for the modulus and 34% for the strength. These values are still substantially higher than the values for the rod composites and this may indicate that the strip composites had achieved better longitudinal fibre orientation, although this was not detectable at the level of examination used here.

#### **4.5.3 General Discussion**

The work presented in this and the previous chapter was undertaken to explore the possibility of obtaining improved mechanical performance of short fibre extruded thermoplastic matrix composites by using high aspect ratio elementary fibres. The work was focussed on kenaf due its importance as a crop in the South East Asia region.

The elementaries obtained from both chemical treatments produced composites with well dispersed fibres, despite a tendency for agglomeration of the elementaries (especially the hydrogen peroxide/acetic acid treated fibres) prior to extrusion. It was also found that there was good fibre-matrix adhesion. Difficulty was experienced, however, in maintaining a uniform fibre fraction along the extruded composites. Moreover, the elementaries broke into fragments during extrusion, with the effect being



most pronounced for the strip composites where the fibre length was reduced by a factor of 10.

None the less, modest improvements of ~20% in the modulus and strength, over that obtained for composites made from the chopped technical fibres, were achieved with the elementary fibres isolated using the hydrogen peroxide/acetic acid treatment. However, no improvement was obtained for the nitric acid treated fibres, even with the less damaging extrusion process used to make the rod composites. The poor performance of the nitric acid treated fibre composites is attributed to their much smaller initial aspect ratio (one tenth of that of the hydrogen peroxide/acetic acid treated fibres) combined with the presence of a higher level of defects resulting from the fibre isolation treatment.

The results are encouraging since the different levels of breakup of the elementaries produced using the two different extrusion processes suggests that there is scope for modifying the process to better retain the initial fibre length. It may also be possible to obtain better fibre alignment which would also lead to improved mechanical performance. Further examination of these possibilities was, however, outside the scope of this project.

## 4.6 Summary

The important findings from this part of the research are summarised below.

- Composites were successfully prepared from the elementary fibres using both single feed and dual feed (separate fibre and matrix feeding systems) extrusion.
- The fibres were well dispersed and well bonded to the matrix. There was no distinct fibre orientation in the extrudates.
- The composites extruded with the single feed system achieved the target fibre fraction, but the fibre fraction was substantially lower in the composites extruded using the dual feed system.
- Difficulty was experienced achieving a constant fibre fraction along the extrudates, especially when using the dual feed system.
- Considerable breakup of the elementary fibres occurred during the extrusion process, especially for the dual feed system where the fibre length was reduced by a factor of 10.

- Improvements of 20% in modulus and strength were obtained for the composites prepared from hydrogen peroxide/acetic acid treated elementaries over the values obtained for the chopped fibre composites.
- The composites prepared from the nitric acid treated elementaries showed no improvement in modulus and strength when compared with the chopped fibre composites extruded as rod while the values were consistently lower for the composites extruded as strip.



**CHAPTER 5**

**TENSILE PROPERTIES OF FLAX FIBRES AND  
UNIDIRECTIONAL FLAX FIBRE/VINYL ESTER  
COMPOSITES**

---



## **5. TENSILE PROPERTIES OF FLAX FIBRES AND UNIDIRECTIONAL FLAX FIBRE/VINYL ESTER COMPOSITES**

### **5.1 Introduction**

This chapter examines the mechanical behaviour of high aspect ratio natural fibre thermoset composites. The work was undertaken to evaluate the possibility of using fibre mechanical grading as an indicator of the performance of the resulting composite. Flax fibres were used as the reinforcement since untwisted flax fibre is available as unidirectional fabrics, which potentially overcome the inherent difficulty of producing well aligned unidirectional composites (Virk, Hall & Summerscales, 2012). Vinyl ester was used as the matrix resin. Single (technical) fibre testing and fibre bundle testing (as used in the textiles industry) were carried out on fibres extracted from the unidirectional fabric. The results obtained were compared with fibre properties determined by back calculating the data obtained from tensile testing of unidirectional composites using the rule of mixtures.

### **5.2 Materials**

The flax fibres were obtained as Biotex unidirectional untreated flax fabric, Figure 5.1, from Composites Evolution Ltd, UK. The fabric had an areal weight of 275 g/m<sup>2</sup> and was made from yarns of untwisted fibres held together by two spiral wrapping

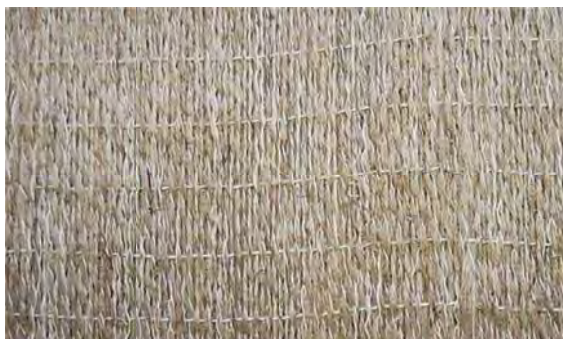


**Figure 5.1:** Biotex unidirectional flax fabric.

threads. The yarns were held in place in the fabric by transverse threads which had been applied every 10 mm, Figure 5.1. ArmorStar® IVSXH210 vinyl ester infusion resin with Arkema Luperox® DHD-9 hardener, supplied by CCP Composites US, was used as the matrix resin when making the composites. Data sheets for the flax fabric and vinyl ester resin are given in Appendix XIV.

## **5.3 Experimental Procedures**

### **5.3.1 Characterisation of Fibres**

#### ***5.3.1.1 Optical and Scanning Electron Microscopy***

The flax fibres were examined using an Olympus SZ-STU2 low power optical microscope and a Hitachi S3400-X scanning electron microscope (SEM). The fibres examined by SEM were first sputter coated with gold using an Emitech K550x sputter coater. The SEM was operated in high vacuum mode at an accelerating voltage of 15 kV.

#### ***5.3.1.2 Measurement of Fibre Length***

The length of the technical fibres was determined for 100 fibres randomly selected from a yarn extracted from the unidirectional fabric. The measurements were made by ruler to an accuracy of 1 mm.

#### ***5.3.1.3 Fibre Defects***

Ten technical fibres were extracted from the unidirectional fabric then cut to a length of approximately 18 mm. The fibres were sputter coated with gold using an Emitech sputter coater, and then examined using a Hitachi S3400-X scanning electron microscope operated in high vacuum mode at an accelerating voltage of 15 kV.

### **5.3.2 Tensile Testing of Single Technical Fibres**

#### ***5.3.2.1 Specimen Preparation***

Single fibre tensile testing was carried out on 113 fibres technical fibres, which had been extracted from the unidirectional fabric. Only fibres having a length of 90 mm or more were used. Each fibre was glued to a 0.6-mm thick paper tab with a 20-mm long slot, as shown in Figures 5.2 and 5.3, using cyanoacrylate adhesive. The specimens

were then conditioned in a humidity chamber at 23°C and 50% relative humidity for a minimum of 24 hours.

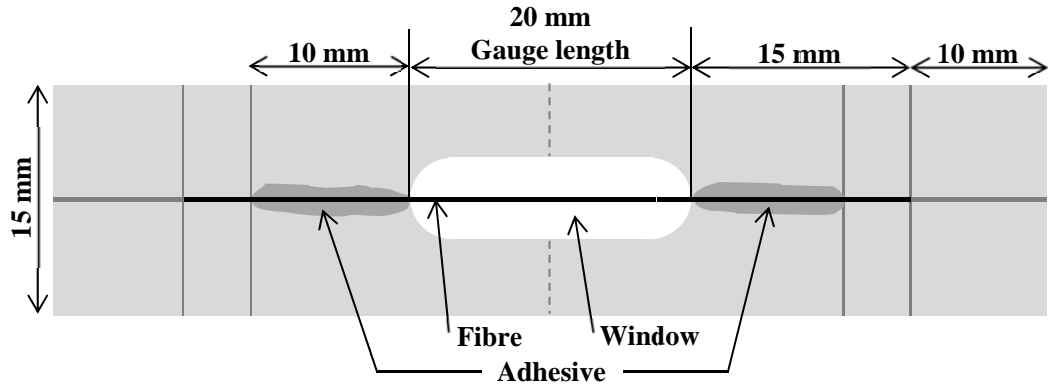


**Figure 5.2:** Schematic diagram of mounting tab for single fibre testing (After Virk, Hall & Summerscales, 2009).



**Figure 5.3:** Photograph of a flax technical fibre specimen for single fibre testing.

### 5.3.2.2 Determination of Fibre Cross-Sectional Area

The diameter of each of the technical fibres was measured, after conditioning, in two orthogonal planes, using a Nikon Eclipse ME600 optical microscope the fibres. The measurements were made from 5x images obtained from 6 successive fields of view along the 20 mm gauge length (the length of the slot) of the mounted specimen. The images were first obtained with the specimens rotated through an angle of +45° about the fibre axis. A second set of images was then obtained with the specimens rotated -45° about the fibre axis. The fibre diameters were measured at 3 approximately equally spaced positions in each of the six fields of view using UTHSCSA Image Tool and the average fibre diameter ( $D$ ) for each specimen then calculated. The measured fibre cross-sectional area ( $A_D$ ) was determined as  $\frac{\pi D^2}{4}$ , which assumes the fibres to be circular in shape.



### 5.3.2.3 Fibre Testing

Prior to testing, the fibre specimens were conditioned once again in the humidity chamber at 23°C and 50% relative humidity for at least 24 hours. Tensile testing was then conducted under ambient conditions of temperature and humidity using a method adapted from ASTM Standard C 1557-03. The tests were carried out using an Instron 5543 universal testing machine, with a 50 N load cell, at a crosshead speed of 0.2 mm/min, using pneumatic grips. The specimens were mounted with the grips extending right up to the end of the slot in the paper tab, as shown in Figure 5.4. The paper tab was then cut on either side of the slot and the test commenced. The tensile modulus of the flax technical fibres was determined at the strain ranges given in Table 5.1. The tensile strength was determined as the maximum stress from the stress-strain curve, while the strain to failure was determined as the strain at break.

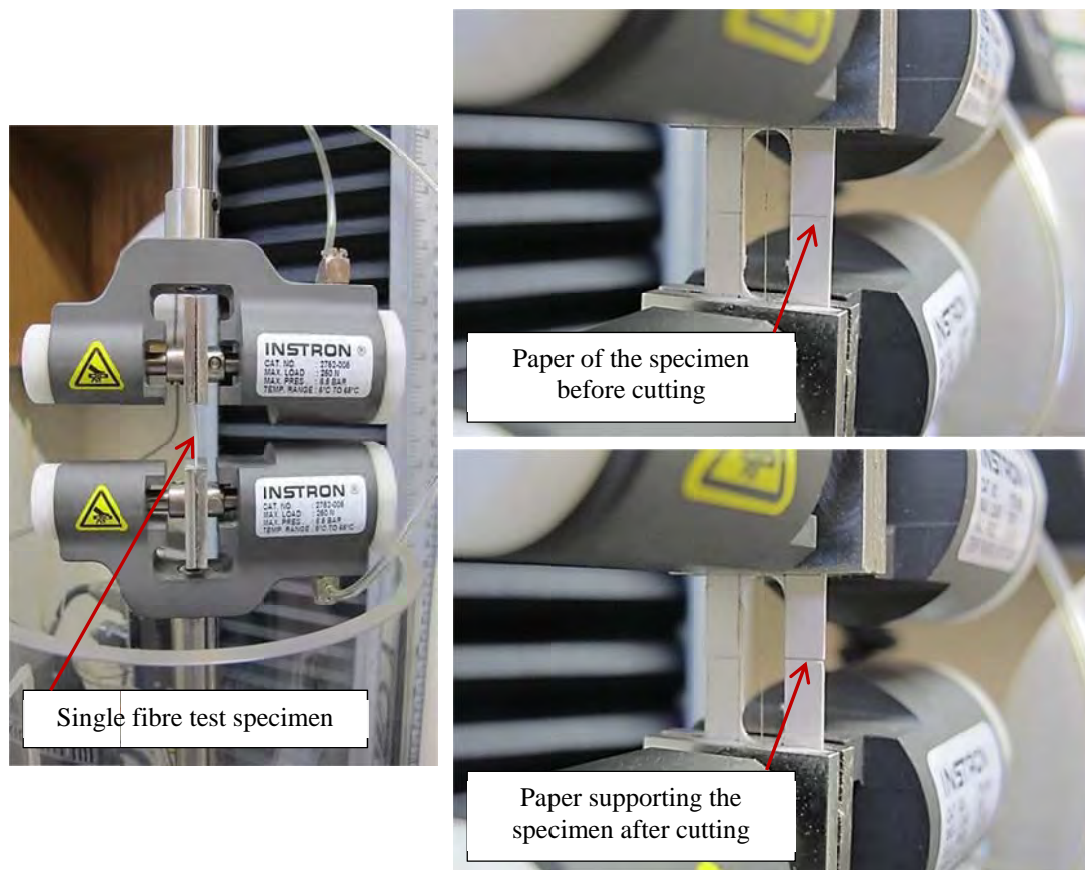


**Figure 5.4:** Single fibre test specimen in a universal testing machine.

**Table 5.1:** Strain ranges used for determination of tensile modulus

Nominal Strain at Break or Percent Elongation at Maximum Load, $\varepsilon$ (%)	Strain Range (%)
$1.2 \leq \varepsilon$	0.5-1.0
$0.6 \leq \varepsilon < 1.2$	0.5-0.7

#### 5.3.2.4 Weibull Analysis

The statistical distribution of the fibre strength and strain to failure was characterised using the two-parameter Weibull probability density function (PDF)

$$f(\sigma) = \frac{\beta}{\eta} \left(\frac{\sigma}{\eta}\right)^{\beta-1} \exp \left[ -\left(\frac{\sigma}{\eta}\right)^{\beta} \right] \quad (5.1)$$

where  $\beta$  is the shape parameter (Weibull modulus),  $\eta$  is the scale parameter (characteristic strength or strain) and  $\sigma$  is strength or failure strain of the fibres. The two-parameter Weibull cumulative distribution function (CDF) is obtained by integration of the Weibull PDF (Virk, Hall & Summerscales, 2009) as follows:

$$F(\sigma) = \int_0^{\sigma} \frac{\beta}{\eta} \left(\frac{\sigma}{\eta}\right)^{\beta-1} \exp \left[ -\left(\frac{\sigma}{\eta}\right)^{\beta} \right] d\sigma \quad (5.2)$$

$$F(\sigma) = 1 - \exp \left[ -\left(\frac{\sigma}{\eta}\right)^{\beta} \right] \quad (5.3)$$

$$F(\sigma) - 1 = -\exp \left[ -\left(\frac{\sigma}{\eta}\right)^{\beta} \right]. \quad (5.4)$$

Multiplying by -1 gives:

$$1 - F(\sigma) = \exp \left[ -\left(\frac{\sigma}{\eta}\right)^{\beta} \right]. \quad (5.5)$$

Taking the natural logarithm of both sides gives:

$$\ln[1 - F(\sigma)] = \ln \left\{ \exp \left[ -\left(\frac{\sigma}{\eta}\right)^{\beta} \right] \right\}. \quad (5.6)$$

As  $\ln[\exp(x)] = x$ ,

$$\ln[1 - F(\sigma)] = -\left(\frac{\sigma}{\eta}\right)^{\beta}. \quad (5.7)$$

Multiplying by -1 gives:

$$-\ln[1 - F(\sigma)] = \left(\frac{\sigma}{\eta}\right)^{\beta}. \quad (5.8)$$

Taking the natural logarithm of both sides gives:

$$\ln\{-\ln[1 - F(\sigma)]\} = \ln \left[ \left(\frac{\sigma}{\eta}\right)^{\beta} \right]. \quad (5.9)$$

Since  $\ln(x^y) = y \ln(x)$ ,

$$\ln\{-\ln[1 - F(\sigma)]\} = \beta \ln\left(\frac{\sigma}{\eta}\right). \quad (5.10)$$

And since  $\ln\left(\frac{x}{y}\right) = \ln(x) - \ln(y)$ ,

$$\ln\{-\ln[1 - F(\sigma)]\} = \beta [\ln(\sigma) - \ln(\eta)] \quad (5.11)$$

$$\ln\{-\ln[1 - F(\sigma)]\} = \beta \ln(\sigma) - \beta \ln(\eta). \quad (5.12)$$

Since  $-\ln(x) = \ln\left(\frac{1}{x}\right)$ ,

$$\ln\left\{\ln\left[\frac{1}{1-F(\sigma)}\right]\right\} = \beta \ln(\sigma) - \beta \ln(\eta). \quad (5.13)$$

Equation 5.13 can be written in the form

$$y = \beta x - \beta \ln(\eta). \quad (5.14)$$

where  $y = \ln\left\{\ln\left[\frac{1}{1-F(\sigma)}\right]\right\}$ , and  $x = \ln(\sigma)$ . The Weibull probability plot can then be plotted as  $y$  versus  $x$  (Murty, Xie & Jiang, 2004). The slope is  $\beta$  and the  $y$ -axis intercept is  $-\beta \ln(\eta)$ . The scale parameter  $\eta$  is then obtained as follows:

$$y \text{ intercept} = -\text{slope} \ln(\eta) \quad (5.15)$$

$$\ln(\eta) = -\frac{y \text{ intercept}}{\text{slope}}. \quad (5.16)$$

Taking the natural logarithm,

$$\ln[\ln(\eta)] = \ln\left(-\frac{y \text{ intercept}}{\text{slope}}\right). \quad (5.17)$$

As  $\ln(x) = \exp(x)$ ,

$$\exp[\ln(\eta)] = \exp\left(-\frac{y \text{ intercept}}{\text{slope}}\right). \quad (5.18)$$

Since  $\exp[\ln(x)] = x$ ,

$$\eta = \exp\left(-\frac{y \text{ intercept}}{\text{slope}}\right). \quad (5.19)$$

It is necessary to rank the data from the lowest value to the highest value when the data is plotted. The cumulative probability of failure ( $F(i, n)$ ) is then assigned to each data point. The values of  $F(i, n)$  are the median rank of the  $i^{\text{th}}$  of  $n$  samples tested (Fothergill, 1990). The median rank is given by

$$F(i, n) = \frac{i-0.3}{n+0.4} = F(\sigma). \quad (5.20)$$

Therefore,  $y$  is transformed into  $\ln\left[\ln\left(\frac{1}{1-\text{Median Rank}}\right)\right]$ .

The shape parameter or Weibull modulus ( $\beta$ ) reveals the variation in strength or strain distribution. A high value of the Weibull modulus indicates only small scatter in

the data. However, if the the Weibull modulus is low, there is large scatter in the data (Sun, Pang, Zhou, Zhang, Zhan & Zheng, 2012).

The scale parameter (characteristic strength or strain) ( $\eta$ ) is an estimator of the average strength or strain (Sun et al., 2012).

#### ***5.3.2.5 Determination of Fibre Area Correction Factor***

Determination of the tensile modulus and strength of fibres requires measurement of the fibre cross-sectional area ( $A_D$ ). This has generally been done by measuring the fibre diameter and then calculating the cross-sectional area assuming the fibres to be circular in shape. However, as pointed out by Virk, Hall & Summerscales (2012) and Thomason et al. (2011), this can lead to considerable error, since the fibres are not circular in cross-section, as shown schematically in Figure 5.5. As a result the tensile strength and modulus of the fibres determined in this way is underestimated. To account for this a fibre area correction factor  $K$  was determined using the method developed by Virk, Hall & Summerscales (2012).



**Figure 5.5:** Schematic diagram of cross-section of a flax technical fibre (Baley, 2002).

To determine the fibre area correction factor, 113 technical fibres were extracted from the unidirectional fabric yarns and mounted in transverse cross-section in epoxy resin. The specimens were then metallographically ground using progressively finer emery paper, then polished on a 3  $\mu\text{m}$  diamond pad and finished on a 1  $\mu\text{m}$  diamond pad. The polished fibre surfaces were subsequently sputter coated with gold using an Emitech K550x gold sputter coater. They were then examined using a Hitachi S3400-X scanning electron microscope (SEM) operated in high vacuum mode at an accelerating voltage of 15 kV. Imaging was done using backscattered electrons to enhance the

contrast. The true cross-sectional areas ( $A_T$ ) of the technical fibres was determined from the images using Image J. To successfully threshold the images it was necessary to improve the contrast further and this was done manually by colouring the fibres black.

The fibre area correction factor ( $K$ ) is given by

$$K = \frac{A_D}{A_T} \quad (5.21)$$

where  $A_D$  and  $A_T$  are the measured and true fibre cross-sectional areas, respectively. Following the method developed by Virk (2010), the fibre area correction factor was calculated from the ratio of the geometric mean of the location parameter of the log-normal distribution of  $A_D$  and  $A_T$ . The log-normal probability density function (PDF) is given by

$$f(A') = \frac{1}{\lambda' \sqrt{2\pi}} \exp \left[ -\frac{1}{2} \left( \frac{A' - \mu'}{\lambda'} \right)^2 \right] \quad (5.22)$$

where  $A' = \ln(A)$  and  $A$  is the fibre area.  $\mu'$  is the location parameter, which is the arithmetic mean of natural logarithms of the fibre areas (the average of  $A'$ ).  $\lambda'$  is also the scale parameter, which is the standard deviation of natural logarithms of the fibre areas (the standard deviation of  $A'$ ). The geometric mean and geometric standard deviation for the fibre area ( $A$ ) are then determined from  $\exp(\mu')$  and  $\exp(\lambda_{A'})$ , respectively. The fibre area correction factor is then given by

$$K = \frac{\exp(\mu'_D)}{\exp(\mu'_T)} = \frac{\mu_D}{\mu_T} \quad (5.23)$$

where  $\mu'_D$  and  $\mu'_T$  are the arithmetic means of the natural logarithms of  $A_D$  and  $A_T$ , respectively and  $\mu_D$  and  $\mu_T$  are the geometric means for  $A_D$  and  $A_T$ , respectively (Virk, 2010).

### 5.3.2.6 Determination of True Modulus and True Strength

Both the elastic modulus and tensile strength are inverse functions of the cross-sectional area. From equation 5.21, the true area  $A_T$  is given by

$$A_T = \frac{A_D}{K} \quad (5.24)$$

Thus the true values of the modulus  $E$  and strength  $\sigma$  are given by

$$E_T = K E_D \quad (5.25)$$

and

$$\sigma_T = K \sigma_D \quad (5.26)$$

where the subscripts  $T$  and  $D$  refer to the true values and the values determined using the measured cross-sectional area, respectively.

### 5.3.3 Testing of Fibre Bundles

#### 5.3.3.1 Introduction

Flat fibre bundle testing is commonly used by the textiles industry to obtain a measure of fibre strength (ASTM D1445/D1445M-12; Burley & Carpenter, 1955). The fibre strength is determined as the breaking force divided by the linear mass density, and is referred to as tenacity. The linear mass density is given in tex (g/1000 m length) and the tenacity is given in gf/tex.

An important feature of the flat fibre bundle test is that it avoids the necessity to determine the fibre cross-sectional area. Assuming that the fibre cross-sectional shape is constant, tenacity (breaking force/linear mass density) can be converted to engineering strength (breaking force/fibre cross-sectional area) (ASTM D 1294-05) if the volumetric density of the fibres is known.

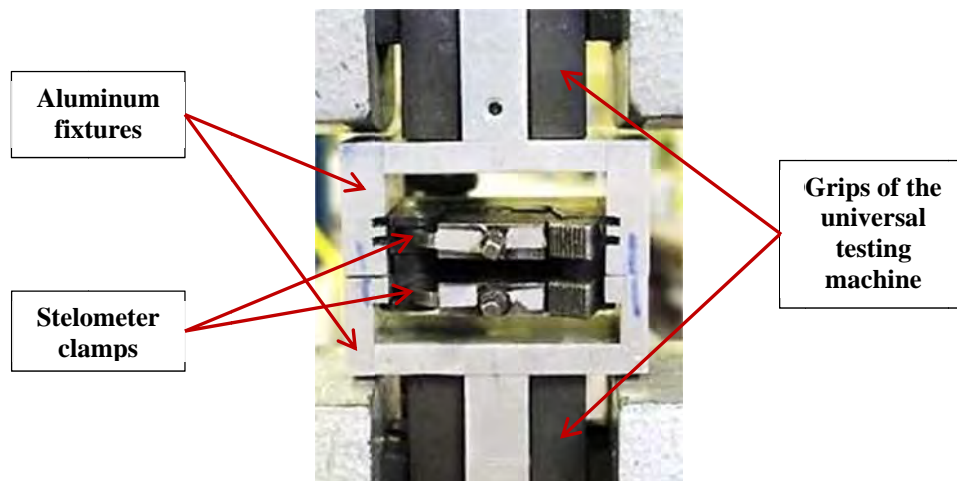


**Figure 5.6:** Set of the aluminium fixtures connecting the Stelometer clamps to the grips of the universal testing machine.

Two instruments have been commonly used for flat fibre bundle tests, these being the Stelometer instrument and the Pressley instrument (ASTM D1445/D1445M-12). Both of these instruments measure the breaking load indirectly and require calibration using standard specimens. ASTM D 2524-95, which covers flat bundle testing of wool fibres, notes that the test can be carried out by inserting the clamps used for gripping the fibres from the Stelometer or Pressley instruments into a universal testing machine and this method was used in the present study. The Stelometer clamps are considered to be particularly good (Foulk, 2010) and the fibre bundle clamps from a

Spinlab Stelometer 154 were used in the tests. A set of aluminium fixtures was fabricated to connect the Stelometer clamps to the grips of the universal testing machine, as shown in Figure 5.6.

The Stelometer clamps can be used with zero gauge length or a gauge length of 3.2 mm. The 3.2-mm gauge length was used in the present work since the results are reported to correlate better with those obtained from yarn testing (ASTM D 1445/D1445M-12).

The test method is intended for determination of breaking strength and elongation at break, but in the present work its usefulness for modulus measurement was also examined.

### 5.3.3.2 Fibre Bundle Preparation

Specimen preparation was carried out using the specialised tools that are provided with the Spinlab Stelometer 154, as well as some standard items, as shown in Figure 5.7. The samples were prepared in accordance with the procedure given in ASTM D1445/D1445M-12.

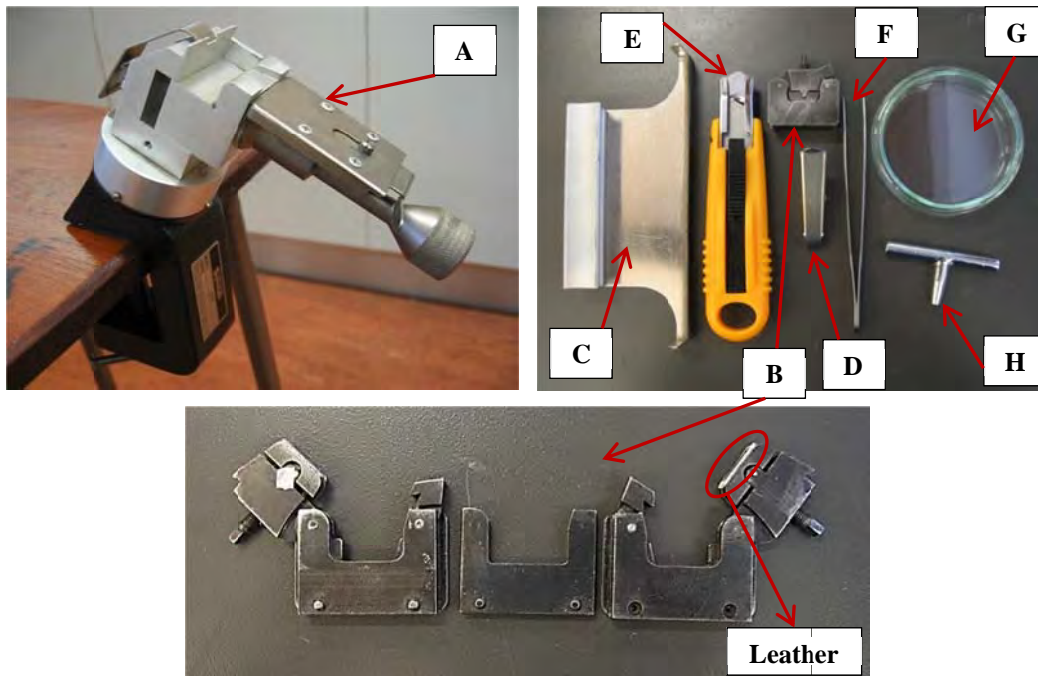


**Figure 5.7:** Tools used for fibre preparation: fibre clamp apparatus (A), Stelometer clamps (B), fine comb (C), small clamp (D), cutting knife (E), pair of tweezers (F), Petri dishes (G) and female Allen key (H).

Yarns were first extracted from the unidirectional fabric and the wrapping threads removed. Fibre bundles were then randomly selected from the yarns and one end of the bundles clamped using a small clamp (item D in Figure 5.7), as shown in Figure 5.8. The fibre bundles were then gently combed using a fine comb (item C in Figure 5.7), as shown in Figure 5.9. After combing, the fibres were aligned and fixed inside the Stelometer clamps using a fibre clamp apparatus (item A in Figure 5.7), as shown in Figure 5.10. The Stelometer clamps were then tightened using the tool shown as item H in Figure 5.7, according to the procedure given in the Stelometer manual (Spinlab, n.d.).



**Figure 5.8:** Clamping the fibre bundles.



**Figure 5.9:** Combing the fibre bundles.

The assembled Stelometer clamps were then removed from the fibre clamp apparatus and the fibres protruding from the sides of the clamps trimmed using a knife. This left a 15 mm length of the fibre bundles (including the 3.2 mm gauge length) inside the assembled Stelometer clamps. Figure 5.11 shows the assembled Stelometer clamps.



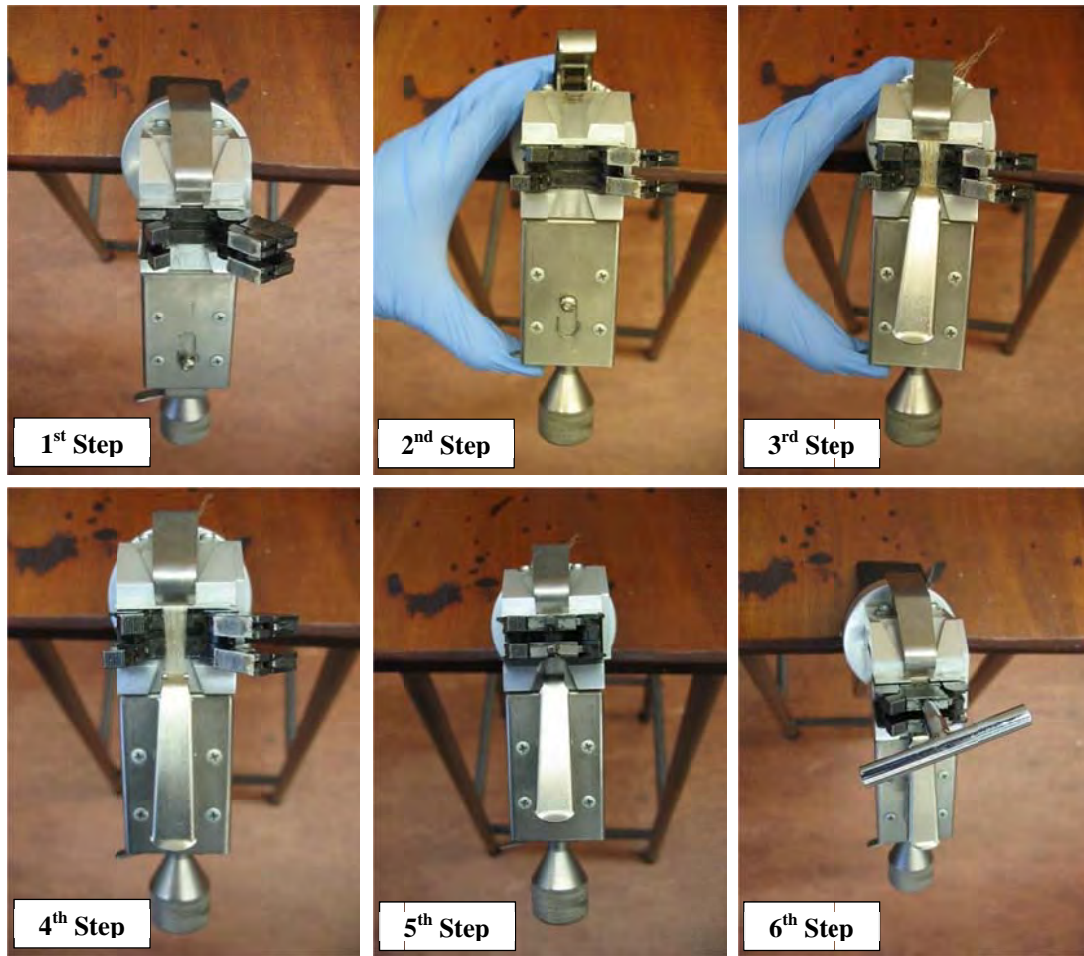


**Figure 5.10:** Steps for aligning and fixing the fibre bundles inside the fibre clamp using the fibre clamp apparatus: 1<sup>st</sup> Step - fixing the fibre clamp in the fibre clamp apparatus using the knob of the clamp apparatus; 2<sup>nd</sup> Step - sliding up the spring and pressing the top part; 3<sup>rd</sup> Step - inserting the fibre bundle held using a small clamp, and fixing the small clamp on the clamp apparatus by releasing the finger from the top part; 4<sup>th</sup> Step - letting the spring pull the fibres across the clamp apparatus by releasing the thumb; 5<sup>th</sup> Step - closing the fibre clamp; 6<sup>th</sup> Step - tightening the fibre clamp using a female Allen key.

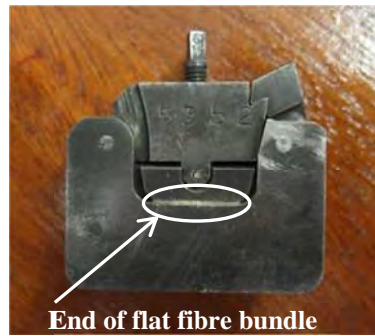


**Figure 5.11:** Assembled Stelometer clamps with fibre bundles held firmly.

### 5.3.3.3 Fibre Bundle Testing

The Stelometer clamps were inserted into a specially fabricated pair of aluminium fixtures which were then fixed into the grips of an Instron 5565 universal testing machine, Figure 5.12. Testing was carried out using a 100 N load cell at a crosshead speed of 10 mm/min. One hundred and five fibre bundle samples were tested under ambient conditions of temperature ranging from 24° to 26°C and relative humidity ranging from 37% to 59%. The tested fibre bundles were subsequently removed from the Stelometer clamps and immediately placed inside a pair of the Petri dishes (item G in Figure 5.7). The fibre bundles were then weighed in grams to 4 decimal places using an electronic balance and their weight was recorded.

After the measurements had been made, the linear mass density in tex was determined as the weight of the tested fibres in milligrams divided by the fibre bundle length in meters. The tenacity of the fibre bundles in gram-force (gf) per tex was determined as the breaking force of the fibres in gf divided by the linear mass density in tex.

The engineering strength  $\sigma$  (load divided by cross sectional area) in MPa can be determined from the measured breaking force  $S$  (gf), the linear mass density  $D$  (mg/m) and the volumetric density  $\rho$  (g/cm<sup>3</sup>) of the fibres if it is assumed that the fibres have constant cross-sectional area along the length used to determine their linear mass density. The strength  $\sigma$  can then be determined as follows:

The breaking force  $F$  in Newtons is given by:

$$F = S \frac{g}{1000} \quad (5.27)$$

where  $S$  is the breaking force given (gf)

and  $g$  is the acceleration due to gravity ( $9.80665 \text{ m/s}^2$ ).

The breaking stress  $\sigma$  in MPa is given by:

$$\sigma = \frac{F}{A} \quad (5.28)$$

where  $A$  is the cross-sectional area (mm).

Assuming constant cross-sectional shape  $A$  can be determined from:

$$A = \frac{D}{1000 \rho} \quad (5.29)$$

where  $D$  is the linear mass density (mg/m or tex)

and  $\rho$  is the volumetric density ( $\text{g/cm}^3$ ).

Thus

$$\sigma = 9.8 \rho \frac{S}{D} \quad (5.30)$$

which reduces to

$$\sigma = 9.8 \rho T \quad (5.31)$$

where  $T$  is the tenacity (gf/tex).

A value of  $1.44 \text{ g/cm}^3$  (Moran, Alvarez, Petrucci, Kenny & Vazquez, 2007) was used for the density  $\rho$  of the flax fibres.

The modulus was calculated as the chord modulus over the strain range of 0.14-0.15 mm/mm. For the calculation, the stress was determined from the tenacity using equation 5.31.

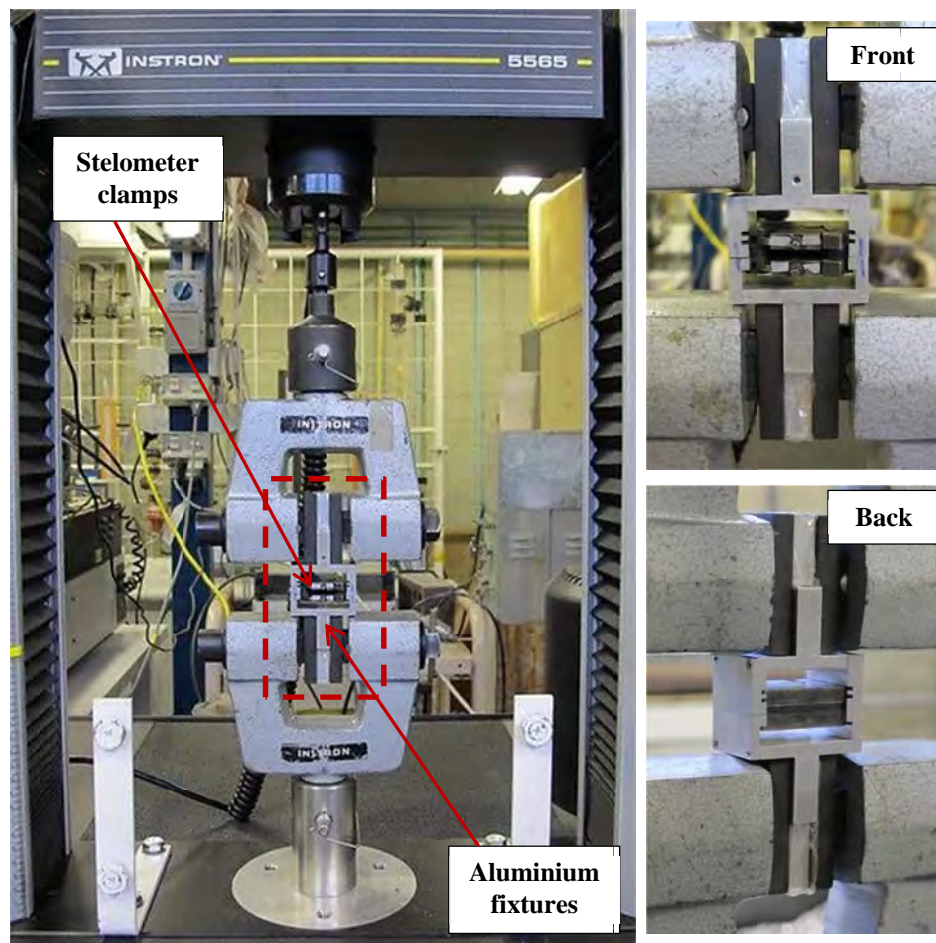


**Figure 5.12:** Stelometer clamps inserted into the aluminium fixtures fixed in the universal testing machine.

#### ***5.3.3.4 Scanning Electron Microscopy of Fractured Fibre Bundles***

Fracture surfaces of the tested fibre bundle specimens were examined using a Hitachi S3400-X scanning electron microscopy (SEM) operated in high vacuum mode at an accelerating voltage of 15 kV. The specimens were sputter coated with gold using an Emitech K550x gold sputter coater before the examination.

### **5.3.4 Unidirectional Flax Fibre-Reinforced Vinyl Ester-Matrix Composites**

#### ***5.3.4.1 Fabrication of Composites***

A unidirectional flax fibre/vinyl ester composite panel was fabricated by the Composites Innovation Centre (CIC), Canada, using rigid cavity vacuum resin transfer

moulding (VaRTM). The composite panel was post cured at 82°C for 1 hour. ArmorStar® IVSXH210 vinyl ester infusion resin catalysed with 1.5 wt% Arkema Luperox® DHD-9 was used as the matrix resin with Biotex unidirectional flax fabric as the reinforcement. The composite panel was fabricated to have a fibre volume fraction  $V_f$  of 30% based on the mass fractions of the resin and the fabric. The volume fraction was determined using the following equation (Huda, Drzal, Mohanty & Misra, 2008):

$$V_f = 100 \frac{w_f/\rho_f}{(w_m/\rho_m)+(w_f/\rho_f)} \quad (5.32)$$

where  $w$  and  $\rho$  are the weight fractions and density, respectively, and the subscripts  $f$  and  $m$  refer to the fibres and matrix, respectively. A value of 1.17 g/cm<sup>3</sup> (Meatherall, 2012) was used for the density of the resin and a value of 1.44 g/cm<sup>3</sup> (Moran et al., 2007) for the density of the fibres. It is noted that the spiral wrapping threads on the yarns and the transverse support threads in the fabric were included in the fibre mass fraction.

A panel of the neat vinyl ester resin post cured for at 82°C for 1 hour was also prepared by the CIC for determination of the properties of the neat resin.

#### **5.3.4.2 Tensile Testing of Composites**

Tensile testing of the cured vinyl ester resin and the 30 volume % unidirectional composites was carried out by the Industrial Technology Centre (ITC), Canada, under ambient laboratory conditions (22°C and approximately 40% relative humidity) using a MTS Landmark load-frame with a Tovey load cell and MTS controller/acquisition software. A mechanical extensometer with a 25.4 mm gauge length was used to measure strain. The extensometer was removed from the specimens after a strain of approximately 0.6% to avoid damage to the extensometer. As a result the strain at failure was not recorded.

Testing was carried out in accordance with ASTM D638 using dog bone shaped specimens having the dimensions shown in Figure 5.13. For the composite samples the longitudinal axis was parallel to the fibre direction. In each case five replicate specimens were tested. The tensile modulus was determined as the chord modulus at a strain range of 0.1% - 0.3% and the ultimate tensile strength determined as the maximum stress from the stress-strain curve.

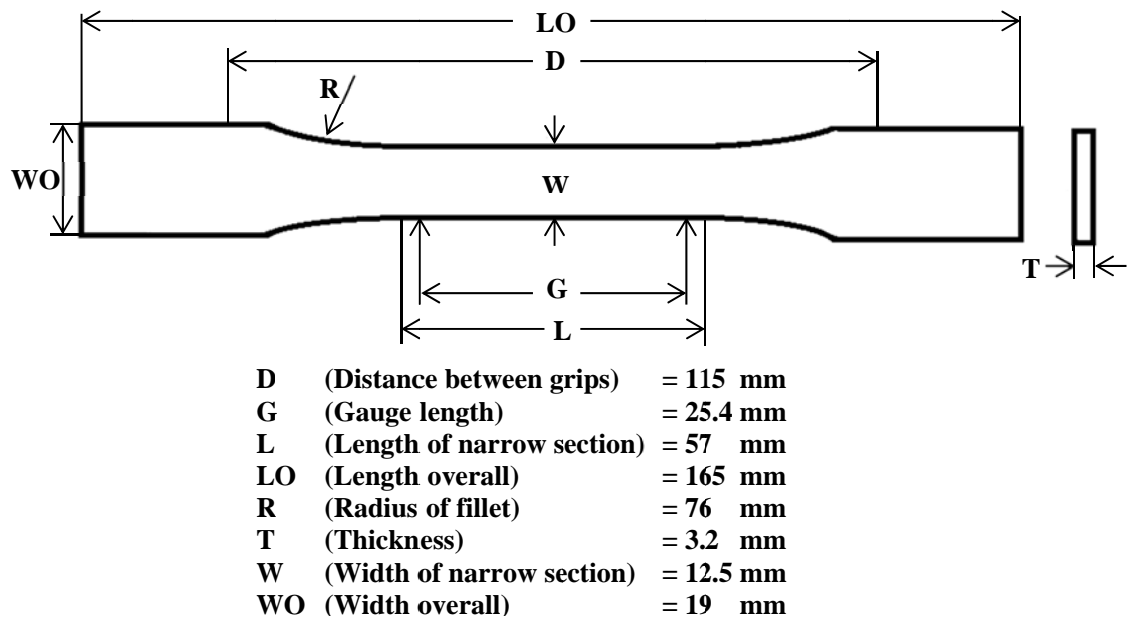


**Figure 5.13:** Schematic diagram of tensile specimen in accordance with ASTM standard D638.

#### **5.3.4.3 Optical and Scanning Electron Microscopy of Composites**

A randomly selected unidirectional flax fibre/vinyl ester composite sample was cut and mounted in epoxy resin on three orthogonal planes, these being the transverse and longitudinal planes and a plane parallel to the specimen surface. The specimens were then metallographically ground using progressively finer emery paper then polished on diamond pads to a 1  $\mu\text{m}$  finish. The polished sections were examined using a Nikon Epiphot 200 optical microscope. The longitudinal and transverse sections were also examined using a Hitachi S3400-X scanning electron microscope (SEM). Prior to examination, the specimens were sputter coated with gold using an Emitech K550x sputter coater. The SEM was operated in high vacuum mode at an accelerating voltage of 15 kV.

#### **5.3.4.4 Fibre Volume Fraction Measurement**

The fibre volume fraction was measured for the transverse section, prepared as described above, using image analysis. The images were obtained from the Hitachi S3400-X SEM, using backscattered electrons (BSE) to improve the contrast. The images were captured from three different locations on the specimen. As noted in Section 5.3.2.5, the images obtained did not have sufficient contrast for accurate

analysis and it was necessary to manually enhance the contrast by colouring the fibres black. Voids were coloured white so as to be included in the matrix fraction. The images were then thresholded and processed using Image J to obtain binary images. The fibre volume fraction was determined as the area fraction in these images.

The fibre volume fraction was determined both including the wrapping threads (wrapping threads coloured the same as the fibres) and excluding the wrapping threads (wrapping threads coloured the same as the matrix).

The volume fraction of flax in the unidirectional fabric was also determined from its weight fraction. This was done by weighing a piece of the fabric 180 mm x 185 mm then removing the wrapping threads and transverse threads and weighing them separately. The volume fraction of flax was determined using the following equation:

$$V_f = 100 \frac{w_r/\rho_r}{(w_f/\rho_f)+(w_r/\rho_r)} \quad (5.33)$$

where  $w$  and  $\rho$  are the weight fractions and density, respectively, and the subscripts  $r$  and  $f$  refer to the wrapping threads and flax fibres, respectively.

#### ***5.3.4.5 Scanning Electron Microscopy of Fracture Surfaces of Composites***

Fracture surfaces of the tested tensile specimen of the unidirectional flax fibre/vinyl ester composites were examined using a Hitachi S3400-X scanning electron microscope (SEM) to assess the fibre-matrix adhesion. The SEM was operated in high vacuum mode at an accelerating voltage of 15 kV. The fracture surfaces were sputter coated with gold using an Emitech K550x gold sputter coater before examination.

### **5.4 Results**

#### **5.4.1 Characterisation of Flax Fabric**

Optical microscope images of a yarn from the unidirectional flax fabric are shown in Figure 5.14. The spiral wrapping thread on the yarn is clearly evident. Two separate counter rotating wrapping threads are in fact present, the first with a spiral angle of approximately 30° and the second with a much shallower angle. Scanning electron microscope images are shown in Figure 5.15 where the individual fibres are readily discernable. The fibres can be seen to be untwisted but are noticeably undulating as a result of the presence of the wrapping thread.



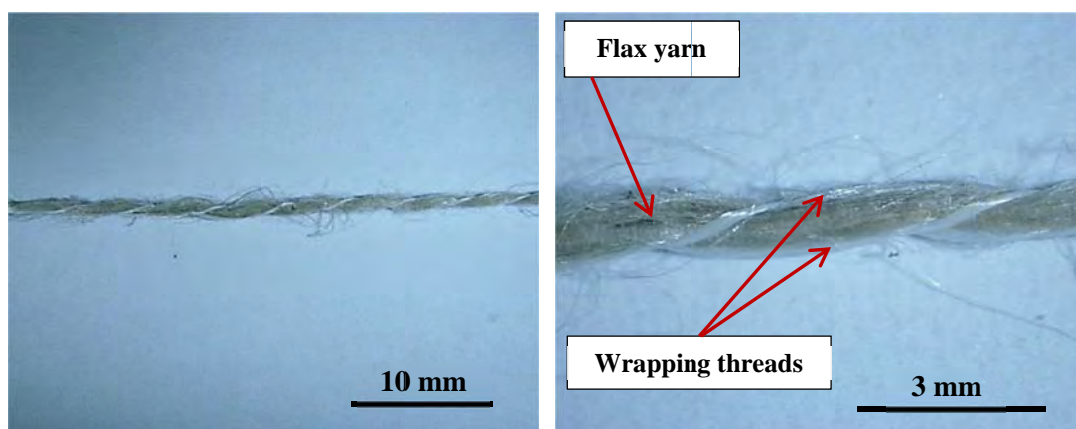


**Figure 5.14:** Optical microscope images of a yarn from the unidirectional flax fabric.

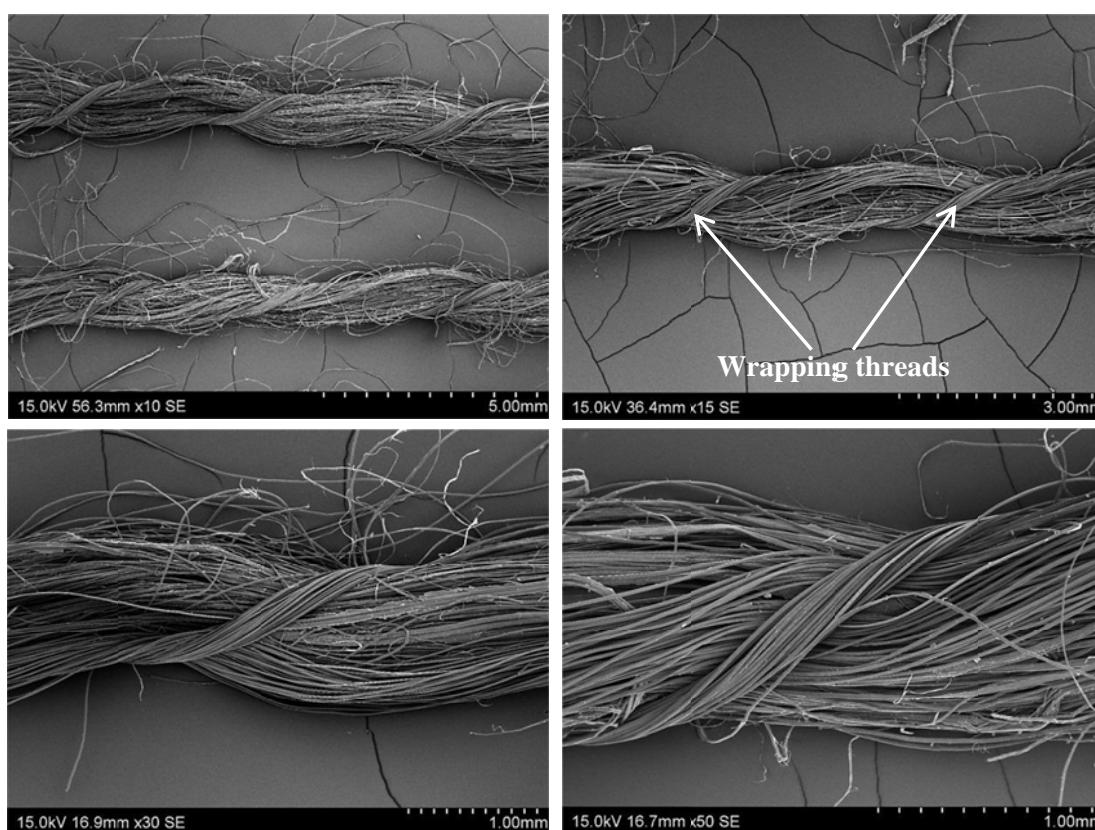


**Figure 5.15:** SEM micrographs of the flax yarns.

No information on the wrapping threads was available from the supplier so they were analysed using FTIR and Raman spectroscopy. The spectra are shown in Figure 5.16 and 5.17. and are consistent with the wrapping thread being made from viscose rayon. The peak assignments for the spectra are given in Appendix XV.



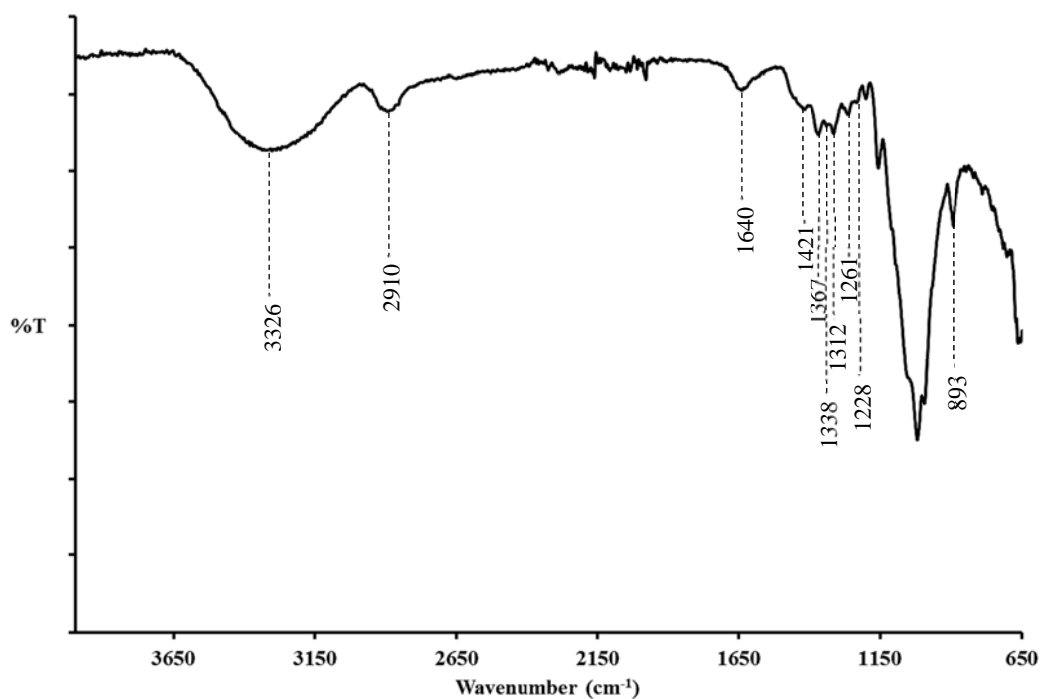


**Figure 5.16:** FTIR spectrum of wrapping threads from flax fabric.

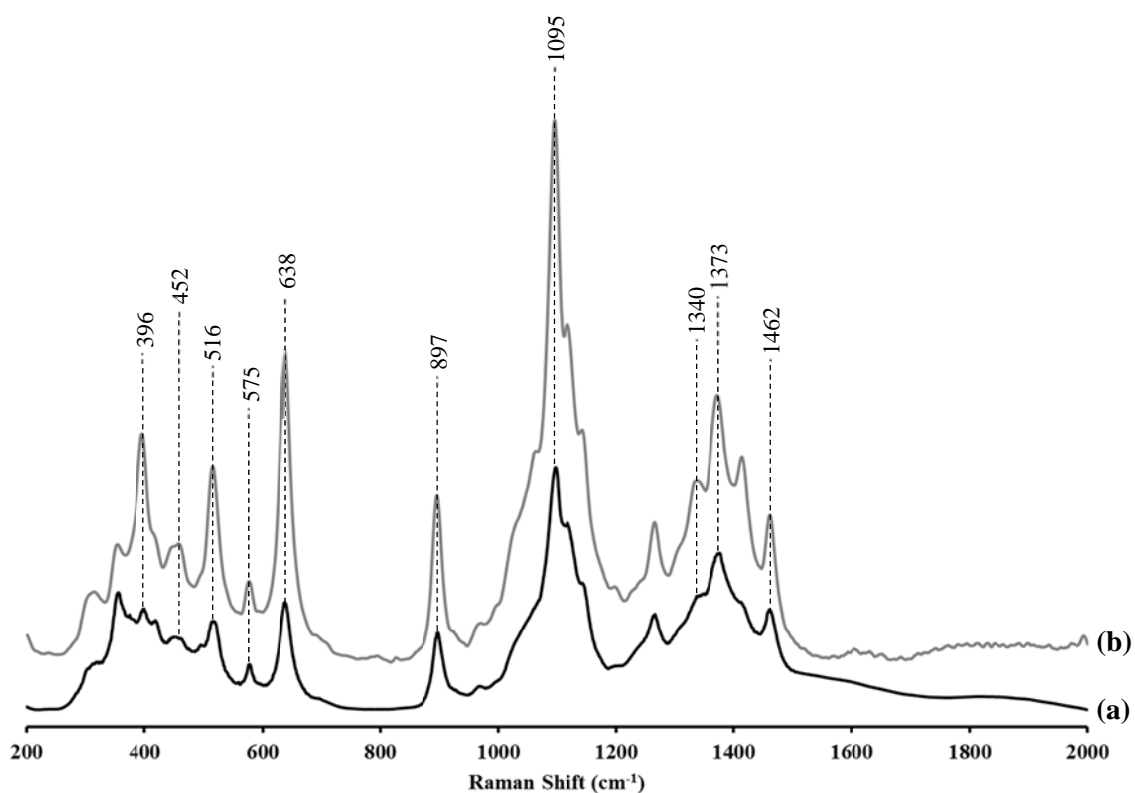


**Figure 5.17:** Raman spectra of wrapping threads from flax fabric using (a) 785-nm and (b) 514-nm excitation.

### 5.4.2 Defect Density of Flax Fibres

The fibre defects were examined in technical fibres extracted from the fabric yarns. The defects observed were kinks, nodes, micro-compressions, and initial breaks, as shown in Figures 5.18 to 5.21, respectively. The defect density was determined for 10 technical fibres over a length of approximately 20 mm and the results are given in Table 5.2. The fibres contained on average 31 defects per mm length, although there was a considerable variability with the standard deviation being 39%.

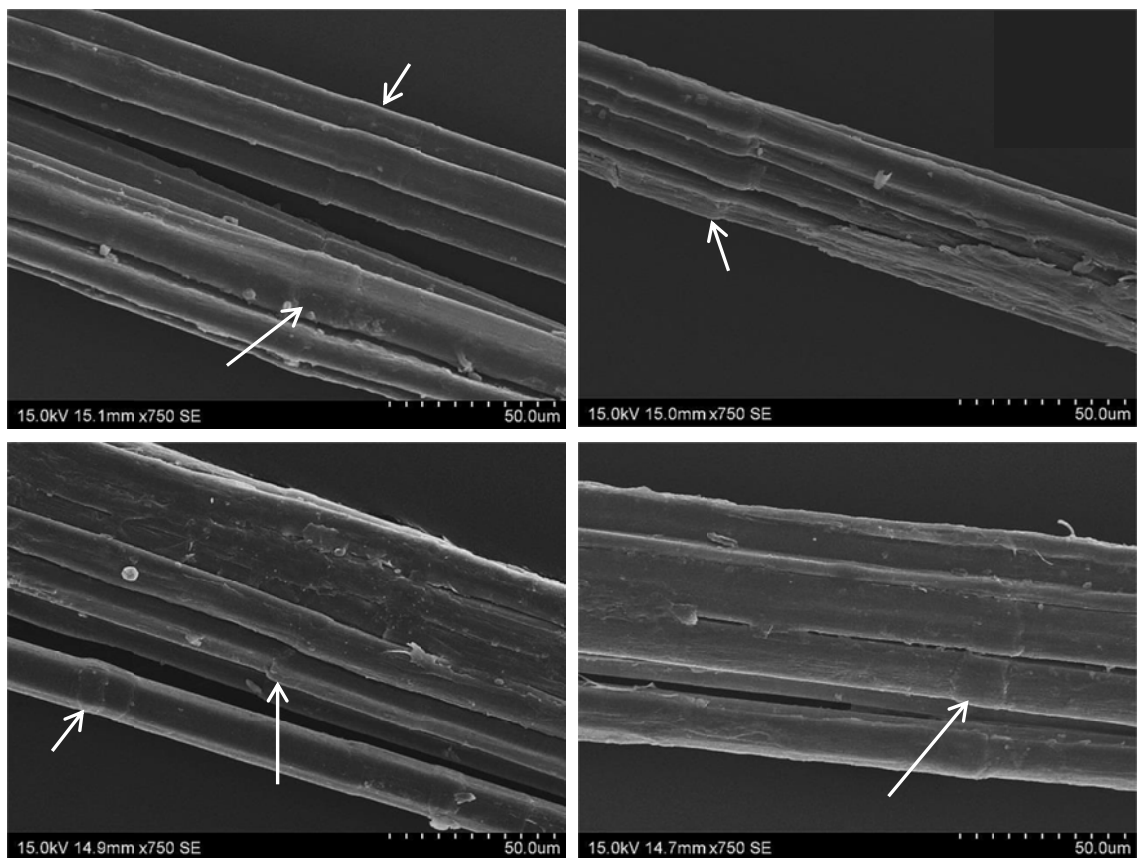


**Figure 5.18:** SEM micrographs of the flax technical fibres showing kinks (arrowed).

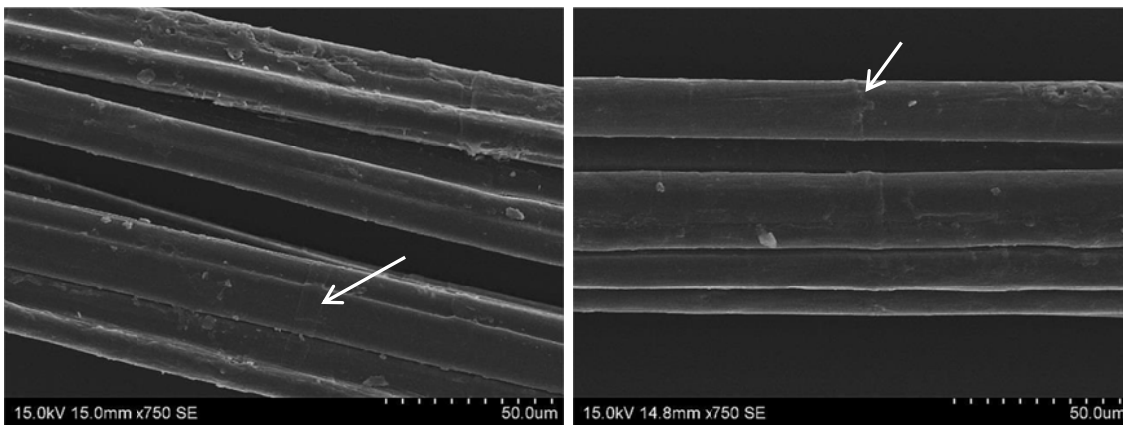


**Figure 5.19:** SEM micrographs of the flax technical fibres showing nodes (arrowed).

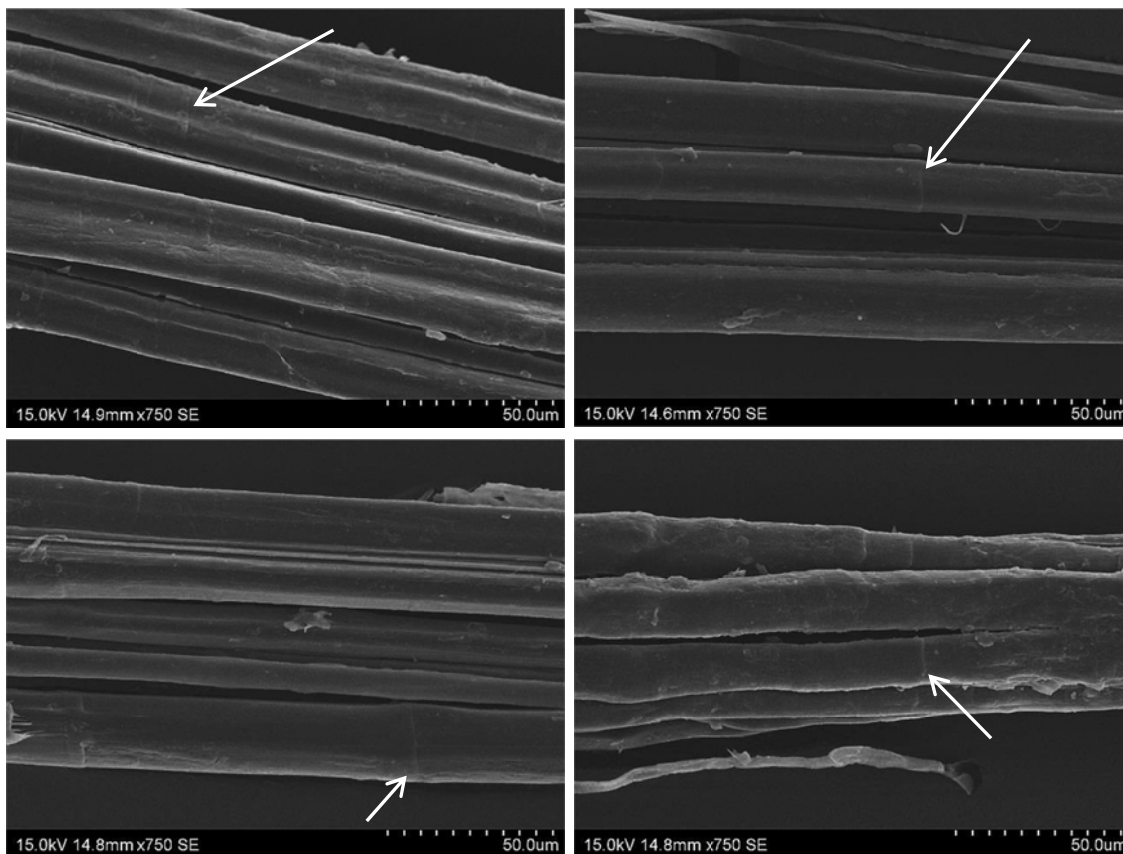


**Figure 5.20:** SEM micrographs of the flax technical fibres showing micro-compressions (arrowed).

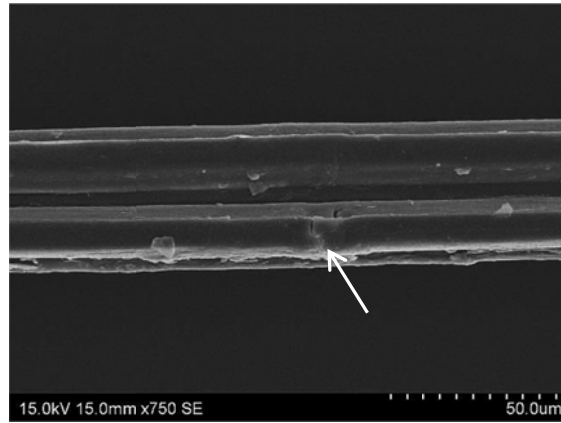


**Figure 5.21:** SEM micrographs of the flax technical fibres showing initial break (arrowed).

**Table 5.2:** Defects in flax technical fibres

Sample No.	Fibre Length (mm)	No. of Defects	Defects/mm
1	17.87	763	43
2	19.03	718	38
3	18.47	819	44
4	15.38	458	30
5	16.66	308	18
6	18.05	286	16
7	17.99	263	15
8	15.91	694	44
9	18.20	406	22
10	17.57	634	36
Average (Defects/mm)			31
SD (Defects/mm)			12
SD (%)			39

### 5.4.3 Flax Technical Fibres

#### 5.4.3.1 Fibre Length

A histogram showing the measured length of the technical fibres is given in Figure 5.22. The data has a normal distribution. The fibre length ranged from 39 mm to

170 mm with the average length being 93 mm with a standard deviation of 25 mm (27%).

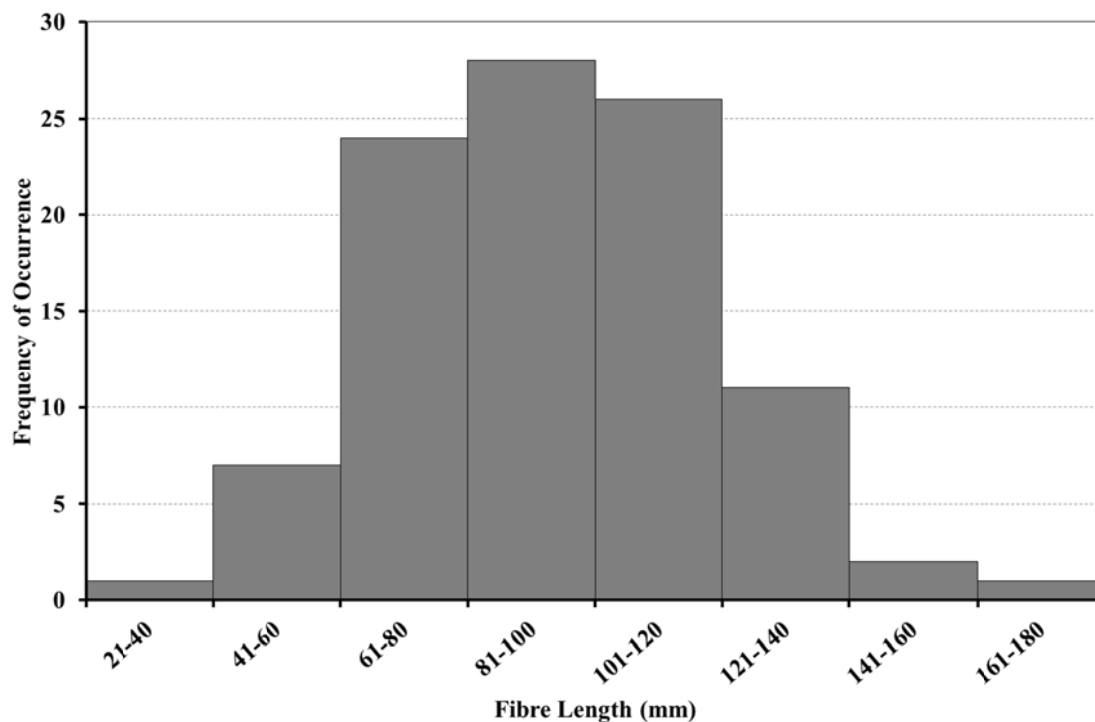


**Figure 5.22:** Histogram showing lengths of flax technical fibres.

#### 5.4.3.2 Diameter and Cross-Sectional Area of Flax Technical Fibres

The average fibre diameter was determined from measurements made in two orthogonal directions at 18 approximately equally spaced locations along the 20 mm gauge length for the 113 technical fibres that were subsequently used for single fibre testing. The fibres had been conditioned at 23°C and 50% relative humidity before being measured. A typical optical microscope image used to measure the fibre diameters is shown in Figure 5.23.

A histogram showing the average fibre diameters is given in Figure 5.24. The distribution can be seen to be positively skewed. There is considerable variability in the fibre diameters, with the minimum and maximum values being 41 and 135  $\mu\text{m}$ , respectively. The overall average diameter was 82  $\mu\text{m}$  with a standard deviation of 21  $\mu\text{m}$ .

The cross-sectional area of the fibres determined from the average fibre diameters and assuming the fibres to be circular in cross-section is shown in Figure 5.25. The positive skewedness is now particularly evident. The minimum and maximum

and cross-sectional areas were 1,290 and 14,356  $\mu\text{m}^2$ , with the average area being 5,631  $\mu\text{m}^2$  with a standard deviation of 2,851  $\mu\text{m}^2$ .

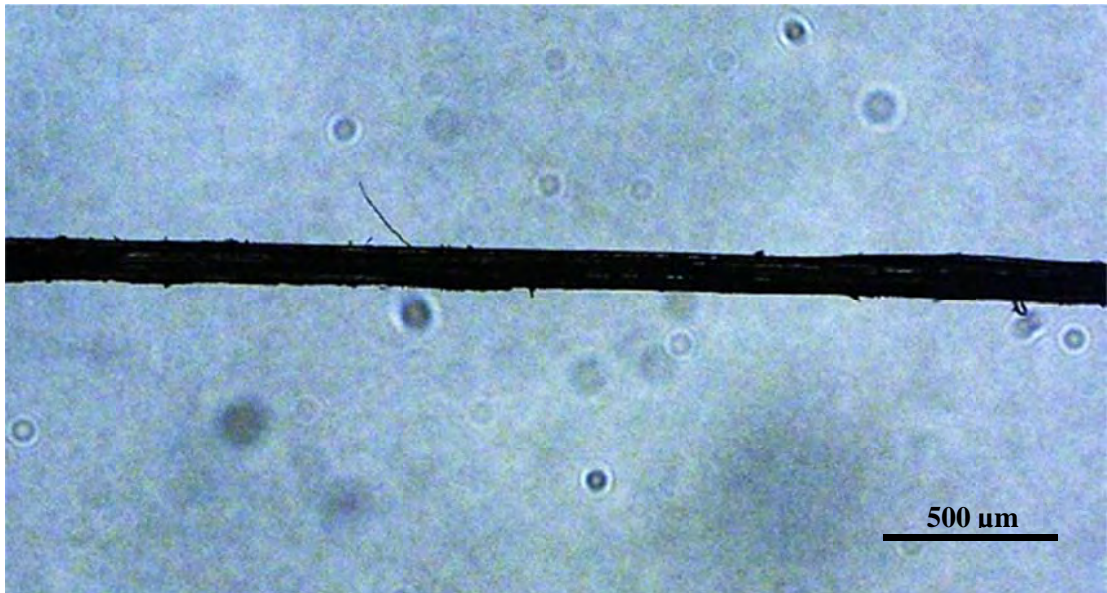


**Figure 5.23:** Typical optical microscope image of flax technical fibre.

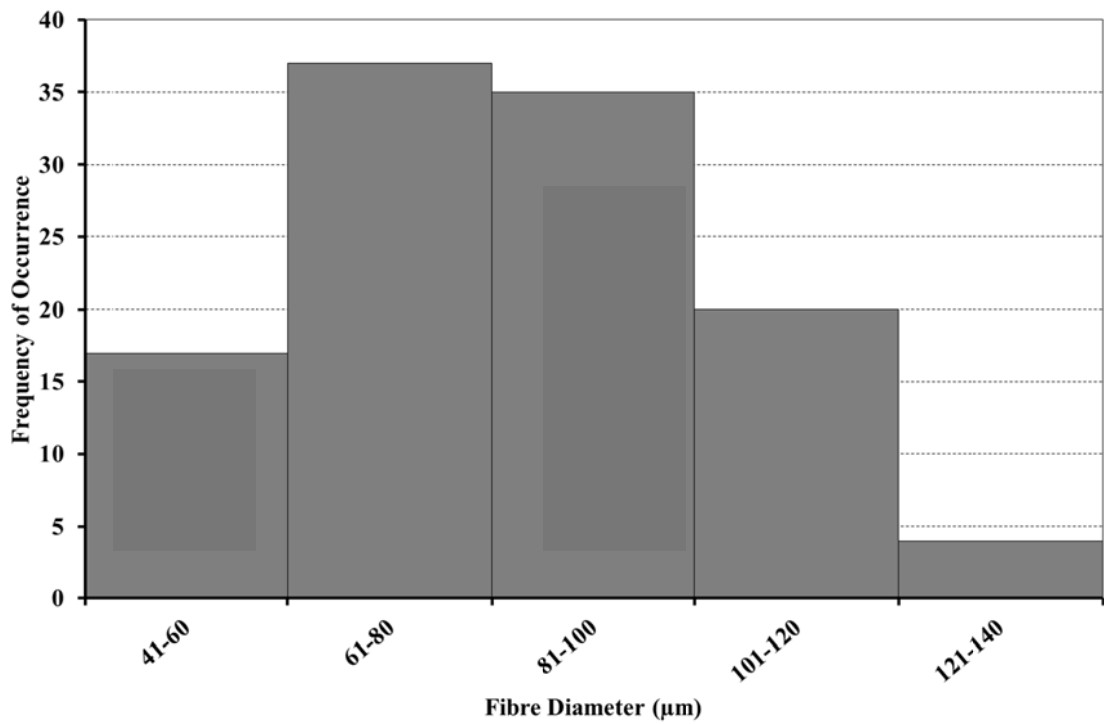


**Figure 5.24:** Histogram of measured diameters of flax technical fibres.

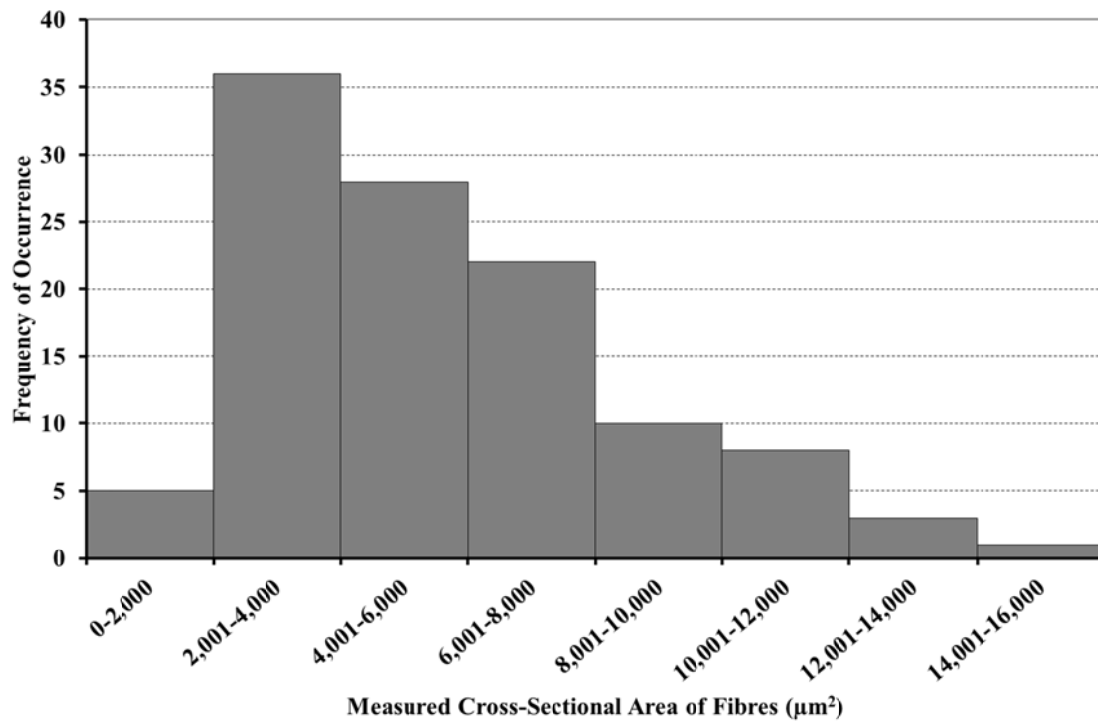


**Figure 5.25:** Histogram of measured cross-sectional areas of flax technical fibres.

#### 5.4.3.3 Fibre Area Correction Factor

Examples of the true cross-sectional shape of the technical fibres are shown in Figure 5.26 while the cross-sectional shape and the true cross-sectional area are given for all 113 fibres examined in Appendix XVI.

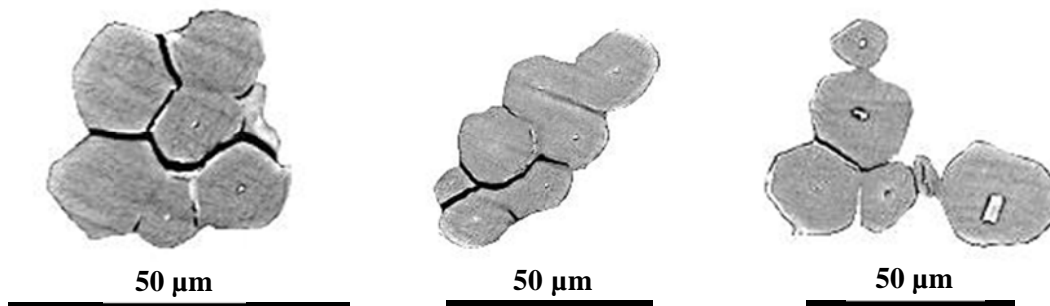


**Figure 5.26:** Examples of cross-sectional shape of technical fibres.

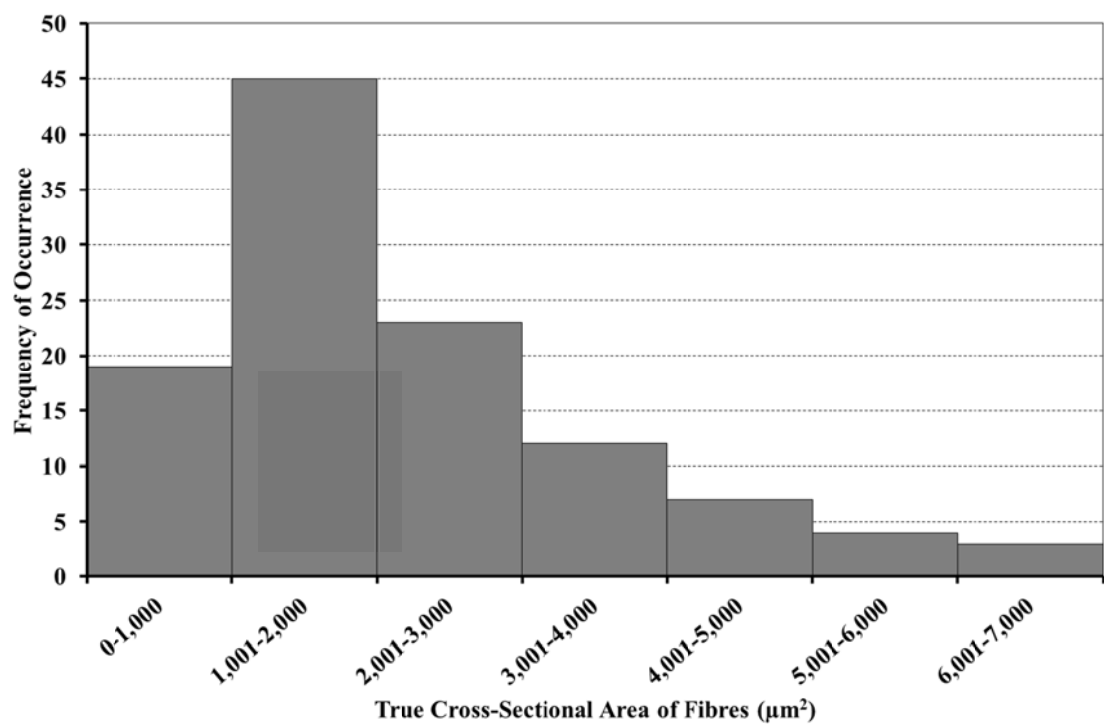


**Figure 5.27:** Histogram of true cross-sectional areas of flax technical fibres.

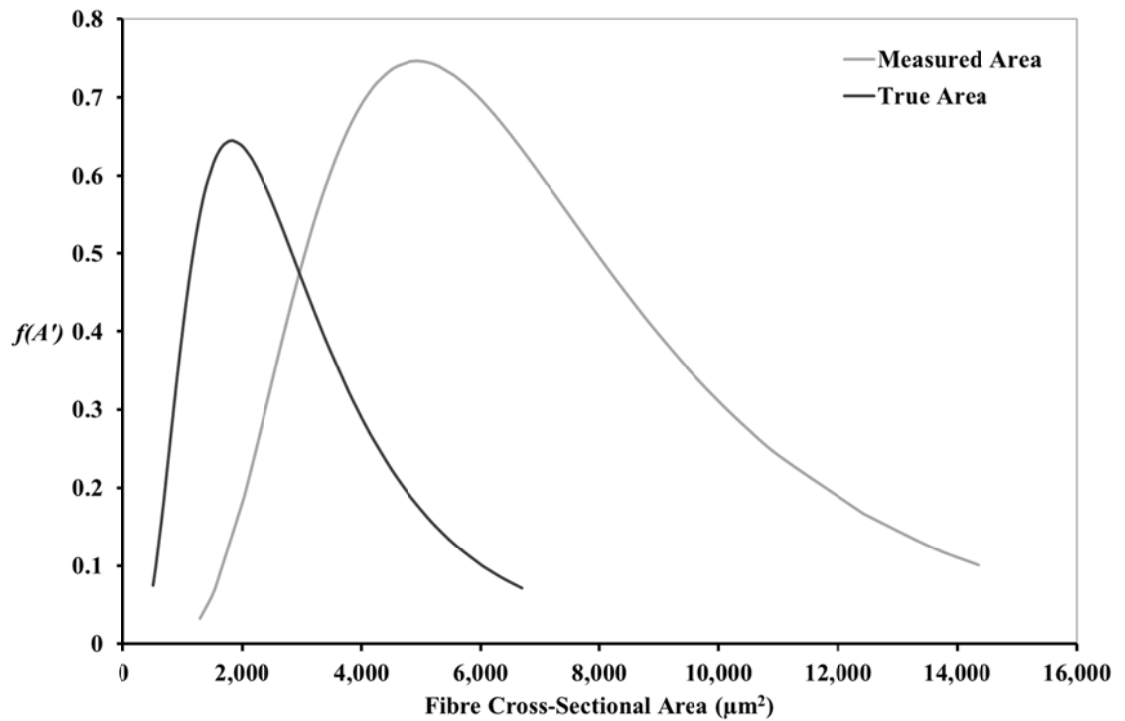


**Figure 5.28:** Log-normal distributions of measured and true cross-sectional areas of flax technical fibres.



A histogram of the true cross-sectional areas of the technical fibres is shown in Figure 5.27. The distribution is again positively skewed, but the values are substantially lower with the minimum and maximum values being 506 and 6,690  $\mu\text{m}^2$  with an average value of 2,205  $\mu\text{m}^2$  and a standard deviation of 1,413  $\mu\text{m}^2$ .

Log-normal distributions of the measured and true cross-sectional areas are shown in Figure 5.28. The data for the log-normal distributions, calculated using equation 5.22 are given in tabulated form in Appendix XVII. The location parameter and scale parameter of the log-normal distributions are given in Table 5.3, together with the geometric mean and geometric standard deviation. The fibre area correction factor ( $K$ ) determined using equation 5.23 was 2.70.

**Table 5.3:** Location parameters, scale parameters, geometric mean and geometric standard deviation of the measured and true cross-sectional areas of the flax technical fibres

	<b>Fibre Cross-Sectional Area</b>	
	<b>Measured Area ( <math>A_D</math> )</b>	<b>True Area ( <math>A_T</math> )</b>
Location parameter ( $\mu'$ )	8.50	7.51
Scale parameter ( $\lambda'$ )	0.53	0.62
Geometric mean ( $\mu$ )	4,929 $\mu\text{m}^2$	1,827 $\mu\text{m}^2$
Geometric standard deviation ( $\lambda$ )	1.71 $\mu\text{m}^2$	1.86 $\mu\text{m}^2$

#### 5.4.3.4 Tensile Properties of Flax Technical Fibres

A technical fibre is shown after testing in Figure 5.29 while representative stress-strain curves are shown in Figure 5.30. In most cases the curves showed an initial

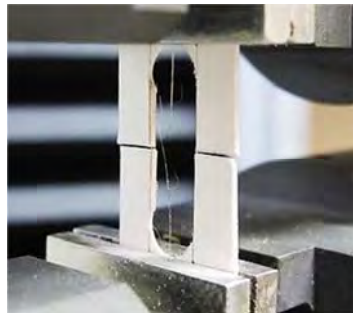


**Figure 5.29:** Tested flax fibre specimen in the universal testing machine.

run-in period (usually to strains of less than 0.005 mm/mm), after which they were linear. Small abrupt load drops (of approximately 3%) were frequently seen towards the end of the test.

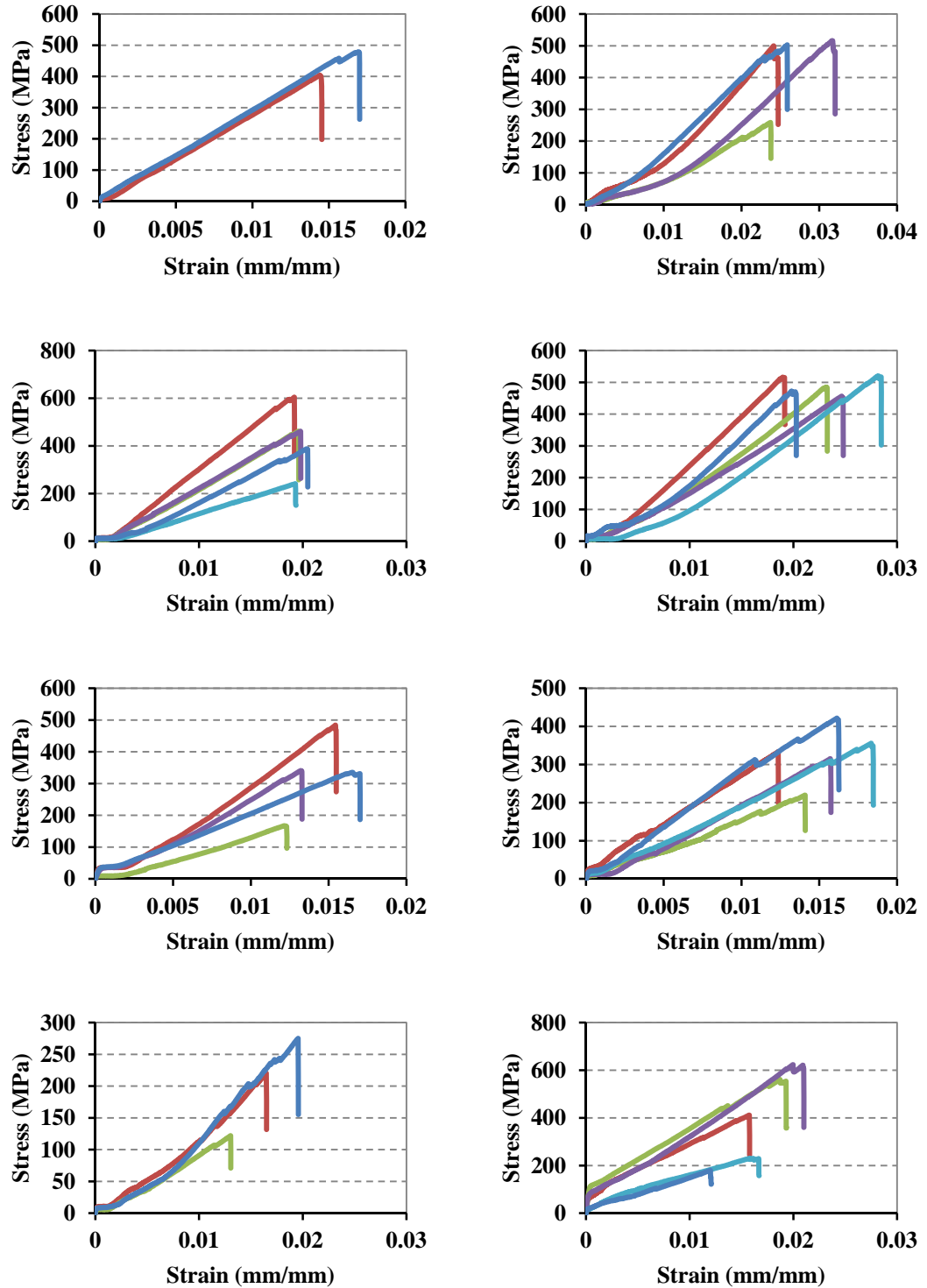


**Figure 5.30:** Representative tensile stress-strain curves of flax technical fibres.

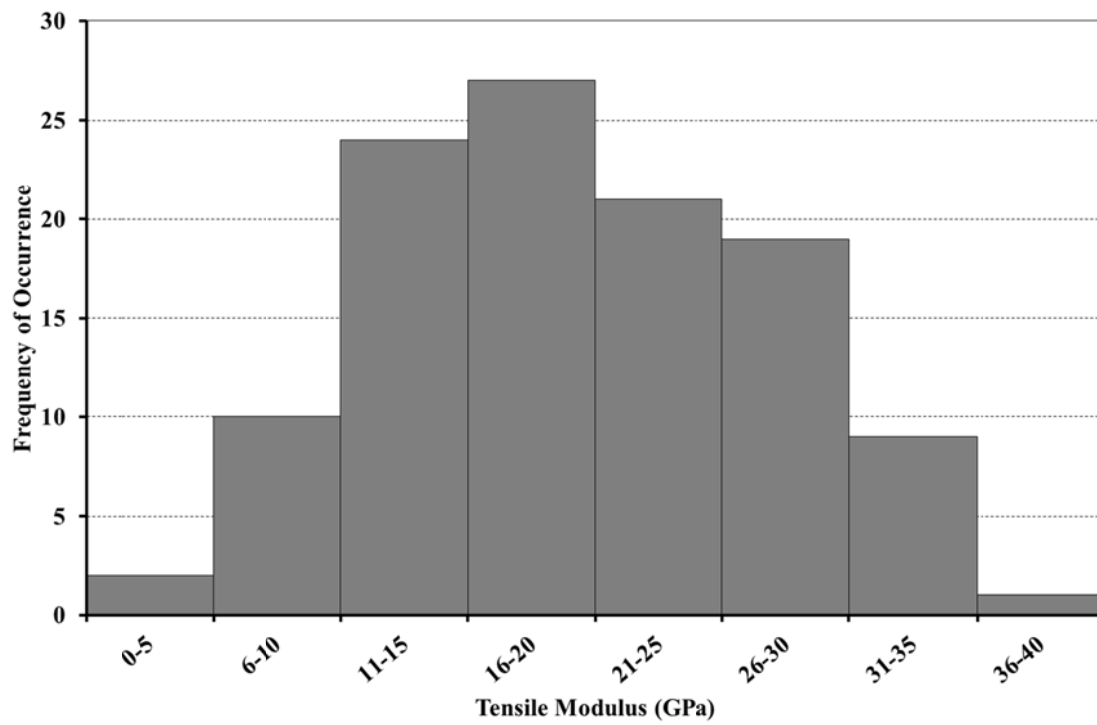


**Figure 5.31:** Histogram of measured tensile modulus of flax technical fibres.

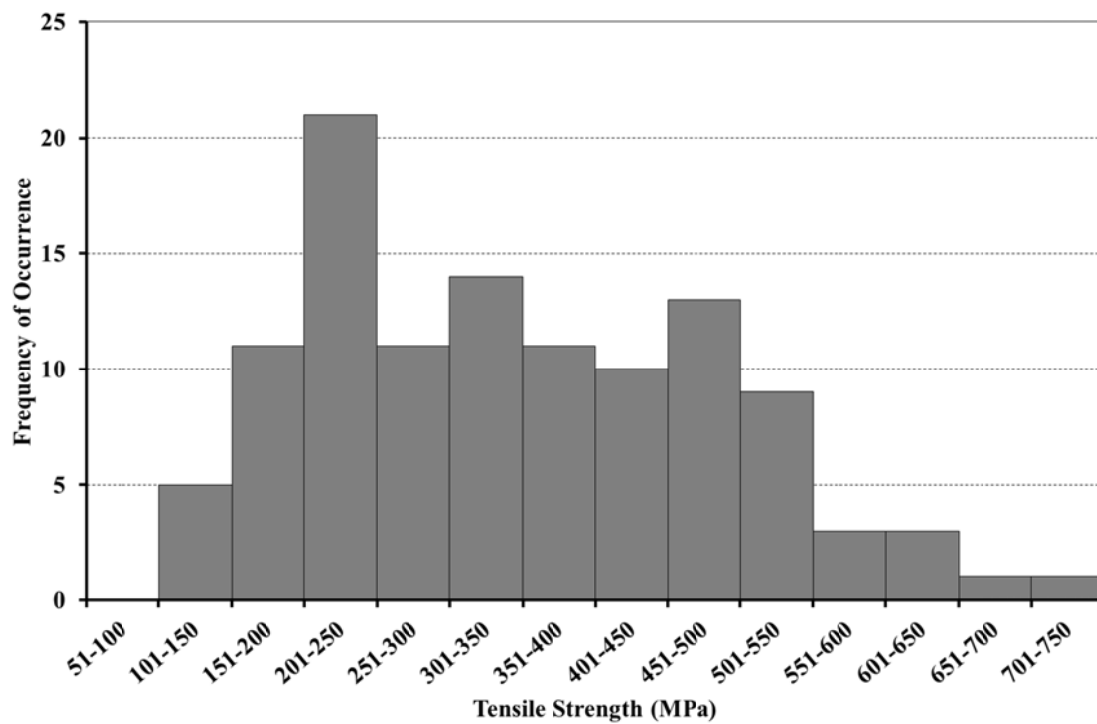


**Figure 5.32:** Histogram of measured tensile strength of flax technical fibres.

Histograms showing the tensile modulus, tensile strength and strain to failure are given in Figures 5.31-5.33. The modulus and strength have been calculated using the measured cross sectional area of the fibres, i.e., the area correction factor has not been applied. The modulus values show a normal distribution but the strength and strain to failure appeared to be slightly positively skewed.

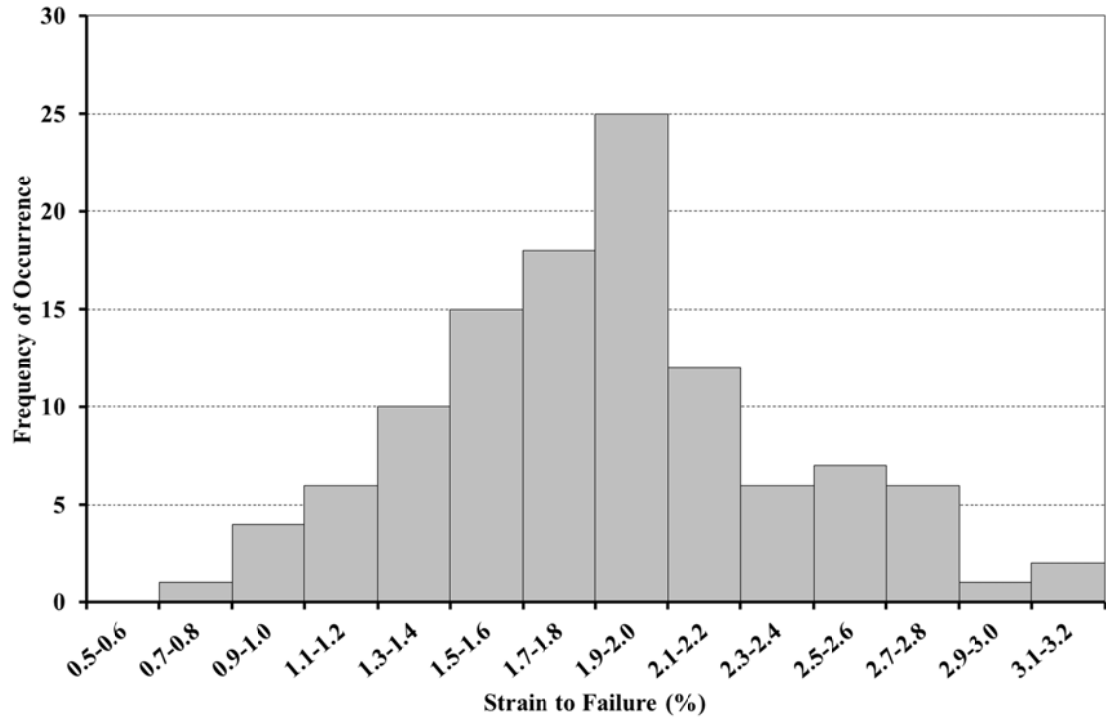


**Figure 5.33:** Histogram of measured strain to failure of flax technical fibres.

**Table 5.4:** Measured tensile properties of flax technical fibres

Property	Average Value	Standard Deviation	Minimum Value	Maximum Value
Modulus (GPa)	19.4	7.4	3.9	36.9
Strength (MPa)	347	136	106	738
Failure Strain (%)	1.8	0.5	0.7	3.2

The minimum and maximum values, together with the average values and the standard deviations are given in Table 5.4. The data shows wide scatter, as is evident from the range of values and also from the standard deviations. The tensile modulus was 19.4 GPa with a standard deviation of 7.4 GPa (38%), the tensile strength was 347 MPa

with a standard deviation of 136 MPa (39%), while the strain to failure was 1.8% with a standard deviation of 0.5% (28% of average value).

**Table 5.5:** True tensile properties of flax technical fibres

<b>Property</b>	<b>Average Value</b>	<b>Standard Deviation</b>	<b>Minimum Value</b>	<b>Maximum Value</b>
Modulus (GPa)	52.4	20.0	10.5	99.6
Strength (MPa)	936	368	286	1993
Failure Strain (%)	1.8	0.5	0.7	3.2

The true tensile properties, determined using the measured area correction factor  $K$  of 2.70, are given in Table 5.5. The true modulus was 52.4 GPa with a standard deviation of 20.0 GPa while the true strength was 936 MPa with a standard deviation of 368 MPa. Strain to failure is independent of cross sectional area so the true strain to failure is the same as the measured strain to failure.

#### **5.4.3.5 Weibull Analysis**

The Weibull probability plots for the true tensile strength and strain to failure of the flax fibres are shown in Figures 5.34 and 5.35, respectively. The data for the Weibull plots, calculated using equations 5.13 and 5.20 are given in tabulated form in Appendix XVIII.

The Weibull modulus was determined from the slope of the Weibull probability plots, while the scale parameter (characteristic strength or strain) was determined from the plots using equation 5.19. The tensile properties and two-parameter Weibull probability ( $\beta$  and  $\eta$ ) are given in Table 5.6.

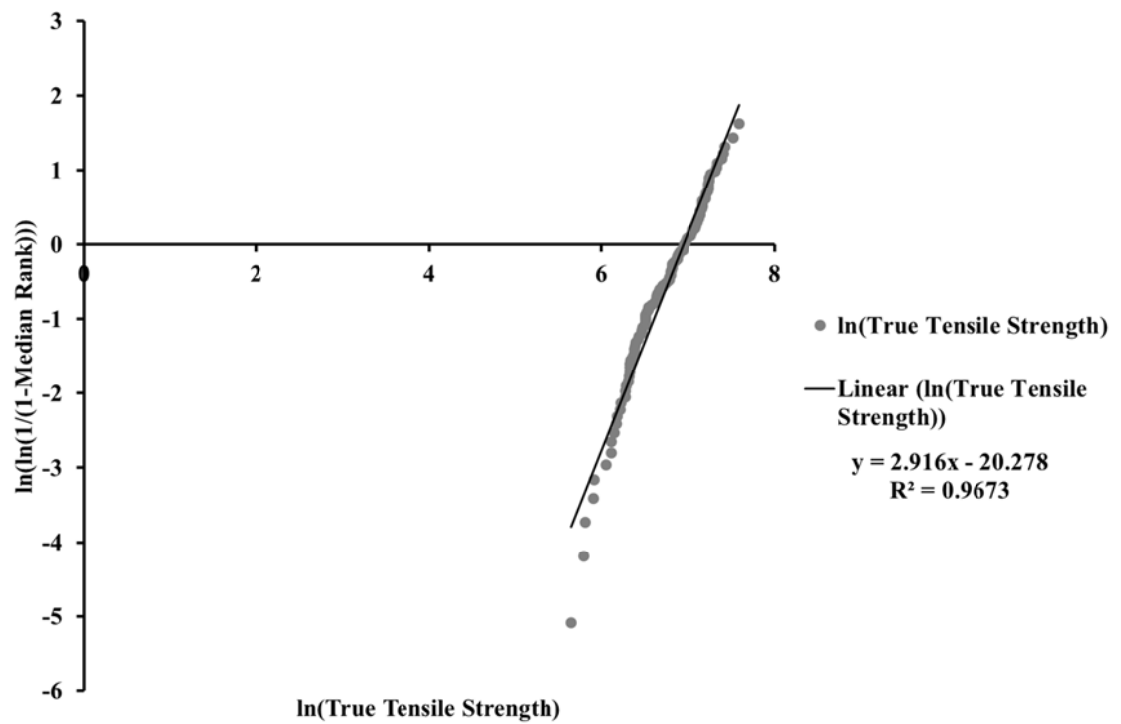


**Figure 5.34:** Weibull probability plot for true tensile strength of flax technical fibres.

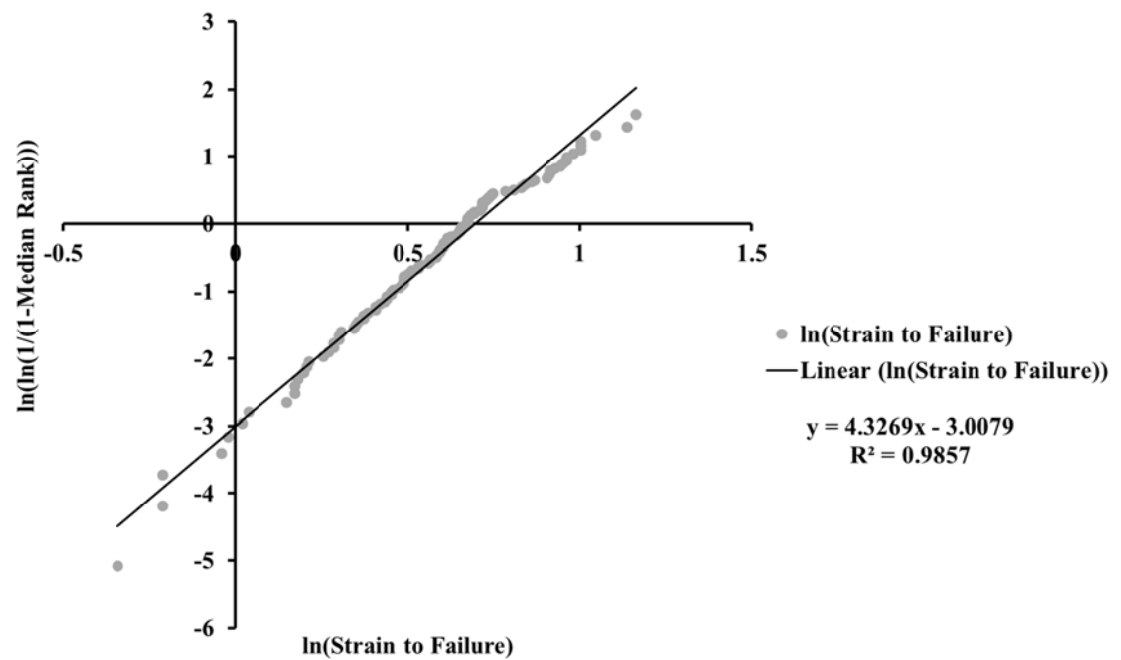


**Figure 5.35:** Weibull probability plot for strain to failure of flax technical fibres.

**Table 5.6:** True tensile properties of flax technical fibres and their Weibull modulus and scale parameters (values in brackets represent one standard deviation)

Tensile Property	Value	Weibull Modulus ( $\beta$ )	Scale Parameter ( $\eta$ )
True strength	936 (368) MPa	2.92	1,047 MPa
Strain to failure	1.83 (0.49)%	4.33	2.00%

## 5.4.4 Testing of Fibre Bundles

### 5.4.4.1 Tensile Properties of Fibre Bundles

Representative stress-strain curves for the flax fibre bundle tests are shown in Figure 5.36. The curves show a distinct run-in period up to a strain of approximately 0.11-0.12 mm/mm. Thereafter, the slope increased rapidly with the curves being essentially linear but then eventually showing a reduction in slope, sometimes with small load drops, before final failure occurred. The run in period is considered to be due to settling in of the Stelometer clamps in the aluminium fixture. The tensile test data for the flax fibre bundles is given in tabulated form in Appendix XIX.

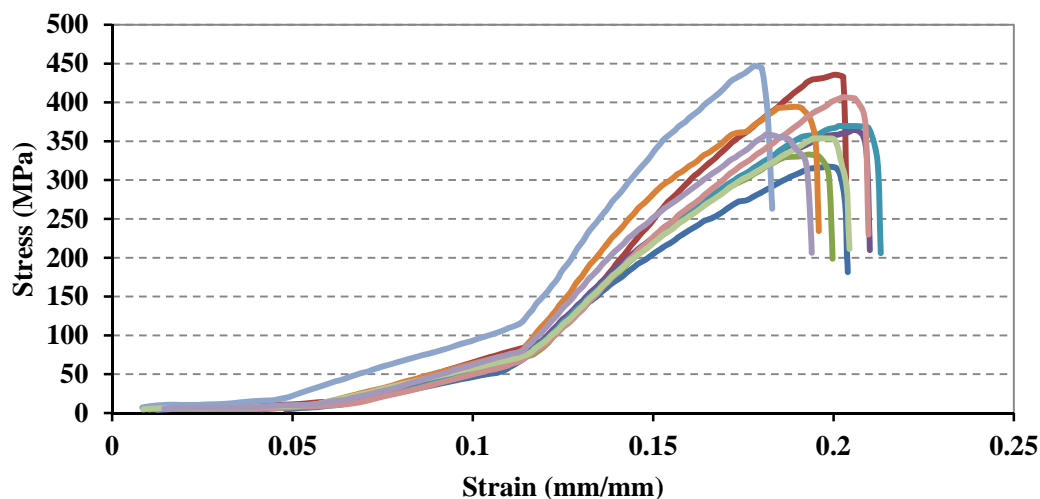


**Figure 5.36:** Representative tensile stress-strain curves of flax fibre bundles.

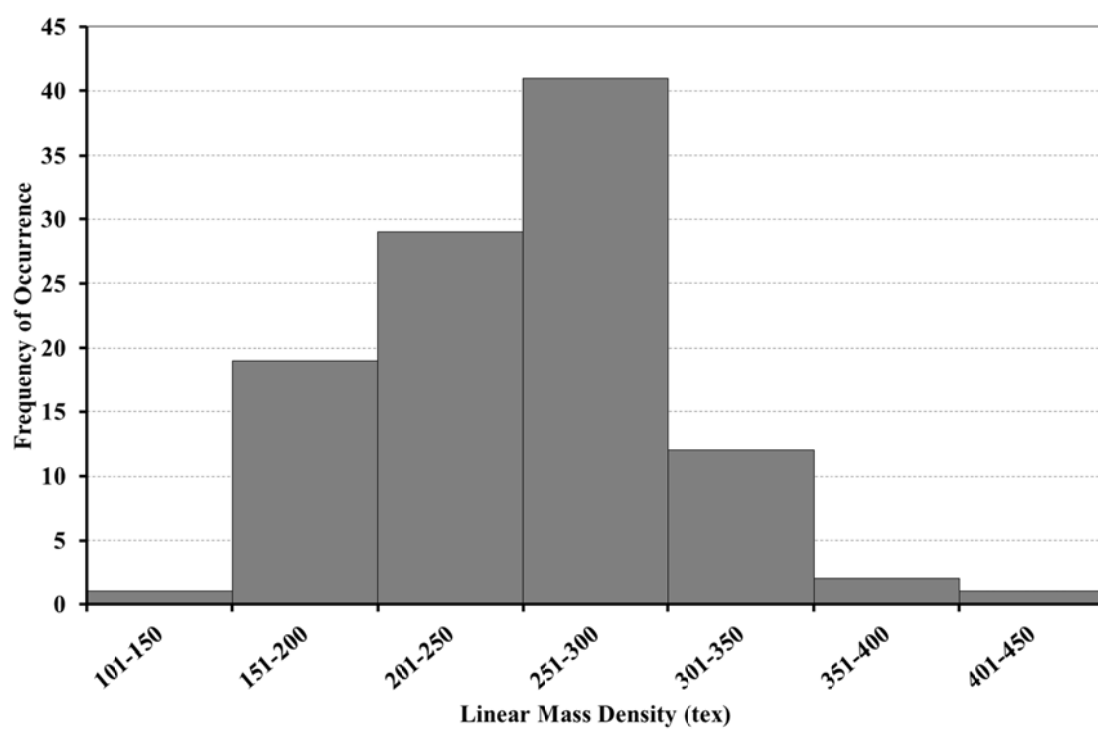


**Figure 5.37:** Histogram of linear mass density of flax fibre bundles.

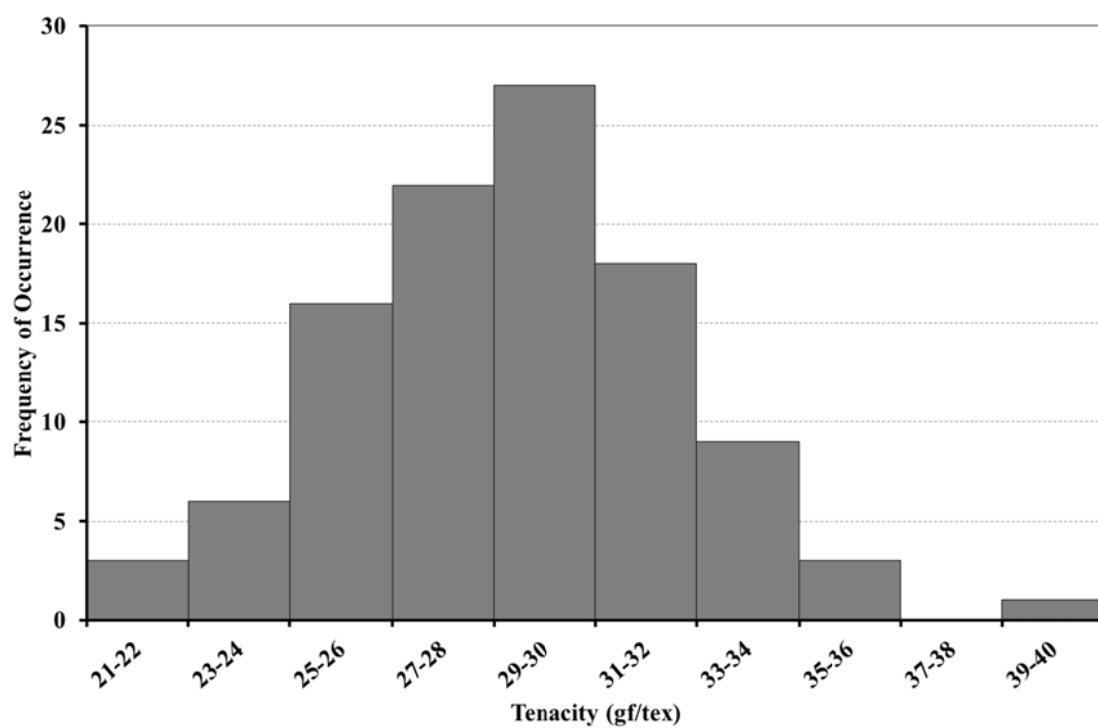


**Figure 5.38:** Histogram of tenacity of flax fibre bundles.



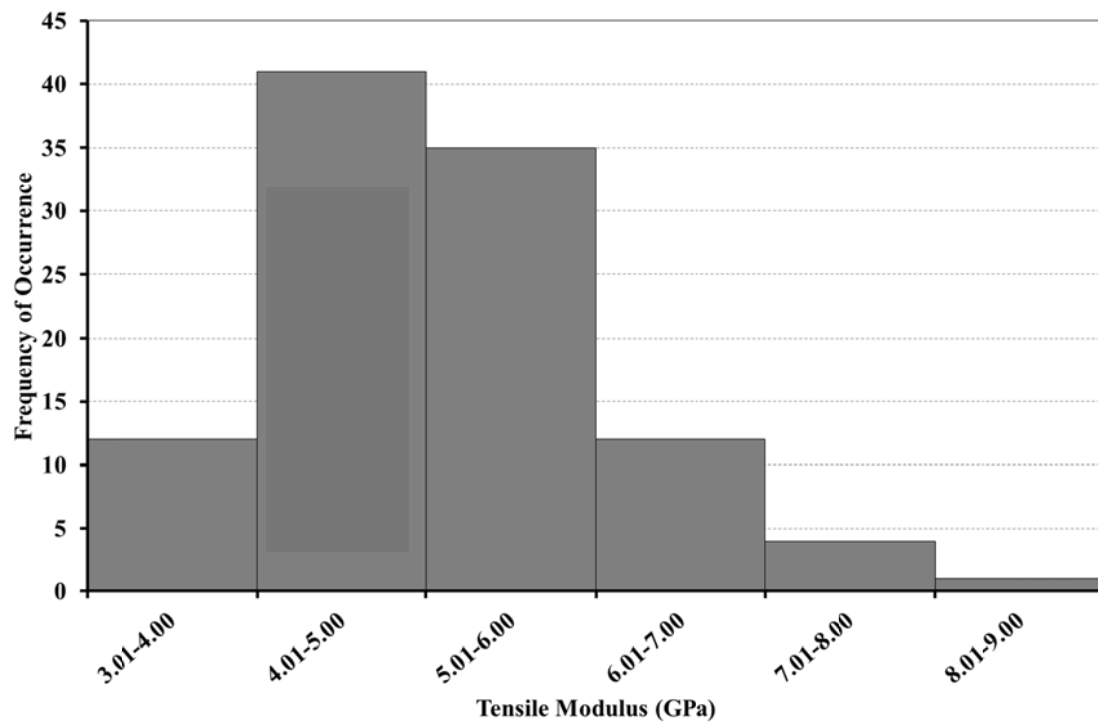


**Figure 5.39:** Histogram of tensile modulus of flax fibre bundles.

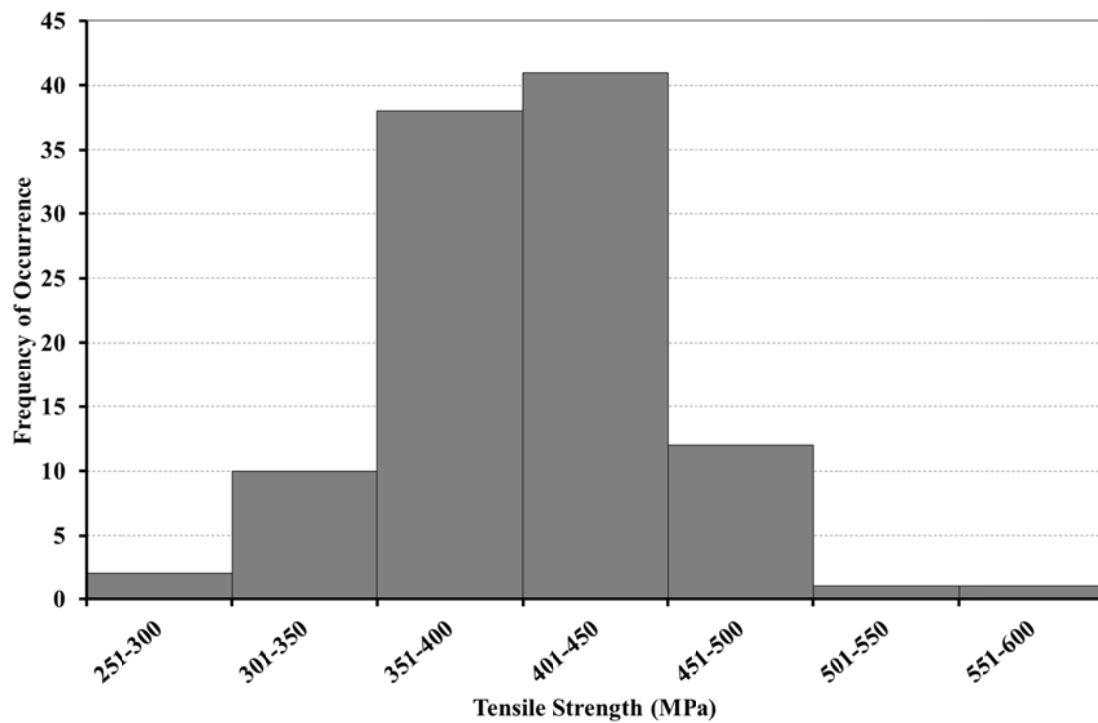


**Figure 5.40:** Histogram of tensile strength of flax fibre bundles.

Histograms showing the linear mass density, the tenacity, the modulus and the strength of the fibre bundles are shown in Figures 5.37-5.40, respectively while the average values, standard deviations, and minimum and maximum values are given in Table 5.6. The test data for all samples is tabulated in Appendix XIX.

**Table 5.7:** Test results for flax fibre bundles

Property	Average Value	Standard Deviation	Minimum Value	Maximum Value
Linear mass density (tex)	251	54	147	427
Tenacity (gf/tex)	28.4	3.3	21.1	39.4
Tensile modulus (GPa)	5.1	1.0	3.0	8.7
Tensile strength (MPa)	401	47	297	556

The distributions appear to be slightly positive-skewed. The fibre bundles had a tenacity of 28.4 gf/tex with a standard deviation of 3.3 gf/tex (12%), a modulus of 5.1 GPa with a standard deviation of 1.0 GPa (20%) and a strength of 401 MPa with standard deviation of 47 MPa (12%).

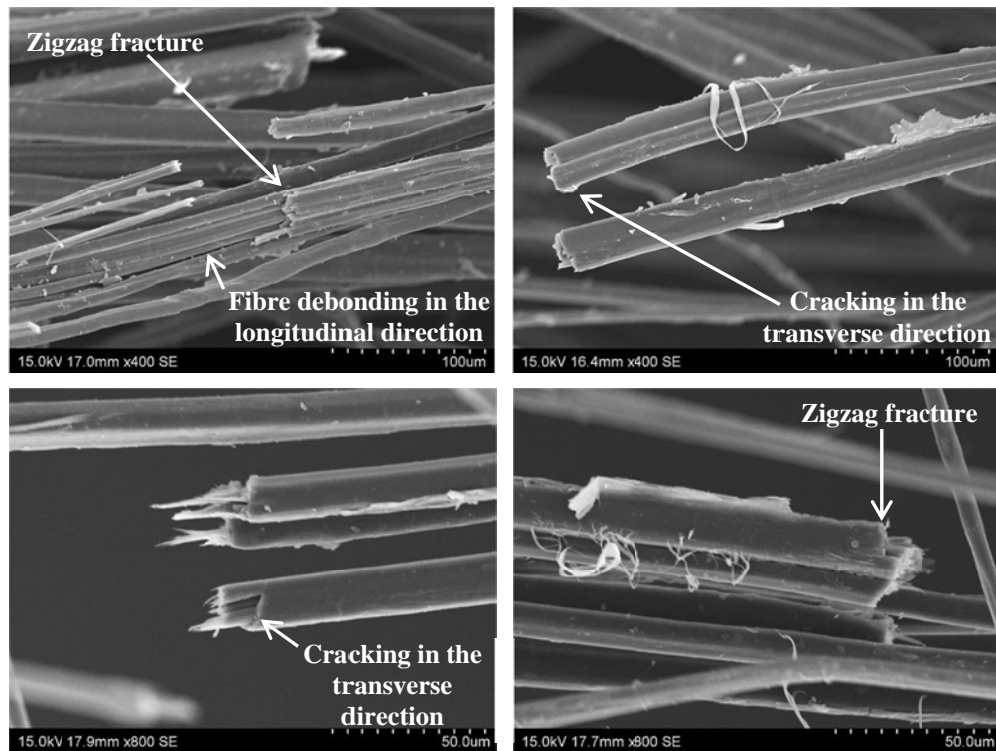


**Figure 5.41:** SEM micrographs of fracture surfaces of tested flax fibre bundles at 400× (top) and 800× (bottom) magnification.

#### 5.4.4.2 Fracture of Fibre Bundles

Examples of typical fractures seen after testing the fibre bundles are shown in Figure 5.41. The fibres show fibre separation in the longitudinal direction, cracking in the transverse direction and zigzag fracture.

#### 5.4.5 Unidirectional Composites

##### 5.4.5.1 Characterisation of Unidirectional Composites

Optical microscope images of the unidirectional composites transverse to the fibre direction are shown in Figure 5.42 while SEM images are shown in Figure 5.43. The flax fibre bundles can be seen to be well dispersed in the matrix resin. The viscose rayon wrapping threads can be readily distinguished from the flax fibres because of their lighter colour (in the optical microscope images) and the absence of a lumen. Some separation of the flax fibres from the matrix is evident in the SEM images, Figure 5.43, indicative of poor bonding.

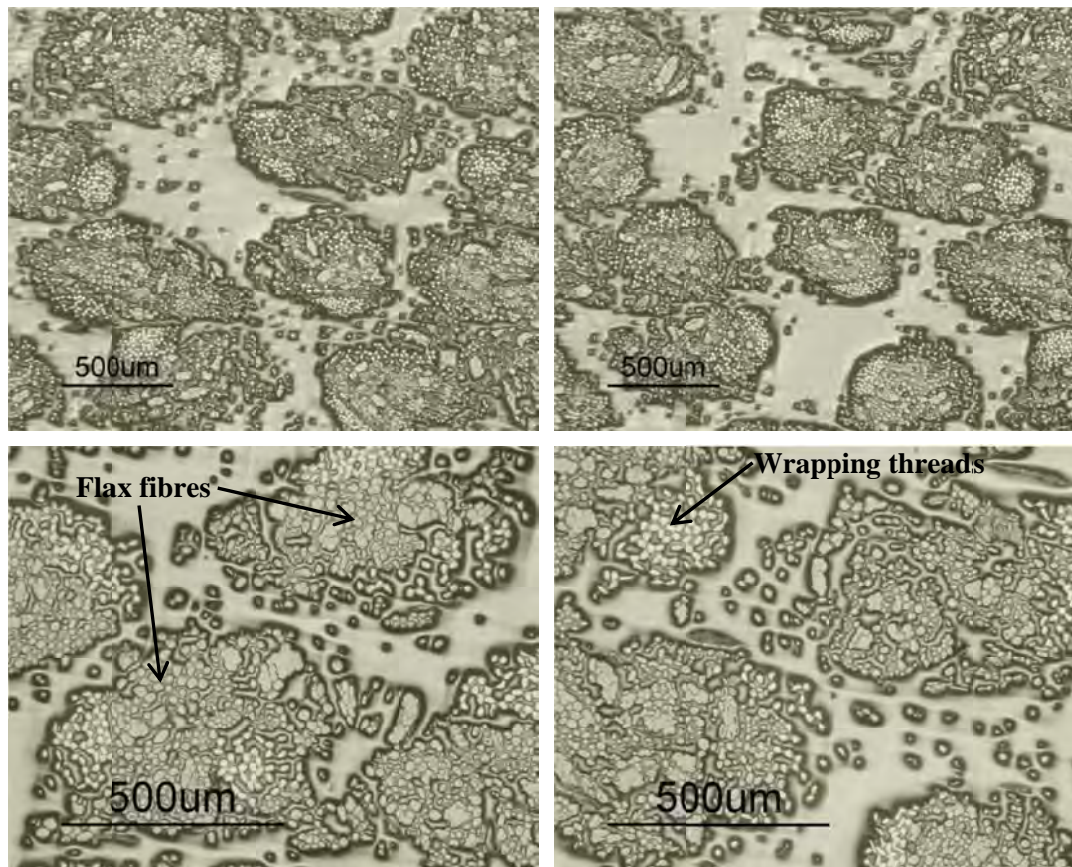


**Figure 5.42:** Optical microscope images of polished unidirectional composites in transverse direction at 5× (top) and 10× (bottom) magnification.

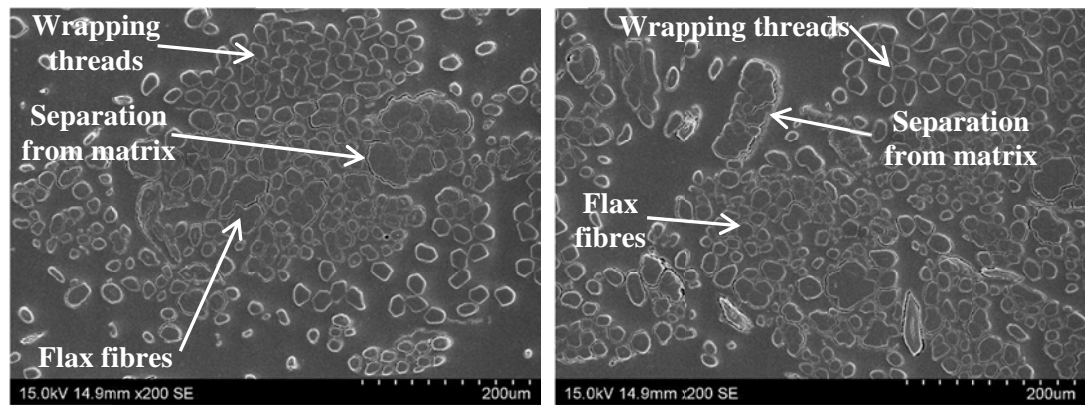


**Figure 5.43:** SEM micrographs of polished unidirectional composites in transverse direction at 200× magnification.

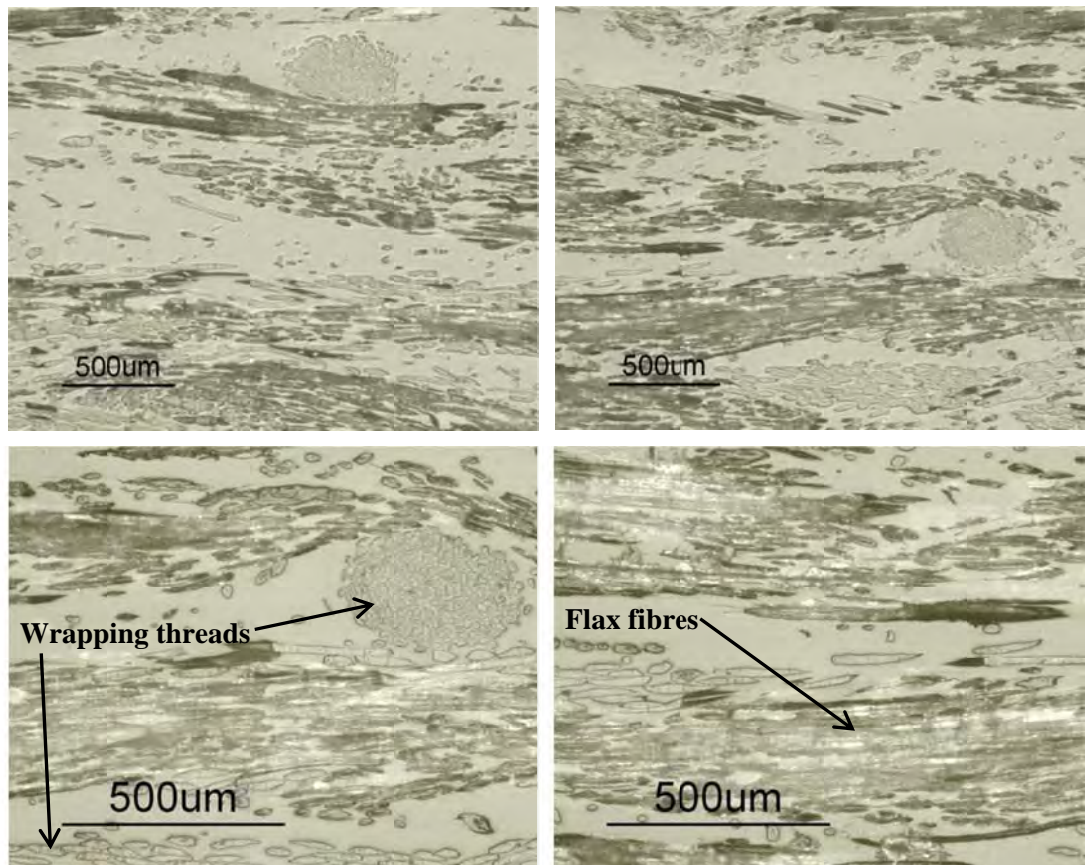


**Figure 5.44:** Optical microscope images of polished unidirectional composites in longitudinal direction at 5× (top) and 10× (bottom) magnification.



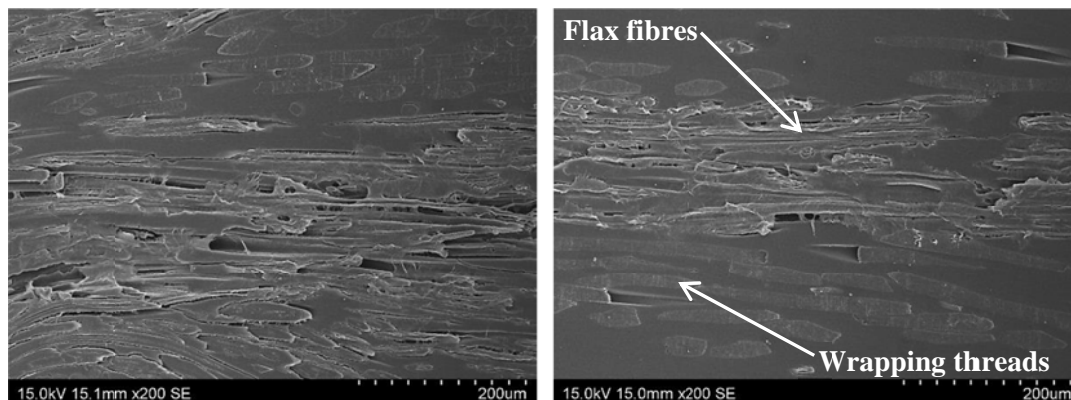


**Figure 5.45:** SEM micrographs of polished unidirectional composites in longitudinal direction at 200 $\times$  magnification.

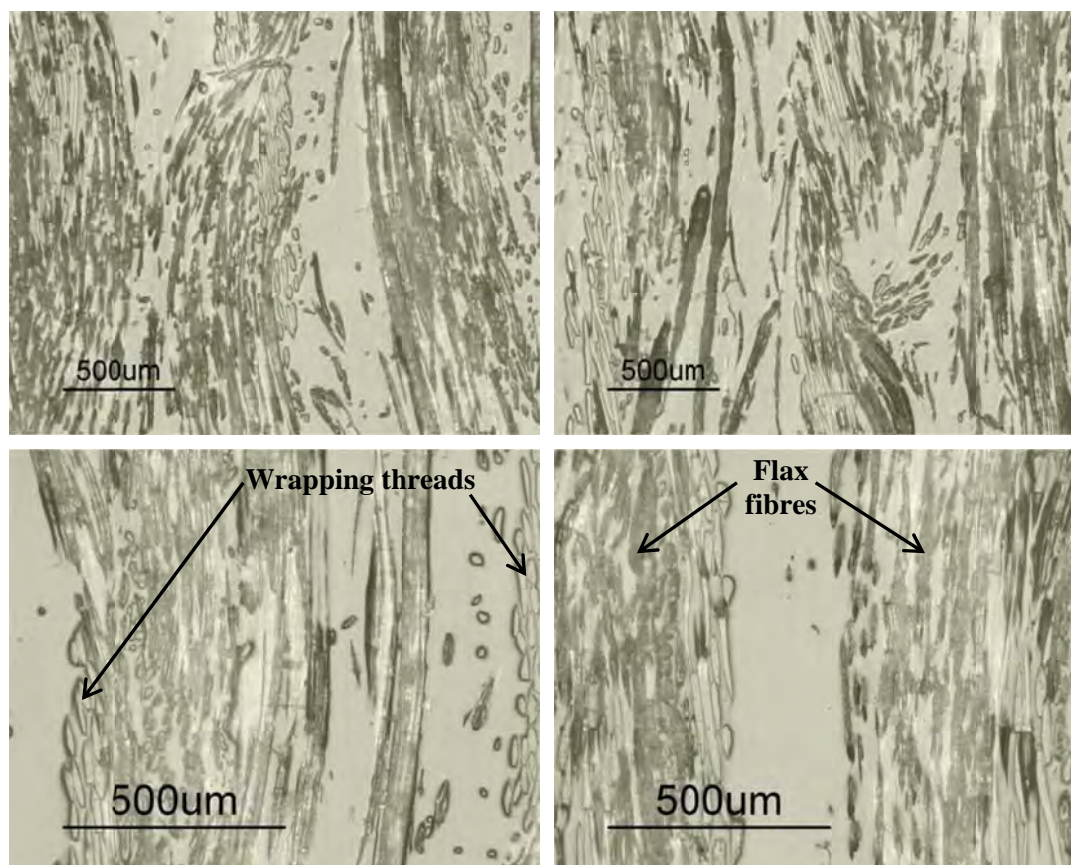


**Figure 5.46:** Optical microscope images of polished unidirectional composites in parallel surface direction at 5 $\times$  (top) and 10 $\times$  (bottom) magnification.

Optical micrographs and SEM images of longitudinal sections perpendicular to the surface of the composites are shown in Figures 5.44 and 5.45 while longitudinal sections parallel to the surface are shown in Figure 5.46. Both longitudinal sections show undulation of the fibres as was also evident in the dry flax yarns shown in Figure 5.15. Separation of the fibres from the matrix is again evident in the SEM micrographs, Figure 5.45. In some cases, this has led to sections of the fibres being removed from the surface during the grinding and polishing process leaving only imprints of their original shape. Some fibrillation of the fibres as a result of grinding and polishing can also be seen.

#### ***5.4.5.2 Fibre Volume Fraction***

The transverse SEM images used for measuring the fibre volume fraction, together with the resulting binary images, both including and excluding the wrapping threads, are given in Figures 5.47 to 5.49 while the results of the measurements are given in Table 5.8. The measured fibre volume fraction with the wrapping threads included was 31.0% with a standard deviation of 1.4% (4.5% of measured value), which is consistent with the targeted value of 30% determined from the weight fractions used to make the composites. The volume fraction of the flax fibres alone (i.e., excluding the wrapping threads) was 25.0% indicating that the wrapping thread made up 19.4 volume % of the fabric.

The volume fraction of the wrapping threads plus the transverse threads was also determined from weight fraction measurements as described in Section 5.3.4.4. The volume fraction was calculated from the weight fraction using equation 5.33. A value of  $1.44 \text{ g/cm}^3$  was used for the density of the flax fibres (Moran et al., 2007) and a value of  $1.49 \text{ g/cm}^3$  for the viscose rayon (Hearle, 2001). The calculated volume fraction of viscose rayon in the flax fabric was 21.0%. This higher volume fraction is to be expected since the transverse threads as well as the wrapping threads have now been included in the viscose rayon fraction.

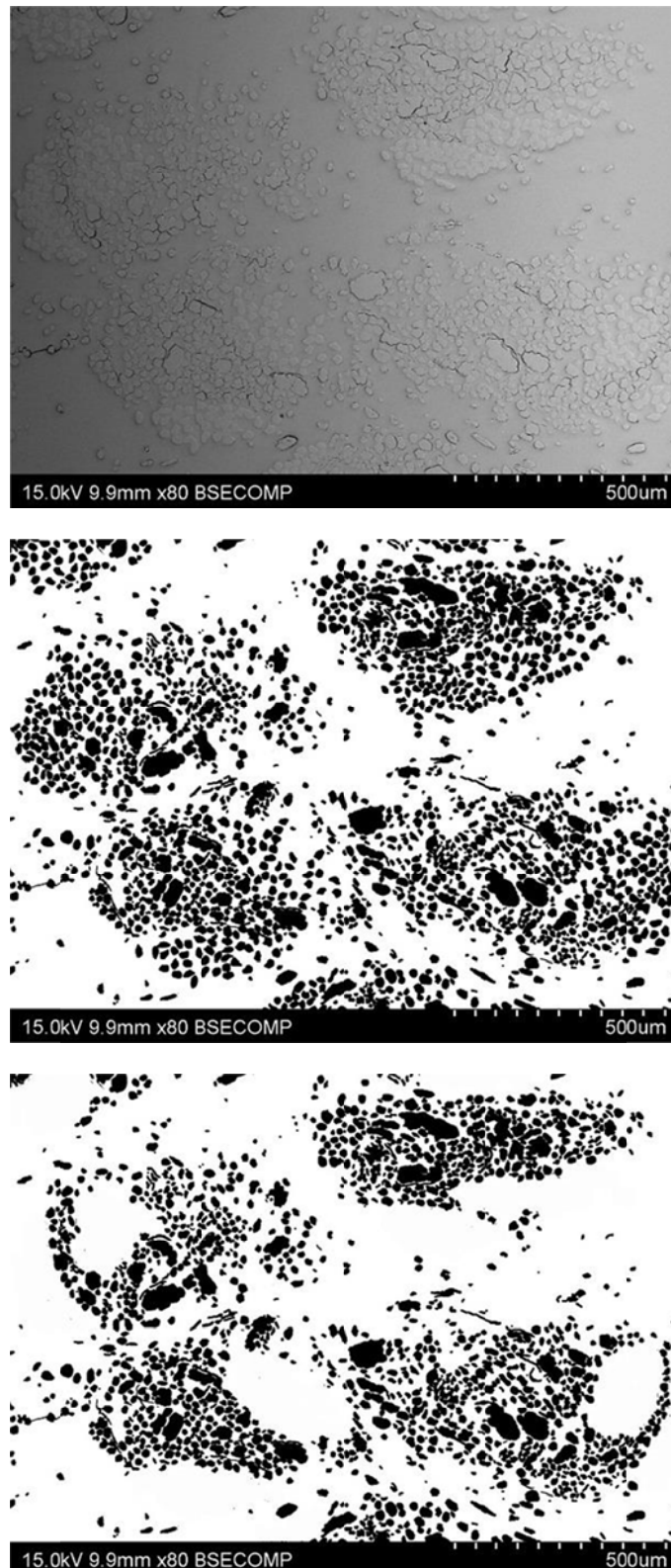


**Figure 5.47:** SEM micrograph (top) of unidirectional composites (Image No. 1) and their binary images including wrapping threads (middle) and excluding wrapping threads (bottom).

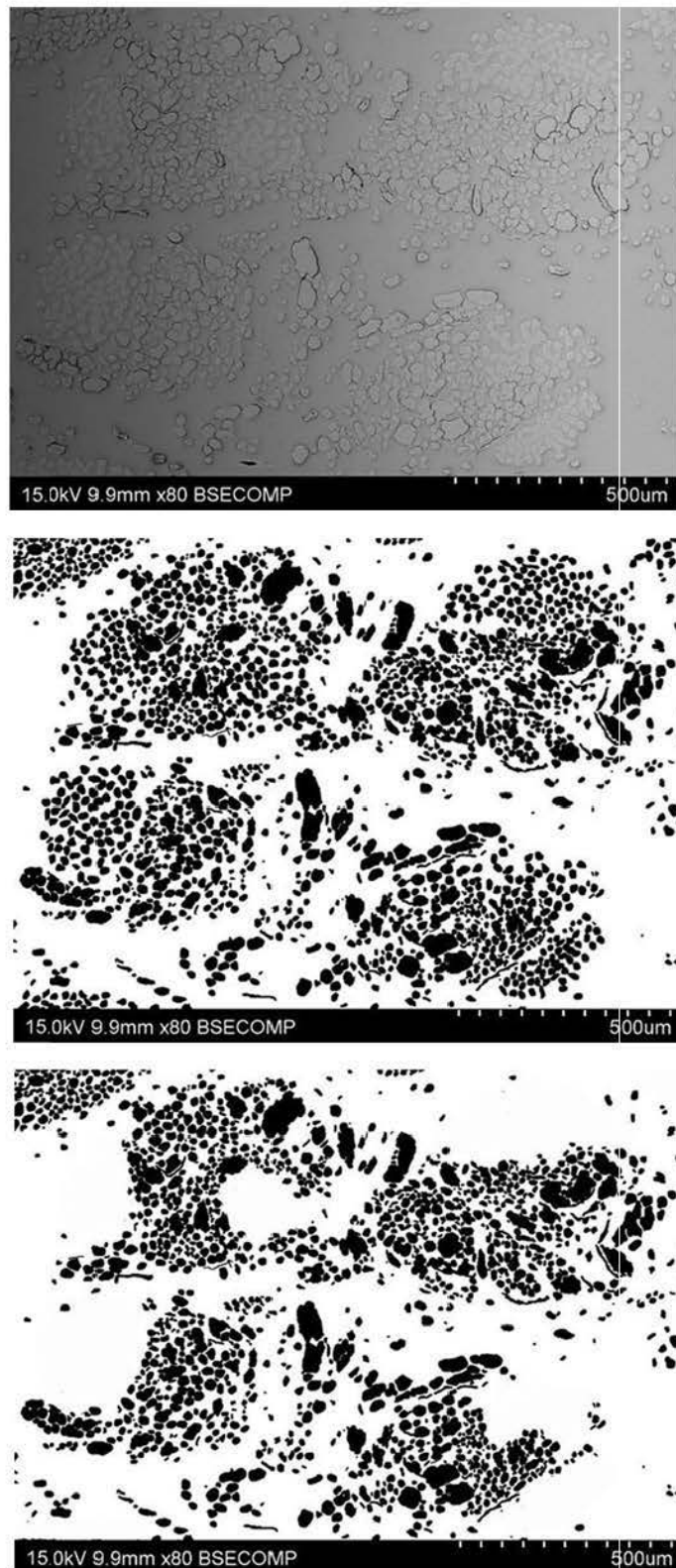


**Figure 5.48:** SEM micrograph (top) of unidirectional composites (Image No. 2) and their binary images including wrapping threads (middle) and excluding wrapping threads (bottom).



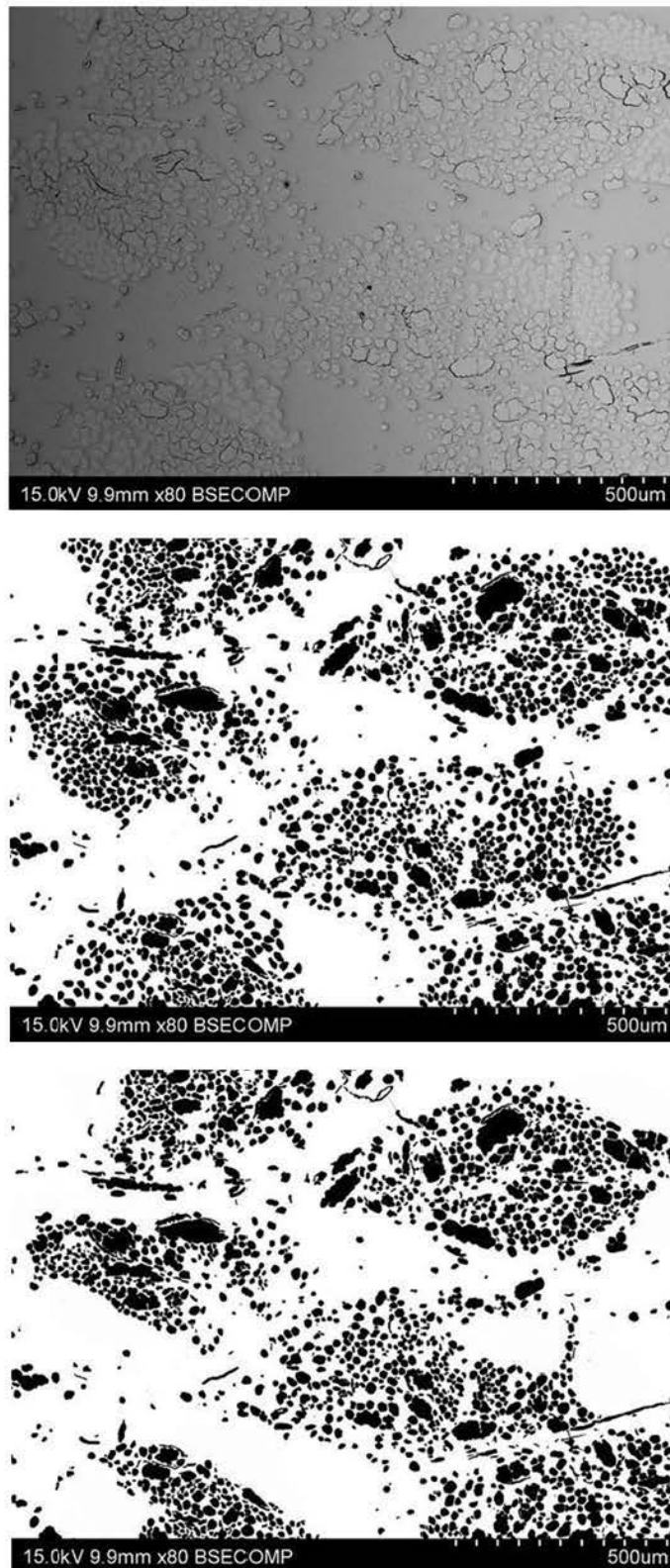


**Figure 5.49:** SEM micrograph (top) of unidirectional composites (Image No. 3) and their binary images including wrapping threads (middle) and excluding wrapping threads (bottom).

**Table 5.8:** Fibre volume fraction of unidirectional composites and flax fibre contents in unidirectional flax fabrics

<b>Image No.</b>	<b>Fibre Volume Fraction (%)</b>		<b>Wrapping thread (%)</b>
	<b>including wrapping threads</b>	<b>excluding wrapping threads</b>	
1	29.4	23.0	21.8
2	32.0	25.5	20.3
3	31.6	26.5	16.1
<b>Average</b>	<b>31.0</b>	<b>25.0</b>	<b>19.4</b>
<b>SD</b>	<b>1.4</b>	<b>1.8</b>	<b>2.9</b>

#### ***5.4.5.3 Tensile Properties of Unidirectional Composites***

The tensile stress-strain curves of the unidirectional composites and neat vinyl ester resin are shown in Figures 5.50 and 5.51, respectively. The strain was recorded only up to 0.6% after which the extensometer was removed. For the composites, the curves all exhibited a knee centred at a strain of approximately 0.2% after which the slope decreased by approximately 40%. However, all the curves of the neat matrix resin were linear.

The measured tensile properties of the neat matrix resin and the unidirectional composites are given in Table 5.9. The resin had a modulus of 3.62 GPa with a standard deviation of 0.02 GPa (0.6%) and a strength of 59.8 MPa with a standard deviation of 4.1 MPa (7%). The modulus of the composites was 13.2 GPa with a standard deviation of 0.4GPa (3%) while the strength was 122 MPa with a standard deviation of 5 MPa (4%).

It is noted that all the specimens failed at the end of the parallel sided section of the dog bone specimens, as shown in Figure 5.52. However, substantial cracking was also seen within the parallel sided region, Figure 5.53 indicating that failure had initiated in this region also. It is therefore considered that the measured values provide a reliable estimate of the strength.

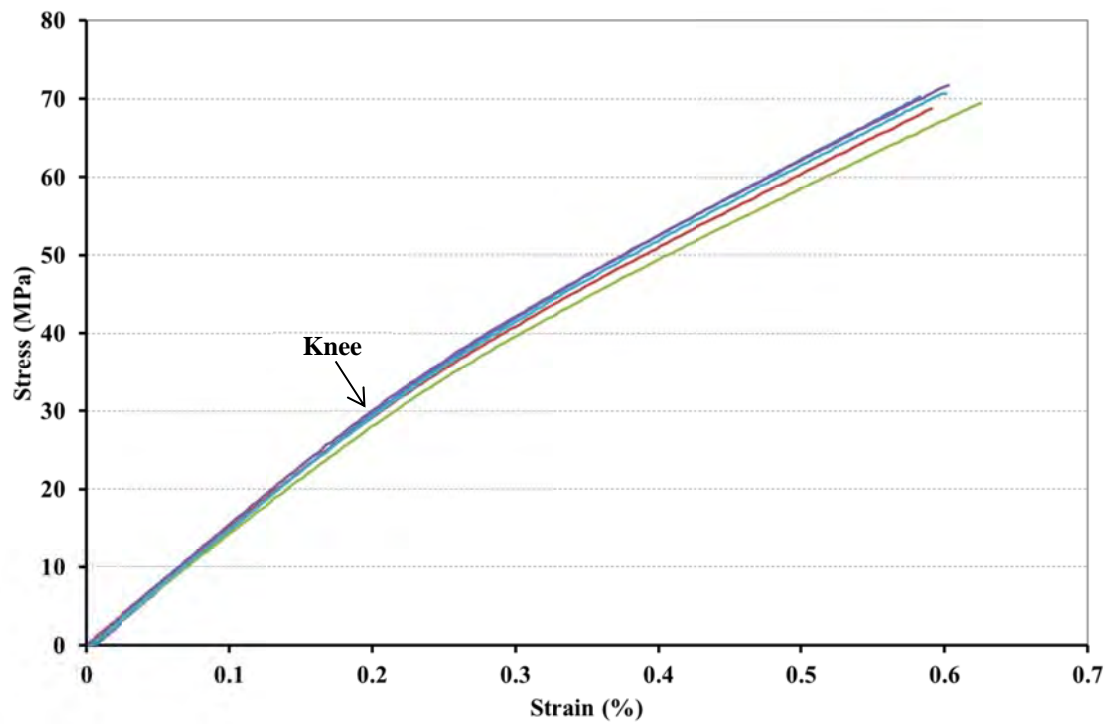


**Figure 5.50:** Tensile stress-strain curves of unidirectional composites.

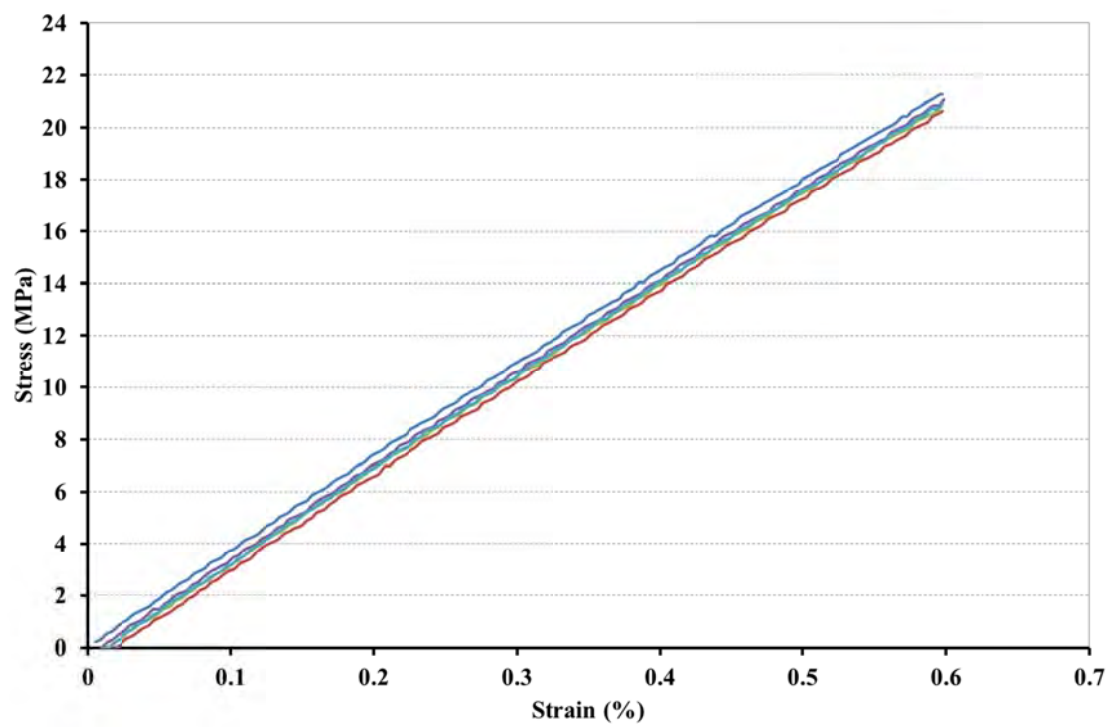


**Figure 5.51:** Tensile stress-strain curves of neat vinyl ester resin.

**Table 5.9:** Measured tensile properties of neat resin and unidirectional composites

Tensile Property	Vinyl ester resin		Flax/vinyl ester composites	
	Average	Standard	Average	Standard
	Value	Deviation	Value	Deviation
Modulus (GPa)	3.62	0.02	13.16	0.42
Strength (MPa)	59.8	4.1	122.4	5.0



**Figure 5.52:** Failed tensile specimens.

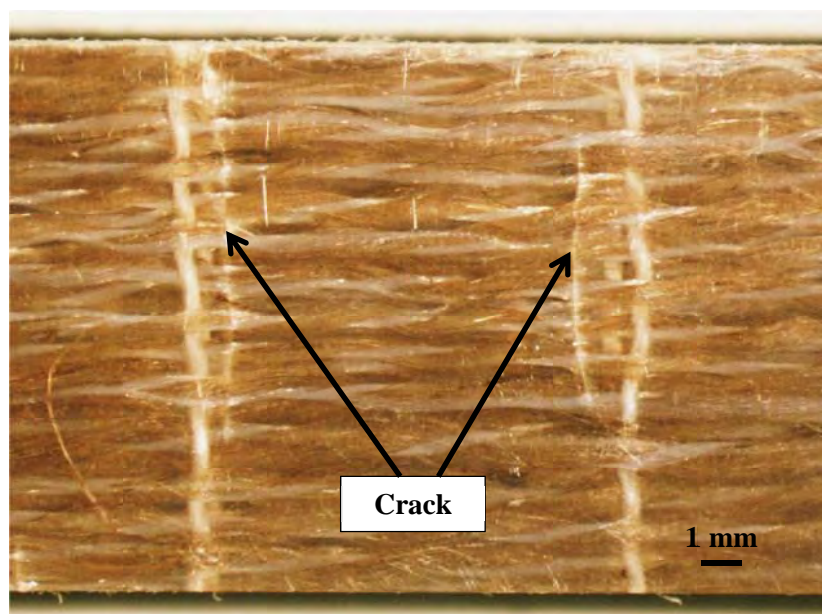


**Figure 5.53:** Cracking in parallel sided region of tensile specimens.

#### 5.4.5.4 Fracture Surface of Composites

SEM micrographs of typical fracture surfaces of the tensile specimens after testing are shown in Figure 5.54. It is clear from the higher magnification images that the matrix resin has impregnated the flax yarns very well.

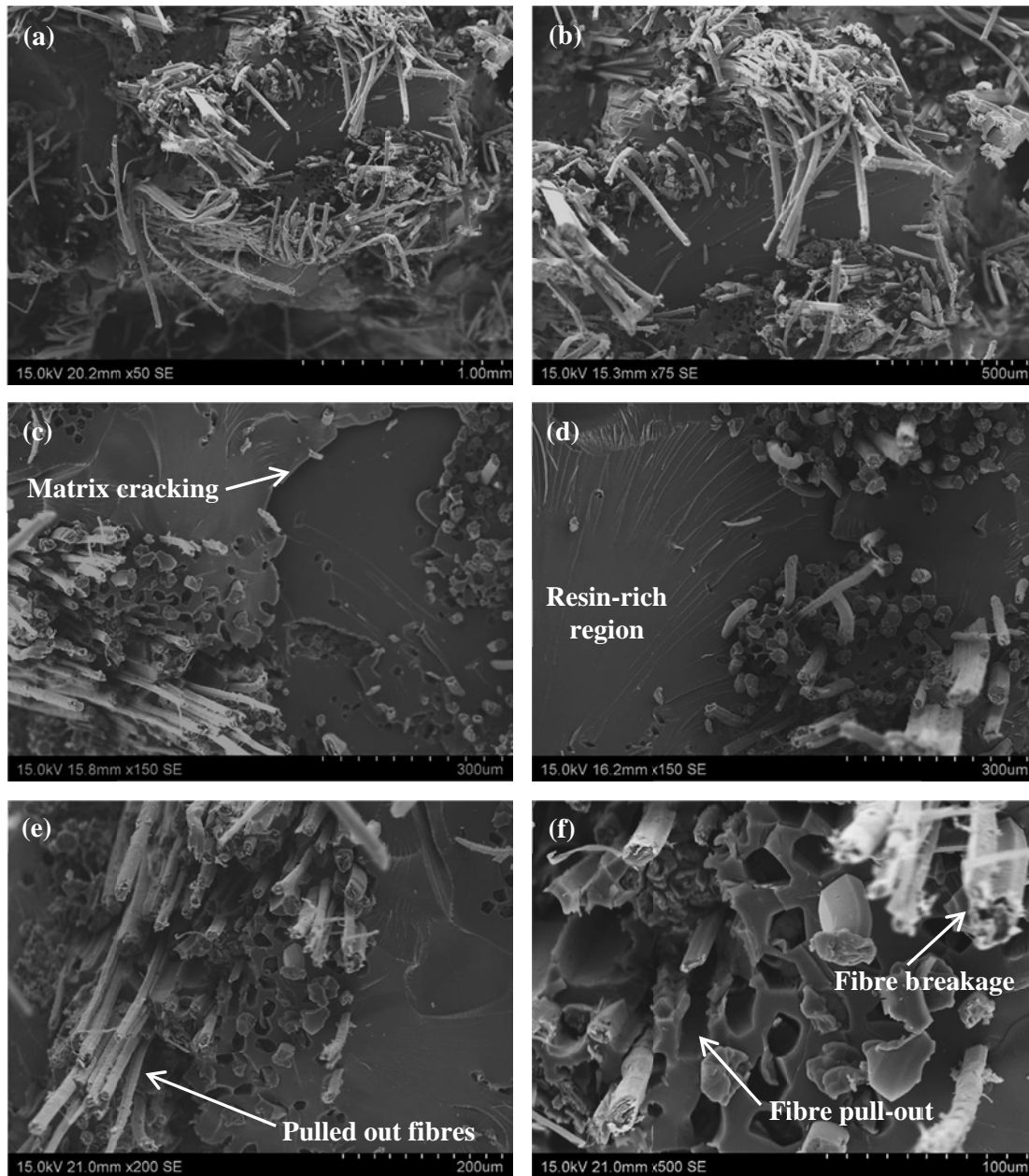


**Figure 5.54:** SEM micrographs of fracture surfaces of unidirectional composites at (a) 50 $\times$ , (b) 75 $\times$ , (c and d) 150 $\times$ , (e) 200 $\times$  and (f) 500 $\times$  magnification.

Fibre pull-out is clearly evident on the fracture surfaces, with broken fibres protruding from the fracture surface and sockets from pulled out fibres remaining on the fracture surface. No evidence of the matrix adhering to the fibres could be seen. These features indicate that poor adhesion had occurred between the flax fibres and the vinyl ester matrix due to incompatibility between the hydrophilic fibres and the hydrophobic polymer matrix. Matrix cracking was sometimes observed in the resin-rich regions.

## **5.5 Discussion**

### **5.5.1 Defects in Flax Fibres**

The types of defect observed in the flax technical fibres were similar to those observed in previous studies (Lamy & Pomel, 2002; Ruys, 2007), as shown for example in Figure 5.55 (Baley, 2002). They were also similar to the defects seen in the kenaf fibres, Section 3.4.3, except for the absence of dislocations and pits.

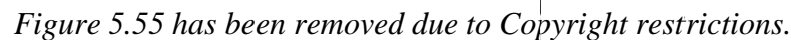


*Figure 5.55 has been removed due to Copyright restrictions.*

**Figure 5.55:** Defects of flax fibres (Baley, 2002).

The measured defect density was 31 defects per millimetre. This is approximately three times the value of 10.9 defects per millimetre found by Ruys (2007) for flax sliver. The higher defect density observed in the present study is attributed to damage induced when making the yarns from which the fibres were extracted.

## **5.5.2 Technical Fibres**

### **5.5.2.1 Fibre Area Correction Factor**

Conventionally, the mechanical properties of technical fibres have been determined assuming the fibres to be circular with a diameter equal to their measured width. As noted by Virk, Hall & Summerscales (2012) and Thomason et al. (2011), this leads to substantial error since the fibres are not generally circular in section, as was confirmed in the present study from a detailed examination of fibre cross-sections.

Accordingly, a fibre area correction factor  $K$  was determined from measurements made on 113 technical fibres using the method developed by Virk, Hall & Summerscales (2009) and subsequently used by Thomason et al. (2011). The results gave a fibre area correction factor of 2.70. This is close to the value of 2.55 obtained by Thomason et al. (2011) for flax fibres. However these values are substantially higher than the value of 1.99 obtained by Thomason et al. (2011) for sisal fibres, the value of 1.47 determined from data published by Terasaki, Goda & Noda (2009) for kenaf fibres and the value of 1.42 obtained by Virk, Hall & Summerscales (2012) for jute fibres. Collectively, these results indicate that the fibre area correction factor varies substantially for different types of fibre.

### **5.5.2.2 Tensile Properties of Technical Fibres**

As noted in Section 5.4.3.4, small abrupt load drops were frequently observed in the stress-strain curves of the technical fibres towards the end of the test. Similar behaviour has also been reported for technical flax fibres by Romhány, Karger-Kocsis & Czigány (2003), although stress strain curves published by other workers do not show detectable load drops (Baley, 2002; Hu et al., 2010). As in the present study, Romhány, Karger-Kocsis & Czigány (2003) found that load drops occurred in only some of the stress strain curves and this may account for their absence in the curves published by Baley (2002) and Hu et al. (2010).

Romhány, Karger-Kocsis & Czigány (2003) considered the load drop to be due to transverse microcracking in the elementary fibres. Their proposed failure mode for the fibres is discussed later in this section. The load drops are also similar to those seen by Ward, Tabil, Panigrahi, Crerar, Powell, Kovacs & Ulrich (n.d.) when testing flax yarns. These authors attributed the load drops to breakage of individual fibres in the yarn. Since these tests were strain-controlled the load will drop when an individual fibre

breaks. Breakage of individual elementary fibres within a technical fibre should likewise produce a load drop, consistent with the proposal of Romhány, Karger-Kocsis & Czigány (2003).

The tensile modulus and strength of the technical fibres, measured assuming a circular cross section (“measured” values), were 19.4 GPa and 347 MPa respectively. The adjusted values taking into account the true fibre cross-sectional area (“true” values) were 52.4 GPa and 936 MPa, respectively. The failure strain (both measured and true) was 1.8%. The individual results showed substantial variability, as is common for natural fibres (Virk, Hall & Summerscales, 2012) with the standard deviations being approximately 40% of the average values for the modulus and strength and approximately 30% for the strain to failure.

The tensile properties of natural fibres (excluding their modulus) vary substantially with test gauge length as shown, for example, by Virk, Hall & Summerscales (2009). For this reason the following discussion is limited to studies which used a 20 mm gauge length, as in the present study. The most relevant data is that obtained for flax by Thomason et al. (2011), since they also used an area correction factor. The flax fibres were conditioned at  $23 \pm 1^\circ\text{C}$  and  $50 \pm 10\%$  relative humidity for 24 hours before the testing, as in the present work. They present results for a gauge length of 20 mm for only three samples; these gave a modulus of 49.8-53.6 GPa, a strength of 611-940 MPa and a strain to failure of 1.23-2.13%. These results are in quite good agreement with the results of the present study.

In their work, Thomason et al. (2011) used the cross-sectional area measured on the remnant section of each fibre attached to the paper tab to determine the modulus and strength. Thus each calculation used the actual cross-sectional shape. The present study used the procedure developed by Virk (2010) which involved multiplying the measured fibre diameter by a constant area correction factor which was determined from other untested fibres from the same batch. This assumes that each fibre differs from being circular by the same factor and does not account for differences from fibre to fibre. Nonetheless, the good agreement with the results obtained by Thomason et al. (2011) indicates that this procedure gives reasonably accurate results.

Romhány, Karger-Kocsis & Czigány (2003) also determined the tensile strength of flax technical fibres with a 20 mm gauge length. Fifty fibres were tested. The fibre cross-sectional area was determined assuming the fibres to be circular in shape (i.e.,



from their measured diameters) so these results are best compared with the “measured” strength from the present study. Romhány, Karger-Kocsis & Czigány (2003) obtained a tensile strength of 613 MPa compared with 347 MPa from the present work. However, their standard deviation of 72% (442 MPa) was almost double that obtained here. The difference in tensile strength may be due to differences in climate, soil conditions, processing techniques, etc (Feng et al., 2001; Munder, Fürll & Hempel, 2005). However, the true significance of this difference is difficult to assess in view of the large variability in their data.

Thomason et al. (2011) also examined the tensile properties of sisal fibres. As with the flax fibres, only three samples were tested at the 20 mm gauge length. The true tensile modulus, true tensile strength and measured failure strain were 16.9-24.1 GPa, 342-765 MPa, and 2.03-3.44%, respectively. These results indicate that the modulus and strength of sisal are significantly lower than those of flax, as has been found by other workers (Bismarck, Mishra & Lampke, 2005).

Virk et al. (2009) measured the tensile properties of jute fibres with a 20 mm gauge length. One hundred fibres were tested. As noted in the previous section, they obtained a fibre area correction factor of 1.42. Using this, their true elastic modulus was 44.0 GPa with a standard deviation of 9.9 GPa (23%), their true strength was 573 MPa with a standard deviation of 199 MPa (35%), and their failure strain was 1.29% with a standard deviation of 0.30% (23%). The true modulus and strength values are substantially lower than those obtained in the present study although the measured values (31.0 GPa and 403 MPa, respectively) are actually higher. This apparent anomaly arises because of the very substantial difference in the area correction factors for flax and jute.

It is noted that when expressed as a percentage, the standard deviations obtained by Virk et al. (2009) were similar to those obtained in the present study for strength and strain to failure but the standard deviation for the modulus was only 61% of that obtained here.

Zakaria (2014) determined the measured tensile properties for thirty untreated kenaf fibres with a 20 mm gauge length. The fibres were conditioned at 23°C and 51% relative humidity for 1 week before testing. The tensile modulus, tensile strength and failure strain were 13.0 GPa with a standard deviation of 5.8 GPa (45%), 184 MPa with a standard deviation of 99 MPa (54%), and 1.3% with a standard deviation of 1.1%

(85%), respectively. These measured strength and modulus values are substantially lower than the “measured” values for flax obtained in the present study, as has been commonly reported (Ashby, 2013; Liu et al., 2007; Bismarck, Mishra & Lampke, 2005).

Xue et al. (2009) also examined the measured tensile properties of 30 kenaf fibres with a 20 mm gauge length. Prior to testing, the fibres were conditioned at 23°C and 30-40% relative humidity for a minimum of 48 hours. Their measured modulus was 12.7-17.2 GPa, their measured tensile strength was 146 to 223 MPa, and their failure strain was 1.12 to 1.46%. These results match well with those of Zakaria (2014).

The Weibull modulus values obtained in the present work were 2.9 for strength and 4.3 for strain to failure. These values are slightly lower than the values obtained by Virk et al. (2009) for jute, which were 3.2 and 5.0, respectively, indicating that the scatter was slightly higher in the present case despite the similarity in number of specimens tested. The values were however higher than those obtained by Romhány, Karger-Kocsis & Czigány (2003) for flax fibres (1.5) and Zakaria (2014) for kenaf fibres (1.9), both of whom only provided a Weibull modulus for strength. Their lower values probably reflect, at least in part, the smaller number of specimens tested (Sullivan & Lauzon, 1986; van der Zwaag, 1989).

### **5.5.3 Fibre Bundle Tests**

#### ***5.5.3.1 Tensile Properties of Fibre Bundles***

Single fibre tests, as discussed in the previous section, are very time consuming and this limits their usefulness as a means of mechanically grading fibre batches. The flat fibre bundle test (ASTM D1445/D1445M-12; Burley and Carpenter, 1955) is reported to be a simpler test for mechanically characterizing fibres (ASTM D1445/D1445M-12; Burley and Carpenter, 1955) and was therefore evaluated using fibres from the same batch of fabric as were used in the single fibre tests. The test was developed more than 50 years ago and has been standardised in ASTM D1445/D1445M-12. It is widely used in the textiles industry for grading cotton.

The tests gave a tenacity of 28.4 gf/tex with a standard deviation of 3.3 gf/tex (12%) which converts to a tensile strength of 401 MPa with a standard deviation of 47 MPa (12%). The calculated modulus was 5.1 GPa with a standard deviation 1.0 GPa (20%). The calculations do not require measurement of cross sectional area since they

use the linear mass density instead. Strength and modulus are determined from the test data using the volumetric density of the fibres, therefore the values obtained do not require correction using the area correction factor. As a result, they should be compared with the true values obtained from single fibre testing. The strength is however half the true strength obtained from the single fibre tests while the modulus is only one tenth the true single fibre value.

The reason for the discrepancy in the modulus value is readily apparent from examination of the stress strain curves given in Figure 5.36. Neglecting the run-in period at the start of the test, the measured strain to failure is still typically about 10% compared with less than 2% for the single fibre tests. ASTM D1445/D1445M-12 notes that slippage of the fibres in the clamps occurs and a correction factor of 0.8 is included in the equation provided for calculating the elongation. This would account for only a small part of the excess strain observed in the present work.

It is considered that the remaining excess strain is due to additional strain occurring in the system. One possibility is shear deformation in the leather pads which are used to face the Stelometer clamps to avoid damage to the fibres, as shown schematically in Figure 5.56. It was necessary to replace the leather pads before the tests were conducted and glove leather was used since it was of an appropriate thickness (0.85 mm). It may be that this leather was excessively compliant. In view of the short gauge length of 3.2 mm, shear deformation of 0.16 mm in the leather facings of each of the two clamps would be sufficient to produce the entire observed strain of 10%.

Thygesen, Madsen, Bjerre & Lilholt (2011) measured the tensile strength of flax and hemp flat fibre bundles using a universal testing machine fitted with Pressley clamps (the clamps from the Pressley instrument). In this case the gauge length used was 3.0 mm and the tested fibre bundle length was 14.8 mm. The fibre bundles were conditioned at  $23 \pm 2^{\circ}\text{C}$  and  $50 \pm 10\%$  relative humidity. The tensile strength ranged from 238 to 482 MPa for the flax fibres, which is in good agreement with the value of 401 MPa obtained in the present study. Somewhat higher values of 396 to 998 MPa were obtained for the hemp fibres. The fibres were reported to have different strengths depending on the type of processing used (dew retting, fungal retting, water retting, scutching, carding and cottonization).

Sengloung, Kaveeta & Müssig (2008) examined the tensile strength of the hemp fibre bundles using a Stelometer at 3.2 mm gauge length. The fibre bundles were

conditioned at 20°C and 65% relative humidity for 24 hours prior to the testing. The tensile strength was 10.9-27.4 cN/tex which equates to 10.7-26.9 gf/tex. This is slightly lower than the value 28.4 gf/tex obtained in the present study.

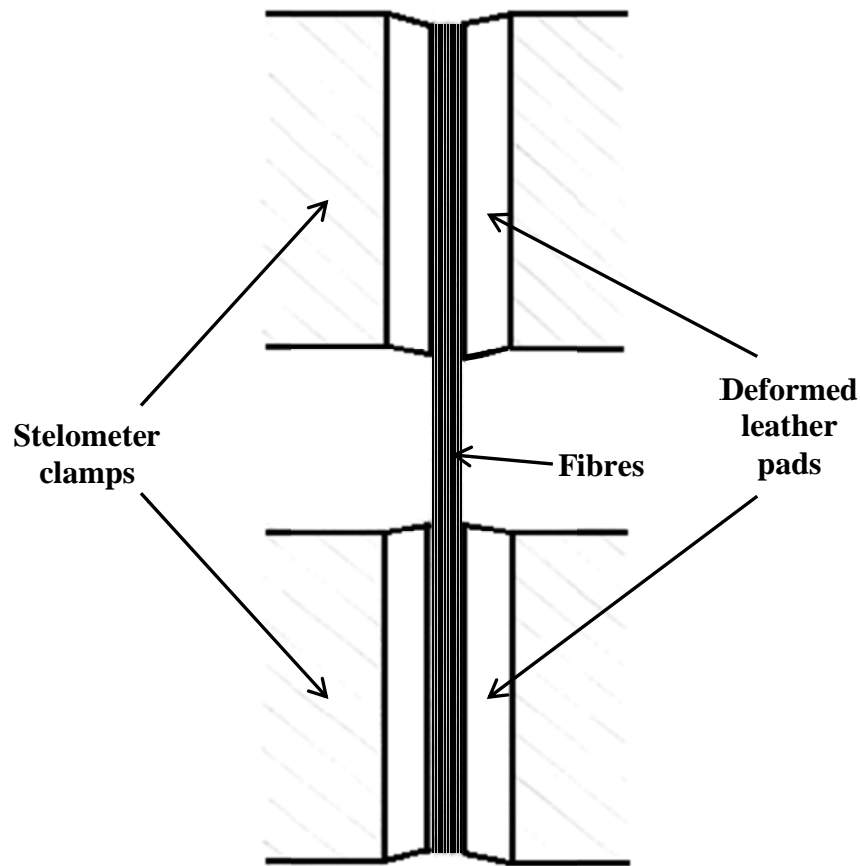


**Figure 5.56:** Shear deformation in the leather pads.

Parmar (2011 & 2012) undertook flat bundle tests on jute (Parmar, 2012) and kenaf (Parmar, 2011) using the same experimental procedure as used in the present study. The jute fibres were from the same batch as those for which the single fibre tests were conducted by Virk et al (2009) while the kenaf fibres were from the same batch as those tested by Zakaria (2014). Fifty tests were conducted in each case. The strength of the jute fibre bundles was 307 MPa with a standard deviation of 66 MPa (21%) while that of the kenaf fibre bundles was 141 MPa with a standard deviation of 25 MPa (18%).

The results from the present study, together with those obtained by Parmar (2011 & 2012), Virk et al. (2009) and Zakaria (2014) are summarized in Table 5.10. It

can be seen that the bundle strength is substantially lower than the single fibre strength in all cases ranging from 43% for flax to 77% for kenaf. The data for kenaf is however an overestimate since the single fibre data does not include an area correction factor. Kenaf is generally considered to be similar to jute. Using the area correction factor of 1.47 for kenaf obtained from the work of Terasaki, Goda & Noda (2009) the bundle strength reduces to 52% of the single fibre strength, Table 5.10.

**Table 5.10:** Comparison of single fibre and bundle strengths

<b>Fibre</b>	<b>Single fibre strength (MPa)</b>	<b>Bundle strength (MPa)</b>	<b>Bundle strength as percentage of single fibre strength (%)</b>
Flax	936	401	43
Jute	573 <sup>1</sup>	307 <sup>2</sup>	54
Kenaf	184 <sup>3</sup>	141 <sup>4</sup>	77
Kenaf (corrected)	270 <sup>5</sup>	141	52

<sup>1</sup>Virk et al. (2009)

<sup>2</sup>Parmar (2012)

<sup>3</sup>Zakaria (2014)

<sup>4</sup>Parmar (2011)

<sup>5</sup>includes area correction factor of 1.47

Daniel & Ishai (1994) report that the bundle strength can be as low as 70% of the average fibre strength but the results above give an average value of only 50%. The data considered by Daniel & Ishai (1994) would almost certainly be data obtained from synthetic fibres. Natural fibres have more scatter in their strength than synthetic fibres, as indicated by their generally lower Weibull moduli (Pardini & Manhani, 2002; Qiu & Schwartz, 1993) and this would be expected to reduce the bundle strength.

The bundle strength is to be expected to be lower than the average single fibre strength since, because of differences in the strength of the individual fibres, the fibres will fail progressively as the load increases. This increases the load on the remaining fibres. Eventually, failure of one fibre will cause the load on the remaining fibres to exceed their strength and catastrophic failure of all the remaining fibres in the bundle will occur. The bundle strength is calculated as the load at catastrophic failure divided by the cross sectional area of all the fibres. Since some of the fibres have already failed

prior to catastrophic bundle failure, the bundle strength will clearly be less than the average strength.

To examine the results further, the fibre bundle strength was modeled for the flax fibres using the results obtained from the single fibre tests. Since the bundle tests carried out in the present work were done under strain control (i.e., loaded using crosshead displacement), the fibres were sorted from the lowest strain to failure to the highest strain to failure. Ten fibre bundles, each with eleven fibres, were then constructed from the set of fibres by taking the results for every tenth fibre. This required that the 113 fibres tested be reduced to a multiple of ten and so the results for the two fibres with the lowest strain to failure and the one with the highest strain to failure were discarded. The first bundle started with the first fibre in the 110 fibre set, the second bundle with the second fibre in the set, etc.

Under strain control, the fibre with lowest strain to failure will break first, followed by the fibre with the second lowest strain to failure, etc. To simulate this, the load in each fibre was calculated at the point of first fibre failure. The load was calculated by multiplying the stress in each fibre by its cross-sectional area. In turn, the stress in each fibre was determined as the product of the modulus of the fibre and strain at the point of first fibre failure. It was noticed that the stress at failure calculated in this manner was not identical to the strength of the fibres and the measured failure strains were adjusted so as to exactly equal the strength divided by the modulus.

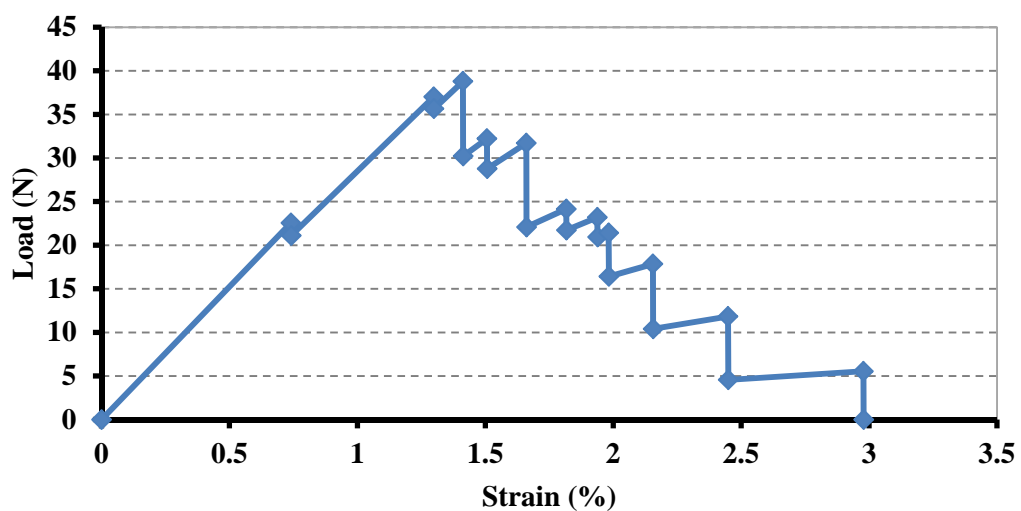


**Figure 5.57:** Simulated load-strain curve for Bundle 9.

Once the load in each fibre was determined, the load at break of the first fibre was then determined as the sum of the load in each fibre. Under strain control, failure of a fibre will lead to a load drop and this was simulated by subtracting the load in that fibre from total load calculated above. The procedure was then repeated for the fibre with second lowest strain to failure, etc, until all fibres had broken. The procedure is illustrated in Figure 5.57. It can be seen that the load rises to a maximum, in this case after the third fibre failure, then decreases. The bundle strength for each of the simulated bundles was determined as the maximum load divided by the sum of the cross sectional area of all eleven fibres in the bundle. The bundle strength for each of the ten simulated bundles, together with the number of fibre breaks required to initiate failure is given in Table 5.11. The curve shown in Figure 5.57 is for Bundle 9 which had the average number of initial fibre breaks and approximately the average fibre bundle strength.

**Table 5.11:** Results from simulated fibre bundle tests

<b>Bundle No.</b>	<b>Bundle Strength (MPa)</b>	<b>Fibre failures required to cause catastrophic failure</b>
1	482	1
2	472	3
3	579	3
4	515	1
5	598	1
6	569	4
7	636	3
8	488	2
9	627	3
10	733	5
<b>Average</b>	<b>570</b>	<b>3</b>
<b>Standard deviation</b>	<b>83</b>	<b>1</b>

The load strain curve shown in Figure 5.57 extends out to a strain of 3% whereas the experimental bundle tests had a typical strain at failure of 10%. As noted above this is considered to be due to additional strain in the system. Assuming this additional strain to be elastic and linearly proportional to stress, the strain was corrected

at each data point to give a strain of 10% at maximum load. The corrected data is plotted in Figure 5.58.

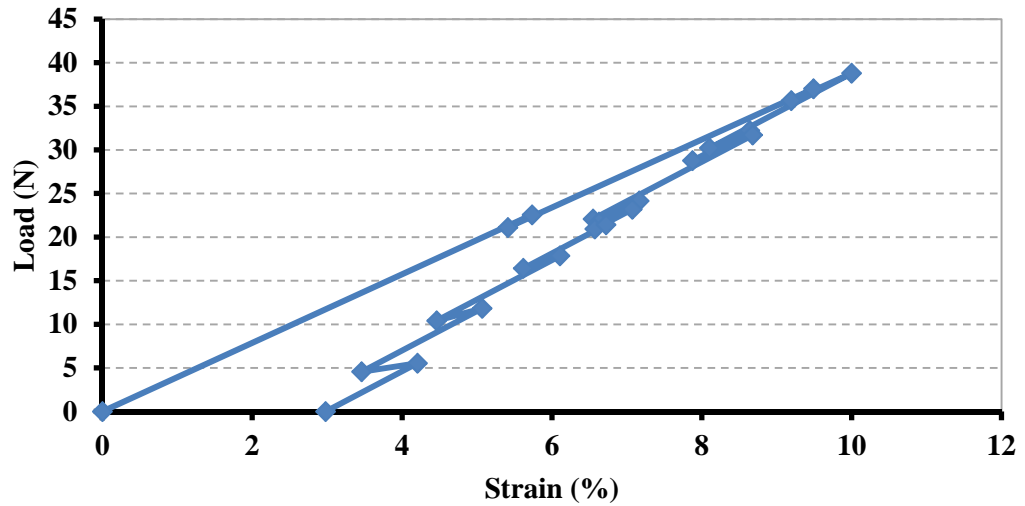


**Figure 5.58:** Corrected simulated load-strain curve for Bundle 9.

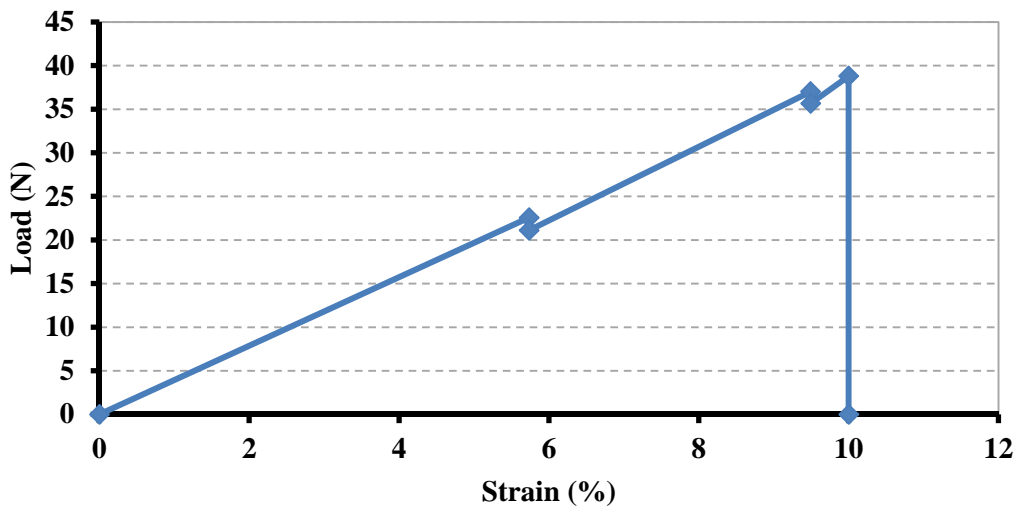


**Figure 5.59:** Simulated experimental load-strain curve for Bundle 9.

In this simulation, each load drop produces a corresponding drop in the additional strain (due to elastic recovery) and the maximum strain now corresponds with the maximum stress. Fibres that broke at strains above the strain at maximum load in Figure 5.57 now break at strains below the strain at maximum load since the additional strain contribution from the system diminishes as the load diminishes. This is because the elastic recovery in the system requires that extra strain occur in the fibres to



compensate for the strain recovery in the system. As a result all remaining fibres will fail once the strain reaches the maximum value in Figure 5.58.

The resulting load displacement curve is shown in Figure 5.59. Since strain drops are not possible under strain control, the load drops associated with fibre failure occur at constant strain. The curve now resembles the curves obtained experimentally, neglecting the effect of run-in

It can be seen from Table 5.11 that failure occurred in the ten simulated bundles after 1 to 5 fibre breaks with the average number of initial breaks being 3. The average bundle strength was 570 MPa which is 42% higher than the measured bundle strength, but still is only 61% of the single fibre strength. It is noted that the effect of gauge length was not taken into account in the simulations. The shorter gauge used for the bundle tests (3.2 mm) than for the single fibre tests (20 mm) should mean that the individual fibres in the bundle tests had on average higher strength than their measured single fibre values. This would increase the simulated bundle strengths, making the difference between the experimental values and simulated values even greater. While qualitatively the simulations give quite good agreement with the experimental observations, it is clear that at a quantitative level the situation is more complex than considered here.

It is noted that the scatter in the results obtained from the bundle tests, both experimental and simulated, was much lower than that obtained from the single fibre tests, as is evident from the standard deviations differing by approximately a factor of 2. This is not surprising since several fibres are involved in the test and this should have an averaging effect. Because of the lower scatter, the bundle test is more discriminating than the single fibre test indicating that it should be more useful for identifying batch to batch variation. It is understood that this is in fact its role in the cotton industry.

### ***5.5.3.2 Fracture of Flax Fibres***

It was not possible to examine the mechanism of fracture in the flax fibres after single fibre testing because the fibres disintegrated when they broke. However, it was possible to examine the fractures in the fibres after bundle testing. The features of the fractured fibres were similar to those reported by other workers (Baley, 2002; Romhány, Karger-Kocsis & Czigány, 2003) with longitudinal separation, transverse fibre cracking and zigzag fracture being observed.

*Figure 5.60 has been removed due to Copyright restrictions.*

**Figure 5.60:** Failure sequence in a flax technical fibre: (a) debonding and fibrillation in the longitudinal direction along the elementary fibres; (b) cracking in the elementary fibres in the transverse direction due to stress concentration; (c) “tearing-type” fracture within and through the elementary fibres; (d) and (e) long-range fracture completed by fracture of the elementary fibres and their constituting microfibrils (Romhány, Karger-Kocsis & Czigány, 2003).

A detailed study of the failure of flax technical fibres has been made by Romhány, Karger-Kocsis & Czigány (2003) using SEM examination during in situ loading. They found that failure started by longitudinal debonding and fibrillation. Fibrillation occurred along the boundaries of the elementary fibres due to break up of the weaker pectin and hemicellulose materials that bind the fibres together, as shown in

Figure 5.60 (a). This was followed by transverse microcracking in the elementary fibres, Figure 5.60 (b). They consider that these processes result in local redistribution of the stresses such that weak sites, which may be quite remote from the initial failure site, now undergo failure. This results in a tearing type process with a transverse crack propagating in a zig-zag direction across the split, fibrillated elementary fibres, Figure 5.60 (c). Fibrillated fibres are shown at higher magnification in Figure 5.61 (Baley 2002).

*Figure 5.61 has been removed due to Copyright restrictions.*

**Figure 5.61:** SEM micrographs of fracture surfaces of tested flax fibres at low (left) and high (right) magnification (Baley, 2002).

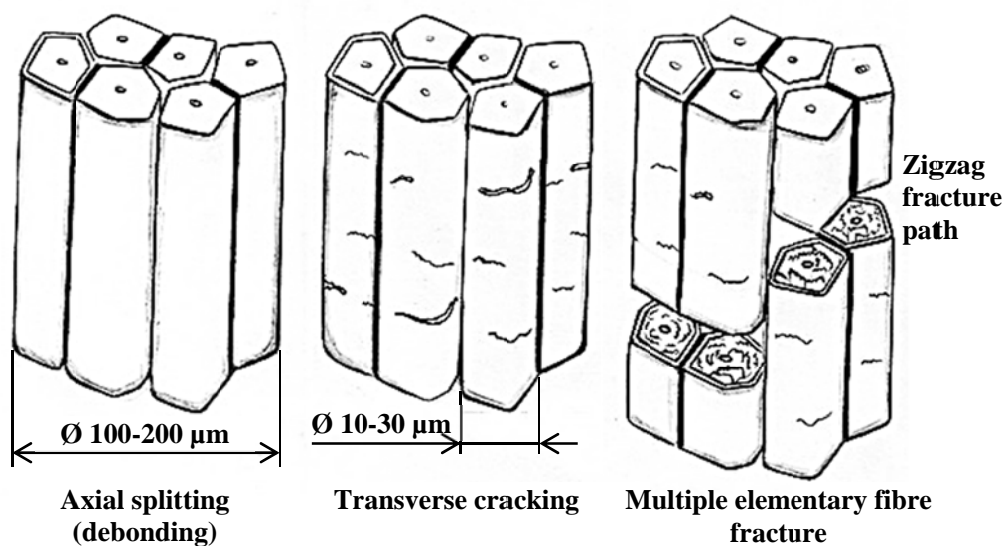


**Figure 5.62:** Diagram showing the failure sequence of flax fibres: axial splitting (debonding), transverse cracking, and multiple elementary fibre fracture (Romhányi, Karger-Kocsis & Czigány, 2003).

The processes described above are shown schematically in Figure 5.62. Eventually multiple fracture of the elementary fibres and their microfibrils occurs, often along a rather long fibre length, resulting in final failure. The final fracture mechanism is consistent with the disintegration of the fibres seen in the single fibre tests in the present study.

## **5.5.4 Unidirectional Flax Fibre/Vinyl Ester Composites**

### ***5.5.4.1 Tensile Properties of Unidirectional Composites***

#### *(5.5.4.1.1) Stress-Strain Behaviour*

The tensile stress-strain curves consisted of two essentially linear regions separated by a distinct knee, Figure 5.50 which occurred at a strain of approximately 0.2%. The slope of the curves decreased by approximately 40% after the knee.

Similar behaviour has been reported previously by Hughes, Carpenter & Hill (2007) for flax fibre/polyester composites, by Ruys (2007) for both flax/epoxy and hemp/epoxy composites, by Abdullah, Khalina & Ali (2011) for kenaf/epoxy composites and by Zakaria (2014) for kenaf/polyester composites.

Hughes, Carpenter & Hill (2007) undertook loading/unloading experiments on either side of the knee, and found that the behaviour of the composite was fully reversible before the knee but that some irreversible behaviour occurred after the knee. They attributed the occurrence of the knee to the behaviour of kink bands present in the fibres during loading. Below the knee, the kink bands were considered to have no effect on the deformation behaviour, but above the knee they were considered to produce microstructural damage to the composite, which reduced its stiffness and produced a component of irreversible behaviour. However, Abdullah, Khalina & Ali (2011) considered that the knee was caused by the behavior of the matrix and did not involve any contribution from the kenaf fibres. This is unlikely to be the case in the present study since the stress strain curves for the matrix material showed no evidence of a knee, Figure 5.51.

#### *(5.5.4.1.2) Calculation of Fibre Modulus and Strength from Composite Tensile Test Data*

The data obtained from tensile testing of the composites was used to calculate the modulus and strength of the fibres, using the rule of mixtures (Daniel & Ishai,

1994), for comparison with the results obtained from the single fibre tests. As noted in Section 5.4.1, the fibres that made up the yarns were not exactly parallel to the yarn direction but had been deformed into a spiral shape by the spiral wrapping threads. This is considered to be due to tension in the wrapping threads causing the yarns to deform into a conforming pattern. The misalignment was taken into account using the Krenchel reinforcing efficiency factor  $\eta$  (Krenchel, 1964, cited in Virk et al., 2012) as used by Virk et al. (2012) for prediction of modulus and by Shah, Shubel & Clifford (2012) for prediction of strength. The Krenchel reinforcing efficiency factor is given by (Krenchel, 1964, cited in Shah, Shubel & Clifford, 2012):

$$\eta = \sum_n a_n \cos^4 \theta_n \quad (5.34)$$

where  $a$  is the fraction of the fibres orientated at an angle  $\theta$  to the loading direction. In the present analysis it is assumed that the all the fibres are oriented at the same angle to the loading direction and  $a$  then becomes equal to 1. Thus, equation 5.34 reduces to

$$\eta = \cos^4 \theta. \quad (5.35)$$

The angular orientation of the fibres in the yarns was, in fact, somewhat variable but it was generally between  $10^\circ$  and  $20^\circ$  and a value of  $15^\circ$  was considered to be a reasonable estimate of  $\theta$ .

The yarns were wrapped with two viscose rayon threads one of which was parallel to the fibres, and thus had an angular orientation of about  $15^\circ$  while the other made an angle of about  $30^\circ$  to the yarn direction. Each of the two threads made up 3% of the volume fraction of the composite and the reinforcement provided by these yarns therefore needed to be considered. This was done by incorporating a contribution from the threads into the rule of mixtures equations, again using the Krenchel factor to account for misalignment with the loading direction. The transverse supporting thread was not considered since it was perpendicular to the loading direction.

A value for the modulus of viscose rayon was required for the calculations. Hearle (2001) gives a range of 4.8-8.8 N/tex which equates to 7.2-13.1 GPa. The mean value of 10.2 GPa was used in the calculations.

Based on the above, the rule of mixtures equations gives the modulus  $E$  and strength  $\sigma$  of the composites as:

$$E_c = E_f V_f \cos^4 \theta_f + E_m V_m + E_{w1} V_{w1} \cos^4 \theta_{w1} + E_{w2} V_{w2} \cos^4 \theta_{w2} \quad (5.36)$$

and

$$\sigma_c = \sigma_f V_f \cos^4 \theta_f + \sigma'_m V_m + \sigma'_{w1} V_{w1} \cos^4 \theta_{w1} + \sigma'_{w2} V_{w2} \cos^4 \theta_{w2} \quad (5.37)$$

where  $V$  is the volume fraction,  $\sigma'$  is the stress in the matrix and wrapping threads at the time of failure, and the subscripts  $c, f, m, w1$  and  $w2$  refer to the composite, the fibres, the matrix and the wrapping threads, respectively. As noted above, the transverse viscose rayon thread was not considered and the matrix volume fraction  $V_m$  was therefore obtained as

$$V_m = 1 - (V_f + V_{w1} + V_{w2}) \quad (5.38)$$

Assuming linear behaviour the stress terms in equation 5.37 can be replaced by

$$\sigma = E\varepsilon \quad (5.39)$$

giving

$$\sigma_c = \sigma_f V_f \cos^4 \theta_f + E_m \varepsilon'_m V_m + E_{w1} \varepsilon'_{w1} V_{w1} \cos^4 \theta_{w1} + E_{w2} \varepsilon'_{w2} V_{w2} \cos^4 \theta_{w2} \quad (5.40)$$

where  $\varepsilon'$  is the strain in the fibres and wrapping threads when the fibres fail.

Assuming isostrain conditions,

$$\varepsilon'_m = \varepsilon'_{w1} = \varepsilon'_{w2} = \varepsilon_f.$$

Equation 5.40 then becomes

$$\sigma_c = \sigma_f V_f \cos^4 \theta_f + E_m \varepsilon_f V_m + E_{w1} \varepsilon_f V_{w1} \cos^4 \theta_{w1} + E_{w2} \varepsilon_f V_{w2} \cos^4 \theta_{w2} \quad (5.41)$$

Equations 5.36 and 5.41 can be rewritten to give the fibre modulus and strength as

$$E_f = \frac{E_c - (E_m V_m - E_{w1} V_{w1} \cos^4 \theta_{w1} - E_{w2} V_{w2} \cos^4 \theta_{w2})}{V_f \cos^4 \theta_f} \quad (5.42)$$

and

$$\sigma_f = \frac{\sigma_c - (E_m \varepsilon_f V_m - E_{w1} \varepsilon_f V_{w1} \cos^4 \theta_{w1} - E_{w2} \varepsilon_f V_{w2} \cos^4 \theta_{w2})}{V_f \cos^4 \theta_f} \quad (5.43)$$

The strength and modulus of the fibres were then calculated using these equations and the data given in Table 5.12. This gave a modulus of 47.0 GPa and a strength of 337 MPa. The value of  $E_m \varepsilon_f$  given in equation 5.43 was slightly higher than the measured strength of the matrix so the latter was used when calculating fibre strength. This anomaly is considered to be due to the assumption of linear behaviour.

The predicted fibre modulus of 47.0 GPa is within 9% of the experimental true value of 52.4 GPa. The calculation was made using the 0.001-0.003 chord modulus from the composite tensile tests since this was the strain range used by Virk et al. (2012). However this strain range spanned the knee of the stress strain curves which

occurred at a strain of  $\sim 0.002$ , Figure 5.50. No knee was, however, observed in the stress strain curves for the fibres, Figure 5.30, and it is therefore considered that the knee is a result of damage occurring in the matrix of the composites, as proposed by Hughes, Carpenter & Hill (2007), rather than being an intrinsic property of the fibres. On this basis, the value of the modulus of the composites before the knee would appear to be more appropriate for determining the fibre modulus for comparison with the single fibre data. Using the strain range of 0.0001-0.0015 for both the composites and the vinyl ester resin gave a value of 55.6 GPa for the modulus of the fibres. This is within 6% of the value obtained from the single fibre tests.

Virk et al. (2012) also obtained good agreement between the experimental and predicted values of the modulus using a fibre area correction factor and the Krenchel reinforcing efficiency factor, as used in the present study, in their work on jute fibre composites. They used the experimentally determined true fibre modulus to calculate the modulus of their composites and obtained agreement within 1%.

**Table 5.12:** Data used for predicting the tensile modulus and strength of the flax fibres

Parameter	Value	Source
$V_f$ (excluding wrapping threads)	0.25	Section 5.4.5.2
$V_{w1}$	0.03	
$V_{w2}$	0.03	
$E_m$	3.62 GPa	Section 5.4.5.3
$E_{w1}$	10.2 GPa	
$E_{w2}$	10.2 GPa	
$E_c$	13.16 GPa	Section 5.4.5.3
$\theta_f$	15°	
$\theta_{w1}$	15°	
$\theta_{w2}$	30°	
$\varepsilon_f$	0.018	
$\sigma_m$	59.8 MPa	Section 5.4.5.3
$\sigma_c$	122.4 MPa	Section 5.4.5.3

In contrast to the predicted modulus, the predicted fibre strength of 337 MPa is very much lower than the experimental true value of 936 MPa. However, the experimental value of fibre strength was determined using a 20 mm gauge length, whereas the average fibre length in the flax yarns used to make the composites was 93 mm. Fibre strength is known to decrease substantially with increasing fibre length (Romhany, Karger-Kocsis & Czigány, 2003; Virk, Hall & Summerscales, 2011) and this needs to be taken into account. Rohmany, Karger-Kocsis & Czigány (2003) used data from testing of flax technical fibres with gauge lengths of 20, 40 and 80 mm, together with additional data for flax technical fibres reported by Stamboulis, Baillie, Garkhail, Van Melick & Peijs (2000) and Bos, Van Den Oever & Peters (2002), and found the following relationship between gauge length  $g$  (mm) and fibre strength  $\sigma$  (MPa):

$$\sigma = Ae^{B/(g+C)} \quad (5.44)$$

where  $A = 12.2$ ,  $B = 883.7$  and  $C = 206.4$ .

This equation was used to determine the ratio of strength at a 20 mm gauge to that at 93 mm. This ratio was then used to convert the true fibre strength of 936 MPa obtained in the present study for a 20 mm gauge length to its equivalent strength at 93 mm, giving a value of 361 MPa. The value of 337 MPa calculated from the composite tests is within 7% of this value and the agreement is again considered to be reasonably good.

## 5.6 General Discussion

The work described in this chapter was undertaken to examine the suitability of using the results obtained from single fibre and flat fibre bundle testing to predict the tensile properties of unidirectional composites made from the fibres. Rather than using the fibre data to predict the composite data, the fibre properties were backed out from the composite data and then compared with the data from the two fibre tests.

For this part of the work, flax was used as the reinforcing fibre since it has now become available as unidirectional fabric made from untwisted yarn and this provided the possibility of producing well aligned unidirectional fibre composites. Unfortunately the fibres were found to adopt a spiral configuration, with a spiral angle of approximately  $15^\circ$  which appeared to result from tension applied to the wrapping yarn, and this needed to be taken into account. Additionally the wrapping threads provided



extra reinforcement and this needed to be accounted for also. The strength data also needed to be adjusted to take into account the effect of fibre length on fibre strength.

The fibre modulus and strength were within 7% of the single fibre values, indicating that the behaviour of the composite can be reasonably well predicted from single fibre test results, as has been reported previously by Virk, Hall & Summerscales (2012) from their study of jute fibre composites. However, as noted by them, it is necessary to use the true cross-sectional area of the fibres, rather than an area based on diameter measurements and the assumption that the fibres are circular in section. This was done in both the present work and that reported by Virk, Hall & Summerscales (2012) by using an experimentally determined fibre area correction factor. The correction factor obtained by Virk, Hall & Summerscales (2012) for jute fibres was 1.42, which is just over half of the value of 2.70 obtained in the present study. The predicted modulus and strength scale in proportion to the correction factor and the good agreement between the experimental and predicted values for both parameters in both studies, despite the large difference in the magnitude of the correction factor, provides strong support for the validity of the procedure.

The bundle tests gave values of strength which were only 43% of the single fibre data. The results from bundle tests carried out by Parmar (2011, 2012) on kenaf and jute fibres, for which data was available for single fibre tests (Zakaria 2014; Virk et al, 2012) conducted on the same fibres using the same gauge length as used in the present study gave similarly low values of 52% and 54%.

The values obtained from the bundle tests would substantially underestimate the behaviour of the composites if used for strength prediction. In addition the bundle test does not provide a value for the elastic modulus of the fibres. However, the results from the bundle test show much lower scatter than those obtained from single fibre testing indicating that the test could be suitable for mechanically grading individual batches of fibres on a relative basis.

## **5.7 Summary**

The important findings from this part of the study are summarised below.

- The fibres were found to have a distinctly non-circular cross-section having an area that was, on average, 2.7 times larger than that calculated from the measured diameter assuming the fibres to be round. This confirms that an area

correction factor needs to be applied to single fibre test data determined using fibre diameter measurements.

- The modulus and strength of the fibres determined using fibre diameter measurements were 19.4 GPa and 347 MPa, respectively, while the strain at failure was 1.8%. The true values of modulus and strength obtained by applying the measured correction factor of 2.70 were 52.4 GPa and 936 MPa, respectively.
- The unidirectional composites with a fibre volume fraction of 25% had a modulus of 13.2 GPa and a strength of 122 MPa.
- The fibre modulus and strength obtained using the rule of mixtures to back out the data from the unidirectional composite tests were within 7% of the true values obtained from the single fibre tests when appropriate account was taken of fibre orientation and fibre length.
- The strength obtained from the bundle tests was only 43% of the true value obtained from the single fibre tests. It was not possible to determine the elastic modulus for the method used.
- The results obtained from the bundle tests showed much smaller scatter than those obtained from single fibre testing. This suggests that the bundle test may be useful for mechanically grading different batches of fibres on a relative basis.



**CHAPTER 6**  
**SUMMARY AND CONCLUSIONS**

---



## 6. SUMMARY AND CONCLUSIONS

The work consisted of two parts. The first involved extraction of the elementary fibres from kenaf fibres to produce high aspect ratio fibres for use in extruded and injection moulded natural fibre thermoplastic composites. High aspect ratio short fibres cannot be obtained by simply chopping the technical fibres because of their much larger diameter.

Two treatments were found to successfully liberate the elementaries, these being treatment in 60% nitric acid and treatment in 20% hydrogen peroxide/acetic acid. The hydrogen peroxide/acetic acid treatment gave a 60% higher yield than the nitric acid treatment and required less time. Moreover, it produced full length elementaries with an average length of 2.3 mm and an average aspect ratio of 180. In contrast, the nitric acid treatment caused the elementaries to break up into much smaller pieces with an average length of 0.2 mm and an average aspect ratio of 15. The nitric acid treated fibres also had double the defect density of the hydrogen peroxide/acetic acid treated fibres.

Both treatments removed lignin, pectin, waxes and extractives from the fibres. They also increased the level of crystallinity, with the increase being greater for the nitric acid treatment than for the hydrogen peroxide/acetic acid treatment. They also increased the hydrophilicity of the fibre surfaces. However both treatments caused some oxidation of the elementaries.

The hydrogen peroxide/acetic acid treatment increased the thermal stability of the fibres with degradation starting at a temperature 50°C higher than for untreated fibres. In contrast the thermal stability was reduced by 70°C for the nitric acid treated fibres.

Extruded HDPE composites containing 40 wt% fibres were prepared using both the nitric acid treated elementaries and those obtained from the hydrogen peroxide/acetic acid treatment. In addition composites were also prepared from chopped technical fibres having an average length of 0.7 mm and an average aspect ratio of 8.

Two different methods were used to extrude the composites. Initially, a single feed extruder was used, but in subsequent work a dual feed extruder was used to allow separate feeding of the fibres and the matrix material in an attempt to improve the quality of the composites. Different dies were used for the two extruders with rod

composites being produced from the single feed extruder and strip composites from the dual feed extruder. Only nitric acid treated and chopped untreated fibres were used for the composites made with the single feed system but hydrogen peroxide/acetic acid treated fibres were also used for the composites made with the dual feed system.

Both processes produced composites with good dispersion of the fibres and good bonding to the matrix. However, some differences between the rod and strip extrudates were observed. The rod composites had a fibre weight fraction of 38%, consistent with the target value of 40%. Difficulties were experienced with the fibre feed in the dual feed system and the fibre fractions in the strip composites were well below the target value. Moreover, severe variation in fibre fraction was encountered in the strip composites with the fibre fraction varying from about 10-50%. A much more consistent fibre fraction was achieved for the rod composites for which the variation was from 31-46%. Considerable breakup of the elementary fibres occurred during the extrusion process, especially for the dual feed system where the fibre length was reduced by a factor of 10.

Differences were also seen in the mechanical behaviour. The rod composites made from the nitric acid treated fibres showed no improvement in mechanical performance over those made from the chopped untreated fibres, with the modulus being identical in the two cases. The strength was actually 9% lower for the nitric acid treated fibre composites than for their untreated fibre counterparts. This is attributed to fragmentation of the elementaries due to chemical attack during the nitric acid treatment together with further breakup of the fibres during the extrusion process.

The strip composites made with nitric acid treated fibres also showed no improvement in mechanical performance over those made from the chopped untreated fibres, with the performance in fact being worse. This is attributed to even greater breakup of the elementaries during the strip extrusion process.

However the strip composites made with the hydrogen peroxide/acetic acid treated fibres showed a modest improvement of ~20% in the modulus and strength, over those obtained for the composites made from the chopped technical fibres. This improvement occurred despite the elementaries being reduced in length by a factor of 10 during the extrusion process.

Overall, the results are encouraging since the different levels of breakup of the elementaries produced using the two different extrusion processes suggests that there is

scope for modifying the process to better retain the initial fibre length. It may also be possible to obtain better fibre alignment which would also lead to improved mechanical performance. Examination of these possibilities would appear to be a fruitful area for further research.

The second part of the work involved an examination of the suitability of using the results obtained from single fibre and flat fibre bundle testing to predict the tensile properties of unidirectional composites made from the flax fibres.

In earlier work, Virk, Hall & Summerscales (2012) had reported that very good agreement could be obtained between the modulus and strength of jute fibre composites and the values predicted from single fibre tests, if proper account were taken of the true fibre cross-sectional shape, the fibre orientation, and the effect of fibre length on fibre strength. Their procedure was evaluated in this part of the study. Flax fibres were used rather than kenaf since unidirectional flax fabric is now available made from untwisted flax yarn, allowing production of well aligned unidirectional laminates. Vinyl ester was used as the matrix resin. The composites were produced by resin transfer moulding and had a fibre volume fraction of 25%.

The present study used the reverse procedure to that used by Virk, Hall & Summerscales (2012) and used data obtained from testing of the composites to predict the properties of the fibres, rather than using fibre data to predict the behaviour of the composites. None the less the two procedures can be considered to be equivalent in testing the validity of the methodology.

The agreement between the predicted and measured values in the present study was within 7%, which is very encouraging. The procedure requires the use of an area correction factor to account for the fibres being non-circular in shape and the modulus and strength scale in direct proportion to this factor. The area correction factor of 2.70 obtained for the flax fibres in the present study was almost twice that of 1.42 reported by Virk, Hall & Summerscales (2012) for their jute fibres. The good agreement from both studies, despite the substantial difference in magnitude of the area correction factor, is considered to provide strong support for the validity of the method.

Because of natural variability in plant fibres, data from one batch of fibres cannot necessarily be used to predict the performance of composites made from a different batch, requiring that single fibre testing be conducted on each different batch.



This is extremely labour intensive and also time consuming and is unlikely to be feasible, either practically or economically.

Batch to batch variation in fibres has long been recognised in the textiles industry and tests such as the flat fibre bundle test have been developed to grade different batches in terms of their mechanical performance. The flax fibre bundle test was therefore conducted on the flax fibres to evaluate its usefulness for predicting fibre properties. The bundle test gave a strength of only 43% of the value obtained by single fibre testing and would substantially underpredict the behaviour of composites made from the fibres. Moreover, it does not allow determination of the fibre modulus. However, since several fibres are present in the tested bundle, there is an averaging effect, which substantially reduces the scatter in results compared to that observed in the single fibre test. As a result the bundle test can discern between smaller differences and may be useful for assessing batch to batch variation. It is also much faster and easier to conduct than single fibre testing.

This suggests an approach that might be viable for predicting the behaviour of natural fibre composites. First, single fibre tests as well as flat bundle tests are conducted on a batch of fibres of the type to be used in the composite. Flat bundle tests are then conducted on all incoming batches and the results compared with those for the original batch. Any differences found could then be used to scale the single fibre test results and the scaled data then used to predict the behaviour of the composites made from each batch. This approach is worthy of further study.

## **REFERENCES**



Abdel Moteleb, M. M., & El Akabawy, Y. K. (1999). Dielectric investigation of some oxyviscoses. *Polymer*, 40(4), 895-903.

Abdul Khalil, H. P. S., Yusra, A. F. I., Bhat, A. H., & Jawaaid, M. (2010). Cell wall ultrastructure, anatomy, lignin distribution, and chemical composition of Malaysian cultivated kenaf fiber. *Industrial Crops and Products*, 31(1), 113-121.

Abdullah, A., Khalina, A., & Ali, A. (2011). Effects of fiber volume fraction on unidirectional kenaf/epoxy composites: The transition region. *Polymer-Plastics Technology and Engineering*, 50(13), 1362-1366.

Agarwal, U. P. (1999). An overview of Raman spectroscopy as applied to lignocellulosic materials *Advances in lignocellulosics characterization* (pp. 201–225). Atlanta: TAPPI Press.

Agarwal, U. P. (2006). Raman imaging to investigate ultrastructure and composition of plant cell walls: distribution of lignin and cellulose in black spruce wood (*Picea mariana*). *Planta*, 224(5), 1141-1153.

Ahmed, S., & Jones, F. (1990). A review of particulate reinforcement theories for polymer composites. *Journal of materials Science*, 25(12), 4933-4942.

Aji, I. S., Sapuan, S. M., Zainudin, E. S., & Abdan, K. (2009). Kenaf fibres as reinforcement for polymeric composites: a review. *International Journal of Mechanical and Materials Engineering*, 4(3), 239-248.

Akil, H. M., Omar, M. F., Mazuki, A. A. M., Safiee, S., Ishak, Z. A. M., & Abu Bakar, A. (2011). Kenaf fiber reinforced composites: A review. *Materials & Design*, 32(8-9), 4107-4121.

Anandjiwala, R. D., & Blouw, S. (2007). Composites from bast fibres - Prospects and potential in the changing market environment. *Journal of Natural Fibers*, 4(2), 91-901.

Ander, P., Daniel, G., Garcia-Lindgren, C., & Marklund, A. (2005). Characterization of industrial and laboratory pulp fibres using HCl, Cellulase and FiberMaster analysis. *Nordic Pulp and Paper Research Journal*, 20(1), 115-121.

Aranguren, M. I., & Reboredo, M. M. (2007). Plant-based reinforcements for thermosets: matrices, processing, and properties. In S. Fakirov & D. Bhattacharyya (Eds.), *Handbook of Engineering Biopolymers: Homopolymers, Blends and Composites* (pp. 193-221): Hanser.

Ashby, M. F. (2013). Chapter 15 - Material profiles *Materials and the Environment (Second Edition)* (pp. 459-595). Boston: Butterworth-Heinemann.

Ashby, M. F., & Jones, D. R. H. (2006). *Engineering Materials* (Third ed. Vol. 2): Butterworth-Heinemann.

Ashton, W. H., & Moser, C. E. (1968). Oxidized cellulose product and method for preparing the same. USA Patent No. 3,364,200.

ASTM C 1557-03 (2008). Standard test method for tensile strength and Young's modulus of fiber: ASTM International.

ASTM D 1294-05 (2005). Standard test method for tensile strength and breaking tenacity of wool fiber bundle 1-in. (25.4-mm) gage length: ASTM International.

ASTM D1445/D1445M-12 (2012). Standard test method for breaking strength and elongation of cotton fibers (flat bundle method): ASTM International.

ASTM D 2524-95 (2008). Standard test method for breaking tenacity of wool fibers, flat bundle method - 1/8-in. (3.2-mm) gage length: ASTM International.

ASTM D638 (2010). Standard test method for tensile properties of plastics: ASTM International.

Atalla, R., & Agarwal, U. (1986). Recording Raman spectra from plant cell walls. *Journal of Raman spectroscopy*, 17(2), 229-231.

Athukorala, Y., Mazza, G., & Oomah, B. D. (2009). Extraction, purification and characterization of wax from flax (*Linum usitatissimum*) straw. *European Journal of Lipid Science and Technology*, 111(7), 705-714.

Ayre, B. G., Stevens, K., Chapman, K. D., Webber Iii, C. L., Dagnon, K. L., & D'Souza, N. A. (2009). Viscoelastic properties of kenaf bast fiber in relation to stem age. *Textile Research Journal*, 79(11), 973-980.

Aziz, S. H., & Ansell, M. P. (2004). The effect of alkalization and fibre alignment on the mechanical and thermal properties of kenaf and hemp bast fibre composites: Part 1 - polyester resin matrix. *Composites Science and Technology*, 64(9), 1219-1230.

Bailar, J. C., Moeller, T., Kleinberg, J., Guss, C. O., Castellion, M. E., & Metz, C. (1989). *Chemistry*. The United States of America: Harcourt Brace Jovanovich, Inc.

Baley, C. (2002). Analysis of the flax fibres tensile behaviour and analysis of the tensile stiffness increase. *Composites Part A: Applied Science and Manufacturing*, 33(7), 939-948.

Baley, C., Le Duigou, A., Bourmaud, A., & Davies, P. (2012). Influence of drying on the mechanical behaviour of flax fibres and their unidirectional composites. *Composites Part A: Applied Science and Manufacturing*, 43(8), 1226-1233.

Bergbreiter, D. E., Franchina, J. G., & Kabza, K. (1999). Hyperbranched grafting on oxidized polyethylene surfaces. *Macromolecules*, 32(15), 4993-4998.

Biagiotti, J., Puglia, D., & Kenny, J. (2004). A Review on Natural Fibre-Based Composites-Part I. *Journal of Natural Fibers*, 1(2), 37-68.

- Bismarck, A., Mishra, S., & Lampke, T. (2005). Plant fibers as reinforcement for green composites. In A. K. Mohanty, M. Misra & L. T. Drzal (Eds.), *Natural fibers, biopolymers, and biocomposites* (pp. 37-108). The United States of America: Taylor & Francis Group.
- Bledzki, A. K., & Gassan, J. (1999). Composites reinforced with cellulose based fibres. *Progress in Polymer Science*, 24(2), 221-274.
- Bledzki, A. K., Jaszkievicz, A., Murr, M., Sperber, V. E., Lutzendorf, R., & Reubmann, T. (2008). Processing techniques for natural- and wood-fibre composites. In K. L. Pickering (Ed.), *Properties and performance of natural-fibre composites*. Cambridge.
- Boeriu, C. G., Bravo, D., Gosselink, R. J. A., & van Dam, J. E. G. (2004). Characterisation of structure-dependent functional properties of lignin with infrared spectroscopy. *Industrial Crops and Products*, 20(2), 205-218.
- Bonatti, P., Ferrari, C., Focher, B., Grippo, C., Torri, G., & Cosentino, C. (2004). Histochemical and supramolecular studies in determining quality of hemp fibres for textile applications. *Euphytica*, 140(1), 55-64.
- Bondeson, D., Kvien, I., & Oksman, K. (2006). Strategies for Preparation of Cellulose Whiskers from Microcrystalline Cellulose as Reinforcement in Nanocomposites. In K. Oksman & M. Sain (Eds.), *Cellulose nanocomposites: processing, characterization, and properties* (pp. 10-25). Washington, DC: American Chemical Society.
- Bos, H., Van Den Oever, M. J., & Peters, O. C. (2002). Tensile and compressive properties of flax fibres for natural fibre reinforced composites. *Journal of materials Science*, 37(8), 1683-1692.
- Brahim, S. B., & Cheikh, R. B. (2007). Influence of fibre orientation and volume fraction on the tensile properties of unidirectional Alfa-polyester composite. *Composites Science and Technology*, 67(1), 140-147.
- Buchert, J., Pere, J., Johansson, L.-S., & Campbell, J. (2001). Analysis of the surface chemistry of linen and cotton fabrics. *Textile Research Journal*, 71(7), 626-629.
- Burley, S. T., & Carpenter, F. (1995). *The evaluation of results obtained on available types of fiber strength testers using various gauge spacings and their relation on yarn strength*. Washington, D.C.: United States Department of Agriculture: Agricultural Marketing Service.
- Calamari, T. A., Tao, J. W., & Akin, D. E. (1999). Some important physical characteristics of kenaf fiber bundles and of the ultimate kenaf fibres. In T. Sellers, N. A. Reichert, E. P. Columbus, M. J. Fuller & K. Williams (Eds.), *Kenaf properties processing and products* (pp. 187-191). Mississippi State: Mississippi State University.
- Campbell, F. C. (2004). The thermoplastic composites: an unfulfilled promise *Manufacturing processes for advanced composites* (pp. 357-397). Oxford, UK: Elsevier Advanced Technology.

- Campbell, F. C. (2010a). Matrix resin systems *Structural composite materials* (pp. 63-100). The United States of America: ASM International.
- Campbell, F. C. (2010b). Thermoset composite fabrication processes *Structural composite materials* (pp. 119-182). The United States of America: ASM International.
- Carlsen, S. (1999). *Effects of freeze drying on paper*.
- Charlet, K., Baley, C., Morvan, C., Jernot, J. P., Gomina, M., & Bréard, J. (2007). Characteristics of Hermès flax fibres as a function of their location in the stem and properties of the derived unidirectional composites. *Composites Part A: Applied Science and Manufacturing*, 38(8), 1912-1921.
- Charlet, K., Eve, S., Jernot, J. P., Gomina, M., & Breard, J. (2009). Tensile deformation of a flax fiber. *Procedia Engineering*, 1(1), 233-236.
- Chattopadhyay, S., Chaki, T., & Bhowmick, A. K. (2001). Structural characterization of electron-beam crosslinked thermoplastic elastomeric films from blends of polyethylene and ethylene-vinyl acetate copolymers. *Journal of Applied Polymer Science*, 81(8), 1936-1950.
- Cheung, H., Ho, M., Lau, K., Cardona, F., & Hui, D. (2009). Natural fibre-reinforced composites for bioengineering and environmental engineering applications. *Composites Part B: Engineering*, 40(7), 655-663.
- Cho, L. (2007). Identification of textile fiber by Raman microspectroscopy. *Forensic Science Journal*, 6(1), 55-62.
- Chu, B., Onclin, M., & Ford, J. (1984). Laser light scattering characterization of polyethylene in 1, 2, 4-trichlorobenzene. *The Journal of Physical Chemistry*, 88(26), 6566-6575.
- Ciannamea, E. M., Stefani, P. M., & Ruseckaite, R. A. (2010). Medium-density particleboards from modified rice husks and soybean protein concentrate-based adhesives. *Bioresource Technology*, 101(2), 818-825.
- Clemons, C., & Sanadi, A. (2007). Instrumented impact testing of kenaf fiber reinforced polypropylene composites: effects of temperature and composition. *Journal of Reinforced Plastics and Composites*, 26(15), 1587.
- Colom, X., & Carrillo, F. (2002). Crystallinity changes in lyocell and viscose-type fibres by caustic treatment. *European Polymer Journal*, 38(11), 2225-2230.
- Costa, S., Borowiak-Palen, E., Kruszyńska, M., Bachmatiuk, A., & Kaleńczuk, R. (2008). Characterization of carbon nanotubes by Raman spectroscopy. *Materials Science-Poland*, 26(2), 433-441.

- Crosky, A., Soatthiyanon, N., Ruys, D., Meatherall, S., & Potter, S. (2014). Thermoset matrix natural fibre-reinforced composites. In A. Hodzic & R. Shanks (Eds.), *Natural fibre composites: Materials, processes and applications* (pp. 233-270): Woodhead Publishing Limited.
- Dai, D., & Fan, M. (2010). Characteristic and performance of elementary hemp fibre. *Materials Sciences and Applications*, 1(6), 336-342.
- Daniel, I. M., & Ishai, O. (1994). *Engineering mechanics of composite materials*. New York: Oxford University Press, Inc.
- Datta, S. K., Bhowmick, A. K., Tripathy, D., & Chaki, T. K. (1996). Effect of electron beam radiation on structural changes of trimethylol propane trimethacrylate, ethylene vinyl acetate, and their blends. *Journal of Applied Polymer Science*, 60(9), 1329-1341.
- de Lange, P. J., de Kreek, A. K., van Linden, A., & Coenjaarts, N. J. (1992). Weathering of wood and protection by chromium studied by XPS. *Surface and interface analysis*, 19(1-12), 397-402.
- Dissanayake, N. P., Summerscales, J., Grove, S., & Singh, M. (2009). Energy use in the production of flax fiber for the reinforcement of composites. *Journal of Natural Fibers*, 6(4), 331-346.
- Dittenber, D. B., & GangaRao, H. V. S. (2012). Critical review of recent publications on use of natural composites in infrastructure. *Composites Part A: Applied Science and Manufacturing*, 43(8), 1419-1429.
- Du, Y., Zhang, J., & Xue, Y. (2008). Temperature-duration effects on tensile properties of kenaf bast fiber bundles. *Forest Products Journal*, 58(9), 59-65.
- Durmuş, A., Woo, M., Kaşgöz, A., Macosko, C. W., & Tsapatsis, M. (2007). Intercalated linear low density polyethylene (LLDPE)/clay nanocomposites prepared with oxidized polyethylene as a new type compatibilizer: Structural, mechanical and barrier properties. *European Polymer Journal*, 43(9), 3737-3749.
- Edeerozey, A. M. M., Akil, H. M., Azhar, A. B., & Ariffin, M. I. Z. (2007). Chemical modification of kenaf fibers *Materials Letters*, 61(10), 2023-2025.
- Edge, M., Allen, N. S., Hayes, M., Riley, P. N. K., Horie, C. V., & Luc-Gardette, J. (1990). Mechanisms of deterioration in cellulose nitrate base archival cinematograph film. *European Polymer Journal*, 26(6), 623-630.
- Ehrensing, D. T. (2008). *Flax*. Oilseed Crops. Department of Crop and Soil Science. Oregon State University.
- Eichhorn, S., Sirichaisit, J., & Young, R. (2001). Deformation mechanisms in cellulose fibres, paper and wood. *Journal of materials Science*, 36(13), 3129-3135.
- English, B., Clemons, C., Stark, N., & Schneider, J. (1996). Waste-wood-derived fillers for plastics. *Notes*.



- Evans, R., Newman, R., Roick, U., Suckling, I., & Wallis, A. (1995). Changes in cellulose crystallinity during kraft pulping. Comparison of infrared, X-ray diffraction and solid state NMR results. *Holzforschung-International Journal of the Biology, Chemistry, Physics and Technology of Wood*, 49(6), 498-504.
- Fan, M. (2010). Characterization and performance of elementary hemp fibres: Factor influencing tensile strength. *BioResources*, 5(4), 2307-2322.
- Feng, D., Caulfield, D. F., & Sanadi, A. R. (2001). Effect of compatibilizer on the structure-property relationships of kenaf-fiber/polypropylene composites. *Polymer Composites*, 22(4), 506-517.
- Focher, B., Palma, M. T., Canetti, M., Torri, G., Cosentino, C., & Gastaldi, G. (2001). Structural differences between non-wood plant celluloses: evidence from solid state NMR, vibrational spectroscopy and X-ray diffractometry. *Industrial Crops and Products*, 13(3), 193-208.
- Fothergill, J. (1990). Estimating the cumulative probability of failure data points to be plotted on Weibull and other probability paper. *Electrical Insulation, IEEE Transactions on*, 25(3), 489-492.
- Foulk, J. (2010). Private communication.
- Foulk, J., Akin, D., Dodd, R., & Ulven, C. (2011). Production of flax fibers for biocomposites. In S. Kalia, B. S. Kaith & I. Kaur (Eds.), *Cellulose fibers: bio- and nano-polymer composites* (pp. 61-95): Springer.
- Franklin, G. (1945). Preparation of thin sections of synthetic resins and wood-resin composites, and a new macerating method for wood. *Nature*, 155(3924), 51.
- Ganster, J., Fink, H. P., & Pinnow, M. (2006). High-tenacity man-made cellulose fibre reinforced thermoplastics - Injection moulding compounds with polypropylene and alternative matrices. *Composites Part A: Applied Science and Manufacturing*, 37(10), 1796-1804.
- Garcia-Jaldon, C., Dupeyre, D., & Vignon, M. R. (1998). Fibres from semi-retted hemp bundles by steam explosion treatment. *Biomass and Bioenergy*, 14(3), 251-260.
- Garside, P., & Wyeth, P. (2003). Identification of cellulosic fibres by FTIR spectroscopy: thread and single fibre analysis by attenuated total reflectance. *Studies in conservation*, 48(4), 269-275.
- Gauthier, A., Derenne, S., Dupont, L., Guillon, E., Largeau, C., Dumonceau, J., & Aplincourt, M. (2002). Characterization and comparison of two ligno-cellulosic substrates by <sup>13</sup>C CP/MAS NMR, XPS, conventional pyrolysis and thermochemolysis. *Analytical and bioanalytical chemistry*, 373(8), 830-838.s
- George, J., Bhagawan, S. S., & Thomas, S. (1997). Effects of environment on the properties of low-density polyethylene composites reinforced with pineapple-leaf fibre. *Composites Science and Technology*, 58(9), 1471-1485.

Gert, E., Morales, A. S., Zubets, O., & Kaputskii, F. (2000). The features of nitric acid 'mercerization' of cellulose. *Cellulose*, 7(1), 57-66.

Gominho, J., Fernandez, J., & Pereira, H. (2001). *Cynara cardunculus* L. - a new fibre crop for pulp and paper production. *Industrial Crops and Products*, 13(1), 1-10.

González, D., Santos, V., & Parajó, J. C. (2011). Silane-treated lignicellulosic fibers as reinforcement material in polylactic acid biocomposites. *Journal of Thermoplastic Composite Materials*, 0(0), 1-8.

Gulmine, J. V., Janissek, P. R., Heise, H. M., & Akcelrud, L. (2002). Polyethylene characterization by FTIR. *Polymer Testing*, 21(5), 557-563.

Gustafsson, J., Ciovica, L., & Peltonen, J. (2003). The ultrastructure of spruce kraft pulps studied by atomic force microscopy (AFM) and X-ray photoelectron spectroscopy (XPS). *Polymer*, 44(3), 661-670.

Gwon, J., Lee, S., Chun, S., Doh, G., & Kim, J. (2010). Effects of chemical treatments of hybrid fillers on the physical and thermal properties of wood plastic composites. *Composites Part A: Applied Science and Manufacturing*.

Han, Y., Han, S., Cho, D., & Kim, H. (2007). Kenaf/polypropylene biocomposites: effects of electron beam irradiation and alkali treatment on kenaf natural fibers. *Composite Interfaces*, 14(6-6), 559-578.

Han, Y., Han, S., Cho, D., & Kim, H. (2008). Dynamic Mechanical Properties of Natural Fiber/Polymer Biocomposites: The Effect of Fiber Treatment with Electron Beam. *Macromolecular Research*, 16(3), 253.

Hänninen, T., Michud, A., & Hughes, M. (2011). Kink bands in bast fibres and their effects on mechanical properties. *Plastics, Rubber and Composites*, 40, 6(7), 307-310.

Harris, B. (1999). *Engineering Composite Materials*. London: IOM Communications Ltd.

Hearle, J. W. S. (2001). Textile Fibers: A Comparative Overview. In K. H. J. Buschow, R. W. Cahn, M. C. Flemings, B. Ilshner, E. J. Kramer, S. Mahajan & P. Veyssière (Eds.), *Encyclopedia of Materials: Science and Technology (Second Edition)* (pp. 9100-9116). Oxford: Elsevier.

Higgins, R. A. (1994). Fibre-reinforced composite materials *The properties of engineering materials* (Second ed., pp. 361-382). New York: Industrial Press Inc.

Holmes-Farley, S. R., & Whitesides, G. M. (1987). Reactivity of carboxylic acid and ester groups in the functionalized interfacial region of " polyethylene carboxylic acid"(PE-CO<sub>2</sub>H) its derivatives: differentiation of the functional groups into shallow and deep subsets based on a comparison of contact angle and ATR-IR measurements. *Langmuir*, 3(1), 62-76.

- Hu, W., Ton-That, M. T., Perrin-Sarazin, F., & Denault, J. (2010). An improved method for single fiber tensile test of natural fibers. *Polymer Engineering & Science*, 50(4), 819-825.
- Huang, M. R., & Li, X. G. (1998). Thermal degradation of cellulose and cellulose esters. *Journal of Applied Polymer Science*, 68(2), 293-304.
- Huda, M. S., Drzal, L. T., Mohanty, A. K., & Misra, M. (2008). Effect of fiber surface-treatments on the properties of laminated biocomposites from poly(lactic acid) (PLA) and kenaf fibers. *Composites Science and Technology*, 68(2), 424-432.
- Hughes, M. (2012). Defects in natural fibres: their origin, characteristics and implications for natural fibre-reinforced composites. *Journal of materials Science*, 47(2), 599-609.
- Hughes, M., Carpenter, J., & Hill, C. (2007). Deformation and fracture behaviour of flax fibre reinforced thermosetting polymer matrix composites. *Journal of materials Science*, 42(7), 2499-2511.
- Hughes, M., Sebe, G., Hague, J., Hill, C., Spear, M., & Mott, L. (2000). An investigation into the effects of micro-compressive defects on interphase behaviour in hemp-epoxy composites using half-fringe photoelasticity. *Composite Interfaces*, 7(1), 13-29.
- Johansson, L.-S., Campbell, J. M., Koljonen, K., & Stenius, P. (1999). Evaluation of surface lignin on cellulose fibers with XPS. *Applied Surface Science*, 144-145(0), 92-95.
- Jonoobi, M., Harun, J., Mathew, A. P., Hussein, M. Z. B., & Oksman, K. (2010). Preparation of cellulose nanofibers with hydrophobic surface characteristics. *Cellulose*, 17(2), 299-307.
- Jonoobi, M., Harun, J., Shakeri, A., Misra, M., & Oksman, K. (2009). Chemical composition, crystallinity, and thermal degradation of bleached and unbleached kenaf bast (*Hibiscus cannabinus*) pulp and nanofibers. *BioResources*, 4(2), 626-639.
- Kabir, M. M., Wang, H., Lau, K. T., & Cardona, F. (2012). Chemical treatments on plant-based natural fibre reinforced polymer composites: An overview. *Composites Part B: Engineering*, 43(7), 2883-2892.
- Kaith, B. S., Mittal, H., Jindal, R., Maiti, M., & Kalia, S. (2011). Environmental benevolent biodegradable polymer: synthesis, biodegradability and applications. In S. Kalia, B. S. Kaith & I. Kaur (Eds.), *Cellulose fibers: Bio- and nano-polymer composites* (pp. 425-451). Heidelberg, Dordrecht, London, New York: Springer.
- Karak, N. (2012). Vegetable oil-based polymer composites *Vegetable oil-based polymers: properties, processing and applications* (pp. 247-270): Woodhead Publishing Limited.

Karnani, R., Krishnan, M., & Narayan, R. (1997). Biofiber reinforced polypropylene composites. *Polymer Engineering & Science*, 37(2), 476-483.

Karus, M., & Kaup, M. (2002). Natural fibres in the European automotive industry. *Journal of Industrial Hemp*, 7(1), 119-131.

Keshk, S. M. A. S., & Haija, M. A. (2011). A new method for producing microcrystalline cellulose from *Gluconacetobacter xylinus* and kenaf. *Carbohydrate Polymers*, 84(4), 1301-1305.

Khasbaatar, A. D., Chun, Y. J., & Choi, U. S. (2007). Synthesis and thermal study on viscose rayon succinate coupled with metals and viscose rayon succinic silane. *Journal of Industrial and Engineering Chemistry*, 13(7), 1109-1116.

Kim, J. K., & Mai, Y. W. (1998). Characterization of interfaces *Engineered interfaces in fiber reinforced composites* (pp. 5-41). Oxford, U.K.: Elsevier Science Ltd.

Kitis, M. (2004). Disinfection of wastewater with peracetic acid: a review. *Environment International*, 30(1), 47-55.

Kobayashi, S., Shoda, S., Donnelly, M. J., & Church, S. P. (1999). Enzymatic synthesis of cellulose. In C. Bucke (Ed.), *Carbohydrate Biotechnology Protocols* (pp. 57-69). Totowa, New Jersey: Humana Press Inc.

Kubo, S., & Kadla, J. F. (2005). Hydrogen bonding in lignin: a Fourier transform infrared model compound study. *Biomacromolecules*, 6(5), 2815-2821.

Kumar, V., & Yang, T. (2002). HNO<sub>3</sub>/H<sub>3</sub>PO<sub>4</sub>-NANO<sub>2</sub> mediated oxidation of cellulose - preparation and characterization of bioabsorbable oxidized celluloses in high yields and with different levels of oxidation. *Carbohydrate Polymers*, 48(4), 403-412.

Laine, J., Stenius, P., Carlsson, G., & Ström, G. (1994). Surface characterization of unbleached kraft pulps by means of ESCA. *Cellulose*, 1(2), 145-160.

Lamy, B., & Pomel, C. (2002). Influence of fiber defects on the stiffness properties of flax fibers-epoxy composite materials. *Journal of Materials Science Letters*, 21(15), 1211-1213.

Lasseguette, E. (2008). Grafting onto microfibrils of native cellulose. *Cellulose*, 15(4), 571-580.

Lattuati-Derieux, A., Egasse, C., Regert, M., Chung, Y. J., & Lavédrine, B. (2009). Characterization and degradation pathways of ancient Korean waxed papers. *Journal of Cultural Heritage*, 10(3), 422-427.

Lee, K.-Y., Delille, A., & Bismarck, A. (2011). Greener surface treatments of natural fibres for the production of renewable composite materials. In S. Kalia, B. S. Kaith & I. Kaur (Eds.), *Cellulose fibers: Bio- and nano-polymer composites*. Heidelberg, Dordrecht, London, New York: Springer.

- Li, X., Tabil, L., & Panigrahi, S. (2007). Chemical treatments of natural fiber for use in natural fiber-reinforced composites: A review. *Journal of Polymers and the Environment*, 15(1), 25-33.
- Li, Y., & Pickering, K. L. (2008). Hemp fibre reinforced composites using chelator and enzyme treatments. *Composites Science and Technology*, 68(15-16), 3293-3298.
- Liu, D., Yuan, X., Bhattacharyya, D., & Easteal, A. (2010). Characterisation of solution cast cellulose nanofibre-reinforced poly (lactic acid). *eXPRESS Polymer Letters*, 4(1), 26-31.
- Liu, W., Drzal, L. T., Mohanty, A. K., & Misra, M. (2007). Influence of processing methods and fiber length on physical properties of kenaf fiber reinforced soy based biocomposites. *Composites Part B: Engineering*, 38(3), 352-359.
- Lora, J. H., & Glasser, W. G. (2002). Recent industrial applications of lignin: A sustainable alternative to nonrenewable materials. *Journal of Polymers and the Environment*, 10(1), 39-48.
- Lundin, T., Cramer, S. M., Falk, R. H., & Felton, C. (2004). Accelerated weathering of natural fiber-filled polyethylene composites. *Journal of materials in civil engineering*, 16, 547.
- Luz, S. M., Del Tio, J., Rocha, G. J. M., Goncalves, A. R., & Del'Arco Jr, A. P. (2008). Cellulose and cellulignin from sugarcane bagasse reinforced polypropylene composites: Effect of acetylation on mechanical and thermal properties. *Composites Part A: Applied Science and Manufacturing*, 39(9), 1362-1369.
- Macko, T., Pasch, H., Kazakevich, Y. V., & Fadeev, A. Y. (2003). Elution behavior of polyethylene in polar mobile phases on a non-polar sorbent. *Journal of Chromatography A*, 988(1), 69-76.
- Mathias, L. J., Hankins, M. G., Bertolucci, C. M., Grubb, T. L., & Muthiah, J. (1992). Thin films of copolymers of ethylene and vinyl acetate. *The Modern Student Laboratory: Fourier Transform Infrared Analysis*, 69(8), A217-A219.
- Matuana, L., Balatinecz, J., Sodhi, R., & Park, C. (2001). Surface characterization of esterified cellulosic fibers by XPS and FTIR spectroscopy. *Wood Science and Technology*, 35(3), 191-201.
- Mazumdar, S. K. (2002). Raw materials for part fabrication *Composites manufacturing: materials, product, and process engineering*. The U.S.: CRC Press LLC.
- Mazumder, B. B., Ohtani, Y., Cheng, Z., & Sameshima, K. (2000). Combination treatment of kenaf bast fiber for high viscosity pulp. *Journal of wood science*, 46(5), 364-370.
- Meatherall, S. (2012). Private communication.

Merdy, P., Guillon, E., Dumonceau, J., & Aplincourt, M. (2002). Characterisation of a wheat straw cell wall residue by various techniques: A comparative study with a synthetic and an extracted lignin. *Analytica Chimica Acta*, 459(1), 133-142.

Merk, S., Blume, A., & Riederer, M. (1997). Phase behaviour and crystallinity of plant cuticular waxes studied by Fourier transform infrared spectroscopy. *Planta*, 204(1), 44-53.

Michielsen, S. (2001). Application of Raman spectroscopy to organic fibers and films. In I. R. Lewis & H. G. M. Edwards (Eds.), *Handbook of Raman spectroscopy from the research laboratory to the process line* (Vol. 28, pp. 749-798). The United States of America: Marcel Dekker, Inc.

Mohanty, A., Drzal, L., & Misra, M. (2002). Engineered natural fiber reinforced polypropylene composites: influence of surface modifications and novel powder impregnation processing. *Journal of Adhesion Science and Technology*, 16(8), 999-1015.

Mohanty, A. K., Misra, M., Drzal, L. T., Selke, S. E., Harte, B. R., & Hinrichsen, G. (2005). Natural fibers, biopolymers, and biocomposites: an introduction. In A. K. Mohanty, M. Misra & L. T. Drzal (Eds.), *Natural fibers, biopolymer, and biocomposites* (pp. 1-36). The United States of America: Taylor & Francis Group.

Moran, J., Alvarez, V., Cyras, V., & Vazquez, A. (2008). Extraction of cellulose and preparation of nanocellulose from sisal fibers. *Cellulose*, 15(1), 149-159.

Moran, J., Alvarez, V., Petrucci, R., Kenny, J., & Vazquez, A. (2007). Mechanical properties of polypropylene composites based on natural fibers subjected to multiple extrusion cycles. *Journal of Applied Polymer Science*, 103(1), 228-237.

Munder, F., Fürll, C., & Hempel, H. (2005). Processing of bast fiber plants for industrial application. In A. K. Mohanty, M. Misra & L. T. Drzal (Eds.), *Natural fibers, biopolymers, and biocomposites* (pp. 109-140). The United States of America: Taylor & Francis Group.

Murty, D. N. P., Xie, M., & Jiang, R. (2004). Overview *Weibull Models* (pp. 3-17). The United States of America: John Wiley & Sons, Inc.

Newman, R. (2004). Homogeneity in cellulose crystallinity between samples of *Pinus radiata* wood. *Holzforschung*, 58(1), 91-96.

Nishino, T. (2004). Natural fibre sources. In C. Baillie (Ed.), *Green composites: polymer composites and the environment*. Cambridge, England: Woodhead Publishing Limited.

Nishino, T., Hirao, K., Kotera, M., Nakamae, K., & Inagaki, H. (2003). Kenaf reinforced biodegradable composite. *Composites Science and Technology*, 63(9), 1281-1286.

- Nosbi, N., Akil, H. M., Mohd Ishak, Z. A., & Abu Bakar, A. (2010). Degradation of compressive properties of pultruded kenaf fiber reinforced composites after immersion in various solutions. *Materials & Design*, 31(10), 4960-4964.
- Ogbonnaya, C. I., Roy-Macauley, H., Nwalozie, M. C., & Annerose, D. J. M. (1997). Physical and histochemical properties of kenaf (*Hibiscus cannabinus* L.) grown under water deficit on a sandy soil. *Industrial Crops and Products*, 7(1), 9-18.
- Oksman, K. (2001). High quality flax fibre composites manufactured by the resin transfer moulding process. *Journal of Reinforced Plastics and Composites*, 20(7), 621-627.
- Oksman, K., Mathew, A. P., Långström, R., Nyström, B., & Joseph, K. (2009). The influence of fibre microstructure on fibre breakage and mechanical properties of natural fibre reinforced polypropylene. *Composites Science and Technology*, 69(11-12), 1847-1853.
- Ooi, B. G., Rambo, A. L., & Hurtado, M. A. (2011). Overcoming the recalcitrance for the conversion of kenaf pulp to glucose via microwave-assisted pre-treatment processes. *International Journal of Molecular Sciences*, 12(3), 1451-1463.
- Orts, W., Shey, J., Imam, S., Glenn, G., Guttman, M., & Revol, J. (2005). Application of cellulose microfibrils in polymer nanocomposites. *Journal of Polymers and the Environment*, 13(4), 301-306.
- Owen, N., & Thomas, D. (1989). Infrared studies of "Hard" and "Soft" woods. *Applied spectroscopy*, 43(3), 451-455.
- Öztürk, I., Irmak, S., Hesenov, A., & Erbatur, O. (2010). Hydrolysis of kenaf (*Hibiscus cannabinus* L.) stems by catalytical thermal treatment in subcritical water. *Biomass and Bioenergy*, 34(11), 1578-1585.
- Padmavathi, T., Naidu, S. V., & Rao, R. (2012). Studies on Mechanical Behavior of Surface Modified Sisal Fibre–Epoxy Composites. *Journal of Reinforced Plastics and Composites*, 31(8), 519-532.
- Pandey, K. K. (1999). A study of chemical structure of soft and hardwood and wood polymers by FTIR spectroscopy. *Journal of Applied Polymer Science*, 71(12), 1969-1975.
- Panthapulakkal, S., & Sain, M. (2007). Agro-residue reinforced high-density polyethylene composites: Fiber characterization and analysis of composite properties. *Composites Part A: Applied Science and Manufacturing*, 38(6), 1445-1454.
- Pardini, L. C., & Manhani, L. G. B. (2002). Influence of the testing gage length on the strength, Young's modulus and Weibull modulus of carbon fibres and glass fibres. *Materials Research*, 5(4), 411-420.

Park, S., Baker, J., Himmel, M., Parilla, P., & Johnson, D. (2010). Cellulose crystallinity index: measurement techniques and their impact on interpreting cellulase performance. *Biotechnology for biofuels*, 3(10), 1-10.

Park, S., Johnson, D., Ishizawa, C., Parilla, P., & Davis, M. (2009). Measuring the crystallinity index of cellulose by solid state  $^{13}\text{C}$  nuclear magnetic resonance. *Cellulose*, 16(4), 641-647.

Parmar, P. A. (2011). *Development of a test for grading bast fibres*. Bachelor of Engineering, University of New South Wales, Sydney, Australia.

Parmar, P. A. (2012). Unpublished research. CRC-ACS, Sydney, Australia.

Pereira, A. L. S., Nascimento, D. M. D., Cordeiro, E. M. S., Morais, J. P. S., Sousa, M. D. S. M., & Rosa, M. D. F. (2010). *Characterization of lignocellulosic materials extracted from the banana pseudostem*. Paper presented at the XII International Macromolecular Colloquium and 7th International Symposium on Natural Polymers and Composites, Brazil.

Qiu, Y., & Schwartz, P. (1993). Micromechanical behavior of Kevlar-149/S-glass hybrid seven-fiber microcomposites: I. Tensile strength of the hybrid composite. *Composites Science and Technology*, 47(3), 289-301.

Ratna Prasad, A. V., & Mohana Rao, K. (2011). Mechanical properties of natural fibre reinforced polyester composites: Jowar, sisal and bamboo. *Materials & Design*, 32(8-9), 4658-4663.

Rautiainen, R., & Alen, R. (2009). Variations in fiber length within a first-thinning Scots pine (*Pinus sylvestris*) stem. *Cellulose*, 16(2), 349-355.

Ray, D., & Rout, J. (2005). Thermoset biocomposites. In A. K. Mohanty, M. Misra & L. T. Drzal (Eds.), *Natural fibers, biopolymers, and biocomposites* (pp. 291-345). The United States of America: Taylor & Francis Group.

Rennekar, S., Zink-Sharp, A., Esker, A. R., Johnson, R. K., & Glasser, W. G. (2006). Novel methods for interfacial modification of cellulose-reinforced composites. In K. Oksman & M. Sain (Eds.), *Cellulose nanocomposites: processing, characterization, and properties* (pp. 78-96). Washington, DC: American Chemical Society.

Rinne, K. T., Boettger, T., Loader, N. J., Robertson, I., Switsur, V. R., & Waterhouse, J. S. (2005). On the purification of alpha-cellulose from resinous wood for stable isotope (H, C and O) analysis. *Chemical Geology*, 222(1-2), 75-82.

Romh ny, G., Karger-Kocsis, J., & Czig ny, T. (2003). Tensile fracture and failure behavior of technical flax fibers. *Journal of Applied Polymer Science*, 90(13), 3638-3645.

Rowell, R., Sanadi, A., Caulfield, D., & Jacobson, R. (1997). Utilization of natural fibers in plastic composites: Problems and opportunities. *Lignocellulosic-Plastic Composites*, Sao Paulo, USP & UNESP, 23-51.



Rowell, R., Sanadi, A., Jacobson, R., & Caulfield, D. (1999). Properties of kenaf/polypropylene composites. *Kenaf Properties, Processing and Products* (pp. 381–392): Mississippi State University, Ag & Bio Engineering.

Rowell, R. M. (2008). Natural fibres: types and properties. In K. L. Pickering (Ed.), *Properties and performance of natural-fibre composites*. Cambridge, England: Woodhead Publishing Limited.

Rowell, R. M., & Han, J. S. (1999). Changes in kenaf properties and chemistry as a function of growing time. In R. M. Rowell, J. S. Han, J. S. Rowell, H. P. Stout, E. S. Miyashita & S. J. Spielvogel (Eds.), *Kenaf properties, porcessing and products* (pp. 33–41).

Ruys, D. (2007). *The influence of bast fibre structure on the mechanical properties of natural fibre Composites*. Doctor of Philosophy, University of New South Wales, Sydney.

Saheb, D., & Jog, J. (1999). Natural fiber polymer composites: A review. *Advances in Polymer Technology*, 18(4), 351–363.

Sain, M., & Panthapulakkal, S. (2004). Green fibre thermoplastic composites. In C. Baillie (Ed.), *Green composites polymer composites and the environment*. Cambridge: CRC Press.

Samal, R. K., & Ray, M. C. (1997). Effect of chemical modifications on FTIR spectra. II. Physicochemical behavior of pineapple leaf fiber (PALF). *Journal of Applied Polymer Science*, 64(11), 2119–2125.

Sanadi, A., Caulfield, D., Jacobson, R., & Rowell, R. (1995). Renewable agricultural fibers as reinforcing fillers in plastics: Mechanical properties of kenaf fiber-polypropylene composites. *Industrial & Engineering Chemistry Research*, 34(5), 1889–1896.

Sandy, M., Manning, A., & Bollet, F. (2010). Changes in the Crystallinity of Cellulose in Response to Changes in Relative Humidity and Acid Treatment. *Restaurator*, 31(1), 1–18.

Saxena, M., Pappu, A., Haque, R., & Sharma, A. (2011) Sisal fiber based polymer composites and their applications. *Cellulose fibers: Bio- and nano-polymer composites* (pp. 589–659). Heidelberg, Dordrecht, London, New York: Springer.

Sayeba, S., Marzouga, I., Hassena, M., Saklia, F., & Rodeslib, S. (2010). Study of water sorption properties for esparto grass ultimate fibre (ALFA fibre). *Journal of the Textile Institute*, 101(1), 19–27.

Segal, L., Creely, L., Martin, A., & Conrad, C. (1959). An empirical method of estimating the degree of crystallinity of native cellulose using the X-ray diffractometer. *Textile Research Journal*, 29, 786–794.

- Sengloung, T., Kaveeta, L., & Müssig, J. (2008). Physical Properties of Traditional Thai Hemp Fiber (*Cannabis sativa* L.). *Journal of Industrial Hemp*, 13(1), 20-36.
- Sgriccia, N., Hawley, M., & Misra, M. (2008). Characterization of natural fiber surfaces and natural fiber composites. *Composites Part A: Applied Science and Manufacturing*, 39(10), 1632-1637.
- Shah, D. U., Schubel, P. J., & Clifford, M. J. (2012). Modelling the effect of yarn twist on the tensile strength of unidirectional plant fibre yarn composites. *Journal of Composite Materials*, 47(4), 425-436.
- Sharma, H. S. S., & Kernaghan, K. (1988). Thermogravimetric analysis of flax fibres. *Thermochimica Acta*, 132(29), 101-109.
- Shchukarev, A., Sundberg, B., Mellerowicz, E., & Persson, P. (2002). XPS study of living tree. *Surface and interface analysis*, 34(1), 284-288.
- Shen, Q., Mikkola, P., & Rosenholm, J. B. (1998). Quantitative characterization of the subsurface acid-base properties of wood by XPS and Fowkes theory. *Colloids and Surfaces A: Physicochemical and Engineering Aspects*, 145(1-3), 235-241.
- Shin, H. K., Jeun, J. P., Kim, H. B., & Kang, P. H. (2012). Isolation of cellulose fibers from kenaf using electron beam. *Radiation Physics and Chemistry*, 81(8), 936-940.
- Silverstein, R. M., Webster, F. X., & Kiemle, D. J. (2005). *Spectrometric identification of organic compounds*. Hoboken, NJ: John Wiley & Sons, Inc.
- Socrates, G. (2001). *Infrared and Raman characteristic group frequencies: tables and charts* (Third ed.): John Wiley & Sons, Ltd.
- Spence, K., Habibi, Y., & Dufresne, A. (2011). Nanocellulose-based composites. In S. Kalia, B. S. Kaith & I. Kaur (Eds.), *Cellulose fibers: bio- and nano-polymer composites* (pp. 179-213). Heidelberg, Dordrecht, London, New York: Springer.
- Spinlab. (n.d.). Stelometer 154: Instrument for measuring fiber strength and elongation.
- Sreekumar, P. A., & Thomas, S. (2008). Matrices for natural -fibre reinforced composites. In K. L. Pickering (Ed.), *Properties and performance of natural-fibre composites*. Cambridge: CRC Press.
- Stamboulis, A., Baillie, C., Garkhail, S., Van Melick, H., & Peijs, T. (2000). Environmental durability of flax fibres and their composites based on polypropylene matrix. *Applied Composite Materials*, 7(5), 273-294.
- Stuart, T., Liu, Q., Hughes, M., McCall, R. D., Sharma, H. S. S., & Norton, A. (2006). Structural biocomposites from flax--Part I: Effect of bio-technical fibre modification on composite properties. *Composites Part A: Applied Science and Manufacturing*, 37(3), 393-404.

Suddell, B. C., & Evans, W. J. (2005). Natural fiber composites in automotive applications. In A. K. Mohanty, M. Misra & L. T. Drzal (Eds.), *Natural fibers, biopolymers, and biocomposites* (pp. 231-259). The United States of America: Taylor & Francis Group.

Sullivan, J. D., & Lauzon, P. H. (1986). Experimental probability estimators for Weibull plots. *Journal of Materials Science Letters*, 5(12), 1245-1247.

Sun, G., Pang, J. H., Zhou, J., Zhang, Y., Zhan, Z., & Zheng, L. (2012). A modified Weibull model for tensile strength distribution of carbon nanotube fibers with strain rate and size effects. *Applied Physics Letters*, 101(13), 131905-1-131905-4.

Tajvidi, M. (2005). Static and dynamic mechanical properties of a kenaf fiber-wood flour/polypropylene hybrid composite. *Journal of Applied Polymer Science*, 98(2), 665-672.

Tajvidi, M., Falk, R., & Hermanson, J. (2005). Time-temperature superposition principle applied to a kenaf-fiber/high-density polyethylene composite. *Journal of Applied Polymer Science*, 97(5), 1995-2004.

Tajvidi, M., Falk, R. H., & Hermanson, J. C. (2006). Effect of natural fibers on thermal and mechanical properties of natural fiber polypropylene composites studied by dynamic mechanical analysis. *Journal of Applied Polymer Science*, 101(6), 4341-4349.

Tajvidi, M., Falk, R. H., Hermanson, J. C., & Felton, C. (2003). *Influence of natural fibers on the phase transitions in high-density polyethylene composites using dynamic mechanical analysis*. Paper presented at the The Seventh International Conference on Woodfiber-Plastic Composites.

Tajvidi, M., Najafi, S. K., & Moteei, N. (2006). Long-term water uptake behavior of natural fiber/polypropylene composites. *Journal of Applied Polymer Science*, 99(5), 2199-2203.

Terasaki, Y., Goda, K., & Noda, J. (2009). *Strength evaluation of natural fibers with variation of within-fiber cross-sectional area*. Paper presented at the ICCM.

Thomas, S., Paul, S. A., Pothan, L. A., & Deepa, B. (2011). Natural fibres: Structure, properties and applications. In S. Kalia, B. S. Kaith & I. Kaur (Eds.), *Cellulose fibers: Bio- and nano-polymer composites* (pp. 3-42). Heidelberg: Springer.

Thomason, J., Carruthers, J., Kelly, J., & Johnson, G. (2011). Fibre cross section determination and variability in sisal and flax and its effects on fibre performance characterisation. *Composites Science and Technology*, 71(7), 1008-1015.

Thygesen, L. G. (2008). Quantification of dislocations in hemp fibers using acid hydrolysis and fiber segment length distributions. *Journal of Materials Science*, 43(4), 1311-1317.

Thygesen, A., Madsen, B., Bjerre, A. B., & Lilholt, H. (2011). Cellulosic fibers: effect of processing on fiber bundle strength. *Journal of Natural Fibers*, 8(3), 161-175.

- Truss, R., & Wood, B. (2011). *X-ray photoelectron spectroscopy (XPS) study of hemp fibre mat*. CRC-ACS.
- Tserki, V., Zafeiropoulos, N. E., Simon, F., & Panayiotou, C. (2005). A study of the effect of acetylation and propionylation surface treatments on natural fibres. *Composites Part A: Applied Science and Manufacturing*, 36(8), 1110-1118.
- Van de Weyenberg, I., Chi Truong, T., Vangrimde, B., & Verpoest, I. (2006). Improving the properties of UD flax fibre reinforced composites by applying an alkaline fibre treatment. *Composites Part A: Applied Science and Manufacturing*, 37(9), 1368-1376.
- Van den Oever, M., Bos, H., & Van Kemenade, M. (2000). Influence of the physical structure of flax fibres on the mechanical properties of flax fibre reinforced polypropylene composites. *Applied Composite Materials*, 7(5), 387-402.
- van der Zwaag, S. (1989). The concept of filament strength and the Weibull modulus. *ASTM Journal of Testing Evaluation*, 17(5), 292-298.
- Vázquez, A., & Alvarez, V. A. (2009). Starch-Cellulose Fiber Composites. In L. Yu (Ed.), *Biodegradable polymer blends and composites from renewable resources* (pp. 241-263). Canada: John Wiley & Sons, Inc.
- Virk, A. S. (2010). *Numerical models for natural fibre composites with stochastic properties*. Doctor of Philosophy, University of Plymouth.
- Virk, A. S., Hall, W., & Summerscales, J. (2009). Multiple Data Set (MDS) weak-link scaling analysis of jute fibres. *Composites Part A: Applied Science and Manufacturing*, 40(11), 1764-1771.
- Virk, A., Hall, W., & Summerscales, J. (2011). Modelling tensile properties of jute fibres. *Materials Science and Technology*, 27(1), 458-460.
- Virk, A., Hall, W., & Summerscales, J. (2012). Modulus and strength prediction for natural fibre composites. *Materials Science and Technology*, 28(7), 864-871.
- Wang, D., Shang, S. b., Song, Z. q., & Lee, M. K. (2010). Evaluation of microcrystalline cellulose prepared from kenaf fibers. *Journal of Industrial and Engineering Chemistry*, 16(1), 152-156.
- Wanjale, S. D., & Jog, J. P. (2011). Polyolefin-based natural fiber composites. In S. Kalia, B. S. Kaith & I. Kaur (Eds.), *Cellulose fibers: Bio- and nano-polymer composites* (pp. 377-398). Heidelberg, Dordrecht, London, New York: Springer.
- Ward, J., Tabil, L. G., Panigrahi, S., Crerar, W. J., Powell, T., Kovacs, A. J., & Ulrich, A. (n.d.). Tensile testing of flax fibers (pp. 1-9). St. Joseph, MI, USA: The Society for engineering in agricultural, food, and biological systems (ASAE).

Watling, K. M., Parr, J. F., Rintoul, L., Brown, C. L., & Sullivan, L. A. (2011). Raman, infrared and XPS study of bamboo phytoliths after chemical digestion. *Spectrochimica Acta Part A: Molecular and Biomolecular Spectroscopy*, 80(1), 106-111.

Wiley, J. H., & Atalla, R. H. (1987). Band assignments in the raman spectra of celluloses. *Carbohydrate research*, 160, 113-129.

Williams, T., Hosur, M., Theodore, M., Netravali, A., Rangari, V., & Jeelani, S. (2011). Time Effects on Morphology and Bonding Ability in Mercerized Natural Fibers for Composite Reinforcement. *International Journal of Polymer Science*, 2011.

Wong, S., & Shanks, R. (2009). Biocomposites of natural fibers and poly(3-hydroxybutyrate) and copolymers: improved mechanical properties through compatibilization at the interface. In L. Yu (Ed.), *Biodegradable polymer blends and composites from renewable resources* (pp. 303-325). Canada: John Wiley & Sons, Inc.

Xue, Y., Du, Y., Elder, S., Wang, K., & Zhang, J. (2009). Temperature and loading rate effects on tensile properties of kenaf bast fiber bundles and composites. *Composites Part B: Engineering*, 40(3), 189-196.

Yang, H.-S., Wolcott, M. P., Kim, H.-S., Kim, S., & Kim, H.-J. (2007). Effect of different compatibilizing agents on the mechanical properties of lignocellulosic material filled polyethylene bio-composites. *Composite Structures*, 79(3), 369-375.

Zafeiropoulos, N. E. (2008). Engineering the fibre-matrix interface in natural-fibre composites. In K. L. Pickering (Ed.), *Properties and performance of natural-fibrecomposites*. Cambridge: CRC Press.

Zafeiropoulos, N., Vickers, P., Baillie, C., & Watts, J. (2003). An experimental investigation of modified and unmodified flax fibres with XPS, ToF-SIMS and ATR-FTIR. *Journal of materials Science*, 38(19), 3903-3914.

Zakaria, M. N. (2014). *Effect of hot water fibre treatment on the properties of kenaf/polyester composites*. (Doctor of Philosophy), University of New South Wales, Sydney, Australia.

Zampaloni, M., Pourboghra, F., Yankovich, S. A., Rodgers, B. N., Moore, J., Drzal, L. T., Misra, M. (2007). Kenaf natural fiber reinforced polypropylene composites: A discussion on manufacturing problems and solutions. *Composites Part A: Applied Science and Manufacturing*, 38(6), 1569-1580.

Zhao, L., & Boluk, Y. (2010). XPS and IGC characterization of steam treated triticale straw. *Applied Surface Science*, 257(1), 180-185.

Zhao, X., van der Heide, E., Zhang, T., & Liu, D. (2010). Delignification of sugarcane bagasse with alkali and peracetic acid and characterization of the pulp. *BioResources*, 5(3), 1565-1580.

Zimniewska, M., Wladyka-Przybylak, M., & Mankowski, J. (2011). Cellulose bast fibers, their structure and properties suitable for composite applications. In S. Kalia, B. S. Kaith & I. Kaur (Eds.), *Cellulose fibers: Bio- and nano-polymer composites* (pp. 97-119). Heidelberg: Springer.



## **Appendix I: Chemical Treatment of Fibres and Alpha-Cellulose**





## I.A EDTA Treatment

Various stages in the EDTA treatment are shown in Figure I.1. While some change in colour of the solution is evident during the process, no breakdown of the technical fibres occurred.

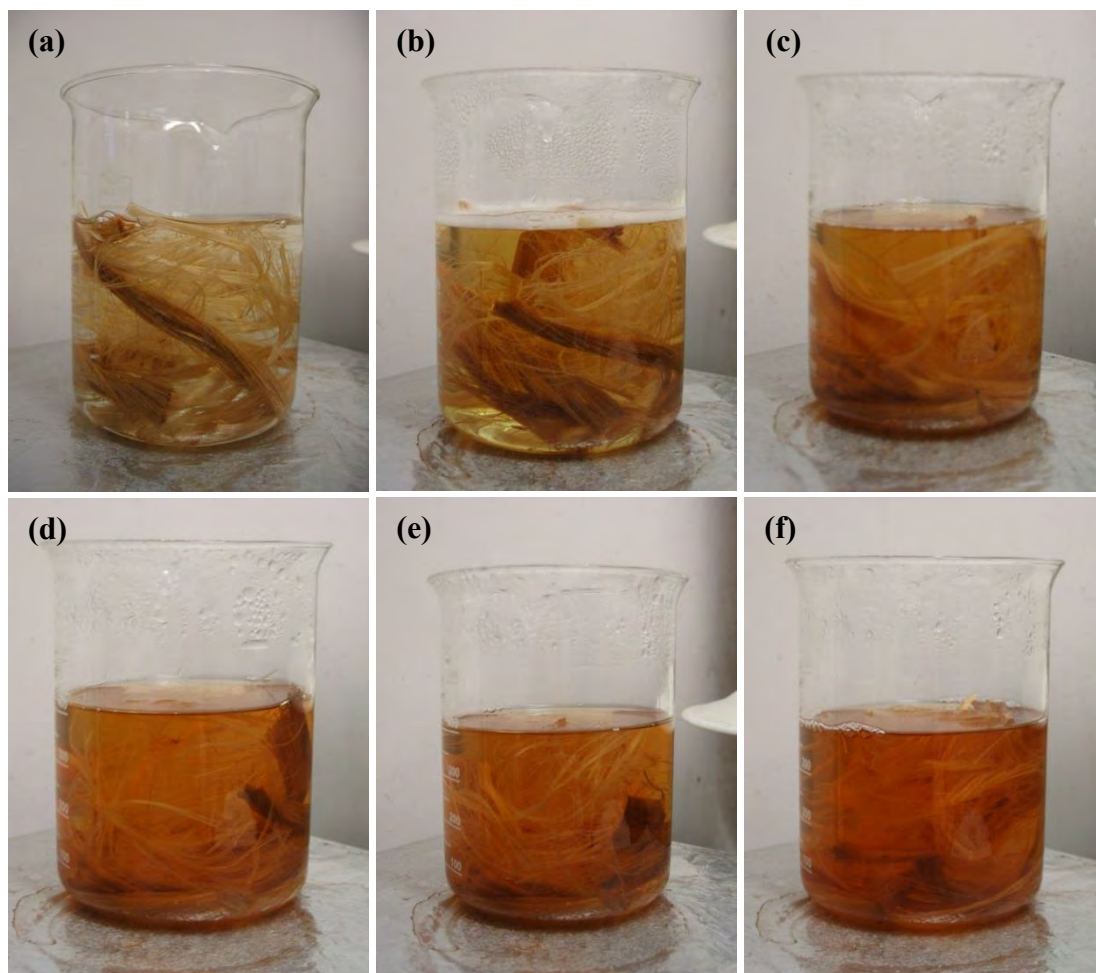


**Figure I.1:** Untreated kenaf fibre bundles immersed in EDTA/NaOH at a pH of 11 (a) at room temperature, (b) after 30 minutes at 60°C, (c) after 3 hours at 60°C, (d) after 5 hours at 60°C, (e) after 7 hours at 60°C, and (f) after 24 hours at 60°C.

## I.B EDTA/Pectinase Treatment

EDTA treated fibres were also subsequently treated with pectinase. Stages in the pectinase treatment are shown in Figure I.2. No break down of the EDTA of the technical fibres occurred during this subsequent treatment.

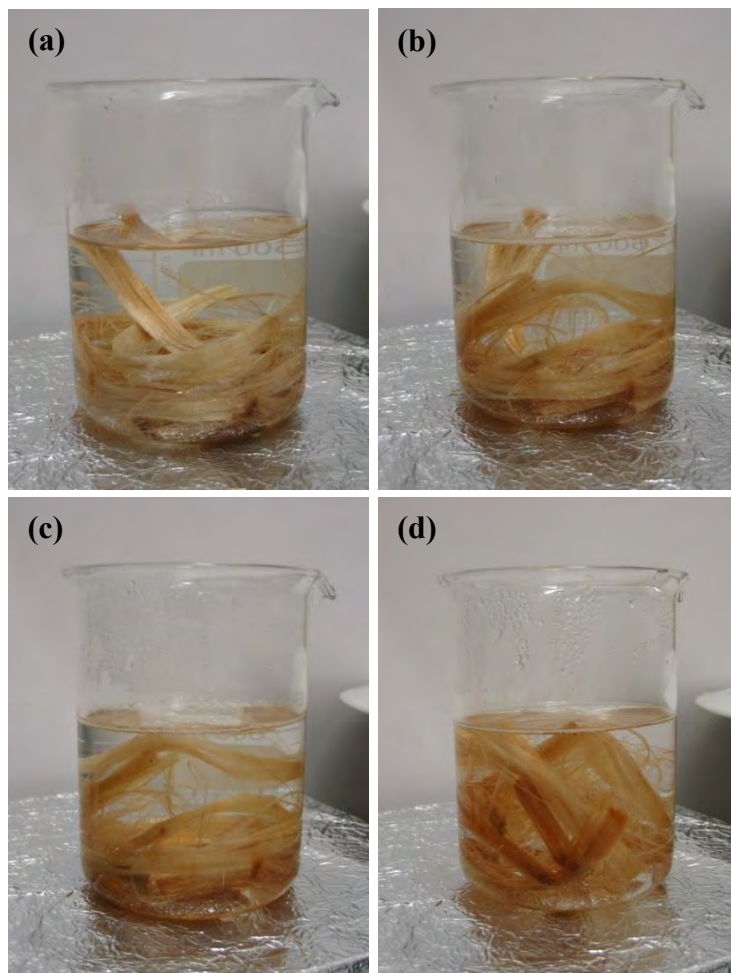


**Figure I.2:** EDTA treated kenaf fibres immersed in  $\text{CH}_3\text{COOH}$  distilled water solution containing Pectinex<sup>®</sup> Ultra SPL at a pH of 4.5, (a) immediately upon immersion, (b) after 30 minutes, (c) after 1 hour and (d) after 2 hours.

## I.C Sulphuric Acid Treatment

Stages during the process of sulphuric acid treatment are shown in Figure I.3. The solution can be seen to have turned black.

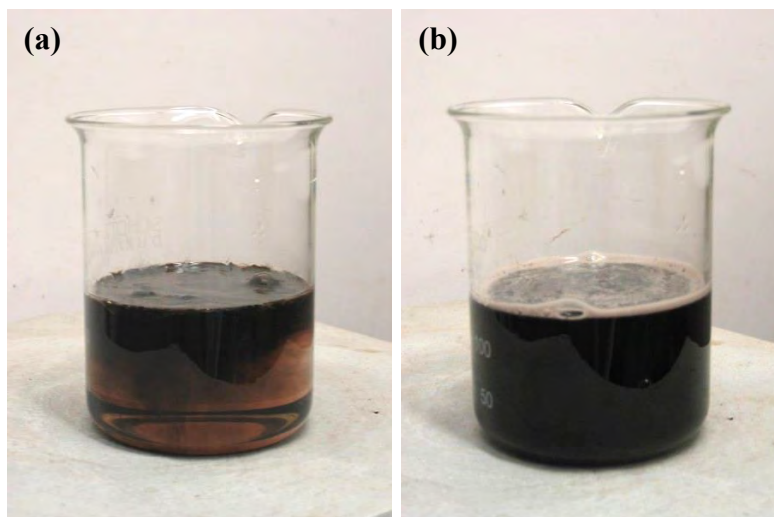


**Figure I.3:** Untreated kenaf fibre bundles immersed in 60%  $\text{H}_2\text{SO}_4$  (a) at room temperature and (b) after 75 minutes at 55°C.

## I.D Nitric Acid Treatment

The nitric acid treatment is shown in Figure I.4. The solution changed from colourless to orange on addition of the fibres, Figure I.4a. On heating, the solution darkened and became cloudy due to the presence of elementary fibres, Figure I.4b. The colour then changed to yellow when the solution was cooled, with the elementary fibres settling to the bottom, Figure I.4c. The elementary fibres were not visible for several days if the solution was not heated.

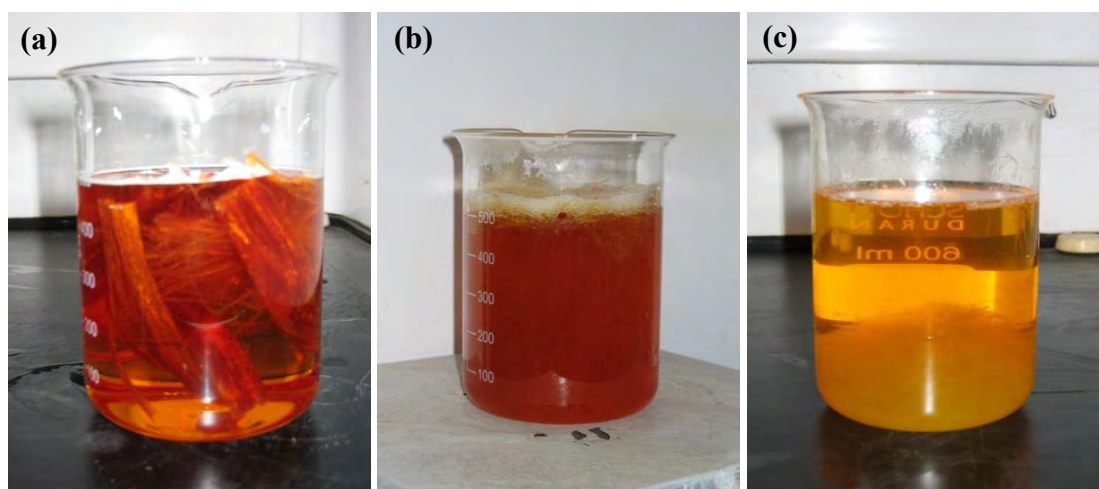


**Figure I.4:** Untreated kenaf fibre bundles (a) immersed in 60%  $\text{HNO}_3$  at room temperature, (b) solution after 30 minutes at  $80^\circ\text{C}$  and (c) solution after cooling to room temperature.

## I.E 30% Hydrogen Peroxide/Glacial Acetic Acid Treatment

Stages in the 30% hydrogen peroxide/glacial acetic acid treatment are shown in Figure I.5. The solution was initially clear, Figure I.5a, but then became yellow in colour, Figure I.5c, eventually again becoming clear and containing white elementary fibres, Figure I.5f.

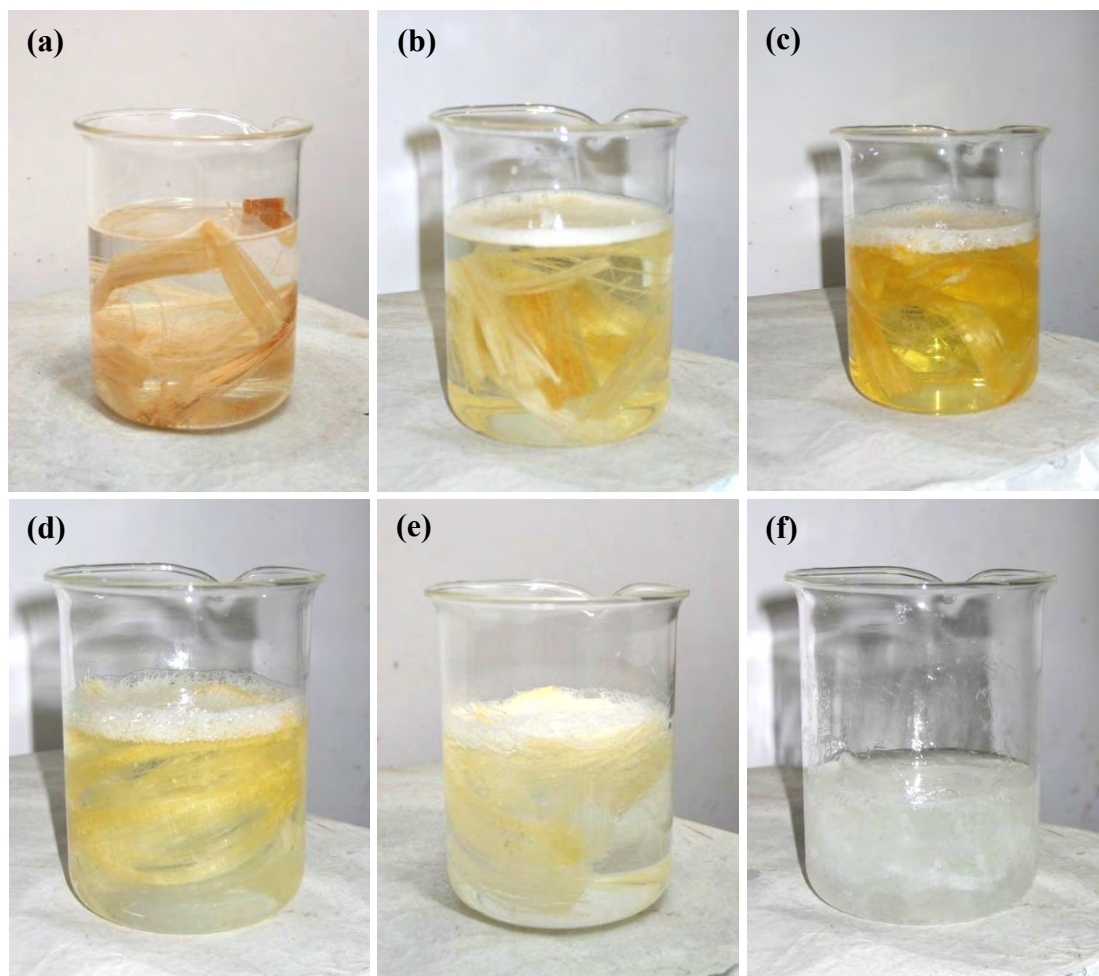


**Figure I.5:** 30%  $\text{H}_2\text{O}_2/\text{CH}_3\text{COOH}$  treatment (a) fibre bundles immersed in solution at room temperature, (b) after 30 minutes at  $60^\circ\text{C}$ , (c) after 3 hours at  $60^\circ\text{C}$ , (d) after 5 hours at  $60^\circ\text{C}$ , (e) after 7 hours at  $60^\circ\text{C}$  and (f) after 24 hours at  $60^\circ\text{C}$ .



## I.F 20% Hydrogen Peroxide/Glacial Acetic Acid Treatment

Stages in the 20% hydrogen peroxide/glacial acetic acid treatment are shown in Figure I.6. The process was similar to that observed for the 30% hydrogen peroxide/glacial acetic acid treatment, with the solution becoming yellowish initially, then becoming clear again with white elementary fibres present.

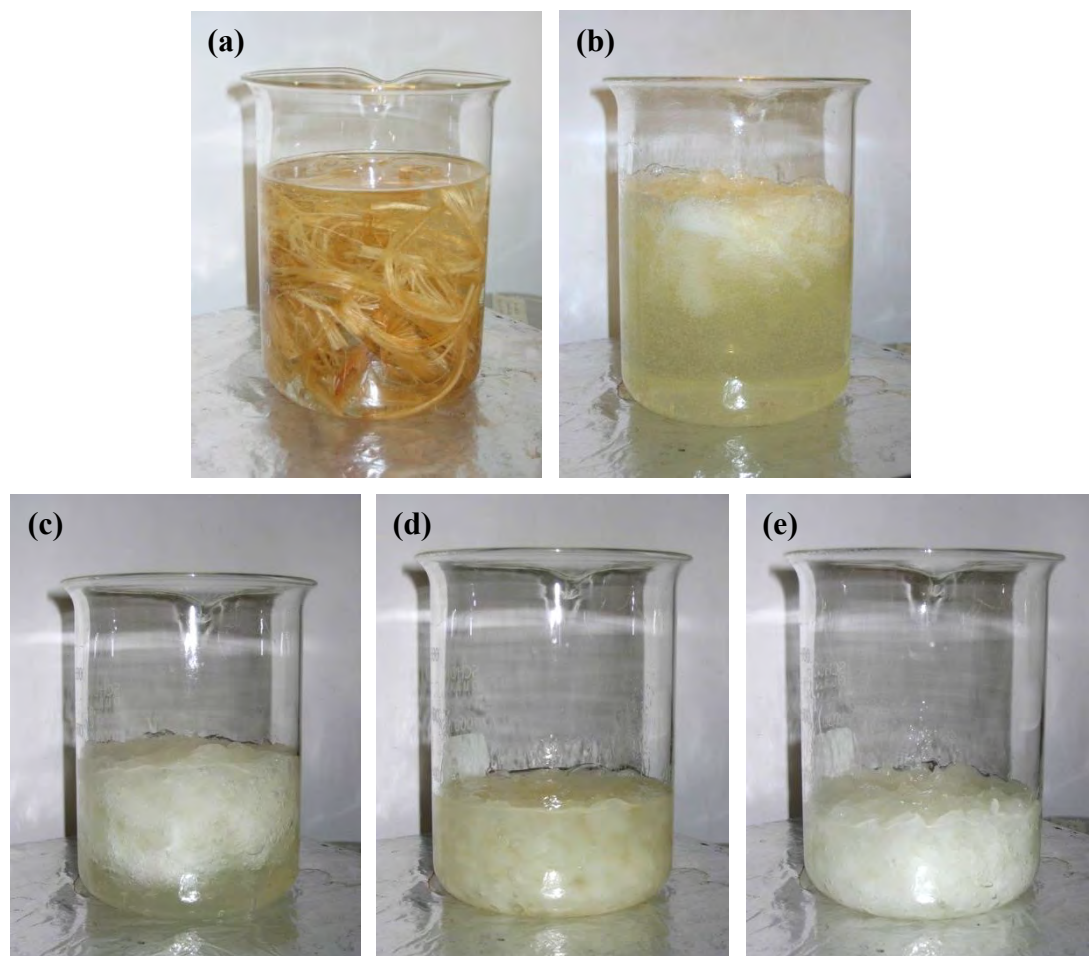


**Figure I.6:** 20%  $\text{H}_2\text{O}_2/\text{CH}_3\text{COOH}$  treatment (a) fibre bundles immersed in solution at room temperature, (b) after 30 minutes at  $98^\circ\text{C}$ , (c) after 3 hours at  $98^\circ\text{C}$ , (d) after 5 hours at  $98^\circ\text{C}$  and (e) after 7 hours at  $98^\circ\text{C}$ .

## I.G Glacial Acetic Acid Treatment

Stages during the glacial acetic acid treatment are shown in Figure I.7. No breakdown of the technical fibres occurred.

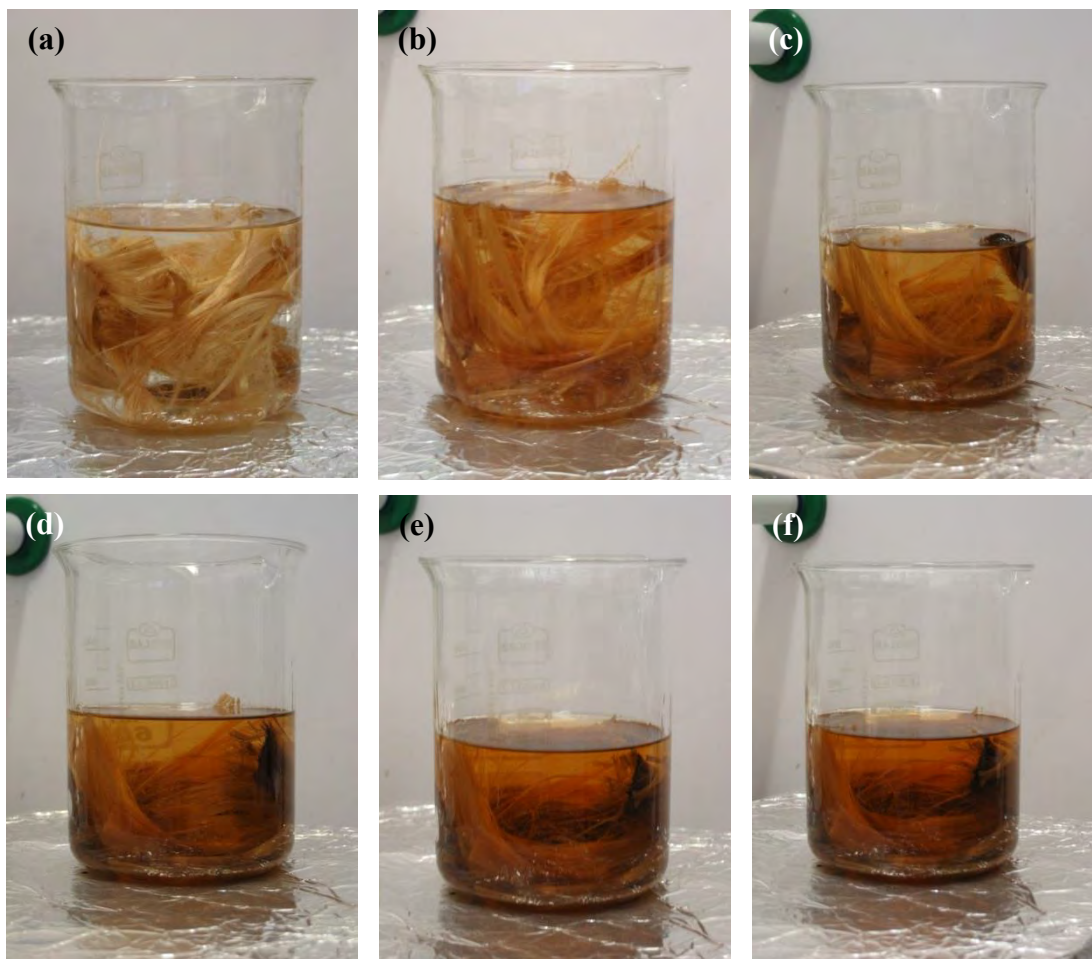


**Figure I.7:** Glacial  $\text{CH}_3\text{COOH}$  treatment (a) fibre bundles immersed in solution at room temperature, (b) after 30 minutes at  $98^\circ\text{C}$ , (c) after 1 hour at  $98^\circ\text{C}$ , (d) after 3 hours at  $98^\circ\text{C}$ , (e) after 5 hours at  $98^\circ\text{C}$  and (f) after 7 hours at  $98^\circ\text{C}$ .



## I.H Nitric Acid and Hydrogen Peroxide/Acetic Acid Treatment of Alpha-Cellulose

Nitric acid treatment of the  $\alpha$ -cellulose is shown at various stages in the process in Figure I.8 while soaking of the  $\alpha$ -cellulose in the hydrogen peroxide/acetic acid solution is shown in Figure I.9.

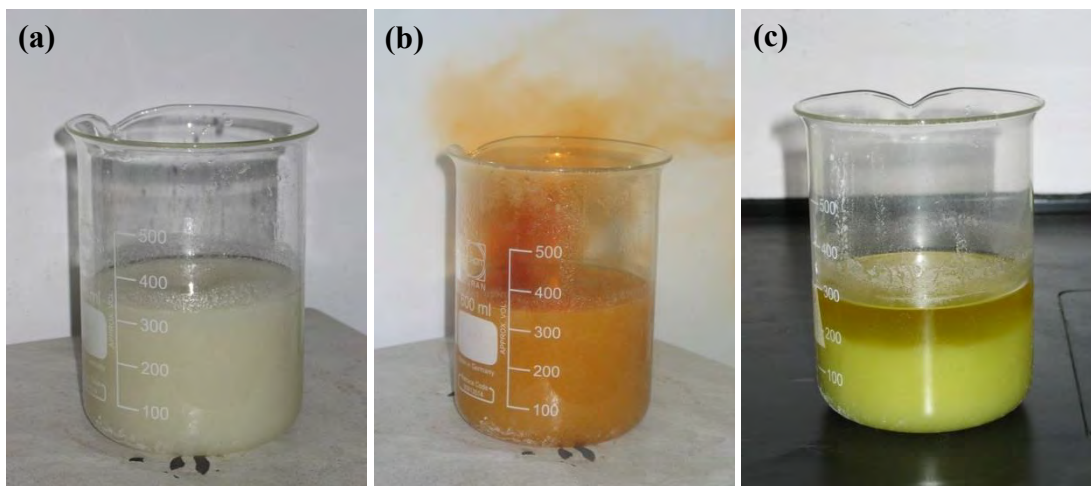


**Figure I.8:**  $\alpha$ -cellulose immersed in 60%  $\text{HNO}_3$  solution (a) at room temperature, (b) after 30 minutes at  $80^\circ\text{C}$  and (c) after cooling to room temperature.



**Figure I.9:**  $\alpha$ -cellulose immersed in a mixture of  $\text{H}_2\text{O}_2$  and  $\text{CH}_3\text{COOH}$ .

For the nitric acid treatment, the solution became distinctly yellow, Figure I.8, as was observed when treating the kenaf fibres, but the  $\alpha$ -cellulose remained its original white colour. No discolouration of either the solution or the  $\alpha$ -cellulose was observed during either the 20% or 30% hydrogen peroxide/acetic acid treatments, Figure I.9.

## **Appendix II: Defects Density of Elementary Kenaf Fibres**



**Table II.1:** Defect density of elementary kenaf fibres

Sample No.	KFTN Fibres			KFTHA1 Fibres			KFTHA2 Fibres		
	Fibre Length (mm)	No. of Defects	Defects/mm	Fibre Length (mm)	No. of Defects	Defects/mm	Fibre Length (mm)	No. of Defects	Defects/mm
1	0.51	5	9.8	2.86	7	2.4	2.34	34	14.5
2	0.22	5	22.7	2.25	5	2.2	3.25	44	13.5
3	0.45	11	24.4	2.56	38	14.8	1.98	30	15.2
4	0.36	10	27.8	2.73	20	7.3	3.44	21	6.1
5	0.59	5	8.5	1.68	37	22.0	1.61	14	8.7
6	0.32	4	12.5	2.75	33	12.0	2.76	44	15.9
7	0.24	8	33.3	1.90	34	17.9	2.91	31	10.7
8	0.44	8	18.2	1.03	23	22.3	2.92	50	17.1
9	0.47	15	31.9	2.30	41	17.8	1.36	23	16.9
10	0.21	4	19.0	1.99	39	19.6	2.64	45	17.0
<b>Average</b>			<b>21</b>				<b>14</b>		
<b>SD</b>			<b>9</b>				<b>8</b>		
<b>%SD</b>			<b>43%</b>				<b>57%</b>		



## **Appendix III: T Test Output for Defect Density of Elementary Kenaf Fibres**



## T Test Output at 95% Confidence Interval for Defect Density of Elementary Kenaf Fibres

### *KFTN versus KFTHA1*

Sample	N	Mean	Std. Deviation	Std. Error Mean	t	df	P value (One-tailed)	Significant?
KFTN	10	20.81	8.795	2.781	1.901	18	0.0367	Yes
KFTHA1	10	13.83	7.579	2.397				

### *KFTN versus KFTHA2*

Sample	N	Mean	Std. Deviation	Std. Error Mean	t	df	P value (One-tailed)	Significant?
KFTN	10	20.81	8.795	2.781	2.390	18	0.0140	Yes
KFTHA2	10	13.56	3.830	1.211				

### *KFTHA1 versus KFTHA2*

Sample	N	Mean	Std. Deviation	Std. Error Mean	t	df	P value (Two-tailed)	Significant?
KFTHA1	10	13.83	7.579	2.397	0.1005	18	0.9210	No
KFTHA2	10	13.56	3.830	1.211				





## **Appendix IV: Material Data Sheets for HDPE and MAPE**





## SPECIALIST TANK GRADE COTENE™ 3925

Rotational Moulding Powder HDPE

Annealed Density (g/cm<sup>3</sup>): 0.941

MFI (g/10min): 3.5

### Product Description:

COTENE™ 3925 is an octene copolymer polyethylene which exhibits an excellent balance of stiffness and strength, mouldability and long term properties. The unique nature of the resin allows for exceptional processability with shorter cycle times compared with conventional polyethylene grades. This combination of properties makes COTENE™ 3925 an ideal material for use in applications such as large above ground tanks as well as underground tanks. COTENE™ 3925 contains a fully formulated stabilisation package (with a minimum UV8 rating).

The COTENE™ 3925 Tank colour range meets Australian food contact requirements (AS2070:1,8) and the Australian potable (drinking) water standard AS4020.

COTENE™ 3925 is available in the COTENE™ Tank colour range, and custom colours on request.

### Key Characteristics:

- ▶ Excellent stiffness
- ▶ Excellent long term creep resistance
- ▶ Excellent flow and processability
- ▶ Excellent impact strength

### Typical Applications:

- ▶ Large water and chemical tanks
- ▶ Underground tanks
- ▶ Pool filters
- ▶ Kayaks

### Physical Characteristics <sup>1</sup>

	Value	Test Method
Melt Flow Index (MFI)	3.5 g /10min	ASTM D 1238
Annealed Density	0.941 g /cm <sup>3</sup>	ASTM D 1505
Softening Point (Vicat)	123 °C	ASTM D 1525
ESCR F50 (100% IGEPAI)	>500 Hrs	ASTM D 1693
ESCR F50 (10% IGEPAI)	- Hrs	ASTM D 1693
Flexural Modulus (1.3mm/min) <sup>2</sup>	815 MPa	ASTM D 790
Tensile Modulus (0.5mm/min) <sup>2</sup>	695 MPa	ASTM D 638
Tensile Strength at Yield (50mm/min)	21 MPa	ASTM D 638
Elongation at Break (50mm/min)	1500 %	ASTM D 638
ARM Impact Strength (3.2mm sample at -40°C) <sup>2</sup>	95 J	ARM Method
Shore Hardness	61 Shore D	ASTM D 2240
UV Rating (50% Retained Tensile Elongation)	8000 Hrs	ASTM 2565

<sup>1</sup> Data values shown are average values for the base resin and should not be used for specification limits.

<sup>2</sup> Impact strength varies with both part thickness and moulding conditions, therefore prototype testing is highly recommended.

<sup>3</sup> Mechanical testing has been performed on 3.2mm compression moulded samples, prepared to ASTM-D1928. Tensile results utilise Type M-II sample dimensions, while flexural testing has been performed on 25.4mm sample width.

ICO Company disclaim responsibility for results of use of this information, which is furnished without charge, or of any product, method or apparatus mentioned herein. It is the users responsibility to make and be guided by their own tests determining the suitability of any such product, method or apparatus for their purpose. No statement or suggestion herein is to be considered a recommendation or inducement of any use, manufacture or sale that may infringe any patents or otherwise in existence.

*Staying ahead by working together and sharing resources*



29-May-08



**Safety Data Sheet in accordance with Regulation (EC) No  
1907/2006****Licocene PE MA 4351 Fine Grain**

Page 1

Substance key: 000000183750  
Version : 1 - 2 / EURevision Date: 05.12.2007  
Date of printing : 16.06.2009**1. Identification of the substance/preparation and of the company/undertaking****Trade name**

Licocene PE MA 4351 Fine Grain

**Material number:** 202386**Use of the substance/preparation.**

Industry sector :	Polymers industry
	Paints, lacquers and varnishes industry
Type of use :	Additive

**Identification of the company**

Clariant Produkte (Deutschland) GmbH

86368 Gersthofen

Telephone no. : +49 6196 757 60

**Information about the substance/preparation**

Division Pigments &amp; Additives

+49 (0)821 479 2521

e-mail: PA.PSGERSTHOFEN@CLARIANT.COM

**Emergency telephone number :** +49 69 305 6418**2. Hazards identification**

According to the present state of knowledge provided this product is handled correctly, there is no danger to humans or the environment

The relevant minimum standards for protective measures in the chemical industry should be observed.

**3. Composition/information on ingredients****Chemical characterization**

ethylene-maleic anhydride copolymer

**CAS number :** 9006-26-2**4. First aid measures****General information**

Seek medical assistance if discomfort continues

**After contact with skin**

After contact with molten product cool quickly with cold water

Do not pull solidified product from skin

Take for medical treatment

**After contact with eyes**

Rinse the affected eye with plenty of water, at the same time keep the unaffected eye well protected.

**Advice to doctor**

**Safety Data Sheet in accordance with Regulation (EC) No  
1907/2006****Licocene PE MA 4351 Fine Grain**

Page 2

Substance key: 000000183750  
Version : 1 - 2 / EURevision Date: 05.12.2007  
Date of printing : 16.06.2009**Symptoms**

Until now no symptoms known so far.

**5. Fire-fighting measures****Suitable extinguishing media**water mist  
foam  
dry powder  
carbon dioxide**Special hazards from the substance itself, its combustion products or from its vapours**

None known.

**Special protective equipment for firefighting**

Impermeable protective clothing (jacket and trousers) with helmet.

**6. Accidental release measures****Environmental precautions**

Do not allow entry to drains, water courses or soil

**Methods for cleaning up/taking up**

Take up mechanically

**7. Handling and storage****Advice on safe handling**Provide suitable exhaust ventilation at processing machines.  
Take precautionary measures against electrostatic loading.**Advice on protection against fire and explosion**Take precautions against accumulation of electrostatic charge  
Observe the general rules of industrial fire protection

Fire class :

B

**8. Exposure controls / personal protection****Occupational exposure controls****General protective measures**

Avoid contact of molten material with skin

**Hygiene measures**Wash hands before breaks and after work.  
At work do not eat, drink, smoke or take drugs.  
Use barrier skin cream.



**Safety Data Sheet in accordance with Regulation (EC) No  
1907/2006****Licocene PE MA 4351 Fine Grain**

Page 3

Substance key: 000000183750  
Version : 1 - 2 / EURevision Date: 05.12.2007  
Date of printing : 16.06.2009

<b>Hand protection :</b>	Nitrile rubber gloves. Minimum breakthrough time (glove): not determined Minimum thickness (glove): not determined Observe the information of the glove manufacturers on permeability and breakthrough times and other workplace requirements
<b>Eye protection :</b>	safety glasses
<b>Body protection :</b>	working clothes

**9. Physical and chemical properties**

<b>Form :</b>	Fine grain / Granulate
<b>Colour :</b>	yellowish
<b>Odour :</b>	not specified
<b>Drop forming point :</b>	approx. 123 °C Method : ASTM D 3954-94
<b>Flash point :</b>	not tested.
<b>Oxidizing properties :</b>	not tested.
<b>Flammability</b>	
<b>Lower explosion limit :</b>	not tested.
<b>Upper explosion limit :</b>	not tested.
<b>Combustion number :</b>	not tested.
<b>Evaporation rate :</b>	not tested.
<b>Vapour pressure :</b>	Not applicable
<b>Density :</b>	approx. 0,99 g/cm <sup>3</sup> (23 °C) Method : ISO 1183
<b>Vapour density in relation to air :</b>	not tested.
<b>Solubility in water :</b>	(20 °C) insoluble
<b>Soluble in ... :</b>	not tested.
<b>pH value :</b>	Not applicable
<b>Acid number (mgKOH/g) :</b>	approx. 46 mg/g
<b>Octanol/water partition coefficient (log Pow) :</b>	not tested.
<b>Viscosity (dynamic) :</b>	approx. 300 mPa.s (140 °C) Method : DIN 53018

**Safety Data Sheet in accordance with Regulation (EC) No  
1907/2006****Licocene PE MA 4351 Fine Grain**

Page 4

Substance key: 000000183750  
Version : 1 - 2 / EURevision Date: 05.12.2007  
Date of printing : 16.06.2009**10. Stability and reactivity****Thermal decomposition :** No decomposition if used as prescribed.**Hazardous reactions**  
No hazardous reactions known.**Hazardous decomposition products**  
No hazardous decomposition products known.**11. Toxicological information****Acute oral toxicity :** LD50 > 2.000 mg/kg (rat)**Remarks**  
The product has not been tested. The statements are derived from products of a similar composition.**12. Ecological information****Remarks**  
Product is insoluble in water  
Harmful effects to fish and bacteria: not harmful  
May be separated out mechanically in treatment plants  
The ecotoxicity of the product has not been tested. The information given is based on products of similar structure or composition.**13. Disposal considerations****Product**  
In accordance with the necessary technical regulations may be dumped or incinerated with household waste, after consultation with site operator and with the responsible authority  
Material may be recycled**Uncleaned packaging**  
Packaging that cannot be cleaned should be disposed of as product waste**14. Transport information**

ADR	not restricted
ADNR	not restricted
RID	not restricted
IATA	not restricted
IMDG	not restricted



**Safety Data Sheet in accordance with Regulation (EC) No  
1907/2006****Licocene PE MA 4351 Fine Grain**

Page 5

Substance key: 000000183750  
Version : 1 - 2 / EURevision Date: 05.12.2007  
Date of printing : 16.06.2009**15. Regulatory information****Labelling in accordance with EC-Directives**

The product does not require a hazard warning label in accordance with EC directives/German regulations on dangerous substances.

**Chemical Safety Assessment**

No Chemical Safety Assessment (CSA) is yet available for the substance, or for the component substances, contained in this product.

**16. Other information**

Decimal notation: "Thousands" places are identified with a dot (example: 2.000 mg/kg means "two thousand mg/kg"). Decimal places are identified with a comma (example: 1,35 g/cm<sup>3</sup>).

The data are based on the current state of our knowledge, and are intended to describe the product with regard to the requirements of safety. The data should not be taken to imply any guarantee of a particular or general specification. It is the responsibility of the user of the product to ensure to his satisfaction that the product is suitable for the intended purpose and method of use. We do not accept responsibility for any harm caused by the use of this information. In all cases, our general conditions of sale apply.

## **Appendix V: Tensile Specimens of Extruded HDPE and Composite Strips after Testing**





**Figure V.1:** Tensile specimens of extruded HDPE strip after testing.



**Figure V.2:** Tensile specimens of extruded UKF/HDPE strip after testing.



**Figure V.3:** Tensile specimens of extruded KFTN/HDPE strip after testing.



**Figure V.4:** Tensile specimens of extruded KFTHA/HDPE strip after testing.



**Figure V.5:** Tensile specimens of hot pressed extruded HDPE (HDPE\_H) strip after testing.



**Figure V.6:** Tensile specimens of hot pressed extruded HDPE/MAPE (HDPE/MAPE\_H) strip after testing.



**Figure V.7:** Tensile specimens of hot pressed extruded UKF/HDPE composites (UKF/HDPE\_H) strip after testing.



**Figure V.8:** Tensile specimens of hot pressed extruded KFTN/HDPE (KFTN/HDPE\_H) strip after testing.



**Figure V.9:** Tensile specimens of hot pressed extruded KFTHA/HDPE (KFTHA/HDPE\_H) strip after testing.



## **Appendix VI: Process for Determining Fibre Weight Fraction of Extruded Composites**





## VI.A Process for Determining Fibre Weight Fraction of Rod Composites

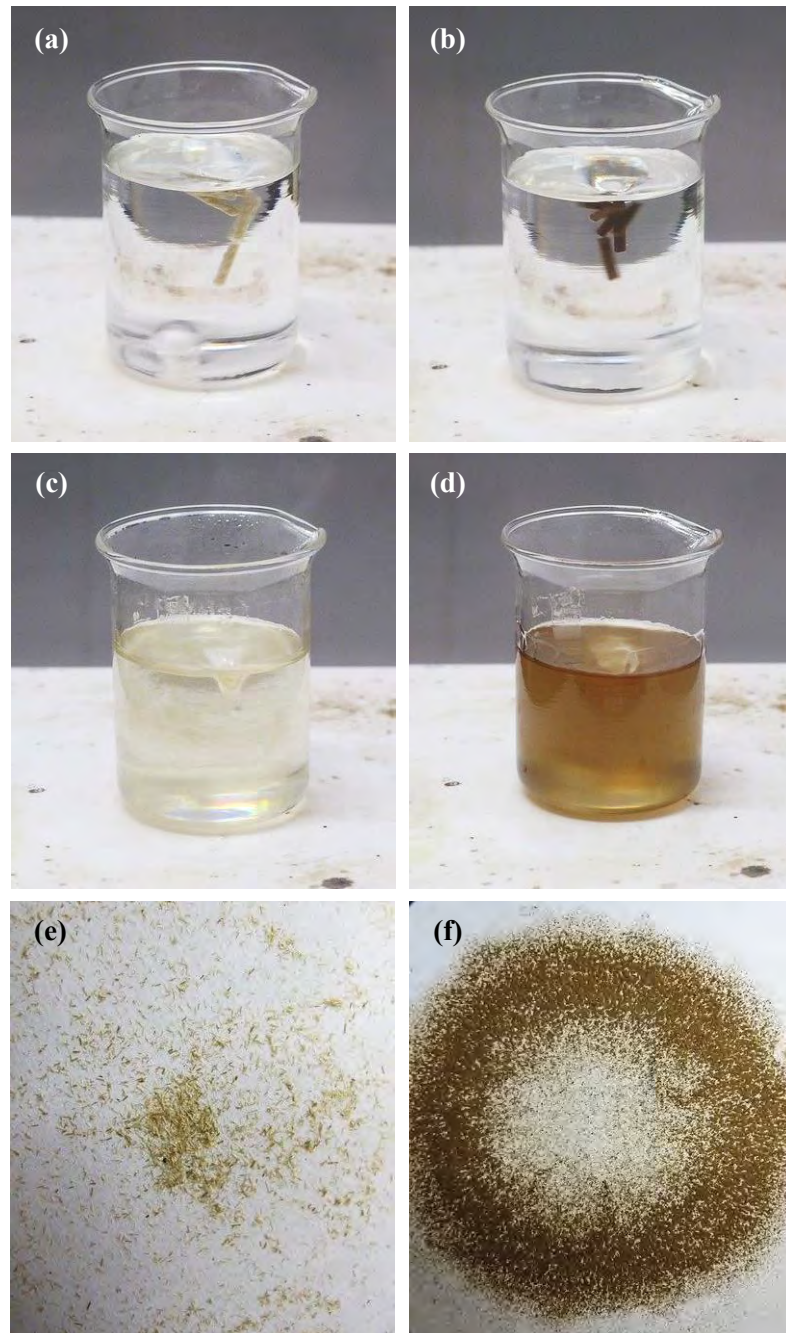


**Figure VI.1:** UKF/HDPE (a) and KFTN/HDPE (b) rod composites immersed in stirred trichlorobenzene, HDPE from UKF/HDPE (c) and KFTN/HDPE (d) dissolved in hot trichlorobenzene, and filtered UKF (e) and KFTN (f) fibres.

## VI.B Process for Determining Fibre Weight Fraction of Strip Composites

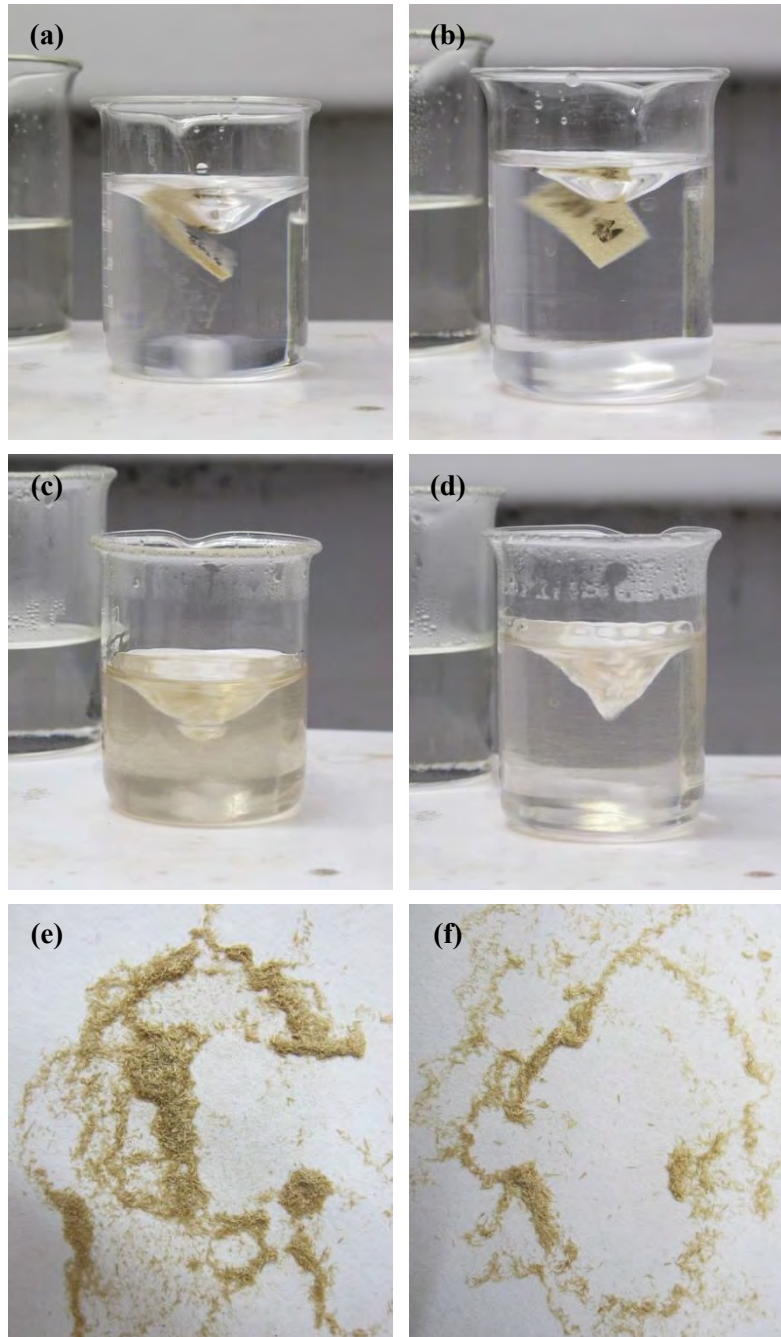


**Figure VI.2:** UKF/HDPE (a) and UKF/HDPE\_H (b) strip composites immersed in stirred trichlorobenzene, HDPE from UKF/HDPE (c) and UKF/HDPE\_H (d) dissolved in hot trichlorobenzene, and filtered UKF fibres from UKF/HDPE (e) and UKF/HDPE\_H (f).

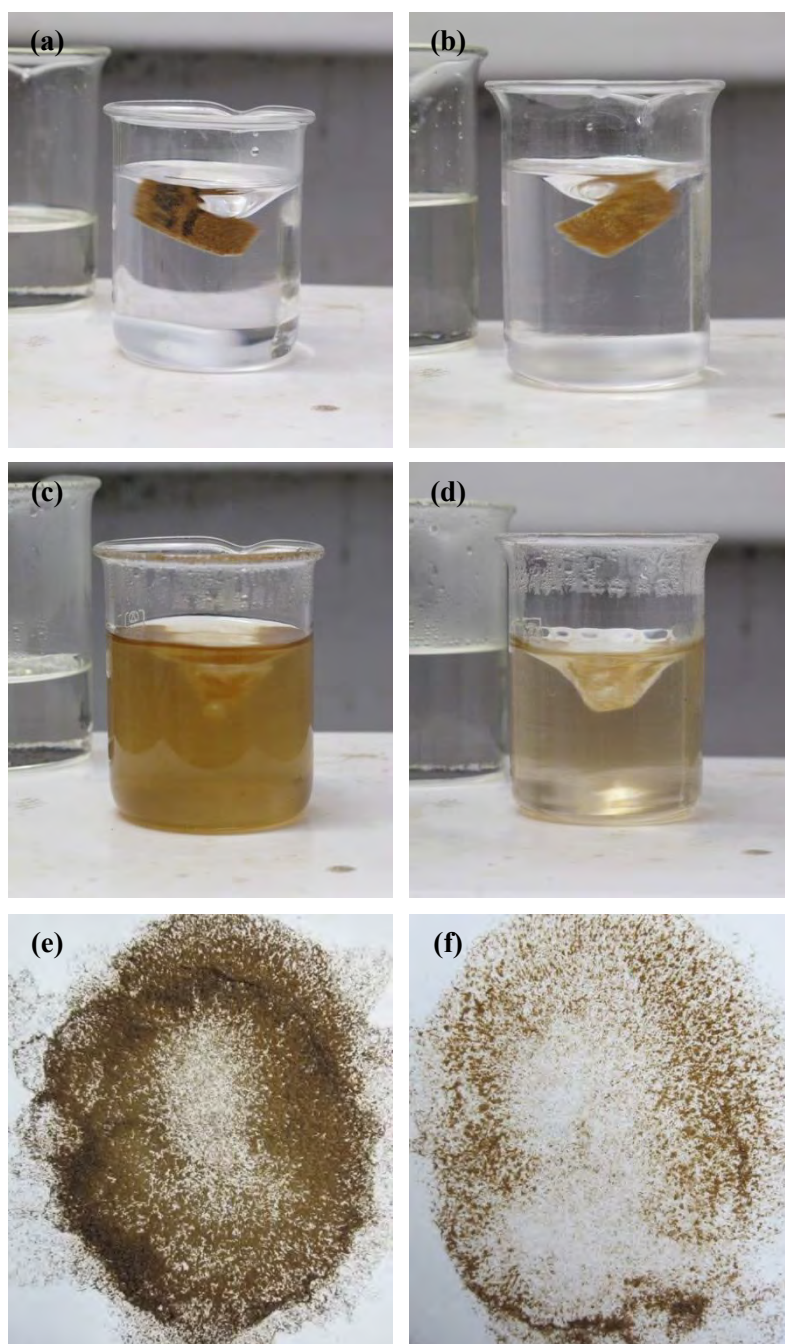


**Figure VI.3:** KFTN/HDPE (a) and KFTN/HDPE\_H (b) strip composites immersed in stirred trichlorobenzene, HDPE from KFTN/HDPE (c) and KFTN/HDPE\_H (d) dissolved in hot trichlorobenzene, and filtered KFTN fibres from KFTN/HDPE (e) and KFTN/HDPE\_H (f).



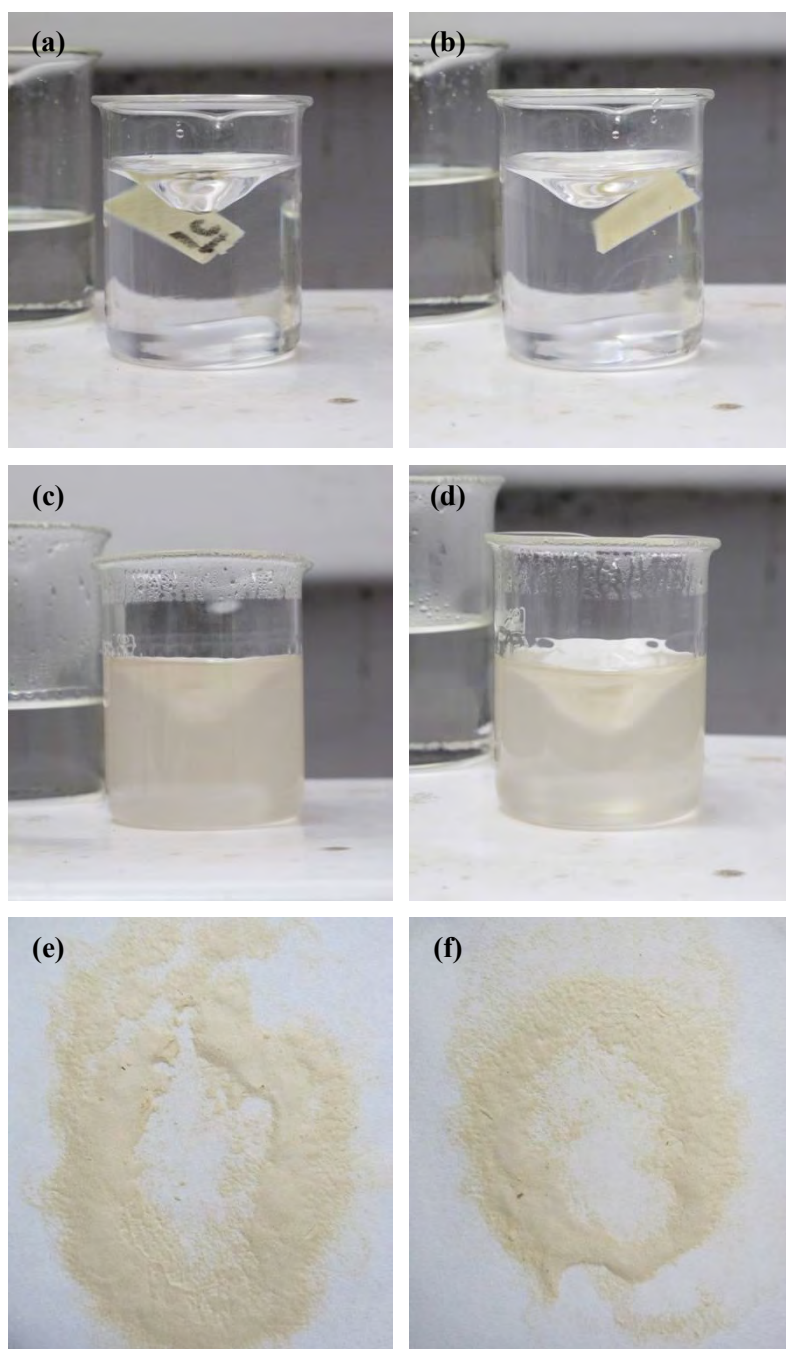


**Figure VI.4:** KFTHA/HDPE (a) and KFTHA/HDPE\_H (b) strip composites immersed in stirred trichlorobenzene, HDPE from KFTHA/HDPE (c) and KFTHA/HDPE\_H (d) dissolved in hot trichlorobenzene, and filtered KFTHA fibres from KFTHA/HDPE (e) and KFTHA/HDPE\_H (f).

## **Appendix VII: Measured Fibre Weight Fractions of Extruded Composites**



**Table VII.1:** Measured fibre weight fractions of extruded kenaf fibre/HDPE rod composite

Sample No.	Fibre Weight Fraction (%)	
	UKF/HDPE	KFTN/HDPE
1	39.20	31.34
2	36.84	36.02
3	33.48	33.85
4	38.22	37.71
5	35.84	27.14
6	34.06	29.77
7	37.42	32.69
8	38.22	31.26
9	35.66	31.87
10	40.20	37.42
11	41.53	37.64
12	37.91	37.86
13	36.80	34.38
14	36.87	31.24
15	33.44	29.53
16	34.64	34.57
17	35.85	38.89
18	33.01	39.93
19	40.64	29.60
20	36.97	30.36
21	33.87	28.84
22	35.96	30.87
<b>Average</b>	<b>36.67</b>	<b>33.31</b>
<b>SD</b>	<b>2.40</b>	<b>3.71</b>



**Table VII.2:** Measured fibre weight fractions of extruded kenaf fibre/HDPE strip composites

<b>Sample Name</b>	<b>Sample No.</b>	<b>Fibre Weight Fraction (%)</b>
UKF/HDPE	1 (3A)	22.42
	2 (3D)	10.56
	3 (3G)	17.55
	4 (3H)	16.52
	<b>Average</b>	<b>16.76</b>
	<b>SD</b>	<b>4.87</b>
KFTN/HDPE	1 (2A)	20.80
	2 (2D)	43.57
	3 (2E)	53.34
	4 (2G)	6.13
	<b>Average</b>	<b>34.35</b>
	<b>SD</b>	<b>24.92</b>
KFTHA/HDPE	1 (1C)	40.16
	2 (1D)	27.70
	3 (1E)	43.51
	4 (1H)	8.85
	<b>Average</b>	<b>30.05</b>
	<b>SD</b>	<b>15.69</b>

**Table VII.3:** Measured fibre weight fraction of hot pressed extruded kenaf fibre/HDPE strip composites

Sample Name	Sample No.	Fibre Weight Fraction (%)
UKF/HDPE_H	1 (7A)	25.67
	2 (7C)	9.82
	3 (7D)	13.54
	4 (7E)	8.55
	<b>Average</b>	<b>14.39</b>
	<b>SD</b>	<b>7.81</b>
KFTN/HDPE_H	1 (8A)	10.92
	2 (8B)	6.96
	3 (8D)	7.25
	4 (8E)	7.08
	<b>Average</b>	<b>8.05</b>
	<b>SD</b>	<b>1.92</b>
KFTHA/HDPE_H	1 (6B)	37.42
	2 (6D)	44.82
	3 (6F)	28.73
	4 (6H)	8.56
	<b>Average</b>	<b>29.88</b>
	<b>SD</b>	<b>15.66</b>



## **Appendix VIII: Process for Soaking Untreated and Treated Kenaf Fibres in Hot Trichlorobenzene**



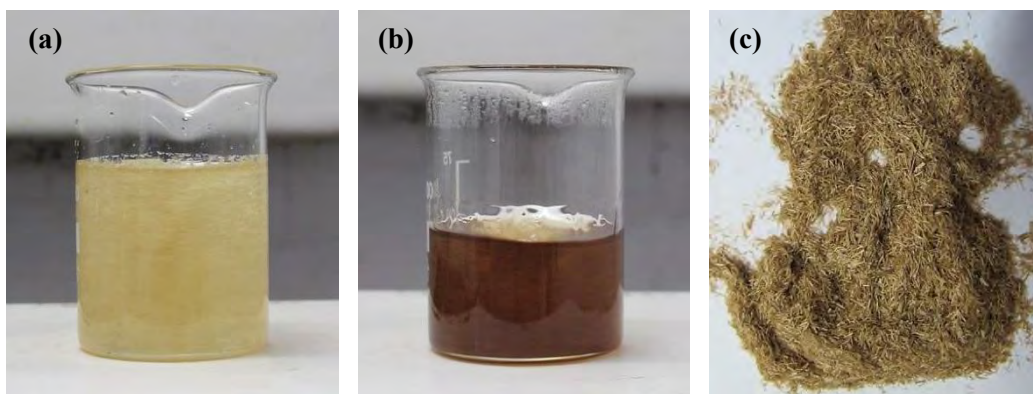


**Figure VIII.1:** (a) UKF fibres immersed in stirred trichlorobenzene, (b) UKF fibres after soaking in hot trichlorobenzene for 1 hour, and (c) filtered UKF fibres.

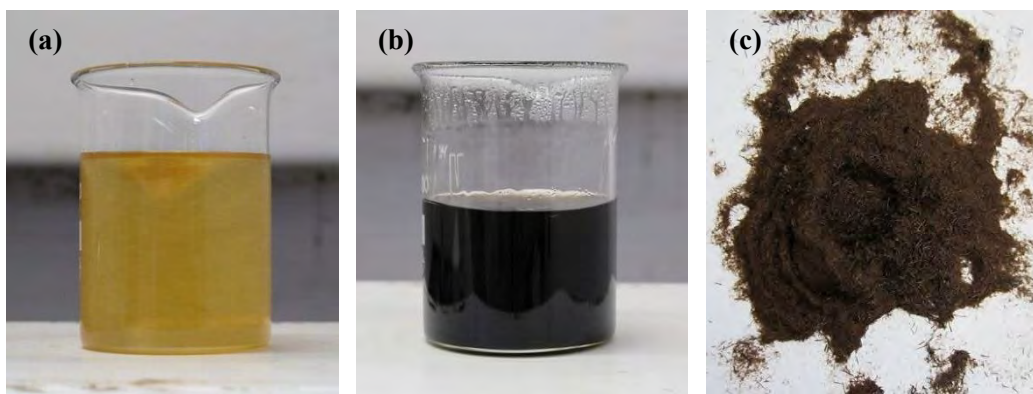


**Figure VIII.2:** (a) KFTN fibres immersed in stirred trichlorobenzene, (b) KFTN fibres after soaking in hot trichlorobenzene for 1 hour, and (c) filtered KFTN fibres.

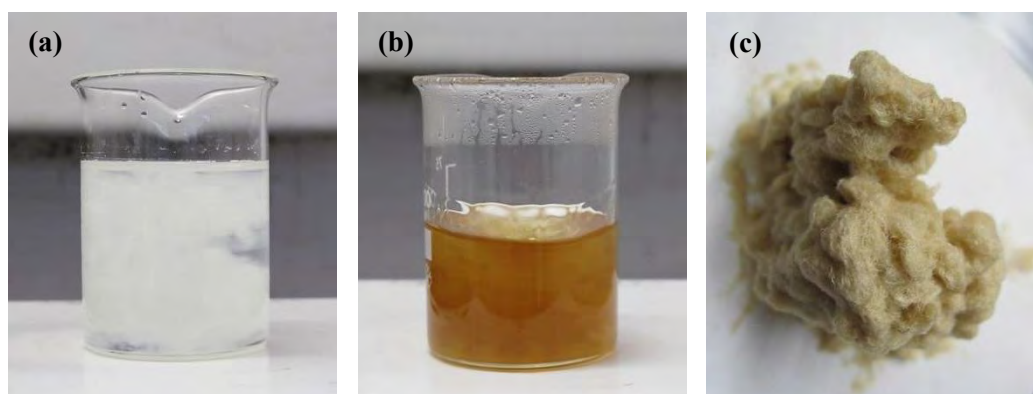


**Figure VIII.3:** (a) KFTHA fibres immersed in stirred trichlorobenzene, (b) KFTHA fibres after soaking in hot trichlorobenzene for 1 hour, and (c) filtered KFTHA fibres.



**Appendix IX: Peak Assignations for FTIR Spectra of  
Residue from Filtered Solution of Untreated and  
Treated Kenaf Fibres Soaked in Hot Trichlorobenzene**





The FTIR spectrum of the residue from the filtered solution of the UKF fibres soaked in hot trichlorobenzene is shown in Figure IX.1, while possible peak assignments are given in Table IX.1. The spectrum of this residue appears to be a combination of the FTIR spectra of lignin (Figure IX.2) and wax (Figure IX.3). Thus, the residue from the filtered solution of the UKF fibres soaked in hot trichlorobenzene was considered to be lignin and wax.

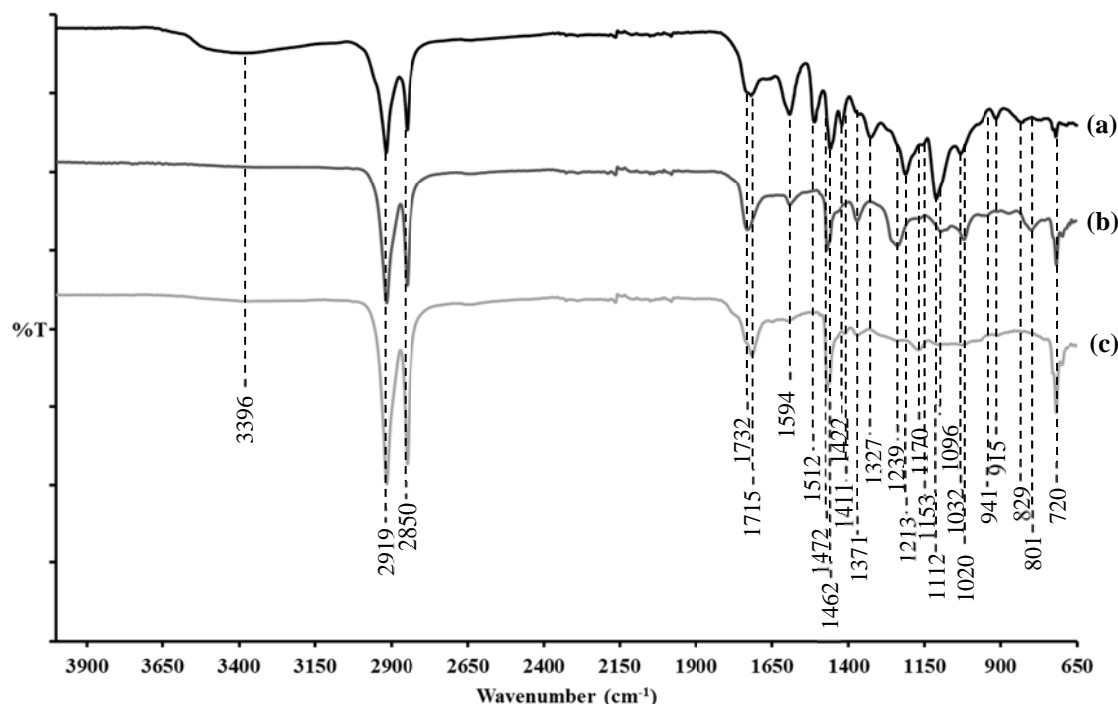


**Figure IX.1:** FTIR spectra of residue from filtered solution of (a) UKF, (b) KFTN and (c) KFTHA fibres soaked in hot trichlorobenzene.

The FTIR spectrum of the residue from the filtered solution of the KFTN fibres soaked in hot trichlorobenzene is shown in Figure IX.1 while possible peak assignments are given in Table IX.2. The FTIR spectrum of this residue tends to resemble that of ethylene-vinyl acetate copolymer (EVA) (Figures IX.4 and IX.5). The chemical structure of EVA is shown in Figure IX.6. The spectrum of this residue also shows some absorption peaks corresponding to disubstituted benzene rings providing further evidence of the presence of EVA.

**Table IX.1:** Possible assignments of peak positions of FTIR band of residue from filtered solution of UKF fibres soaked in hot trichlorobenzene

Peak Position (cm <sup>-1</sup> )	Possible assignment
3,396	O-H stretching vibrations (the average stretching of intermolecular hydrogen bonding) in lignin <sup>1</sup>
2,919	C-H stretching vibrations in lignin <sup>2</sup> and asymmetric $\nu\text{CH}_2$ in wax <sup>3</sup>
2,850	C-H stretching vibrations in lignin <sup>2</sup> and symmetric $\nu\text{CH}_2$ in wax <sup>3</sup>
1,715	Unconjugated C=O stretching vibrations in lignin <sup>2</sup>
1,594	Aromatic skeletal vibrations combined with C=O stretching vibrations in lignin <sup>1</sup>
1,512	Aromatic skeletal vibrations in lignin <sup>1</sup>
1,462	C-H deformation combined with aromatic ring vibrations in lignin <sup>4</sup> and -C-H in wax <sup>5</sup>
1,422	C-H in-plane deformation combined with aromatic ring stretching vibrations in lignin <sup>2</sup>
1,371	$\delta\text{CH}_2$ in-plane deformation vibrations i.e. bending vibrations in wax <sup>6</sup>
1,327	C-O vibrations of the syringyl ring in lignin <sup>1</sup>
1,213	C-C and C-O stretching vibrations in lignin <sup>1</sup>
1,153	Aromatic C-H in-plane deformation in the guaiacyl ring in lignin <sup>1</sup>
1,112	Aromatic C-H deformation in the syringyl ring in lignin <sup>1</sup>
1,032	Aromatic C-H deformation (C-O, C-C stretching vibrations and C-OH bending vibrations in polysaccharides) in lignin <sup>4</sup>
915	C-H out-of-plane vibrations in lignin <sup>2</sup>
829	C-H out-of-plane vibrations of guaiacyl units in lignin <sup>4</sup>
720	Doublet $\gamma\text{CH}_2$ (out-of-plane deformation vibrations i.e. rocking vibrations) in wax <sup>6</sup>

<sup>1</sup> Kubo & Kadla (2005)

<sup>2</sup> Pandey (1999)

<sup>3</sup> Merk, Blume & Riederer (1997)

<sup>4</sup> Boeriu et al. (2004)

<sup>5</sup> Athukorala, Mazza & Oomah (2009)

<sup>6</sup> Lattuat-Derieux et al. (2009)

*Figure IX.2 has been removed due to Copyright restrictions.*

**Figure IX.2:** FTIR spectrum of softwood lignin (SKL) and hardwood lignin (HKL)  
(Kubo & Kadla, 2005).

*Figure IX.3 has been removed due to Copyright restrictions.*

**Figure IX.3:** FTIR spectrum of reconstituted cuticular wax from *Hedera helix* leaves  
(Merk, Blume & Riederer, 1997).

**Table IX.2:** Possible assignments of peak positions of FTIR band of residue from filtered solution of KFTN fibres soaked in hot trichlorobenzene

Peak Position (cm <sup>-1</sup> )	Possible assignment
2,919	CH <sub>2</sub> asymmetric stretching vibrations <sup>1</sup> in EVA <sup>2</sup>
2,850	CH <sub>2</sub> symmetric stretching vibrations <sup>1</sup> in EVA <sup>2</sup>
1,732	Symmetric C=O stretching vibrations of ester groups in EVA <sup>3,4</sup>
1,594	C=C aromatic stretching vibrations in benzene <sup>5</sup>
1,472	>CH <sub>2</sub> scissor vibrations in EVA <sup>3</sup>
1,371	C-H bending vibrations of CH <sub>3</sub> in EVA <sup>3</sup>
1,239	C-O stretching vibrations of ester and acids in EVA <sup>3</sup>
1,096	C-O-C stretching vibrations of ether in EVA <sup>3</sup> and/or C-H in-plane bending vibrations of <i>p</i> -substituted benzene <sup>5</sup>
1,020	=C-O-C stretching vibrations of ester and acids in EVA <sup>3</sup> and/or C-H in-plane bending vibrations in <i>p</i> -substituted benzene <sup>5</sup>
941	C-H deformation of acetate in EVA <sup>3</sup>
801	C-H out-of-plane bending vibrations in <i>m</i> -substituted benzene <sup>5</sup>
720	Rocking deformation in EVA <sup>3</sup>

<sup>1</sup> Gulmine et al. (2002)

<sup>2</sup> Mathias et al. (1992)

<sup>3</sup> Chattopadhyay, Chaki & Bhowmick (2001)

<sup>4</sup> Datta et al. (1996)

<sup>5</sup> Socrates (2001)

The FTIR spectrum of the residue from the filtered solution of the KFTHA fibres soaked in hot trichlorobenzene is shown in Figure IX.1, while possible peak assignments are given in Table IX.3. The spectrum of this residue is similar to that of oxidized polyethylene (Figure IX.7). The chemical structure of oxidized polyethylene is shown in Figure IX.8. This is considered to indicate that the residue was a substance similar to oxidised polyethylene, possibly oxidized wax.

*Figure IX.4 has been removed due to Copyright restrictions.*

**Figure IX.4:** FTIR spectra of ethylene-vinyl acetate copolymer containing nominal vinyl acetate 40 wt% (A), 33 wt% (B), 18 wt% (C) and 14 wt% (D) in the range of 4,000-500  $\text{cm}^{-1}$  (Mathias, Hankins, Bertolucci, Grubb & Muthiah, 1992).

*Figure IX.5 has been removed due to Copyright restrictions.*

**Figure IX.5:** FTIR spectra of polyethylene (PE), ethylene-vinyl acetate copolymer (EVA) and PE:EVA blend (50:50) in the range of 2,000-500 cm<sup>-1</sup> (Chattopadhyay, Chaki & Bhowmick, 2001).

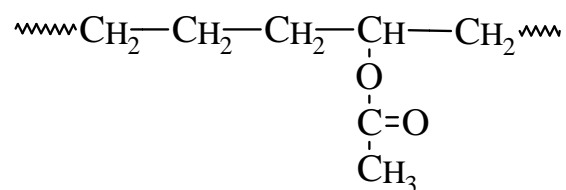


**Figure IX.6:** Chemical structure of ethylene-vinyl acetate copolymer (EVA) (Datta, Bhowmick, Tripathy & Chaki, 1996).

**Table IX.3:** Possible assignments of peak positions of FTIR band of residue from filtered solution of KFTHA fibres soaked in hot trichlorobenzene

Peak Position (cm <sup>-1</sup> )	Possible assignment
2,919	CH <sub>2</sub> asymmetric stretching vibrations in polyethylene <sup>1</sup>
2,850	CH <sub>2</sub> symmetric stretching vibrations in polyethylene <sup>1</sup>
1,732	Symmetric C=O stretching vibrations of ester groups in oxidised polyethylene <sup>2</sup>
1,715	Symmetric C=O stretching vibrations of carboxylic groups in oxidised polyethylene <sup>2</sup>
1,472	Bending deformation in polyethylene <sup>1</sup>
1,462	Bending deformation in polyethylene <sup>1</sup>
1,411	Long chain saturated ketones (R <sub>1</sub> R <sub>2</sub> C=O) in oxidised polyethylene <sup>2</sup>
1,371	Symmetric deformation in polyethylene <sup>1</sup>
1,170	Wagging deformation in polyethylene <sup>1</sup>
720	Rocking deformation in polyethylene <sup>1</sup>

<sup>1</sup> Gulmine et al. (2002)

<sup>2</sup> Durmuş et al. (2007)



*Figure IX.7 has been removed due to Copyright restrictions.*

**Figure IX.7:** FTIR spectrum of oxidised polyethylene in the range of (a) 3,200-1,000  $\text{cm}^{-1}$  (Bergbreiter, Franchina, & Kabza, 1999) and (b) 2,000-400  $\text{cm}^{-1}$  (Durmuş, Woo, Kaşgöz, Macosko & Tsapatsis, 2007).

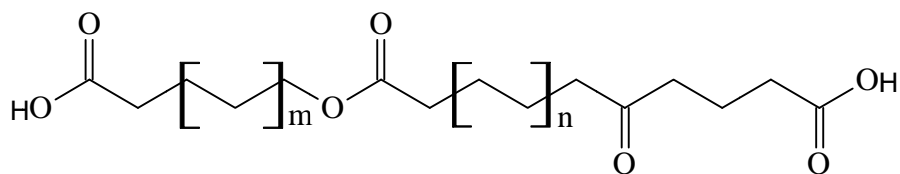


**Figure IX.8:** Chemical structure of oxidised polyethylene (Durmuş et al., 2007).

## **Appendix X: SEM Micrographs of Transverse Sections of Extruded Composites**





**Figure X.1:** SEM micrographs of transverse section of UKF/HDPE rod composite (Sample no. 1 and End A).

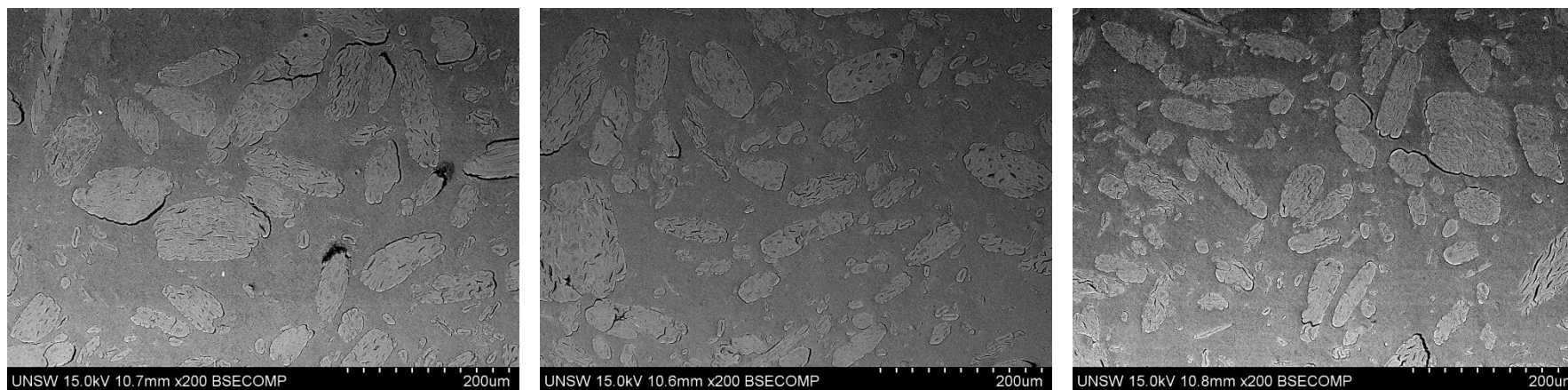


**Figure X.2:** SEM micrographs of transverse section of UKF/HDPE rod composite (Sample no. 1 and End B).

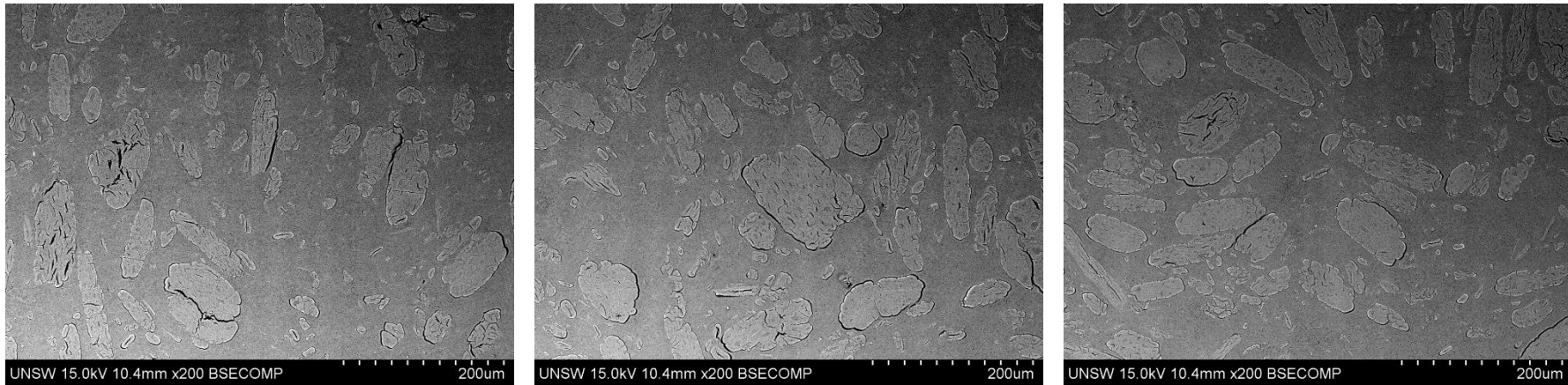


**Figure X.3:** SEM micrographs of transverse section of UKF/HDPE rod composite (Sample no. 2 and End A).



**Figure X.4:** SEM micrographs of transverse section of UKF/HDPE rod composite (Sample no. 2 and End B).

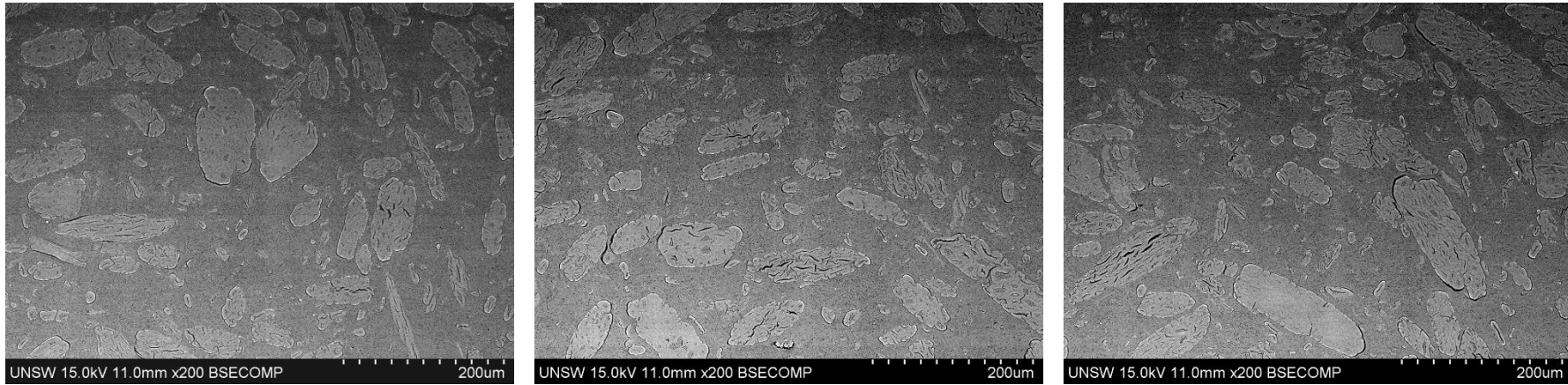


**Figure X.5:** SEM micrographs of transverse section of UKF/HDPE rod composite (Sample no. 3 and End A).

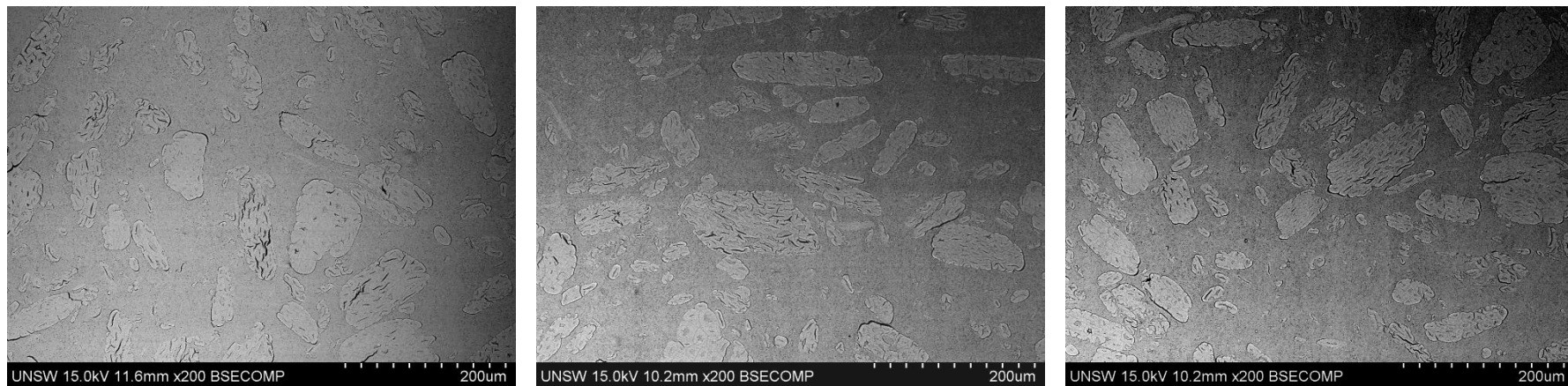


**Figure X.6:** SEM micrographs of transverse section of UKF/HDPE rod composite (Sample no. 3 and End B).



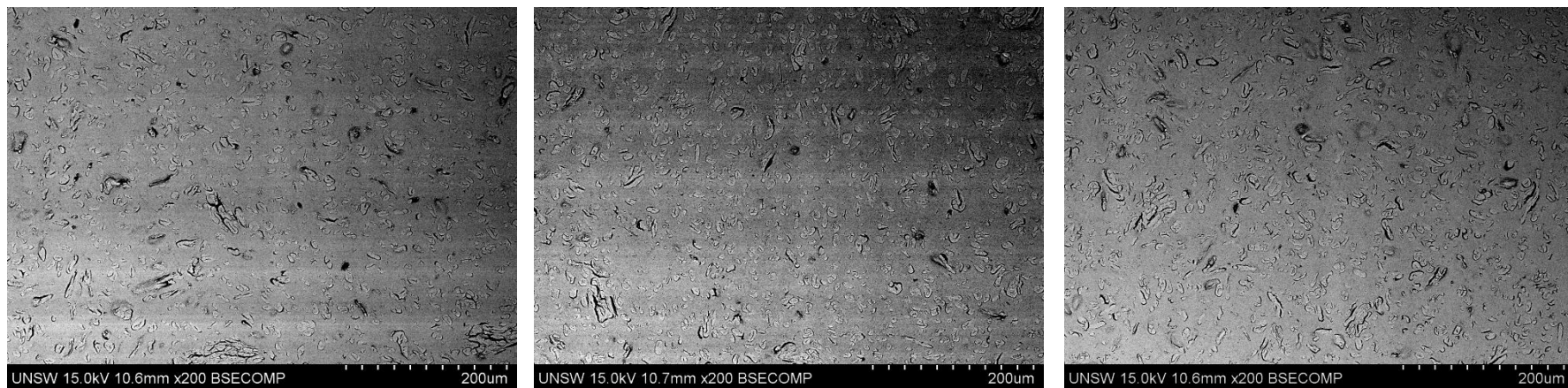


**Figure X.7:** SEM micrographs of transverse section of KFTN/HDPE rod composite (Sample no. 1 and End A).

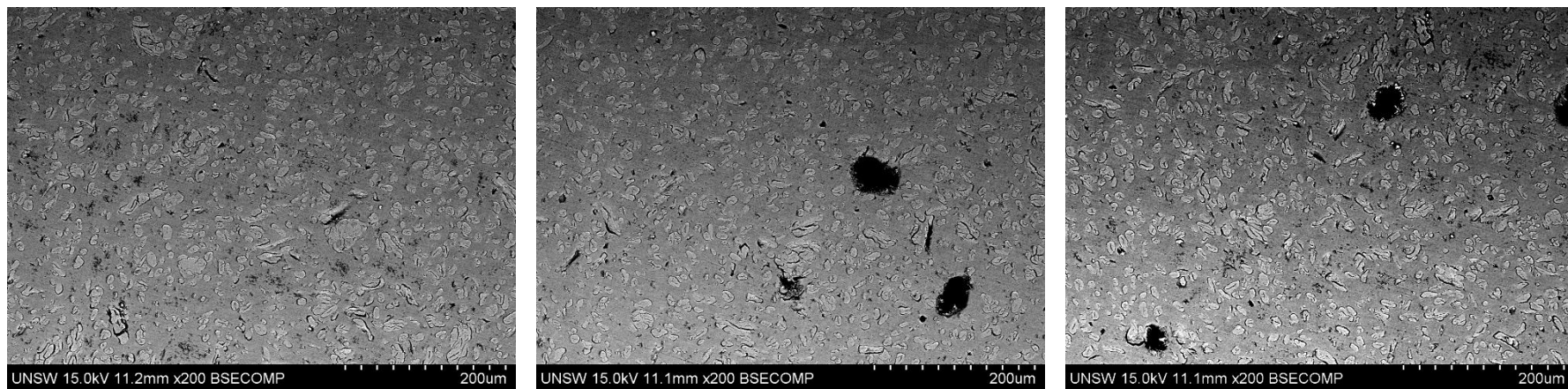


**Figure X.8:** SEM micrographs of transverse section of KFTN/HDPE rod composite (Sample no. 1 and End B).

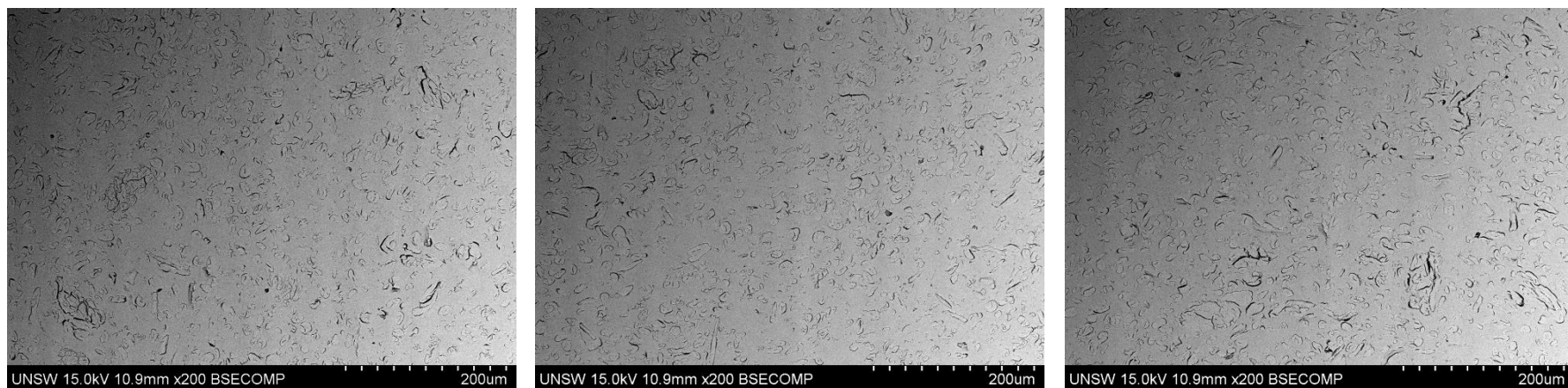


**Figure X.9:** SEM micrographs of transverse section of KFTN/HDPE rod composite (Sample no. 2 and End A).

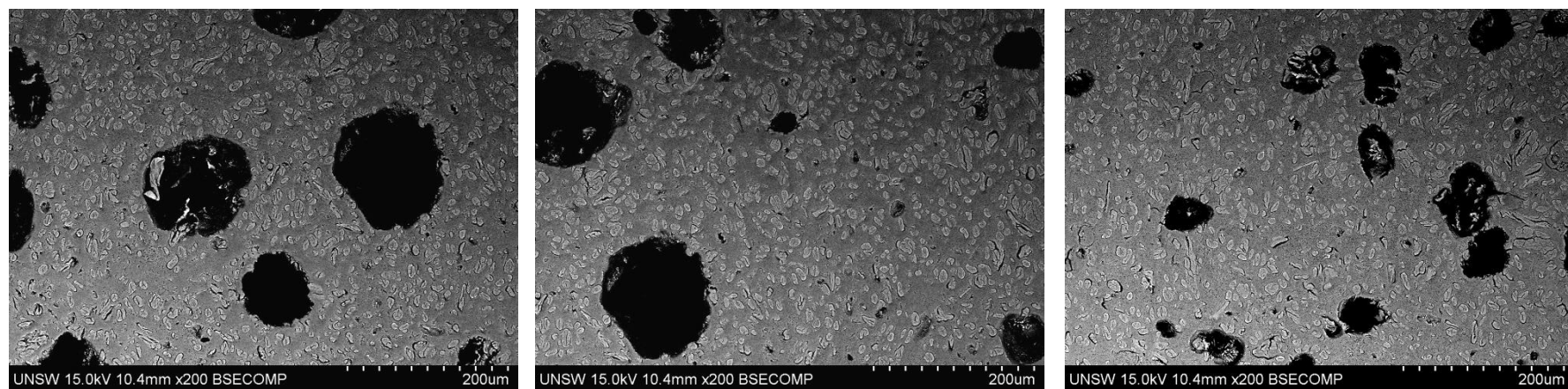


**Figure X.10:** SEM micrographs of transverse section of KFTN/HDPE rod composite (Sample no. 2 and End B).



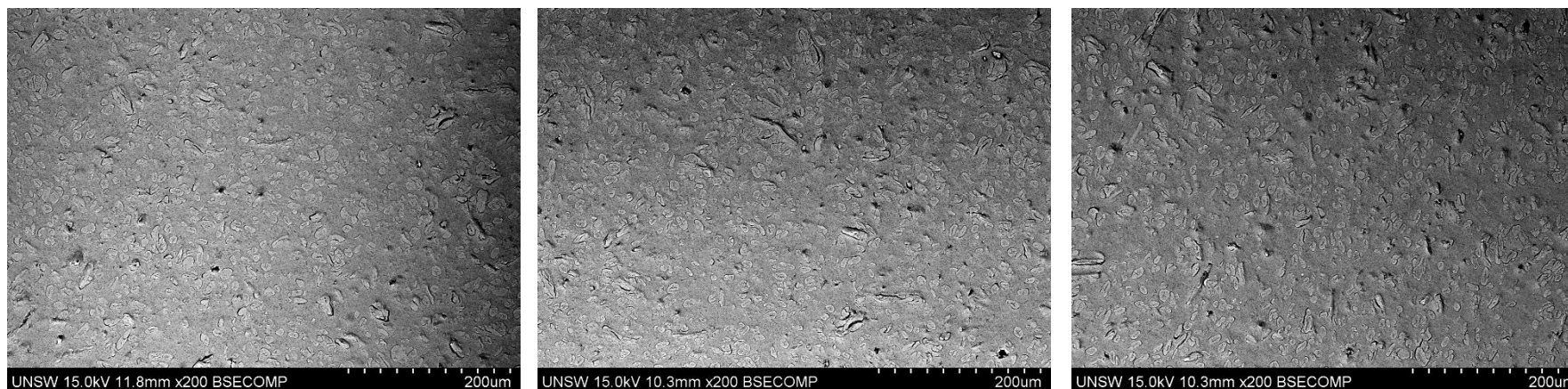


**Figure X.11:** SEM micrographs of transverse section of KFTN/HDPE rod composite (Sample no. 3 and End A).

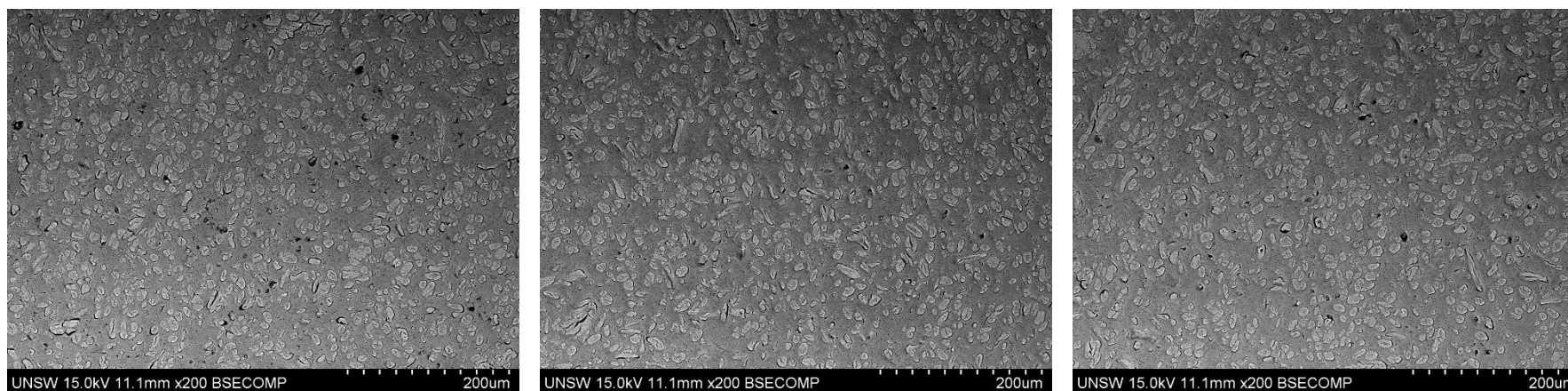


**Figure X.12:** SEM micrographs of transverse section of KFTN/HDPE rod composite (Sample no. 3 and End B).

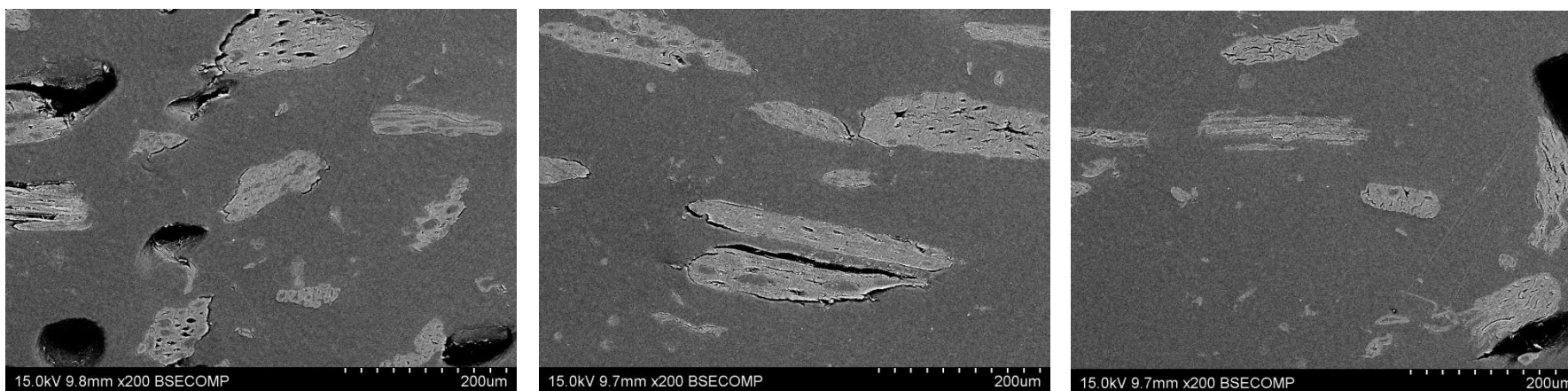


**Figure X.13:** SEM micrographs of transverse section of UKF/HDPE strip composite (Sample no. 1 (3B)).



**Figure X.14:** SEM micrographs of transverse section of UKF/HDPE strip composite (Sample no. 2 (3D)).

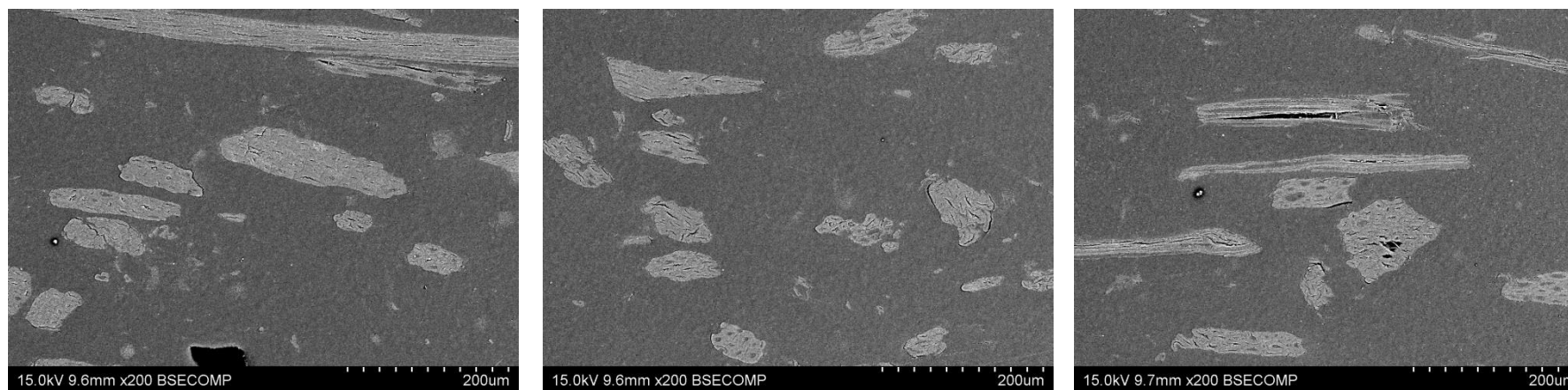


**Figure X.15:** SEM micrographs of transverse section of UKF/HDPE strip composite (Sample no. 3 (3G)).

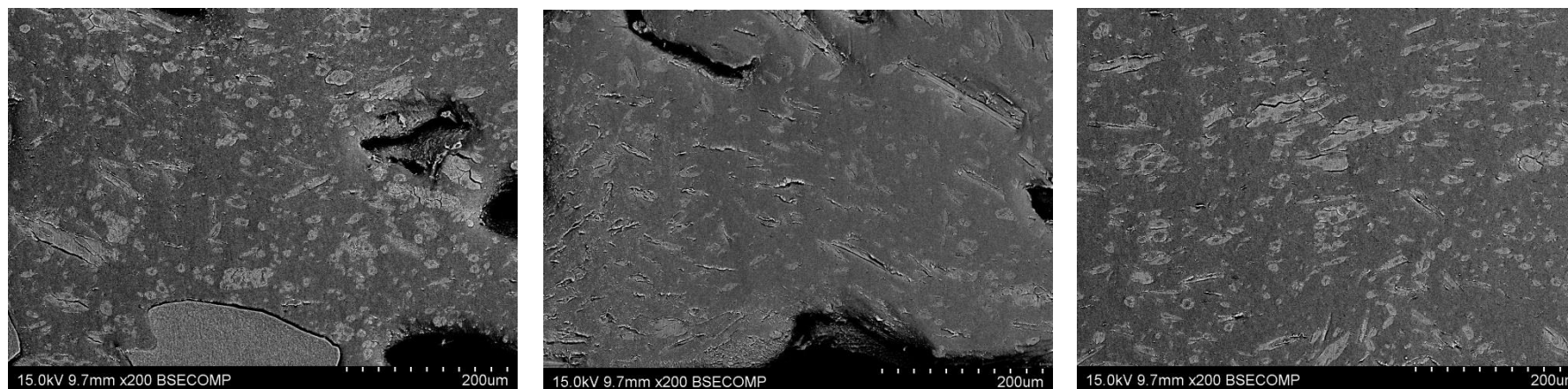


**Figure X.16:** SEM micrographs of transverse section of KFTN/HDPE strip composite (Sample no. 1 (2B)).



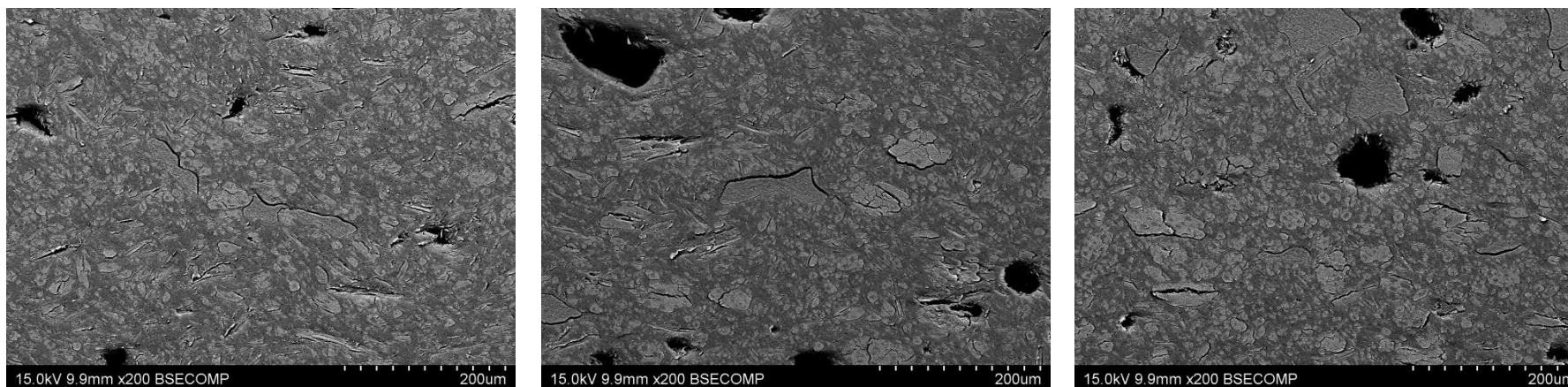


**Figure X.17:** SEM micrographs of transverse section of KFTN/HDPE strip composite (Sample no. 2 (2D)).

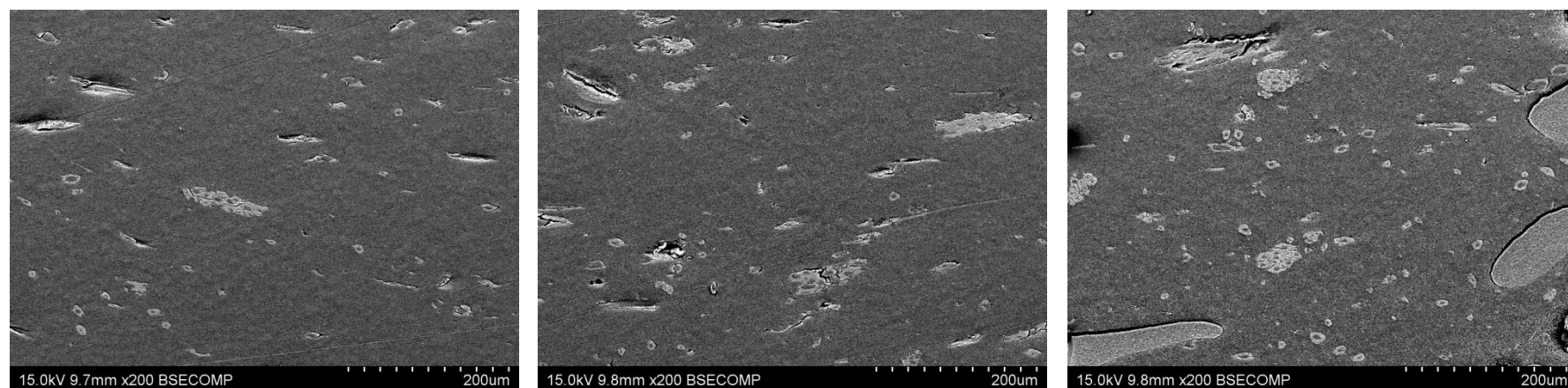


**Figure X.18:** SEM micrographs of transverse section of KFTN/HDPE strip composite (Sample no. 3 (2H)).

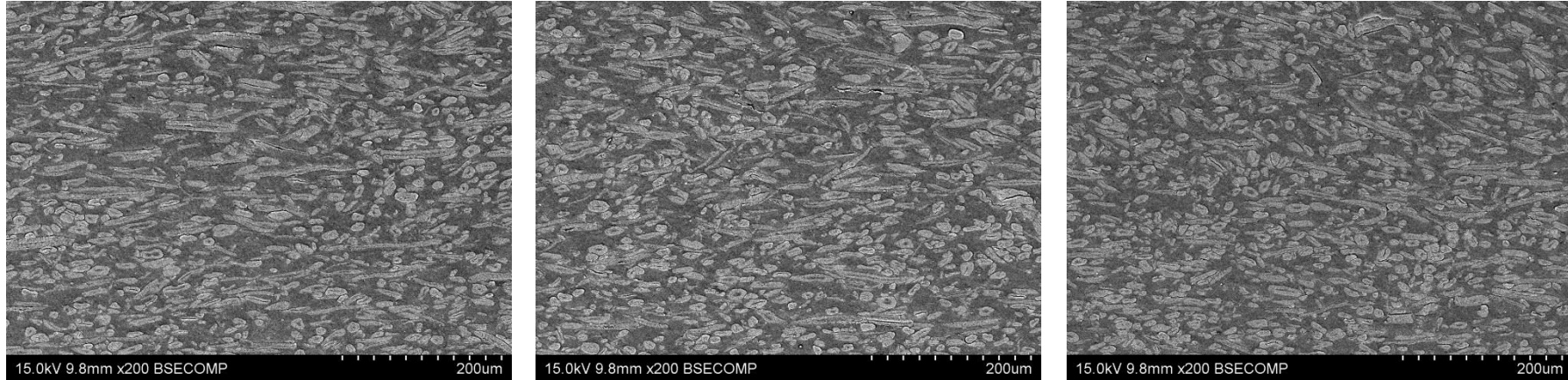


**Figure X.19:** SEM micrographs of transverse section of KFTHA/HDPE strip composite (Sample no. 1 (1A)).

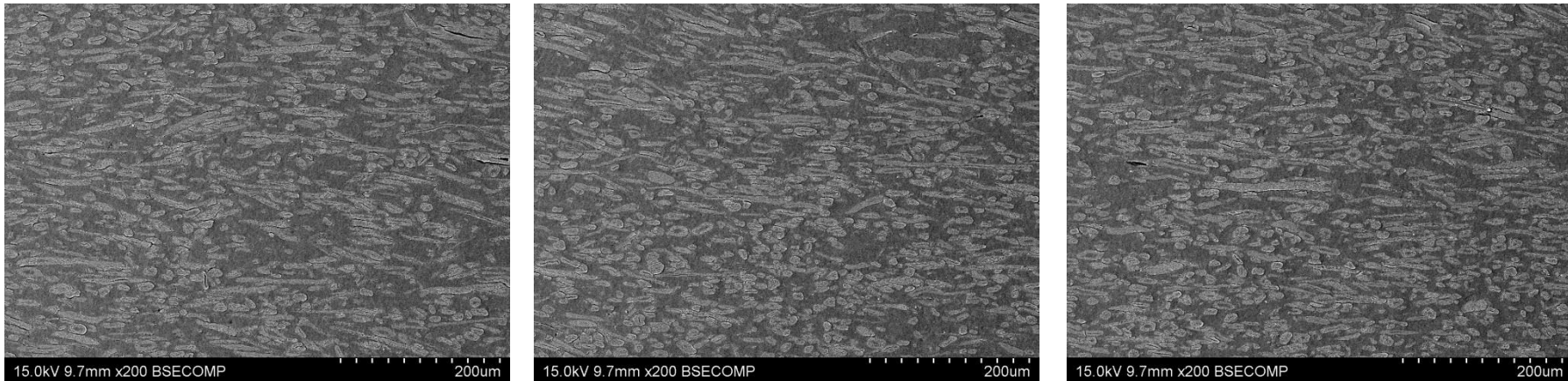


**Figure X.20:** SEM micrographs of transverse section of KFTHA/HDPE strip composite (Sample no. 2 (1E)).

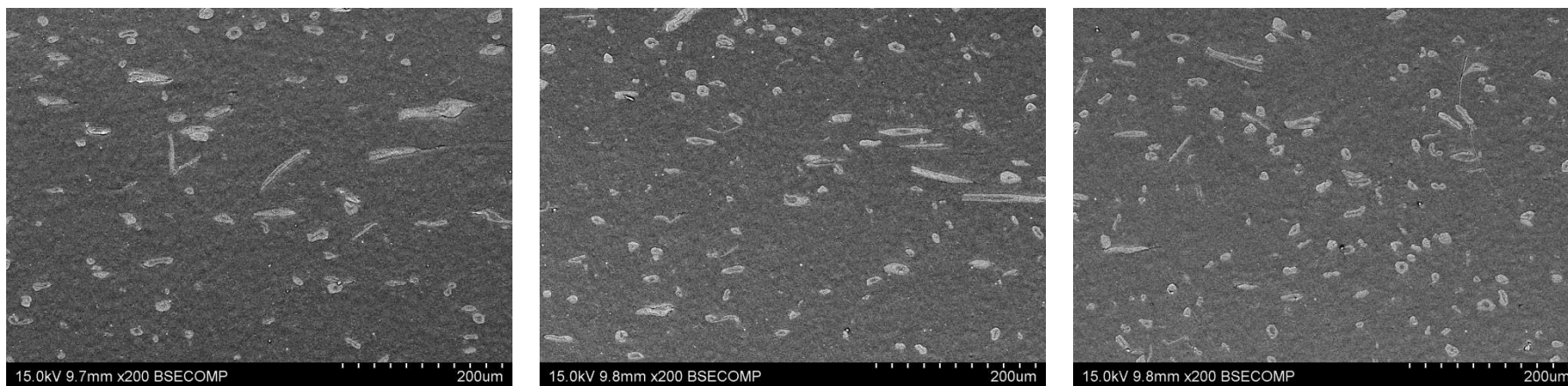


**Figure X.21:** SEM micrographs of transverse section of KFTHA/HDPE strip composite (Sample no. 3 (1H)).

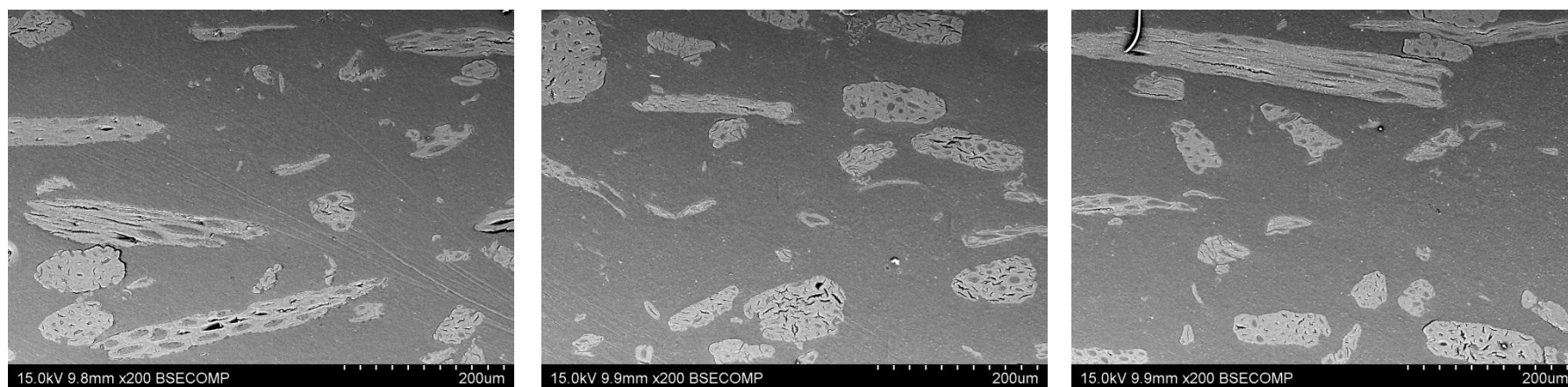


**Figure X.22:** SEM micrographs of transverse section of UKF/HDPE\_H strip composite (Sample no. 1 (7A)).

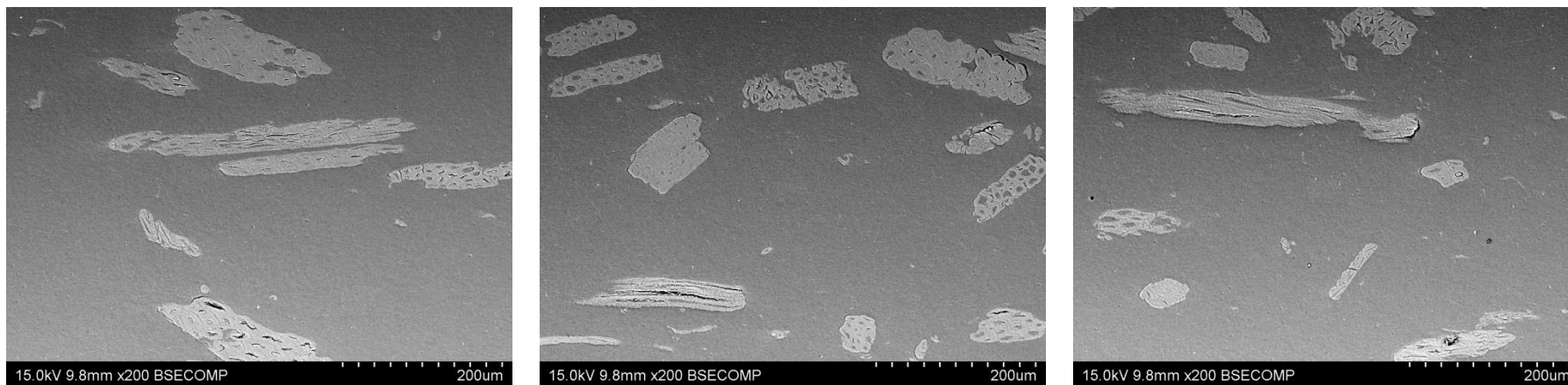


**Figure X.23:** SEM micrographs of transverse section of UKF/HDPE\_H strip composite (Sample no. 2 (7C)).



**Figure X.24:** SEM micrographs of transverse section of UKF/HDPE\_H strip composite (Sample no. 3 (7D)).





**Figure X.25:** SEM micrographs of transverse section of KFTN/HDPE\_H strip composite (Sample no. 1 (8A)).



**Figure X.26:** SEM micrographs of transverse section of KFTN/HDPE\_H strip composite (Sample no. 2 (8C)).



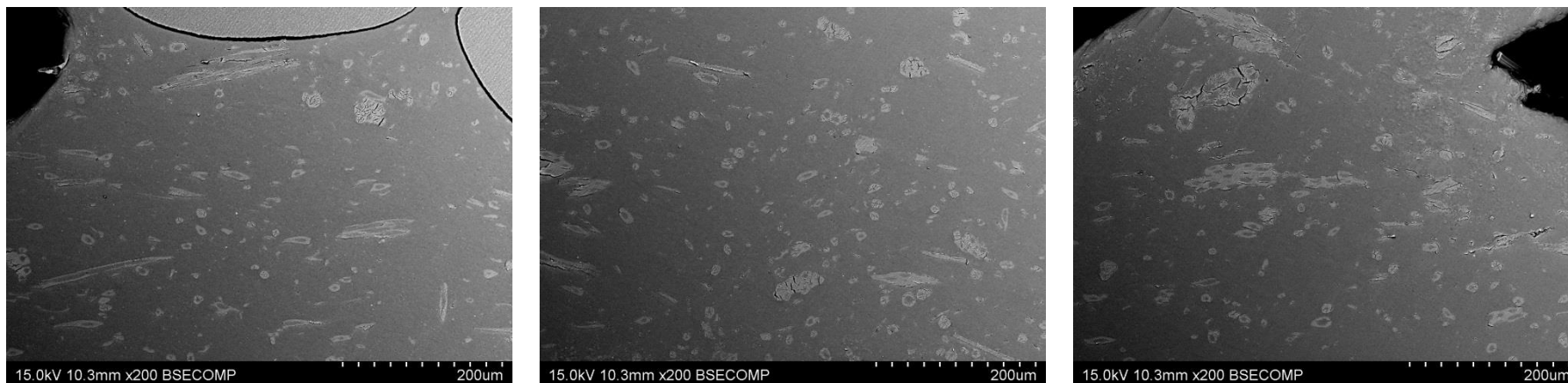


**Figure X.27:** SEM micrographs of transverse section of KFTN/HDPE\_H strip composite (Sample no. 3 (8E)).

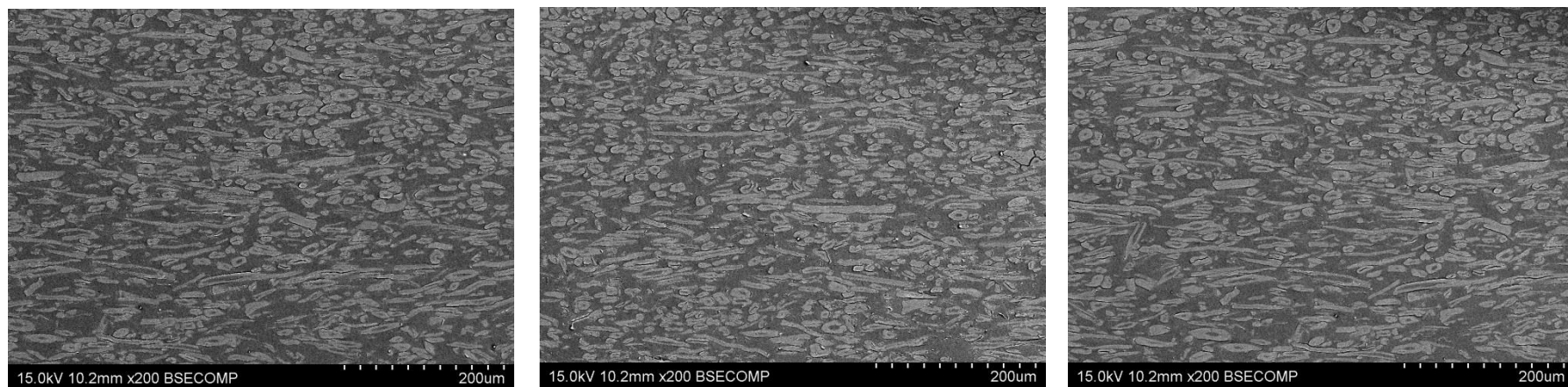


**Figure X.28:** SEM micrographs of transverse section of KFTHA/HDPE\_H strip composite (Sample no. 1 (6D)).

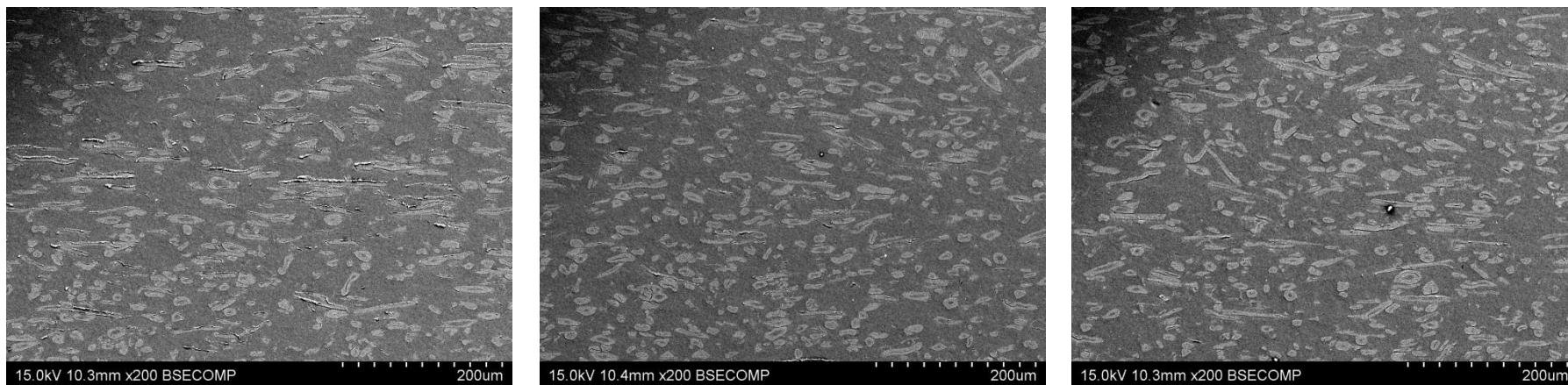


**Figure X.29:** SEM micrographs of transverse section of KFTHA/HDPE\_H strip composite (Sample no. 2 (6F)).

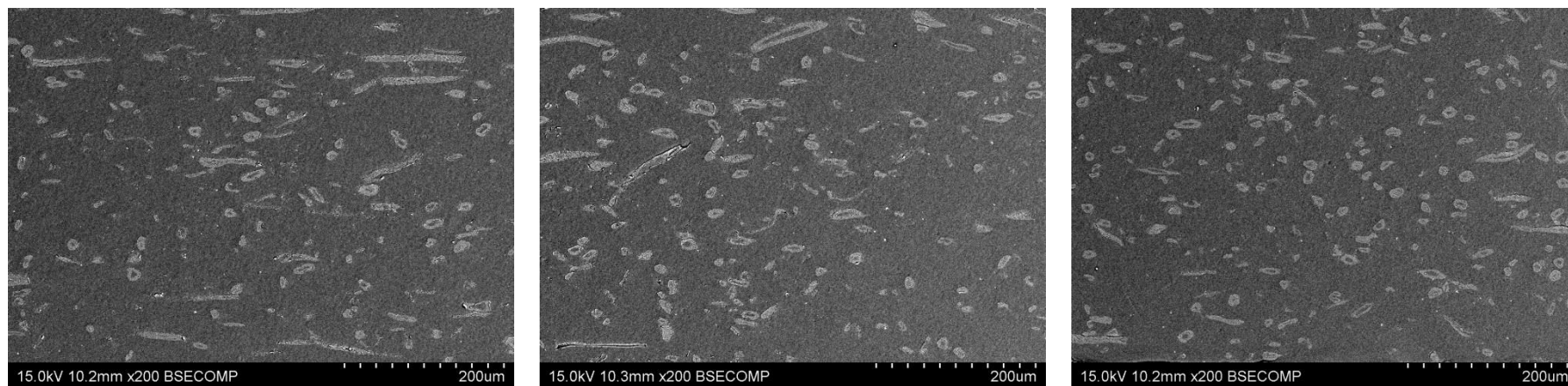


**Figure X.30:** SEM micrographs of transverse section of KFTHA/HDPE\_H strip composite (Sample no. 3 (6H)).



## **Appendix XI: SEM Micrographs of Longitudinal Section of Extruded Composites**



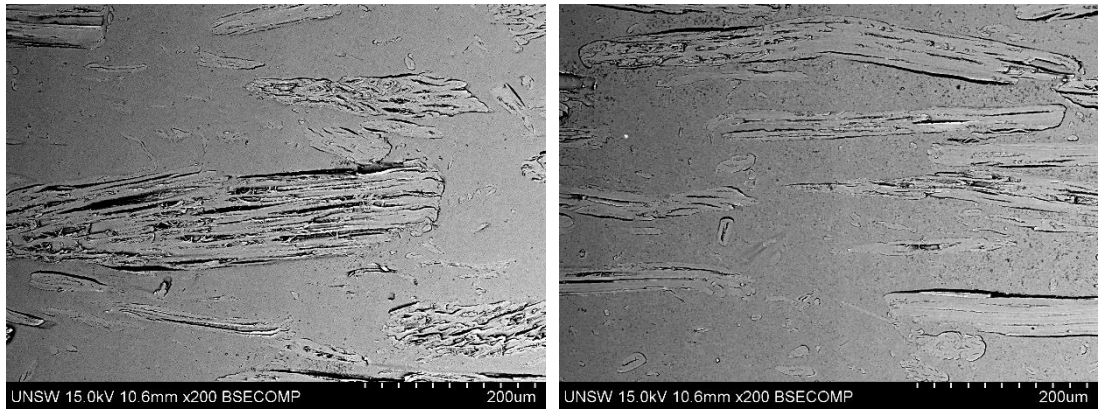


**Figure XI.1:** SEM micrographs of longitudinal section of UKF/HDPE rod composite at centre of specimen (Sample no. 1 and End A).

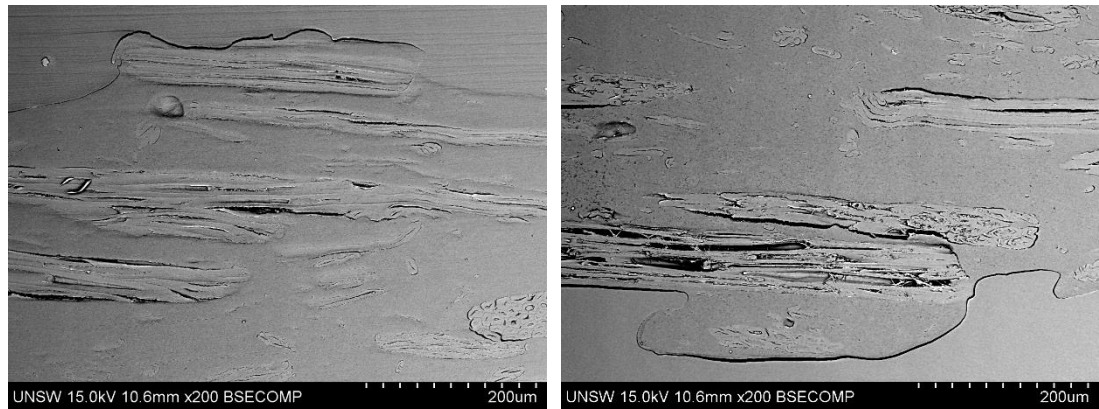


**Figure XI.2:** SEM micrographs of longitudinal section of UKF/HDPE rod composite at edge of specimen (Sample no. 1 and End A).

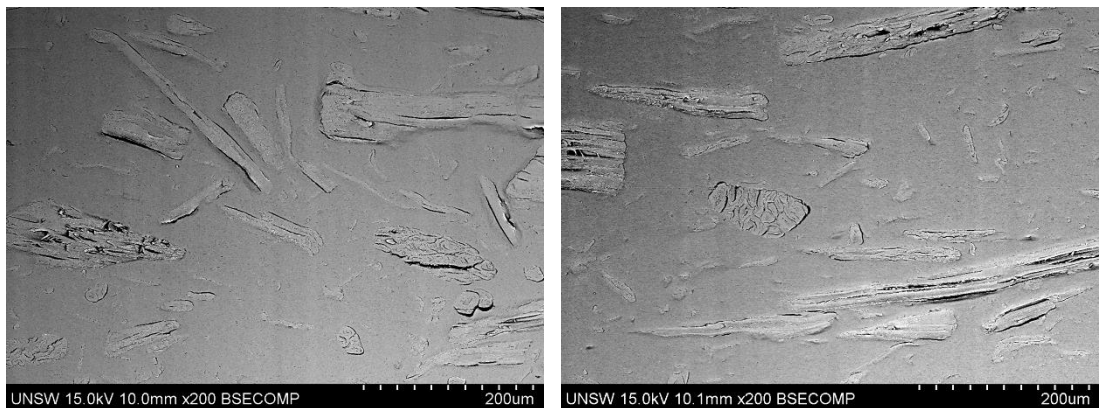


**Figure XI.3:** SEM micrographs of longitudinal section of UKF/HDPE rod composite at centre of specimen (Sample no. 1 and End B).

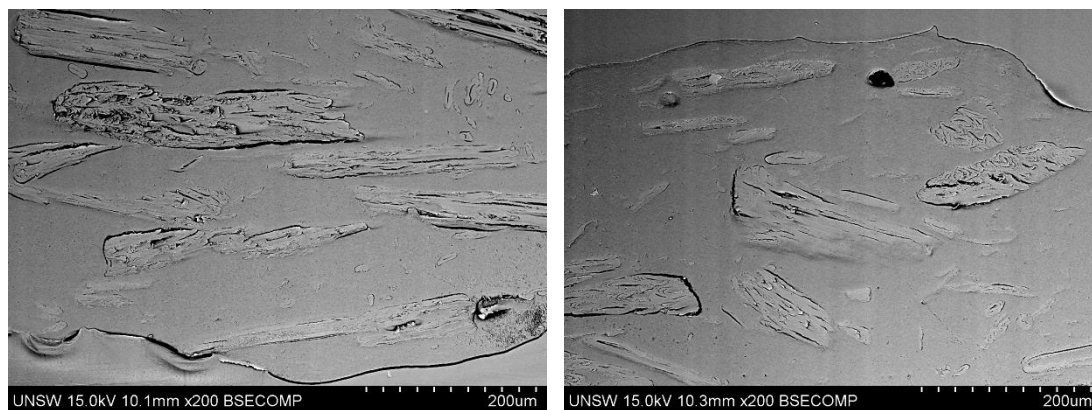


**Figure XI.4:** SEM micrographs of longitudinal section of UKF/HDPE rod composite at edge of specimen (Sample no. 1 and End B).

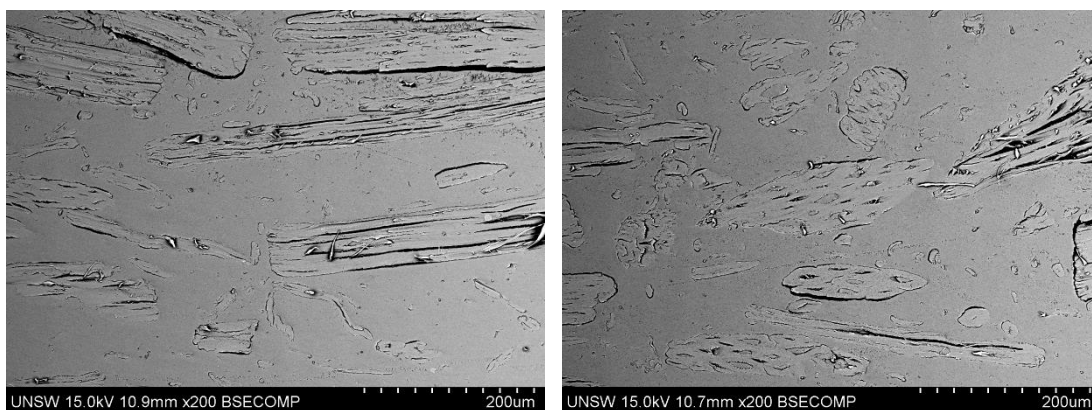


**Figure XI.5:** SEM micrographs of longitudinal section of UKF/HDPE rod composite at centre of specimen (Sample no. 2 and End A).

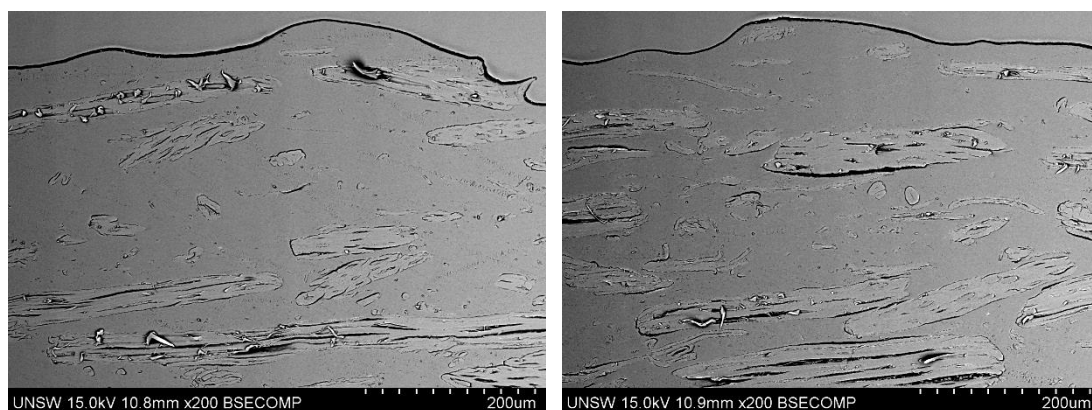


**Figure XI.6:** SEM micrographs of longitudinal section of UKF/HDPE rod composite at edge of specimen (Sample no. 2 and End A).



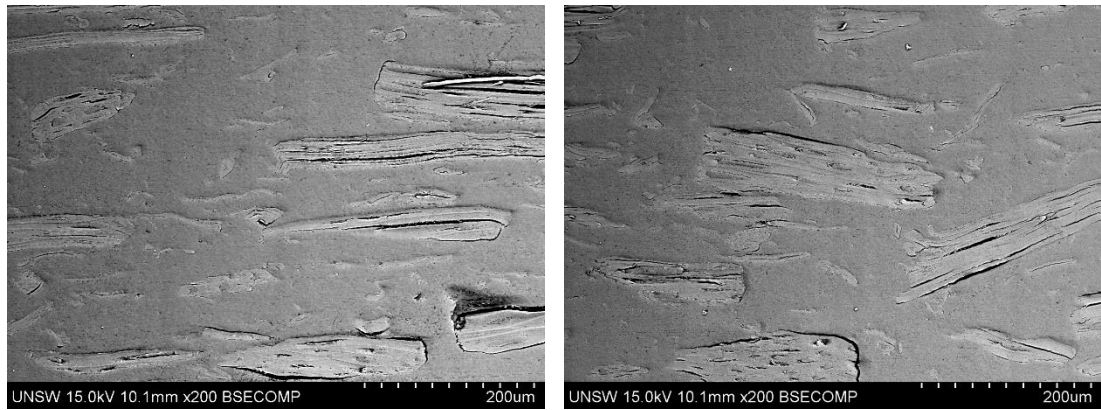


**Figure XI.7:** SEM micrographs of longitudinal section of UKF/HDPE rod composite at centre of specimen (Sample no. 2 and End B).

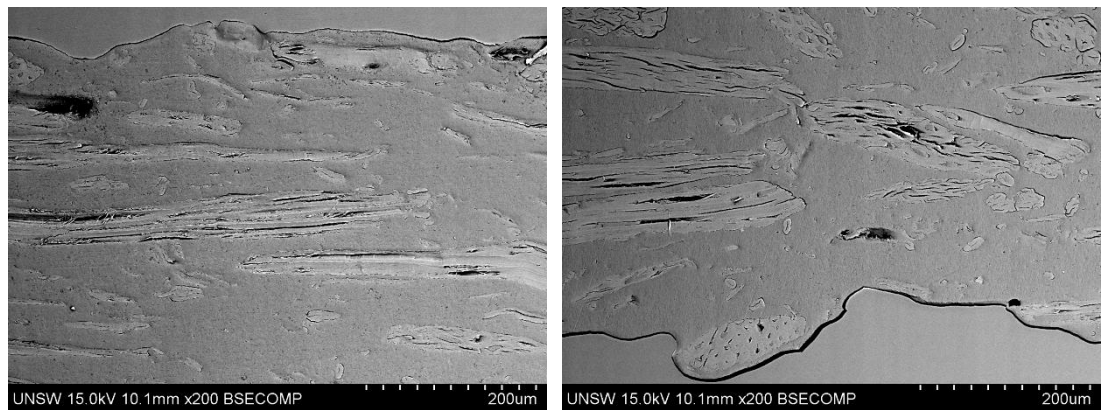


**Figure XI.8:** SEM micrographs of longitudinal section of UKF/HDPE rod composite at edge of specimen (Sample no. 2 and End B).

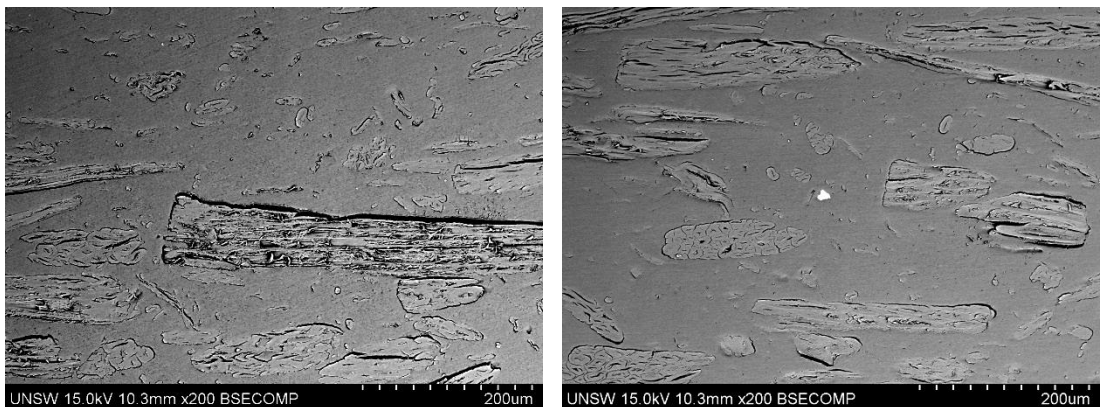


**Figure XI.9:** SEM micrographs of longitudinal section of UKF/HDPE rod composite at centre of specimen (Sample no. 3 and End A).



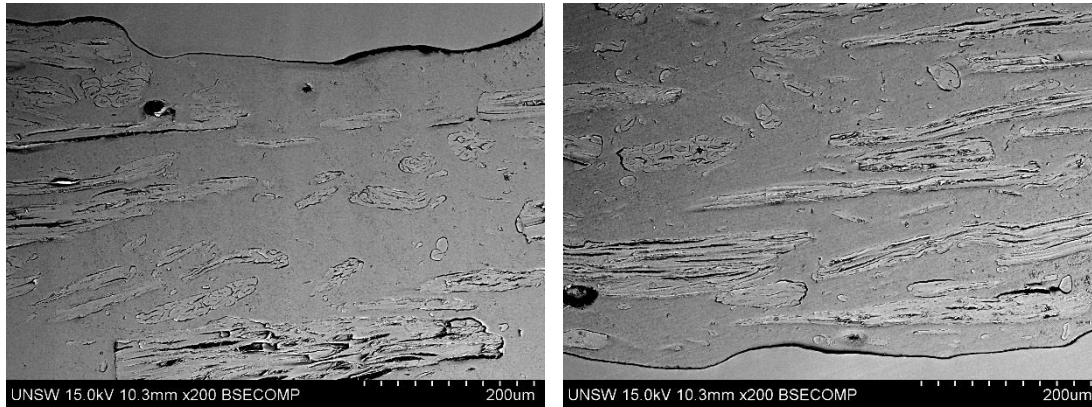


**Figure XI.10:** SEM micrographs of longitudinal section of UKF/HDPE rod composite at edge of specimen (Sample no. 3 and End A).

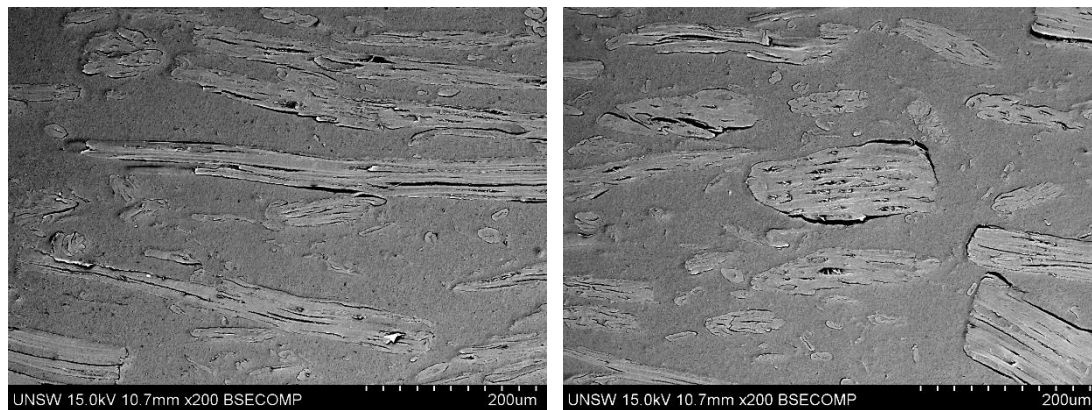


**Figure XI.11:** SEM micrographs of longitudinal section of UKF/HDPE rod composite at centre of specimen (Sample no. 3 and End B).

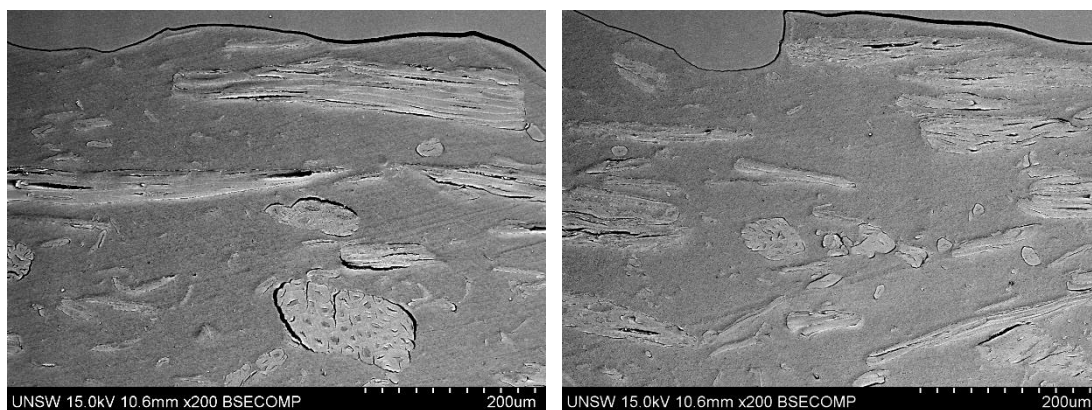


**Figure XI.12:** SEM micrographs of longitudinal section of UKF/HDPE rod composite at edge of specimen (Sample no. 3 and End B).

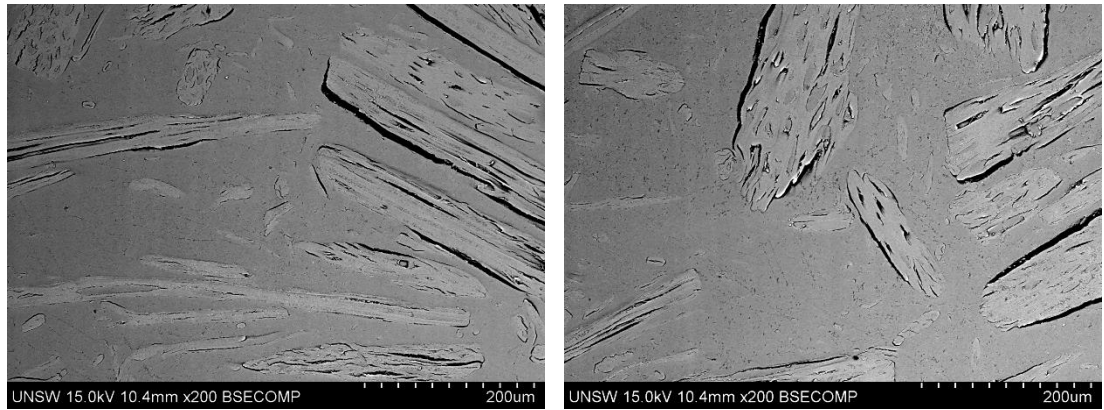


**Figure XI.13:** SEM micrographs of longitudinal section of UKF/HDPE rod composite at centre of specimen (Sample no. 4 and End A).

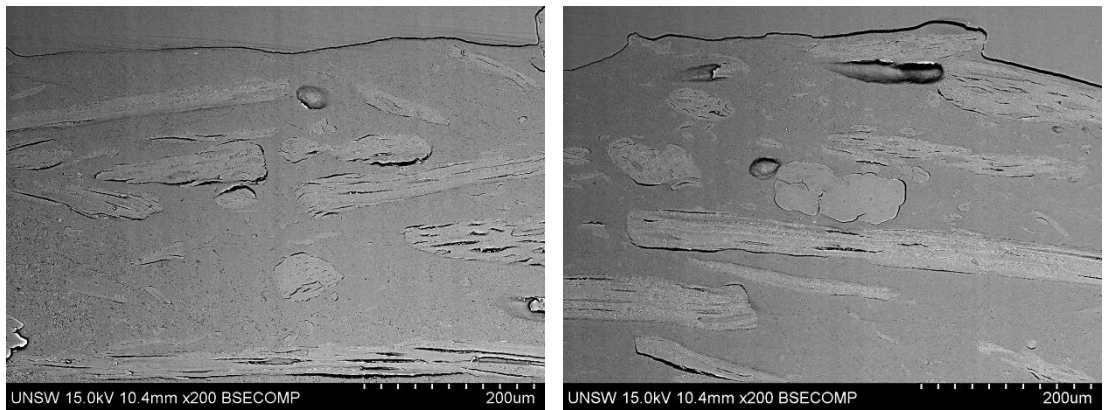


**Figure XI.14:** SEM micrographs of longitudinal section of UKF/HDPE rod composite at edge of specimen (Sample no. 4 and End A).

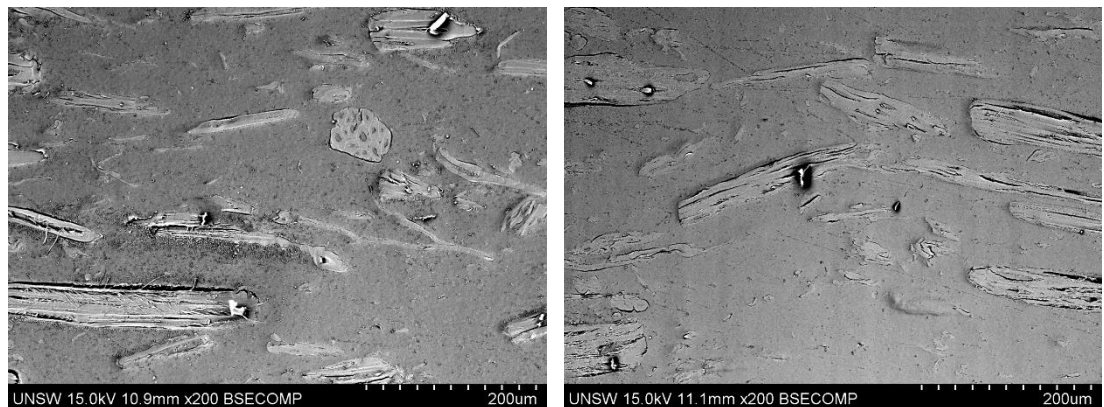


**Figure XI.15:** SEM micrographs of longitudinal section of UKF/HDPE rod composite at centre of specimen (Sample no. 4 and End B).

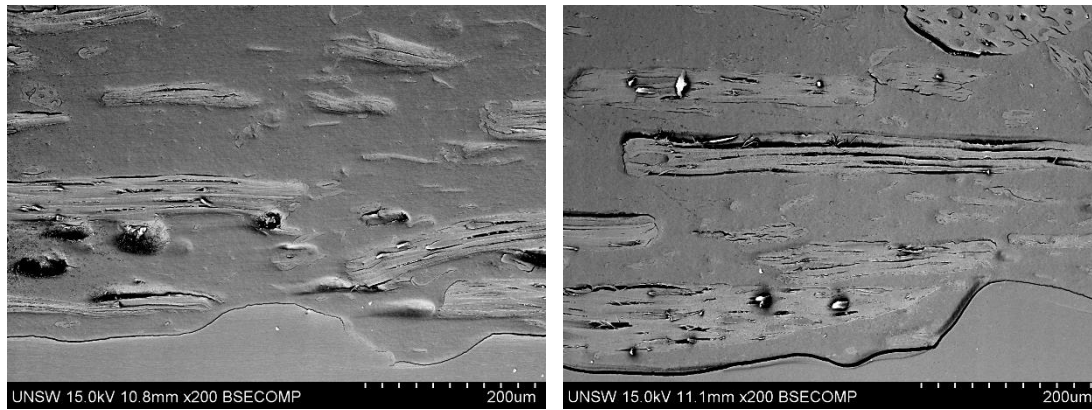


**Figure XI.16:** SEM micrographs of longitudinal section of UKF/HDPE rod composite at edge of specimen (Sample no. 4 and End B).

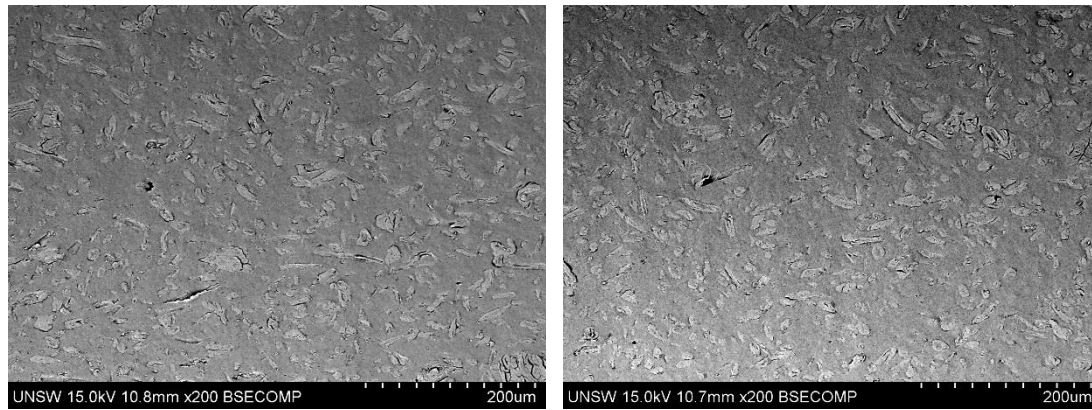


**Figure XI.17:** SEM micrographs of longitudinal section of KFTN/HDPE rod composite at centre of specimen (Sample no. 1 and End A).

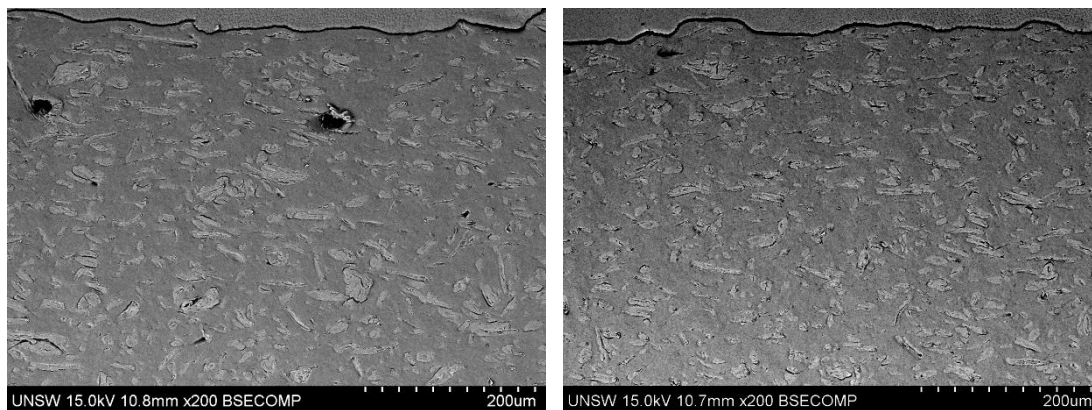


**Figure XI.18:** SEM micrographs of longitudinal section of KFTN/HDPE rod composite at edge of specimen (Sample no. 1 and End A).

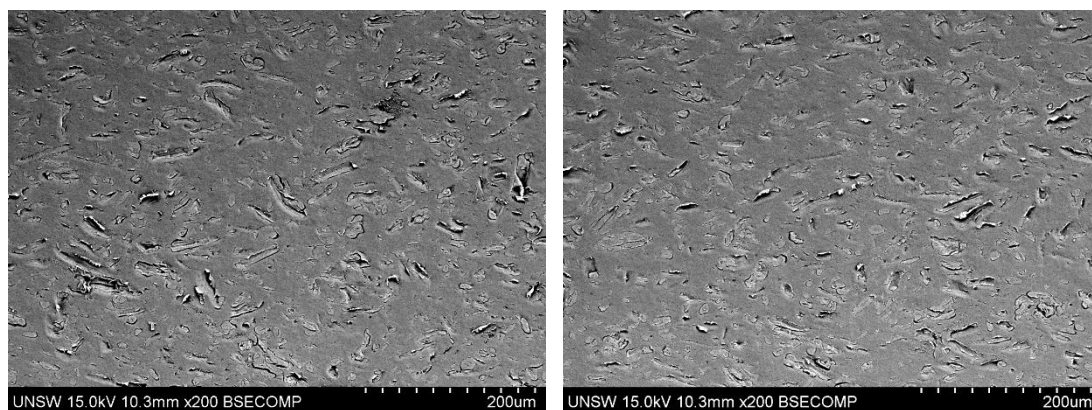


**Figure XI.19:** SEM micrographs of longitudinal section of KFTN/HDPE rod composite at centre of specimen (Sample no. 1 and End B).

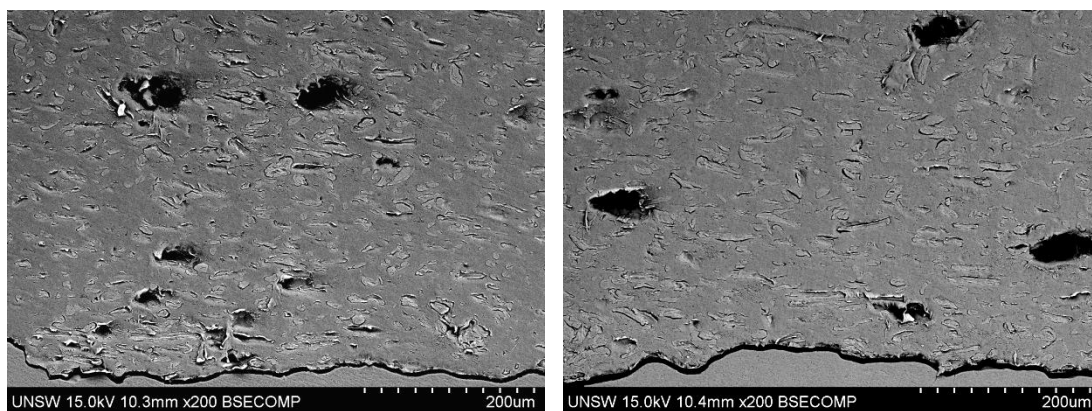


**Figure XI.20:** SEM micrographs of longitudinal section of KFTN/HDPE rod composite at edge of specimen (Sample no. 1 and End B).

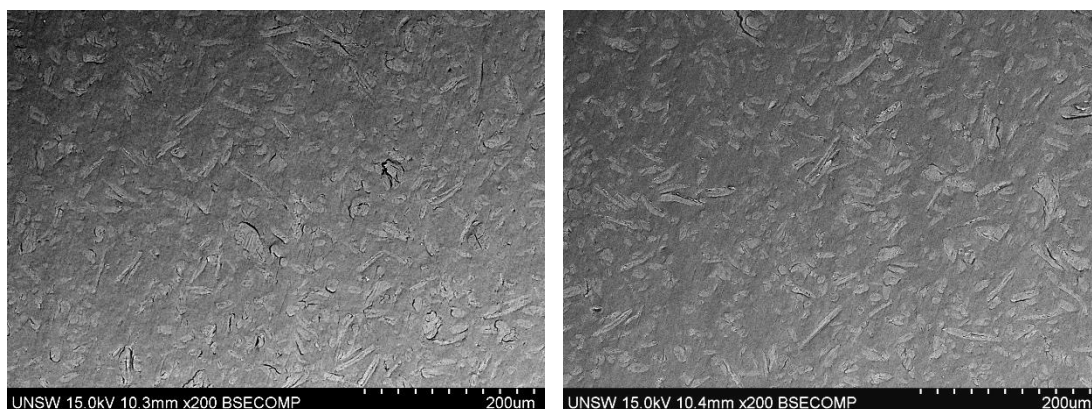


**Figure XI.21:** SEM micrographs of longitudinal section of KFTN/HDPE rod composite at centre of specimen (Sample no. 2 and End A).



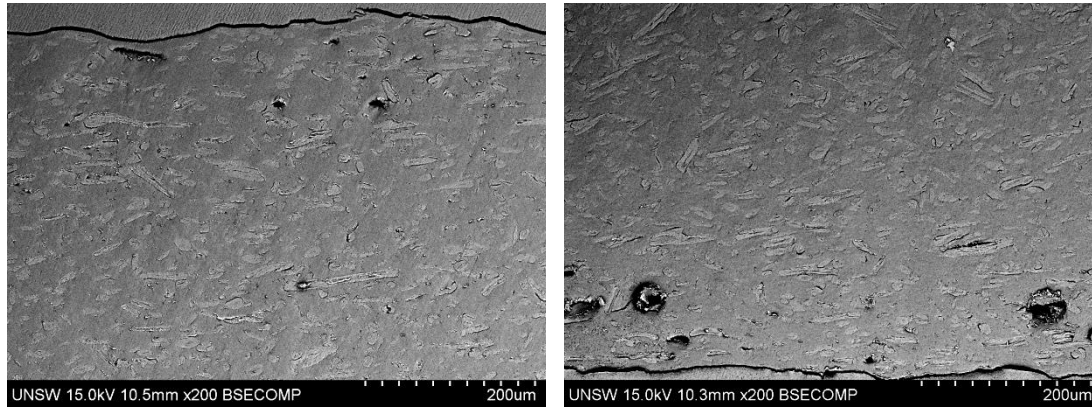


**Figure XI.22:** SEM micrographs of longitudinal section of KFTN/HDPE rod composite at edge of specimen (Sample no. 2 and End A).

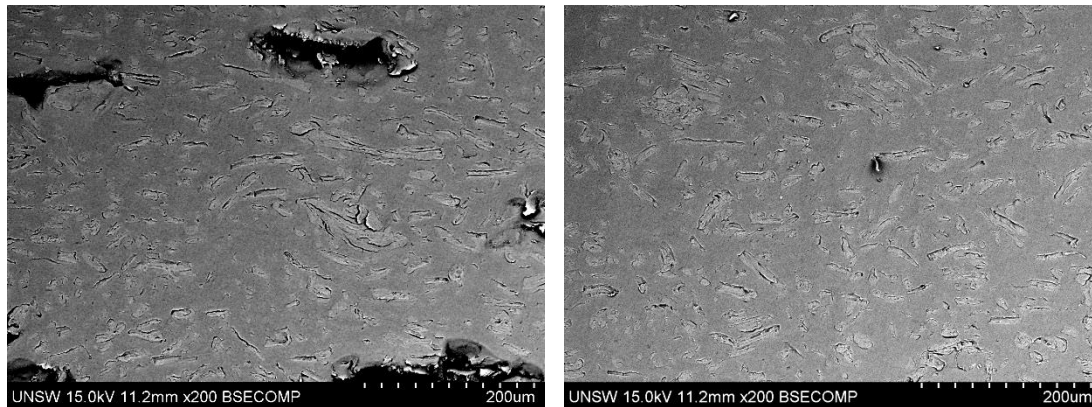


**Figure XI.23:** SEM micrographs of longitudinal section of KFTN/HDPE rod composite at centre of specimen (Sample no. 2 and End B).

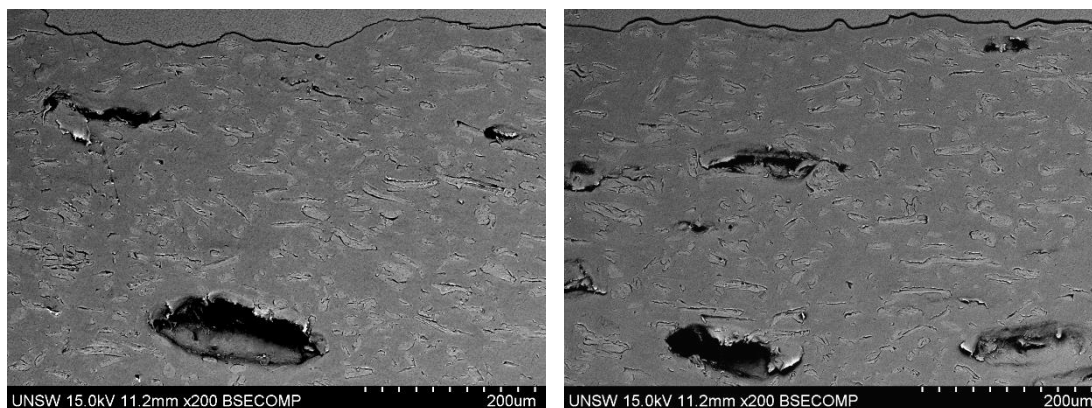


**Figure XI.24:** SEM micrographs of longitudinal section of KFTN/HDPE rod composite at edge of specimen (Sample no. 2 and End B).

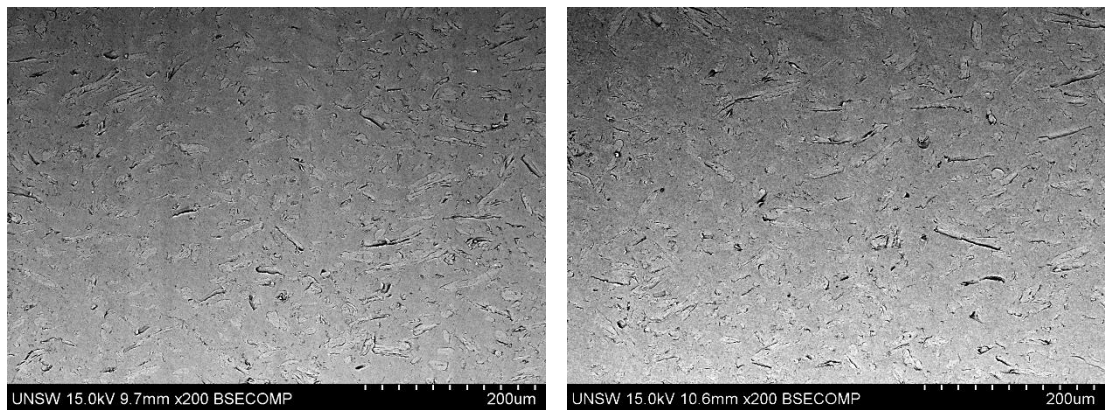


**Figure XI.25:** SEM micrographs of longitudinal section of KFTN/HDPE rod composite at centre of specimen (Sample no. 3 and End A).

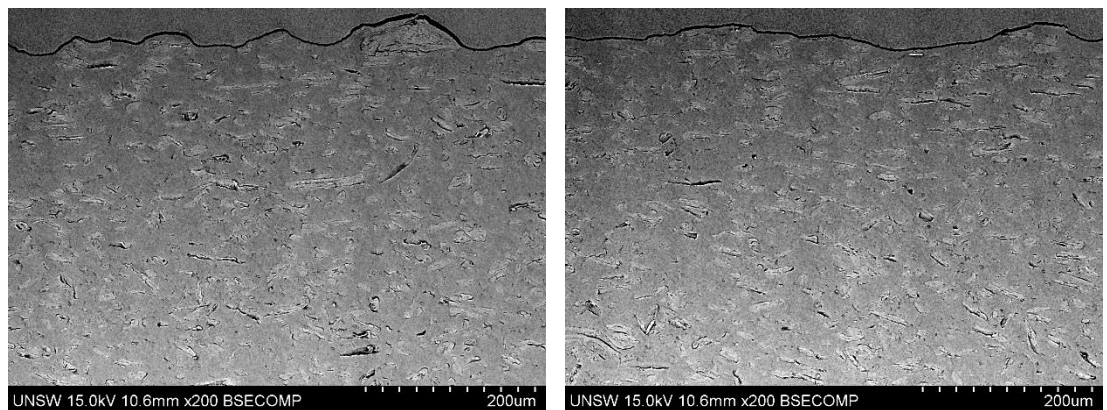


**Figure XI.26:** SEM micrographs of longitudinal section of KFTN/HDPE rod composite at edge of specimen (Sample no. 3 and End A).

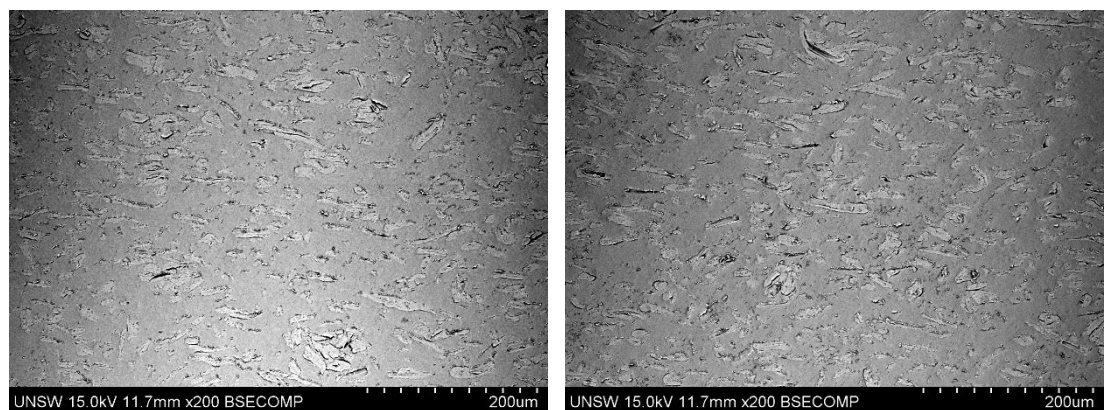


**Figure XI.27:** SEM micrographs of longitudinal section of KFTN/HDPE rod composite at centre of specimen (Sample no. 3 and End B).

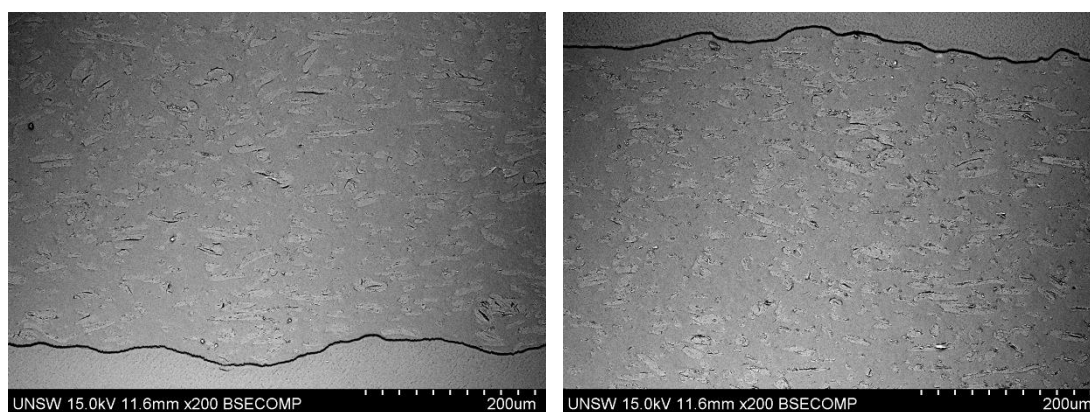


**Figure XI.28:** SEM micrographs of longitudinal section of KFTN/HDPE rod composite at edge of specimen (Sample no. 3 and End B).

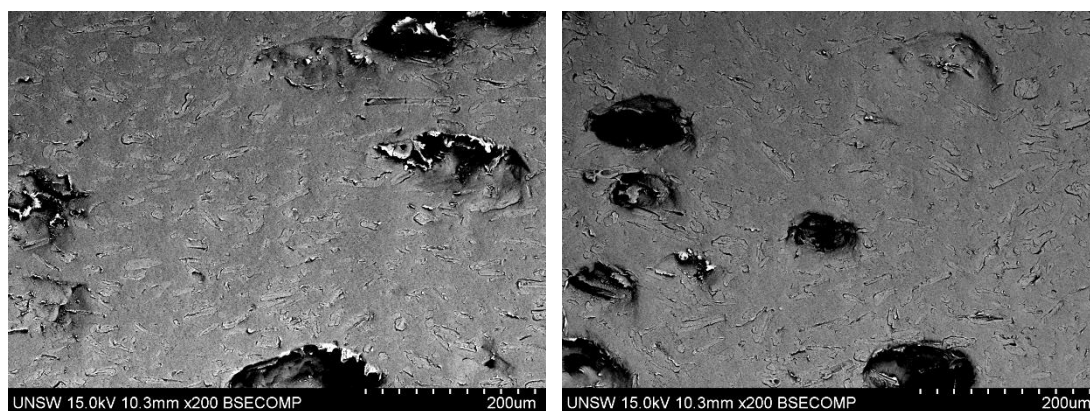


**Figure XI.29:** SEM micrographs of longitudinal section of KFTN/HDPE rod composite at centre of specimen (Sample no. 4 and End A).

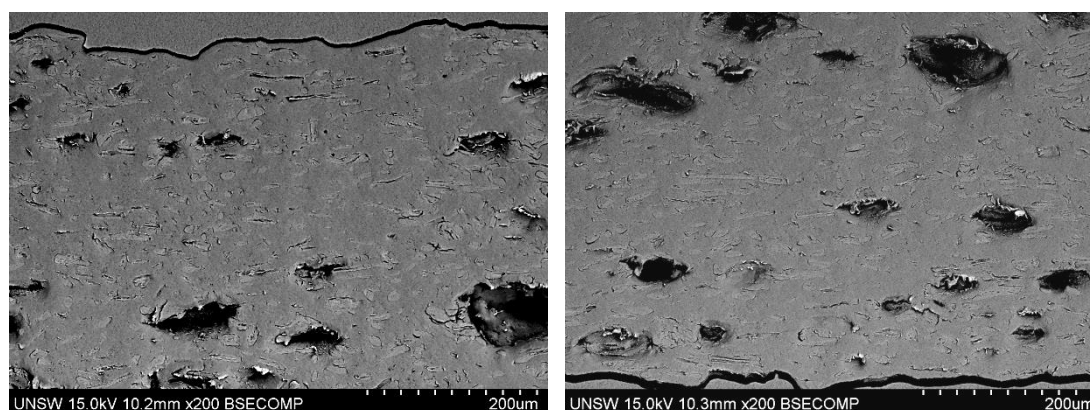


**Figure XI.30:** SEM micrographs of longitudinal section of KFTN/HDPE rod composite at edge of specimen (Sample no. 4 and End A).

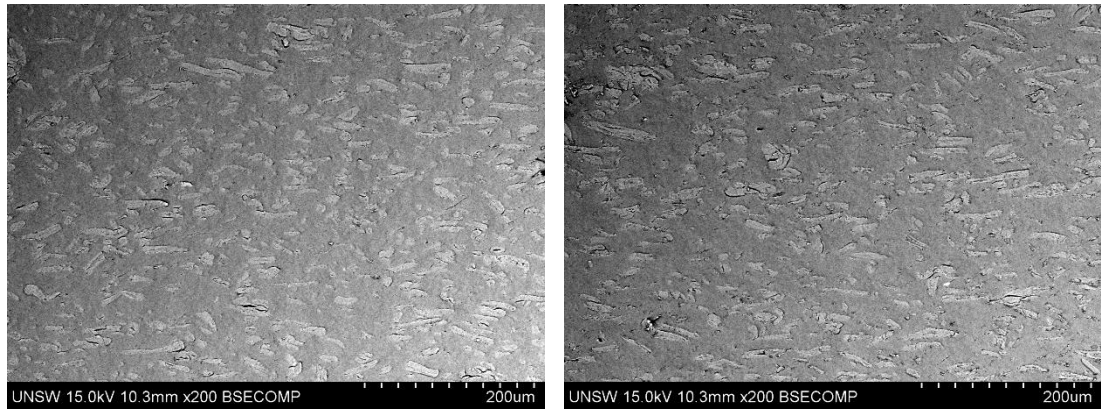


**Figure XI.31:** SEM micrographs of longitudinal section of KFTN/HDPE rod composite at centre of specimen (Sample no. 4 and End B).

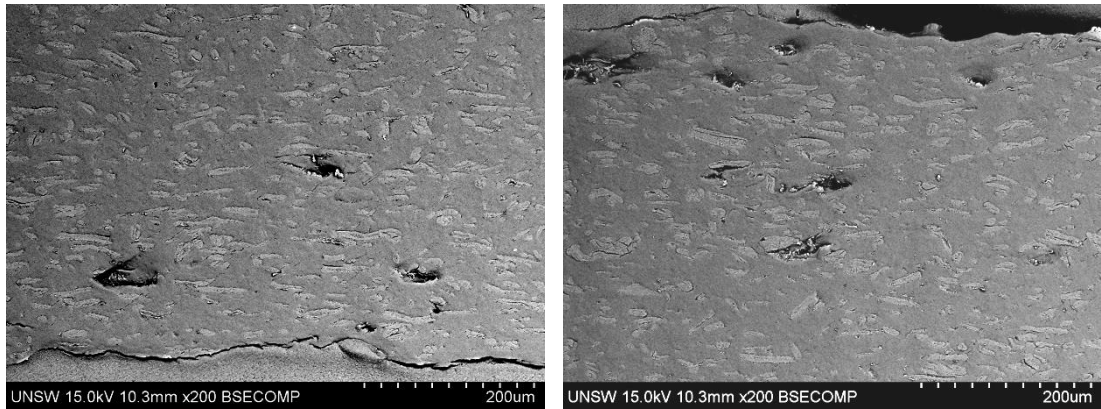


**Figure XI.32:** SEM micrographs of longitudinal section of KFTN/HDPE rod composite at edge of specimen (Sample no. 4 and End B).

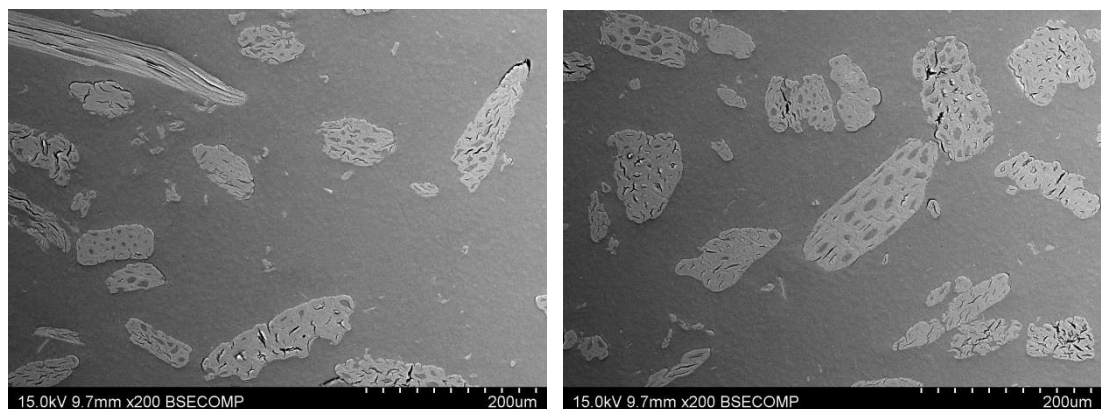


**Figure XI.33:** SEM micrographs of longitudinal section of UKF/HDPE strip composite at centre of specimen (Sample no. 1 (3A)).



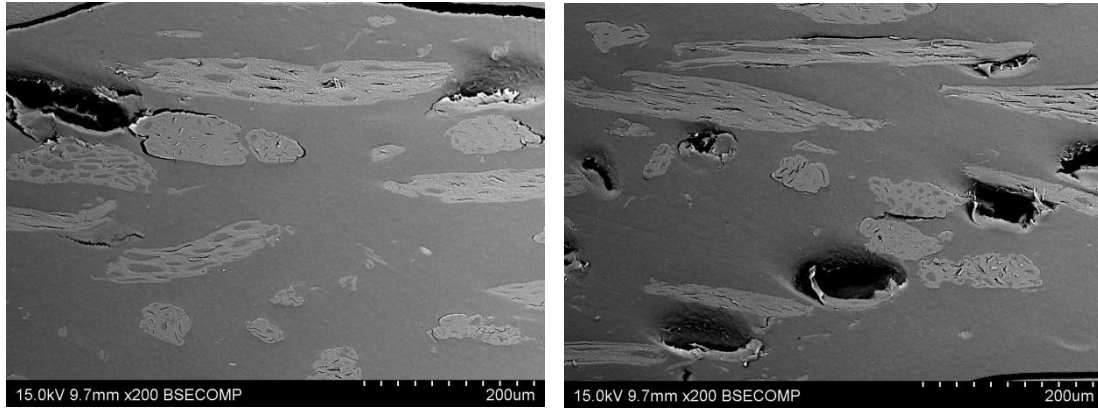


**Figure XI.34:** SEM micrographs of longitudinal section of UKF/HDPE strip composite at edge of specimen (Sample no. 1 (3A)).

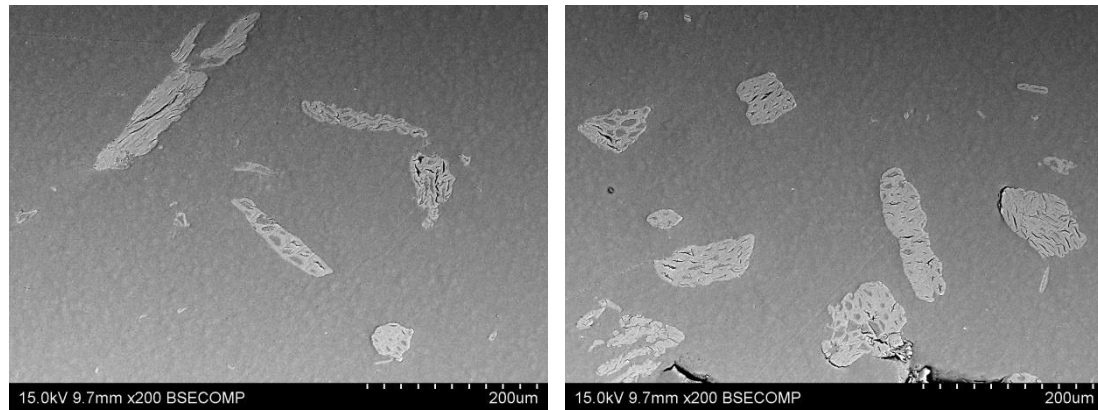


**Figure XI.35:** SEM micrographs of longitudinal section of UKF/HDPE strip composite at centre of specimen (Sample no. 2 (3C)).

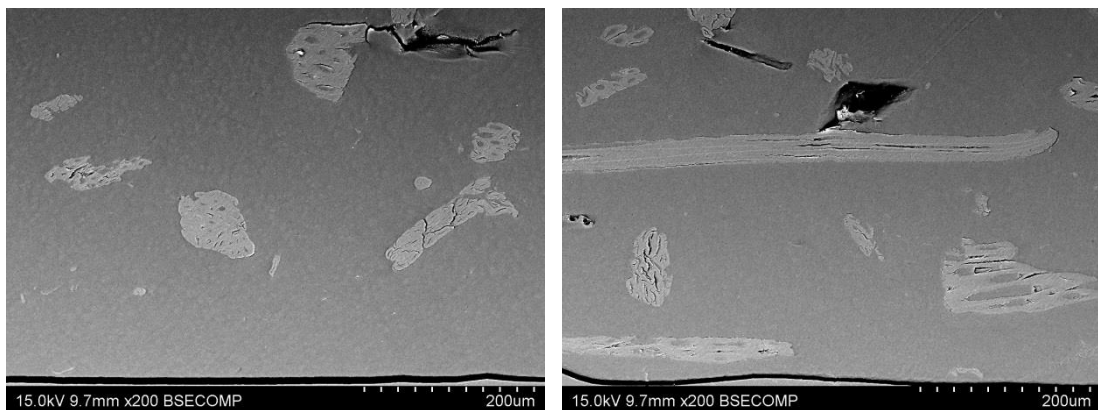


**Figure XI.36:** SEM micrographs of longitudinal section of UKF/HDPE strip composite at edge of specimen (Sample no. 2 (3C)).

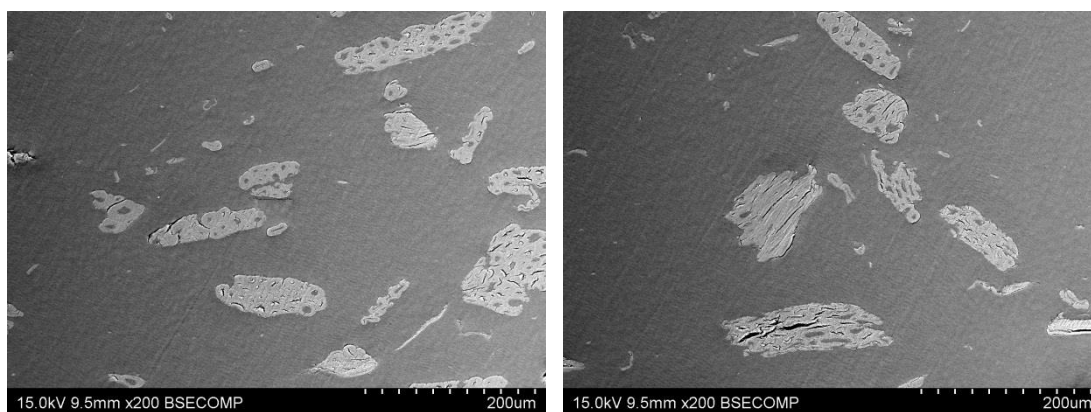


**Figure XI.37:** SEM micrographs of longitudinal section of UKF/HDPE strip composite at centre of specimen (Sample no. 3 (3H)).

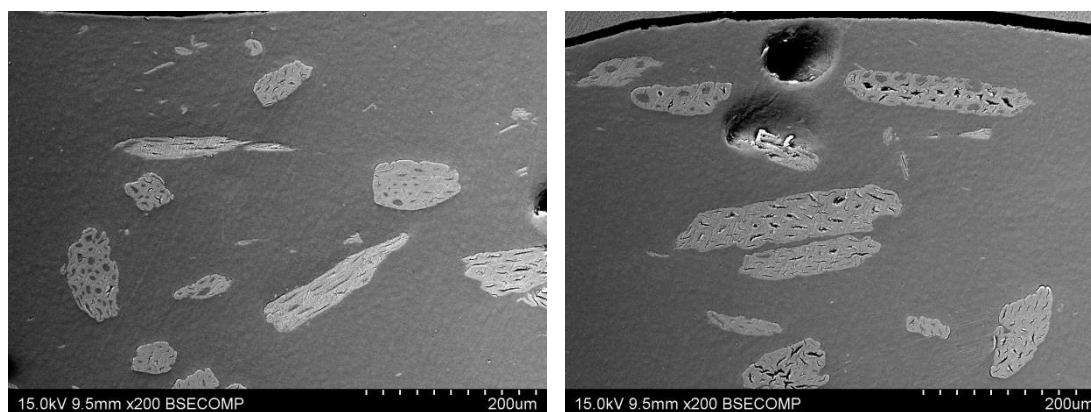


**Figure XI.38:** SEM micrographs of longitudinal section of UKF/HDPE strip composite at edge of specimen (Sample no. 3 (3H)).

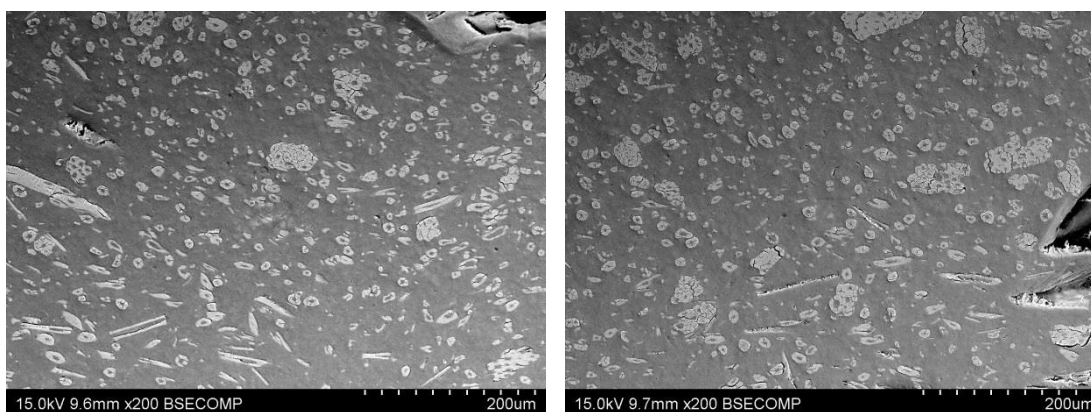


**Figure XI.39:** SEM micrographs of longitudinal section of KFTN/HDPE strip composite at centre of specimen (Sample no. 1 (2A)).

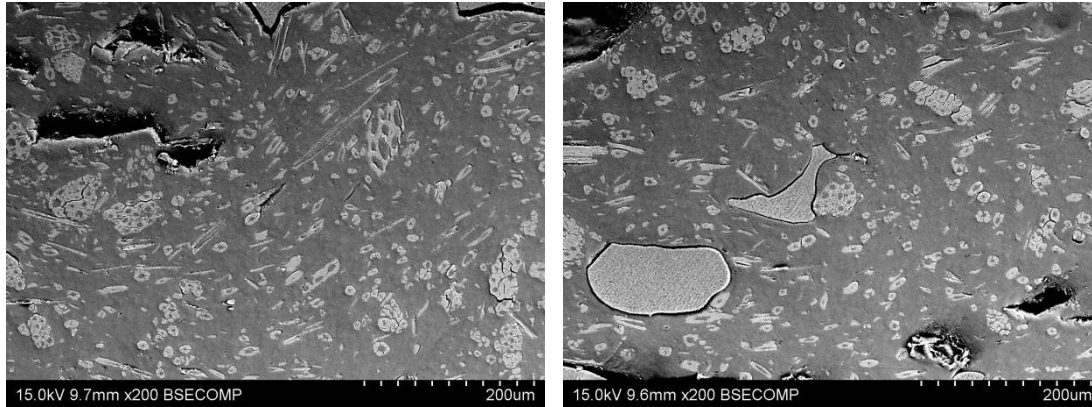


**Figure XI.40:** SEM micrographs of longitudinal section of KFTN/HDPE strip composite at edge of specimen (Sample no. 1 (2A)).

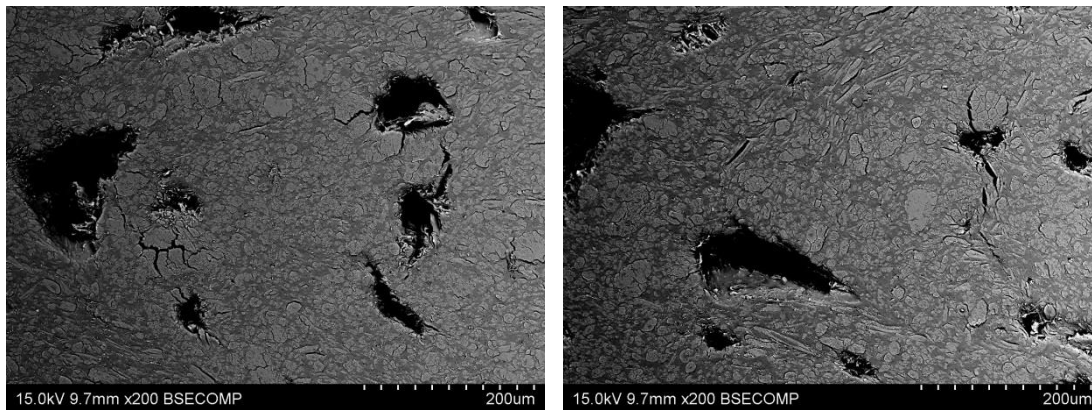


**Figure XI.41:** SEM micrographs of longitudinal section of KFTN/HDPE strip composite at centre of specimen (Sample no. 2 (2E)).

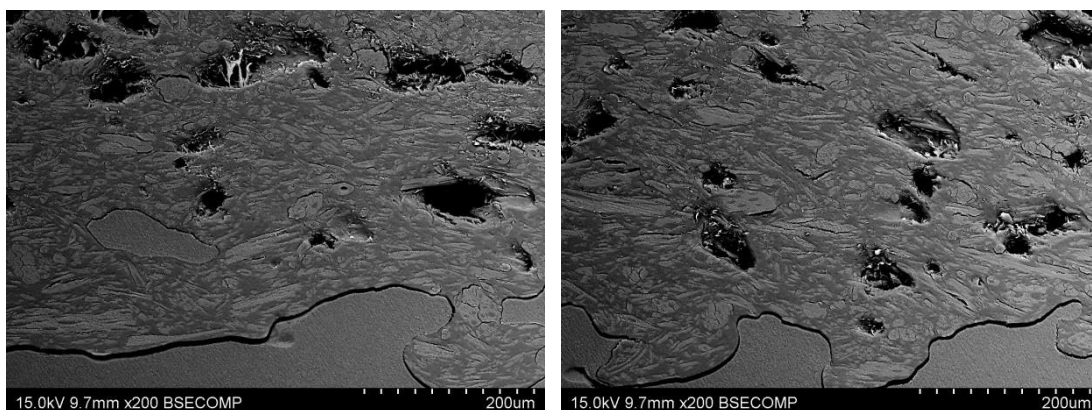


**Figure XI.42:** SEM micrographs of longitudinal section of KFTN/HDPE strip composite at edge of specimen (Sample no. 2 (2E)).

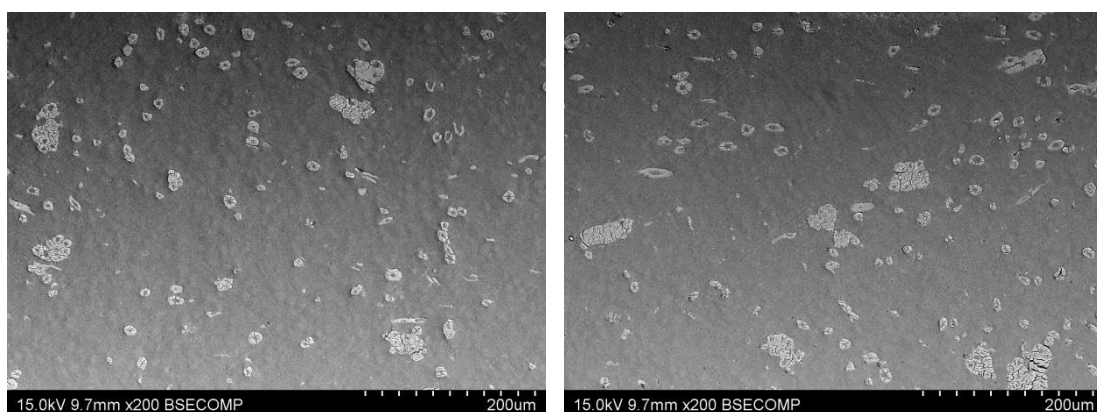


**Figure XI.43:** SEM micrographs of longitudinal section of KFTN/HDPE strip composite at centre of specimen (Sample no. 3 (2G)).

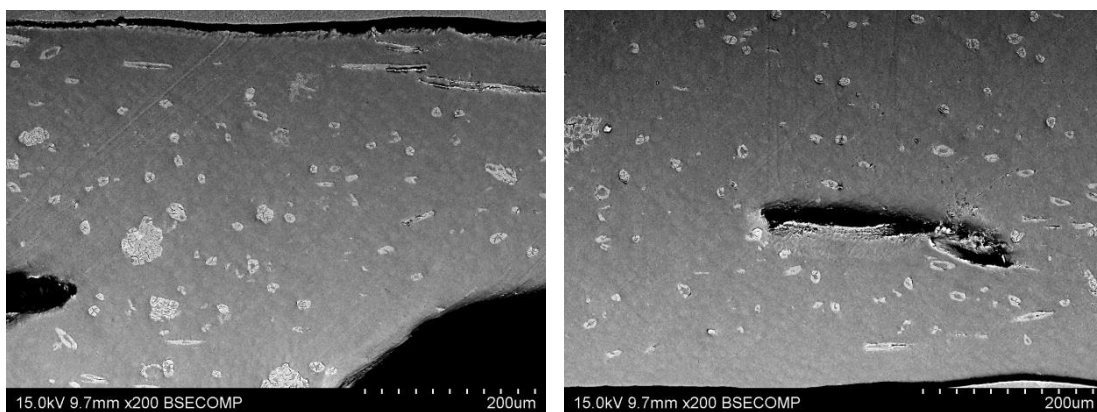


**Figure XI.44:** SEM micrographs of longitudinal section of KFTN/HDPE strip composite at edge of specimen (Sample no. 3 (2G)).

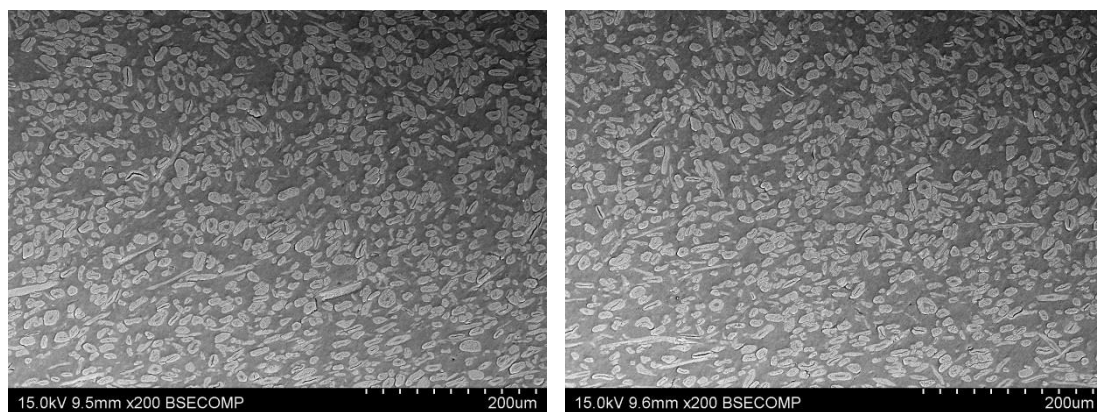


**Figure XI.45:** SEM micrographs of longitudinal section of KFTHA/HDPE strip composite at centre of specimen (Sample no. 1 (1C)).



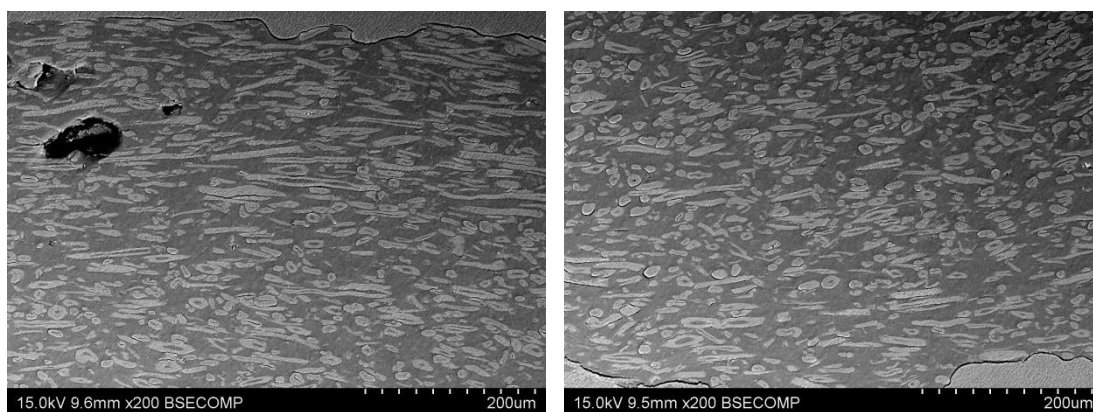


**Figure XI.46:** SEM micrographs of longitudinal section of KFTHA/HDPE strip composite at edge of specimen (Sample no. 1 (1C)).

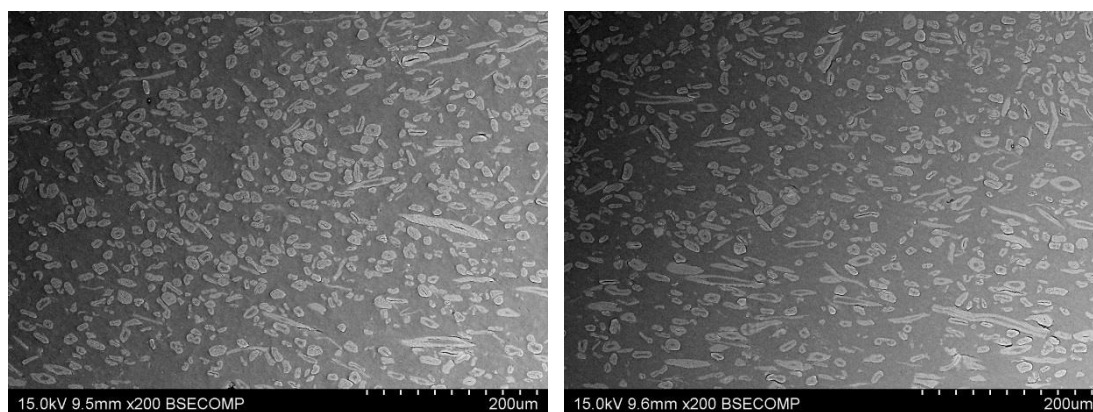


**Figure XI.47:** SEM micrographs of longitudinal section of KFTHA/HDPE strip composite at centre of specimen (Sample no. 2 (1D)).

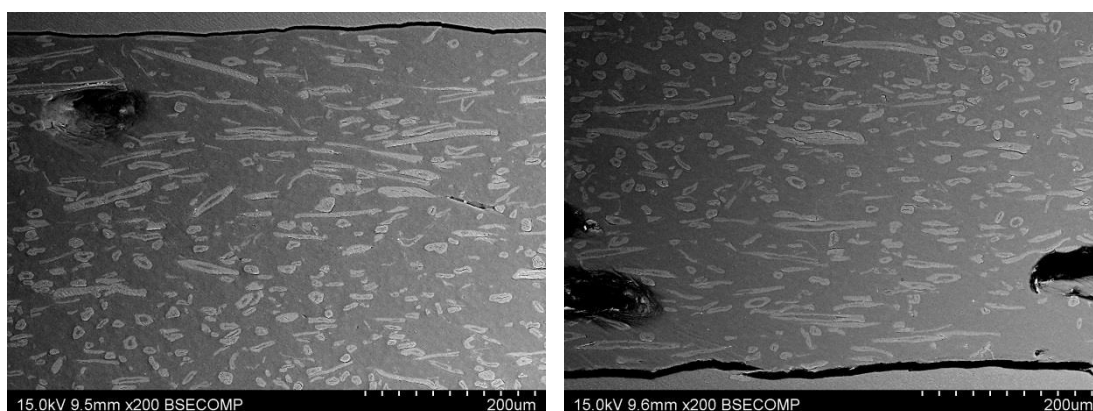


**Figure XI.48:** SEM micrographs of longitudinal section of KFTHA/HDPE strip composite at edge of specimen (Sample no. 2 (1D)).

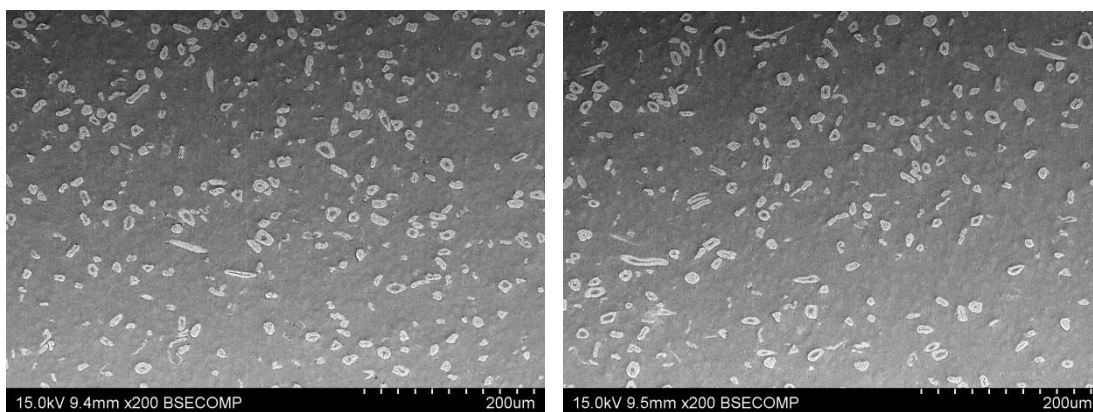


**Figure XI.49:** SEM micrographs of longitudinal section of KFTHA/HDPE strip composite at centre of specimen (Sample no. 3 (1G)).

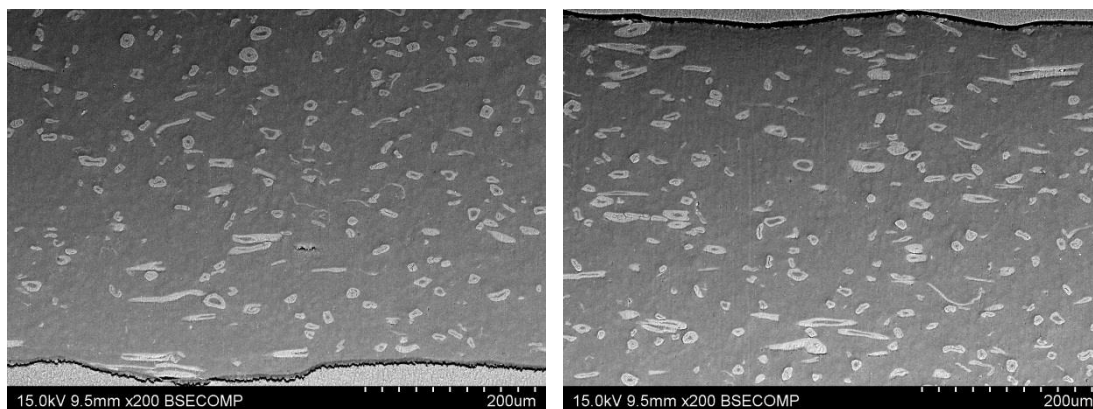


**Figure XI.50:** SEM micrographs of longitudinal section of KFTHA/HDPE strip composite at edge of specimen (Sample no. 3 (1G)).

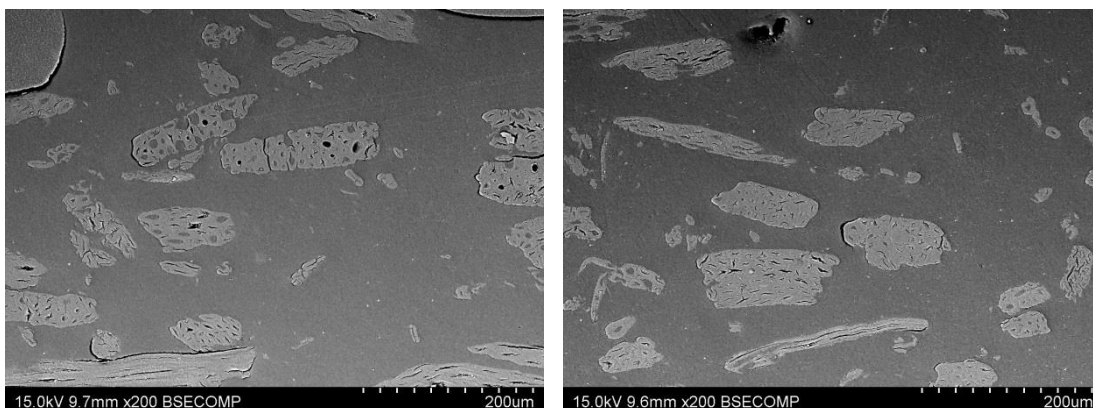


**Figure XI.51:** SEM micrographs of longitudinal section of UKF/HDPE\_H strip composite at centre of specimen (Sample no. 1 (7B)).

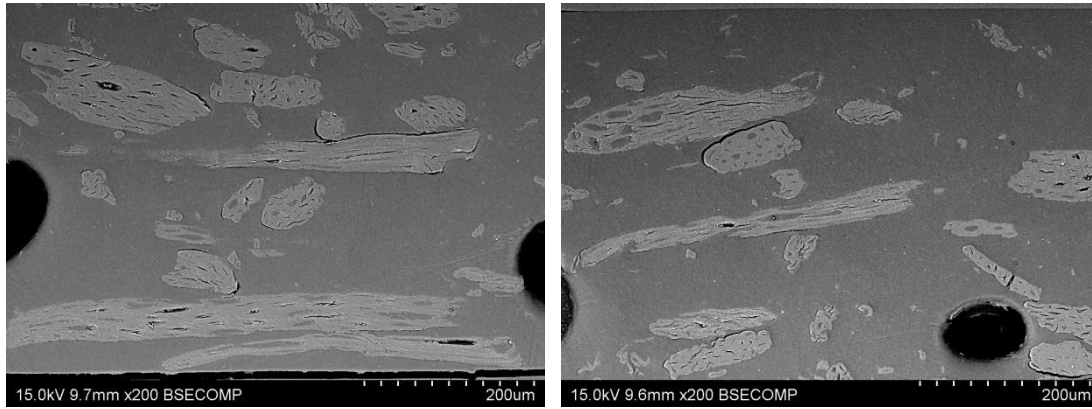


**Figure XI.52:** SEM micrographs of longitudinal section of UKF/HDPE\_H strip composite at edge of specimen (Sample no. 1 (7B)).

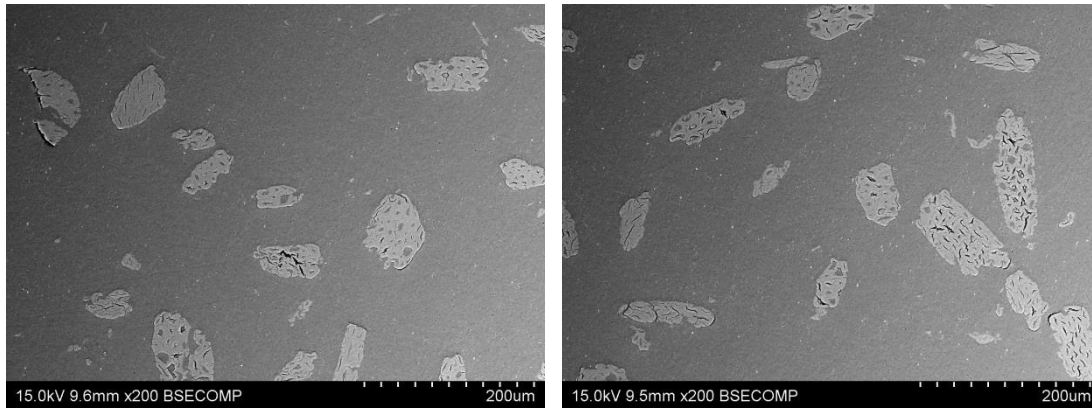


**Figure XI.53:** SEM micrographs of longitudinal section of UKF/HDPE\_H strip composite at centre of specimen (Sample no. 2 (7E)).

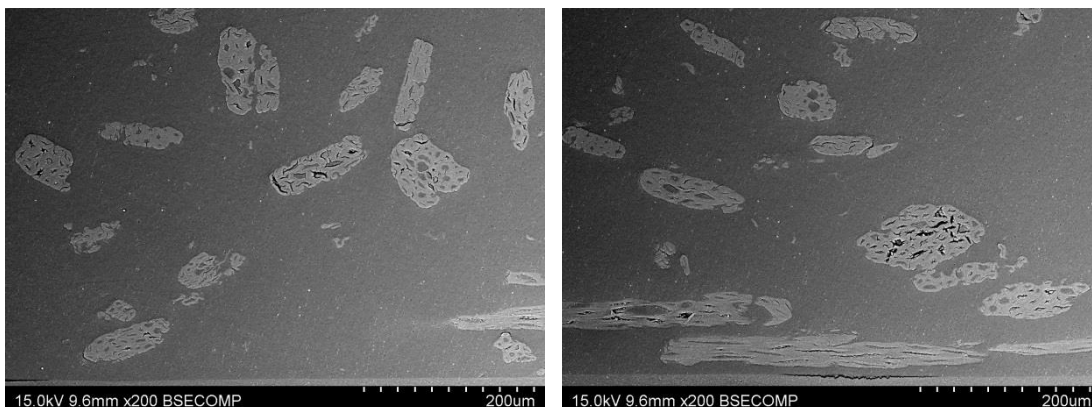


**Figure XI.54:** SEM micrographs of longitudinal section of UKF/HDPE\_H strip composite at edge of specimen (Sample no. 2 (7E)).

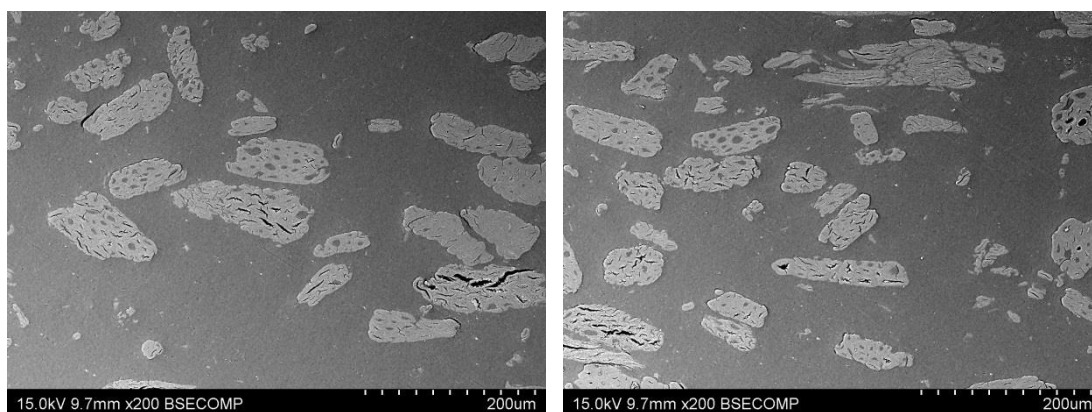


**Figure XI.55:** SEM micrographs of longitudinal section of UKF/HDPE\_H strip composite at centre of specimen (Sample no. 3 (7G)).

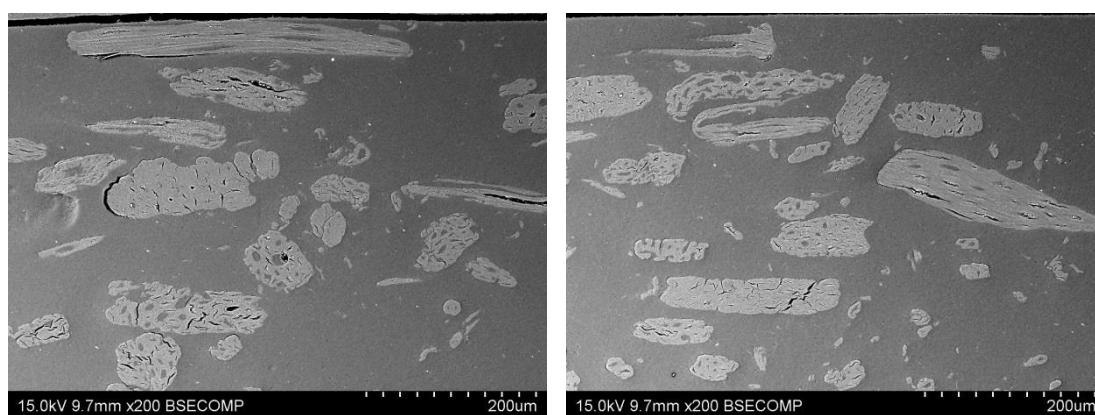


**Figure XI.56:** SEM micrographs of longitudinal section of UKF/HDPE\_H strip composite at edge of specimen (Sample no. 3 (7G)).

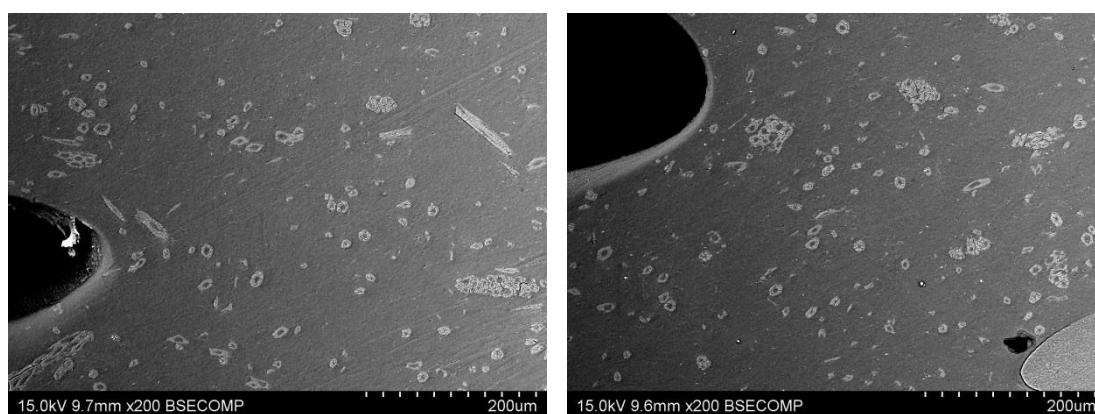


**Figure XI.57:** SEM micrographs of longitudinal section of KFTN/HDPE\_H strip composite at centre of specimen (Sample no. 1 (8B)).



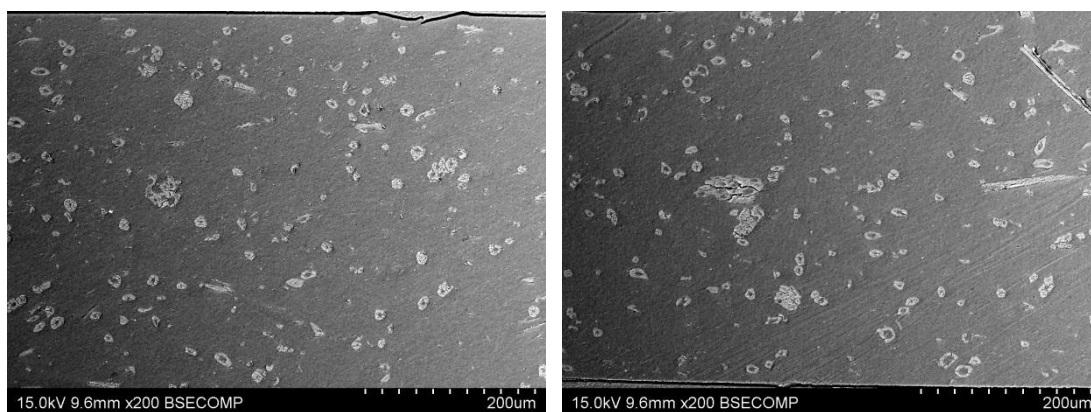


**Figure XI.58:** SEM micrographs of longitudinal section of KFTN/HDPE\_H strip composite at edge of specimen (Sample no. 1 (8B)).

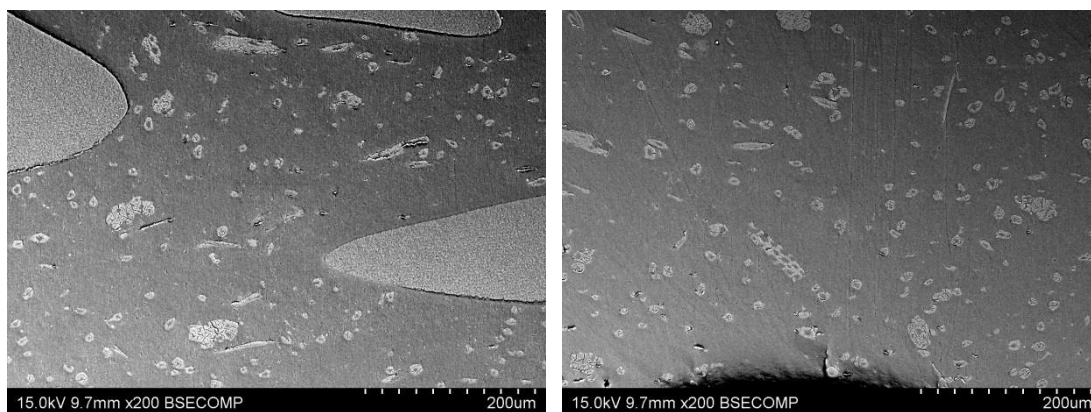


**Figure XI.59:** SEM micrographs of longitudinal section of KFTN/HDPE\_H strip composite at centre of specimen (Sample no. 2 (8D)).

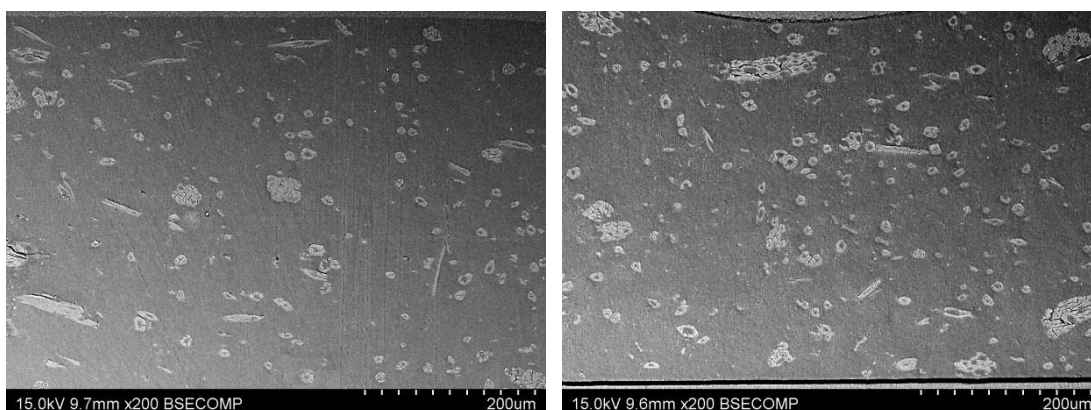


**Figure XI.60:** SEM micrographs of longitudinal section of KFTN/HDPE\_H strip composite at edge of specimen (Sample no. 2 (8D)).

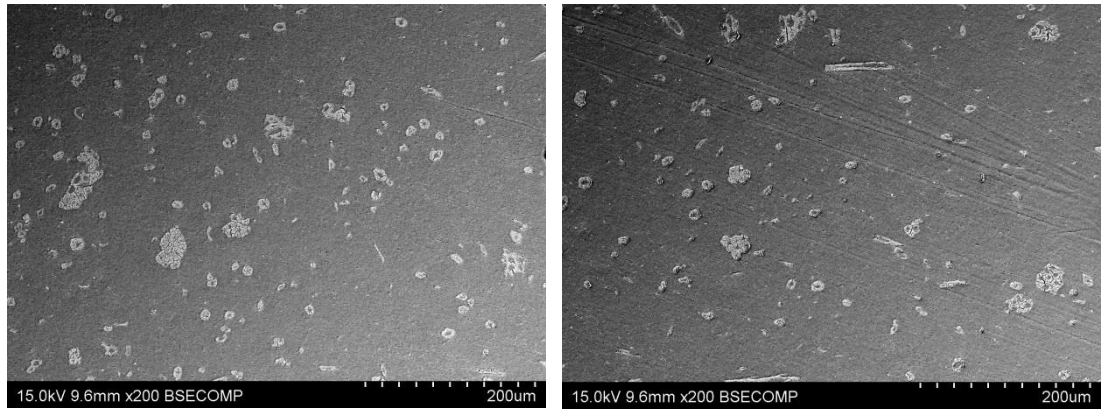


**Figure XI.61:** SEM micrographs of longitudinal section of KFTN/HDPE\_H strip composite at centre of specimen (Sample no. 3 (8F)).

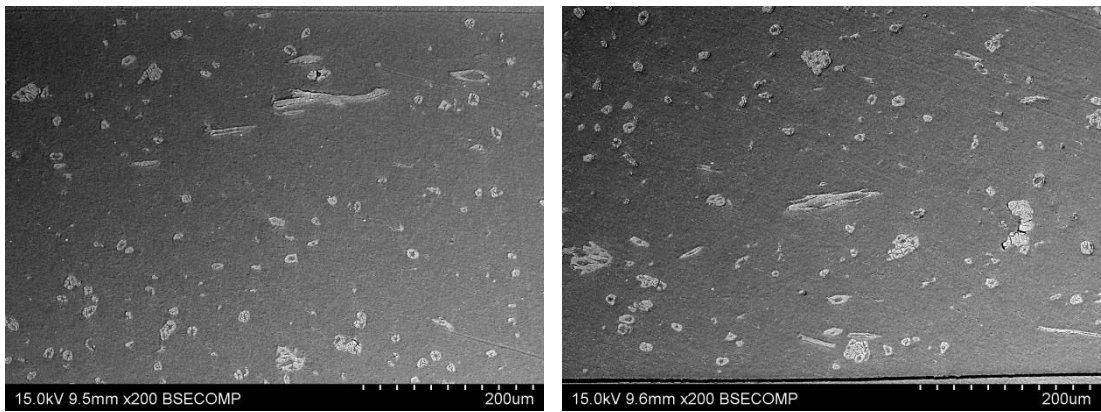


**Figure XI.62:** SEM micrographs of longitudinal section of KFTN/HDPE\_H strip composite at edge of specimen (Sample no. 3 (8F)).

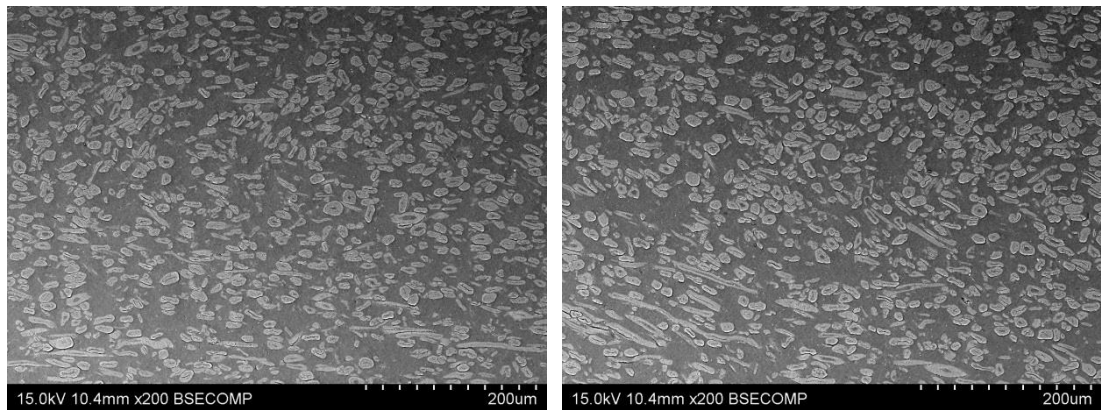


**Figure XI.63:** SEM micrographs of longitudinal section of KFTHA/HDPE\_H strip composite at centre of specimen (Sample no. 1 (6B)).

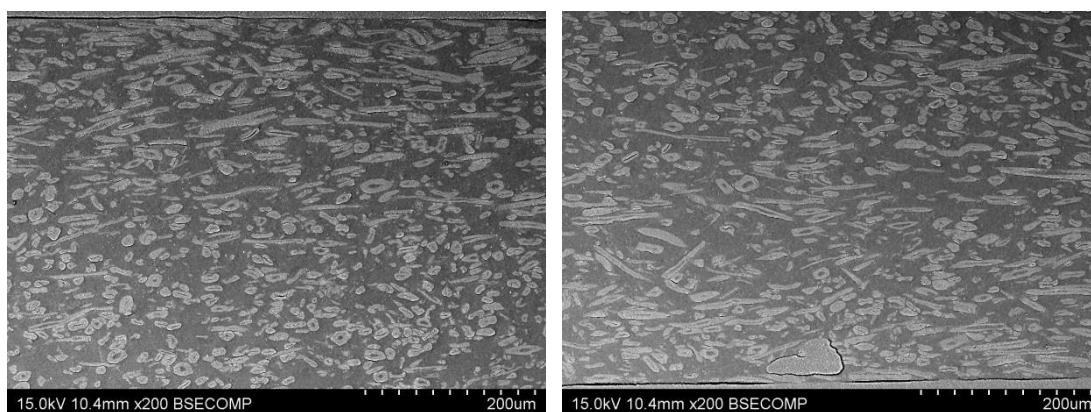


**Figure XI.64:** SEM micrographs of longitudinal section of KFTHA/HDPE\_H strip composite at edge of specimen (Sample no. 1 (6B)).

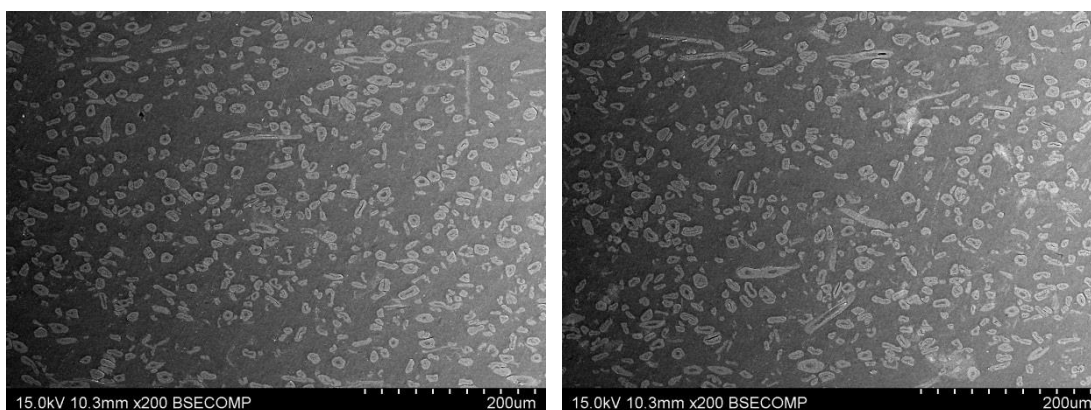


**Figure XI.65:** SEM micrographs of longitudinal section of KFTHA/HDPE\_H strip composite at centre of specimen (Sample no. 2 (6E)).

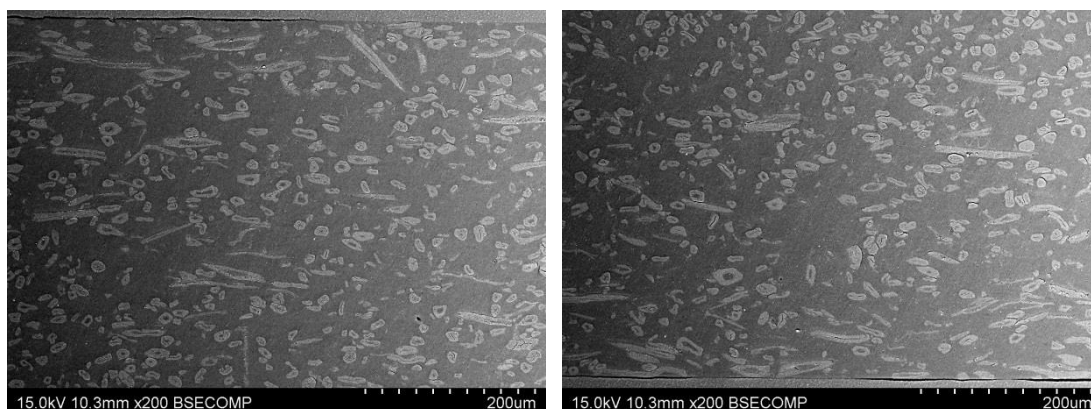


**Figure XI.66:** SEM micrographs of longitudinal section of KFTHA/HDPE\_H strip composite at edge of specimen (Sample no. 2 (6E)).

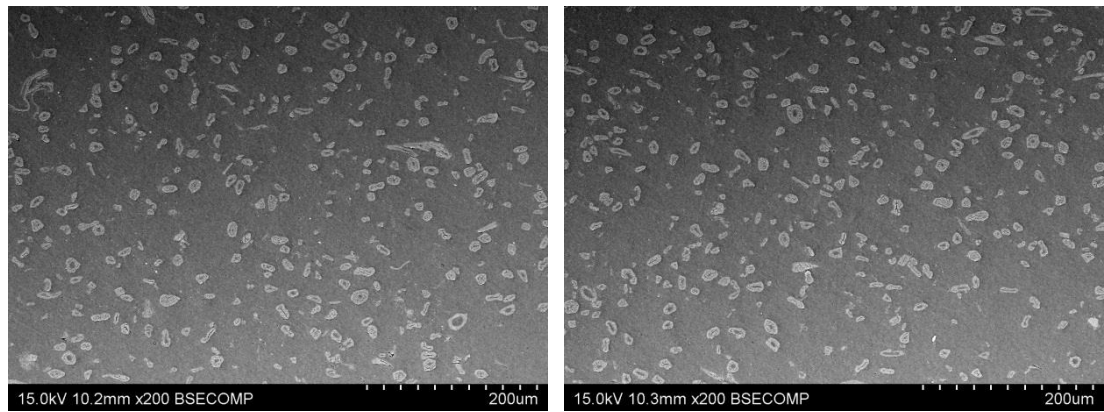


**Figure XI.67:** SEM micrographs of longitudinal section of KFTHA/HDPE\_H strip composite at centre of specimen (Sample no. 3 (6G)).

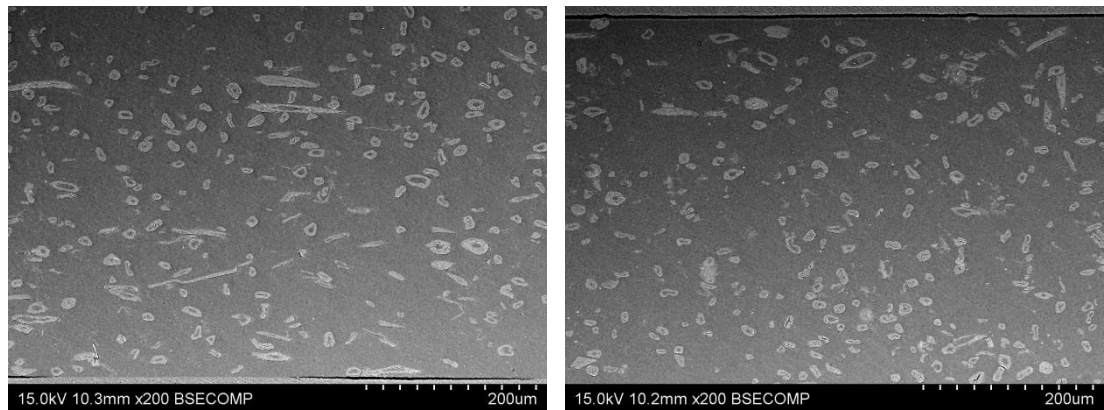


**Figure XI.68:** SEM micrographs of longitudinal section of KFTHA/HDPE\_H strip composite at edge of specimen (Sample no. 3 (6G)).



**Appendix XII: T Test and One-Way Analysis of Variance (ANOVA) Output for Tensile Property Test Data for Extruded HDPE and Short Kenaf Fibre/HDPE Rod Composites**



## **T Test and One-Way Analysis of Variance (ANOVA) Output at 95% Confidence Interval for Tensile Properties of Extruded HDPE and Short Kenaf Fibre/HDPE Rod Composites**

### **Tensile Modulus**

*All of the Extruded Rods*

<b>ANOVA Table</b>	<b>Sum of Squares</b>	<b>df</b>	<b>Mean Square</b>	<b>F</b>	<b>Sig.</b>
Between groups	0.03587	2	0.01793	22.48	< 0.0001
Within groups	0.03749	47	0.0007976		
Total	0.07335	49			

<b>Tukey's Multiple Comparison Test</b>	<b>Mean Difference</b>	<b>q</b>	<b>Significant (p &lt; 0.05)</b>	<b>95% Confidence Interval of diff.</b>
HDPE vs UKF/HDPE	-0.08703	9.462	Yes	-0.1185 to -0.05555
HDPE vs KFTN/HDPE	-0.07198	7.827	Yes	-0.1035 to -0.04051
UKF/HDPE vs KFTN/HDPE	0.01505	2.499	No	-0.005562 to 0.03565



## ***Effects of Reinforcements***

### ***1. HDPE versus UKF/HDPE***

<b>Sample</b>	<b>N</b>	<b>Mean</b>	<b>Std. Deviation</b>	<b>Std. Error Mean</b>	<b>t</b>	<b>df</b>	<b>P value (One-tailed)</b>	<b>Significant?</b>
HDPE	6	0.2383	0.009331	0.003809	6.611	26	< 0.0001	Yes
UKF/HDPE	22	0.3254	0.03148	0.006711				

### ***2. HDPE versus KFTN/HDPE***

<b>Sample</b>	<b>N</b>	<b>Mean</b>	<b>Std. Deviation</b>	<b>Std. Error Mean</b>	<b>t</b>	<b>df</b>	<b>P value (One-tailed)</b>	<b>Significant?</b>
HDPE	6	0.2383	0.009331	0.003809	6.171	26	< 0.0001	Yes
KFTN/HDPE	22	0.3103	0.02781	0.005929				

## ***Effects of Kenaf Fibre Types***

<b>Sample</b>	<b>N</b>	<b>Mean</b>	<b>Std. Deviation</b>	<b>Std. Error Mean</b>	<b>t</b>	<b>df</b>	<b>P value (One-tailed)</b>	<b>Significant?</b>
UKF/HDPE	22	0.3254	0.03148	0.006711	1.680	42	0.1004	No
KFTN/HDPE	22	0.3103	0.02781	0.005929				

## **Tensile Strength**

### ***All of the Extruded Rods***

<b>ANOVA Table</b>	<b>Sum of Squares</b>	<b>df</b>	<b>Mean Square</b>	<b>F</b>	<b>Sig.</b>
Between groups	105.1	2	52.57	7.103	0.0020
Within groups	347.8	47	7.400		
Total	452.9	49			

<b>Tukey's Multiple Comparison Test</b>	<b>Mean Difference</b>	<b>q</b>	<b>Significant (p &lt; 0.05)</b>	<b>95% Confidence Interval of diff.</b>
HDPE vs UKF/HDPE	-4.332	4.889	Yes	-7.364 to -1.299
HDPE vs KFTN/HDPE	-2.240	2.528	No	-5.272 to 0.7924
UKF/HDPE vs KFTN/HDPE	2.092	3.607	Yes	0.1068 to 4.077

## ***Effects of Reinforcements***

### ***1. HDPE versus UKF/HDPE***

<b>Sample</b>	<b>N</b>	<b>Mean</b>	<b>Std. Deviation</b>	<b>Std. Error Mean</b>	<b>t</b>	<b>df</b>	<b>P value (One-tailed)</b>	<b>Significant?</b>
HDPE	6	19.11	1.615	0.6593	4.625	26	< 0.0001	Yes
UKF/HDPE	22	23.44	2.121	0.4521				

### ***2. HDPE versus KFTN/HDPE***

<b>Sample</b>	<b>N</b>	<b>Mean</b>	<b>Std. Deviation</b>	<b>Std. Error Mean</b>	<b>t</b>	<b>df</b>	<b>P value (Two-tailed)</b>	<b>Significant?</b>
HDPE	6	19.11	1.615	0.6593	1.558	26	0.1314	No
KFTN/HDPE	22	21.35	3.383	0.7212				

## ***Effects of Kenaf Fibre Types***

<b>Sample</b>	<b>N</b>	<b>Mean</b>	<b>Std. Deviation</b>	<b>Std. Error Mean</b>	<b>t</b>	<b>df</b>	<b>P value (One-tailed)</b>	<b>Significant?</b>
UKF/HDPE	22	23.44	2.121	0.4521	2.457	42	0.0091	Yes
KFTN/HDPE	22	21.35	3.383	0.7212				

## **Strain at Maximum Stress**

### ***All of the Extruded Rods***

<b>ANOVA Table</b>	<b>Sum of Squares</b>	<b>df</b>	<b>Mean Square</b>	<b>F</b>	<b>Sig.</b>
Between groups	2218	2	1109	200.8	< 0.0001
Within groups	259.6	47	5.523		
Total	2478	49			

<b>Tukey's Multiple Comparison Test</b>	<b>Mean Difference</b>	<b>q</b>	<b>Significant (p &lt; 0.05)</b>	<b>95% Confidence Interval of diff.</b>
HDPE vs UKF/HDPE	20.90	27.31	Yes	18.28 to 23.52
HDPE vs KFTN/HDPE	20.01	26.15	Yes	17.39 to 22.63
UKF/HDPE vs KFTN/HDPE	-0.8850	1.766	No	-2.600 to 0.8298

## ***Effects of Reinforcements***

### ***1. HDPE versus UKF/HDPE***

<b>Sample</b>	<b>N</b>	<b>Mean</b>	<b>Std. Deviation</b>	<b>Std. Error Mean</b>	<b>t</b>	<b>df</b>	<b>P value (One-tailed)</b>	<b>Significant?</b>
HDPE	6	30.25	4.192	1.711	21.02	26	< 0.0001	Yes
UKF/HDPE	22	9.352	1.261	0.2687				

### ***2. HDPE versus KFTN/HDPE***

<b>Sample</b>	<b>N</b>	<b>Mean</b>	<b>Std. Deviation</b>	<b>Std. Error Mean</b>	<b>t</b>	<b>df</b>	<b>P value (One-tailed)</b>	<b>Significant?</b>
HDPE	6	30.25	4.192	1.711	14.73	26	< 0.0001	Yes
KFTN/HDPE	22	10.24	2.567	0.5472				

## ***Effects of Kenaf Fibre Types***

<b>Sample</b>	<b>N</b>	<b>Mean</b>	<b>Std. Deviation</b>	<b>Std. Error Mean</b>	<b>t</b>	<b>df</b>	<b>P value (Two-tailed)</b>	<b>Significant?</b>
UKF/HDPE	22	9.352	1.261	0.2687	1.452	42	0.1540	No
KFTN/HDPE	22	10.24	2.567	0.5472				

**Appendix XIII: Tensile Stress-Strain Curves of  
Extruded HDPE and Short Kenaf Fibre/HDPE Strip  
Composites**



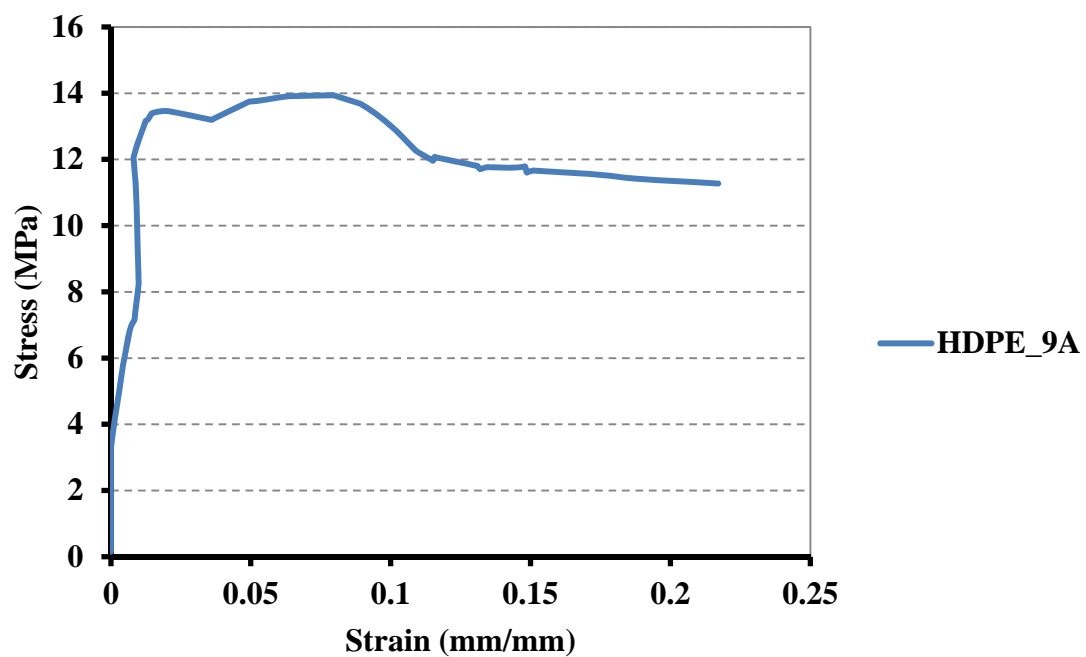


**Figure XIII.1:** Tensile stress-strain curve of extruded HDPE strip.

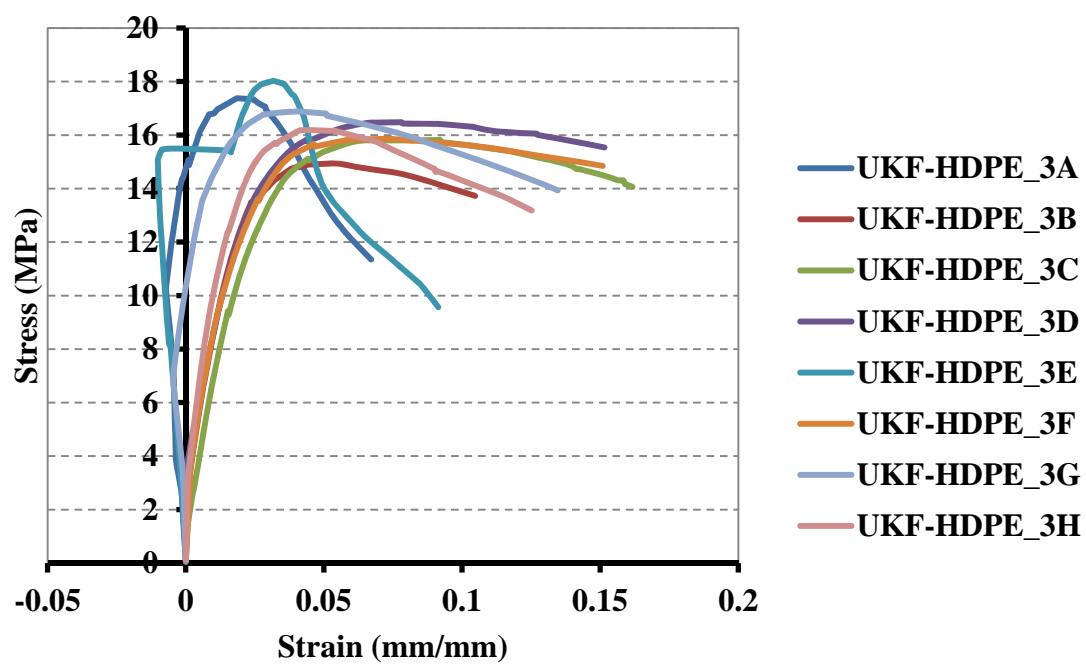


**Figure XIII.2:** Tensile stress-strain curves of extruded UKF/HDPE strip composites.



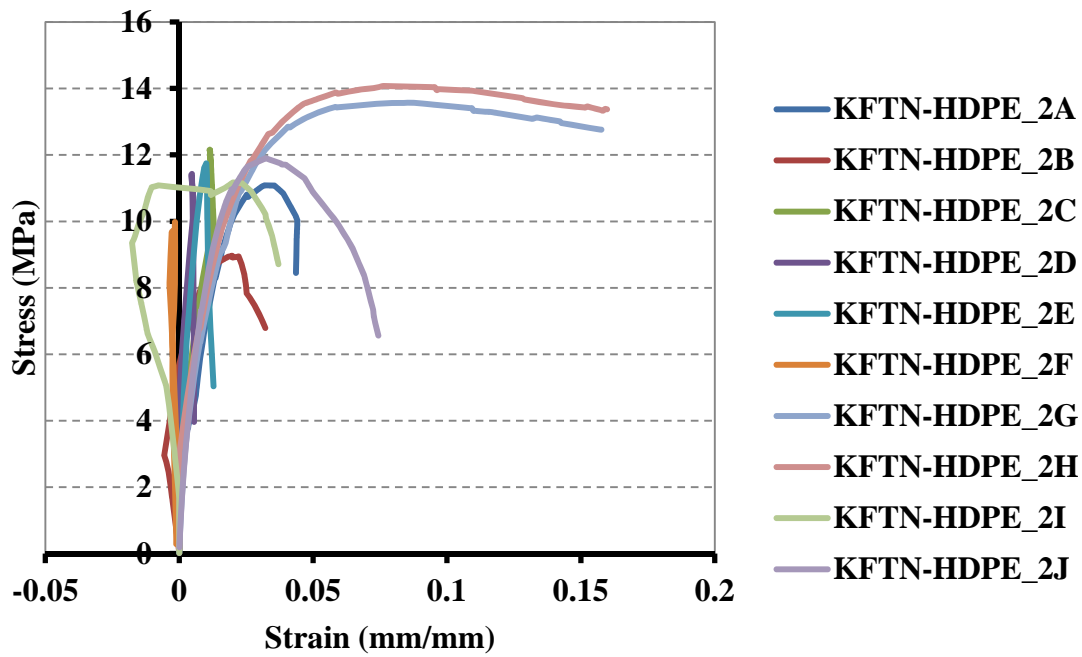


**Figure XIII.3:** Tensile stress-strain curves of extruded KFTN/HDPE strip composites.

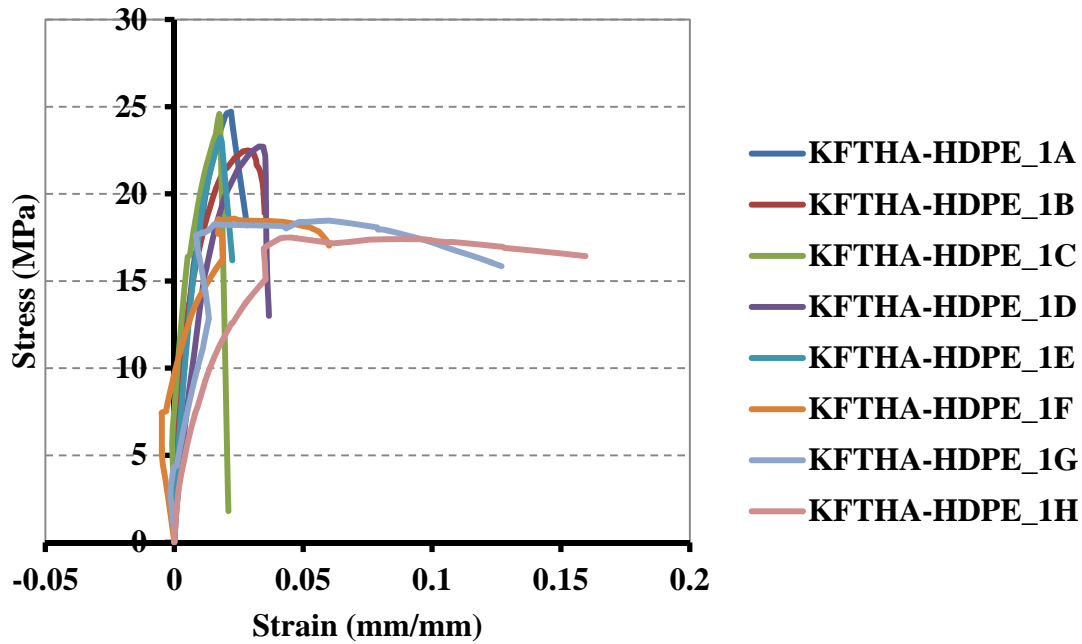


**Figure XIII.4:** Tensile stress-strain curves of extruded KFTHA/HDPE strip composites.

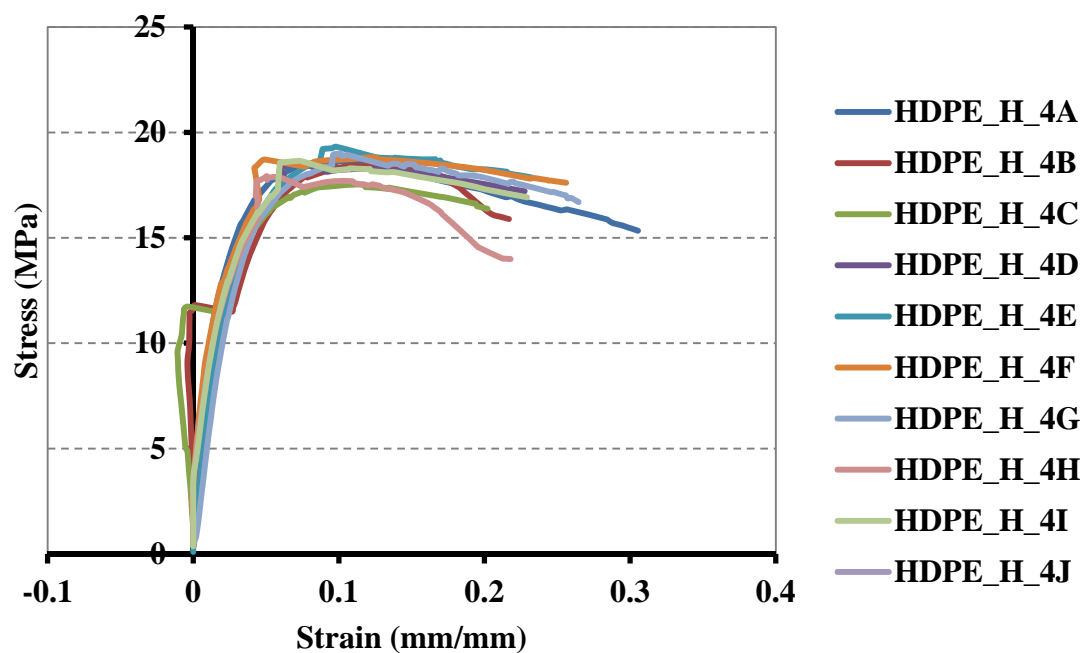


**Figure XIII.5:** Tensile stress-strain curves of hot pressed extruded HDPE (HDPE\_H) strips.

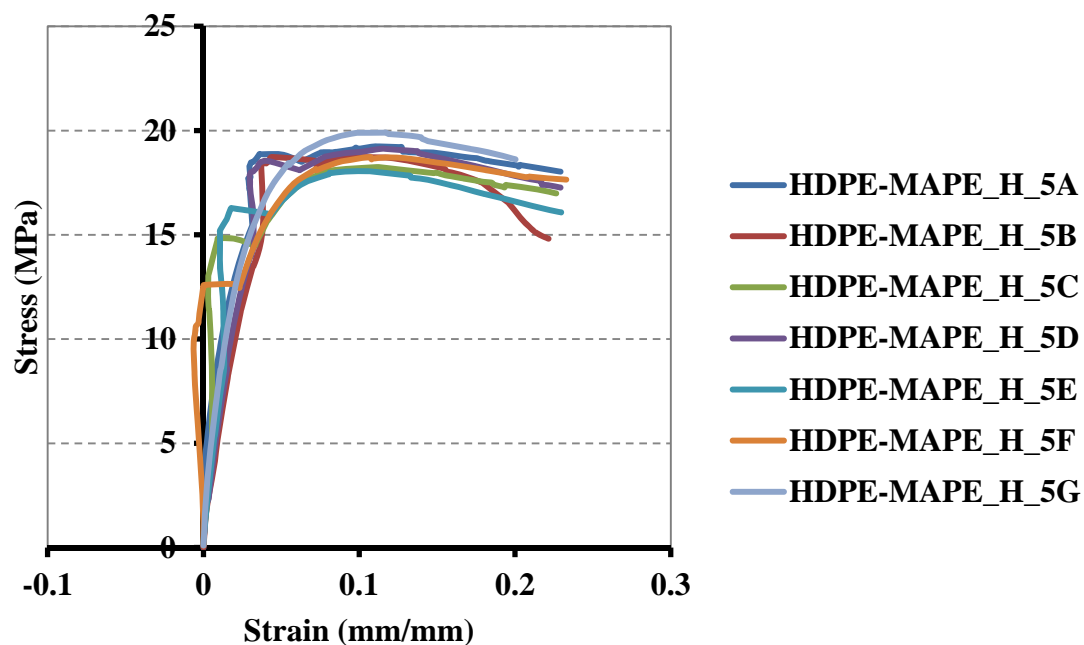


**Figure XIII.6:** Tensile stress-strain curves of hot pressed extruded HDPE/MAPE (HDPE/MAPE\_H) strips.

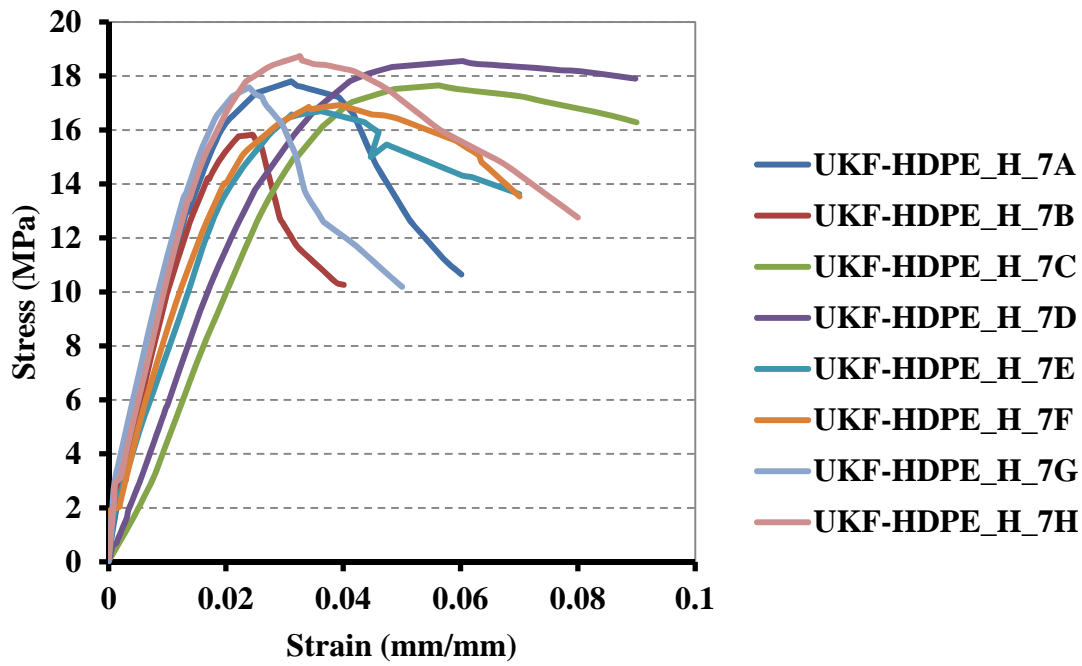


**Figure XIII.7:** Tensile stress-strain curves of hot pressed extruded UKF/HDPE (UKF/HDPE\_H) strip composites.

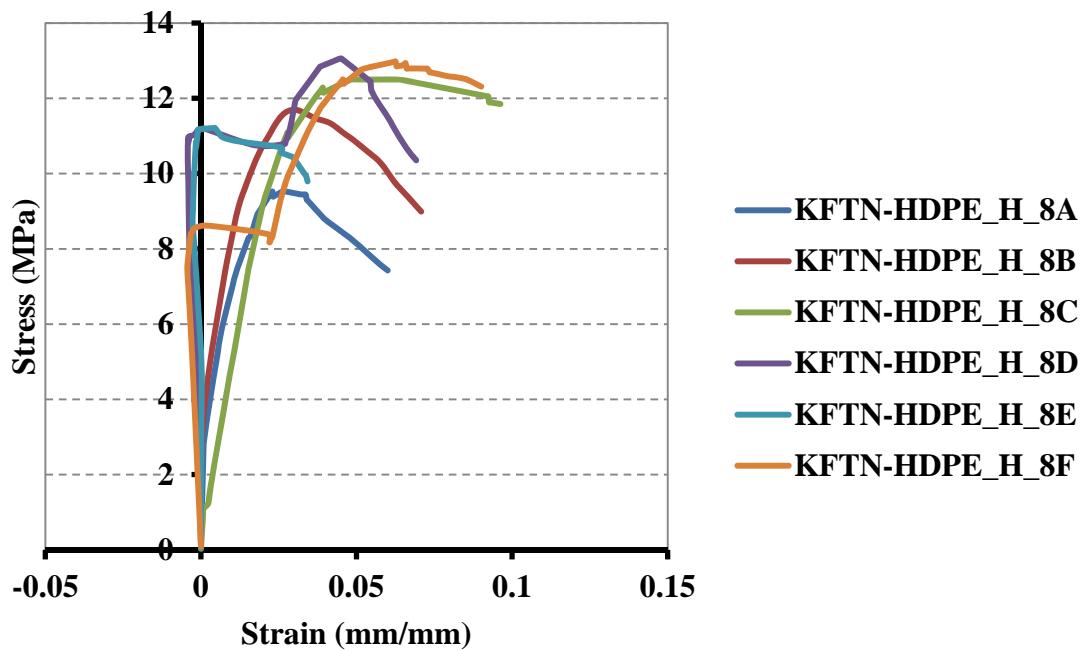


**Figure XIII.8:** Tensile stress-strain curves of hot pressed extruded KFTN/HDPE (KFTN/HDPE\_H) strip composites.

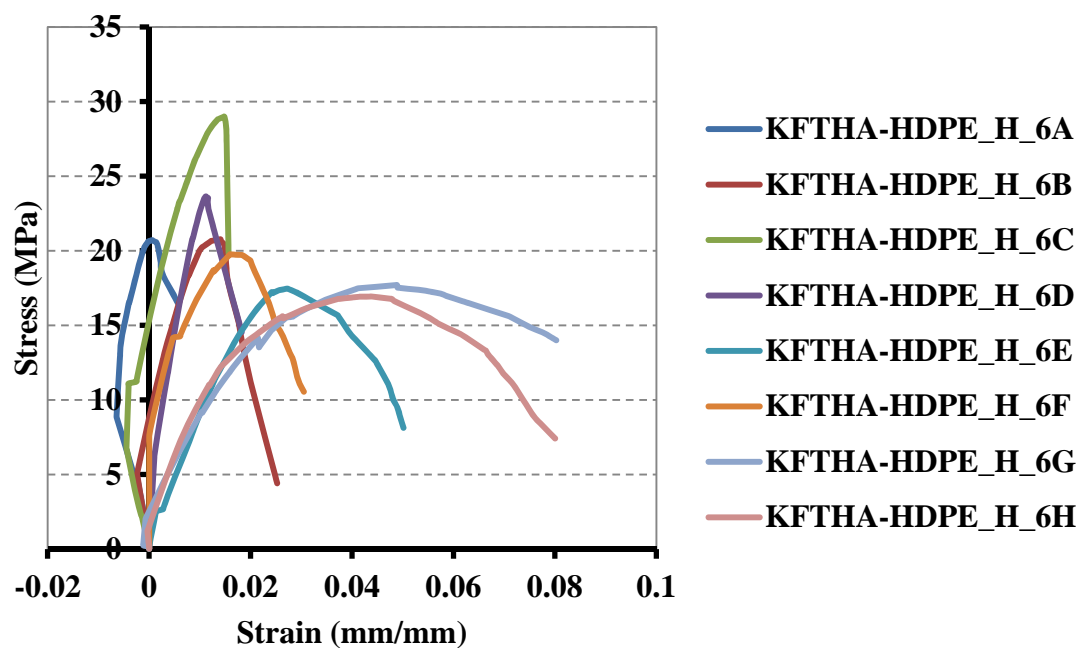


**Figure XIII.9:** Tensile stress-strain curves of hot pressed extruded KFTHA/HDPE (KFTHA/HDPE\_H) strip composites.



## **Appendix XIV: Material Data Sheets for Flax Fabric and Vinyl Ester Resin**



## Biotex Flax Technical Information



### Yarn

Linear Density	250tex	Standard
	125-2000tex	On request

Processing	Typical processes include filament winding and pultrusion, processed in the same way as glass fibre.	
------------	--	--

### Fabrics

Woven Fabrics	2x2 twill	Standard
	4x4 hopsack	Standard
	Others	On request

Non-Crimp Fabrics	Unidirectional	Standard
	+/-45 biaxial	Standard
	Others	On request

Fabric Weight	420-520gsm	Standard (depending on weave style)
	250-800gsm	On request

Fabric Width	1.25m	Standard
	Up to 3m	On request (woven fabrics only)

Processing	Typical processes for include hand lay-up, vacuum infusion and RTM with standard resins or bio-based resins. Processing is carried out in the same way as with glass fibre.	
------------	---	--

### Typical Properties

	UD flax-polyester laminate (0 dir)	Biaxial flax-polyester laminate (0 dir)	Woven flax-polyester laminate (0 dir)	
Density	1.30g/cm <sup>3</sup>	1.30g/cm <sup>3</sup>	1.24g/cm <sup>3</sup>	
Tensile Modulus	18.8GPa	8.7GPa	7.2GPa	(ISO 527-4)
Tensile Strength	174MPa	85MPa	68.3MPa	(ISO 527-4)
Tensile Elongation	1.5%	1.7%	2.5%	(ISO 527-4)
Flexural Modulus	15.1GPa	6.8GPa	4.0GPa	(ISO 14125)
Flexural Strength	196MPa	135MPa	97.4MPa	(ISO 14125)
Charpy Impact (flat)	TBC	TBC	28.0kJ/m <sup>2</sup>	(ISO 179-1 U)
Charpy Impact (edge)	TBC	TBC	27.7kJ/m <sup>2</sup>	(ISO 179-1 U)

Data for laminates made from 30-33vol% Biotex flax fabrics and unsaturated polyester by the vacuum infusion process and tested at ambient temperature.





**ArmorStar® VE**  
VE MC • VE SX • VE BX

## IVSXH210

### Vinyl Ester Infusion Resin

Copyright 2010

#### Description

ArmorStar® IVSXH210 is a pre-promoted, vinyl ester blended resin containing styrene monomer. It is formulated for building reinforced plastic parts using closed molding processes and specifically infusion processes such as vacuum bagging, SCRIMP®, and resin injection.

#### Features and Benefits

ArmorStar® IVSXH210 offers the following features:

- Low viscosity for good fiber wetting and mold filling performance
- Rapid fill times
- Rapid cure and Barcol development for quick demold
- Excellent strength and toughness for crack resistance
- High heat distortion temperature (HDT)
- Superior blister resistance
- Good surface cosmetics
- Compatible with standard catalyst and CHP/MEKP blends

#### Typical Liquid Properties (at 77°F)

Liquid properties of ArmorStar® IVSXH210 are shown below. These values may or may not be manufacturing control criteria; they are listed for a reference guide only. Particular batches will not conform exactly to the numbers listed because storage conditions, temperature changes, age, testing equipment (type and procedure) can each have a significant effect on the results. Products outside of these readings can perform acceptably. Final suitability of this product is in the end use performance.

Test	ArmorStar® IVSXH210
Viscosity <sup>1</sup>	100 cps
Gel Time <sup>2</sup>	20 minutes

CCP Composites US • P.O. Box 419389 • Kansas City • Missouri • 64141-6389  
Tel. 800-821-3590 • Tel. 816-391-6000 • Fax 816-391-6337 • [www.ccpcompositesus.com](http://www.ccpcompositesus.com)

## IVSXH210 - Copyright 2010

Weight per Gallon	9.0
-------------------	-----

<sup>1</sup>Brookfield RVF #2 at 50 rpm<sup>2</sup>100 g mass, 1.50% Luperox® DDM-9**Physical Properties**

The physical properties of ArmorStar® IVSXH210 are shown below. The properties given below are for well cured castings and laminates. Resin and laminates at different stages of cure will have varying properties.

Test	Test Method <sup>1</sup>	Neat Resin Casting <sup>2</sup>	Laminate <sup>3</sup>
Tensile Strength	ASTM D638	9,500 psi	16,000 psi
Tensile Modulus		580,000 psi	1,460,000 psi
Tensile Elongation		2.4%	1.6%
Flexural Strength	ASTM D790	16,000 psi	31,000 psi
Flexural Modulus		590,000 psi	1,290,000 psi
Glass Transition Temperature, Tg	CCP-22-TAS-TM-3008 (DMA)	230°F (110°C)	—

<sup>1</sup>All tests run per internal CCP test methods. These methods are similar to the ASTM Method listed above.<sup>2</sup>Neat resin casting catalyzed with 1.5% Arkema Luperox® DHD-9. The casting cured for 16 hours at room temperature and was post cured for 4 hours at 150°F.<sup>3</sup>Laminate - Resin initiated with 1.5% Arkema Luperox® DHD-9. The laminate schedule was 2 plies of 1.5 oz. CSM. Glass content was 35-37%. The panel was cured for 16 hours at room temperature and post cured for 4 hours at 150°F.**Application**

The cure rate of thermoset resins depends on a number of factors including the product's age, temperature, catalyst type, catalyst level and ambient humidity. When used in a closed molding application the laminate cure rate also depends on reinforcement content and laminate thickness as well as other factors. For these reasons, we recommend that customer's check the cure rate in your plant.

AarmorStar® IVSXH210 is quality control tested using Arkema Luperox® DDM-9 but can be used with a variety of peroxide initiators. When making thin laminates (<150 mils) Luperox® DDM-9 or a equivalent catalyst such as NOROX® MEKP-9, NOROX® MEKP-9H, Akzo Nobel CADOX L-50a and CADOX D-50 are recommended. Arkema Luperox® DHD-9, Syrgis NOROX® MEKP-925, NOROX® MEKP-925H and Chemtura HP-90 may also be used but gel and cure times may vary.

For thicker laminates cumene hydroperoxide/methyl ethyl ketone peroxide blends such as Arkema's Luperox® KC-70 and KC-50 can be used to reduce exotherm without negatively affecting the final cure of the composite.



IVSXH210 - Copyright 2010

The MEKP catalyst level should not exceed 2.4% or fall below 0.9% for proper cure. A catalyst level of 1.5% at 77°F is considered ideal. Contact your catalyst supplier or your CCP representative for acceptable catalyst ranges for MEKP/CHP blends. This product should not be used when temperature conditions are below 60°F, as curing may be adversely affected.

**Caution**

Do not add any material other than the recommended organic peroxide to this product without the advice of a representative of CCP Composites US.

**Storage**

AzorStar® IVSXH210 has a shelf life of three months from date of shipment from CCP when stored at 73°F or below in a closed, factory-sealed, opaque container, and out of direct sunlight. The usage life is cut in half for every 20°F over 73°F.

## **Appendix XV: Identification of Wrapping Threads Using Fourier Transforms Infrared (FTIR) and Raman Spectroscopy**



## XV.A Experimental Procedures

Wrapping threads were removed from the unidirectional flax fabrics. They were then identified using a Perkin Elmer Spotlight 400 FTIR microscope within universal attenuated total reflectance (ATR) mode in the range of 4,000-650  $\text{cm}^{-1}$ , with a resolution of 4  $\text{cm}^{-1}$ .

The wrapping threads were also identified using a Perkin Elmer Ramanstation 785-nm (near-IR) laser-based Raman spectrometer and a Renishaw inVia Raman microscope 514-nm (green light) laser-based Raman spectrometer. The Raman spectrum measurement conditions used are shown in Table XV.1.

**Table XV.1:** The Raman spectrum measurement conditions

Condition	Instrument	
	785-nm (near-IR) laser-based Raman spectrometer	514-nm (green light) laser-based Raman spectrometer
Excitation source	785-nm (near IR) laser	514-nm (green light) laser
Laser energy (%)	100	100
Microscope objective	50 times	50 times
Exposure time (per second)	30	4
Spectrum range or Raman shift ( $\text{cm}^{-1}$ )	200-2,000	200-2,000

## XV.B Results

The FTIR spectrum of the wrapping threads is shown in Figure XV.1. The possible peak assignments of the spectrum are given in Table XV.2. The spectrum was the same as that of viscose rayon.

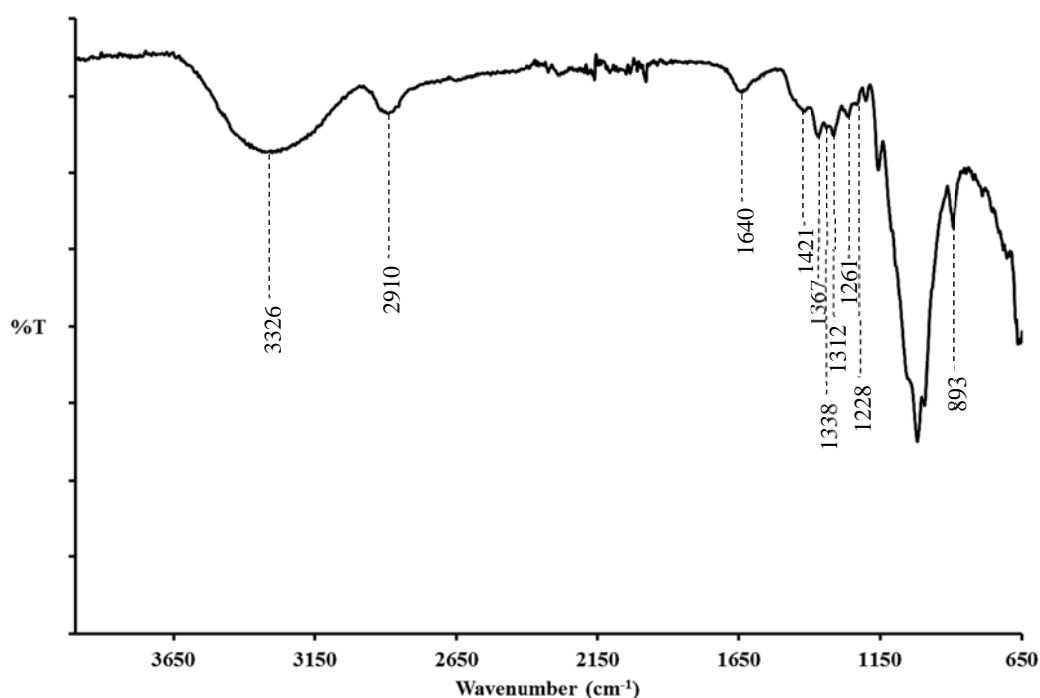


**Figure XV.1:** FTIR spectrum of wrapping threads from flax fabric.

**Table XV.2:** Possible assignments of peak positions of FTIR spectrum of wrapping threads from flax fabric

Wavenumber (cm <sup>-1</sup> )	Possible assignment
3,326	O-H stretching vibrations <sup>1</sup>
2,910	CH <sub>2</sub> stretching vibrations <sup>1</sup>
1,640	O-H bending vibrations due to water absorption <sup>1</sup>
1,421	δ CH <sub>2</sub> symmetric bending vibrations due to cellulose II and amorphous cellulose <sup>2</sup>
1,367	C-H bending vibrations <sup>2</sup>
1,338	C-OH in plane bending vibrations <sup>2</sup>
1,312	CH <sub>2</sub> wagging vibrations due to crystalline cellulose (cellulose I and cellulose II) <sup>2</sup>
1,261	C-H bending vibrations <sup>2</sup>
1,228	C-OH in plane bending vibrations <sup>2</sup>
893	γ (COC) in plane and symmetric stretching vibrations <sup>2</sup>

<sup>1</sup>Khasbaatar, Chun & Choi (2007)

<sup>2</sup>Colom & Carrillo, (2002)

*Figure XV.2 has been removed due to Copyright restrictions.*

**Figure XV.2:** FTIR spectrum of viscose rayon (Colom & Carrillo, 2002).

*Figure XV.3 has been removed due to Copyright restrictions.*

**Figure XV.3:** FTIR spectrum of viscose rayon (Kobayashi et al., 1999).

The Raman spectra of the wrapping threads are shown in Figure XV.4 while the possible assignments of peak positions are shown in Table XV.3. The wrapping threads were again identified to be viscose rayon as the spectra of the wrapping threads were similar to the spectrum of viscose rayon as shown in Figure XV.5.



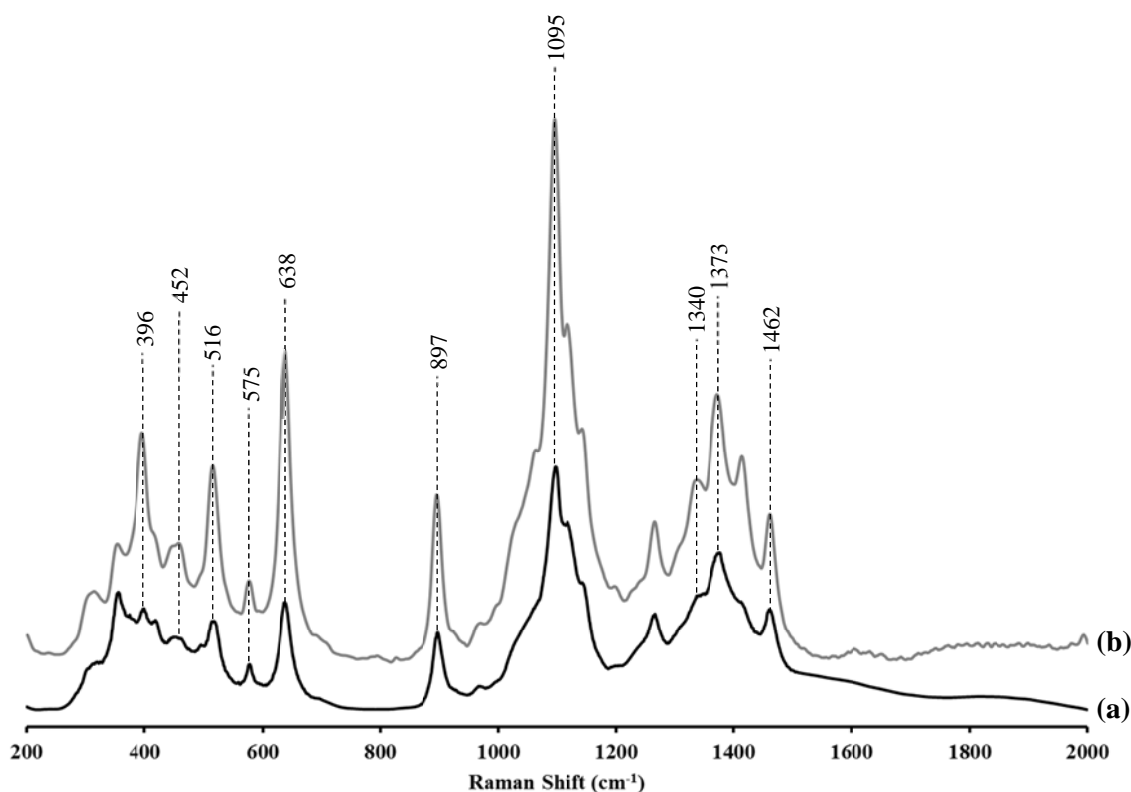


**Figure XV.4:** Raman spectra of wrapping threads from the flax fabrics using (a) 785-nm and (b) 514-nm excitation.

**Table XV.3:** Possible assignments of peak positions of Raman spectra of wrapping threads from flax fabric (Cho, 2007)

Wavenumber (cm <sup>-1</sup> )	Possible assignment
379-516	Skeletal C-O-C, C-C-C, O-C-C and O-C-O bending vibrations
638	C-S-C stretching vibrations due to the xanthate derivative which was incompletely regenerated back into the cellulose form during the rayon process
897	C-O-C in plane symmetric vibrations
1,095	C-C and C-O stretching vibrations
1,340 and 1,373	H-C-C, H-C-O and H-O-C bending vibrations
1,462	H-C-H and H-O-C bending vibrations

*Figure XV.5 has been removed due to Copyright restrictions.*

**Figure XV.5:** Raman spectrum of viscose rayon (Cho, 2007).

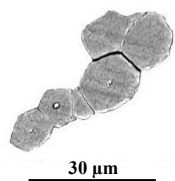


## **Appendix XVI: SEM Images of Cross-Sections of Flax Technical Fibres**

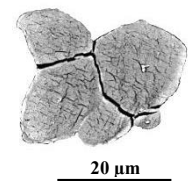




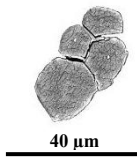
**Magnification:**  $\times 800$   
**Area ( $A_T$ ):**  $506 \mu\text{m}^2$



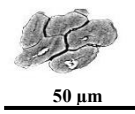
**Magnification:**  $\times 1,500$   
**Area ( $A_T$ ):**  $513 \mu\text{m}^2$



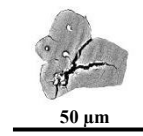
**Magnification:**  $\times 2,000$   
**Area ( $A_T$ ):**  $534 \mu\text{m}^2$



**Magnification:**  $\times 1,200$   
**Area ( $A_T$ ):**  $543 \mu\text{m}^2$



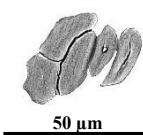
**Magnification:**  $\times 1,000$   
**Area ( $A_T$ ):**  $551 \mu\text{m}^2$



**Magnification:**  $\times 1,000$   
**Area ( $A_T$ ):**  $660 \mu\text{m}^2$



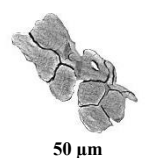
**Magnification:**  $\times 1,200$   
**Area ( $A_T$ ):**  $719 \mu\text{m}^2$



**Magnification:**  $\times 1,000$   
**Area ( $A_T$ ):**  $783 \mu\text{m}^2$



**Magnification:**  $\times 900$   
**Area ( $A_T$ ):**  $802 \mu\text{m}^2$



**Magnification:**  $\times 1,000$   
**Area ( $A_T$ ):**  $803 \mu\text{m}^2$



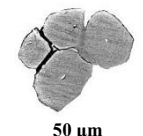
**Magnification:**  $\times 900$   
**Area ( $A_T$ ):**  $833 \mu\text{m}^2$



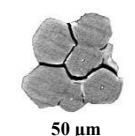
**Magnification:**  $\times 1,000$   
**Area ( $A_T$ ):**  $855 \mu\text{m}^2$



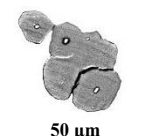
**Magnification:**  $\times 500$   
**Area ( $A_T$ ):**  $875 \mu\text{m}^2$



**Magnification:**  $\times 1,000$   
**Area ( $A_T$ ):**  $910 \mu\text{m}^2$



**Magnification:**  $\times 1,000$   
**Area ( $A_T$ ):**  $917 \mu\text{m}^2$



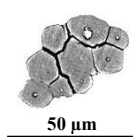
**Magnification:**  $\times 900$   
**Area ( $A_T$ ):**  $922 \mu\text{m}^2$



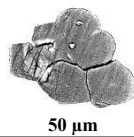
**Magnification:**  $\times 600$   
**Area ( $A_T$ ):**  $928 \mu\text{m}^2$



**Magnification:**  $\times 1,000$   
**Area ( $A_T$ ):**  $951 \mu\text{m}^2$



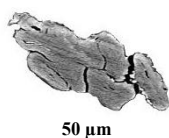
**Magnification:**  $\times 900$   
**Area ( $A_T$ ):**  $964 \mu\text{m}^2$



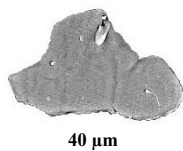
**Magnification:**  $\times 1,000$   
**Area ( $A_T$ ):**  $1,005 \mu\text{m}^2$



**Magnification:**  $\times 800$   
**Area ( $A_T$ ):**  $1,017 \mu\text{m}^2$



**Magnification:**  $\times 1,000$   
**Area ( $A_T$ ):**  $1,024 \mu\text{m}^2$



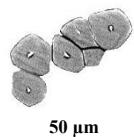
**Magnification:**  $\times 1,200$   
**Area ( $A_T$ ):**  $1,033 \mu\text{m}^2$



**Magnification:**  $\times 800$   
**Area ( $A_T$ ):**  $1,046 \mu\text{m}^2$



**Magnification:**  $\times 800$   
**Area ( $A_T$ ):**  $1,075 \mu\text{m}^2$



**Magnification:**  $\times 800$   
**Area ( $A_T$ ):**  $1,079 \mu\text{m}^2$



**Magnification:**  $\times 800$   
**Area ( $A_T$ ):**  $1,123 \mu\text{m}^2$



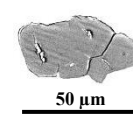
**Magnification:**  $\times 800$   
**Area ( $A_T$ ):**  $1,131 \mu\text{m}^2$



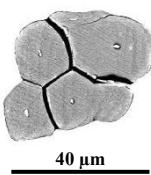
**Magnification:**  $\times 700$   
**Area ( $A_T$ ):**  $1,136 \mu\text{m}^2$



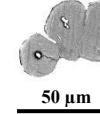
**Magnification:**  $\times 600$   
**Area ( $A_T$ ):**  $1,157 \mu\text{m}^2$



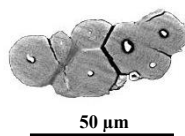
**Magnification:**  $\times 800$   
**Area ( $A_T$ ):**  $1,160 \mu\text{m}^2$



**Magnification:**  $\times 1,200$   
**Area ( $A_T$ ):**  $1,229 \mu\text{m}^2$



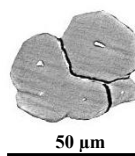
**Magnification:**  $\times 700$   
**Area ( $A_T$ ):**  $1,234 \mu\text{m}^2$



**Magnification:**  $\times 1,000$   
**Area ( $A_T$ ):**  $1,284 \mu\text{m}^2$



**Magnification:**  $\times 700$   
**Area ( $A_T$ ):**  $1,306 \mu\text{m}^2$



**Magnification:**  $\times 1,000$   
**Area ( $A_T$ ):**  $1,337 \mu\text{m}^2$



50  $\mu\text{m}$

**Magnification:**  $\times 800$   
**Area ( $A_T$ ):**  $1,361 \mu\text{m}^2$



50  $\mu\text{m}$

**Magnification:**  $\times 600$   
**Area ( $A_T$ ):**  $1,374 \mu\text{m}^2$



100  $\mu\text{m}$

**Magnification:**  $\times 500$   
**Area ( $A_T$ ):**  $1,400 \mu\text{m}^2$



50  $\mu\text{m}$

**Magnification:**  $\times 600$   
**Area ( $A_T$ ):**  $1,408 \mu\text{m}^2$



50  $\mu\text{m}$

**Magnification:**  $\times 600$   
**Area ( $A_T$ ):**  $1,420 \mu\text{m}^2$



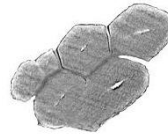
50  $\mu\text{m}$

**Magnification:**  $\times 800$   
**Area ( $A_T$ ):**  $1,518 \mu\text{m}^2$



100  $\mu\text{m}$

**Magnification:**  $\times 500$   
**Area ( $A_T$ ):**  $1,518 \mu\text{m}^2$



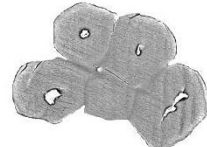
50  $\mu\text{m}$

**Magnification:**  $\times 1,000$   
**Area ( $A_T$ ):**  $1,527 \mu\text{m}^2$



50  $\mu\text{m}$

**Magnification:**  $\times 700$   
**Area ( $A_T$ ):**  $1,528 \mu\text{m}^2$



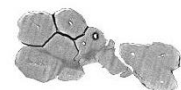
40  $\mu\text{m}$

**Magnification:**  $\times 1,200$   
**Area ( $A_T$ ):**  $1,542 \mu\text{m}^2$



50  $\mu\text{m}$

**Magnification:**  $\times 600$   
**Area ( $A_T$ ):**  $1,542 \mu\text{m}^2$



50  $\mu\text{m}$

**Magnification:**  $\times 800$   
**Area ( $A_T$ ):**  $1,544 \mu\text{m}^2$



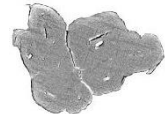
50  $\mu\text{m}$

**Magnification:**  $\times 700$   
**Area ( $A_T$ ):**  $1,568 \mu\text{m}^2$



50  $\mu\text{m}$

**Magnification:**  $\times 700$   
**Area ( $A_T$ ):**  $1,578 \mu\text{m}^2$



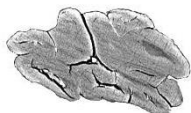
50  $\mu\text{m}$

**Magnification:**  $\times 900$   
**Area ( $A_T$ ):**  $1,583 \mu\text{m}^2$



50  $\mu\text{m}$

**Magnification:**  $\times 700$   
**Area ( $A_T$ ):**  $1,630 \mu\text{m}^2$



50  $\mu\text{m}$

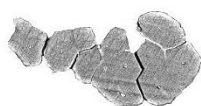
**Magnification:**  $\times 1,000$   
**Area ( $A_T$ ):**  $1,650 \mu\text{m}^2$



100  $\mu\text{m}$

**Magnification:**  $\times 500$   
**Area ( $A_T$ ):**  $1,671 \mu\text{m}^2$





**Magnification:**  $\times 900$   
**Area ( $A_T$ ):**  $1,681 \mu\text{m}^2$



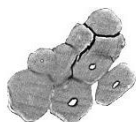
**Magnification:**  $\times 500$   
**Area ( $A_T$ ):**  $1,682 \mu\text{m}^2$



**Magnification:**  $\times 700$   
**Area ( $A_T$ ):**  $1,691 \mu\text{m}^2$



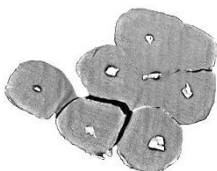
**Magnification:**  $\times 1,000$   
**Area ( $A_T$ ):**  $1,697 \mu\text{m}^2$



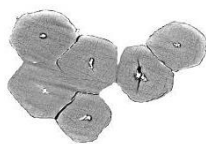
**Magnification:**  $\times 800$   
**Area ( $A_T$ ):**  $1,697 \mu\text{m}^2$



**Magnification:**  $\times 600$   
**Area ( $A_T$ ):**  $1,770 \mu\text{m}^2$



**Magnification:**  $\times 1,200$   
**Area ( $A_T$ ):**  $1,815 \mu\text{m}^2$



**Magnification:**  $\times 1,000$   
**Area ( $A_T$ ):**  $1,832 \mu\text{m}^2$



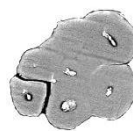
**Magnification:**  $\times 600$   
**Area ( $A_T$ ):**  $1,848 \mu\text{m}^2$



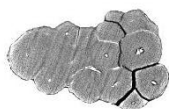
**Magnification:**  $\times 800$   
**Area ( $A_T$ ):**  $1,992 \mu\text{m}^2$



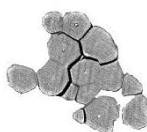
**Magnification:**  $\times 500$   
**Area ( $A_T$ ):**  $2,129 \mu\text{m}^2$



**Magnification:**  $\times 800$   
**Area ( $A_T$ ):**  $2,188 \mu\text{m}^2$



**Magnification:**  $\times 800$   
**Area ( $A_T$ ):**  $2,191 \mu\text{m}^2$



**Magnification:**  $\times 700$   
**Area ( $A_T$ ):**  $2,227 \mu\text{m}^2$



**Magnification:**  $\times 800$   
**Area ( $A_T$ ):**  $2,241 \mu\text{m}^2$



**Magnification:**  $\times 500$   
**Area ( $A_T$ ):**  $2,312 \mu\text{m}^2$



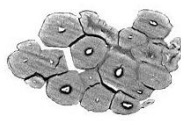
**Magnification:**  $\times 600$   
**Area ( $A_T$ ):**  $2,387 \mu\text{m}^2$



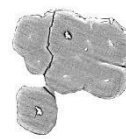
**Magnification:**  $\times 700$   
**Area ( $A_T$ ):**  $2,389 \mu\text{m}^2$



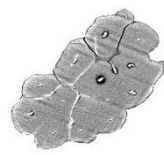
**Magnification:**  $\times 800$   
**Area ( $A_T$ ):**  $2,427 \mu\text{m}^2$



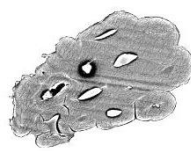
**Magnification:**  $\times 800$   
**Area ( $A_T$ ):**  $2,450 \mu\text{m}^2$



**Magnification:**  $\times 700$   
**Area ( $A_T$ ):**  $2,472 \mu\text{m}^2$



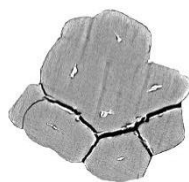
**Magnification:**  $\times 800$   
**Area ( $A_T$ ):**  $2,480 \mu\text{m}^2$



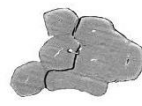
**Magnification:**  $\times 900$   
**Area ( $A_T$ ):**  $2,501 \mu\text{m}^2$



**Magnification:**  $\times 700$   
**Area ( $A_T$ ):**  $2,517 \mu\text{m}^2$



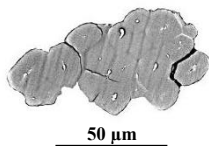
**Magnification:**  $\times 1,000$   
**Area ( $A_T$ ):**  $2,521 \mu\text{m}^2$



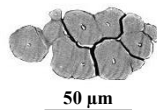
**Magnification:**  $\times 600$   
**Area ( $A_T$ ):**  $2,618 \mu\text{m}^2$



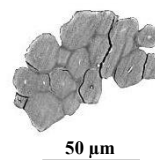
**Magnification:**  $\times 500$   
**Area ( $A_T$ ):**  $2,618 \mu\text{m}^2$



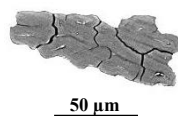
**Magnification:**  $\times 800$   
**Area ( $A_T$ ):**  $2,672 \mu\text{m}^2$



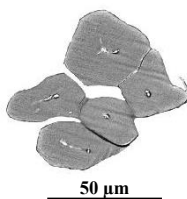
**Magnification:**  $\times 600$   
**Area ( $A_T$ ):**  $2,712 \mu\text{m}^2$



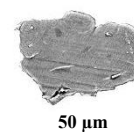
**Magnification:**  $\times 700$   
**Area ( $A_T$ ):**  $2,725 \mu\text{m}^2$



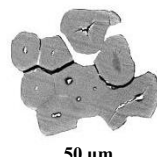
**Magnification:**  $\times 600$   
**Area ( $A_T$ ):**  $2,830 \mu\text{m}^2$



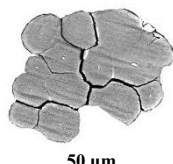
**Magnification:**  $\times 800$   
**Area ( $A_T$ ):**  $2,918 \mu\text{m}^2$



**Magnification:**  $\times 600$   
**Area ( $A_T$ ):**  $2,932 \mu\text{m}^2$



**Magnification:**  $\times 700$   
**Area ( $A_T$ ):**  $3,005 \mu\text{m}^2$



**Magnification:**  $\times 800$   
**Area ( $A_T$ ):**  $3,013 \mu\text{m}^2$



**Magnification:**  $\times 500$   
**Area ( $A_T$ ):**  $3,022 \mu\text{m}^2$



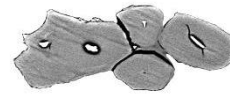
50  $\mu\text{m}$

**Magnification:**  $\times 600$   
**Area ( $A_T$ ):**  $3,035 \mu\text{m}^2$



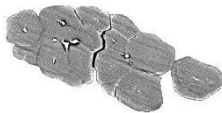
50  $\mu\text{m}$

**Magnification:**  $\times 600$   
**Area ( $A_T$ ):**  $3,198 \mu\text{m}^2$



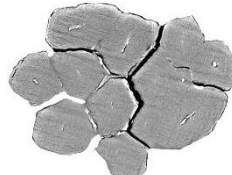
50  $\mu\text{m}$

**Magnification:**  $\times 700$   
**Area ( $A_T$ ):**  $3,247 \mu\text{m}^2$



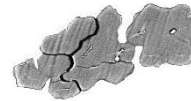
50  $\mu\text{m}$

**Magnification:**  $\times 700$   
**Area ( $A_T$ ):**  $3,286 \mu\text{m}^2$



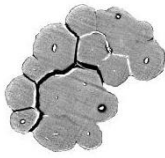
50  $\mu\text{m}$

**Magnification:**  $\times 1,000$   
**Area ( $A_T$ ):**  $3,309 \mu\text{m}^2$



50  $\mu\text{m}$

**Magnification:**  $\times 600$   
**Area ( $A_T$ ):**  $3,462 \mu\text{m}^2$



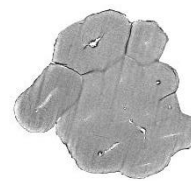
50  $\mu\text{m}$

**Magnification:**  $\times 700$   
**Area ( $A_T$ ):**  $3,778 \mu\text{m}^2$



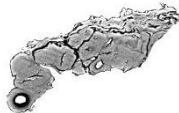
50  $\mu\text{m}$

**Magnification:**  $\times 600$   
**Area ( $A_T$ ):**  $3,819 \mu\text{m}^2$



50  $\mu\text{m}$

**Magnification:**  $\times 800$   
**Area ( $A_T$ ):**  $3,990 \mu\text{m}^2$



100  $\mu\text{m}$

**Magnification:**  $\times 500$   
**Area ( $A_T$ ):**  $4,048 \mu\text{m}^2$



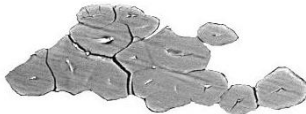
50  $\mu\text{m}$

**Magnification:**  $\times 600$   
**Area ( $A_T$ ):**  $4,107 \mu\text{m}^2$



100  $\mu\text{m}$

**Magnification:**  $\times 500$   
**Area ( $A_T$ ):**  $4,175 \mu\text{m}^2$



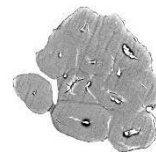
50  $\mu\text{m}$

**Magnification:**  $\times 700$   
**Area ( $A_T$ ):**  $4,502 \mu\text{m}^2$



100  $\mu\text{m}$

**Magnification:**  $\times 500$   
**Area ( $A_T$ ):**  $4,783 \mu\text{m}^2$



50  $\mu\text{m}$

**Magnification:**  $\times 600$   
**Area ( $A_T$ ):**  $4,848 \mu\text{m}^2$



100  $\mu\text{m}$

**Magnification:**  $\times 500$   
**Area ( $A_T$ ):**  $4,863 \mu\text{m}^2$



50  $\mu\text{m}$

**Magnification:**  $\times 600$   
**Area ( $A_T$ ):**  $5,122 \mu\text{m}^2$

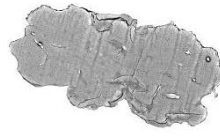


100  $\mu\text{m}$

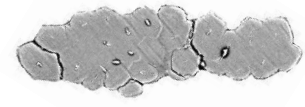
**Magnification:**  $\times 500$   
**Area ( $A_T$ ):**  $5,353 \mu\text{m}^2$



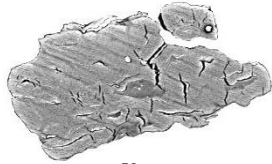
**Magnification:**  $\times 500$   
**Area ( $A_T$ ):**  $5,595 \mu\text{m}^2$



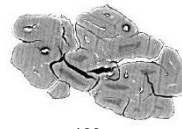
**Magnification:**  $\times 600$   
**Area ( $A_T$ ):**  $5,986 \mu\text{m}^2$



**Magnification:**  $\times 600$   
**Area ( $A_T$ ):**  $6,102 \mu\text{m}^2$



**Magnification:**  $\times 700$   
**Area ( $A_T$ ):**  $6,372 \mu\text{m}^2$



**Magnification:**  $\times 500$   
**Area ( $A_T$ ):**  $6,690 \mu\text{m}^2$



**Appendix XVII: Calculations for the Log-Normal  
Distributions of Measured and True Cross-Sectional  
Areas of Flax Technical Fibres**



## XVII.A Calculations for the Log-Normal Distribution of Measured Cross-Sectional Area of Flax Technical Fibres

Rank	Measured Area ( $\mu\text{m}^2$ ) ( $A_D$ )	$A'_D = \ln(A_D)$	$f(A'_D)$
1	1290	7.162	0.0322
2	1475	7.297	0.0585
3	1504	7.316	0.0633
4	1527	7.331	0.0676
5	1547	7.344	0.0712
6	2027	7.614	0.1874
7	2041	7.621	0.1914
8	2104	7.651	0.2099
9	2251	7.719	0.2547
10	2357	7.765	0.2881
11	2447	7.803	0.3165
12	2512	7.829	0.3371
13	2546	7.842	0.3478
14	2579	7.855	0.3581
15	2666	7.888	0.3856
16	2682	7.894	0.3903
17	2756	7.922	0.4133
18	2865	7.960	0.4461
19	2905	7.974	0.4575
20	2950	7.989	0.4706
21	2980	8.000	0.4794
22	3164	8.059	0.5292
23	3190	8.068	0.5360
24	3218	8.077	0.5431
25	3307	8.104	0.5650
26	3317	8.107	0.5673
27	3417	8.137	0.5903
28	3427	8.139	0.5923
29	3433	8.141	0.5937



Rank	Measured Area ( $\mu\text{m}^2$ ) ( $A_D$ )	$A'_D = \ln(A_D)$	$f(A'_D)$
30	3454	8.147	0.5983
31	3486	8.157	0.6051
32	3510	8.163	0.6101
33	3564	8.179	0.6210
34	3634	8.198	0.6344
35	3741	8.227	0.6535
36	3807	8.245	0.6642
37	3807	8.245	0.6642
38	3834	8.252	0.6684
39	3851	8.256	0.6709
40	3919	8.274	0.6808
41	3998	8.293	0.6913
42	4046	8.305	0.6973
43	4071	8.312	0.7002
44	4176	8.337	0.7114
45	4191	8.341	0.7128
46	4207	8.344	0.7144
47	4218	8.347	0.7154
48	4248	8.354	0.7181
49	4258	8.357	0.7190
50	4525	8.417	0.7369
51	4810	8.478	0.7457
52	4846	8.486	0.7461
53	4885	8.494	0.7463
54	4945	8.506	0.7464
55	5029	8.523	0.7459
56	5130	8.543	0.7443
57	5208	8.558	0.7425
58	5285	8.573	0.7401
59	5293	8.574	0.7398
60	5305	8.576	0.7394

Rank	Measured Area ( $\mu\text{m}^2$ ) ( $A_D$ )	$A'_D = \ln(A_D)$	$f(A'_D)$
61	5548	8.621	0.7284
62	5549	8.621	0.7283
63	5563	8.624	0.7275
64	5595	8.630	0.7257
65	5739	8.655	0.7168
66	5797	8.665	0.7128
67	5950	8.691	0.7015
68	5959	8.693	0.7008
69	5994	8.698	0.6981
70	6062	8.710	0.6925
71	6179	8.729	0.6826
72	6180	8.729	0.6824
73	6232	8.737	0.6779
74	6302	8.749	0.6716
75	6372	8.760	0.6650
76	6469	8.775	0.6558
77	6514	8.782	0.6515
78	6693	8.809	0.6336
79	6721	8.813	0.6307
80	6729	8.814	0.6299
81	6800	8.825	0.6226
82	6980	8.851	0.6038
83	7218	8.884	0.5786
84	7252	8.889	0.5749
85	7332	8.900	0.5663
86	7454	8.916	0.5532
87	7716	8.951	0.5252
88	7725	8.952	0.5242
89	7809	8.963	0.5152
90	7860	8.970	0.5098
91	7940	8.980	0.5014

Rank	Measured Area ( $\mu\text{m}^2$ ) ( $A_D$ )	$A'_D = \ln(A_D)$	$f(A'_D)$
92	8009	8.988	0.4941
93	8040	8.992	0.4908
94	8116	9.002	0.4829
95	8174	9.009	0.4769
96	8270	9.020	0.4670
97	8831	9.086	0.4116
98	9414	9.150	0.3586
99	9693	9.179	0.3352
100	9731	9.183	0.3321
101	9826	9.193	0.3244
102	10079	9.218	0.3048
103	10123	9.223	0.3015
104	10323	9.242	0.2867
105	10455	9.255	0.2774
106	10455	9.255	0.2774
107	10495	9.259	0.2746
108	10496	9.259	0.2745
109	11029	9.308	0.2398
110	12429	9.428	0.1669
111	12430	9.428	0.1669
112	13551	9.514	0.1246
113	14356	9.572	0.1010
<b>Average</b>	<b>5631</b>	<b>8.503</b>	
<b>SD</b>	<b>2864</b>	<b>0.534</b>	

- Mean ( $A_D$ ) = 5,631  $\mu\text{m}^2$  with a standard deviation of 2,864  $\mu\text{m}^2$
- Location parameter ( $\mu'_D$ ) = 8.50
- Scale parameter ( $\lambda'_D$ ) = 0.53
- Geometric mean ( $\mu_D = \exp(\mu'_D)$ ) = 4,929  $\mu\text{m}^2$
- Geometric standard deviation ( $\lambda_D = \exp(\lambda'_D)$ ) = 1.71  $\mu\text{m}^2$

## XVII.B Calculations for the Log-Normal Distribution of True Cross-Sectional Area of Flax Technical Fibres

Rank	True Area ( $\mu\text{m}^2$ ) ( $A_T$ )	$A'_T = \ln(A_T)$	$f(A'_T)$
1	506	6.226	0.0747
2	513	6.240	0.0783
3	534	6.280	0.0891
4	543	6.298	0.0944
5	551	6.312	0.0986
6	660	6.492	0.1664
7	719	6.578	0.2069
8	783	6.663	0.2524
9	802	6.687	0.2656
10	803	6.689	0.2669
11	833	6.725	0.2881
12	855	6.751	0.3033
13	875	6.774	0.3176
14	910	6.813	0.3418
15	917	6.821	0.3464
16	922	6.826	0.3498
17	928	6.833	0.3540
18	951	6.858	0.3695
19	964	6.871	0.3781
20	1005	6.913	0.4046
21	1017	6.924	0.4117
22	1024	6.932	0.4162
23	1033	6.940	0.4214
24	1046	6.952	0.4292
25	1075	6.980	0.4465
26	1079	6.984	0.4487
27	1123	7.024	0.4734
28	1131	7.031	0.4774
29	1136	7.035	0.4802

Rank	True Area ( $\mu\text{m}^2$ ) ( $A_T$ )	$A'_T = \ln(A_T)$	$f(A'_T)$
30	1157	7.053	0.4907
31	1160	7.056	0.4926
32	1229	7.114	0.5253
33	1237	7.120	0.5286
34	1284	7.158	0.5481
35	1306	7.175	0.5567
36	1337	7.198	0.5677
37	1361	7.216	0.5758
38	1374	7.225	0.5799
39	1400	7.245	0.5880
40	1408	7.250	0.5902
41	1420	7.258	0.5936
42	1518	7.325	0.6166
43	1518	7.325	0.6167
44	1527	7.331	0.6183
45	1528	7.332	0.6186
46	1542	7.341	0.6211
47	1542	7.341	0.6212
48	1544	7.342	0.6216
49	1568	7.357	0.6255
50	1578	7.364	0.6272
51	1583	7.367	0.6278
52	1630	7.397	0.6341
53	1650	7.409	0.6363
54	1671	7.421	0.6383
55	1681	7.427	0.6392
56	1682	7.428	0.6393
57	1691	7.433	0.6399
58	1697	7.436	0.6404
59	1697	7.437	0.6404
60	1770	7.479	0.6441

Rank	True Area ( $\mu\text{m}^2$ ) ( $A_T$ )	$A'_T = \ln(A_T)$	$f(A'_T)$
61	1815	7.504	0.6449
62	1832	7.513	0.6450
63	1848	7.522	0.6449
64	1992	7.597	0.6387
65	2129	7.664	0.6255
66	2188	7.691	0.6182
67	2191	7.692	0.6177
68	2227	7.708	0.6128
69	2241	7.715	0.6108
70	2312	7.746	0.6000
71	2387	7.778	0.5875
72	2389	7.779	0.5871
73	2427	7.794	0.5806
74	2450	7.804	0.5764
75	2472	7.813	0.5723
76	2480	7.816	0.5708
77	2501	7.824	0.5671
78	2517	7.831	0.5641
79	2521	7.832	0.5633
80	2618	7.870	0.5447
81	2618	7.870	0.5446
82	2672	7.890	0.5341
83	2712	7.905	0.5260
84	2725	7.910	0.5235
85	2830	7.948	0.5023
86	2918	7.979	0.4843
87	2932	7.983	0.4815
88	3005	8.008	0.4667
89	3013	8.011	0.4652
90	3022	8.014	0.4633
91	3035	8.018	0.4606

Rank	True Area ( $\mu\text{m}^2$ ) ( $A_T$ )	$A'_T = \ln(A_T)$	$f(A'_T)$
92	3198	8.070	0.4282
93	3247	8.085	0.4188
94	3286	8.097	0.4112
95	3309	8.104	0.4068
96	3462	8.149	0.3783
97	3778	8.237	0.3236
98	3819	8.248	0.3170
99	3990	8.291	0.2906
100	4048	8.306	0.2821
101	4107	8.320	0.2737
102	4175	8.337	0.2641
103	4502	8.412	0.2228
104	4783	8.473	0.1922
105	4848	8.486	0.1858
106	4863	8.489	0.1844
107	5122	8.541	0.1609
108	5353	8.585	0.1425
109	5595	8.630	0.1255
110	5986	8.697	0.1024
111	6102	8.716	0.0964
112	6372	8.760	0.0839
113	6690	8.808	0.0714
<b>Average</b>	<b>2205</b>	<b>7.510</b>	
<b>SD</b>	<b>1413</b>	<b>0.619</b>	

- Mean ( $A_T$ ) = 2,205  $\mu\text{m}^2$  with a standard deviation of 1,413  $\mu\text{m}^2$
- Location parameter ( $\mu'_T$ ) = 7.51
- Scale parameter ( $\lambda'_T$ ) = 0.62
- Geometric mean ( $\mu_T = \exp(\mu'_T)$ ) = 1,827  $\mu\text{m}^2$
- Geometric standard deviation ( $\lambda_T = \exp(\lambda'_T)$ ) = 1.86  $\mu\text{m}^2$

**Appendix XVIII: Calculations for the Weibull Probability Plot for True Tensile Strength and Strain to Failure of Flax Technical Fibres**





Rank (i)	Median Rank ( $F(\sigma_D)$ ) n = 113	1 – Median Rank	ln[-ln(1 – Median Rank)]	Tensile Strength ( $\sigma_D$ ) (MPa)	ln (Tensile Strength) ( $\ln(\sigma_D)$ )	True Tensile Strength ( $\sigma_T$ ) (MPa)	ln (True Tensile Strength) ( $\ln(\sigma_T)$ )	Strain to Failure (%)	ln (Strain to Failure)
1	0.006	0.994	-5.085	105.79	4.661	285.63	5.655	0.71	-0.342
2	0.015	0.985	-4.193	121.88	4.803	329.08	5.796	0.81	-0.211
3	0.024	0.976	-3.726	124.53	4.825	336.23	5.818	0.81	-0.211
4	0.033	0.967	-3.406	136.86	4.919	369.52	5.912	0.96	-0.041
5	0.041	0.959	-3.162	137.32	4.922	370.76	5.916	0.98	-0.020
6	0.050	0.950	-2.965	157.26	5.058	424.60	6.051	1.02	0.020
7	0.059	0.941	-2.799	166.99	5.118	450.87	6.111	1.04	0.039
8	0.068	0.932	-2.655	168.02	5.124	453.65	6.117	1.16	0.148
9	0.077	0.923	-2.528	173.06	5.154	467.26	6.147	1.19	0.174
10	0.086	0.914	-2.414	177.49	5.179	479.22	6.172	1.19	0.174
11	0.094	0.906	-2.312	179.86	5.192	485.62	6.185	1.20	0.182
12	0.103	0.897	-2.217	186.70	5.230	504.09	6.223	1.22	0.199
13	0.112	0.888	-2.131	187.46	5.234	506.14	6.227	1.23	0.207
14	0.121	0.879	-2.050	197.06	5.284	532.06	6.277	1.24	0.215
15	0.130	0.870	-1.974	197.79	5.287	534.03	6.280	1.29	0.255

Rank (i)	Median Rank ( $F(\sigma_D)$ ) n = 113	1 – Median Rank	ln[-ln(1 – Median Rank)]	Tensile Strength ( $\sigma_D$ ) (MPa)	ln (Tensile Strength) ( $\ln(\sigma_D)$ )	True Tensile Strength ( $\sigma_T$ ) (MPa)	ln (True Tensile Strength) ( $\ln(\sigma_T)$ )	Strain to Failure (%)	ln (Strain to Failure)
16	0.138	0.862	-1.904	199.12	5.294	537.62	6.287	1.31	0.270
17	0.147	0.853	-1.837	204.18	5.319	551.29	6.312	1.33	0.285
18	0.156	0.844	-1.774	205.87	5.327	555.85	6.320	1.33	0.285
19	0.165	0.835	-1.714	207.39	5.335	559.95	6.328	1.35	0.300
20	0.174	0.826	-1.656	207.89	5.337	561.30	6.330	1.35	0.300
21	0.183	0.817	-1.602	208.55	5.340	563.09	6.333	1.36	0.307
22	0.191	0.809	-1.549	209.35	5.344	565.25	6.337	1.41	0.344
23	0.200	0.800	-1.499	215.33	5.372	581.39	6.365	1.42	0.351
24	0.209	0.791	-1.451	219.30	5.390	592.11	6.384	1.43	0.358
25	0.218	0.782	-1.404	219.51	5.391	592.68	6.385	1.45	0.372
26	0.227	0.773	-1.359	220.39	5.395	595.05	6.389	1.45	0.372
27	0.235	0.765	-1.315	222.60	5.405	601.02	6.399	1.47	0.385
28	0.244	0.756	-1.273	228.00	5.429	615.60	6.423	1.50	0.405
29	0.253	0.747	-1.232	230.22	5.439	621.59	6.432	1.50	0.405
30	0.262	0.738	-1.192	238.52	5.474	644.00	6.468	1.52	0.419

<b>Rank (i)</b>	<b>Median Rank (<math>F(\sigma_D)</math>) n = 113</b>	<b>1 – Median Rank</b>	<b>ln[-ln(1 – Median Rank)]</b>	<b>Tensile Strength (<math>\sigma_D</math>) (MPa)</b>	<b>ln (Tensile Strength) (<math>\ln(\sigma_D)</math>)</b>	<b>True Tensile Strength (<math>\sigma_T</math>) (MPa)</b>	<b>ln (True Tensile Strength) (<math>\ln(\sigma_T)</math>)</b>	<b>Strain to Failure (%)</b>	<b>ln (Strain to Failure)</b>
31	0.271	0.729	-1.153	238.84	5.476	644.87	6.469	1.54	0.432
32	0.280	0.720	-1.115	241.09	5.485	650.94	6.478	1.55	0.438
33	0.288	0.712	-1.078	247.32	5.511	667.76	6.504	1.55	0.438
34	0.297	0.703	-1.042	248.67	5.516	671.41	6.509	1.57	0.451
35	0.306	0.694	-1.007	248.79	5.517	671.73	6.510	1.57	0.451
36	0.315	0.685	-0.973	249.46	5.519	673.54	6.513	1.58	0.457
37	0.324	0.676	-0.939	249.50	5.519	673.65	6.513	1.61	0.476
38	0.332	0.668	-0.906	252.61	5.532	682.05	6.525	1.62	0.482
39	0.341	0.659	-0.874	258.00	5.553	696.60	6.546	1.63	0.489
40	0.350	0.650	-0.842	258.55	5.555	698.09	6.548	1.63	0.489
41	0.359	0.641	-0.811	268.03	5.591	723.68	6.584	1.63	0.489
42	0.368	0.632	-0.780	275.12	5.617	742.82	6.610	1.63	0.489
43	0.377	0.623	-0.750	280.61	5.637	757.65	6.630	1.65	0.501
44	0.385	0.615	-0.720	283.18	5.646	764.59	6.639	1.66	0.507
45	0.394	0.606	-0.691	284.12	5.649	767.12	6.643	1.67	0.513

Rank (i)	Median Rank ( $F(\sigma_D)$ ) n = 113	1 – Median Rank	$\ln[-\ln(1 - \text{Median Rank})]$	Tensile Strength ( $\sigma_D$ ) (MPa)	$\ln$ (Tensile Strength) ( $\ln(\sigma_D)$ )	True Tensile Strength ( $\sigma_T$ ) (MPa)	$\ln$ (True Tensile Strength) ( $\ln(\sigma_T)$ )	Strain to Failure (%)	$\ln$ (Strain to Failure)
46	0.403	0.597	-0.662	286.01	5.656	772.23	6.649	1.70	0.531
47	0.412	0.588	-0.634	291.06	5.674	785.86	6.667	1.70	0.531
48	0.421	0.579	-0.605	292.20	5.677	788.94	6.671	1.71	0.536
49	0.429	0.571	-0.578	302.71	5.713	817.32	6.706	1.75	0.560
50	0.438	0.562	-0.550	303.61	5.716	819.75	6.709	1.76	0.565
51	0.447	0.553	-0.523	315.19	5.753	851.01	6.746	1.76	0.565
52	0.456	0.544	-0.497	322.51	5.776	870.78	6.769	1.79	0.582
53	0.465	0.535	-0.470	328.46	5.794	886.84	6.788	1.79	0.582
54	0.474	0.526	-0.444	329.34	5.797	889.22	6.790	1.80	0.588
55	0.482	0.518	-0.418	332.49	5.807	897.72	6.800	1.81	0.593
56	0.491	0.509	-0.392	333.66	5.810	900.88	6.803	1.81	0.593
57	0.500	0.500	-0.367	335.07	5.814	904.69	6.808	1.82	0.599
58	0.509	0.491	-0.341	337.82	5.823	912.11	6.816	1.83	0.604
59	0.518	0.482	-0.316	338.57	5.825	914.14	6.818	1.83	0.604
60	0.526	0.474	-0.291	340.27	5.830	918.73	6.823	1.83	0.604

<b>Rank (i)</b>	<b>Median Rank (<math>F(\sigma_D)</math>) n = 113</b>	<b>1 – Median Rank</b>	<b>ln[-ln(1 – Median Rank)]</b>	<b>Tensile Strength (<math>\sigma_D</math>) (MPa)</b>	<b>ln (Tensile Strength) (<math>\ln(\sigma_D)</math>)</b>	<b>True Tensile Strength (<math>\sigma_T</math>) (MPa)</b>	<b>ln (True Tensile Strength) (<math>\ln(\sigma_T)</math>)</b>	<b>Strain to Failure (%)</b>	<b>ln (Strain to Failure)</b>
61	0.535	0.465	-0.266	340.69	5.831	919.86	6.824	1.85	0.615
62	0.544	0.456	-0.241	344.38	5.842	929.83	6.835	1.85	0.615
63	0.553	0.447	-0.217	355.63	5.874	960.20	6.867	1.85	0.615
64	0.562	0.438	-0.192	360.23	5.887	972.62	6.880	1.87	0.626
65	0.571	0.429	-0.168	361.12	5.889	975.02	6.882	1.90	0.642
66	0.579	0.421	-0.144	365.16	5.900	985.93	6.894	1.91	0.647
67	0.588	0.412	-0.120	367.89	5.908	993.30	6.901	1.92	0.652
68	0.597	0.403	-0.096	373.93	5.924	1009.61	6.917	1.92	0.652
69	0.606	0.394	-0.072	387.27	5.959	1045.63	6.952	1.93	0.658
70	0.615	0.385	-0.048	387.78	5.960	1047.01	6.954	1.93	0.658
71	0.623	0.377	-0.024	389.90	5.966	1052.73	6.959	1.95	0.668
72	0.632	0.368	0.000	390.89	5.968	1055.40	6.962	1.96	0.673
73	0.641	0.359	0.024	395.77	5.981	1068.58	6.974	1.96	0.673
74	0.650	0.350	0.048	400.66	5.993	1081.78	6.986	1.96	0.673
75	0.659	0.341	0.072	404.10	6.002	1091.07	6.995	1.96	0.673

Rank (i)	Median Rank ( $F(\sigma_D)$ ) n = 113	1 – Median Rank	$\ln[-\ln(1 - \text{Median Rank})]$	Tensile Strength ( $\sigma_D$ ) (MPa)	$\ln$ (Tensile Strength) ( $\ln(\sigma_D)$ )	True Tensile Strength ( $\sigma_T$ ) (MPa)	$\ln$ (True Tensile Strength) ( $\ln(\sigma_T)$ )	Strain to Failure (%)	$\ln$ (Strain to Failure)
76	0.668	0.332	0.096	411.46	6.020	1110.94	7.013	1.97	0.678
77	0.676	0.324	0.121	421.59	6.044	1138.29	7.037	1.98	0.683
78	0.685	0.315	0.145	426.08	6.055	1150.42	7.048	2.00	0.693
79	0.694	0.306	0.169	429.32	6.062	1159.16	7.055	2.00	0.693
80	0.703	0.297	0.193	430.07	6.064	1161.19	7.057	2.03	0.708
81	0.712	0.288	0.218	443.33	6.094	1196.99	7.088	2.04	0.713
82	0.720	0.280	0.243	445.34	6.099	1202.42	7.092	2.05	0.718
83	0.729	0.271	0.267	446.55	6.102	1205.69	7.095	2.05	0.718
84	0.738	0.262	0.293	455.00	6.120	1228.50	7.114	2.05	0.718
85	0.747	0.253	0.318	456.43	6.123	1232.36	7.117	2.05	0.718
86	0.756	0.244	0.343	460.99	6.133	1244.67	7.127	2.07	0.728
87	0.765	0.235	0.369	461.24	6.134	1245.35	7.127	2.08	0.732
88	0.773	0.227	0.395	470.85	6.155	1271.30	7.148	2.09	0.737
89	0.782	0.218	0.421	471.92	6.157	1274.18	7.150	2.10	0.742
90	0.791	0.209	0.448	472.20	6.157	1274.94	7.151	2.11	0.747

<b>Rank (i)</b>	<b>Median Rank (<math>F(\sigma_D)</math>) n = 113</b>	<b>1 – Median Rank</b>	<b>ln[-ln(1 – Median Rank)]</b>	<b>Tensile Strength (<math>\sigma_D</math>) (MPa)</b>	<b>ln (Tensile Strength) (<math>\ln(\sigma_D)</math>)</b>	<b>True Tensile Strength (<math>\sigma_T</math>) (MPa)</b>	<b>ln (True Tensile Strength) (<math>\ln(\sigma_T)</math>)</b>	<b>Strain to Failure (%)</b>	<b>ln (Strain to Failure)</b>
91	0.800	0.200	0.475	478.63	6.171	1292.30	7.164	2.19	0.784
92	0.809	0.191	0.503	483.15	6.180	1304.51	7.174	2.24	0.806
93	0.817	0.183	0.531	483.54	6.181	1305.56	7.174	2.29	0.829
94	0.826	0.174	0.560	483.82	6.182	1306.31	7.175	2.30	0.833
95	0.835	0.165	0.589	484.64	6.183	1308.53	7.177	2.32	0.842
96	0.844	0.156	0.619	499.68	6.214	1349.14	7.207	2.36	0.859
97	0.853	0.147	0.650	502.26	6.219	1356.10	7.212	2.38	0.867
98	0.862	0.138	0.682	502.92	6.220	1357.88	7.214	2.47	0.904
99	0.870	0.130	0.714	514.00	6.242	1387.80	7.235	2.48	0.908
100	0.879	0.121	0.748	515.79	6.246	1392.63	7.239	2.49	0.912
101	0.888	0.112	0.784	516.27	6.247	1393.93	7.240	2.49	0.912
102	0.897	0.103	0.820	516.74	6.248	1395.20	7.241	2.53	0.928
103	0.906	0.094	0.859	519.99	6.254	1403.97	7.247	2.57	0.944
104	0.914	0.086	0.900	520.72	6.255	1405.94	7.248	2.59	0.952
105	0.923	0.077	0.943	532.95	6.278	1438.97	7.272	2.62	0.963



<b>Rank (i)</b>	<b>Median Rank (<math>F(\sigma_D)</math>) n = 113</b>	<b>1 – Median Rank</b>	<b>ln[-ln(1 – Median Rank)]</b>	<b>Tensile Strength (<math>\sigma_D</math>) (MPa)</b>	<b>ln (Tensile Strength) (<math>\ln(\sigma_D)</math>)</b>	<b>True Tensile Strength (<math>\sigma_T</math>) (MPa)</b>	<b>ln (True Tensile Strength) (<math>\ln(\sigma_T)</math>)</b>	<b>Strain to Failure (%)</b>	<b>ln (Strain to Failure)</b>
106	0.932	0.068	0.989	561.36	6.330	1515.67	7.324	2.62	0.963
107	0.941	0.059	1.040	570.06	6.346	1539.16	7.339	2.67	0.982
108	0.950	0.050	1.095	573.86	6.352	1549.42	7.346	2.73	1.004
109	0.959	0.041	1.158	604.24	6.404	1631.45	7.397	2.73	1.004
110	0.967	0.033	1.230	612.44	6.417	1653.59	7.411	2.73	1.004
111	0.976	0.024	1.318	623.32	6.435	1682.96	7.428	2.85	1.047
112	0.985	0.015	1.435	685.47	6.530	1850.77	7.523	3.12	1.138
113	0.994	0.006	1.627	738.32	6.604	1993.46	7.598	3.20	1.163

## **Appendix XIX: Tensile Test Data for Flax Fibre Bundles**



<b>Specimen No.</b>	<b>Temperature of Testing (°C)</b>	<b>RH of Testing (%)</b>	<b>Weight of Specimen (mg)</b>	<b>Breaking Load (gf)</b>	<b>Linear Mass Density (tex)</b>	<b>Tenacity (gf/tex)</b>	<b>Tensile Modulus (GPa)</b>	<b>Tensile Strength (MPa)</b>
1	26	37	5.7	9429	380.00	24.81	3.016	350.13
2	26	37	4.2	7372	280.00	26.33	4.960	371.51
3	26	37	3.3	6542	220.00	29.74	5.317	419.61
4	26	37	4.9	7681	326.67	23.51	3.598	331.77
5	26	37	4.2	8574	280.00	30.62	4.236	432.08
6	26	59	3.9	8225	260.00	31.63	4.988	446.36
7	26	59	2.7	5216	180.00	28.98	6.457	408.89
8	26	59	2.7	5003	180.00	27.79	7.190	392.17
9	26	59	5.0	9725	333.33	29.17	4.258	411.67
10	26	59	4.8	9420	320.00	29.44	4.215	415.38
11	26	59	3.8	7714	253.33	30.45	4.551	429.65
12	26	59	4.1	7287	273.33	26.66	4.726	376.20
13	26	59	4.4	9243	293.33	31.51	4.338	444.64
14	26	59	2.7	5008	180.00	27.82	5.353	392.60
15	26	59	4.9	8675	326.67	26.55	3.777	374.70

<b>Specimen No.</b>	<b>Temperature of Testing (°C)</b>	<b>RH of Testing (%)</b>	<b>Weight of Specimen (mg)</b>	<b>Breaking Load (gf)</b>	<b>Linear Mass Density (tex)</b>	<b>Tenacity (gf/tex)</b>	<b>Tensile Modulus (GPa)</b>	<b>Tensile Strength (MPa)</b>
16	26	59	2.3	4901	153.33	31.96	7.709	451.00
17	26	59	3.7	8023	246.67	32.53	5.276	458.98
18	26	59	4.0	7478	266.67	28.04	4.804	395.72
19	26	59	3.6	7623	240.00	31.76	5.287	448.17
20	26	59	3.5	7562	233.33	32.41	5.743	457.33
21	24	49.5	3.6	7411	240.00	30.88	5.504	435.75
22	24	49.5	3.8	8018	253.33	31.65	5.196	446.58
23	24	49.5	2.3	5455	153.33	35.57	8.732	501.96
24	24	49.5	3.3	5457	220.00	24.80	5.830	349.98
25	24	49.5	4.2	5896	280.00	21.06	4.147	297.12
26	24	49.5	4.3	7782	286.67	27.15	4.387	383.04
27	24	49.5	2.7	5264	180.00	29.24	6.257	412.62
28	24	49.5	4.3	8161	286.67	28.47	4.427	401.70
29	24	49.5	4.4	7353	293.33	25.07	4.095	353.69
30	24	49.5	6.4	9355	426.67	21.93	3.210	309.38

<b>Specimen No.</b>	<b>Temperature of Testing (°C)</b>	<b>RH of Testing (%)</b>	<b>Weight of Specimen (mg)</b>	<b>Breaking Load (gf)</b>	<b>Linear Mass Density (tex)</b>	<b>Tenacity (gf/tex)</b>	<b>Tensile Modulus (GPa)</b>	<b>Tensile Strength (MPa)</b>
31	24	49.5	3.4	6520	226.67	28.76	5.271	405.86
32	24	49.5	5.6	8400	373.33	22.50	3.335	317.48
33	24	49.5	4.7	7393	313.33	23.60	3.975	332.94
34	24	49.5	4.9	8446	326.67	25.86	3.836	364.83
35	24	49.5	4.6	8035	306.67	26.20	3.992	369.70
36	24	49.5	3.5	6522	233.33	27.95	4.973	394.44
37	24	51	3.1	6550	206.67	31.69	5.605	447.19
38	24	51	4.4	8455	293.33	28.82	4.541	406.73
39	24	51	4.8	8019	320.00	25.06	3.675	353.60
40	24	51	4.2	7118	280.00	25.42	4.042	358.74
41	24	51	3.8	5350	253.33	21.12	3.843	297.98
42	24	51	3.3	5600	220.00	25.45	5.173	359.18
43	24	51	3.8	8148	253.33	32.16	4.586	453.85
44	24	51	4.1	8055	273.33	29.47	4.496	415.84
45	24	51	4.7	8920	313.33	28.47	4.338	401.69

<b>Specimen No.</b>	<b>Temperature of Testing (°C)</b>	<b>RH of Testing (%)</b>	<b>Weight of Specimen (mg)</b>	<b>Breaking Load (gf)</b>	<b>Linear Mass Density (tex)</b>	<b>Tenacity (gf/tex)</b>	<b>Tensile Modulus (GPa)</b>	<b>Tensile Strength (MPa)</b>
46	24	51	3.9	7381	260.00	28.39	4.423	400.56
47	25	55	4.7	8158	313.33	26.04	4.095	367.38
48	25	55	2.8	5521	186.67	29.58	6.558	417.35
49	25	55	4.3	7734	286.67	26.98	4.837	380.69
50	25	55	4.0	6748	266.67	25.31	4.454	357.09
51	25	55	3.5	7699	233.33	33.00	5.150	465.58
52	25	55	3.0	5850	200.00	29.25	5.709	412.75
53	25	55	4.3	7775	286.67	27.12	4.265	382.71
54	25	55	2.5	5396	166.67	32.38	6.507	456.87
55	25	55	3.9	7928	260.00	30.49	5.058	430.28
56	25	55	3.4	5694	226.67	25.12	5.122	354.46
57	25	52	3.8	6189	253.33	24.43	5.341	344.71
58	25	52	3.2	5522	213.33	25.88	6.002	365.24
59	25	52	3.1	6581	206.67	31.84	6.154	449.33
60	25	52	3.1	5484	206.67	26.54	6.348	374.44

<b>Specimen No.</b>	<b>Temperature of Testing (°C)</b>	<b>RH of Testing (%)</b>	<b>Weight of Specimen (mg)</b>	<b>Breaking Load (gf)</b>	<b>Linear Mass Density (tex)</b>	<b>Tenacity (gf/tex)</b>	<b>Tensile Modulus (GPa)</b>	<b>Tensile Strength (MPa)</b>
61	25	52	2.9	6067	193.33	31.38	5.963	442.80
62	25	52	4.1	7789	273.33	28.50	5.054	402.10
63	25	52	3.0	6166	200.00	30.83	5.642	435.06
64	25	52	4.2	8286	280.00	29.59	4.764	417.56
65	25	52	5.2	8118	346.67	23.42	3.854	330.43
66	25	52	3.3	6356	220.00	28.89	5.403	407.67
67	25	52	4.4	7714	293.33	26.30	4.742	371.09
68	25	52	5.1	10015	340.00	29.46	3.616	415.63
69	25	52	3.4	6119	226.67	26.99	5.400	380.91
70	25	52	4.2	6709	280.00	23.96	4.282	338.09
71	25	52	3.4	6000	226.67	26.47	5.486	373.51
72	25	52	3.6	7518	240.00	31.33	5.503	442.02
73	25	52	2.5	5303	166.67	31.82	7.197	448.97
74	25	52	4.2	8586	280.00	30.66	4.839	432.67
75	25	52	3.7	6228	246.67	25.25	4.521	356.28



<b>Specimen No.</b>	<b>Temperature of Testing (°C)</b>	<b>RH of Testing (%)</b>	<b>Weight of Specimen (mg)</b>	<b>Breaking Load (gf)</b>	<b>Linear Mass Density (tex)</b>	<b>Tenacity (gf/tex)</b>	<b>Tensile Modulus (GPa)</b>	<b>Tensile Strength (MPa)</b>
76	25	52	4.0	6743	266.67	25.28	4.988	356.78
77	25	52	4.2	6803	280.00	24.30	4.434	342.82
78	25	52	3.5	7129	233.33	30.55	5.255	431.11
79	25	52	2.8	4678	186.67	25.06	5.920	353.65
80	25	52	3.6	6288	240.00	26.20	5.269	369.69
81	25	52	2.9	7618	193.33	39.40	6.991	556.02
82	25	52	3.3	7557	220.00	34.35	5.755	484.71
83	25	52	3.3	6581	220.00	29.91	5.845	422.12
84	25	52	3.8	7420	253.33	29.29	5.009	413.27
85	25	52	4.3	6720	286.67	23.44	4.436	330.77
86	25	57.5	2.5	5594	166.67	33.57	6.647	473.64
87	25	57.5	3.3	7683	220.00	34.92	6.002	492.77
88	25	57.5	3.9	7015	260.00	26.98	5.082	380.74
89	25	57.5	4.5	8185	300.00	27.28	4.683	384.98
90	25	57.5	2.8	5143	186.67	27.55	5.830	388.79

<b>Specimen No.</b>	<b>Temperature of Testing (°C)</b>	<b>RH of Testing (%)</b>	<b>Weight of Specimen (mg)</b>	<b>Breaking Load (gf)</b>	<b>Linear Mass Density (tex)</b>	<b>Tenacity (gf/tex)</b>	<b>Tensile Modulus (GPa)</b>	<b>Tensile Strength (MPa)</b>
91	25	57.5	3.2	6355	213.33	29.79	6.109	420.33
92	25	57.5	3.5	7831	233.33	33.56	5.527	473.58
93	25	57.5	4.5	7934	300.00	26.45	4.177	373.18
94	25	57.5	2.2	4913	146.67	33.49	7.117	472.63
95	25	57.5	3.5	6440	233.33	27.60	4.672	389.47
96	25	57.5	2.7	5370	180.00	29.83	5.736	420.98
97	25	57.5	4.3	7485	286.67	26.11	4.554	368.45
98	25	57.5	3.9	6503	260.00	25.01	4.823	352.91
99	25	57.5	3.8	8327	253.33	32.87	4.810	463.81
100	25	57.5	2.5	5214	166.67	31.28	5.982	441.40
101	25	57.5	3.1	6124	206.67	29.63	5.880	418.14
102	25	57.5	4.2	7841	280.00	28.00	4.156	395.13
103	25	57.5	2.3	4340	153.33	28.30	6.085	399.37
104	25	57.5	3.9	7381	260.00	28.39	4.830	400.58
105	25	57.5	4.2	8160	280.00	29.14	4.306	411.23

